

# Industrial Applications of Surface Analysis

**Lawrence A. Casper, EDITOR**

*Honeywell-Solid State  
Development Center*

**Cedric J. Powell, EDITOR**

*National Bureau of Standards*

Based on a symposium jointly  
sponsored by the Divisions of  
Industrial and Engineering Chemistry,  
Colloid and Surface Chemistry,  
Petroleum Chemistry, and  
Paper and Textile Chemistry  
at the 182nd Meeting of  
the American Chemical Society,  
New York, New York,  
August 23–28, 1981

TP  
156  
S95  
153  
1982

## TECHNICAL LIBRARY

ADVANCED MICRO DEVICES

901 Thompson Place

P. O. Box 453

Sunnyvale, CA 94086

A C S S Y M P O S I U M S E R I E S **199**

AMERICAN CHEMICAL SOCIETY

WASHINGTON, D. C.

1982



### Library of Congress Cataloging in Publication Data

Industrial applications of surface analysis.

(ACS symposium series, ISSN 0097-6156; 199)

"Based on a symposium jointly sponsored by the Divisions of Industrial and Engineering Chemistry, Colloid and Surface Chemistry, Petroleum Chemistry, and Paper and Textile Chemistry at the 182nd Meeting of the American Chemical Society, New York, New York, August 23-28, 1981."

Includes index.

I. Surfaces (Technology)—Analysis—Industrial applications—Congresses.

I. Casper, Lawrence A., 1945- . II. Powell, Cedric J., 1935- . III. American Chemical Society. IV. American Chemical Society. Division of Industrial and Engineering Chemistry. V. Series.

TP156.S95153 1982 660.2'9453 82-16290  
ISBN 0-8412-0735-6 ACSMC8 199 1-438 1982

Copyright © 1982

American Chemical Society

All Rights Reserved. The appearance of the code at the bottom of the first page of each article in this volume indicates the copyright owner's consent that reprographic copies of the article may be made for personal or internal use or for the personal or internal use of specific clients. This consent is given on the condition, however, that the copier pay the stated per copy fee through the Copyright Clearance Center, Inc. for copying beyond that permitted by Sections 107 or 108 of the U.S. Copyright Law. This consent does not extend to copying or transmission by any means—graphic or electronic—for any other purpose, such as for general distribution, for advertising or promotional purposes, for creating new collective work, for resale, or for information storage and retrieval systems. The copying fee for each chapter is indicated in the code at the bottom of the first page of the chapter.

The citation of trade names and/or names of manufacturers in this publication is not to be construed as an endorsement or as approval by ACS of the commercial products or services referenced herein; nor should the mere reference herein to any drawing, specification, chemical process, or other data be regarded as a license or as a conveyance of any right or permission, to the holder, reader, or any other person or corporation, to manufacture, reproduce, use, or sell any patented invention or copyrighted work that may in any way be related thereto.

PRINTED IN THE UNITED STATES OF AMERICA

Second printing 1984

# ACS Symposium Series

**M. Joan Comstock**, *Series Editor*

## *Advisory Board*

David L. Allara

Marvin Margoshes

Robert Baker

Robert Ory

Donald D. Dollberg

Leon Petrakis

Robert E. Feeney

Theodore Provder

Brian M. Harney

Charles N. Satterfield

W. Jeffrey Howe

Dennis Schuetzle

James D. Idol, Jr.

Davis L. Temple, Jr.

Herbert D. Kaesz

Gunter Zweig

## FOREWORD

The ACS SYMPOSIUM SERIES was founded in 1974 to provide a medium for publishing symposia quickly in book form. The format of the Series parallels that of the continuing ADVANCES IN CHEMISTRY SERIES except that in order to save time the papers are not typeset but are reproduced as they are submitted by the authors in camera-ready form. Papers are reviewed under the supervision of the Editors with the assistance of the Series Advisory Board and are selected to maintain the integrity of the symposia; however, verbatim reproductions of previously published papers are not accepted. Both reviews and reports of research are acceptable since symposia may embrace both types of presentation.

## PREFACE

**T**HIS BOOK COMPILES AND DESCRIBES much of the recent growth in developments and techniques in the fields of surface science and surface analysis. In the past decade, techniques, once mainly of interest to academia, have been adapted to solve a variety of industrial research and development problems. Advanced surface-characterization methods have moved quickly out of the research laboratory and into commercial instrument manufacture. Indeed, this growth has generated a highly specialized, even bewildering, array of techniques—an alphabet soup of techniques in fact.

Recent developments in surface-characterization methods have been made possible to a great extent by technological advances in areas such as lasers, ultra-high vacuum, charged-particle optics, and computer science. The surface-analysis techniques are commonly used to probe the interface between two phases after one phase is removed, but there is now a growing demand for additional methods for in situ interface characterization.

Paralleling the growth in techniques has been an equally rapid growth in the industrial use of surface-characterization methods. Surface and interface properties and processes are now recognized as crucial to many technologies. New processes, devices, and materials have been developed for new or improved products; to minimize degradation or failure; and in response to such national concerns as energy production, shortage of critical materials, and protection of the environment. The automotive industry, for example, may involve many “surface-intensive” components ranging from the exhaust catalytic converter to composite materials in the body. In this and other industries, surface and interface characterization and analysis are employed for failure analysis, process and device development, and process control. The present trend in industry, of increased use of surface and interface characterization is expected to continue as long as economic growth is tied to the advancement of technology.

This book provides an overview of the industrial applications of surface analysis. The range of its uses is so broad that we have not attempted to provide comprehensive coverage. Instead, we have presented some of the topics significant to the industrial sectors and to the energy technologies to illustrate the range of surface analysis methods and their relative utility in solving surface and interface problems.

Included in the book is the symposium's keynote address by C. B. Duke, followed by several introductory chapters for the scientist or engineer not familiar with surface-analysis techniques. The following chapters offer detailed discussions of a wide range of research and development problems in industry. Each author was asked to identify the relevant problems, to indicate where possible the relative utility of different analytical techniques for these problems, and to identify problem areas where new or improved techniques are required. Thus, the book provides a broad review of significant technological phenomena and of the surface-analysis techniques useful for elucidating important problems.

LAWRENCE A. CASPER

Idaho National Engineering Laboratory

Idaho Falls, ID 83415

(Currently with Honeywell-Solid State Development Center

Plymouth, MN 55441)

CEDRIC J. POWELL

National Bureau of Standards

Washington, DC 20234

April 27, 1982

# Surface Analysis: Prologue and Perspective

C. B. DUKE

Xerox Webster Research Center, Rochester, NY 14644

This paper is a synopsis of the introductory lecture at the American Chemical Society Symposium on "Industrial Applications of Surface Analysis." Following a review of the objectives of surface analysis, an outline is given of the design principles for measurements to achieve these objectives. Then common techniques for surface analysis are surveyed briefly. An example of the application of these techniques in microelectronics is indicated. The paper concludes with an assessment of the major advances in surface analysis during the past decade and an indication of the major current trends which could lead to comparable advances during the coming decade.

The main purpose of this Introductory lecture is to set the stage for the detailed papers which follow by indicating broadly the objectives, principles and methods of modern surface analysis. A secondary objective is to provide some perspective on the major developments in modern surface analysis methods during the past decade, and on the prospects for their future development during the coming decade.

## Objectives of Surface Analysis

The objectives of surface analysis, articulated nearly a decade ago (1, 2) and reiterated many times since (3-6), are determinations of the composition, structure, atomistic dynamics and electronic structure of the "surface" regions of a material, usually a solid. Perhaps unfortunately, the concept of a "surface" is not well defined, especially for most samples of industrial interest, because the structure and composition of a material often deviate from their ideal bulk values for depths of microns and in a spatially inhomogeneous fashion. Since each

0097-6156/82/0199-0001\$06.00/0

© 1982 American Chemical Society

In Industrial Applications of Surface Analysis; Casper, L., et al.;  
ACS Symposium Series; American Chemical Society: Washington, DC, 1982.

individual surface analysis spectroscopy exhibits its own depth and areal resolution, each provides its own unique "view" of the inhomogeneous surface region of a solid (2, 7, 8). This fact is a major barrier to quantitative surface analysis, and as such has motivated considerable efforts to establish calibration standards (6, 9). Our emphasis is on the spectroscopic experiments themselves (2, 5, 7, 8,) rather than on their applications per se, which is the main topic of the other papers in this symposium.

Compositional analysis involves the determination of three quantities. The most fundamental of these is the elemental identity of surface species, i.e., the atomic number of each species. It also is desirable to know, however, the chemical identities of these species. For example, is CO adsorbed as a molecule or is it dissociated into separate C and O complexes with the substrate. Finally, it is necessary to determine the approximate spatial location of the various chemical species. Are they "on top" an otherwise undisturbed substrate? Do they reconstruct the substrate or diffuse into it, e.g., along grain boundaries? Or perhaps they form localized islands or even macroscopic segregated phases at various positions across the surface. An important trend in modern compositional analysis is the increasing demand for spatial resolution laterally across the surface on a scale ( $d \lesssim 0.1 \mu\text{m} = 10^3 \text{Å}$ ) comparable to the dimensions of modern integrated circuits (10-12). Compositional analysis is by far the most extensively used form of surface analysis and is the subject of most of the papers in this symposium as well as of numerous reviews in the literature (5-9, 13, 14).

As in the case of surface composition, the specification of surface structure involves three levels of information. For atomically flat single-crystal surfaces, the structure is specified by the atomic geometry in each cell of the surface unit mesh, information available essentially only from low-energy electron diffraction (LEED) intensity analysis (15, 16). All real surfaces contain defects, however, in the form of steps, dislocations, and grain boundaries, for example. These either can be imaged directly (17) or, more commonly, inferred from LEED measurements (18, 19). Finally, the "Macroscopic" topography of the sample on dimensions of 100Å and above is typically determined by scanning electron microscopy (SEM) for 100Å  $\lesssim d \lesssim 10^5 \text{Å}$  and by optical microscopy for still larger dimensions. A new trend in surface structure analysis is the determination of the "local" atomic structure associated with given elemental species by analysis of photoelectron-induced diffraction effects (16, 20). Of these various techniques, only SEM is widely used industrially. Therefore determinations of the atomic geometries of surfaces are available for a relatively small number of rather ideal single-crystal systems studied by LEED and other methods in ultra high vacuum (5, 16). These systems do not include the



vast majority of those considered at this symposium. In spite of this limitation, however, surface structure analyses can provide valuable clues about the interplay between chemical bonding and kinetics which can be extrapolated from model systems to those of technological interest. An example of such a case is developed later during our discussion of metal-semiconductor contacts.

From the perspective of this symposium, analysis of the atomic dynamics and electronic structure of surfaces constitutes an even more exotic topic than surface atomic geometry. In both cases attention has been focused on a small number of model systems, e.g., single crystal transition metal and semiconductor surfaces, using rather specialized experimental facilities. General reviews have appeared for both atomic surface dynamics (21) and spectroscopic measurements of the electronic structure of single-crystal surfaces (3, 22). An important emerging trend in the latter area is the use of synchrotron radiation for studying surface electronic structure via photoemission spectroscopy (23). Moreover, the use of the very intense synchrotron radiation sources also will enable major improvements in the application of core-level photoemission for surface chemical analysis (13).

### Principles of Surface Analysis

The design of a comprehensive set of measurements for the analysis of a surface involves three main considerations. First, the surface must remain stable (i.e., unmodified) during the course of measurements of its properties. Second, the experiments used to examine the sample must be sensitive to its surface (as opposed to bulk) properties. Third, since each individual measurement provides its own view of surface composition and structure, multiple complementary techniques are commonly employed to provide a suitably complete description of a given surface or interface.

The combined considerations of surface stability and multiple techniques lead to the consequence that most surface analysis is carried out in ultra-high vacuum (UHV,  $p \lesssim 10^{-10}$  Torr) vacuum chambers which typically contain an ion gun, one or more electron guns, and possibly a UV or X-ray source as well as detectors embodying the capability for energy analysis suitable for electrons, ions or both, and some means of measuring the pressure and composition of the residual gases in the vacuum (24). Most instruments designed specifically for routine surface analysis also embody vacuum interlocks for sample insertion and removal. A versatile UHV instrument designed to analyze surfaces prepared in situ in the UHV chamber is described in reference four. Descriptions of similar instruments are given in the other papers in this symposium.

Surface sensitivity is achieved by performing scattering or emission experiments using incident or exit species which inter-

act strongly with the samples. Both electrons (2, 25, 26) and ions (2, 14, 27, 28) of suitable energies are appropriate for this purpose. Comparisons of their relative merits for surface analysis may be found in the literature (13, 14, 29, 30). In both cases it is the large inelastic scattering cross sections of these entities which require that their elastic scattering or emission be dominated by contributions from the surface region of the solid. Thus, the measurement of elastic electron or ion scattering cross sections or of sharp line photoemission or Auger emission spectra is an effective vehicle for insuring that the scattering or emission originated in the surface region of the sample. It is beyond the scope of this introductory paper to present detailed models of electron- and ion-solid interactions and scattering. Extensive quantitative models of electron-solid scattering have been developed and tested in the literature during the past few decades as reviewed elsewhere (2, 15, 25, 26). The theory of ion-solid interactions is well developed for fast ( $E \gtrsim 10^6$  eV) ions in those cases (e.g., backscattering from thin films) for which neutralization can be neglected (27, 31). Models of ion neutralization and of secondary ionization are, however, in a rather rudimentary state at the present time (14, 27, 32).

#### Methods of Surface Analysis

The experimental measurements commonly utilized to determine the composition, structure, and dynamics of surfaces can be grouped conveniently into three broad classes. The first consists of scattering and emission experiments from "planar" (i.e., macroscopic surface area,  $A \gtrsim 1 \text{ mm}^2$ , but possibly irregularly shaped) surfaces (1, 4). In such techniques beams of electrons, photons, ions or neutrals are directed toward the surface while the yields (and often the energy and/or angular distributions) from the surface of one or more of these entities are measured. We include in this category the extraction of any of these entities from the surface by heat (e.g., thermal desorption of neutrals) or electric fields (e.g., field-induced desorption of ions). The second class consists of field emission and ionization experiments conducted by applying a strong electric field to a needle-shaped sample and imaging the resultant emission of electrons or ions on a spherical screen, thereby achieving a magnification roughly equal to the ratio of the radius of the screen to that of the tip of the needle (22, 33, 34). The third class consists of measurements of the consequences of the chemical reaction of some external species with a surface. We refer to members of this class as "chemical reaction" (as opposed to UHV) surface analysis methods. They span a wide range of specific measurements including adsorption isotherms, titration experiments, cyclic voltammetry in electrochemical cells, and reactive ion scattering.

In this symposium emphasis is placed on the first class of methods. Isolated examples of the third class are discussed. Consideration of the second class is omitted entirely. Indeed, the scope of the symposium is perhaps best described as encompassing the more widespread techniques of surface compositional analysis as applied to materials science and electrochemistry oriented problems. Many modern surface analysis methods, e.g., those embodying tip sample geometries (21, 22, 33, 34), those based on synchrotron radiation (23, 35), and those dealing with surface structure (15-20) and dynamics (3, 21-23), as opposed to surface composition, are not represented in the symposium program even though many of them enjoy "industrial applications" in the areas of electronics, metallurgy and catalytic chemistry.

Finally, in order to relate the acronyms for the various techniques to the scattering and emission experiments on which they are based, we present in Table I an indication of the relationship between these acronyms, the type of information which they provide, and the scattering or emission experiment which they designate. The definition of the acronyms is given in Table II. These tables embody only "commonly used" methods. Considerably more extensive lists may be found elsewhere in the literature (1, 5-9, 20, 30, 36). Unfortunately, all authors do not use the same acronyms. Therefore Tables I and II are a guide to but not a glossary of the acronyms used in other papers in this symposium.

### Role of Surface Structure in Microelectronics: An Example

Since most of the papers in this symposium deal primarily with the role of surface composition in industrial applications, in this section we depart from that path to consider an example of the role of surface structure in the performance microelectronics devices.

The atomic geometry of a surface or interface is, in certain respects, its most fundamental property. Since most surfaces and interfaces are metastable, especially those of technological interest, their composition and structure depends on their process history. Their structures determine, moreover, the "interesting" interfacial properties which are utilized in specific applications, e.g., reactivity and specificity in catalysis or Schottky barrier height in metal-semiconductor contacts. In addition, the interface structure is measurable by one or more of the techniques noted earlier. Therefore the structure of an interface is a measurable link between the process used to prepare it and the electronic and chemical properties which determine its utility.

While a number of techniques like ion scattering and depth profiling via secondary ion mass spectrometry, Auger electron spectroscopy or X-ray photoelectron spectroscopy can be used to

TABLE I: SELECTED MODERN METHODS OF SURFACE ANALYSIS:  
PROPERTIES, EXPERIMENTS AND ACRONYMS.

The symbol F designates electric fields; T, the temperature; e, electrons; I, ions; A, atoms; and  $\gamma$  photons.

PROPERTY	TIP GEOMETRY (Imaging)	PLANAR GEOMETRY (Statistical)
Atomic, Chemical Composition	F $\rightarrow$ I (atom probe)	e $\rightarrow$ e' (AES) $\gamma$ $\rightarrow$ e (XPS = ESCA) I $\rightarrow$ I (ISS, RBS = HEIS) I $\rightarrow$ I' (SIMS) $\gamma$ $\rightarrow$ $\gamma'$ (IR, RAMAN) I $\rightarrow$ $\gamma'$ (IIXS) T $\rightarrow$ A (TDS)
Atomic Geometry	A + F $\rightarrow$ I (FIM)	e $\rightarrow$ e (LEED, RHEED) e $\rightarrow$ e' (SEM) $\gamma$ $\rightarrow$ e (SEXAFS, ARPES)
Atomic Dynamics	A + F $\rightarrow$ I (FIM)	e $\rightarrow$ e (LEED) e $\rightarrow$ e' (EELS) $\gamma$ $\rightarrow$ $\gamma'$ (IR, RAMAN)
Electronic Structure	F $\rightarrow$ e (FEED)	$\gamma$ $\rightarrow$ e (XPS, UPS, SRPES) e $\rightarrow$ e' (ILEED, AES) I $\rightarrow$ e' (INS)

TABLE II: DEFINITIONS OF THE ACRONYMS IN TABLE I

<u>ACRONYM</u>	<u>DEFINITION</u>
AES	Auger Electron Spectroscopy
ARPES	Angle Resolved Photoemission Spectroscopy
EELS	Electron Energy Loss Spectroscopy
ESCA	Electron Spectroscopy for Chemical Analysis
FEED	Field Emission Energy Distribution (Spectroscopy)
FIM	Field Ion Microscopy
HEIS	High-Energy Ion Scattering
IIXS	Ion-Induced X-Ray Spectroscopy
ILEED	Inelastic Low-Energy Electron Diffraction
INS	Ion Neutralization Spectroscopy
IR	Infra-Red (Adsorption Spectroscopy)
ISS	Ion Scattering Spectroscopy
LEED	(Elastic) Low-Energy Electron Diffraction
RAMAN	Raman (Scattering Spectroscopy)
RBS	Rutherford Backscattering Spectroscopy
RHEED	Reflection High-Energy Electron Diffraction
SEM	Scanning Electron Microscopy
SEXAFS	Surface (Sensitive) Extended X-Ray Absorption Fine Structure
SIMS	Secondary Ion Mass Spectroscopy
SRPES	Synchrotron Radiation Photoemission Spectroscopy
TDS	Thermal Desorption Spectroscopy
UPS	Ultraviolet Photoemission Spectroscopy
XPS	X-Ray Photoemission Spectroscopy

examine the composition profiles normal to a semiconductor interface, evaluations of the atomic geometries of these interfaces are more difficult. Consider, for example, the GaAs/Al contacts of importance for fast digital electronics (37, 38) or the GaAs/Al<sub>0.5</sub>Ga<sub>0.5</sub>As interfaces involved in semiconductor laser technology (38).<sup>x</sup> The best structure analysis of the former has been achieved by X-ray total internal reflectance (39), in which case the structures of the first eighteen layers of Al on GaAs(100) were inaccessible. The sharpness of the latter type interfaces has been assessed by X-ray diffraction from periodic arrays of these interfaces grown by molecular beam epitaxy (40). This technique gives the average Ga and Al composition of layers parallel to the interface and hence provides a high-resolution (roughly 5 Å or two atomic layers) non-destructive profiling method. The high degree of specialty of the techniques used in these structure analyses in spite of the broad technical importance of the interfaces illustrates well the difficulty and the current state-of-the-art of solid-solid interface structure determination.

During the past year the LEED intensity analysis technique has been extended to encompass Al overlayers on GaAs(110) (41, 42). It is found that upon annealing Al deposited on GaAs(110), Al replaces the Ga first in the second atomic layer, next in the third, then in the first, revealing a complicated interplay between the energetically favored bulk Al-for-Ga replacement reaction and the kinetic limitations on Al and Ga diffusion. Moreover, the AlAs surface layer forms a cap on the GaAs substrate, hindering further diffusion in accordance with known activation energies (40) and measurements on Au/GaAs contacts (43). Thus, we are led to the concept that the deposition and reaction of a few monolayers of a reactive metal onto a semiconductor substrate can lead to a diffusion barrier at the interface and to profound changes in its electrical properties. This idea is related, of course, to the well-known technique of using heavily doped surface layers several hundred Angstroms deep to generate ohmic contacts (44). In the present case, however, it is the influence of monolayer quantities of deposited metal which is being considered.

Studies of the electrical characteristics of Au contacts on InP(110) (45), GaAs(110) (45), CdS(10 $\bar{1}$ 0) (46), and CdSe(10 $\bar{1}$ 0) (46) confirm the expectations based on the insight gleaned from our examination of replacement reactions on GaAs(110). The presence of a few monolayers of reactive metal (e.g., Al or Ni) prior to deposition of the Au suppresses the diffusion of the semiconductor species through the Au overlayer and reduces the asymmetry of the I-V characteristic of the Schottky barrier, making it more "ohmic". Indeed, a few monolayers of Al on CdSe(10 $\bar{1}$ 0) renders the resulting Au/Al/CdSe composite contact completely ohmic (46). Thus, studies of semiconductor-metal interface structure in this case led to a new technique for

Schottky barrier height modulation and stabilization as a "by product" of the original studies. Moreover, since these results are thought to follow from replacement reactions in the vicinity of the interface, they reflect the importance of surface structure as well as composition at semiconductor interfaces.

### Perspective

During the past decade improvements in both instrumentation and procedures for data interpretation have extended greatly the range of applications of surface analysis. Perhaps of most importance, the reliability of both electronics and vacuum apparatus have improved to the point that it is no longer a rare occurrence to have all (or most) of the sources, detectors, and manipulators in a vacuum instrument simultaneously functioning. Therefore multiple-technique analysis has gone from an uncommon laboratory accomplishment to a routine surface analysis procedure. The instrumentation for the individual measurements also has improved in both reliability and performance. The advent of computer (most recently microprocessor) control and vacuum interlocks for sample insertion has increased significantly the productivity and thruput of a typical UHV analytical facility. Indeed, these two capabilities plus the development of ion-erosion techniques for depth profiling are primarily responsible for UHV analysis making the transition from a laboratory procedure used for in situ measurements during surface science experiments to widespread utilization as a tool for analytical chemistry. Finally, the data-analysis procedures also have been improved, aided greatly by computer controlled automated data acquisition and manipulation. Serious efforts have been made to develop AES, XPS and RBS as quantitative elemental surface analysis techniques (9, 13, 14, 27, 31). XPS has long been the leading technique for extracting information on the chemical analysis of surfaces, but AES (47) and ISS (48) increasingly are being applied for this purpose also. LEED structure analyses, which were just emerging a decade ago (1, 15), are now commonplace and have been verified in model systems by a wide variety of independent techniques (16). Therefore the major trends in surface analysis during the past decade were the continuing improvements in the reliability, productivity and thruput of instrumentation used for this purpose and in the reliability and diversity of the algorithms and procedures used to extract quantitative composition and structure information from measured scattering and emission spectra.

The coming decade probably will be the scene of still further reliability and productivity improvements as local microprocessor instrument control and data handling become more pervasive and complex. Unlike the past decade, however, for which the ultimately developed surface analysis techniques were well recognized at the outset (1), the coming decade may be the

scene of more innovation. The use of synchrotron radiation as a phonon source will become increasingly commonplace (23, 35), and will not only greatly enhance the effectiveness of "traditional" techniques like XPS and IR but also will enable new spectroscopies like SEXAFS and photoelectron diffraction which probe the local geometrical structure of surface species without the need for single-crystal samples. Scanning techniques for local composition and structure analysis will become increasingly prevalent, being driven, e.g., by the need for spatial information in the microelectronics industry. Indeed the combined trends toward larger wafers and smaller circuits may drive that industry toward complete "vacuum" processing and in situ surface analysis (10, 49). Similarly, pressures to fabricate improved electrochemical and photovoltaic cells are likely to induce the development of photon based techniques for interface analysis so that vacuum is not required for analysis per se (50). Thus, in the coming decade it seems reasonable to anticipate more diversity with the further development of vacuum processing and analysis for some applications (e.g., microelectronics) but also with the development of novel photon-based "remote" interface analysis techniques for others (e.g., electrochemistry, catalytic chemistry). One result we may anticipate with confidence: the techniques which we are discussing in this symposium will appear as much if not more like fossils in 1991 as the thermal desorption and work function measurements of 1971 appear to us today in our era of XPS, AES, RBS, SIMS, LEED, EELS and other electron, ion and photon based spectroscopies which give a truly microscopic picture of the composition and structure of vacuum surfaces.

#### Literature Cited

1. Duke, C.B. and Park, R.L. Physics Today 1972, 25 (8), 23.
2. Duke, C.B. in "Dynamic Aspects of Surface Physics; Proceedings of the International School of Physics 'Enrico Fermi', Course LVIII"; Goodman, F.O. ed; Editrice Compositori: Bologna, 1974; pp 52-98.
3. Eastman, D.E. and Nathan, M.I. Physics Today 1975, 28 (4), 44.
4. Duke, C.B., in "McGraw Hill Encyclopedia of Science and Technology"; McGraw Hill: New York, 1977; Vol. 13, pp 332-333.
5. Somorjai, G.A. and Van Hove, M.A. "Adsorbed Monolayers on Solid Surfaces"; Springer Verlag: Berlin, 1979.
6. Powell, C.J. Applications of Surface Sci. 1978 1, 143.
7. Park, R.L. Physics Today 1975, 28 (4), 52.
8. Park, R.L., in "Surface Physics of Materials"; Blakely, J.M., ed; Academic Press: New York, 1975; pp 377-418.



9. McIntyre, N.S., ed.; "Quantitative Surface Analysis of Materials"; American Society for Testing and Materials: Philadelphia, 1978.
10. Capece, R.P. Electronics November 23, 1978, 111.
11. Broers, A.N. Physics Today 1979, 32 (11), 39.
12. Brady, T.E. and Hovland, C.T. J. Vac. Sci. Technol. 1981, 18, 339.
13. Chang, C.C. J. Vac. Sci. Technol. 1981, 18, 276.
14. Reuter, W. and Baglin, J.E.E. J. Vac. Sci. Technol. 1981 18, 282.
15. Duke, C.B. Adv. Chem. Phys. 1974, 27, 1.
16. Duke, C.B. Appl. Surface Sci. (to be published).
17. Young, R.D. Physics Today 1971, 24 (11), 42.
18. Henzler, M. in "Electron Spectroscopy for Surface Analysis"; Ibach, H. ed.; Springer Verlag: Berlin, 1977; pp 117-149.
19. Lu, T.M. and Lagally, M.G. Surface Sci. 1980, 99, 695.
20. McKee, C.S. Chemical Physics of Solids and Their Surfaces 1980, 8, 41.
21. Ehrlich, G. Physics Today, 1981, 34 (6), 44.
22. Plummer, E.W., Gadzuk, J.W. and Penn, D.R. Physics Today 1975, 28 (4), 63.
23. Eastman, D.E. and Himpsel, F.J. Physics Today 1981, 34 (5), 64.
24. Physics Today 1972, 25 (8).
25. Duke, C.B. Crit. Rev. Solid State Sci. 1974, 4, 371.
26. Duke, C.B. Comments Sol. State Phys. 1975, 6, 141.
27. Chu, W.K., Mayer, J.W., Nicholet, M-A., Buck, T.M., Amsel, G. and Eisen, F. Thin Solid Films 1973, 17, 1.
28. Benninghoven, A. Surface Sci. 1973, 35, 427.
29. Benninghoven, A. Appl. Phys. 1973, 1, 3.
30. Coburn, J.W. and Kay, E. Crit. Rev. Solid State Sci. 1974, 4, 561.
31. Chu, W.K., Mayer, J.W., and Nicholet, M-A. "Backscattering Spectrometry"; Academic: New York, 1978.
32. Hagstrum, H.D. J. Vac. Sci. Technol. 1975, 12, 7.
33. Mueller, E.W. in "Dynamic Aspects of Surface Physics; Proceedings of the International School of Physics 'Enrico Fermi', Course LVIII"; Goodman, F.O. ed; Editrice Compositori: Bologna, 1974; pp. 3-22.
34. Mueller, E.W. in "Dynamic Aspects of Surface Physics; Proceedings of the International School of Physics 'Enrico Fermi', Course LVIII"; Goodman, F.O. ed; Editrice Compositori: Bologna, 1974; pp 23-51.
35. Sparks, C.J. Jr. Physics Today 1981, 34 (5), 40.
36. McRae, E.G. and Hagstrum, H.D. in "Treatise on Solid State Chemistry"; Hannay, N.B. ed.; Plenum: New York, 1976; Vol. 6A, pp 57-163.
37. Wieder, H.H. J. Vac. Sci. Technol. 1980,17, 1009.

38. Holonyak, N. Jr., Stillman, G.E., and Wolfe, C.W. J. Electrochem. Soc. 1978, 125, 487C.
39. Marra, W.C., Eisenberger, P., and Cho, A.Y. J. Appl. Phys. 1979, 50 6927.
40. Flemming, R.M., McWham, D.B., Gossard, A.C., Wiegmann, W., and Logan, R.A. J. Appl. Phys. 1980 51, 357.
41. Duke, C.B., Paton, A., Meyer, R.J., Brillson, L.J., Kahn, A., Kanani, D., Carelli, J., Yeh, J.L., Margaritondo, G., and Katnani, A.D. Phys. Rev. Lett. 1981 46, 440.
42. Kahn, A., Kanani, D., Carelli, J., Yeh, J.L., Duke, C.B., Meyer, R.J., Paton, A., and Brillson, L.J. J. Vac. Sci. Technol. 1981, 18, 792.
43. Brillson, L.J., Margaritondo, G., and Stoffel, N.G. Phys. Rev. Lett. 1980, 44, 667.
44. Wood, C.E.C. J. Vac. Sci. Technol. 1981, 18, 772.
45. Brillson, L.J., Brucker, C.F., Katnani, A.D., Stoffel, N.G., and Margaritondo, G. Appl. Phys. Lett. 1981, 38, 784.
46. Brucker, C.F., and Brillson, L.J. Appl. Phys. Lett. 1981, 39, 67.
47. Madden, H.H. J. Vac. Sci. Technol. 1981, 18, 677.
48. McCune, R.C. J. Vac. Sci. Technol. 1981, 18, 700.
49. Duke, C.B. J. Vac. Sci. Technol. 1980, 17, 1.
50. Duke, C.B. Surface Sci. 1980, 101, 624.

RECEIVED May 21, 1982

# Ultra-High Vacuum Techniques of Surface Characterization

C. R. BRUNDLE

IBM Research Laboratory, San Jose, CA 95193

Four UHV spectroscopies used for the compositional and chemical analysis of surfaces are discussed. These are X-ray Photoemission, Auger Spectroscopy, Secondary Ion Mass Spectroscopy, and Ion Scattering (both low and high energy). Descriptions of the basic processes and information contents are given, followed by a comparative discussion of the surface sensitivities, advantages and disadvantages of each spectroscopy.

The purpose of this short review is to introduce and put into perspective the ultra-high vacuum (UHV) techniques of surface characterization that appear in the later application chapters. The techniques discussed are X-Ray Photoemission (XPS or ESCA); Auger Electron Spectroscopy (AES); Secondary Ion Mass Spectroscopy (SIMS); and Ion Scattering (IS). IS is usually split into two categories: low and high energy ion scattering. High energy ion scattering is more commonly referred to as Rutherford Backscattering Spectroscopy (RBS).

The outline of the chapter is as follows. In the next section, we discuss why certain techniques are designated as "Ultra-High Vacuum," while others are not, and what the factors are determining whether studies should be done at UHV or not. In later sections, a description of the basic processes involved is given, followed by a discussion of the information content available, and a similar discussion on surface sensitivities. Finally, the last section lists the relative advantages and disadvantages of the techniques.

Some comments should be made on areas which are not included. No discussion is given on specific instrumentation. There is virtually no discussion of *structural* characterization of surfaces, the emphasis being on elemental and chemical composition analysis. For this reason, several techniques which are primarily structural tools, are not discussed at all (e.g., Low Energy Electron Diffraction, LEED (1), Surface Extended X-Ray Absorption Fine Structure SEXAFS (2), and neutron scattering (3)), and the structural analysis capabilities of XPS (4), SIMS (5), and Ion Scattering (6) are not covered.

0097-6156/82/0199-0013\$06.00/0

© 1982 American Chemical Society

In Industrial Applications of Surface Analysis; Casper, L., et al.;  
ACS Symposium Series; American Chemical Society: Washington, DC, 1982.

### Why UHV?

By UHV, one usually means a pressure of  $10^{-9}$  Torr or better. This is an operational definition which arises because at this residual pressure, a surface which is very reactive (i.e., which has a high sticking probability for the residual gases), such as Ni, Fe, W, will take fifteen minutes to a few hours of time to become contaminated to monolayer quantities, i.e., long enough to make some measurements while the surface is still clean. If one is interested, therefore, in the initial coverage stages of CO adsorption on clean Ni, one *must* work under UHV conditions. Many material surfaces are rather unreactive to many gases, however, e.g., Si, GaAs, and some polymer surfaces towards oxygen. In such cases, it is not as necessary to work at UHV. Likewise, if one is not interested in initial adsorption phenomena but more extensive interaction (such as corrosion) or simply in characterizing an "as inserted" surface, UHV requirements can be relaxed.

None of the techniques described here *has* to be performed at UHV from an instrumental or fundamental physics point of view. It is necessary that interactions of the probing or signal species (photons, ions, or electrons) with residual gases do not interfere with the surface measurements and there may be some subsidiary instrument factor to be considered (e.g., What pressure will your x-ray source operate at?; Will your electron gun filament burn out?; Will your electron multiplier degrade?), but it is quite possible to work at pressures up to  $10^{-3}$  Torr and with some instrumental ingenuity up to  $10^{-1}$  Torr. Of course, in the practical world, one is often interested in reactions at these pressures and much higher (atmospheric and above or aqueous environments), and then all the techniques described here become unusable, and one must rely on the photon-in, photon-out spectroscopies described in later chapters. RBS, in its usual form, is not usually considered a true surface technique. It is typically one for situations where surface layers of 100's to 1,000's of Å are involved and therefore it is *usually* quite unnecessary to go to UHV conditions (7). However, in the last few years, work has been published which demonstrates that with refinements, the technique is one of the most powerful for quantitative and structural information at the surface monolayer level. Obviously, if used for this type of work, UHV requirements become important.

### Basic Description of the UHV Techniques

**XPS.** The basic XPS process (8) is illustrated in the electronic energy level diagram of Figure 1. The soft x-ray  $h\nu$ , has the possibility of ejecting any electron that has a B.E. of less than  $h\nu$ . The zeroth approximation is that every electron orbital level of energy  $\epsilon$ , will give rise to a peak in the XPS spectrum characterized by a binding energy, B.E.= $\epsilon$ . This is not strictly true because on removing one electron from an n-electron system, the remaining n-1 electrons do not remain "frozen" but relax towards the hole created by the loss of the electron. Thus, B.E.< $\epsilon$ . In addition, it is this *final state relaxation* which is directly responsible for the probability of a two-electron process, in which an electron is promoted from one of the valence level molecular orbitals (M.O.) to an unoccupied higher valence level simultaneously with the removal of the core electron, becoming greater than zero. This results in two (or more) peaks ("main" peak and "shake-up" peak) appearing in the photoelectron spectrum for one  $\epsilon$  value, as illustrated in Figure 1(b).

Another final-state effect which gives rise to an increase in the number of photoemission peaks is multiplet splitting. If the valence levels contain unpaired

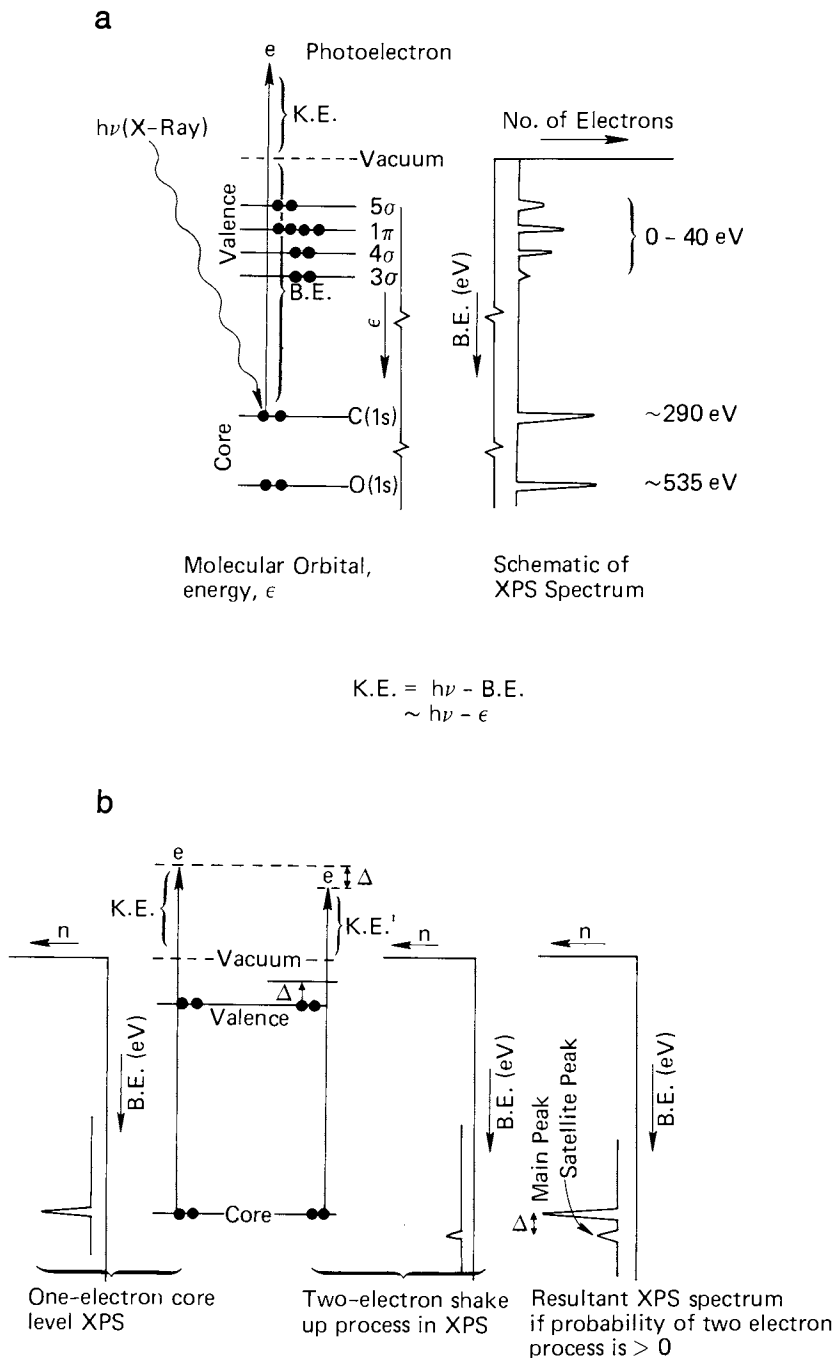


Figure 1. Schemes of the photoemission process (a) and the resultant XPS spectrum using CO as an example. Scheme of a core-level shake-up process in XPS (b).

electrons, (such is often the case for transition metal materials) removal of a core-electron by XPS results in two possible final states with the spin of the remaining core-electron either "up" or "down". The coupling with the unpaired spins of the valence levels will be different for "up" or "down" and so the final state energies and hence the experimentally determined B.E.'s will be different resulting in more than one peak in the photoemission process for a given initial state,  $\epsilon$ .

AES. The basic AES process (9) is illustrated in Figure 2. The decay of a core-hole state by the capture of an electron from a higher lying level (valence or core - a valence level capture is illustrated in the figure) may provide enough energy to eject another electron (valence or core), the Auger electron. The K.E. of the ejected electron is *independent* of the process by which the original core-hole was produced, as indicated in Figure 2. For this reason, AES can be performed either using electrons (1-5 keV typically) or soft x-rays (an XPS x-ray source) to produce the initial hole state. In practice (10), electrons are used more often than soft x-rays for reasons of cost, source intensity, and, very importantly, in many cases, spatial resolution. Anyone performing XPS will obtain x-ray induced Auger spectra as a free extra in his spectra, however, and this method of obtaining AES does offer some advantages to offset the disadvantage of poorer lateral resolution. Since we start with a core-hole, all the original core-hole effects of shake-up structure and multiplet splitting will also show up in AES, in addition to extra structures caused by the possibility of valence level excitation occurring during the Auger decay process.

SIMS. In the SIMS process (11), a beam of energetic ions, typically of 1-20 KeV energy and usually either  $\text{Ar}^+$  or  $\text{O}^+$  strikes the sample surface, penetrates into the sub-surface and loses its energy by a series of inelastic collisions with the substrate atoms (collision cascade). The energy transferred from the lattice is sufficient to cause particles to eject from the surface. Most of these will be neutrals, but a small fraction are positive or negative ions (the secondary ions) which can be mass-analyzed in a quadrupole mass spectrometer. The species ejected from the surface will be a mixture of single atoms and clusters of atoms, e.g.,  $\text{M}^+$ ,  $\text{M}_2^+$ ,  $\text{M}_3^+$ , etc. The objective of SIMS is to derive something about the original surface atomic or chemical composition from the intensities and cluster distributions of the detected ions. Unfortunately, there is not as yet a good understanding of the basic physics involved in determining whether an atom (or cluster) will ultimately appear as an ion or neutral.

IS. The ion-scattering process (6,22) is illustrated in Figure 3. It is essentially a billiard-ball binary collision game. In contrast to SIMS, in which the secondary ejected particles are examined, here the scattered primary ion is energy analyzed. In the low energy version, Ion Scattering Spectrometry, (ISS) 1-5 keV  $\text{H}^+$  or other noble gas ions are used. The single-collision binary scattering takes place entirely at the surface (though primary ions penetrate further - see SIMS) and the incoming and outgoing energies ( $E_0$  and  $E_3$ ) are determined by conservation of mass and momentum, such that, at a scattering angle of  $90^\circ$ ,

$$\frac{E_3}{E_0} = \frac{M_3 - M_1}{M_3 + M_1} \quad (1)$$

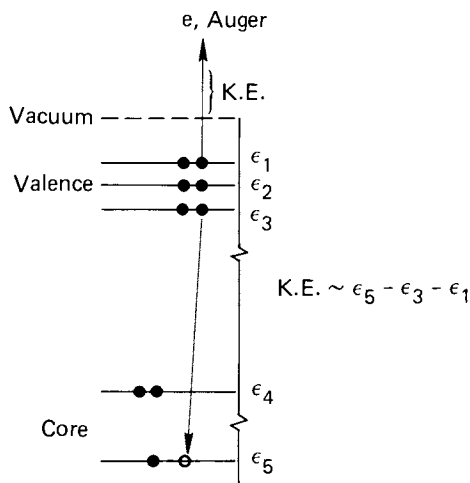


Figure 2. Scheme of the Auger process. A valence-level involved Auger emission is illustrated here, but the two electrons involved also could have come from core level,  $\epsilon_4$ , provided  $\epsilon_5 - 2\epsilon_4 > 0$ .

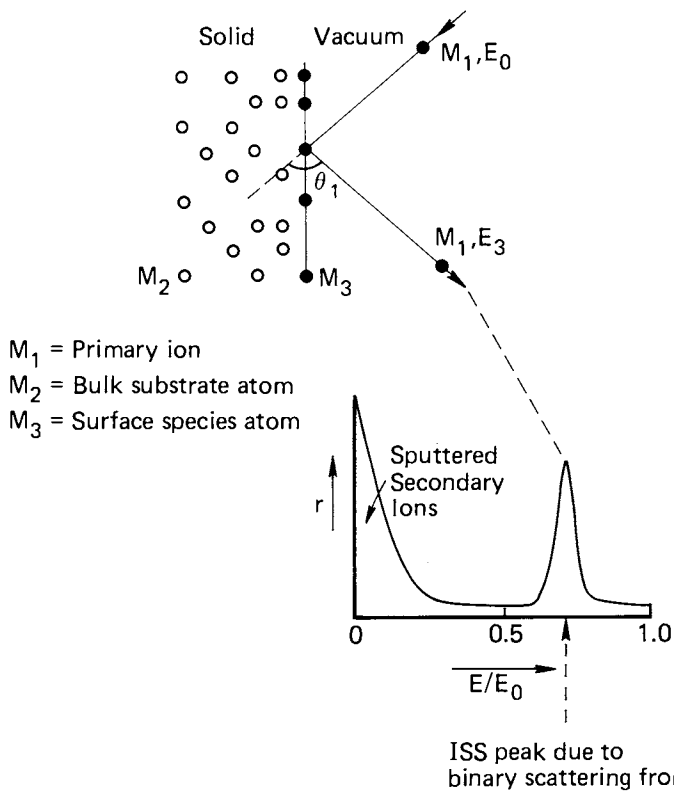


Figure 3. Scheme of the ISS process. No peak due to scattering from substrate atom,  $M_2$ , will appear in the spectrum unless it also is present in the top layer.

where  $M_1$  is the mass of the primary particle and  $M_3$  the mass of the surface atom involved in the binary collision. The equation is a reduced form of the more general equations, that applies at angles other than  $90^\circ$ .

$$\frac{E_3}{E_0} = \frac{1}{\left(1 + \frac{M_3}{M_1}\right)^2} \left\{ \cos \theta_1 + \left[ \left(\frac{M_3}{M_1}\right)^2 - \sin^2 \theta_1 \right]^{1/2} \right\}^2 \quad (2)$$

A schematic representation of the ISS spectrum observed is shown in Figure 3(b).

In the high energy version of ion scattering, RBS, 1-3 MeV  $\text{He}^+$  ions are used. The scattering process is again binary and the same relationships of Eq. (1) hold. However, at this energy, the back-scattering mechanism is from the nucleus (Rutherford scattering). This means that ions directly striking the nucleus are back-scattered, but most of the ions suffer small angle scattering, lose small amounts of energy, travel on into the lattice and after a series of such collisions, will be eventually backscattered and come out again and be detected. The general form of the spectrum obtained for the same sample situation as for ISS in Figure 3 is as in Figure 4. The surface atom, mass  $M_3$ , will be represented by a peak, but the substrate atoms,  $M_2$ , cause a step with decreasing  $E_1/E_0$  values corresponding to ions,  $M_1$ , which have been backscattered after ever deeper penetration into the substrate,  $M_2$ .

### Information Content

**XPS.** As indicated in Figure 1, core-level B.E.'s are characteristic of individual atoms and so one obtains an atomic identification directly from the determined B.E. value. In addition, the core-level photoionization cross-sections are reasonably well-established, both theoretically (13) and experimentally (14), and since the core-levels are atomic in nature, there are no significant variations with chemical environment of the atoms, which means that the atom composition analysis can be made quantitative. All elements which have core-levels, i.e., everything but hydrogen and helium can be detected, though the magnitude of the cross-sections and hence the relative sensitivities to the different elements varies by  $\sim 10^2$ .

The *absolute* sensitivity, i.e., the number of atoms required to give a detectable signal is not good by analytical standards. For typical instruments,  $10^{13}$ - $10^{14}$  atoms are required. Since the sampling area is of the order of  $0.5 \text{ cm}^2$ , this corresponds to  $\sim 0.5$  to 5% of a monolayer as the detection limit if all the  $10^{13}$ - $10^{14}$  atoms are in the top layer.

In addition to atomic identification, information on the chemical environment of the atom is available from three main sources. Most useful is the chemical shift phenomenon. Small differences in B.E. (0-10 eV) occur with differences in the chemical environment of the atom. For metallic species, different oxidation states are usually distinguishable in this manner (15) and for nonmetallic species, such as C, significant variations are observed depending on the electronegativities of the ligands (16). Chemical shifts can be handled in some cases by theoretical means (8), but for most practical situations, a large empirical database is the means of assigning shifts to particular chemical environments. The other two most common means of providing chemical information are from the shake-up and multiplet



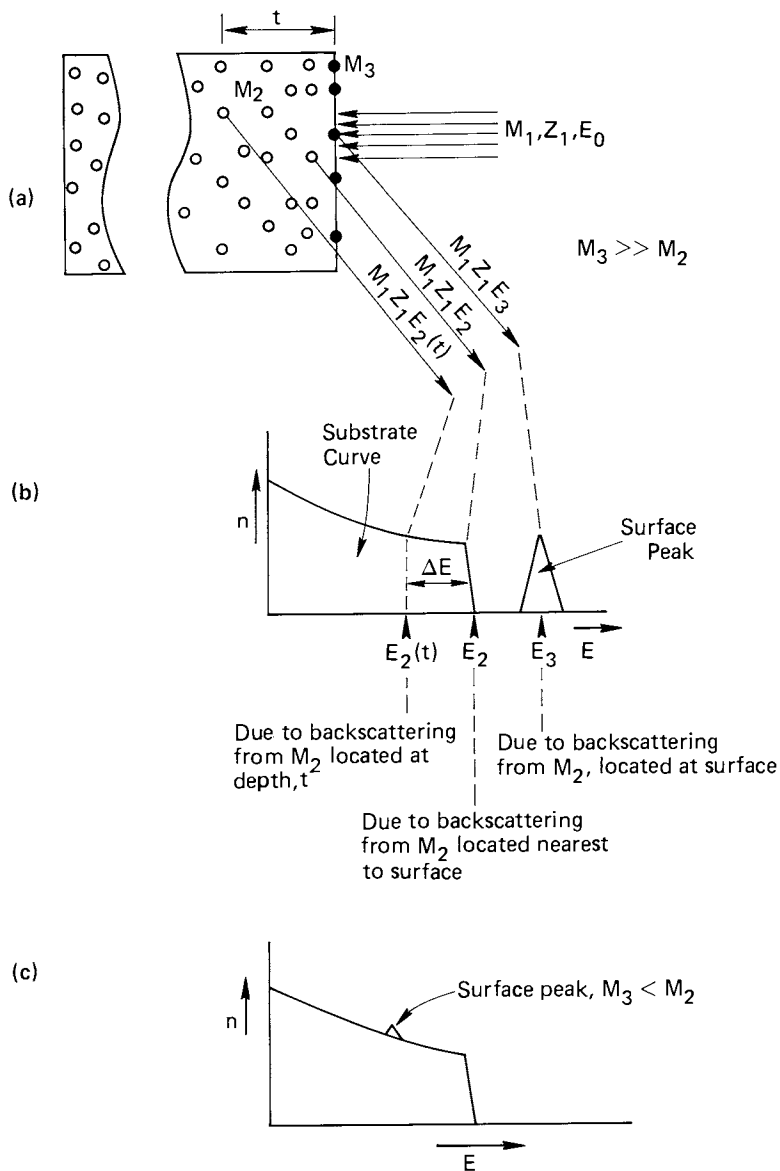


Figure 4. Scheme of the RBS process (a). A spectrum where the surface layer atoms,  $M_3$ , are much heavier than the substrate atoms,  $M_2$  (b). A spectrum where the surface layer atoms are lighter than the substrate atoms (c).

splitting phenomena. Since these effects are caused by electron transitions between occupied and unoccupied valence levels and since valence level energies are characteristic of the molecular or chemical state rather than the atomic state, the presence of structure due to shake-up and multiplet splitting provides additional fingerprinting of the chemical environment of an atom.

**AES.** Atomic identification is provided in an analogous manner to XPS. In Figure 2,  $\epsilon_5$  is a core level and the Auger KE is largely determined by its energy. In general, the Auger K.E. is approximately  $\epsilon_x - \epsilon_y - \epsilon_z$  where  $\epsilon_x$  is the B.E. of the initial core-hole level, and  $\epsilon_y$  and  $\epsilon_z$  are the energies of the higher lying electrons involved in the Auger process. The quantitative capabilities are in poorer shape than XPS for several reasons. First, the process is more complex, involving three electron levels instead of one. The core-level photoionization or electron impact cross-section has to be folded with the Auger decay channel probability. The latter is not as well-known as photoionization cross-sections, which makes quantitative analysis from first principles more difficult. Experimental standards are also less well-established and finally the usual manner of recording Auger spectra in the first derivative mode and measuring peak-to-peak heights can introduce large errors owing to line-shape changes. (In XPS, the areas under the "main" and all satellite peaks are summed.)

All the chemical shift, shake-up and multiplet splitting information of XPS is, in principle, available in AES (9,10). The interpretation is more complex, however, because of the three levels involved in the process. In practice, Auger chemical shifts, etc., have not been nearly so widely exploited as they have in XPS. The empirical database is to date much more limited and again the habit of recording in the first derivative mode, often with poor resolution (to increase sensitivity for fast semi-quantitative elemental analyses) has obscured the usefulness of the chemical information. The exceptions to these remarks are usually from XPS practitioners who take their x-ray induced Auger data in the same manner as the XPS data and treat the analysis on an equal footing (9).

It should be pointed out that the chemical shifts observed in AES are not usually the same as in XPS for the same atoms in the same chemical state. Often, they are larger because of the two-hole nature of the final state in the Auger process. The difference between the XPS and Auger chemical shift has been termed the Auger parameter (17) and is an additional useful guide to the chemical state of the atom concerned.

**SIMS.** SIMS is performed in either of two distinct modes, "static" or "dynamic". The information content depends on which mode one is using (assuming typical usage in each mode). The more commonly used mode, especially in analytical laboratories, is the "dynamic" one (18). Here, the sputtering rate is kept high so that whatever information is obtained corresponds to a profile throughout a sputtered depth. The objective of these measurements is usually to obtain an atomic composition depth profile. Thus, for instance, a typical example from the semiconductor industry would be an in-depth concentration profiling of boron in silicon, performed by monitoring the intensity of the most intense B containing secondary ions ( $B^+$ ) in the SIMS spectrum. The depth profile range might be of the order of 100's to 1,000's of Å and the raw data would consist of a plot of observed  $B^+$  and  $SiO^+$  secondary ion intensities as a function of sputter time (19). To transform this to a composition versus depth-profile, two conversions are required: time to depth and intensity to concentration. The time-to-depth conversion problem

is not limited to SIMS but is common to all profiling measurements involving sputtering and is usually done by simply measuring the depth of a deep sputter crater with a stylus technique and assuming a constant sputter rate. This has some potential inaccuracies, as briefly discussed at the end of the next section. The intensity to concentration conversion is done by either using homogeneously bulk doped standard samples of known density or ion-implanted samples of known dose for calibration. An important point here is to recognize that secondary ion yields are a very strong function of the *chemical* state of the elements in the surface, so that if the chemical state of the element being profiled changes as a function of depth, then the observed atomic concentration profile of that element will be distorted by secondary ion yield changes. For example, the secondary ion yield of  $\text{Ni}^+$  from a clean Ni sample has been quoted as being  $\sim 10^2$  times smaller than that of  $\text{Ni}^+$  from an oxygen covered Ni surface (11). (The total sputter yield does not change significantly; there is simply a change in the number which are ejected as ions as opposed to neutrals.) In practice, such large artifacts can be mostly overcome for the atomic composition profiling measurements by keeping the surface in a constant chemical state during profiling. This is usually achieved by using an  $\text{O}_2^+$  primary beam, which oxidizes the surface as well as sputtering it (18,19). As can be seen from the above quoted Ni example, oxidized surfaces generally give much higher ion yields so that the SIMS sensitivity is also increased by using the  $\text{O}_2^+$  beam. Using  $\text{O}_2^+$  beams can also introduce artifacts, however, such as when profiling alloys where one component undergoes preferential oxidation and surface segregation.

The main advantage of SIMS over other profiling techniques is its large dynamic range. For example, a calibrated B in Si depth profile is shown in Figure 5 (19). The concentrations span four orders of magnitude and the detection limit is  $\sim 5 \times 10^{15}$  atoms/cm<sup>3</sup>, far below the detection limits of XPS or AES. Further significant advantages that SIMS has over XPS and AES are the ability to detect hydrogen and isotopically labelled elements. In terms of spatial resolution, SIMS is intermediate between AES and XPS in its capabilities.

In static SIMS, the primary beam current density is kept sufficiently low, such that the sputtering rate is small compared to the data collection rate (11). To achieve this, it is necessary to make the beam as large as possible ( $\sim 0.5$  cm), or to raster the beam over a large area. Spatial resolution is therefore sacrificed. In any case at the low current densities and low energies (typically 1 KeV for static SIMS compared to  $\sim 20$  KeV for dynamic SIMS) used, it is not possible to focus on small spot sizes. Inert primary beams such as  $\text{Ar}^+$  or  $\text{Xe}^+$  are used. The objectives of static SIMS measurements are usually different from dynamic measurements. The relative intensities of all the monomer and cluster ions are measured and from these information not only on the elemental composition, but on the chemical state and short range order of the surface species can sometimes be extracted. For example, for CO adsorption on Ni, CO containing secondary ions will be observed in SIMS if the CO is molecularly adsorbed, whereas no such species are observed if the CO is dissociated on the surface (20). Similarly, large intact organic molecules are often identified by the presence of a parent ion SIMS peak. For dissociated species, the nature of the fragment concerned can often be identified. For example, the presence of atomic oxygen can be distinguished from OH (20). For alloys preferential adsorption to, or oxidation of, one component can be identified from the large enhancements in SIMS yield observed for that component. At present, however, none of these chemical identification features is on a very sound quantitative footing

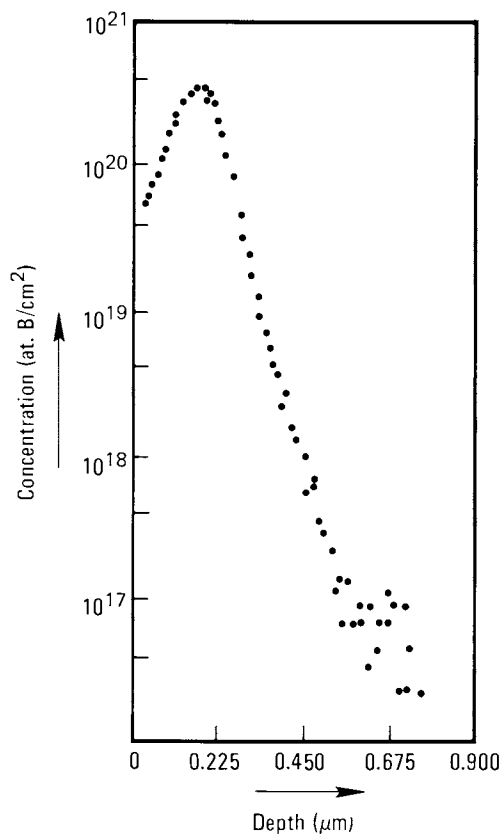


Figure 5. Indepth SIMS concentration profile of B in Si showing a dynamic measuring range of  $10^4$  (19).

because of the tremendous and poorly understood changes in ion yields with change in chemical state.

IS. ISS provides an atomic identification only (see Figure 3(b)) since the binary collision carries no direct chemical information though chemical effects can influence ion yields through changes in neutralization rates. In principle, all elements can be detected from a measurement of  $E_3/E_0$ , but in practice, elemental resolution is a limiting factor (6,12).  $\text{He}^+$  primary beams are most commonly used and since the best resolution is obtained for  $M_1 \approx M_3$  (see Eq. (1)), unit mass resolution can not be achieved with  $\text{He}^+$  for heavy target atoms. The resolution at high mass can be retrieved by going to heavier primary ions ( $\text{Ar}^+$ ,  $\text{Ne}^+$ ). Other factors which affect resolution are the energy resolving power of the analyser and the angle,  $\theta_1$ . For  $\theta_1$  of  $<90^\circ$ , mass resolution decreases drastically (see Eq. (2)). Commercial instruments are usually designed to operate at  $90^\circ$  scattering angle using  $\text{He}^+$ . Under these conditions, the resolution is limited, being inadequate to resolve Ni from Zn. However, the use of high scattering angles ( $90^\circ$  or greater) and low mass primary ions keeps to a minimum the features in the spectra which arise from multiple scattering and shadowing effects and therefore simplifies interpretations for compositional analysis. Low angle scattering using heavier ions ( $\text{Ar}^+$ ) accentuates these effects and also greatly increases the scattering cross-sections. Such shadowing and multiple scattering effects are, in fact, used for *structural determinations* (6). Since IS is a mass spectrometric technique, it has, like SIMS, the capability of detecting isotopically labelled elements, subject to the constraints of resolution described above. Absolute and relative sensitivities of elements in ISS depend on two factors: the scattering cross-sections for the incident ion and the ion-neutralization probability. Scattering cross-sections increase with increasing  $M_1/M_3$  and with decreased scattering angle, but values cannot be accurately calculated. Neutralization of the incident ion as it approaches the surface can occur by several mechanisms, the most probable being Auger ion neutralization. This effect reduces the detected scattered ion current and is strongly dependent on the incident ion species and the composition of the sample. Like SIMS, therefore, quantitative analysis is difficult unless we use well-defined standards for calibration purposes. This has not often been done and there are indications that some qualitative conclusions concerning the presence or absence of adsorbate species above substrate surfaces may, therefore, be in error.

In RBS (high energy ion scattering), atomic identification considerations are similar to ISS but now since a nuclear scattering process is involved, scattering cross-sections are accurately known (Rutherford cross-sections), and ion neutralization is not important because the solid state detectors used in this energy range are sensitive to both ions and neutrals. The measurements then become quantitative (21). However, the incident 1 MeV ions can penetrate long distances before being back-scattered and therefore, in its usual mode, RBS is not very surface sensitive and does not require UHV conditions. In favorable cases, however, for example, a heavy element,  $M_3$ , on a light substrate,  $M_2$ , such as illustrated in Figure 4(a) and (b), it is still possible to detect low surface concentrations from the surface peak. For light elements on heavy substrates, the surface peak rides on the substrate step-structure (Figure 4(c)) and also the cross-section for the light element is much smaller, greatly increasing the amount required in the surface layer for detection.

Factors affecting the depth resolution and surface sensitivity in RBS are discussed further in the following section.

### Surface Sensitivities

A technique can be surface sensitive for two reasons. Either the detected signal comes only from the surface region or it comes from the surface plus bulk but it is possible to distinguish the surface component from the bulk. In XPS and AES, the signals we are interested in are those electrons which are detected without suffering inelastic collisions and which therefore appear at their original characteristic energies in the electron spectrum. The mean free path length for inelastic scattering is short so these electrons can only have originated from near the surface and the techniques are thus surface sensitive. The exact thickness from which the detected electrons can escape depends on several parameters; the electron kinetic energy, the nature of the solid (shortest in metals, largest in organic materials), and the geometry of the experiment. These factors have been discussed several times elsewhere (8,22). Varying the K.E. of the detected electrons by varying the incident photon energy,  $h\nu$  or the angle of detection of the photoelectrons (23) provides a means of varying the depth from which the signal is generated. The sampled depth can vary from a few Å to  $\sim 100\text{Å}$  taking all the above items into consideration.

For SIMS in the static mode using relatively low energy ions (typically 1-3 KeV), the majority of ejected secondary ions is believed to come from the first atomic layer and nothing from beyond the third layer (5). It is, therefore, comparable to XPS and AES in their most surface sensitive conditions (low angle, low KE). In the dynamic mode, the fast sputtering rate and the consequent interface broadening effects (see next section) muddy the definition of surface sensitivity since the surface is rapidly changing. A better figure of merit would be the depth resolved. This is likely to be on the order of  $\sim 20\text{Å}$  near the vacuum-surface interface and will increase with the depth sputtered owing to sputter broadening effects. At  $1000\text{Å}$  depth, a figure of  $\sim 100\text{Å}$  is common, or a depth resolution of  $\sim 10\%$ .

ISS has the greatest surface sensitivity in terms of depth sampled (but not in terms of lowest limits of detection. SIMS is much superior here.) Though the impinging  $\text{He}^+$  ions can penetrate the lattice, the single-collision binary events occur entirely with atoms from the top-most atomic layer so the ISS spectrum is restricted to that layer. The detection limit is of the order of  $10^{-2}$ - $10^{-3}$  monolayers.

RBS is quite different from ISS in its surface sensitivity characteristics, as mentioned in the previous section. Referring to Figure 4, if  $M_3$  were Pb and  $M_2$  Si (spectrum represented schematically in Figure 4(b)), a surface peak would be detectable for Pb concentrations as low as  $10^{12}$  atom/cm<sup>2</sup>, which means  $10^{-3}$  monolayers if they were all located exactly on the surface, as drawn in Figure 4(a). For a situation at the opposite extreme, (a low Z layer on a high Z substrate) say a hydrocarbon on copper (schematically indicated spectrum 4c), some  $10^{15}$ - $10^{16}$  atoms/cm<sup>2</sup> would be required (1-10 monolayers) for detection in the "surface" peak. Rutherford scattering cross-sections are several orders of magnitude lower than for electronic scattering processes and as the MeV  $\text{He}^+$  or  $\text{H}^+$  ions penetrate into the solid, the major energy-loss mechanism is through electronic interactions. The rate of energy loss with distance,  $x$ ,  $dE/dx$ , depends on  $M_1$  and  $M_2$ , but it is a well-known quantity and may be obtained from tables. The total amount of energy lost through these low-angle forward-scattering electron

interactions for an ion which ultimately undergoes a Rutherford backscattering process and is detected in the RBS spectrum can therefore be used to determine thicknesses. However, as traditionally used, the depth resolution of RBS is very poor. This is usually an *instrumental* limitation. Solid state detectors are used which have poor energy resolution, which from the following equations, can be seen to translate directly into depth resolution.

$$E_0(t) = E_0 - t \left( \frac{dE}{dx} \right)_{E_0} \quad (3)$$

where  $E_0(t)$  is the energy of the incident particle,  $M_1$ , at depth  $t$  prior to backscattering. The final energy of  $M_1$  after backscattering from substrate atoms,  $M_2$ , at depth,  $t$ , and returning out to the detector is given by

$$E_2(t) = \left( \frac{M_2 - M_1}{M_2 + M_1} \right)^2 E_0(t) + \frac{t}{\cos \theta} \left( \frac{dE}{dx} \right) \quad (4)$$

for normal incidence. Thus, in Figure 4(b), the energy spread,  $\Delta E$ , of the "peak" corresponding to scattering from  $M_2$  is a direct measure of the thickness of the material. If the energy resolution of the instrument ( $\Delta E/E$ ) is poor, then the depth resolution is poor. Typical depth resolutions are 50-150Å because of detector resolution limitations. Therefore, in the example quoted above of Pb on Si, though as little as  $10^{12}$  atom/cm<sup>2</sup> of Pb could be identified as being "in a surface layer," one could not distinguish  $10^{12}$  atoms/cm<sup>2</sup> in the top monolayer from  $10^{12}$  atoms/cm<sup>2</sup> dispersed over the depth resolution (30-100Å).

Channelling and Blocking in RBS. For single-crystal materials, channelling and blocking methods allow one to convert RBS from a technique which is primarily usable in measuring depth-distributions over 100's-1,000'sÅ to one with routine monolayer and sub-monolayer sensitivity. The basis of the approach (21) is shown in Figure 6(a). The incoming beam is aligned with a major crystallographic axis of the sample. Ions impinging close to the *nucleus* of a surface atom are backscattered and detected, but all others suffer small-angle collisions and are channeled away from the atom and into the bulk. The second atom down on the crystallographic axis is in the "shadow cone" of the top atom and there is little probability of Rutherford backscattering occurring from it. The exact probability depends on the radius of the shadow cone,  $R$ , and the vibrational amplitude of the atoms and can be calculated. Increased surface sensitivity is obtained by essentially suppressing the bulk signal. Thus, the number of atoms "per string" contributing to the RBS signal in an aligned experiment can be calculated. The result of such an alignment experiment is indicated in Figure 6(b) where nonaligned and aligned RBS spectra for W are shown (21). The step distribution of the nonaligned experiment has been replaced by a surface peak and a suppressed bulk signal in the aligned experiment. From the area under the peak, the number of atoms "per string" contributing to the peak was calculated and found to be larger than that expected for a bulk W crystal. This is because the top layer of W atoms is, in fact, reconstructed with the W atoms laterally displaced from their bulk positions, thereby reducing the shadowing effect of the first row atom on the second row atoms located in bulk positions. The dotted curve in Figure 6(c) shows the effect of adsorbing H on the W surface. The shadowing effect from the H itself is negligible, the large decrease in W surface peak being

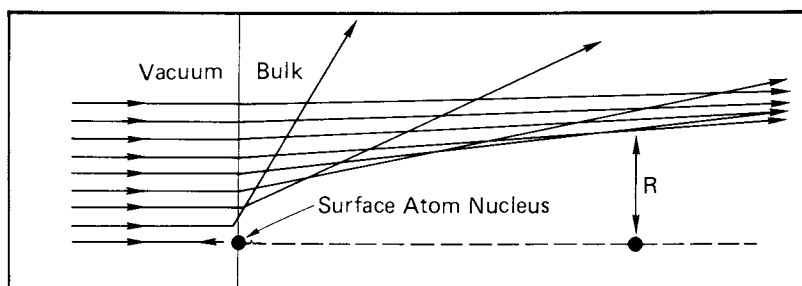


Figure 6a. Formation of a shadow cone, radius  $R$ , (one half shown only) at an atom in the second row for an aligned incident beam. (Reproduced, with permission, from Ref. 21. Copyright 1981, CRC Press.)

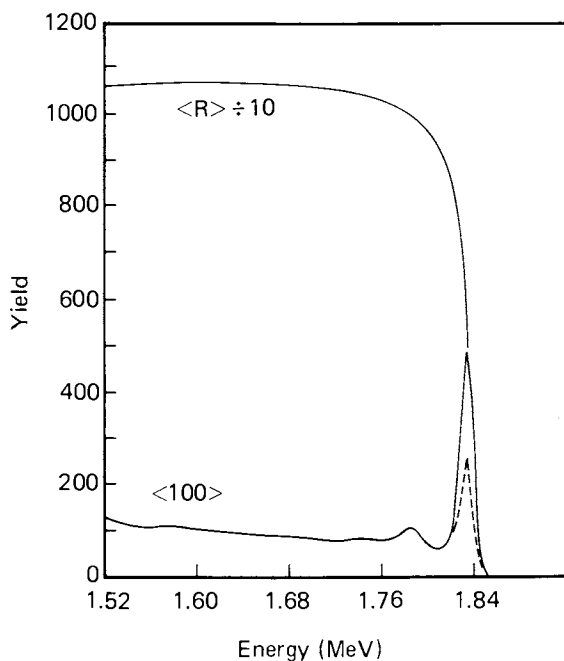


Figure 6b. Scattering spectrum for 2 MeV  $He^+$  on a  $W(100)$  crystal.  $\langle R \rangle$  represents the nonaligned spectrum, 100 the  $(100)$  channeling direction spectrum. The dashed curve represents the channeled spectrum after hydrogen adsorption. (Reproduced, with permission, from Ref. 21. Copyright 1981, CRC Press.)



caused by the top W atoms moving back to their bulk positions under the influence of the H adsorption.

Blocking experiments in RBS are conceptually the same as channelling. In addition to aligning the incident beam, a movable detector scans the scattering angles of the emergent beam. At the angle where a surface atom is directly aligned with ions backscattering from an atom beneath (blocking direction) the back-scattering yield will decrease due to shadowing by the surface atoms. The concentration and the geometric location of the surface atoms can be determined by such experiments.

The instrumental requirements for channelling and blocking experiment are much more severe than for standard RBS. A scattering chamber with high precision double-alignment capabilities is needed, which since it is used for sub-monolayer studies, must also be capable of achieving UHV. A movable detector is required. Both the depth resolution of thickness determinations made from the energy spread of the RBS peaks and the surface peak/bulk background ratio are therefore enhanced. Working at these energies excludes the use of the standard solid state detectors, however, since their energy resolution is far too poor ( $\sim 20$  keV), and one must go to electrostatic detectors, as for ISS. For measurements made with 100 KeV ions using both channelling and blocking, it becomes possible to observe sub-monolayer quantities of light elements on heavy substrates and determine concentrations accurately. For example, two studies of oxygen on Ni(110) (24) and Ni(100) (25), have recently been performed where the oxygen coverage is monitored directly from the oxygen RBS peak between 0 and 1.6 monolayer coverage.

**Depth Profiling by Ion Milling.** From the preceding discussion, it is clear that the four techniques can sample differing thicknesses into the bulk, and that for XPS, AES, and RBS, the thicknesses sampled depend rather strongly on the parameters chosen for the experiment. ISS always samples only the top monolayer; static SIMS mostly the top monolayer; XPS and AES between 1-20 monolayers, depending on materials and operating parameters; and RBS 1 - many hundred monolayers depending upon operating conditions.

Very often, we require more information than simply the elemental and chemical composition within the probing depth of the technique. One may require a depth distribution through that probing depth or information to a thickness far beyond the probing depth. In the case of RBS operated in its nonaligned mode, the latter requirement is unlikely since the probing depth is so deep, and the depth distribution within that probing depth is provided from the energy width of the RBS peaks (albeit with very poor depth-resolution). In the case of XPS and AES, a depth distribution through the probing depth can be obtained nondestructively by actually varying the probing depth by varying angles (23) (also photon energy for XPS). For all other cases, i.e., XPS and AES beyond the limit of their probing depth and for SIMS and ISS always, the depth distribution must be obtained by removing surface layers and taking fresh measurements. This is most commonly done by Ar<sup>+</sup> sputtering (or in the case of dynamic SIMS and ISS sputtering by whatever primary ion is being used). Time-of-sputtering then has to be converted to a depth scale, as discussed earlier for SIMS. This calibration is usually done by either physically measuring the sputtered depth after extensive sputtering (0.1-1  $\mu\text{m}$  required), or determining the time required to sputter through a known thickness of material. Unfortunately, materials sputter at very different rates so in the latter method, a fresh calibration is really required for each material.

If conversion of time-to-depth sputtered were the only problem, things would not be too bad since often relative concentrations as a function of depth are the main concern with the absolute value of the depth being of lesser importance. Many artifacts are introduced by the sputtering process itself, however, and these have to be carefully considered in evaluating any profile obtained using sputtering. The major artifacts are mentioned briefly below.

- (a) "*Knock-on*" effects. In addition to removing material, sputtering will drive some into the bulk. This has the effect of broadening any interface widths measured.
- (b) *Surface roughening*. A flat surface will become progressively roughened during sputtering owing to either macroscopic differences in sputtering rate or differences in sputtering yields for different elements (see below). Profiled interfaces again become artificially broadened, the effect getting worse the further one has to sputter before reaching the interface.
- (c) *Preferential sputtering; chemical changes*. Different elements may sputter at different rates so the composition within the probing depth at any given sputter depth may not be representative of the original composition at that depth. The preferential sputtering may also induce severe *chemical* as well as elemental changes. For instance, extensive sputtering of  $\text{Fe}_2\text{O}_3$  by  $\text{Ar}^+$  will yield a mixture of  $\text{Fe}^0$  (metal),  $\text{Fe}^{\text{II}}$  and  $\text{Fe}^{\text{III}}$  oxidation states at the surface owing to preferential loss of O (26).
- (d) *Radiation induced chemical reactions*. The interaction of energetic ions with the surface may cause reactions to occur at the surface (either between species on the surface, or between surface and gas) which would not otherwise occur.
- (e) *Ion enhanced diffusion*. Certain elements undergo greatly enhanced diffusion under the influence of charged bombardment.
- (f) *Sputter re-deposition*. If large amounts of material are being removed by sputtering, some may eventually be redeposited on the surface. This is largely an instrumental configuration problem which can be overcome with care.

### Comparative Advantages and Disadvantages of the UHV Techniques

In this section, the advantages and disadvantages of XPS, AES, SIMS and the two types of Ion Scattering are listed. For most practical applications, compromises are usually made in the use of the techniques; resolution for sensitivity; speed for detail, etc. The discussion here refers to typical usage situations rather than extremes. As in most surface studies, it is usually advantageous to combine two or more of the techniques in one system. First, it is generally more cost effective since a significant part of the cost relates to the vacuum systems and sample manipulation and treatment capabilities. Secondly, the preparation of an identical surface in two different systems cannot be guaranteed and therefore greater faith is generally placed in complementary studies by two techniques if they are performed simultaneously on a single surface.

## XPS

### Advantages

1. Sub-monolayer sensitivity; probing depth 1-20 monolayers, depending on material and experimental parameters.
2. Detection of all elements, except H, with reasonably well-known cross-sections without strong matrix effects.
3. Quantitative elemental analysis; often limited in practical situations by the combination of an unknown depth distribution over the probing depth, which itself may not be known to better than a factor of 2.
4. Excellent chemical information from the use of chemical shifts and satellite structure in conjunction with a well-documented database on standard compounds.
5. X-ray beam damage is not often a problem.

### Disadvantages

1. Very poor lateral resolution; sample areas studied usually vary from 0.5 mm<sup>2</sup> to 1 cm<sup>2</sup>.
2. Typical data collection is slow compared to typical AES. This is partly because more detailed information is usually collected for XPS and partly because of the low brightness of x-ray sources.
3. In depth profiling using Ar<sup>+</sup> sputtering, it is not easy to take the XPS data while actually sputtering.

## AES

### Advantages

1. Submonolayer sensitivity as for XPS and He.
2. Detection of all elements except H and He. Cross-sections not as well-known as for XPS. Matrix effects when valence levels are involved in the Auger transitions.
3. Fast, semi-quantitative elemental analysis (less accurate than XPS owing to a combination of less well-known cross-sections, and the manner in which the data are usually taken). Simultaneous Ar<sup>+</sup> profiling.
4. Some chemical information from chemical shifts, line shapes, etc. Not often fully exploited.
5. Excellent lateral resolutions (0.05 μm).

### Disadvantages

1. Severe electron beam induced beam damage in many cases (e.g., organics, oxides, chemisorbed molecules).
2. Poorer understanding of chemical shifts, etc. and lack of extensive database limit chemical information.

## SIMS

### Advantages

1. Extreme surface sensitivity for some elements ( $10^{-6}$  monolayer). Probing depth restricted to top monolayer in the nondestructive static mode.
2. Detection of all elements, including H; isotope identification.
3. Moderately good lateral resolutions ( $1\ \mu\text{m}$ ).
4. Simultaneous depth profiling in the dynamic mode.
5. In the dynamic mode, the only technique with sufficient sensitivity to profile dopant-level concentrations in semiconductors.
6. Limited chemical information (at present) from relative intensities of cluster ions.

### Disadvantages

1. Intrinsically destructive.
2. SIMS process not well-understood. Major problem is the huge variation in a given SIMS ion intensity with changes in chemical or physical environment. This makes quantitative elemental analysis difficult.

## ISS

### Advantages

1. Single binary collision interactions, and therefore probing depth, restricted to top monolayer.  $10^{-2}$ - $10^{-3}$  monolayer sensitivity.
2. Detection of all elements except H and He.
3. Isotope separation.

### Disadvantages

1. Scattering cross-sections and ion-neutralization cross-sections not well understood. ISS can therefore be quantitative only when calibrated against some other technique, or when using standards.
2. No chemical information available in most cases.
3. Intrinsically destructive
4. Moderate lateral resolution ( $100\ \mu\text{m}$ ).
5. Poor mass resolution for high mass elements.

**RBS****Advantages**

1. Quantitative because of accurately known Rutherford cross-sections.
2. Using medium energies (100-300 keV) and double alignment instrumentation becomes a quantitative elemental analysis tool with sub-monolayer sensitivity. It has excellent *structural* analysis capabilities.
3. Beam damage is usually very small.

**Disadvantages**

1. Expensive, requiring an accelerator.
2. Standard RBS (nonaligned experiments) is not very surface sensitive and is therefore not usually performed under UHV conditions.
3. No direct chemical information.
4. Channelling and blocking experiments, and therefore the true surface sensitive capabilities of RBS, are restricted to single crystals.
5. Poor lateral resolution (~1 mm).

**Literature Cited**

1. Ertl, G.; Küppers J. "Low Energy Electrons and Surface Chemistry"; Verlag Chemie: Weinheim, 1974.
2. Stohr, J. E. Surface Science, to be published.
3. Suzanne, J.; Coulomb, J. P.; Bienfait, M.; Matecki, M.; Thomy, A.; Croset, B.; Marti, C. Phys. Rev. Lett. 1978, **41**, 760.
4. Fadley, C. S. Progress in Surface Science, to be published 1982.
5. Winograd, N.; Garrison, B. J. Accts. of Chemical Research 1980, **13**, 406.
6. Armour, D. G. Vacuum, to be published.
7. Chu, W-K.; Mayer, J. A.; Nicolet, M. A. "Backscattering Spectrometry"; Academic Press: New York, 1978.
8. Fadley, C. S.; in "Electron Spectroscopy, Theory Techniques, and Applications"; Vol. 2, Eds. Brundle, C. R. and Baker, A. D.; Academic Press: London, 1978.
9. Fuggle, J. C. in "Electron Spectroscopy, Theory Techniques, and Applications"; Vol. 4, Eds. Brundle, C. R. and Baker, A. D.; Academic Press: London, 1981.
10. McGuire, G. E.; Holloway, P. H. "Electron Spectroscopy, Theory Techniques, and Applications"; Vol. 4, Eds. Brundle, C. R. and Baker, A. D.; Academic Press: London, 1978.
11. Benninghoven A. "Critical Reviews in Solid State Sciences"; CRC Press, Inc.: Cleveland, Ohio, 1978.
12. Taglauer, E.; Heiland, W. Appl. Phys. 1976, **9**, 261.
13. Scofield, J. H.; J. Electron. Spectr. 1976, **8**, 129.
14. Evans, S.; Pritchard, R. G.; Thomas, J. M.; J. Electron Spectr. 1978, **14**, 341.
15. Holm, R.; Storp, S.; Appl. Phys. 1977, **12**, 101.

16. Dilks, A. "Electron Spectroscopy, Theory Techniques, and Applications"; Vol. 4, Eds. Brundle, C. R. and Baker, A. D.; Academic Press: London, 1978.
17. Wagner, C. D.; Faraday Disc. 1975, 60, 291.
18. Yu, M. L.; Reuter, W.; J. Appl. Phys. 1981, 52, 1478.
19. Kempf, J.; Kans, G. IBM Technical Report TR 28.105
20. Hopster, H.; Brundle, C. R. J. Vac. Sci. Tech. 1979, 16, 518.
21. Feldman, L. C.; "MeV Ion Scattering for Surface Structure Determination," in Surface Science: Recent Progress and Perspectives; CRC Press, Inc.: Cleveland, Ohio, 1981.
22. Brundle, C. R. J. Vac. Sci. Tech. 1974, 11, 212.
23. Brundle, C. R.; Silverman; Madix, R. J. J. Vac. Sci. Tech. 1979, 16, 474.
24. Smeenk, R. G.; Tromp, R. M.; Frenken, J. W. M.; Saris, F. W.; Surface Science, in press.
25. Smeenk, R. G.; Tromp, R. M.; Savis, F. W.; Surface Science 1981, 107, 429.
26. Chuang, T. J.; Brundle, C. R.; Wandelt, K.; Thin Solid Films 1978, 53, 19.

RECEIVED June 1, 1982

# Analysis of Surfaces and Thin Films by IR, Raman, and Optical Spectroscopy

D. L. ALLARA

Bell Laboratories, Murray Hill, NJ 07974

Surface analysis techniques using light as a probe are often desirable because of their non-destructive tendencies, particularly for organic films, and their ability to operate under a variety of ambient conditions such as gas pressures from ultra high vacuum to atmospheres. Several photon techniques are available which provide sufficient signal-to-noise ratios for detection and characterization of surface species and thin films. For cases in which the adsorbates are polyatomic molecules infrared (IR) and Raman spectroscopies are most useful because of the large amount of structural information available in vibrational spectra. For less chemically complex films, such as native oxide overlayers, or for molecules with strong electronic transitions, ultraviolet (UV)-visible spectroscopy may be the best choice. Reflection infrared techniques, both internal and external, have been developed to the point where they are rather straightforward to use both experimentally and theoretically. The reflection IR techniques have been applied to a range of problems including catalysis, polymer degradation and adhesion. Infrared emission and surface electromagnetic wave propagation are little used but offer interesting possibilities in special circumstances. Surface Raman is a very new field and several methods are rapidly evolving for obtaining vibrational spectra of surface films. These methods include the use of a special Raman enhancing metal substrate structures (usually silver), two wave scattering (Raman Gain) and internal reflection wave-guide mode excitation. In the area of UV-visible spectroscopy, reflectance or ellipsometry can be used. While scanning UV-visible ellipsometry has yet to be widely used it has been clearly demonstrated to be a convenient and very useful technique for analysis of inorganic surface films.

An important part of modern technology revolves around phenomena at material interfaces. A detailed knowledge of the chemical and physical nature of interfaces is of great value in solving existing problems and creating new developments based on these

0097-6156/82/0199-0033\$06.00/0

© 1982 American Chemical Society

In Industrial Applications of Surface Analysis; Casper, L., et al.;  
ACS Symposium Series; American Chemical Society: Washington, DC, 1982.

phenomena. Whereas twenty years ago means of obtaining atomic and molecular scale information at interfaces were virtually non-existent it is common now to obtain such information from several different types of experiments particularly for the cases in which one of the phases is a solid and the other a gas. When the gas phase is at extremely low pressures, viz, ultra high vacuum (UHV), detailed studies can be made of the solid surface structure by the ever growing number of ion and electron spectroscopies and it is this type of interface which has been the focus of most studies. However, when we turn to the gas-solid interface at high gas pressures and the solid-solid and solid-liquid interfaces, these techniques are virtually inapplicable without some prior and usually permanent chemical and/or physical alteration of the sample. A less popular but potentially quite useful class of spectroscopies which use photon probes offers additional possibilities for surface analysis in all the above cases. This type of spectroscopy will be the subject of this paper. I have directed my discussion to those workers who are currently using the typical ion and electron spectroscopies and would like to know of other types of techniques which could assist them in solving their problems of surface analysis. To this end I shall present a broad view of available and developing techniques that involve the measurement of photon interactions with surfaces over the range of ultraviolet through infrared wavelengths. New techniques with synchrotron generated X-ray beams are being developed and utilized but will be excluded for brevity. As a preliminary, I wish to discuss briefly several important contrasting requirements and problems of ion and electron spectroscopies and photon spectroscopies. This knowledge is necessary in order to select which types of analyses to use for a given problem.

The first consideration is that of what we mean by a "surface". The most convenient definition for the present purposes is that depth region of the solid measured from the outermost interface which is probed by the particular analysis method. Thus the surface of a typical material as defined by common techniques such as X-ray photoelectron emission or Auger spectroscopy is a layer roughly 3-40Å in thickness, the so-called escape depth of the emitted electron. Most ion and electron spectroscopies in fact define surfaces in the region of from one monolayer to less than 100Å. In contrast, photon spectroscopies generally probe to a depth which is at least some significant fraction of the wavelength of the photon. In the ultraviolet-infrared (UV-IR) regions this means that surface information can range from at least many hundreds of angstroms to as much as several micrometers into the solid phase with the interesting exception of surface enhanced Raman spectroscopy (SERS) which will be discussed in a later section. Thus the term "surface analysis" can be somewhat nebulous unless the physical nature of the measuring technique is known or appropriate empirical calibrations have been made. However, in many cases of interest one needs to characterize a thin surface layer of very different characteristics than the supporting substrate, e.g. a polymer film, an organic deposit or a metal oxide layer on a metal. In such cases the substrate may not interfere with the analysis spectroscopically because its interaction is observed in a different energy region of the photon probe than the region of interest for the film. For these cases "surface sensitivity" does not matter and rather the overall sensitivity of a technique to analyze the species of interest is important. A more complicated case of interest involves the analysis of interfaces and interphases between two solid phases. When this region of interest is buried beyond 50-100Å below the outer vacuum or ambient interface most common neutral and charged particle spectroscopies are inapplicable. One approach is to sputter material away to reach the interface of interest. However, as discussed below this can cause significant chemical damage to the interface. In contrast, photons can be capable of deep



penetration (see above). The obvious requirement for photon spectroscopies is that the light required for analysis be allowed to escape in some usable fashion and that the region of interest have a significantly different response than the rest of the sample. An example of a useful case that I have studied is the polymer-metal interface where the metal can act as a reflector and the interfacial species yield some different spectral features than those found in bulk film.

A second consideration is the ambient environment required for analysis. All techniques using particles require moderate or high vacuum conditions, i.e. pressures of  $\sim 10^{-5}$  torr or lower. However, techniques using only photons work in any fluid environment, including liquids, with the provision, of course, that the wavelengths of interest are not appreciably absorbed or emitted by the environment. Thus *in situ* studies of such phenomena as catalysis and corrosion in typical ambient environments are possible with photon spectroscopy. Further, in many cases the surface film to be studied will be quite air stable and analysis outside of a vacuum chamber can result in a great savings in time and effort.

The final consideration I will discuss is that of unwanted side effects caused by energy transfer from the probing particle or photon to the sample. For highly stable surfaces and films such as those of most simple inorganic materials the "beam" damage is usually negligible as regards the desired result from most analytical techniques. However, for organic surfaces and films severe damage of the subtle organic bonding structures by ion, electron or neutral atom bombardment often renders hopeless the task of obtaining useful chemical, as opposed to atom composition, information about these structures. This can be due to collisional energy transfer effects and/or charge withdrawal or injection effects. However, photons at typical fluxes used for analysis in the UV-IR region usually do not cause damage. The two major exceptions to note here are analyses of molecules highly sensitive to photochemical reaction, most usually because of UV chromophores, and the conditions of surface Raman techniques which use intense laser beams generated at visible wavelengths which may induce photochemistry in molecules normally of low photochemical reactivity. A discussion of these problems will be dealt with in the later section on Raman spectroscopies. It should also be mentioned that X-ray beam damage in X-ray photoemission is normally not a controlling factor in using this technique for typical organic surfaces.

The above discussion highlights some advantages and problems of photon spectroscopies in surface analysis. A major problem historically has been the lack of sensitivity for observing monolayer amounts of materials, i.e.  $\sim 10^{15}$  molecules/cm<sup>2</sup>. Recent advances in spectrometers, detectors and the discoveries of new physical processes for the interaction of light with surfaces have dramatically altered the situation. In the sections to follow I will discuss several photon spectroscopies which have developed to the point of being able to yield surface information. The techniques, in order of presentation, are IR and UV-visible absorption and Raman scattering. These will be divided into classes and each class will be discussed from the point of view of general principles, capabilities, ease of the experiment, special problems, instructive applications and future developments. Each of these fields has its own extensive literature and within the extent of this paper a full coverage of these topics is impossible. The intent of this paper is to create an awareness of the breadth of techniques and to provide key references to give the reader an entrance into the literature. The general slant of this paper will be towards surface analysis of typical samples of practical interest as opposed to UHV prepared samples.

### *Infrared Spectroscopy*

Infrared spectra yield useful information about the vibrational properties of molecular structures. For complicated organic species this information can be extremely valuable in identifying specific chemical groups and changes thereof due to surface reactions. There are four different techniques that I will discuss; internal and external reflection, emission and surface wave propagation.

*Reflection.* The two reflection techniques will be discussed together because the physical natures of both are so similar. Both techniques depend upon the generation of a standing electromagnetic wave at an interface where a beam of light is reflected. For parallel layer samples this process can be accurately described in terms of macroscopic electromagnetic theory (1). The only variables are the initial angle of incidence of the chosen wavelength of light, the optical dielectric response (refractive and absorption indices) of each medium through which the light passes and the thickness of each layer. The qualitative descriptions usually given for reflection spectroscopy come from calculations using this theory.

In internal reflection a beam of light of the frequency or frequencies of interest is guided along the inside of an IR transparent slab (generally of high refractive index such as silicon or thallium bromiodide) via internal reflections as shown in Fig. 1. The power lost at each frequency through interaction with a film of absorbing material on the surfaces of the slab is measured. High sensitivity is obtained by using a sufficiently thin slab to generate multiple reflections (usually 25-50). The electric field intensity decays with increasing distance from the interface (an evanescent wave) and effectively extends to a distance, shown as  $d_p$  in Fig. 1, of several micrometers from the slab face. Any film located within this region can be probed. The distance  $d_p$  depends upon the refractive index of the slab, the angle of incidence and the wavelength (2). This technique is well developed and has been thoroughly explained elsewhere (2). It can be used quantitatively with calibrations and is a simple experiment that can be carried out using inexpensive commercial attachments to standard IR spectrometers. Internal reflection infrared spectroscopy is limited in application to surface films on IR transparent materials which can be cut and polished to the required slab dimensions. Typical materials used for mid-IR internal reflection elements are silicon, germanium, thallium bromiodide (KRS-5), sapphire, and zinc selenide. The technique cannot be applied to substrates such as bulk metals unless very thin ( $\sim < 100 \text{ \AA}$ ) films of these materials can be smoothly placed on the reflection element such that some of the evanescent wave can penetrate through this layer to the adsorbate. This is often not appropriate or practical for many experiments. For cases of soft materials such as many organic polymers the reflection element can be firmly clamped against the polymer surface to give optical contact and the surface regions up to several micrometers into the polymer can be examined. Some varied examples of applications are found in studies of silicon oxide film structure, (3, 4) fluorination of polyolefin surfaces, (5) adsorption of CO on thin evaporated palladium films (6) and adhesion mechanisms (7). The usefulness of the method can be illustrated with the study of Sung, Lee and Sung (7) of the role of silane coupling agents as adhesion promoters at aluminum oxide-polymer interfaces. Single crystal aluminum oxide (sapphire) optical elements were treated with solutions of silane coupling agents. Films from several hundred to about one thousand Angstroms were examined by internal reflection spectroscopy between  $\sim 2000$  to  $4000 \text{ cm}^{-1}$ . The spectra indicate that the thin films are highly crosslinked polysiloxane networks. To examine the regions below  $2000 \text{ cm}^{-1}$ , where the sapphire

elements are highly absorbing, a KRS-5 element was placed parallel to the sapphire-film structure and the evanescent wave from the KRS-5 used to obtain the film spectrum. With this modification evidence was obtained to substantiate the crosslinked structure and to show that some unreacted Si-OH groups are present, which indicates that crosslinking is not complete. This type of information is important in understanding the nature of metal-polymer adhesion when siloxane coupling agents are used as adhesion promoters. Other interesting applications can be found in several reviews (2, 8, 9, 10, 11). Future applications should continue to grow, particularly as more sensitive IR spectrometers such as Fourier Transform instruments become more common.

In external reflection infrared a beam of light is reflected off a metal surface as shown in Fig. 2. The power lost by interaction of the standing wave at and near the metal surface with an overlayer film or adsorbed monolayer gives rise to an absorption spectrum. Typically in ambient environment experiments the metal will have an overlayer of oxide and the film of interest may be this oxide and/or additional overlayers of corrosion products, polymer or organic deposits, for example. The electric field intensity extends continuously above the surface and there is no limit to the thickness of the sample which can be probed. Again, as with internal reflection, relatively inexpensive commercial attachments are available for most spectrometers to allow external reflection experiments. To obtain sufficient signal-to-noise ratios for the observation of typical organic monolayers one must use either Fourier transform spectrometers (12, 13) or dispersive spectrometers with wavelength (14) or polarization modulation (15, 16, 17, 18) in conjunction with very sensitive, quiet and fast state-of-the-art detectors such as intrinsic photoconductors of which mercury cadmium telluride is a typical example. For films considerably thicker than  $\sim 100\text{\AA}$  standard spectrometers can be used. Quantitative calculations of band shapes and intensities can be made from macroscopic electromagnetic theory (19) as discussed earlier for the case of internal reflection. A knowledge of the real ( $n$ ) and imaginary ( $k$ ) parts of the complex optical constant for each layer, as shown in Fig. 2, is necessary. For quantitative intensity calculations involving adsorbed molecules with optical properties different than the free molecules specific knowledge of the adsorption interaction must be known to evaluate the required optical functions. For many multilayer films bulk and thin-film optical functions are virtually identical and calculations of such quantities as the amount of adsorbed material can be made reasonably well (19).

Applications of the external reflection technique to surface analysis have been reviewed (12, 20). Representative of a broad range of applications are studies of polymer film degradation at metal surfaces, (21) adhesion, (22) bonding of polymer monolayers, (23) oxidation of metals, (24) corrosion coatings (25) and catalysis (26). This list is not intended to be comprehensive but rather illustrative. An example from work in this laboratory is the characterization of poly(acrylic acid) (PAA) monolayer structures on native-oxide-covered evaporated aluminum (23). Different thickness layers (thicknesses were measured by visible wavelength ellipsometry, a technique discussed in a following section) of various molecular weights of PAA were adsorbed from ethanol solution onto the above substrates. The reflection IR spectra obtained show that for thick films (hundreds of Angstroms) only the bulk PAA spectrum is observed. However, for films of monolayer thickness,  $\sim 5\text{-}10\text{\AA}$ , a strong contribution at  $\sim 1620\text{ cm}^{-1}$  is observed, a position appropriate for the carboxylate ion. A spectrum of an  $\sim 10\text{\AA}$  film is shown in Fig. 3. Using estimates of the optical constants for the carboxylate and carboxylic acid C=O stretching frequencies calculations indicated that about one-half the bulk PAA acid groups are ionized to carboxylate in the monolayer.

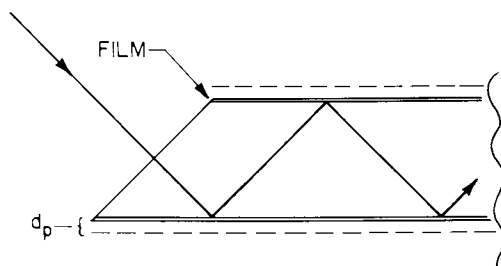


Figure 1. A description of the internal reflection experiment. The quantity,  $d_p$ , is the penetration depth of the surface evanescent field away from the slab face.

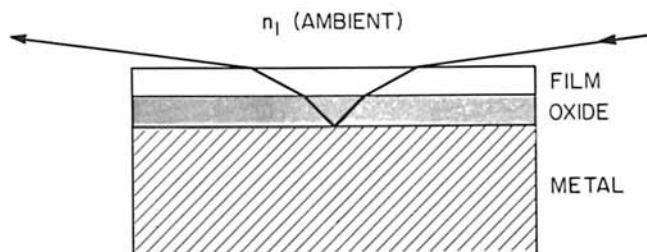


Figure 2. A description of the external reflection experiment for an oxide coated metal with an overlayer film. The complex refractive indices,  $\hat{n} = n + ik$ , for each phase are as follows: film,  $\hat{n}_2 = n_2 + ik_2$ ; oxide,  $\hat{n}_3 = n_3 + ik_3$ ; and metal,  $\hat{n}_4 = n_4 + ik_4$ .

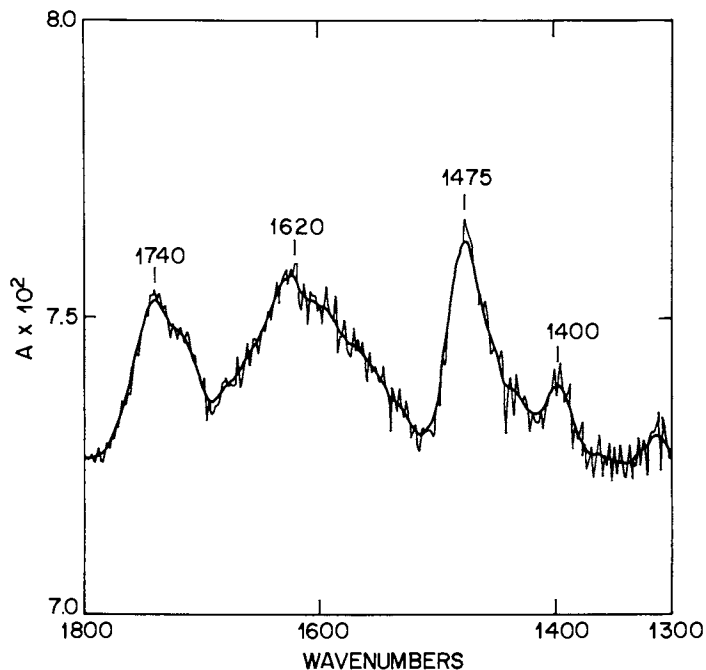


Figure 3. External reflection IR spectrum of an  $\sim 10$ -Å film of poly(acrylic acid) on native-oxide-covered, evaporated aluminum. The jagged line is the unsmoothed spectrum at  $2\text{ cm}^{-1}$  resolution. The major peak assignments are:  $1740\text{ cm}^{-1}$ , unionized carboxylic acid,  $\text{C}=\text{O}$  stretch; and  $1620\text{ cm}^{-1}$ , the carboxylate ion asymmetric stretch;  $1475\text{ cm}^{-1}$ ,  $\text{CH}_2$  bending. (Reproduced, with permission, from Ref. 23. Copyright 1980, Plenum Publishing Co.)

Presumably, these groups are chemisorbed to the aluminum oxide surface and the remaining un-ionized acid groups are pointed away from the surface. Reaction of these un-ionized groups with thermally generated aluminum atoms in a vacuum environment to form an aluminum carboxylate salt showed that the latter structure is reasonable. An interesting and potentially important application of external reflection spectroscopy is the recent report of an *in situ* study of the electrochemical liquid-solid interface (27). It is safe to say that during the next few years a growing number of applications of external reflection infrared spectroscopy to surface and thin film analysis should be forthcoming particularly as more sensitive instrumentation becomes available in many laboratories.

*Emission.* All samples which absorb infrared radiation to give absorption spectra also emit at the same frequencies, even in the absence of external radiation, and in principle the infrared spectrum can be obtained by detection of this emission. In fact at first glance this seems a particularly useful way of getting the spectrum of surface films because a flat, reflecting surface should not be necessary as with reflection spectroscopy and thus the spectrum of an odd shaped, rough object could in principle be measured. However, there are two factors which are serious considerations. First the emission is a function of temperature and at ambient temperature the absolute level of emission from surface films near monolayer thickness is extremely weak compared to the levels easily measured with standard IR spectrometers. Second, every part of the optical system, also at room temperature, is emitting unwanted and interfering infrared radiation along with the sample. There are basically three ways to overcome these problems: heat the sample, cool the spectrometer or look at thick films with high emission levels. All three approaches have been tried but only a few studies of surface analysis by emission have been reported and these mostly have dealt with heated samples. An interesting example is the study of fuel and lubricant deposits on fuel lines in which the actual fuel line part was directly examined using a microspectrophotometer which could focus on small regions of the sample (28). A useful discussion of the application of emission IR has been given by Chase (29). Recently, my co-workers and I have been successful in observing the 300K emission spectrum of a monolayer of p-nitrobenzoic acid chemisorbed on oxide covered copper using a liquid nitrogen cooled Fourier transform IR spectrometer (30). This experiment proved to be fairly difficult but demonstrates the potential for monolayer, thin film surface analysis. Most important, a 90Å film of poly(methyl methacrylate) on an extremely rough and non-reflective copper surface also gave a high quality spectrum (30). This sample is not capable of analysis by reflection (diffuse or specular) techniques. Although there are some restrictions on the general use of emission IR for surface analysis, as pointed out above, the technique should be capable of solving some problems particularly for rough and/or odd shaped samples, and also particularly when surface films exceed monolayer amounts and/or the sample can be heated.

*Surface Electromagnetic Wave Propagation.* The external reflection techniques depend upon the presence of a standing wave generated by reflection of a light beam from a metal surface. It is also possible by passing the incoming beam at a specific angle through a prism of a given index of refraction to launch a propagating wave along the surface of the metal at the ambient interface. For metals such as copper using mid-IR radiation this propagation distance can be several cm in length. The light can be coupled out through another or the same prism and directed into a detector. This so-called surface electromagnetic wave can interact with a film on the surface and give

rise to absorption spectra. A typical experimental schematic is shown in Fig. 4. With this particular configuration a small gap between the prism and the metal surface is necessary to couple the light into the metal surface. The penetration of the surface field into an overlayer film is similar to that for external reflection. A general review of this technique has been made by Bell (31). The optical efficiency is usually low and a strong source is needed to provide sufficient signal to the detector. Further, the coupling efficiency is very dependent on the wavelength of the beam, the optical positioning of the sample and the prism refractive index so that monochromatic light of a particular wavelength is required for a measurement at each fixed sample configuration. The use of a laser solves both problems and provides sufficient sensitivity and low noise to carry out submonolayer analysis. However, the use of a laser limits the ability to do broad regions of the spectrum. Some examples of studies using laser sources include Langmuir-Blodgett films on copper, (32) oxide films on metals, (33) benzene and cellulose acetate films on copper (34) and hydrogen chemisorbed on tungsten under UHV conditions (35). The technique has not seen widespread use because of the extra complexity of the optics, primarily coupling prisms, and the narrow band capabilities of lasers. With this latter problem in mind Schlesinger and Sievers (36) recently have developed a method with broadband capabilities. The experiment is more difficult to assemble than typical external reflection IR but the sensitivity for surface films is claimed to be an order of magnitude better (36). It appears that with very intense broadband sources the spectra will be of better quality than those of external reflection (35). If the broadband modification is improved further there exists the potential for some useful general applications. In specific applications where high sensitivity analysis is required, such as for submonolayer films, over a narrow wavelength range laser-surface-wave spectroscopy could be very useful.

#### *UV-Visible Reflection Spectroscopy*

Light of UV-visible frequencies, henceforth for convenience referred to as the optical region, can be used to probe the electronic characteristics of thin films and/or substrates much as infrared reflection spectroscopy probes vibrational characteristics. This is of particular interest for materials such as metals, semiconductors and organic molecules with observable electronic transitions. Optical spectra can be obtained directly by either internal or external reflection-absorption techniques (reflectance spectroscopy). A modification of reflection spectroscopy called ellipsometry in which the polarization properties of reflected light are measured gives the above information and in addition can yield information on the thickness of overlayers even when they are non-absorbing. Ellipsometry appears to be a more powerful tool than reflectance spectroscopy and will be discussed at greater lengths. As with the IR spectroscopies the probing depth of the optical frequency photon into a solid or a thick film will be much larger than a surface monolayer thickness except that the probing distance for the optical wavelengths is correspondingly shorter than for the IR, i.e. in the neighborhood of many hundreds to a few thousands of Angstroms compared to micrometers.

**Reflectance.** Both internal and external reflectance spectroscopy are relatively simple experiments to perform. Commercially available attachments for standard UV-visible spectrometers can be used. For films with strong electronic transitions reasonable spectra can be obtained. The theory for external and internal reflectance is the same as that for the IR and can be found elsewhere (2, 37). The techniques have not been very popular in their applications to surface analysis. The major reason appears to be

that spectra are generally broad, featureless and accordingly of little use in analyzing molecular groups and their arrangements on surfaces. The major uses for external reflectance have been in electrochemical systems (37).

*Ellipsometry.* Ellipsometry is a modification of external reflection spectroscopy in which one measures the changes in the state of polarization of the light upon reflection rather than the reflected power. The reflecting beam of light can be considered in terms of its sinusoidal electric fields. In general, the complex component of the electric field which is parallel to the sample surface ( $E_p$ ) suffers a different loss in intensity and change in phase with reflection than the component lying in the plane of reflection ( $E_s$ ). This difference shifts the polarization state of the light. This effect is shown schematically in Fig. 5. Ellipsometry has several advantages over reflectance measurements, particularly in the optical region. The primary advantage is that the former is intrinsically a "double-beam" measurement with a built-in internal reference whereas the latter is an absolute power-loss measurement. Accordingly the experimental accuracy of ellipsometric data can be significantly greater than reflectance data. In addition, ellipsometric data yield both the imaginary part (the absorbed light or the usual absorption spectrum) and the real part (the refractive index, normally only a perturbation on absorption spectra and not easily untangled with accuracy) of the optical functions. The theory of ellipsometric measurements and data analysis is well known and can be found in several reviews (38, 39, 40). The experiment is reasonably simple and consists of first passing a well collimated monochromatic beam of unpolarized light through optical polarizer elements to obtain a known state of polarization. This light is then reflected off the sample, passed through a further polarizer system which is varied to analyze the changed polarization state, and finally directed into a photo-detector. However, for spectral analysis with reasonable resolution over a wide range of wavelengths it is necessary that the experiment be interfaced with a computer. The data handling also requires a computer since the equations are complicated algebraically and calculation of optical properties are best done numerically. The only requirement of the sample is that it reflect light specularly. Any material including metals and non-metals can be analyzed in principle. It is possible, for cases where one can assume flat parallel overlayers on the substrate, to calculate both the optical properties and film thickness from ellipsometric spectra. The measured dielectric functions are quite sensitive to the presence of even submonolayer adsorbates and ellipsometry data can be obtained with sufficient precision to determine the structures of complex multi-overlayer thin films. For example, electrochemically grown anodic oxide layers on GaAs give spectra which have been analyzed (41) for a specific growth condition in terms of a best fit model consisting of an inner 0.3Å layer of amorphous arsenic under an 1152Å oxide overlayer containing a small fraction of amorphous arsenic (~0.2%) and ~1.5% voids and a 68Å outer oxide layer with 15% void space. Such a detailed analysis of a complicated interface provides strong support for the use of the technique. Other examples can be found elsewhere (42-45). The future of this technique for surface analysis looks extremely promising particularly in the field of semiconductor technology (42) but should find applications in a variety of other areas.

### *Raman Spectroscopy*

Raman spectroscopy is based upon the Raman effect in which light, usually of visible wavelengths and chosen to be monochromatic, interacts with a sample to give rise to a small fraction of inelastically scattered radiation (of shifted frequencies). In



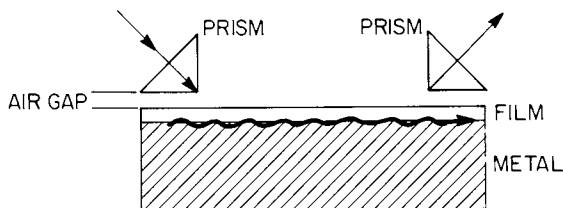


Figure 4. A typical experimental configuration of surface electromagnetic wave propagation spectroscopy. A surface wave is launched along the surface of a metal using a coupling prism separated by an air gap. The light is coupled out to a detector through another prism.

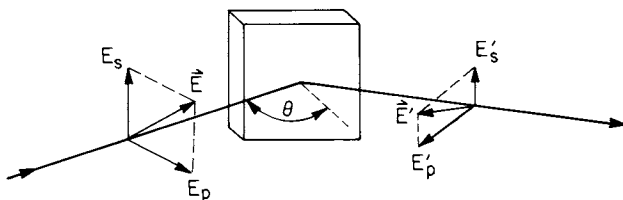


Figure 5. A description of the electric field amplitudes in an ellipsometry experiment. Upon reflection at the angle of the two complex components of the electric field,  $\vec{E}_s$  and  $\vec{E}_p$  assume the different values,  $\vec{E}'_s$  and  $\vec{E}'_p$ , according to the optical properties of the surface.

the usual case of spontaneous Raman scattering this shifted light is spectrally analyzed and the magnitude of the shifts can be directly related to the spacing of vibrational levels of the samples. This gives a vibrational spectrum as with IR spectroscopy except that the vibrational bands have different intensities and sometimes slightly different frequencies than in the IR. These differences are well understood for simple molecular structures and in fact the combination of both types of spectra for the same sample can provide quite a powerful tool for structural characterization. The Raman scattering process is quite inefficient and it was not until the application of lasers with higher input power than traditional sources that scattered light could be produced to provide good quality spectra. Even with laser irradiation the typical sample may consist of several grams of material. When one considers that a typical amount of a monolayer is about  $10^{14}$ - $10^{15}$  molecules/cm<sup>2</sup> (less than  $\mu\text{g}$  quantities) it is easy to understand why the technique was thought useless for surface analysis until a few years ago. Recently, several methods have been developed which are capable of generating Raman spectra of monolayers and thin films. These techniques depend upon an enhancement of the electromagnetic field intensity of the exciting source beam at the sample surface, an increase in the efficiency of the scattering process arising from a specific electronic or chemical interaction between the surface and the adsorbate and/or a decrease in the noise and background emission effects in the experiment.

*Surface Enhanced Raman.* Several years ago a huge enhancement was reported for the Raman spectrum of pyridine adsorbed from solution onto an silver electrode in an aqueous electrochemical environment (46). A large number of experiments rapidly followed (47, 48) which showed that the normal Raman effect could be enhanced by factors of  $10^4$  to  $10^7$  when molecules were adsorbed on or near electrochemically, mechanically or otherwise roughened silver surfaces of vacuum-deposited silver structures and discrete silver particles. Some success in enhancing scattering also has been achieved for Cu and Au, (48) Ag-Pd alloys, (49) Pt (50) and Ni (50, 51). There are reports of enhanced scattering on liquid mercury (52, 53). Spectra have been obtained on Ag with a variety of molecules although there are no definitive reports of phonon spectra from materials such as metal oxides or semiconductors. The experiments, excluding special surface preparations, are relatively easy to run with standard lasers, focusing optics, monochromators and detection systems, all designed for use in the visible wavelength region. For cases where one wishes to study surface films on specially roughened or prepared silver, copper or gold surfaces the method looks very promising and the vibrational spectra can be, in fact, of better quality than corresponding IR reflection spectra. The more general problem, however, involves the measurement of a spectrum of a thin film or monolayer on a variable substrate which would include metals, semiconductors, metal oxides, etc. Our own recent work (54) has shown that in fact this is possible through the use of a rough, vacuum deposited and thin (hundred of angstroms) overlayer of CaF<sub>2</sub> covering the sample (surface and adsorbate) of interest (generally a flat plate specimen) with a final top layer of thin, vacuum deposited silver. This structure acts like a surface amplifier or antenna for the incoming and emitted radiation fields and enhances Raman signals of the substrate surface film sample. Both small organic molecule monolayers and polymer films have given good spectra (54). In some cases silver island structures can be deposited directly on the surface films with good results. Whereas, optical techniques usually probe at distances of a few thousand angstroms into a material the surface-enhanced technique described above has been shown to penetrate only a few hundred angstroms or less away from the top silver overlayer. Thus the "surface sensitivity" of this technique is at

least an order of magnitude closer to the surface sensitivity of the ion and electron techniques. Future developments in the area look promising but some definitive applications of analyses of specific samples are needed to establish the practical aspects of the technique.

*Internal Reflection Raman.* Recently, internal reflection techniques have been utilized to produce enhancement of the electromagnetic field strengths of a Raman excitation beam at the surfaces of optically transparent slabs. This enhancement can result in sufficient Raman scattering signals to provide useful spectra for thicker than monolayer samples, such as polymer films, at the slab interface. Iwamoto and co-workers (55) have reported the observation of a Raman spectrum of a nominally 60Å thick film of polystyrene on a sapphire plate using a single internal reflection of a 4880Å laser beam (see Fig. 1) to excite the surface film. Using their optimum conditions for sample and optical geometries they were able to show a measurement penetration ("surface sensitivity") of ~4000Å into the film as measured from the sapphire film interface. Rabolt, Santo and Swalen (56) have obtained spectra for 800Å films of polystyrene on bilayer glass slabs using several hundred or more internal reflections (waveguide modes) of the excitation beam. Their experimental arrangement is similar to that in Fig. 4 except the wave propagates along the glass interface rather than along a metal surface. Other workers (57) have reported a spectrum from a 75Å Langmuir-Blodgett type of film on a thin (400Å) silver film deposited on a rutile prism. The up-to-several orders of magnitude enhancements of the thin film spectra by these methods are due to the well understood properties of electromagnetic radiation fields at smooth material interfaces. The complications of surface roughness and surface-adsorbate interactions are not factors as with the surface-enhanced Raman effects. The present lack of capability to see monolayer films is a detraction but improvements to this end are possible. The fact that this technique should be generally applicable to a variety of films and film substrates should encourage further attempts to obtain monolayer spectra.

*Stimulated Raman Gain.* Whereas the Raman processes described so far involve spontaneous, incoherent emission, i.e., the Raman emission emanates from individual molecular centers radiating in all directions independently of one another, there exist other Raman processes which involve coherent phenomena. Motivated to some extent by the complexities of surface-enhanced Raman spectroscopy, attempts have been made to utilize stimulated Raman gain spectroscopy to analyze monolayer quantity films. The technique involves the crossing of two high-intensity, synchronously-pumped, mode-locked laser beams of slightly different visible frequencies. The sample surface to be analyzed is placed in the mixing region of the two beams. When the difference in frequencies of the beams is coincident with the frequency of a Raman active vibrational mode one beam gains power at the expense of the other. The reflected or transmitted (depending upon the type of sample) beams are separated optically and the power change measured as a function of beam frequency difference giving rise to a Raman spectrum. The several orders of magnitude higher sensitivity of this method relative to normal spontaneous Raman spectroscopy is due primarily to the ability to measure small changes in the probing beam power level much more precisely than the corresponding changes in the power level of diffusely scattered light in the spontaneous experiment. Levine and co-workers (58) have reported a high sensitivity measurement of the 520  $\text{cm}^{-1}$  band of a 20Å film of Si on sapphire. Heritage and Allara (59) have

observed vibrational features near  $1610\text{ cm}^{-1}$  of a chemisorbed monolayer of p-nitrobenzoic acid on an aluminum oxide film. Although these studies point the way towards a sensitive technique with general applicability to a variety of surfaces there are several problems which presently limit the usefulness. First the spectral scan width is limited to about  $100\text{ cm}^{-1}$ . Secondly the experiment is complex and requires a significant effort to set up. In spite of these difficulties practical applications of this potentially useful spectroscopy may be expected in the future.

#### Literature Cited

1. For example, see Born, M.; and Wolf, E. "Principles of Optics", Pergamon Press, New York, 1975.
2. For example, see Harrick, N. J. "Internal Reflection Spectroscopy", John Wiley and Sons, New York, 1967.
3. Harstein, A.; DiMaria, D. J.; Dong, D. W.; Kucza, J. A. *J. Appl. Phys.* 51 3860 (1980).
4. Hass, G. A.; Pankey, T.; Holm, R. T. *J. Appl. Phys.* 47 1185 (1976).
5. Blackwell, C. S.; Degen, P. J.; Osterholtz, F. D. *Appl. Spectrosc.* 32 480 (1978).
6. Rice, R. W.; Haller, G. L. *J. Catalysis* 40 249 (1975).
7. Paik Sung, C. S.; Lee, S. H.; Sung, N. H. *Polymer Science and Technology* 12B 757 (1980).
8. Haller, G. L.; Rice, R. W.; Wan, Z. C. *Catalysis Revs.* 13 259 (1976).
9. Zolotarev, V. M.; Lygin, V. I.; Tarasevich, B. N. *Russ. Chem. Rev.* 50 14 (1981).
10. Harrick, N. J. in "Characterization of Metal and Polymer Surfaces" ed. by L. H. Lee, Vol. 2, Academic Press, New York, 1977, p 153.
11. Jakobsen, R. J. in "Fourier Transform Infrared Spectroscopy" ed. by J. R. Ferraro and L. J. Basile, Vol. 2, Academic Press, New York, 1979, chap. 5.
12. For example see, Allara, D. L. in "Vibrational Spectroscopies for Adsorbed Species" ed. by M. L. Hair and A. T. Bell, Symposium Series, Vol. 137, American Chemical Society, Washington, DC, 1980, chap. 3.
13. Marcott, C. "Proceedings of the 1981 International Conference on Fourier Transform Infrared Spectroscopy", SPIE Proceedings 289 121 (1981).
14. Pritchard, J.; Catterick, T.; Gupta, R. K. *Surface Sci.* 53 1 (1975).
15. See Feydek, J. D.; Dignam, M. J. in "Vibrational Spectroscopies for Adsorbed Species", ed. by M. L. Hair and A. T. Bell, ACS Symposium Series, Vol. 137, American Chemical Society, Washington, DC, 1980, Chap. 5.
16. Bradshaw, A. M.; Hoffman, F. *Surface Sci.* 52 449 (1975).
17. Golden, W. G.; Dunn, D. S.; Overend, J. *J. Phys. Chem.* 82 843 (1978).
18. Marcott, C. A. *Appl. Spectrosc.*, in press, 1982.
19. Allara, D. L.; Baca, A.; Pryde, C. A. *Macromolecules*, 11 1215 (1978).
20. Tompkins, H. G. in "Methods of Surface Analysis ed. by A. W. Czanderna Elsevier, New York, 1975, Vol. 1, Chap. 10.
21. Allara, D. L. in "Characterization of Metal and Polymer Surfaces", ed. by L. H. Lee, Academic Press, New York, 1977, Vol. 2, p 193.
22. Boerio, F. J.; Gosselin, C. A.; Dillingham, R. G.; Liu, H. W. *J. Adhesion*, 13 159 (1982).
23. Allara, D. L. *Polymer Science and Technology* 12B 751 (1980)
24. Mertens, F. P. *Surface Science* 71 161 (1978)
25. Handke, M.; Stock, A.; Lorenzelli, V.; Bonora, P. L. *J. Materials Science* 16 307 (1981).

26. Baudais, F. L.; Borschke, A. J.; Fedyk, J. D.; Dignam, M. J. *Surface Science* 100 210 (1980)
27. Bewick, A.; Kunitatsu, K.; Robinson, J.; Russell, J. W. *J. Electroanal. Chem.* 119 175 (1981).
28. Lauer, J. L.; Keller, L. E. "Proceedings of the 1981 International Conference on Fourier Transform Infrared Spectroscopy", SPIE Proceedings 289 87 (1981).
29. Chase, D. B. *Appl. Spectrosc.* 35 77 (1981).
30. Allara, D. L.; Teicher, D.; Durana, J. F. *Chem. Phys. Lett.* 84 20 (1981).
31. Bell, R. J.; Alexander, R. W.; Ward, C. A. in "Vibrational Spectroscopies for Adsorbed Species" ed. by A. T. Bell and M. L. Hair, ACS Symposium Series, Vol. 137, American Chemical Society, Washington, DC, 1980 Chap. 6.
32. Zhizhin, G. N.; Morozov, N. N.; Moskaleva, M. A.; Sigarov, A. A.; Shomina, E. V.; Yakovlev, V. A.; Grigos, V. I. *Thin Solid Films* 70 163 (1980).
33. Zhizhin, G. N.; Moskaleva, M. A.; Firsov, E. I.; Shomina, E. V.; Yakovlev, V. A. *Sov. Phys. JETP* 52 282 (1980)
34. Bhasin, K.; Bryan, D.; Alexander, R. W.; Bell, R. J. *J. Chem. Phys.* 64 5019 (1976)
35. Chabal, Y. J.; Sievers, A. J. *Phys. Rev. B* 24 2921 (1981)
36. Schlesinger, Z.; Sievers, A. J. *Surface Sci.* 102 L29 (1981).
37. McIntyre, J. D. E. in "Optical Properties of Solids, New Developments" ed. by B. O. Seraphin, Elsevier, New York, 1976, chap. 11; and in "Advances in Electrochemistry and Electrochemical Engineering", Vol. 9, ed. by P. Delahay and C. W. Tobias, Wiley, New York, 1973 pp 61-66
38. Azzam, R. M. A.; Bashara, N. M. "Ellipsometry and Polarized Light", North-Holland, Amsterdam, 1977.
39. Aspnes, D. E. in "Optical Properties of Solids: New Developments", ed. by B. O. Seraphin, North-Holland, Amsterdam, 1976, Chap. 15.
40. Neal, W. E. J. *Appl. Surf. Sci.* 2 445 (1979).
41. Aspnes, D. E.; Schwartz, G. P.; Gualtieri, G. J.; Studna, A. A.; Schwartz, B. J. *Electrochem. Soc.* 128 590 (1981).
42. Theeten, J. B.; Aspnes, D. E. *Annual Reviews of Material Science*, 11 97 (1981).
43. Aspnes, D. E. *Surface Sci.* 101 84 (1980)
44. Hottier, F.; Laurence, G. *Appl. Phys. Lett.* 38 863 (1981)
45. Habraken, F. H. P. M.; Gijzeman, O. L. J.; Bootsma, G. A. *Surface Sci.* 96 482 (1980).
46. Jeanmaire, D. L.; Van Duyne, R. P. *J. Electroanal. Chem.* 84 1 (1977).
47. For a review of some earlier work see Van Duyne, R. P. in "Chemical and Biological Applications of Lasers", Vol. 4, ed. by C. B. Moore, Academic Press, New York, 1979, Chap. 5.
48. "Surface Enhanced Raman Scattering", ed. by R. K. Chang and T. E. Furtak, Plenum, New York, 1981.
49. Furtak, T. E.; Kester, J. *Phys. Rev. Lett.* 45 1652 (1980).
50. Yamada, H.; Yamamoto, Y. *Chem. Phys. Lett.* 77 520 (1980).
51. Krasser, W.; Ervens, H.; Fadimi, A.; Renouprex, A. J. *J. Raman Spec.* 9 80 (1980).
52. Naaman, R.; Buelow, S. J.; Cheshnovsky, O.; Herschbach, D. R. *J. Phys. Chem.* 84 2692 (1980).
53. Sanchez, L. A.; Birke, R. L.; Lombardi, J. R. *Chem. Phys. Lett.* 79 219 (1981).
54. Murray, C. A.; Allara, D. L.; Rhinewine, M. *Phys. Rev. Lett.* 46 57 (1981); C. A. Murray and D. L. Allara, *J. Chem. Phys.*, 76 1290 (1982).

## Near Surface Analysis with Energetic Ion Beams

C. R. GOSSETT

Naval Research Laboratory, Condensed Matter and Radiation Sciences Division,  
Washington, DC 20375

A review is given of some representative methods and results for near surface analysis of elemental composition vs. depth as determined by Rutherford backscattering and related ion beam techniques. Examples are given from new applications in the areas of thin film and ion implantation technologies, which are used to tailor the near-surface composition to beneficially modify such surface-sensitive properties as friction, wear, oxidation and resistance to corrosion. Profiling by energetic ion beam methods is useful in optimizing the effect or in studies to understand the mechanisms. The advantages and limitations of this analysis method are explored with discussion of ion-excited x-ray analysis and nuclear reaction analysis as alternative or auxiliary approaches.

The field of materials analysis by energetic ion beams has begun to mature in the last decade after arising within the nuclear physics community. The basic method, Rutherford backscattering, has been the subject of a text (1), and the field has also engendered a useful handbook (2). Publications are scattered throughout the literature with much of the output in articles relating to the properties of materials. In these the ion beam analysis may form only a part of the work. New developments in technique and applications continue and have been the subject of a series of international conferences (see for example (3) for the latest of these).

For the purposes of this symposium this paper will attempt to summarize the main features of the technique, drawing on the author's own work to demonstrate both the range of applicability and the limitations. In addition to Ruther-

This chapter not subject to U.S. copyright.  
Published 1982 American Chemical Society.

ford backscattering two auxiliary ion beam techniques will also be discussed.

A principal distinction between energetic ion beam analysis and other analysis techniques presented at this symposium is one of the energy scale involved. While chemical binding effects are in the range of electron volts and the "surface-sensitive" techniques are at most restricted to within a few orders of magnitude of this, most energetic ion beam analyses are conducted in the range of a few million electron volts for the primary ions. This vast difference in the energy range has a number of important consequences for the analysis method.

First, because of the large energy difference, this method is completely insensitive to chemical binding effects. While other conventional surface analysis techniques which are sensitive to the chemical state are unquestionably frequently required, it is also true that methods thus dependent on the chemical state may suffer from difficulties in calibration, particularly in transition regions where an element is found in more than one chemical state. Energetic ion beam analysis, on the other hand, offers an absolute technique independent of these effects. As such, this technique and other conventional techniques (e.g. Auger, ESCA etc.) may often prove to be complementary, each supplying information not available by the other techniques.

Second, because the high energies provide penetration of solid materials to depths of several micrometers, this technique is not strictly a "surface analysis" method so much as a "near-surface analysis." When information is required on the composition, not only of the outermost surface, but also of the depth region within a few micrometers below the surface, such as in cases where the surface may be expected to be removed in use by wear or corrosion, then the composition in immediately underlying regions may be of importance. In these cases where a composition vs. depth (profile) is required, surface-sensitive techniques may of course be applied, provided that a method of successively removing surface layers by abrasion, etching, or sputtering is supplied to determine the profile. The greater penetration of the energetic ion beam, on the other hand, does not require removal of material to obtain a profile, as it depends only upon the relatively well understood energy loss phenomena for ions in matter to determine the depth at which atoms of a particular species are located. In this sense, this method is not destructive, although it may in some circumstances affect the material under study and may not always qualify as totally "nondestructive".

Third, the requirement of accelerating an ion to the MeV range of energies must necessarily entail a larger size, more expensive and often more complex acceleration apparatus. Thus, the technique of energetic ion beam analysis grew in the

environment of nuclear physics laboratories where such accelerators proliferated in the past few decades in support of the low energy nuclear physics research. This same environment was responsible for generating much of the available information on specific useful nuclear reactions and on the energy loss of ions in materials which is so important to the applications of the technique. In more recent years, as the technique has become better established, many of these older facilities have been converted to materials analysis and much of the current accelerator production is dedicated to this field and the related field of modification of materials by ion implantation.

#### Elastic Backscattering Analysis

The use of elastic backscattering, which is the primary technique for energetic ion beam analysis, is the normal method of choice when it will produce satisfactory results. Some other ion beam techniques which may be useful in supplementing backscattering in specific cases will be discussed later in this paper.

Backscattering analysis requires the previously mentioned accelerator and the associated energy selection, focusing and positioning apparatus. The incident ions, usually a stable isotope of hydrogen or helium, are formed into a well collimated beam of monoenergetic particles. Beyond this the requirements are relatively simple. Generally analyses are conducted in a moderately high (e.g.  $10^{-6}$  Torr) vacuum, because of the energy losses even in gaseous matter, although in special cases of volatile substances or even liquids, analyses have been provided in partial atmospheres of inert gasses. The other required apparatus for the experiment are: (1) a small surface barrier diode detector for detecting the scattered ions and for measuring their energy; (2) associated electronics, including a multichannel analyzer system or equivalent on-line computer for converting the electrical pulses from the detector into a spectrum of count vs. energy; and (3) a means of positioning a sample to intercept the accelerated ion beam in a known relationship to the detector. The latter arrangement typically includes provision to place successively several samples in position without breaking the vacuum and usually a means of changing the orientation of the sample with respect to the beam direction.

The theoretical foundation upon which backscattering stands is extremely straight-forward. The primary mechanism is the elastic collision process. The conservation of energy and momentum provide nonrelativistically that the ratio of the energy of the scattered ion,  $E_1$ , to that of the incident ion,  $E_0$ , is:



$$\frac{E_1}{E_0} = \frac{M_1^2}{(M_1 + M_2)^2} \left\{ \cos \theta \pm \left[ \left( \frac{M_2}{M_1} \right)^2 - \sin^2 \theta \right]^{1/2} \right\}^2, \quad (1)$$

where the subscripts 1 and 2 refer to the scattered ion and the scattering atom, respectively,  $M$  is the mass, and  $\theta$  is the scattering angle. Scattering angles from about  $135^\circ$  to nearly  $180^\circ$  are generally used to enhance the separation in energy for different masses, but it will also be noted that the energy separation of adjacent mass numbers will become less sensitive at higher masses.

Thin Film Example. As an illustration of the method, Figure 1 shows a backscattering spectrum for a study of a thin  $\text{MoS}_2$  film sputter-deposited for solid lubrication purposes. Since this analysis is of a relatively thin layer it provides a good example of the effect of the elastic collision process in identifying the elements present within the thin film. In this case the mass four isotope of helium (i.e., an alpha particle) scattered into a narrow angular range at a definite backward angle will have an energy uniquely dependent upon the mass of the nucleus from which it scattered as calculated by Equation 1. This determines the grouping of the energy of the scattered ions into the peaks, each labeled with the symbol for the relevant element.

A second consideration, not as apparent in Figure 1, where the film is very thin, is the role of energy loss considerations in defining the depth below the surface at which the particular scattering event took place. This energy loss is due to inelastic collisions of the ions with the electrons of the atoms present in the film. In the case illustrated in Figure 1 the atoms were all within a very thin near-surface layer and the peaks show an energy width not significantly greater than the energy resolution of the detector system. However, for thicker layers, both the incoming ion and the scattered ion lose energy in traversing the distance between the surface and the scattering site giving rise to a distribution of energies. There now exists a large amount of experimental and theoretical information on this energy loss process for passage of the commonly used analysis ion beams into most elements. Thus, with a knowledge of the stopping power known to an accuracy of 10-15% or better it is possible with a monoenergetic incident beam to quantify the depth at which the scattering event took place in terms of the energy loss of the scattered ion compared to an ion scattered at the surface, for which no inelastic losses occurred.

A large amount of information may be determined from energy spectra such as that shown in Figure 1. If the bombard-

ing energy is low enough (i.e., below about 3 MeV for helium ions for all but lightest elements) the elastic collision process giving rise to the backscattering is due entirely to the electrostatic repulsive forces between the ion and the nucleus and does not involve an actual contact of the two. In this case the backscattering is called Rutherford backscattering. The great advantage of the purely electrostatic scattering is that its probability depends only on the square of the atomic number of the nucleus and not on specific nuclear properties. Therefore for any given element the cross section or probability of scattering at the prescribed angle is directly and simply calculable. This means that comparisons with standards are not required other than for a single elemental sample to establish the solid angle subtended by the detector. The consequence of this is that given the beam energy, scattering angle, total integrated beam charge, and elemental identification from the peak positions, the number of atoms/cm<sup>2</sup> of each element present can be readily and directly calculated from the total number of counts in each peak.

It should be noted that a  $Z^2$  dependence of the cross section makes the process very sensitive for heavier elements but proportionately less so for lighter elements. This effect can be observed in Figure 1 when it is noted that the Au peak indicates the presence of only about 0.04% Au compared to about 50% for the O peak. In the latter case the sensitivity is further degraded by the superposition of the O peak from the thin film with the distribution from the thick underlying Si substrate. It should be further noted here that the Si substrate is prevented from interfering with other elements by the special preparation of the substrate by placing a film of C on its surface before deposition of the sample thin film. This technique is useful when one has the opportunity to choose the substrate.

In thicker uniform samples the peaks at each mass broaden out with a relatively flat-topped distribution. By calculations based upon the energy loss process described above, it is possible to relate the energy of the scattered ion to the depth below the surface for the scattering interaction. In this way the observed distribution may be related to the composition vs. depth of the particular element within the sample layer.

Thick Film Example. As the peaks become thicker the possibility of interference of the distributions from two or more of the elements is also increased. This is particularly true for heavier elements which inherently appear closer together in terms of the energy of the scattered ions. A particularly difficult example of this situation is shown in Figure 2, again for a sputter-deposited solid lubricant film, in this case a thicker layer on a steel substrate. Figure 2

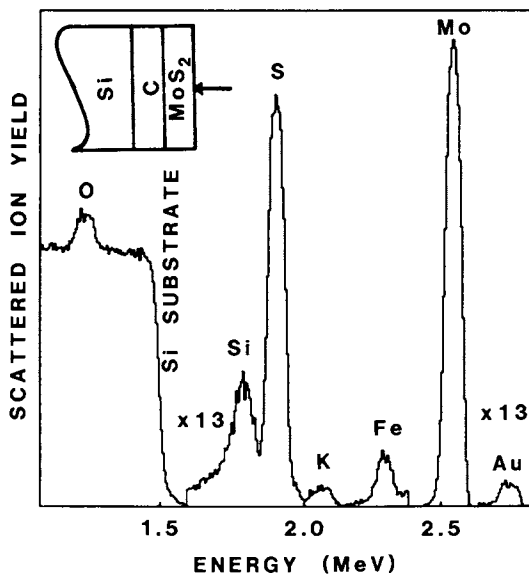


Figure 1. A Rutherford backscattering spectrum for a thin ( $40\mu\text{g}/\text{cm}^2$ )  $\text{MoS}_2$  sputter-deposited film. Conditions:  $^4\text{He}^+$  ions normally incident at 3.0 MeV, and scattered ions detected at a  $135^\circ$  angle by a surface-barrier diode detector. Note the scale factor for other than the Mo peak and the Si substrate. The sample layer configuration is indicated at the upper left.

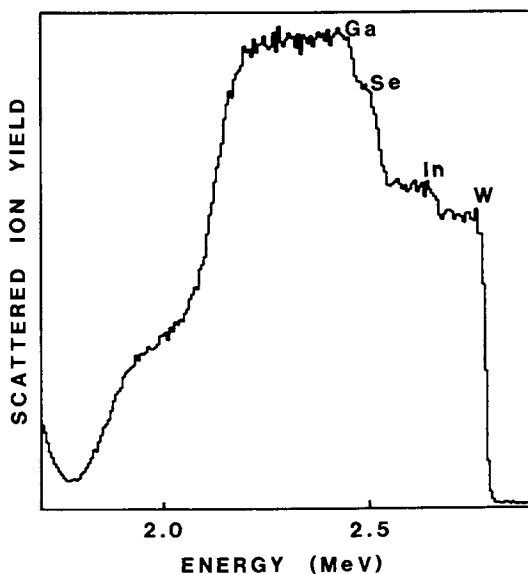


Figure 2. A partial Rutherford backscattering spectrum for a relatively thick ( $430\mu\text{g}/\text{cm}^2$ ) sputter-deposited solid lubricant thin film with conditions as in Fig. 1.

shows a higher energy portion of the spectrum and demonstrates discernable edges for the four (labeled) elements involved. It should be noted that in the case where the thickness of the layer is greater than the resolution of the detector, the height of the edges may be related to the number of atoms/cm<sup>3</sup> of that particular element at the surface. Thus, it is possible even when the distributions overlap to determine from the edge heights the composition of the film, at least at or near the surface. Because in this spectrum the distributions from the four elements considerably overlap it is more difficult to determine the detailed profile. However, the appearance of the combined distribution suggests that the elements are nearly uniformly distributed throughout the depth of the film.

The problem of overlapping distributions arises from the fact that it is impossible to distinguish uniquely or simply from the energy of a single scattered ion, whether: (1) the scattering is from the lighter element near the surface, or (2) from a heavier element at a greater depth below the surface. Although individual scattered ions can not be thus distinguished, in the aggregate they can frequently be identified, as in the case of the edges shown in Figure 2 and discussed above.

Because all phases of the interaction of the incident energetic ion beam with materials, including kinematics and cross section of the elastic collision and the energy losses by means of inelastic interaction with the electrons are readily calculable, the analysis lends itself to computer simulation. One of the first such programs, developed at IBM (4), is used at NRL, while other programs have also been developed at a number of other laboratories.

Figure 3 shows a computer simulation for the spectrum shown in Figure 2 and illustrates how the individual distributions (i.e., the lower curves identified by involved element) add to produce the observed total distribution shown as the upper curve. It is seen that the computer fit is relatively good and that the assumption of uniformity (the individual elemental compositions do not vary by more than 10% throughout the depth except at the back edge) was warranted. Although the simulation conclusions are not necessarily unique they generally may give a reasonable description of even complex overlap situations. However, since the processes simulated require a fair amount of computation, the direct deconvolution of a spectrum by such techniques is not generally possible. In practice, computer fits such as those shown are determined by a series of trials of successive approximations to the observed distribution. As such, they are relatively time-consuming and may not be universally applied except where circumstances warrant.

Implantation Example. An even more complex example may be cited from the use of ion implantation as applied for modifying the surface-sensitive properties of metals. The use of ion implantation in the semiconductor industry is well known as a means of producing well controlled and reproducible doping of semiconductor materials. Also, for metals by means of ion implantation it is often possible to produce near the surface an entirely different alloy from that of the bulk, as in a stainless steel, by the addition of Cr or other common alloying elements. In such cases it is obviously necessary to know what concentration profile results from the implantation of one or more elements into the near surface region. Although the computational capabilities for predicting the distribution of an element implanted under given conditions have improved considerably in recent years, there are a number of factors which are not yet well understood or for which information may not be available in many cases. These effects may strongly influence the resulting depth concentration profile, particularly if more than one implantation is performed. These effects include, but are not limited to, dilution, ion induced mixing and surface sputtering. The latter many become a factor in these cases because of the relatively larger fluences required to change the near surface composition in the 1 - 50 at % range.

Figure 4 provides an example of the result of a duplex implantation into a commonly used bearing alloy. The small peak at the left of the diagram which is due to P, the lighter of the two implanted elements, is subject to easy interpretation. From this peak the conditions of the P implantation (i.e., the total atoms present and the parameters of its nearly Gaussian distribution) may be determined. As in earlier examples the presence of the peak on a large background from the bulk materials present in the alloy requires excellent statistics (through longer exposure to the analyzing beam) in order to reduce the statistical uncertainties in subtracting this background. Due to the proximity in mass of the major component of the steel, Fe, and the other implanted element, Cr, the interpretation of the major leading edge due to the Fe is not at all clear from initial inspection. The lower intensity distribution above the Fe edge is due to a small percentage (about 4 wt %) of Mo in the base alloy.

A solution of this problem is provided by the computer simulation shown in Figure 5, where the distributions of the individual elements are shown labeled in the bottom of the figure and the top curve is the sum of these for comparison with Figure 4. What is observed is a new phenomenon compared to the simpler thin film case shown earlier, i.e., the presence of a dilution effect in the base materials caused by the implantation of the two ion species. This may be readily

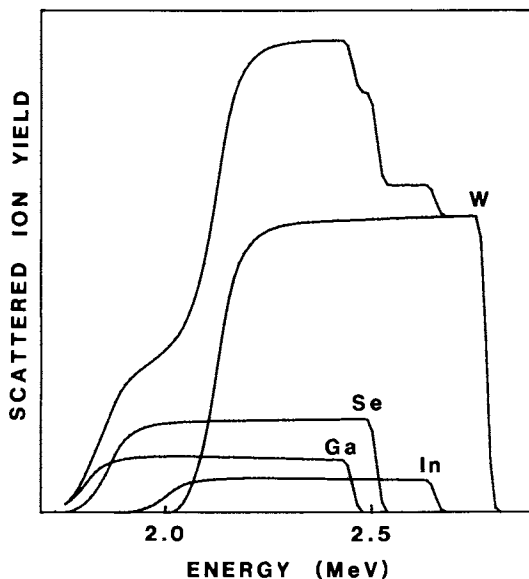


Figure 3. A computer simulation of the partial spectrum from Fig. 2. The lower labeled curves are the individual distributions, and the upper curve is their sum.

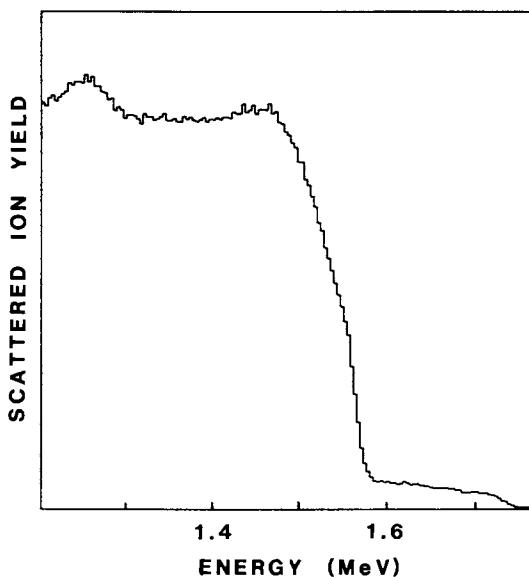


Figure 4. A partial Rutherford backscattering spectrum of an M-50 steel sample successively implanted with  $2 \times 10^{17}$   $^{52}\text{Cr}$  atoms/cm<sup>2</sup> at 150 keV and with  $1 \times 10^{17}$   $^{31}\text{P}$  atoms/cm<sup>2</sup> at 40 keV. Conditions:  $^4\text{He}^+$  ions normally incident at an energy of 2.0 MeV, and scattered ions detected at a 135° angle by a surface-barrier diode detector.

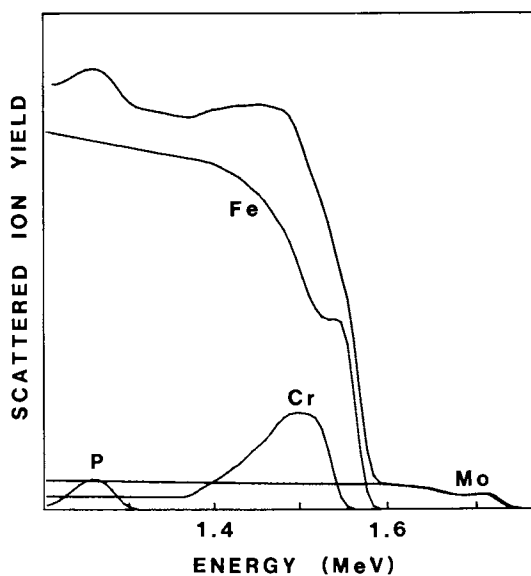


Figure 5. A computer simulation of the partial spectrum from Fig. 4.

observed in the Fe distribution and also in the weaker Mo distribution from the base components. The other small percentage component, Cr, in the original alloy is identical with one of the implanted ions, but its presence is manifest in the tail shown to the left of the Cr peak.

The P peak to the left shows the expected nearly Gaussian distribution with a width consistent with the relatively lower energy (40 keV) with which it was implanted, producing a distribution near the surface. The Cr distribution, on the other hand, is clearly considerably distorted from a Gaussian distribution, due in this case to sputtering which is significant for this fluence ( $2 \times 10^{17}$   $^{52}\text{Cr}$  atoms/cm<sup>2</sup>). This sputtering results in raising the percentage of Cr at the surface relative to the peak as is apparent by the appearance of a definite edge at the high energy (surface) end of the Cr distribution. This edge is slightly displaced from the Fe edge due to their mass difference. It is the superposition of the displaced Cr peak with the dilution dip in the Fe distribution which gives rise to the peculiar shape of the observed distribution of Figure 4. Although the computer simulation shown here is instructive in explaining the effects leading to the observed distribution, it will in most cases produce sufficient uncertainties in the elemental composition profiles as to make other methods preferable in a case which proves this difficult for backscattering analysis. Fortunately in this case a specific nuclear reaction is available to profile the Cr and this reaction will be described later.

The examples of backscattering analysis that have been cited demonstrate some of the principal limitations of the method which are here summarized. (1) The energy separation of ions scattered from neighboring elements becomes smaller the higher the mass. This effect may lead to identification and/or overlap problems. (2) The cross section for elastic scattering varies with  $Z^2$ , making it more difficult to observe lighter elements. This problem is exacerbated by the fact that distributions from light elements may frequently be superimposed on large distributions from the bulk materials or from a substrate, unless special substrate provision can be made. (3) When the thickness of layers of material are sufficiently great or constituent elements are insufficiently separated in mass the possibility of overlap exists which may degrade the quality of information on the depth distribution available, but may not necessarily prevent a determination of composition at least at the surface.

Ion Induced x-ray. Auxiliary techniques may be used to obviate some of the difficulties or limitations of backscattering analysis outlined above. One such technique is ion induced x-ray analysis, a relatively simple technique to apply in an



accelerator laboratory. The instrumentation consists of a cooled lithium drifted silicon detector, usually in its own vacuum container and separated from the accelerator vacuum by thin Be windows. The electronics and multichannel analyzer requirements are similar to those for ion energy detection, and if sufficient equipment is available, an x-ray spectrum may frequently be accumulated simultaneously with the backscattering spectrum. Unlike the backscattering, however, the energies of the observed x-rays are characteristic only of the elements present and not of their depth distribution. In this laboratory this method is used principally to provide positive elemental identifications in cases where high mass numbers cause difficulties using elastic backscattering or in some cases to identify weaker components which may be masked by other elements in overlapping backscattering distributions.

However, it is possible to get quantitative information on the total quantity of a given element present from the x-ray data. Generally corrections are necessary for decreasing cross section and increasing x-ray absorption as a function of depth in the material, except for cases of elements known to be present only in a thin layer near the surface. As this information is generally available from the backscattering analysis the two techniques may be used in conjunction and it may be possible to produce better results for the total quantity from the x-ray data, such as case of the sample for which a backscattering analysis is shown in Figures 2 and 3. The ion induced x-ray spectrum from this solid lubricant sample is shown in Figure 6 in a semi-logarithmic display. Although this spectrum shows considerable complexity due to multiple K, L, or M peaks from the several elements present, at least one well isolated peak is available for purposes of quantification for practically all elements. In any case, the presence of the particular peaks does provide positive identification of the elements in the sample.

#### Nuclear Reaction Analysis

An additional approach that may help when interferences occur in backscattering spectra or when weak lighter element distributions are obscured by large backgrounds is the use of a selective nuclear reaction to determine the profile of that particular element only. By careful selection of the bombarding ion species and energy it is often possible to find such a selective nuclear reaction so as to preclude interference from other elements which may cause problems in the backscattering case. Recourse to nuclear reactions is, however, resorted to only in cases of necessity, as nuclear reactions generally suffer from cross sections several orders of magnitude lower than the equivalent Rutherford elastic scattering. As a consequence of this and the added complexity of nuclear

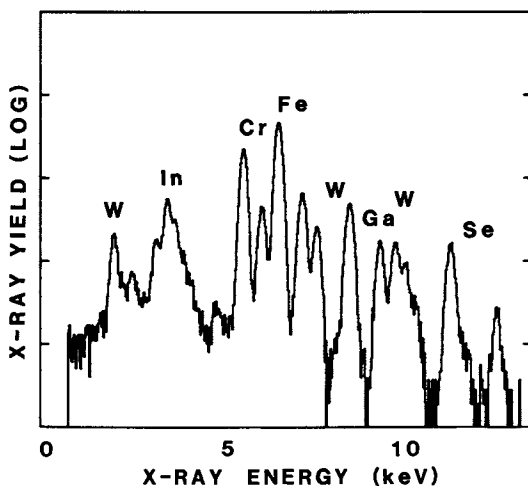


Figure 6. An ion induced x-ray spectrum for the sample shown in Fig. 2. Conditions:  ${}^1\text{H}^+$  ions incident at an energy of 3.0 MeV, and scattered ions detected at a  $45^\circ$  angle to the normal sample. X-rays detected at a  $90^\circ$  angle to the beam with a Si(Li) detector.

reaction analysis, such methods are generally much more time consuming. The conceptually more difficult subject of nuclear reactions may be divided into two classes to simplify the discussion.

Nonresonant Reactions. The so-called "nonresonant" reactions in use bear a close resemblance to the backscattering techniques previously described. In this case the bombarding ion type and energy are selected to be sufficient to actually penetrate the nucleus and initiate a reaction, rather than remaining outside the nucleus as in the Rutherford backscattering case. The cross section for the reaction then becomes a complex function of the nuclear excited states and thus not subject to simple calculation. Indeed in this case it is necessary to experimentally measure the cross sections as a function of energy in the region of interest, or more usually to use a standard of a pure element or compound of known stoichiometry to calibrate the reaction yield for comparison. This is not completely straight forward in the case of moderately fluctuating cross sections as proper allowance must be taken computationally of the differing energy losses in the two different materials.

One of the primary distinctions of this type of reaction is the fact that usually the detected particle (this term rather than ion will be used henceforth in conformity to nuclear physics usage) is normally of a different element or isotope than the incident particle which initiates the reaction. Typical reactions may be  $(p,\alpha)$ ,  $(d,p)$ ,  $(d,\alpha)$ ,  $({}^3\text{He},p)$ , or  $({}^3\text{He},\alpha)$  where  $p = {}^1\text{H}^+$ ,  $d = {}^2\text{H}^+$ , and  $\alpha = {}^4\text{He}^+$  or  ${}^4\text{He}^{++}$ . These reactions are largely restricted to light elements ( $Z < 10$ ) by energy considerations in order to allow penetration of the nucleus with low energy ( $< 5$  MeV) particle beams. Generally then, to profile a particular element a specific reaction will be chosen which fulfills as many as possible of the following factors: (1) the reaction must be exoergic with a large positive Q-value (energy release) to assure that the outgoing particle will have a large enough energy to place it higher in the energy spectrum than the elastically scattered particles from any elements in the sample. (2) The cross section must be as large as possible to provide good yield and must be as smooth or slowly varying as possible to facilitate comparison with the standard. Frequently, in addition to the choice of energy, a choice of the angle with respect to the beam at which the particles are observed may improve these factors. (3) Possible interference with particles from other light elements which may be present should be avoided. This is usually easy since other light elements are normally present only as surface contaminants except in organic materials, and in any event can usually be avoided by proper choice of bombarding particle and energy.

(4) If it is necessary to profile with good depth resolution it is preferable that one of the particles be an isotope of He, as the greater stopping power will increase the energy loss for this particle and thus enhance the depth resolution.

N Implantation Example. Experimentally the measurements are conducted similarly to the backscattering technique. The same type of detector is used, although often thicker to accommodate the higher energy and hence greater range of the particles, particularly for a hydrogen isotope. An example for a  $\text{Si}_3\text{N}_4$  standard for the  $^{14}\text{N}(\text{d},\alpha)^{12}\text{C}$  reaction is shown in Figure 7 in a semi-logarithmic representation. The detector does not distinguish between particle types and the various groups seen are due to competing (d,p) and higher-excited state (d, $\alpha$ ) groups. The elastically scattered deuterons give rise to the highest peak at the extreme low energy end. The groups of interest are marked  $\alpha_0$  and  $\alpha_1$ , corresponding to reactions proceeding to the ground state and 4.43 MeV first excited state of  $^{12}\text{C}$ , respectively. Because of very large Q values these groups stand out above the others and are suitable for use in profiling work. The  $\alpha_1$  group is often used because it has a relatively flat cross section over an extended energy range.

Figure 8 shows an application of this technique to a measurement of N implanted into a tool steel, specifically an end mill, to ascertain the stability of the N under the rigorous conditions at the cutting edge. The figure shows the same very small portion of the energy spectrum taken at two points on the end mill: one at the cutting end where overheating occurred (b) and the second on the cutting edge farther from the region which overheated (a). The portion of the spectra displayed in each case corresponds to only a small part of the spectrum of Figure 7, specifically from the higher energy edge of the  $\alpha_1$  group along the flat portion. As can be seen the cool end (a) retained the N in the nearly "as implanted" condition in a narrow layer near the surface, while for the hot end (b) the heat has caused the N to diffuse, greatly reducing the capability of the N in inhibiting wear.

C Implantation Example. Another example of using a light element to affect surface properties is the implantation of C into a Ti6Al4V alloy in an attempt to enhance fatigue characteristics. The (d,p) reaction is the usual standard for profiling C, but this reaction suffers from a lack of high depth resolution due to the fact that it utilizes only H isotopes which have lower stopping power. This provides a problem in that, in the relative "dirty" vacuum systems of accelerators, C is deposited as a ubiquitous surface contaminant in a graphitic form by the action of the beam, even with cryotrapping arrangements. The problem then is distinguishing

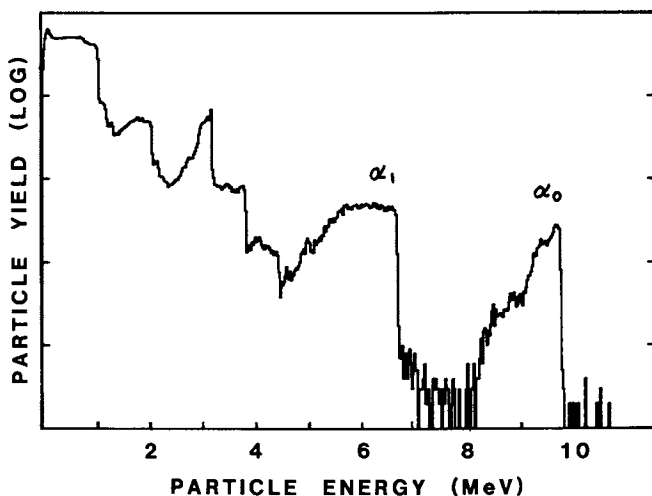


Figure 7. A spectrum of particles resulting from nuclear reactions and scattering from a thick  $\text{Si}_3\text{N}_4$  standard. Conditions:  $^2\text{H}^+$  ions normally incident at an energy of 1.41 MeV, and resulting reaction particles detected at a  $165^\circ$  angle by a surface-barrier diode detector. The particle group marked  $\alpha_1$  is from the  $^{14}\text{N}(d,\alpha)^{12}\text{C}$  reaction and is used to profile N in samples.

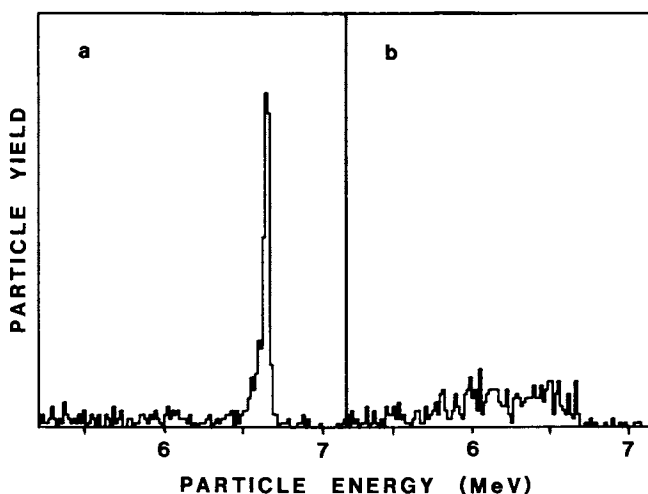


Figure 8. Partial spectra of particles resulting from the  $^{14}\text{N}(d,\alpha)^{12}\text{C}$  reaction at two positions on a  $^{14}\text{N}$  implanted cutting edge of an end mill tool. Key: a, the end was not overheated and retains the as implanted N; and b, the end was overheated in use and caused diffusion of the N. Conditions are as in Fig. 7.

the surface C, added by the analysis technique, from that deliberately introduced into the near surface region of the sample.

The solution to the problem, which was reported recently (5), is the use of a ( $^3\text{He},\alpha$ ) reaction which through the greater stopping power of the He isotopes provides enhanced depth resolution. The result is shown in Figure 9 which is a profile of a relatively shallow C implant in the Ti alloy.

The technique here is of particular interest since it utilizes a magnetic spectrometer with a position-sensitive detector rather than the usual surface-barrier energy detector. This double-focusing spectrometer, which has a very reasonable solid angle of acceptance, is sometimes used in profiling because of its inherently higher energy resolution. However, in this case the use of a magnetic momentum measuring device rather than a purely energy measuring device is necessary because for this reaction at backward angles the energy of the alpha particles is actually below that of the bombarding  $^3\text{He}$  particles elastically scattered from the Ti alloy. However, because of the higher momentum due to the mass four observed reaction particle compared to the mass three scattered particles, the alpha particles may be observed in the region of interest, resulting in the spectrum shown.

Resonant Nuclear Reaction. A second class of nuclear reaction useful in profiling the near surface region is the so called "resonant" reaction, in which a narrow isolated resonance in the yield of the selected reaction is used to probe the number of atoms of this nucleus within a narrow depth interval of the sample. The profile is then generated by accumulating data at a series of different bombarding energies, each corresponding to a different depth below the surface of the sample for the resonance, according to the energy loss process for the incident particles.

This method is of course restricted to nuclei which provide a satisfactory resonance, usually with a (p, $\gamma$ ) or (p, $\alpha$ ) reaction. These are most often found in the region of elements between  $Z = 10$  and  $Z = 28$ , although a few examples exist for lighter elements. Unfortunately above Ni there are no nuclear reaction techniques which have proved satisfactory for profiling purposes.

Cr Implantation Example. Fortunately for those interested in profiling implanted elements in steels, the principal isotope of Fe contributes very little yield from the (p, $\gamma$ ) reaction in the energy region of interest, whereas at least Ti, Cr, and Ni (6) among others have an appropriate resonance. To measure the gamma-ray yield it is often necessary to use a high-resolution gamma-ray detector such as Ge(Li) or hyperpure

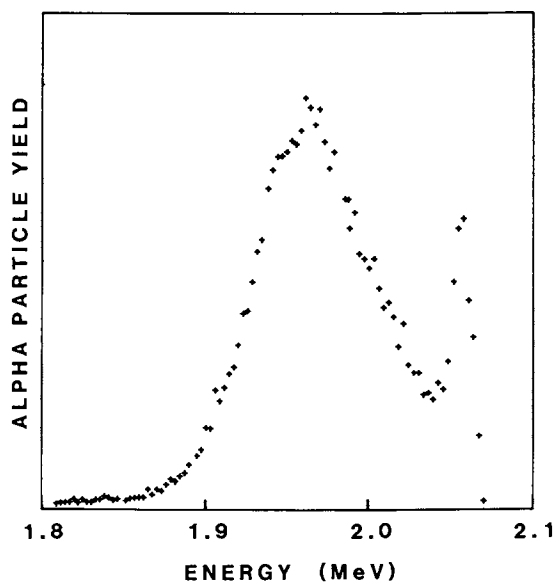


Figure 9. A partial spectrum of  $\alpha$  particles resulting from the  $^{12}\text{C}(^3\text{He},\alpha_0)^{11}\text{C}$  reaction as applied to a Ti6Al4V alloy sample implanted with  $3 \times 10^{17}$   $^{12}\text{C}$  atoms/cm<sup>2</sup> at 75 keV. Conditions:  $^3\text{He}^+$  ions normally incident at an energy of 2.775 MeV, and resulting reaction particles detected at a  $135^\circ$  angle with a magnetic spectrometer. The higher energy peak is due to surface contamination and is resolved from the implanted distribution. (Reproduced, with permission, from Ref. 5. Copyright, North-Holland Publishing Co.)

Ge in order to be able to clearly distinguish only transitions produced by the resonance of interest. Such detectors, self contained in their own cryostat, again utilize electronics and multichannel analyzer similar to the other cases.

An example of this technique is shown in Figure 10 where distributions for Cr implanted in Fe are shown at two different fluences to demonstrate the effect of sputtering on the profile at higher fluences. The lower curve is for a fluence producing negligible effect from the sputtering whereas the upper curve shows the typical distortion effects characterized by a raising of the surface concentration due to sputtering.

### Conclusions

It has been shown that energetic ion beams may be utilized to "nondestructively" determine the profile of composition vs. depth in a wide variety of near surface situations. The major difficulties and limitations of the method have been delineated with descriptions of alternative methods applicable in difficult cases. The advantages of using these techniques as complementary to other surface analysis methods has also been pointed out.

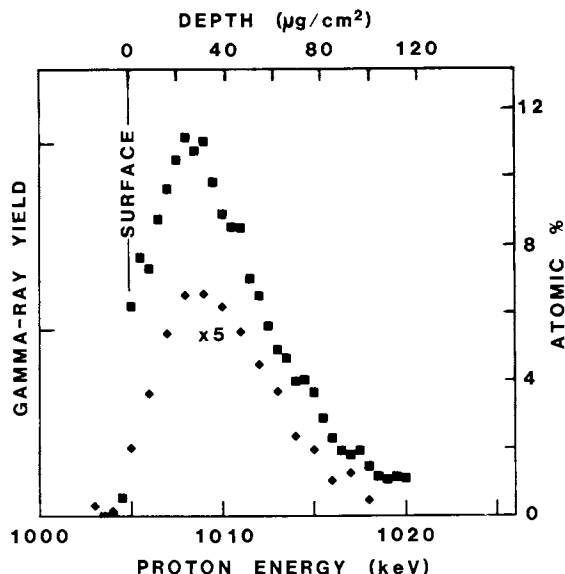


Figure 10. Profiles generated from the 1005-keV resonance of the  $^{52}\text{Cr}(p,\gamma)^{53}\text{Mn}$  reaction in pure Fe samples implanted with fluences of  $1 \times 10^{17}$  and  $1 \times 10^{18}$   $^{52}\text{Cr}$  atoms/cm $^2$  at 150 keV. (Note the scale factor for the latter.) The incident energy at which the  $\gamma$ -ray yield for each point was obtained is on the lower abscissa scale and an equivalent depth scale is on the upper. Conditions:  $^1\text{H}^+$  ions normally incident, and  $\gamma$ -rays detected at a  $0^\circ$  angle to the beam with a Ge(Li) detector. (Reproduced, with permission, from Ref. 6. Copyright 1980, North-Holland Publishing Co.)



Literature Cited

1. Chu, W-K.; Mayer, J. W.; Nicolet, M.-A. "Backscattering Spectrometry"; Academic Press: New York, NY, 1978.
2. Mayer, J. W.; Rimini, E., Eds.; "Ion Beam Handbook for Materials Analysis"; Academic Press, New York, NY, 1977.
3. King, B., Ed.; "Proceedings of the 5th International Conference on Ion Beam Analysis" (Sydney, Australia, 16-20 February 1981); to be published in Nucl. Instrum. Methods.
4. Zeigler, J. F.; Lever, R. F.; Hirvonen, J. K. "Computer Analysis of Nuclear Backscattering," p. 163 in "Ion Beam Surface Layer Analysis," ed. by O. Meyer, G. Linker, and F. Kappeler; Plenum Press: New York, NY, 1976.
5. Gossett, C. R.; to be published in (3).
6. Gossett, C. R. Nucl. Instrum. Methods 1980, 168, 217.

RECEIVED April 5, 1982

# Characterization of Solid Surfaces by Wet Chemical Techniques

FREDERICK M. FOWKES

Lehigh University, Department of Chemistry, Bethlehem, PA 18015

Some very important surface properties of solids can be properly characterized only by certain wet chemical techniques, some of which are currently under rapid improvement. Studies of adsorption from solution allow determination of the surface density of adsorbing sites, and the characterization of the surface forces involved (the energy of dispersion forces,  $\gamma^d$ ; the strength of acidic or basic sites; and the surface density of coulombic charge). Adsorption studies can now be extended with some newer spectroscopic tools (Fourier-transform infra-red spectroscopy, laser Raman spectroscopy, and solid NMR spectroscopy), as well as convenient modern versions of older techniques (Doppler electrophoresis, flow micro-calorimetry, and automated ellipsometry).

Measurements of the strength of surface acids and bases can now be used to determine their Drago E and C constants.

The surface analysis of solids has benefited greatly from the introduction of various high vacuum techniques, from electron microscopy through LEED, AES, ESCA, ISS, SIMS, etc. These techniques have given detailed information on atomic composition and structure, but rather limited information on the capability for chemical reactivity of surface groups. This latter type of information has much practical value, and is often more easily obtained by wet chemical techniques than high vacuum techniques.

The assessment of surface reactivity of solids involves determination of the number of each kind of sites and ability to interact with reactive molecules. The interactions are of two kinds; the general interactions of the London dispersion forces (1) and the specific interactions. Most of the specific interactions are some kind of acid-base phenomenon; this category

includes chelation, coordination, hydrogen-bonding, and the complexes between nucleophiles and electrophilic sites which are so important in catalysis. Most of these complexes with ordinary organic molecules have enthalpies of formation of 1-15 Kcal/mole and consequently disassociate appreciably with rise of temperature or dissociate upon reduction of pressure. Thus acidic sites on an inorganic catalyst may well adsorb amines strongly from organic solvents but in a vacuum system the amines evaporate off and are generally not observed by vacuum techniques. The surface acid sites cannot be readily observed by the various surface analytical vacuum devices. For instance ESCA gives chemical reactivity information but can't observe hydrogen. On the other hand a number of "wet" chemical techniques can be used to gain information about the complexes formed between reactive surface sites and test molecules. Some of these techniques determine energies of interaction by spectroscopic shifts in the UV, visible, or IR (including Raman). Others determine enthalpies of interaction by calorimetry of temperature-dependence of formation constants, or adsorption isotherms. Energies of complexation can also be determined from a variety of other techniques such as gas chromatography.

The surface properties of importance for adsorbents, catalysts, adherent surfaces, and corrodable surfaces are those properties which control interactions with adsorbable species. These interactions always involve dispersion force interactions and may or may not involve specific interactions. The ability of a surface to interact with another material can be determined at present best by observing its interactions with test materials, and these observations are never done in high vacuum and generally involve wet chemical techniques.

### London Dispersion Force Interaction

The London dispersion forces are present and important in most adsorption processes and in adhesive interactions between dissimilar materials. The free energy of interaction per unit area between materials 1 and 2 in contact is  $-W_{12}$  where  $W_{12}$  is the "work of adhesion". At an interface where acid-base interactions occur, the total work of adhesion is the sum of the contributions of dispersion forces,  $W_{12}^d$ , and acid-base interactions,  $W_{12}^{ab}$ . It has been shown that  $W_{12}^d$  can be precisely calculated from the dispersion force contributions to the surface free energy of the two materials ( $\gamma_1^d$  and  $\gamma_2^d$ ):

$$W_{12}^d = 2\sqrt{\gamma_1^d \gamma_2^d} \quad (1)$$

For a solid surface S the value of  $\gamma_S^d$  can be determined by measuring the work of adhesion  $W_{LS}^d$  to a test liquid L of known  $\gamma_L^d$  which has no specific interactions with the solid surface. The work of adhesion of liquid L to solid S is determinably by:

$$W_{SL} = \gamma_L (1 + \cos\theta) + \pi_e \quad (2)$$

where  $\theta$  is the equilibrium angle of contact of the liquid on the solid and  $\pi_e$  is the reduction of the surface free energy of the solid caused by adsorption of the liquid vapor at the equilibrium vapor pressure  $p_0$  of the liquid

$$\pi_e = RT \int_0^1 \Gamma_L d \ln p/p_0 \quad (3)$$

where  $\Gamma_L$  is the surface concentration of adsorbed vapor in moles per unit area.

On low energy surfaces such as polyethylene, polypropylene, or polytetrafluoroethylene many liquids have finite contact angles and  $\pi_e$  values are generally zero (3). On high energy surfaces such as most mineral oxides most liquids have no contact angle,  $\pi_e$  values are quite appreciable and

$$W_{LS} = 2\gamma_L + \pi_e \quad (4)$$

The measurement of contact angles is a wet chemical technique and since  $\pi_e$  is determined with a liquid film adsorbed from vapor in equilibrium with the liquid, it could also qualify as a wet chemical technique in contrast with vacuum techniques.

The aim of these determinations is to find  $\gamma_S^d$ , from which  $W_{SL}^d$  values for a wide variety of liquids can be calculated from equation (1). Calorimetric heats of immersion (1) may also be used to determine  $\gamma_S^d$ .

### Acid-Base Interaction at Interfaces

For many decades we have been using the word "polar" to describe specific surface interactions such as hydrogen-bonding at interfaces, a vestige of the once-popular notion that dipole interactions were the main contribution to hydrogen-bonding. It is now at least twenty years since the strength of hydrogen-bonds was demonstrated to be completely unrelated to the magnitude of the permanent dipole moments of the molecules forming hydrogen-bonds (4), but the use of the word "polar" lingers on.

Hydrogen-bonds have been found to be a member of the family of acid-base interactions, with enthalpies of hydrogen-bonding precisely calculable from the Drago  $E_A$  and  $C_A$  constants for the hydrogen-donor and the Drago  $E_B$  and  $C_B$  constants for the hydrogen-acceptor (6). Some hydrogen bonds are very weak, such as those between water and benzene, for which  $\Delta H^{ab}$  is -1.2 Kcal/mole; this is because the  $\pi$ -electrons of aromatic rings are rather weak bases (weak electron-donors or hydrogen-acceptors). On the other hand the hydrogen bonds which develop between strongly acidic hydrogens and strong bases may have enthalpies as great as 20 Kcal/mole, and involve actual hydrogen transfer from the acid

to the base. In all of these interactions the enthalpy of hydrogen bonding is predictable usually to within  $\pm 0.2$  Kcal/mole, by the Drago correlation:

$$-\Delta H = C_A C_B + E_A E_B \quad (5)$$

Other important acid-base interactions at interfaces involve acidic sites other than "active hydrogens". For instance, all cations are electro-acceptors and are therefore Lewis acids, with an acid strength often proportional to the ionic charge and inversely proportional to the ionic radius; thus trivalent ions of small radii tend to be strongly acidic. Of course the electron-accepting sites must actually be low energy vacant orbitals, so transition metal ions with vacant d-orbitals often display strong Lewis acid character. Lewis acid sites also include electrophilic sites in organic molecules, such as the electrophilic carbons of ketones, esters, carbonates, and nitriles, the electrophilic phosphorus atoms of organic phosphates or the electrophilic nitrogens in nitro groups. Chlorinated or fluorinated hydrocarbons generally are found to be appreciably acidic, including some without hydrogens, such as carbon tetrachloride.

Basic sites are electrons in high energy orbitals, usually on oxygens (ethers, carbonyl oxygens, alcohols), nitrogens (amines, amides, nitriles),  $\pi$ -electron sites (olefins, aromatics), and the heavier elements of the nitrogen and oxygen series. All anions are bases, with the anions of the weaker acids being the stronger bases.

The surface acidity or basicity (or both) of organic solids is more easily understood today than that of inorganic solids, for acidic and basic sites of organic molecules have had much more study, mainly in solution, and often with spectral techniques such as NMR which have been more successful for solutions than for solids, at least until recent introduction of "magic angle" spinning NMR probes for solids. The study of the acidity and basicity of inorganic solid surfaces is most important, but is still in a pioneering stage, with the possible exception of certain commercially important solids such as cracking catalysts and carbon blacks.

#### Indicator Dye Techniques for Surfaces Acidity and Basicity

Following a suggestion by C. Walling (7) to use Hammett acidity indicators (8) for measuring acid strengths of colorless inorganic solids, Johnson (9), Benesi (10), and others (11) developed procedures for determining the distribution of acid strengths of surface acidic sites on cracking catalysts, modified silica, and clays (12). The indicators are a series of hydrocarbon-soluble organic bases which form brightly colored complexes with acids, and are listed in Table I.

Table I  
Hammett Acidity Indicators (8-12)

Indicator	$pK_a$ in water	Basic Color	Acidic Color
Neutral Red	+6.8	Yellow	Blue
Phenylazonaphthylamine	+4.0	Yellow	Red
Butter yellow	+3.3	Yellow	Red
Benzeneazodiphenylamine	+1.5	Yellow	Purple
Dieinmalacetone	-3.0	Yellow	Red
Benzalacetophenone	-5.6	Colorless	Yellow
Anthraquinone	-8.2	Colorless	Yellow

A more extensive list is given in Tanabe's book (11) on "Solid Acids and Bases", and the author has extended the list upwards to include Nile Blue A ( $pK_a \sim 9.5$ ) and Rhodamine B ( $pK_a \sim 10-11$ ).

The original scheme of Hammett (8) was to define an acidity scale for non-aqueous media ( $H_o$ ) such that

$$H_o = pK_a + \log [B]/[BH^+] \quad (6)$$

in which the  $pK_a$  in water was used even though the solvent is typically benzene or toluene, and where B represents the basic form of the indicator and  $BH^+$  the acidic. Johnson (9) and Benesi (10) titrated silica-alumina catalysts with n-butylamine, using the above indicators to determine  $H_o$  values. Figure 1 shows the results of such an n-butylamine titration of three clays (kaolinite, attapulgite, and bentonite), illustrating their differences in surface acidity (12).

However it is now clear that acid strength is not a single-valued function, that different kinds of bases will tend to rank acid strengths differently, depending on their "hardness" or "softness". This is illustrated by the work of Kobayashi (13), who used a spectroscopic method of determining  $[B]/[BH^+]$  on a sample of silica-alumina titrated with n-butylamine and one titrated with pyridine (Figure 2). Evidently the acidity of indicators and of individual acid sites on solids needs at least two constants for complete characterization of acid strength.

Johnson (9) had proposed that one could titrate the acidity of colored solids by adding white solid acids and then titrate while observing the color changes on the white solid acids. This idea is based on the assumption that the colored and white solids do not interact with each other but only with the titrant and dyes. This assumption has been used for many years without challenge, but T. Fabish (14) has just recently shown that carbon blacks do indeed interact with silica-alumina particles and can appreciably change their surface acidity.

Surface basicity can also be examined by indicator dyes, but there has been much less study of surface basicity than of surface acidity. Phenolphthalein, bromothymol blue and various nitro-anilines have been used to assess the effect of dehydration on the basicity of alkaline earth oxides or hydroxides, using benzoic

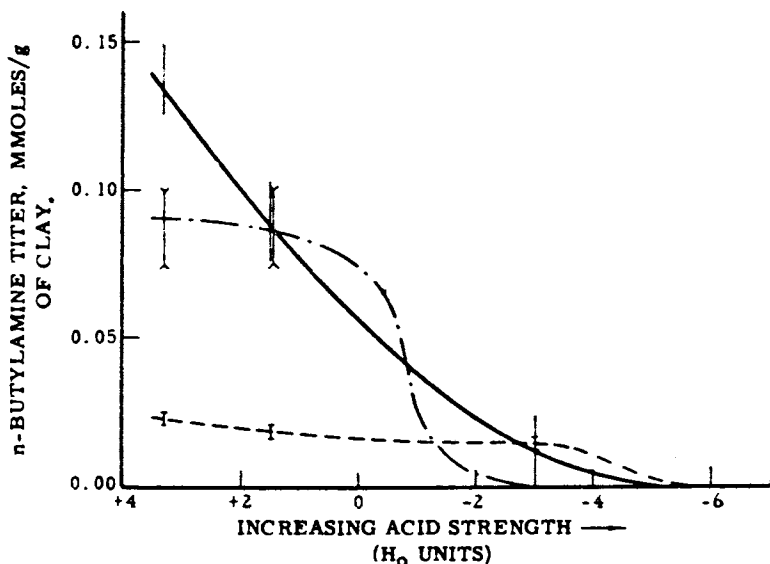


Figure 1. Butylamine titration vs. acid strength for clays dried at 120°C. Key: —, attapulgite; — · —, montmorillonite; ---, kaolinite; and vertical lines denote titer uncertainties. (Reproduced from Ref. 10. Copyright 1957, American Chemical Society.)

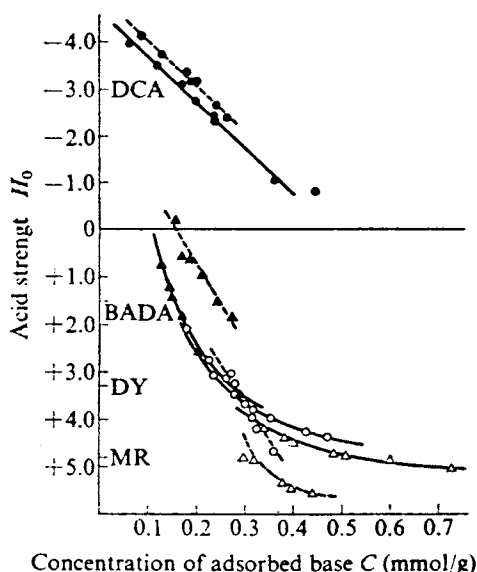


Figure 2. Values of  $H_0$  for  $\text{SiO}_2 \cdot \text{Al}_2\text{O}_3$  at different concentrations of adsorbed organic base. Key: —●—, dicinnamalacetone (DCA)/pyridine; ---●---, DCA/n-butylamine; —▲—, benzeneazodiphenylamine (BADA)/pyridine; ---▲---, BADA/n-butylamine; —○—, dimethyl yellow; ---○---, dimethyl yellow/n-butylamine; —△—, methyl red/pyridine; ---△---, methyl red/n-butylamine. (Reproduced, with permission, from Ref. 11. Copyright 1970, Academic Press.)

acid as titrant (15,16), as illustrated in Figure 3. M.M. Davies proposed an ethyl ester of tetrabromophenolphthalein for detection of basic groups (7); this is a hydrocarbon-soluble light yellow acid which is blue to purple in its complex with basic sites. We have used this dye successfully to determine concentrations of basic sites on glass fibers, using trifluoroacetic acid as titrant (18).

At present the dye techniques are very useful and economical but are somewhat approximate. Advances in use of indicator dyes for measuring surface acidity and basicity may be expected to include a two-parameter measure of acid or base strength similar to the E and C equation of Drago, and the use of fluorescent indicators for colored solids.

#### Titration of Surface Sites on Carbon Blacks

The chemically active sites on the surface of carbon blacks and charcoals are most important to their usefulness. These blacks, formed by pyrolysis of hydrocarbons, are largely fused ring aromatic structures with oxygenated groups such as phenols, quinones, carboxylic acids, esters and lactones residing on the surfaces (19-21). The degree of oxidation determines the chemical properties of the surface. Carbon blacks which have been heated to very high temperatures in the absence of oxygen become graphitized and "function as a Lewis base capable of  $\pi$ -complexing a proton to form its conjugate acid. Aqueous slurries of graphitized carbon blacks containing no surface oxygen have pH values ranging from 8.5 to 10.0 depending on the black" (21). Oxidation of carbon black surfaces produces surface acidity which gives aqueous slurries steadily decreasing pH values with increase in oxygen content. Aqueous slurries of carbon blacks with 6% oxygen have pH values as low as 3.3.

Most of the surface analyses of carbon blacks are done by wet chemical techniques.

Many of the detailed studies of the four classes of oxygen compounds (phenols, quinones, carboxylic acids, and esters or lactones) have involved well-known organic reactions of these surface groups, such as the condensation reactions of the quinone groups with analine, hydroxylamine, or diazomethane, or the gas-evolution reactions of the phenolic groups with lithium aluminum hydride, diazomethane, or methylmagnesium iodide (19). Several of these reactions can be used to titrate specific groups; for instance the content of "active hydrogens" (phenolic and carboxylic acids) can be determined by measuring the volume of hydrogen evolved from carbon blacks heated to 80°C. in a solution of lithium aluminum hydride in a high-boiling ester (21).

Aqueous titrations of the phenolic and carboxylic surface acids are successful routine laboratory techniques involving agitation of slurried carbon black in alkaline aqueous solutions for hours or even days, followed by back-titration. Figure 4



Figure 3. Values of  $H_0$  for alkaline earth metal oxides titrated with benzoic acid in benzene, using nitroaniline indicators. Key: a, MgO; b, CaO; and c, SiO. (Reproduced, with permission, from Ref. 11. Copyright 1970, Academic Press.)

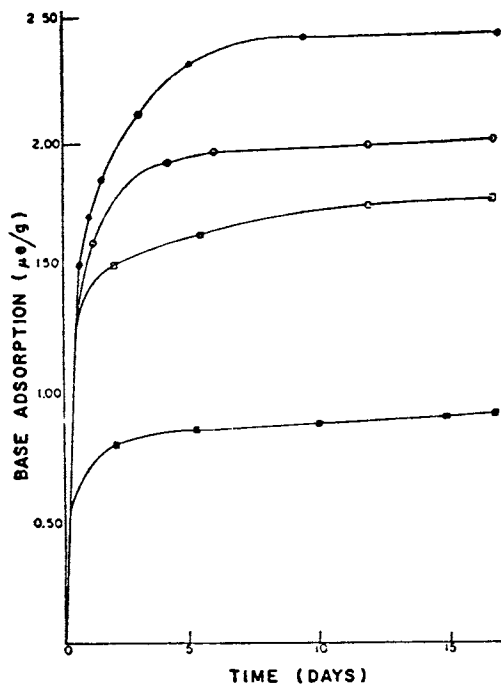
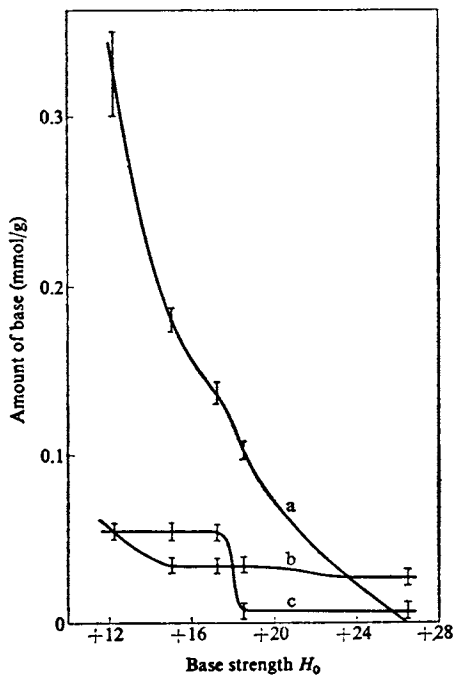


Figure 4. Neutralization of carbon black surface acids on black pearls (2) in aqueous sodium hydroxide. Key:  $\bullet$ —, 1.0 N;  $\circ$ —, 0.2 N;  $\square$ —, 0.1 N; and  $\blacksquare$ —, 0.02 N. (Reproduced from Ref. 21. Copyright 1971, American Chemical Society.)

shows the results obtained with slurries of a high color channel black (surface area of 744 m<sup>2</sup>/g) agitated for several hours in different concentrations of sodium hydroxide. The amount of acidity neutralized is appreciably greater with the more basic solutions, suggesting an appreciable concentration of very weakly acidic surface sites. However one should bear in mind that as acidic hydrogens are dissociated, the resulting surface anions become more concentrated and a high negative surface potential develops which increases the energy required to dissociate acidic hydrogens. This effect is quite analogous to the dissociation of the three acidic hydrogens in phosphoric acid with pK<sub>a</sub>'s of 2.12, 7.21, and 12.67; each of the three are identical, but the energy for dissociation increases with increasing anionic charge. One arbitrary technique for delineation of strong and weak acid sites is to agitate a slurry of carbon black in 0.1 N sodium bicarbonate (pH 8.2) or in 0.1 N sodium carbonate (pH 11.1) and after four hours of agitation, add excess hydrochloric acid, boil off the carbon dioxide, and then back titrate with sodium hydroxide (21). The results of such an acid titration are shown in Table 2, together with the total acidity, determined by hydrogen evolution upon treatment with lithium aluminum hydride in a high-boiling ether at 80°C. (21).

Table 2 also shows surface concentration of quinones and esters or lactones, often referred to as "neutral oxygen compounds" in the rubber literature; actually these are basic oxygens, but not basic in an aqueous environment. The quinone content is estimated from the amount of carbon monoxide evolved in pyrolysis minus the weak acid content (presumed to be phenolic acids, not neutralized at pH 8.2), and the ester and lactone content is estimated from the carbon dioxide evolved in pyrolysis minus the strong acid content (presumed to be carboxylic acids neutralized at pH 8.2).

#### Titration of Ionic Groups on Latex Particles

In the polymerization of latexes such as polystyrene the free radical initiators contribute covalently bonded hydrophilic end groups at each end of every polymer molecule and these hydrophilic groups tend to accumulate in the surface of latex particles where they influence latex properties. The techniques developed for titration of these hydrophilic sites on latex particles may be of general application however.

Latexes initiated with persulfate normally have terminal sulfate groups, but these can be hydrolyzed to alcohols and then oxidized to carboxyl groups. Terminal alcohol groups also result from hydrogen peroxide or hydroperoxide initiated polymerization. Ottewill and Shaw (22) first showed by electrophoresis that latexes stripped of salts and emulsifiers by dialysis have both strong and weak acid sites. Van den Hul and Vanderhoff (23) then found that conductometric titrations were most effective for

Table 2  
Analysis of Chemically Reactive Sites on Carbon Blacks<sup>21</sup>

Carbon black	m <sup>2</sup> /g	pH	Total acids <sup>a</sup> (meq/g)	Strong Acids <sup>b</sup> (meq/g)	Weaker acids <sup>c</sup> (meq/g)	Total weak acids <sup>d</sup> (meq/g)	Quinones (meq/g)	Esters, Lactones (meq/g)
Black Pearls 2	744	3.3	2.45	0.45	0.36	2.00	2.74	0.02
Black Pearls A	299	3.5	1.58	0.28	0.22	1.30	2.23	0.30
Black Pearls 74	332	5.4	0.95	0.06	0.08	0.89	0.42	0.12
Spheron	112	-	0.94	0.16	-	0.78	1.57	0.14
Vulcan 9	124	-	0.84	0.00	-	0.84	-	-
Vulcan 6	114	7.4	0.58	0.02	0.00	0.56	0.00	0.16
Regal 600	108	7.8	0.54	0.02	0.00	0.52	0.00	0.11
Sterling S	23	8.3	0.18	0.00	0.00	0.18	0.00	0.05
Regal SRF	30	8.3	0.21	0.00	0.00	0.21	0.07	0.07
Sterling MT	6	8.4	0.10	0.00	0.00	0.10	0.03	0.02

a. Total acids by LiAlH<sub>4</sub>

b. Strong acids neutralized in 0.1N NaHCO<sub>3</sub>

c. Weaker acids neutralized in 0.1N Na<sub>2</sub>CO<sub>3</sub>

d. (a-b)

distinguishing and determining quantitatively the surface concentrations of the strongly acidic  $\text{RSO}_4\text{H}$  sites, the weakly acidic  $\text{RCOOH}$  sites, and even the  $\text{ROH}$  sites after oxidation to  $\text{RCOOH}$  sites with ionic silver catalysts. Dialysis (22) has been supplanted with ion exchange (23), and further improved by serum replacement (24). In these conductometric titrations the surface acids are titrated with aqueous sodium hydroxide (see Figure 5). The strong acids are quite conductive because of the high mobility of the hydrogen ion, and as titration by sodium hydroxide proceeds the conductivity decreases sharply. At the end point the conductivity rises sharply if no weak acids are present, but more gradually if they are present, and then steeply at the end point for the weak acids. The difficulties in titrating weak acids potentiometrically, evidenced by Figure 4 for carbon blacks, do not arise in conductometric titration when low ionic strengths are attainable. Perhaps these techniques could be useful for pigments, clays, adsorbents, catalysts, carbon, or even coal. Conductometric titrations are quantitative measurements of acid site concentration, but are only qualitative measurements of acid strength.

#### Spectral Measurement of Acid-Base Complexes on Metals

Metal oxides have surface sites which are acidic, basic, or both and these characteristics control important properties such as lubrication, adhesion, and corrosion. Some of the newer infrared techniques such as laser-Raman and Fourier transform infrared reflection spectroscopy are important tools for assessing just how organic acids and bases interact with the oxide films on metal surfaces. Illustrations are given for the adsorption of acidic organic species onto aluminum or iron surfaces, using Fourier transform infrared reflection spectroscopy.

Allara has made a number of FTIR reflection spectroscopic studies of organic acids adsorbing onto oxide films on aluminum. Aluminum has been known to adsorb acids more strongly than bases for some years (25), but details of this interaction are much more accessible by FTIR spectroscopy. Allara first studied films of polyacrylic acid ( $\text{MW} \sim 2000$ ) adsorbed from ethanol onto freshly evaporated aluminum films with 20 Å oxide films. He found that the carbonyl stretch peak of 1712 wave numbers observed in transmission through the polyacrylic acid disappeared from the reflection spectrum of this acid on aluminum and two prominent new peaks appeared, at 1740 and 1620 wave numbers. (26) The  $1740 \text{ cm}^{-1}$  peak is well known to result from carboxylic acid groups which are not hydrogen-bonded, the  $1712 \text{ cm}^{-1}$  peak results from carboxylic acid dimers, and Allara gives good reasons for assigning the  $1620 \text{ cm}^{-1}$  peak to the carbonyl stretching of the aluminum carboxylate. These spectra show that about half the acrylic acid groups form aluminum acrylate bonds and the other half are too far apart to form hydrogen-bonding dimers. Allara speculated that

the free carboxylic acid groups were in the surface of the polymer; to prove it be exposed the sample to metal atom vapors of about  $10^{-7}$  torr and found that Al, Pb, and In vapors shifted the free acid peak to the carboxylate region with the aluminum carboxylate peak at about  $1610\text{ cm}^{-1}$ .

In other studies Allara (27) used FTIR reflection to study the interaction of the oxide film of aluminum with acetic acid in which the aluminum acetate carbonyl stretch peak was found at  $1590\text{ cm}^{-1}$ , in excellent agreement with the  $1589\text{ cm}^{-1}$  peak determined by inelastic electron tunnelling spectroscopy (IETS), another modern technique for vibrational spectra at metal interfaces. The spectra of acetic acid adsorbed on copper oxide or indium oxide were about the same.

Jakobsen used FTIR with attenuated total reflection (ATR) to study the spectra of stearic acid adsorbing onto a 50-100 Å film of iron sputtered onto a germanium ATR prism (28). The species initially adsorbed from hexadecane were the hydrogen-bonded form (probably the dimer) with a strong carbonyl stretching peak at  $1720\text{ cm}^{-1}$ , and a growing (ferric) stearate carbonyl peak at  $1540\text{ cm}^{-1}$ , but at no time was free stearic acid carbonyl stretch peak ( $\sim 1740\text{ cm}^{-1}$ ) observed. Thus the dimer appears to react directly with the surface to produce ferric stearate, in which the stearate ion acts as a strong base complexed with a ferric ion (a Lewis acid site). Thus the mechanism of stearic acid adsorption on iron oxide may be rather more complex than expected, probably involving donation of a carboxyl hydrogen to an FeOFe site, producing a basic carboxylate anion, an FeOH site and an  $\text{Fe}^+$  site.

### Heats of Adsorption of Acids and Bases on Inorganic Surfaces

Adsorption of organic molecules from solution in organic solvents onto inorganic surfaces has been shown to be governed by acid-base interactions between solute and inorganic surface (30). It has been found that basic polymers such as polymethylmethacrylate (PMMA) adsorb only onto acidic solids (such as silica) and then only from solvents less basic than the polymer and less acidic than the acidic solid (Figure 6). Similarly it has been found that acidic polymers such as chlorinated polyvinylchloride (CPVC) adsorb only onto basic solids (such as calcium carbonate) and then only from solvents less acidic than the polymer and less basic than the inorganic solid. Those two polymers have also been used to provide an approximate determination of the ratio of acidic surface sites to basic surface sites in a series of iron-containing pigments, for iron oxides tend to have both kinds of sites (31).

Figure 6 shows the amounts of PMMA adsorbed onto silica gel powders from six solvents of known basicity or acidity, chosen from Drago's tables. Carbon tetrachloride was the most neutral solvent, benzene a very weak base, and dioxane and

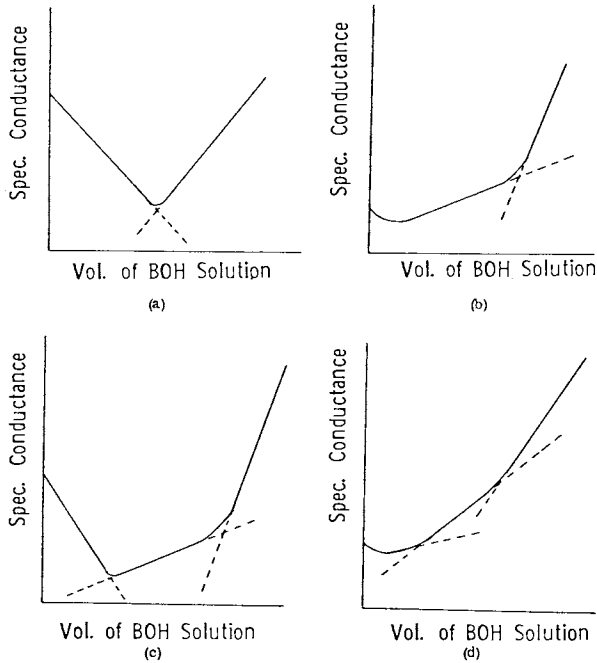


Figure 5. Conductometric titration of polystyrene latex with strong base. Key: a, strong acid sites; b, weak acid sites; c, both strong and weak acid sites; and d, weak acid and very weak acid sites (from Ref. 38.)

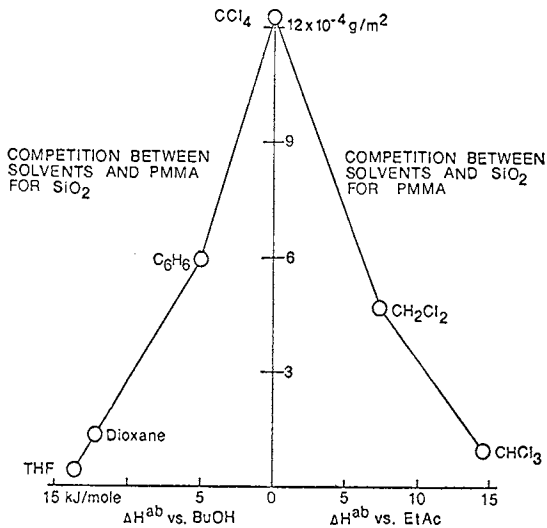


Figure 6. Adsorption of polymethyl methacrylate onto silica gel from basic, neutral, and acidic solvents at 23°C. (Reproduced, with permission, from Ref. 30. Copyright 1978, IEC Products.)

tetrahydrofuran stronger bases; the basicity is measured in this diagram by the enthalpy of interaction with t-butanol, a weak acid. On the right side of the diagram the acidity of dichloromethane and of chloroform is measured by their enthalpy of interaction with ethyl acetate, a weak base. It is clear from the left side of Figure 6 that the competition for adsorption onto silica between the basic polymer and basic solvents is determined by their relative basic strengths, and that very little polymer adsorbs when the solvent is the stronger base. Similarly it is clear from the right side of Figure 6 that the competition between the acidic solvents and the acidic SiOH sites on silica for complexing with the basic ester sites of PMMA is determined by their relative acid strengths, and that very little polymer adsorbs when the solvent is more acidic than the SiOH sites of silica. Quite similar results were found for the adsorption of CPVC onto calcium carbonate; strong adsorption occurred only with neutral solvents and not with chloroform or any of the basic solvents (30). These findings illustrate how completely the acid-base interactions control adsorption from organic solvents onto inorganic surfaces.

For decades such adsorption had been assumed to involve dipole interactions and interacting sites were termed "polar." It is quite clear in the above studies that dipoles in the polymers and in the solid surfaces do not contribute measurably to adsorption. Even from carbon tetrachloride, the solvent most favorable to adsorption, the amount of basic polymer (PMMA) that adsorbed onto basic calcium carbonate was only 2.5% of the amount that adsorbed on the same area of silica surface. Similarly, the amount of acidic polymer (CPVC) that adsorbed onto the acidic silica from any of the six solvents was less than 0.2% of the amount that adsorbed from carbon tetrachloride or dichloromethane onto the same area of basic calcium carbonate. It is concluded that adsorption of organic acids or bases from neutral organic solvents onto inorganic solids is governed entirely by acid-base interactions and is quite independent of dipole phenomena. It is therefore proposed that heats of adsorption are actually enthalpies of acid-base interaction and should therefore be subject to the Drago correlation:

$$-\Delta H = C_A C_B + E_A E_B \quad (5)$$

Test of this proposal are under way, using bases of known  $C_B$  and  $E_B$  from Drago's tables, and measuring heats of adsorption on iron oxide and on silica from solutions in various hydrocarbons.

### Iron Oxides

Iron oxides have been known to adsorb either acids or bases (25). The ratio of acidic to basic sites can be estimated by a method developed by Manson and Straume (31), based on the adsorption of

PMMA and CPVC from neutral solvents (30). The results obtained with four pigments containing iron oxide are shown in Table 3. In general iron oxides are found to be predominantly acidic, but certain alloys may actually be mainly basic, as shown in the table for pigment #3. The performance of these pigments in dispersions correlated very well with the degree of surface acidity.

Table 3  
Ratio of Acidic to Basic Sites in Pigments

Pigment	1	2	3	4
<u>PMMA Adsorbed</u> (mg/g)	30	97	35	6
<u>CPVC Adsorbed</u> (mg/g)	0.09	1.7	8.5	61
<u>%PMMA Adsorbed</u>	99.7	98	80	9
<u>%CPVC Adsorbed</u>	0.3	2	20	91

The acidic sites on iron oxides are believed to be FeOH sites (32), much like the well-known SiOH sites on silica. Heats of adsorption on iron oxide of bases of known  $C_B$  and  $E_B$ , having appreciably different ratios of  $C_B$  to  $E_B$  ("hardness" or "softness"), allow estimation of the  $C_A$  and  $E_A$  for the acidic sites of iron oxide. Our initial studies were done by measuring adsorption isotherms at two or more temperatures (Figure 7) and from the temperature coefficient of the equilibrium constant  $K$  the enthalpy of adsorption was calculated. In Figure 7 the adsorption data is plotted as a Langmuir isotherm:

$$\frac{C}{\Gamma} = \frac{1}{\Gamma_m K} + \frac{C}{\Gamma_m} \quad (7)$$

where  $C$  is the bulk concentration in equilibrium with surface concentration  $\Gamma$ ,  $\Gamma_m$  is the maximum surface coverage, and  $K$  is the equilibrium constant

$$K = \frac{\Gamma}{(\Gamma_m - \Gamma)C} \quad (8)$$

The graph shown in Figure 7 is a plot of  $C/\Gamma$  versus  $C$ , which has a slope of  $1/\Gamma_m$  and intercept  $1/\Gamma_m K$  from which  $\Gamma_m$  and  $K$  are calculable. The heat of adsorption  $\Delta H_{ads}$  is calculable from:

$$\Delta H_{ads} = \frac{RT_1 T_2}{T_2 - T_1} \ln \frac{(K \text{ at } T_2)}{(K \text{ at } T_1)} \quad (9)$$

If the adsorption data give a straight line as in Figure 7 it means that all sites adsorb equally strongly; in this case that all acid sites are of equal acid strength. If half the sites were more strongly acidic the left half of the line would be depressed and two slopes would be observed; this is indeed what we found with Cab-0-Sil silica where it is well-known that there are two types of SiOH, the less acidic adjacent silanols being hydrogen-bonded.



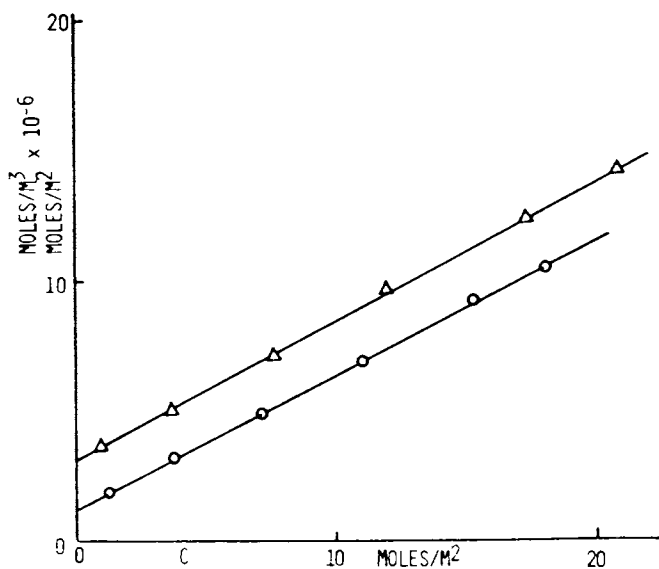


Figure 7. Langmuir isotherms for adsorption of pyridine from cyclohexane onto ferric oxide. Conditions: heat of adsorption,  $-8.8$  kcal/mol; and area per pyridine,  $87 \text{ \AA}^2$ . Key:  $\Delta$ ,  $45^\circ\text{C}$ ; and  $\circ$ ,  $25^\circ\text{C}$ . (Reproduced, with permission, from Ref. 33. Copyright 1981, NACE.)

The Langmuir isotherm also tends to deviate from a straight line if the adsorbed molecules crowd each other too much and thereby raise their Gibbs free energy. Such an effect would tend to cause the higher points of the plot to curve upwards from the straight line. No such deviation resulted in Figure 7 because the area per molecule was  $88 \text{ \AA}^2$ , nearly twice the tightest packing for pyridine.

A graph similar to Figure 7 resulted with adsorption of triethylamine onto the same iron oxide, with  $\Delta H^{\text{ads}} = -13.1 \text{ Kcal/mole}$  and  $\Gamma_m$  corresponding to  $167 \text{ \AA}^2$ . Using Drago's values of  $C_B$  and  $E_B$  for triethylamine, 11.09 and 0.99 respectively, in units of  $(\text{Kcal/mole})^{1/2}$ , we can write equation (5) as:

$$E_A = -\Delta H^{\text{ads}} - C_A \left( \frac{C_B}{E_B} \right) = +13.1 - C_A \left( \frac{11.09}{0.99} \right) \quad (10)$$

and for pyridine

$$E_A = +8.8 - C_A \left( \frac{6.40}{1.17} \right) \quad (11)$$

Equations (10) and (11) predict  $E_A = 2.04$  and  $C_A = 1.0$ , in units of  $(\text{Kcal/mole})^{1/2}$ , indicating that the acid sites are soft acids, somewhat stronger than iodine.

There are shortcomings in this work, however, and we expect to solve these soon. Adsorption is a slower process than most of us realize (25), and at  $25^\circ\text{C}$  the adsorption of pyridine onto iron oxide takes about three days to reach equilibrium. The results of Figure 7 with pyridine and those with triethylamine were obtained in about one hour. However  $\Gamma_m$  was the same for the two temperatures, for the slopes are exactly equal for the two lines. We are now using a flow microcalorimeter to measure the evolution of heat upon adsorption and we are adding a UV sensor to detect concentration changes; this combination should give accurate heats of adsorption and desorption. We will then be able to compare these direct measurements of heats of adsorption with those obtained from the temperature coefficients of adsorption isotherms.

The above values of  $E_A$  and  $C_A$  for iron oxide can be used to predict heats of adsorption with other bases of known  $E_B$  and  $C_B$ . The heat of adsorption of ethyl sulfide should be  $-8.1 \text{ Kcal/mole}$ , tetrahydrofuran  $-6.3 \text{ Kcal/mole}$ , and p-xylene  $-2.6 \text{ Kcal/mole}$ ; the expected accuracy of such predictions is  $\pm 0.2 \text{ Kcal/mole}$ .

### Silica

Results similar to Figure 7 have been obtained with triethylamine adsorption from cyclohexane onto Hi-Sil, a silica gel with a high surface density of silanol groups (34). This is in contrast with Cab-0-Sil, a silica gel known to have a lower surface concentration of silanol groups, some of which are stronger acids

because they are not sufficiently close to others to form hydrogen-bonds. The Langmuir plot for adsorption on Cab-0-Sil has a bent knee shape, indicating about half the sites are more strongly acidic. The time allowed for adsorption was one day and and fairly saturated surface concentrations of triethylamine were observed; the  $\Gamma_m$  values correspond to  $54.5 \text{ \AA}^2$  at  $25^\circ$  and  $54.2 \text{ \AA}^2$  at  $50^\circ\text{C}$ .

Langmuir plots for pyridine adsorption from cyclohexane onto Hi-Sil were not entirely straight lines, for half of the molecules were slightly more strongly adsorbed. These adsorbed films were tightly packed; the  $\Gamma_m$  values corresponded to 30.2 and  $30.7 \text{ \AA}^2$  per pyridine molecule at  $50^\circ$  and  $25^\circ$ , respectively.

The temperature coefficient for both the pyridine and triethylamine adsorption was small, and will need checking by calorimetric measurements.

### Aluminum Oxide

Adsorption of test acids and bases from solution in hydrocarbons onto polished aluminum has been studied by ellipsometry (35). The surface was actually a film of native aluminum oxide; it did not adsorb pyridine but did adsorb chloroform showing the oxide to have no acid sites, but basic sites. Treatment of the aluminum oxide with aqueous carbonate solutions clearly enhanced the basicity, as evidenced by stronger adsorption of chloroform. By observing the temperature coefficient of adsorption isotherms with ellipsometry one can actually determine heats of adsorption on a square centimeter of flat surface.

### Glass Surfaces

As mentioned in a foregoing section, indicator dye techniques showed sodium containing glass fibers to have no acidic sites, but a high density of strongly basic sites. In the flow microcalorimeter we observed no adsorption of pyridine but strong adsorption of chloroform, confirming the suspicion that silicate groups are quite basic and not acidic like the silanols of quartz surfaces, (36).

### Electrophoretic Methods for Detecting Surface Acidity and Basicity

J. Bolger proposed that the isoelectric pH in water could be used to rank the acidic or basic surface properties of oxides (37) and there is much merit in the suggestion. Certainly the basicity of aluminum oxide is predicted by its isoelectric pH of 9.0 and the acidity of silica is predicted by its isoelectric pH of 3.0. However when a surface has both basic and acidic sites like many iron oxides, the isoelectric pH's near 7 do not really tell the whole story.

We propose doing electrophoresis in organic liquids of known

acidity or basicity (3) such as those in Drago's tables, but avoiding liquids that have both acidic and basic sites (such as water, alcohols, ketones, nitriles, nitrobenzene, or any other associated liquid). For instance, pyridine and triethylamine have only basic functionality, and any acidic particles dispersed in these liquids would become negatively charged, with a larger zeta-potential for the more strongly acidic. Similarly basic particles dispersed in acidic liquids such as chloroform will become positively charged, with larger zeta potentials for the more basic particles. The zeta potentials develop by proton-transfer or electron-transfer, as has been proved in some detail (3). An advantage over the aqueous electrophoresis is that powders with both acidic and basic sites will not appear neutral, but the acidity and basicity can be assessed separately.

### Conclusions

The surface reactivity of solids is, to a large extent, a function of site concentration and the acidic or basic strength of sites, properties more easily determinable by a variety of wet chemical techniques than by vacuum instrumentation. The determination of the Drago E and C parameters of surface sites appears to offer more predictability of surface reactivity than other techniques.

### Acknowledgment

Grateful acknowledgment is expressed to the Office of Naval Research who provided support for the research reported herein.

### Literature Cited

1. Fowkes, F. M., Ind. Eng. Chem. 1964, Dec., 40.
2. Boyd, G. E.; Livingston, H. K. J. Amer. Chem. Soc. 1942, 64 2383.
3. Fowkes, F. M.; Anderson, F. W.; Moore, R. J.; Jinnai, H.; Mostafa, M. A. Colloids and Surfaces in Reprographic Technologies, ACS Symposium Series (1982) ed. by M. L. Hair & M.D. Croucher.
4. Pimentel, G. C. The Hydrogen Bond (W. H. Freeman, SF, 1960).
5. Fowkes, F. M., presented at Bronsted Symposium, 178th ACS Meeting, (Sept. 12, 1979).
6. Drago, R. S.; Vogel, G. C.; Needham, T. E. J. Am. Chem. Soc. 1971, 93, 6014; Drago, R. S.; Parr and Chamberlain 1977, 99, 3203.
7. Walling, C. J. Am. Chem. Soc. 1950, 72, 1164.
8. Hammett, L. P.; Deyrup A. J. J. Am. Chem. Soc. 1932, 54, 2721.
9. Johnson, O. J. Phys. Chem. 1955, 59, 827.
10. Benesi, H. A. J. Phys. Chem 1957, 61, 970.
11. Tanabe, K. "Solid Acids and Bases" (Academic Press, 1970).

12. Fowkes, F. M.; Benesi, H. A.; Ryland, L. B.; Sawyer, W. M.; Loeffler, E. S.; Folckemer, F. M.; Johnson, M.R.; Sun, Y.F. J. Agric. & Food Chem. 1960, 8, 203.
13. Kobayashi J.; Higuchi, I.; Shokubai (Tokyo) 1968, 10, 123.
14. Fabish, T. J. Abstract #73, Div. of Colloid and Surface Chem. 182nd ACS Meeting (Aug. 1981).
15. Saito, K.; Tanabe, K. Shokubai (Tokyo) 1969, 11, 206.
16. Take, J.; Kikuchi,; Yoneda, Y. Shokubai, 1968, 10, 127.
17. Davies, M. M. J. Research Bur. Stds. 1955, 54, 309.
18. Fowkes, F. M.; Knitter, K. unpublished results.
19. Donnet, J. B.; Voet, A. Carbon Black (Dekker, 1976).
20. Rivin, D. Rubber Chem. Technol. 1963, 36, 729.
21. Rivin, D. Rubber Chem. Technol 1971, 44, 307.
22. Ottewill, R. H.; Shaw, J. N., Kolloid Z.u.Z. Polymer, 1967, 218, 34.
23. van den Hul, H.J.; Vanderhoff, J.W. Br. Polymer J., 1970, 2, 121, J. Electroanalytical Chem. 1972, 37, 161.
24. Ahmed, S. M.; El-Aasser, M.S.; Pauli, G.H.; Poehlein, G. W.; Vanderhoff, J. W. J. Coll. Interf. Sci. 1980, 73, 388.
25. Fowkes, F.M. J. Phys. Chem. 1960, 64, 726.
26. Allara, D. L. Adhesion and Adsorption of Polymers, ed. by L.-H. Lee (Plenum, 1980) Vol. B, p.751.
27. Allara, D. L. Vibrational Spectroscopies for Adsorbed Species ACS Symp. Ser. 137 (ed. by A. T. Bell and M. L. Hair), 1980, 37.
28. Jacobsen, R. J. Fourier Transform Infrared Spectroscopy, ed. by J. R. Ferraro and L. J. Basile Vol. 2, 174-7.
29. Tanabe, K. "Solid Acids and Bases", Academic Press, 1970, 19-23.
30. Fowkes, F. M.; Mostafa, M. A. IEC Prod R & D, 1978, 17, 3.
31. Manson, J. A.; Straume, M. private communication
32. Lorenzelli, V.; Rossi, P. F.; Busca, G.; Cotena, N. Heterogeneous Catalysis 1979, 1, 463.
33. Fowkes, F. M.; Sun, C.-Y.; Joslin, S. T. Corrosion Control by Organic Coatings ed. by H. Leidheiser, Jr. (NACE, 1981) p. 1.
34. Fowkes, F. M.; McCarthy, D. C. to be published.
35. Fowkes, F. M.; Casper, L. A. to be published.
36. Joslin, S. T., private communication.
37. Bolger, J. C.; Michaels, A. S. Interface Conversion Polymer Coatings ed. by P. Weiss (Elsevier, NY, 1968) pp3-60.

RECEIVED April 19, 1982

## Prospects in the Analysis of Chemically Modified Electrodes

DALE H. KARWEIK, CHARLES W. MILLER, MARC D. PORTER,  
and THEODORE KUWANA

Ohio State University, Department of Chemistry, Columbus, OH 43210

Powerful methods of analyzing surfaces at atomic and molecular levels developed in recent years have allowed the electrochemist to begin rationally exploring various means of chemically modifying the electrode surface to promote catalysis. Many of these surface methods require that the sample be probed in high and ultra-high vacuum to obtain a signal and to maintain sample integrity. On the other hand, electrochemists have felt the need to develop in situ surface methods to provide complementary information. The combined sets of techniques, in solo and ensemble performances, have provided descriptions of the surface topography, atomic speciation, molecular speciation, and structure and bonding of the mediator on the surface and/or at the solution interface. Although each method has provided remarkably accurate correlations with the observed electrochemical behavior of the chemically modified surface, it is the "global" description that will accelerate the rational development of efficient, competitive electrocatalysts.

An area currently very active in electrochemical research deals with the design, fabrication and applications of chemically modified electrodes (CME's). The attractiveness of CME's stems from their potential to replace precious metals such as Pt in electrocatalysis for energy production (1-9), energy storage (10-13), electrosynthesis (14-19), electroanalysis (20-28), and other purposes (29-31). One approach has been to "immobilize", either by covalent attachment, strong adsorption or incorporation into polymeric structures, electrochemically active molecules, called mediators, which act as electron transfer bridges between the electrode surface and the solution species. It has been

0097-6156/82/0199-0089\$08.75/0

© 1982 American Chemical Society

found that the ec catalytic mechanism (21) describes the mediated electron transfer sequence and provides a rational approach to the design of electrocatalysis systems via preliminary studies of the homogeneous reaction of the mediator with the solution species. There are several examples in the literature that describe such studies and subsequent translations of homogeneous into heterogeneous catalysis via surface immobilization. The mechanism, and hence, a description of the interaction of the mediator with the electrode and the solution substrate are of fundamental interest. Such a description relies, in part, on the ability to fully characterize the CME surface. A wide variety of chemical modifications on various conducting support surfaces presents the analytical chemist with a unique set of problems that are difficult to solve by available methods. These problems arise because the surface functionalities and the molecules attached via modification are: a) labile, b) present at thicknesses of less than a monolayer to a few layers, thereby presenting an inherently poor signal/noise ratio for atomic and molecular methods; c) usually "bound" by more than one means, i.e. adsorbed, covalently linked, or incorporated into a carbon lattice; d) most likely oriented in more than one way on either a "clean" or "dirty" and complex surface; and e) used in contact with a solution phase while analytical information may be derived predominately from vacuum spectroscopic methods. These problems require an investigator to consider such things as sensitivity of detection, the damage created by the probe beam, the type of information, i.e. atomic or molecular, and the level of quantitation of the method or methods selected for CME surface analysis. Additional problems are introduced when the support is graphitic or carbonaceous such as those on which we have focused our attention. The carbon-based supports offer versatility and wide choice of surface functionalities that can be manipulated with known chemistry. Also, carbon should remain plentiful and cost effective. However, the signal to "noise" ratio is unfavorable when one is trying to ascertain the type and quantity of carbon contained in an introduced functionality or mediator on a carbon-based support.

This paper will survey the current status of surface analysis in the examination of chemically modified electrode surfaces. In doing so, we shall take selected examples from our laboratory and the literature to illustrate some of the methods that have been employed to answer questions about surface topography, atomic and molecular speciation, and molecular orientation and bonding.

### The "Alphabet Soup" Of Methods

The "ideal" surface analytical method would produce information that would identify the types and quantities of chemical groups or functionalities and their spatial

distributions. If it were a spectroscopic method, the spectrum would contain bands or peaks directly identified with groups as derived from known samples. The mode of surface "bonding" with the moiety containing the group(s) would be derivable from the shape or shift of these bands. Perhaps the dependence of the intensity and "polarization" as a function of the angular dependence of the input and output signals would provide information about the orientation of the particular moiety on the CME surface. The ideal method would also allow in situ analysis so that the nature of the interaction(s) between the CME surface and the solution reactant could be defined. Of course, sensitivity and spatial resolution must be sufficiently high to observe submonolayers of material and their distribution.

Since such an ideal surface method does not presently exist, the alternative has been to use several methods in concert, such as those listed in Table I, to obtain a "global" view of the surface. This alphabet soup compilation of methods is familiar to most surface scientists. However, the equipment, facility and manpower costs are such that most locations have only a limited selection available. Collaborative efforts including the use of instrumentation at regional centers offer access to sophisticated instrumentation perhaps unavailable locally. However, the possibility of surface contamination and changes incurred during sample transit can compromise the surface integrity. In any case, the use of multiple spectroscopic methods with cross-correlation of information is the best approach today. Clearly it would be ideal if one could perform analyses using several methods at each step of the CME life starting from the initial pretreatments through the synthetic steps of modification; and also, before, during and after electrochemical usage. In the text to follow, we shall survey what has been done to determine surface topography, atomic and molecular speciation, and structure/bonding of moieties created by various electrode surface modifications.

### Surface Topography

Scanning electron microscopy (SEM) has been the most widely used technique for defining the surfaces of CME's. The principal aims have been to (a) screen conductor samples prior to usage for desirable features such as smoothness; i.e. lack of cracks, holes, cleavages; (b) monitor any introduction of surface roughness or etching during modification steps; (c) determine the macro-scale homogeneity and completeness of surface coverage, particularly for polymeric materials; and (d) monitor the effect of electrochemistry.

For example, SEM examination of carbon surfaces has shown considerable difference between those of polished glassy carbon (GC) and pyrolytic graphite. The surface of pyrolytic graphite is "pebbled" and uneven (32) while the glassy carbon can be



Table I. Prospective Methods for the Analysis of Chemically Modified Electrodes

A. Surface Topography

SEM Scanning Electron Microscopy  
STEM Scanning Transmission Electron Microscopy

B. Atomic Speciation

XPS X-Ray Photoelectron Spectroscopy  
AES Auger Electron Spectroscopy

C. Molecular Speciation

XPS X-Ray Photoelectron Spectroscopy  
IR Infra-Red Spectroscopy, including  
FTIR Fourier Transform IR  
PAS-IR IR Photo Acoustic Spectroscopy  
RS Raman Spectroscopy  
Fl Fluorescence  
SE UV-VIS Spectroelectrochemistry

D. Structure and Bonding

XPS X-Ray Photoelectron Spectroscopy  
IETS Inelastic Tunneling Spectroscopy  
TDMS Thermal Desorption Spectroscopy  
EXAFS Extended X-ray Absorption Fine Structure  
RS Raman Spectroscopy  
IR Infra-Red Spectroscopy

polished to a microscopically flat plane as may be seen in the micrographs of Figure 1. Variation in the quality of the surface also occurs with the source and manufacturing method. In glassy carbon from Tokai (Tokai Carbon Co., Ltd., Tokyo), surface "pits" (33) are observed and these pits increase in number and size as the heat treatment limit increases, i.e. GC-10 to GC-30. Thus, the high temperature GC-30 with its rougher surface may be undesirable for modification at monolayer coverages.

The effect of various radio frequency (RF) plasma treatments on glassy carbon surfaces has been recently detailed (33). Reactive gases such as oxygen not only etched the surface but also seemingly caused the rupture of voids close to the surface of GC samples with the higher heat treatment limits. Less reactive gases such as water vapor, nitrogen, carbon dioxide and ammonia produced a much lower amount of surface damage with some pits appearing to result from surface ablation. SEM has also been used to verify the absence of polymer formation (34) where it could have been a competing form of modification.

A more recent and wide spread usage of SEM has been to evaluate the quality of polymerically coated electrode surfaces. For example, it has been used to verify the production of smooth, pore and defect free polymeric films on indium oxide, tin oxide, Pt/Pt oxide, and carbon surfaces (35-38). Polypyrrole on Pt (39) produced an uneven film with spheroids of polymer on the surface at sites of preferential growth. On Au perylene formed films with 100 angstrom microcrystalline domains without evidence of channels or pin holes (40). Further, a dependence on the support geometry and roughness has been reported for viologen polymers on Au foils and minigrids (41-42). The clearest SEM evidence of pin holes to date has been obtained for polyvinyl ferrocene films on Pt which showed 0.5 micron diameter holes (43). Finally, SEM has indicated gross changes in a functionalized polystyrene film that were caused by swelling of the polymer during electrolysis (44). The extent of swelling which remained after the polymer was dried was estimated to be ca. 15%.

Better spatial definition can be attained using transmission microscopy but the opaqueness of the electrode support negates its effectiveness. The spatial distribution of elements on the surface can be resolved with a scanning Auger microprobe. The problem of electron beam damage to the modified surface has prevented widespread usage.

### Atomic Speciation

XPS and to a lesser extent, Auger electron spectroscopy (AES) have been applied to detect the presence of and to determine the extent of surface modification. Most of these qualitative and semi-quantitative studies have monitored certain elements which occurred in the mediator and not on the unmodified surface. The sustained presence of such element(s) following

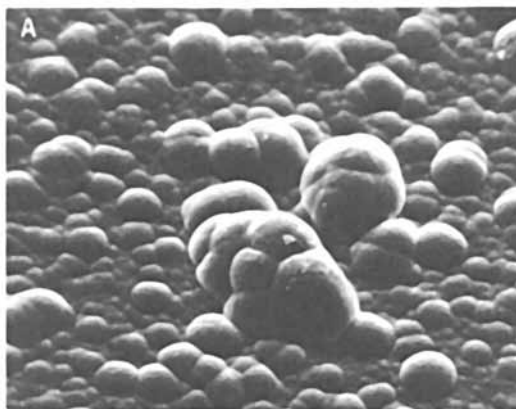


*Figure 1A. SEM of an untreated pyrolytic graphite electrode with  $\times 200$  magnification. (Reproduced from Ref. 32. Copyright 1977, American Chemical Society.)*

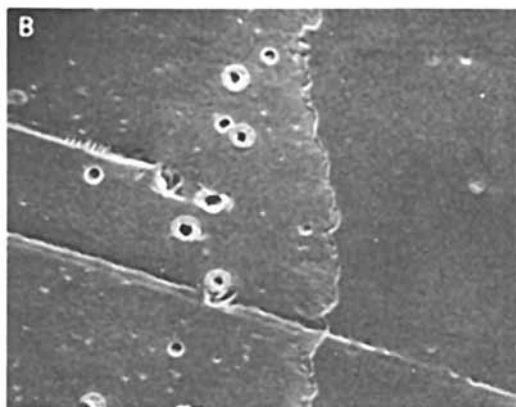


*Figure 1B. SEM of an O<sub>2</sub> rf plasma treated glassy carbon electrode  $\times 500$  magnification. The right side of the glassy carbon surface was protected and so exhibits the structure of an untreated electrode. (Reproduced from Ref. 33. Copyright 1981, American Chemical Society.)*

washing and/or after electrolysis has been considered *prima facie* evidence for the covalent attachment of the mediator (45-54). In a more restricted manner, AES has been similarly used (34,55). AES has also been successfully used to verify the cleanliness of special surfaces, i.e. single crystal Pt electrodes (56-57), prior to and following electrochemical studies. XPS derived "proof" of covalent bonding has been less convincing in a few cases where very high background levels of the selected element (58) or where significant overlap of the support and modifier peaks precluded the acquisition of good XPS spectra (59). Further, it has difficult to distinguish between covalent bonding and strong adsorption in most cases via XPS. Off-surface fluorescence measurements have provided data to determine the relative amounts of the two modes of immobilization in one case (60). Wider usage of fluorescence methods is predicted.

While XPS signals may not provide conclusive proof of covalent attachment, they can be correlated, and hence supported, by electrochemical data. For example, a cyclic voltammetric study of 33 immobilized charge-transfer mediators and their solution analogs indicated that the redox potential of the immobilized species was shifted by ca. 36 mV compared to similar ones in solution (49). Tetrathiafulvalene carboxylic acid immobilized through an alkyl-amine silane (51) and aminophenyl ferrocene bound with a butyryl chloride silane (54) also showed a behavior atypical of solution species. In these 35 cases, the electrochemical behavior was interpreted to be due to surface "immobilized" species with no evidence of adsorption. These results were consistent with the elemental XPS data. Similar results have been obtained using cyanuric chloride as the linking agent for methylaminopropyl viologen (61), ortho-tolidine (62), and hydroxy- and bishydroxy-methylferrocene (63,64). The XPS spectral associated with the fabrication and use of a hydroxymethyl ferrocene modified electrode are shown in Figure 2. There is a clear progression of expected elements appearing in the spectra as the carbon surface is pretreated and functionalized, the cyanuric chloride introduced, hydroxymethyl ferrocene attached, and finally, after electrochemical usage. An electrode taken through all of the synthetic steps produced electrochemistry identified with the formal potential of the electroactive ferrocene moiety whereas a control, treated identically except for the omission of cyanuric chloride, exhibited only background electrochemistry (see Figures 3, and 4). The last XPS spectrum in Figure 2 verifies the stability of the attached hydroxylvinylferrocene to electrolysis. In other cases, the mediator linkage has been unstable to electrolysis with concomittant loss of XPS signal and electrochemical activity (65,66).

Another important aspect of XPS atomic speciation involves the use of elemental intensities to determine the thickness of mediator layers. Initial attempts have included qualitative

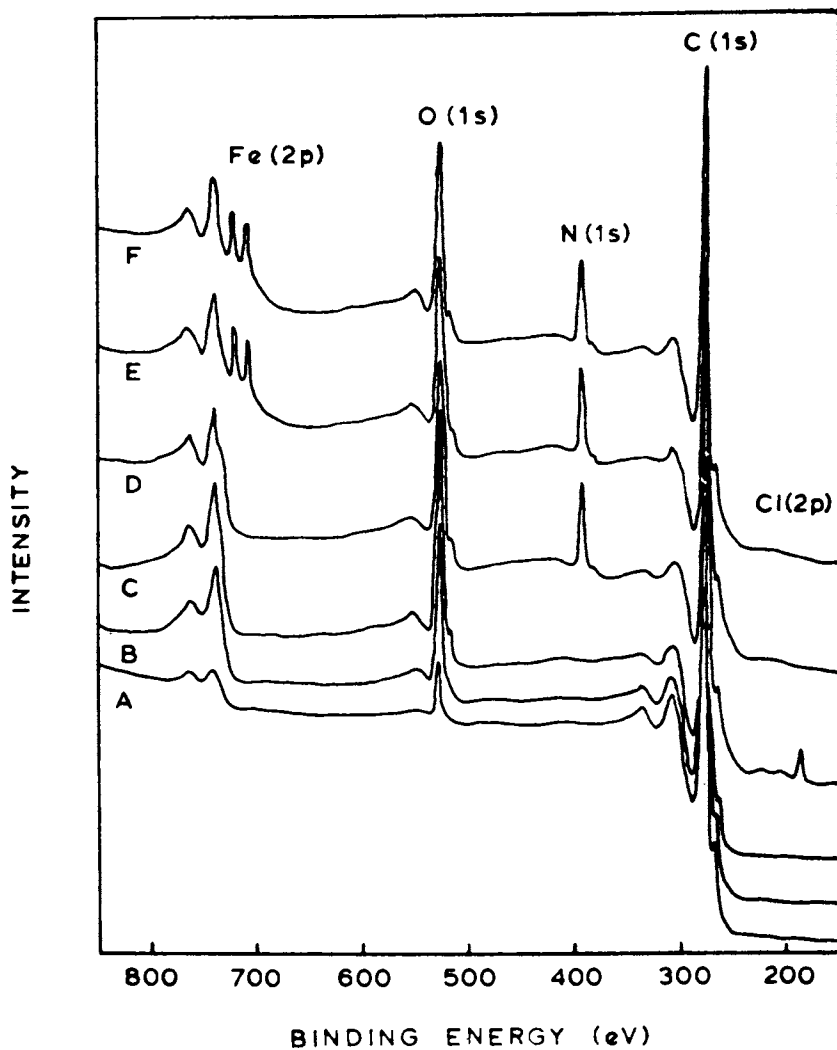


Figure 2. Low-resolution XPS spectra of a pyrolytic graphite electrode surface. Key: A, prior to modification; B, following a 1-h  $O_2$  rf plasma treatment; C, after reduction with  $LiAlH_4$ ; D, after modification with cyanuric chloride; E, after attachment of hydroxymethyl ferrocene; and F, following electrolysis in pH 7 phosphate buffer.

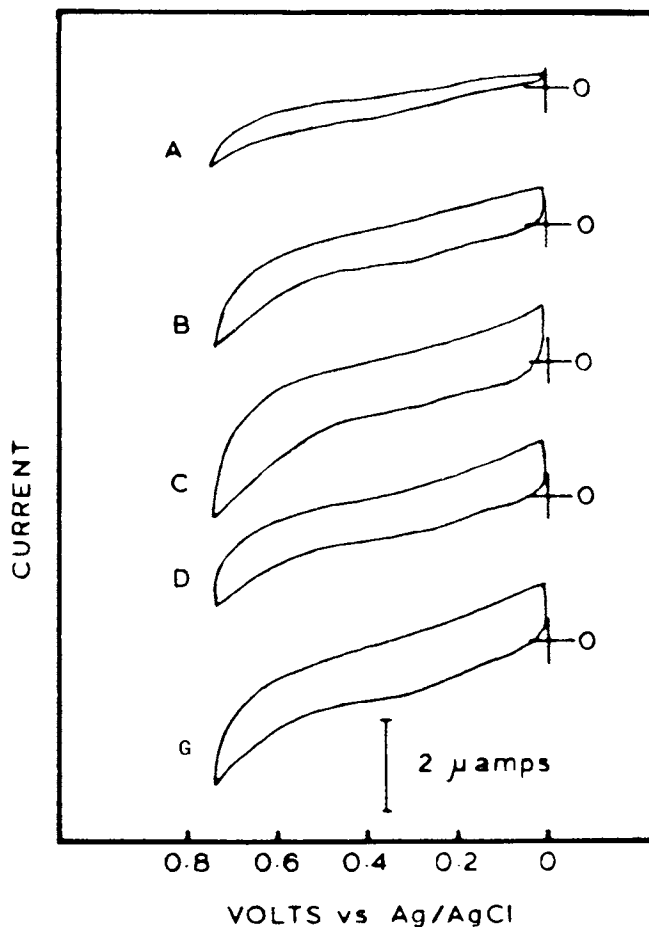


Figure 3. Cyclic voltammograms of a pyrolytic graphite electrode in pH 7 phosphate buffer following the listed reaction steps. Traces A–D correspond to the reaction steps cited in Fig. 2; and trace G corresponds to a control electrode produced by omitting step D before reacting with hydroxymethyl ferrocene. The potential scale is referenced to Ag/AgCl (saturated KCl). All traces were recorded with a 50 mV/s scan rate. (Reproduced from Ref. 64. Copyright 1978, American Chemical Society.)

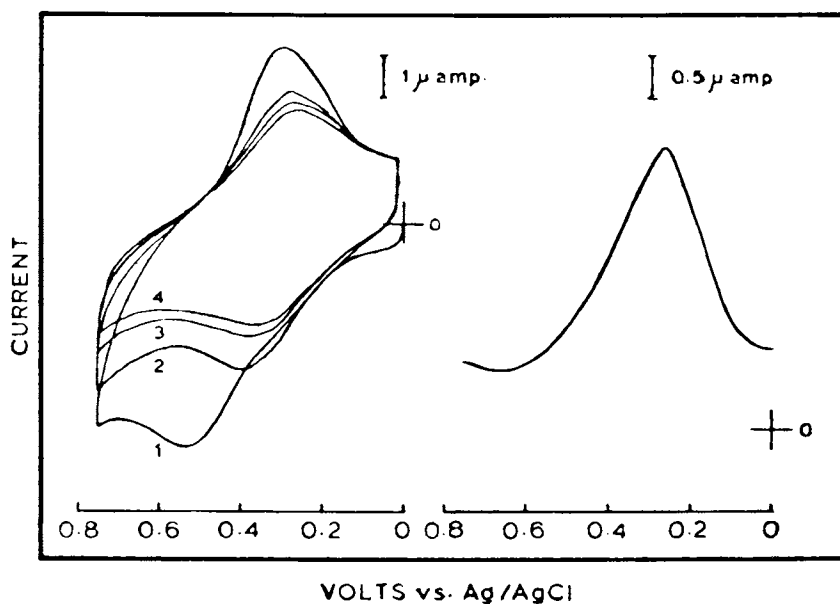


Figure 4. Cyclic voltammogram and differential pulse polarogram of electrodes prepared as in Fig. 2, spectrum E. Recorded using solution conditions from Fig. 3. The differential pulse polarogram was recorded with a scan rate of 2 mV/s.

statements about the absence or attenuation of the signal intensities from the support element (39,67,68) or of the increases in the peaks due to elements of the mediator as a function of immobilization reaction time (69). These initial attempts were followed by more quantitative measurements of thickness. Calculations using relative intensities provided reasonable estimates of the thickness when continuous coverages were obtained (70-72). In one notable case there proved to be a linear correlation between the XPS signal and the electrochemically determined coverage (73). Other investigations have not obtained estimates of thickness that correlated well with other experimental observations (74,75) probably due to discontinuity or inhomogeneity in the films. Another interesting case recently was reported (76) in which initial intense XPS signals for the modifier elements were monitored during depth profiling by sputtering. The profile indicated a multilayer incorporation of the modifier which extended into the support material.

The most recent advance in the determination of film thickness has employed angular resolved XPS measurements following the work of Fadley (77-80). Notable experiments of this type have been performed on supports coated with polymeric films (81,82). In an initial report (81) the intensity ratio of the mediator elements from the outer polymer layer to a separate set of elements from the inner polymer layer increased with the decrease in the emission angle as expected and predicted by theory. The XPS spectra and the intensity ratios are reproduced in Figure 5. The results clearly support the presence of a distinct bilayer structure. This approach has been applied in a more quantitative manner (82) to determine film thicknesses. The thicknesses of six different polymer films on Pt supports were measured and correlated with coverages that were determined from coulometric measurements. Plots of the relative intensities of the naked Pt surface and of Pt supports coated with each of the polymers, as shown in Figure 6, provided the raw data for the calculation of the film thicknesses. Two of the films yielded excellent correlation between the XPS and coulometric results. Ambiguities in this elegant approach resulted from inaccurate penetration depths, discontinuous films or poor electrochemical estimates of the surface coverage (inactive or isolated mediator sites). At the present, this method provides the most promising approach for determining CME thicknesses.

### Molecular Speciation

The molecular nature of the CME surface and of the support during the synthetic steps in the attachment of a mediator is critical to the understanding and rational design of CME's. XPS will continue to be the principal method for probing the surface to determine the nature of the molecular species (i.e. functional



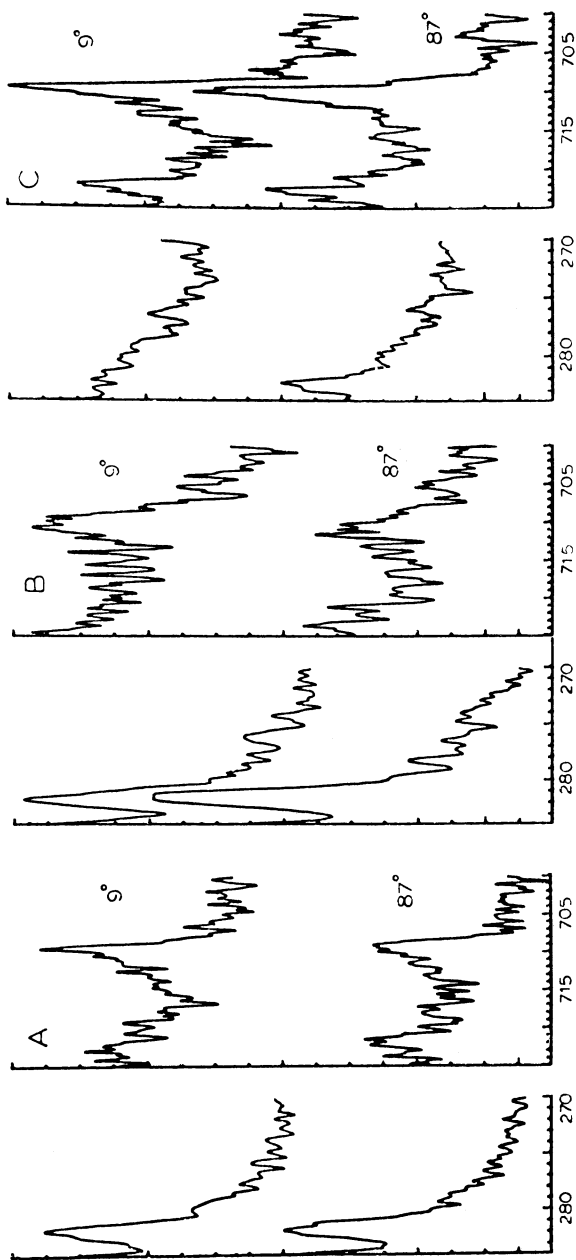


Figure 5. XPS spectra as a function of emission angle for Ru 3d 5/2 (BE = 281 eV) and Fe 2p 3/2 (BE = 710 eV). Key: A, a copolymer layer of 4-vinyl-4'-methyl-2,2'-bipyridine complexes of Ru(II), I, and Fe(II), II, two bilayer films with Pt/II structures where R = 0.98; B, R = 0.39; and C, R = 0.0. The thickness of the outer film, II, is ca. 3 × larger in C than in B. The intensity ratio is defined as R = Ru/Fe at 9°, and Ru/Fe at 87°. (Reproduced from Ref. 81. Copyright 1981, American Chemical Society.)

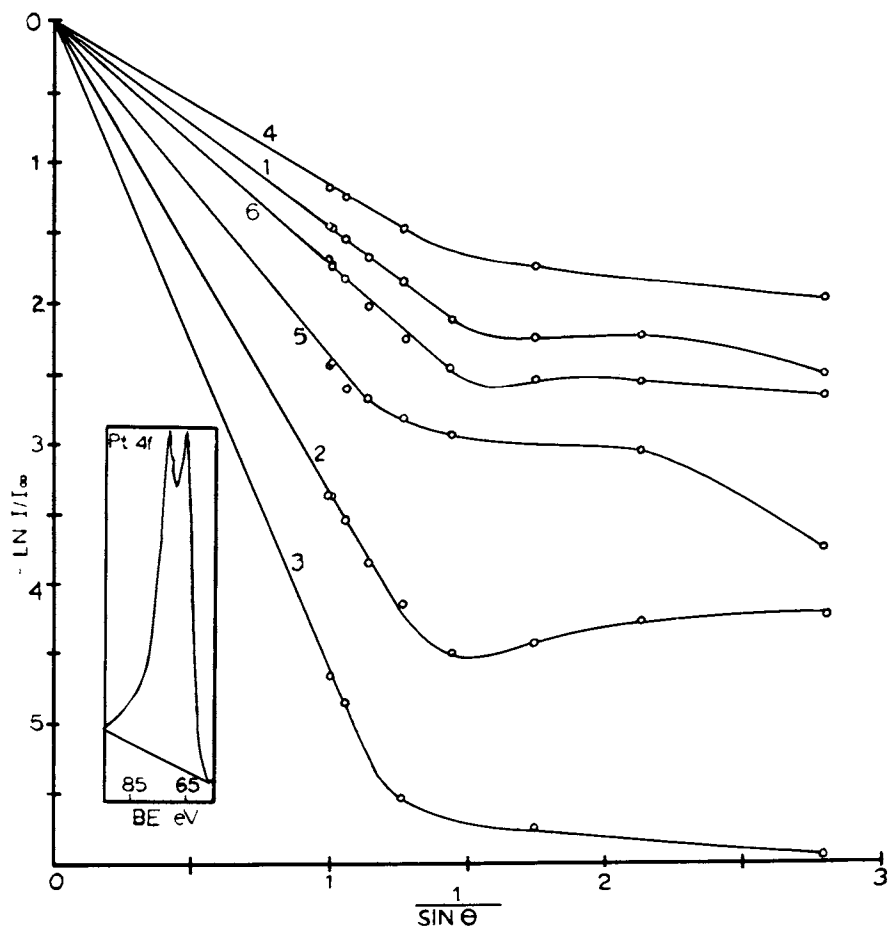


Figure 6. Plots of the relative intensities of Pt 4f(5/2 + 7/2) photoelectrons from naked Pt and from Pt coated with 6 polymer films. Intensities are given as integrated peak areas. (Reproduced from Ref. 82. Copyright 1981, American Chemical Society.)

groups) for several reasons. XPS and AES have the highest proven surface sensitivities and hence, have the greatest chance for detecting changes due to surface modification. It should be realized, however, that XPS is inherently an atomic technique which must be interpreted to obtain molecular information, i.e. through the chemical shift and the corrected atomic ratios. Despite the fact that XPS spectra have been very useful, there are no literature reports in which it has provided sufficient information to give an unequivocal definition of the molecular species. It is clear that complementary measurements using other types of spectroscopy in addition to the use of chemical standards and mathematical methods will be necessary to provide a molecular description of surfaces.

A primitive approach to molecular speciation involves identification of the molecular functionalities through the binding energies (BE's) of their constituent elements. This approach has been used to identify electropolymerized poly-pyrrole (9) and N-(O-hydroxybenzyl)aniline/tyrosine (84) films. In the latter case the identification was confirmed with multi-reflection IR spectroscopy. Both examples used either monomers or model compounds as references to generate known comparison spectra. The BE's and peak shapes have also been used to identify the presence of the ferricinium ion on freshly prepared surfaces (85). In this way the identification is similar to fingerprinting.

Frequently, identifications have been reinforced with the aid of chemical labeling. A surface bound pyridine moiety has been labeled by methylation to produce a large chemical shift due to the formation of a quaternary salt (86). The quaternary shift could be removed and restored by reduction and reoxidation of the surface species. Similar modifications using acid and base treatments to protonate and deprotonate surface amines have been demonstrated (87). However, some surface preparations have behaved differently than expected (88), possibly due to polymer formation. Other labels have been used to identify functionalities (89) following the lead of derivitization reactions used in analytical chromatography (90). Although this approach has been widely used (2,15,29,33,36,89), there is no direct evidence that these labels can provide quantitation of surface functionalities. Statistically significant, quantitative determinations of the reaction yield of derivitization with respect to the surface moiety are lacking. Similar reagents can often give quite different results on nearly identical surfaces (87).

The principal difficulty with the previous approaches to molecular speciation has been less with what was attempted and more with the inability to control the sample surface. A recent study of RF plasma treated surfaces has shown that the surface composition can change on exposure to laboratory air and water vapor (91,92). The development of a sample isolation/ treatment/

transfer system (91) has permitted a more controlled approach to molecular speciation. This sample handling system potentially allows electrodes to be pretreated, modified, and electrochemically studied without ever leaving an extended vacuum transfer system. The vacuum specifications for the sample handling system and the XPS/ AES spectrometer interfaced to it are given in Table II.

Our laboratory's approach to molecular speciation is initiated with the acquisition of high quality, signal averaged, high resolution XPS spectra via a computerized spectrometer (92). Storage of the digitized spectra allows extensive data manipulation to be performed while attempting to extract molecular speciation information. In most cases digital smoothing of the spectra with a non-linear least-squares algorithm (93,94) is used prior to further data manipulation. The first comparisons attempted are usually between sample and reference spectra. Homopolymers have been chosen as the principal references for comparisons with modified carbon surfaces because they appear, at the present time, to be the only authenticated samples with carbon based functionalities in a high concentration (95,96,97). As with other forms of spectroscopy, difference spectra provide a sensitive method for detecting and locating small changes. For example, changes produced by electrode surface treatments can be isolated by subtracting the spectrum of the untreated surface from that of the surface following treatment. Such an approach has been quite effective in determining the identity of a platinum oxide film on a complex electrode surface (98). Alternately, the binding energy (BE) and the full width at half the maximum (FWHM) parameters derived from the deconvolution of homopolymers or other standard spectra can be useful in providing the starting points and the reasonable ranges necessary for the deconvolution of complex spectra.

Such a comprehensive approach has been applied to the study of the surface composition produced by oxidizing RF plasmas and by post plasma treatments of glassy carbon electrodes. A typical high resolution carbon XPS spectrum of the oxygen RF plasma treated surface is shown in Figure 7a. Comparison of this spectrum to that of a homopolymer reference (95,96,97) indicates that this surface contains ketone (or quinone) and hydroxyl (or phenol) -like surface functionalities. Inclusion of a small amount of moisture in the oxygen RF plasma (USP grade) reduced the definition of the valley at ca. 1.5 eV higher BE than the main peak indicating an increased hydroxyl concentration. The changes produced by the plasmas are graphically illustrated in the difference spectra of 7a' and 7b'. When water vapor is used in the RF plasma, less modification occurs (see Figure 7d and 7d'). Significantly, there are less ketone -like functionalities present with respect to the hydroxyl -like ones. Spectral changes suggest that it is possible to produce a predominantly hydroxylic surface which subsequently was accomplished by an

Table II. Sample Transfer and Isolation System Vacuum Performance

A. Base Pressure	$3 \times 10^{-9}$ torr
B. Analyzer Bell Jar Pressure (typical)	
a. Normal Operation	$5 \times 10^{-10}$ torr
b. During Sample Transfer	$5 \times 10^{-9}$ torr
C. Evacuation Timing	
a. Following Sample Introduction from Atmospheric Pressure	
To 10 mtorr	ca. 4 min.
To $5 \times 10^{-7}$ torr	ca. 6 min.
b. Following Plasma Treatment at 100 mtorr	
To 10 mtorr	ca. 2 min.
To $5 \times 10^{-7}$ torr	ca. 4 min.

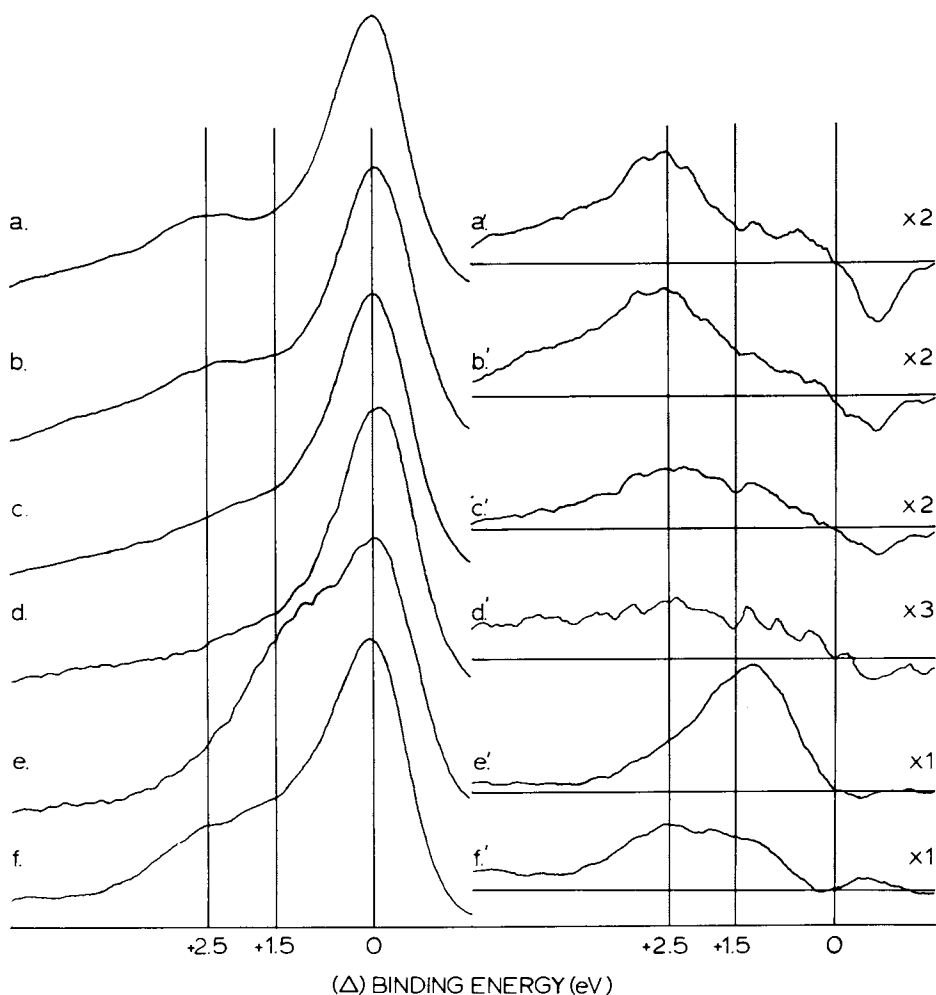


Figure 7. High resolution carbon, C1s, spectra from Tokai glassy carbon samples following smoothing and baseline subtraction for various treatments. The treatments include: a, O (Linde, 99.6%) RFP; b, O (liquid carbonic, USP grade) RFP; c, sample a following 90-min exposure to double distilled, degassed water vapor; d, double distilled, degassed water vapor RFP; e, sample d following post plasma treatment with a reducing agent (Vitride) at 50°C for 4 h; and f, sample c treated using the same conditions as in e. RFP treatment conditions: gas pressure, 100 ( $\pm 20$ ) mtorr; and applied rf power, 35 W. The primed spectra are difference spectra obtained by subtracting the as polished C1s spectrum from each of the spectra shown. (Reproduced, with permission, from Ref. 22. Copyright 1981, Pergamon Press.)

off-line reduction using a mild reducing agent (Vitride, TM, Hexcell Corp., Zeeland, MI)(99). This result could not be reproduced by the alternate preparations shown in Figure 7. The identity of the surface functionality was confirmed by comparing the spectrum from the modified surface, reproduced from Figure 7e, to that from an authentic polyvinyl alcohol reference sample. These spectra plus the difference spectrum are shown in Figure 8. With the exception of a small mismatch at higher BE's due in part to the higher BE "tail" characteristic of glassy carbon, the two spectra are nearly identical. Further, the BE's from the difference spectra and the optimized parameters (BE's and FWHM's from the polyvinyl alcohol spectrum, Figure 9a) can be used to synthesize a summation spectrum, as shown in Figure 9b, which very closely matches the experimental spectrum. Component 3 corresponds to a ketone -like group and its BE coincides with the small negative peak detectable in the difference spectrum of Figure 8. We conclude that the small amount of surface ketone remained after the Vitride reduction. The fourth peak is most likely an artifact caused by the high BE "tail" of the main glassy carbon peak. Correction of the experimental spectrum for this "tail" will result in a slight diminution of the relative areas of components 2 and 3. However, the predominant functionality on the surface is clearly a hydroxylic species similar to the alcohol groups found in the polyvinyl alcohol homopolymer.

Even with resolution enhancement (100,101) XPS does not exhibit "group" frequencies with sufficient resolution to distinguish between individual types of closely related surface functionalities (102), i.e. differentiating between alcohols and ethers or between esters and lactones. This realization has provided an impetus for developing optical methods, principally electronic and vibrational spectroscopy, for surface analysis. Such methods offer the advantage that they do not necessarily require a vacuum and thus can be used to monitor in situ experiments (103). Thus, these methods provide a continuity between the surfaces studied by vacuum methods, i.e. XPS, and those participating in interfacial electrocatalysis. Finally, they offer an independent source of quantitative calibration for the XPS signals. The major question remaining is whether the optical methods are sufficiently sensitive to detect either the presence of or changes in monolayer and submonolayer modifications. For example, seven modified microscope slides had to be stacked to produce a measurable absorbance in one report (104). On the other hand, fluorescence measurements of submonolayer coverages of adsorbed tetraphenylporphinato zinc(II) have been used to follow its electrochemistry (105). Another ex situ study on a variety of modified surfaces has shown similar sensitivities while being used to confirm the presence of the desired changes (106).

The remaining optical methods have been used primarily as an

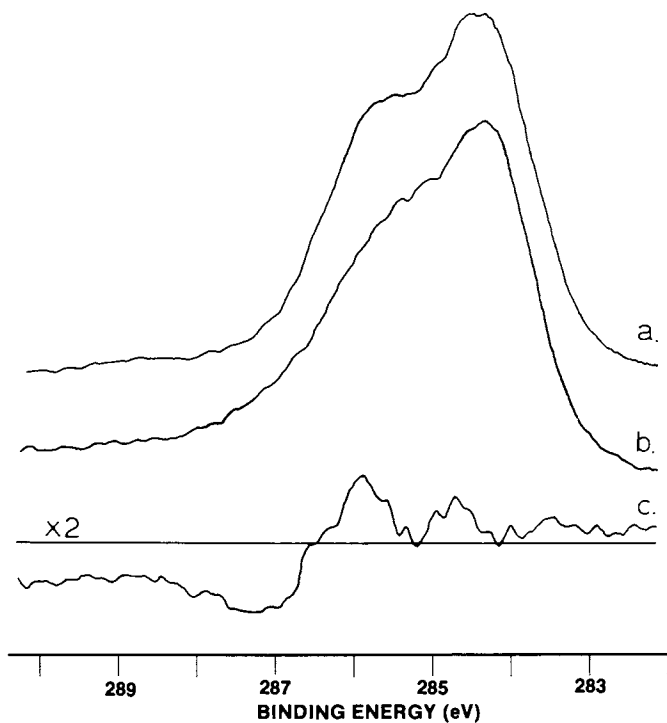


Figure 8. Carbon, C1s, spectra. Key: a, from a polyvinyl alcohol homopolymer reference sample; b, a spectrum of a modified glassy carbon surface corresponding to Fig. 7, spectrum e; and c, the difference spectrum obtained by subtracting b from a, magnified 2 $\times$ . (Reproduced, with permission, from Ref. 22. Copyright 1981, Pergamon Press.)



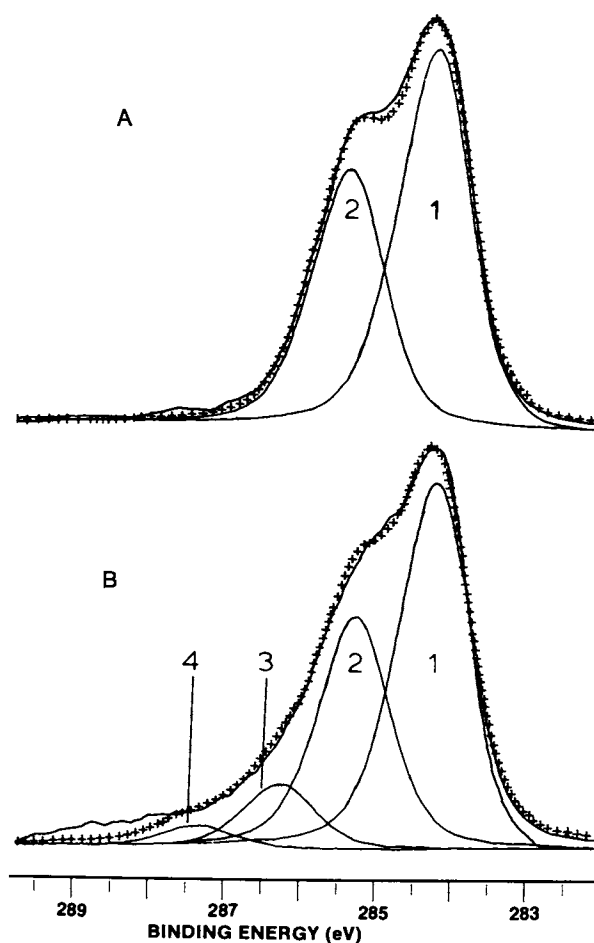


Figure 9. A, a spectrum of polyvinyl alcohol corresponding to Figure 8, spectrum a. Conditions: deconvoluted into component 1 (59.55%), BE = 284.1; and component 2 (40.45%), BE = 285.55 eV. B, a spectrum corresponding to Figure 8, spectrum b. Conditions: deconvoluted using parameters from Figure 9 spectrum a, component 1 (53.32%), BE = 284.10 eV; component 2 (34.17%), BE = 285.45 eV; component 3 (9.43%), BE = 286.40 eV; and component 4 (3.07%), BE = 287.50 eV; all peaks have FWHM of 1.45 eV. The numbers indicated above in parentheses are the total area percentages for each component.  $\times\times\times$  indicates spectra calculated from the individual components. (Reproduced, with permission, from Ref. 92. Copyright 1981, Pergamon Press.)

extension of conventional spectroelectrochemistry (107,108,109) to determine the concentration of electroactive surface mediators (110) and to confirm the identities of their redox states (7,111,112,113,114). Although similar to the solution spectra, the absorption (7,111,112) and reflectance (113,114) spectra of the surface species frequently have been shifted in wavelength (106,114). Despite some small spectral differences, the similarities have been sufficient to confirm the slow step in the electrochemistry of immobilized cobalt porphyrin mediators (113) and to identify the intermediates involved in a tetrathiafulvalene polymer coated electrode (7). A polyxylylviologen -polystyrenesulfonate co-polymer coated electrode, on the other hand, showed no changes in the position of the peaks in the absorption spectra upon immobilization (111). Presumably this indicated an absence of interactions between neighboring viologen moieties. Similar spectral results have been obtained using photoacoustic spectroscopy (PAS). Heptyl viologen adsorbed on Pt exhibited an unshifted spectrum which correlated with the electrochemical results (115). Unfortunately, PAS has not seen sufficient usage to fully assess its potential in the study of CME's.

The effect of immobilization on the molar absorptivity needs to be carefully assessed. One report has implied that immobilization may have reduced the molar absorptivity and the basicity of an acid-base indicator synthesized on the surface. Despite this caveat, absorption spectra have been obtained *ex situ* to evaluate the surface coverage of a silyl bound tris-(bipyridyl) ruthenium complex (ca. 1000 monolayers thick) on a dry electrode (110).

The application of vibrational spectroscopic methods, i.e. infra-red (IR) and Raman (RS), to investigate CME surfaces remains sparse. The time appears opportune for IR since it has been applied to heterogeneous catalysts (116) and possesses well documented group frequencies (117,118). These advantages are enhanced further by the possibility of using Fourier transform and/or photoacoustic modes of detection which possess better sensitivities and signal to noise ratios. Considerable recent attention has been devoted to laser RS following the observation of surface enhanced Raman spectra produced on silver (119,120,121,122) and related surfaces (123). Other, possibly more important, advantages of laser Raman spectroscopy have also been discussed recently (124,125). Seemingly, the most popular applications have involved the study of adsorbed biological components on silver electrodes (125,126,127). Internal reflection resonance Raman (128) has been applied to the examination of methylene blue adsorption on tin oxide. Differences in the orientations and polymorphism have been identified on vapor deposited thick films of iron phthalocyanines supported on glassy carbon (129). These "bulk" differences correlated directly with the ability of the film to catalyze

oxygen reduction. However no differences were detected from the surface layer as a function of the potential applied. In addition to these studies RS has also been applied to graphitic and carbon surfaces (130,131). Recently, RS spectra from chemically modified carbon surfaces were observed as shown in Figure 10 (132). The most prominent lines in the spectra are those characteristic of the carbon surface at 1585 (+10) and 1385 (+10) cm. Although the source and the identity of the fine structure have not been established, their presence in the spectra is correlated with the surface treatments and, hence, most likely reflects changes in the nature of the surface functionalities.

### Structure And Bonding

A major challenge remaining is an experimental description of the mediator bonding and interaction(s) at the CME/ solution interface. Such a description clearly requires an in situ measurement method. The analysis of this problem is complicated by the complex nature of the real catalyst surface which, at present, defies crystallographic analysis in either two or three dimensions.

To date the only studies approaching a description of the surface bonding have employed either labeling studies in concert with XPS or with special methods to obtain vibrational spectra. The labeling studies sought to determine the bonding and preferred orientation, in one example, of tetrakis (p-aminophenyl) porphyrin to a modified carbon surface through a determination of the average number of free amine groups remaining after immobilization (133,134). Whether the average of two out of the four possible sites per molecule represented a preferred orientation or the maximum registry between the surface acid chloride site and the pendant porphyrin amines is not clear. Another vibrational spectroscopic method that has been applied is inelastic electron tunneling spectroscopy (IETS). This method requires a special layered structure which could incorporate a model structure of a CME. The vibrational spectrum that results may be interpreted, with appropriate caveats, to determine the number and type of bonds present between the immobilized moiety and the surface. An example of an application of this method on a CME model surface was presented by Diaz (135) who probed a silane treated alumina surface. In addition to confirming the presence of the silane- surface bonding, it was also possible to infer the presence of intermolecular hydrogen bonding. Because of the sample requirements (need an thin overlayer of a conductor above the CME) inelastic electron tunneling spectroscopy may see only limited use for the direct investigation of CME surfaces although it may prove valuable for use with model surfaces.

Three additional spectroscopic methods which are yet untried

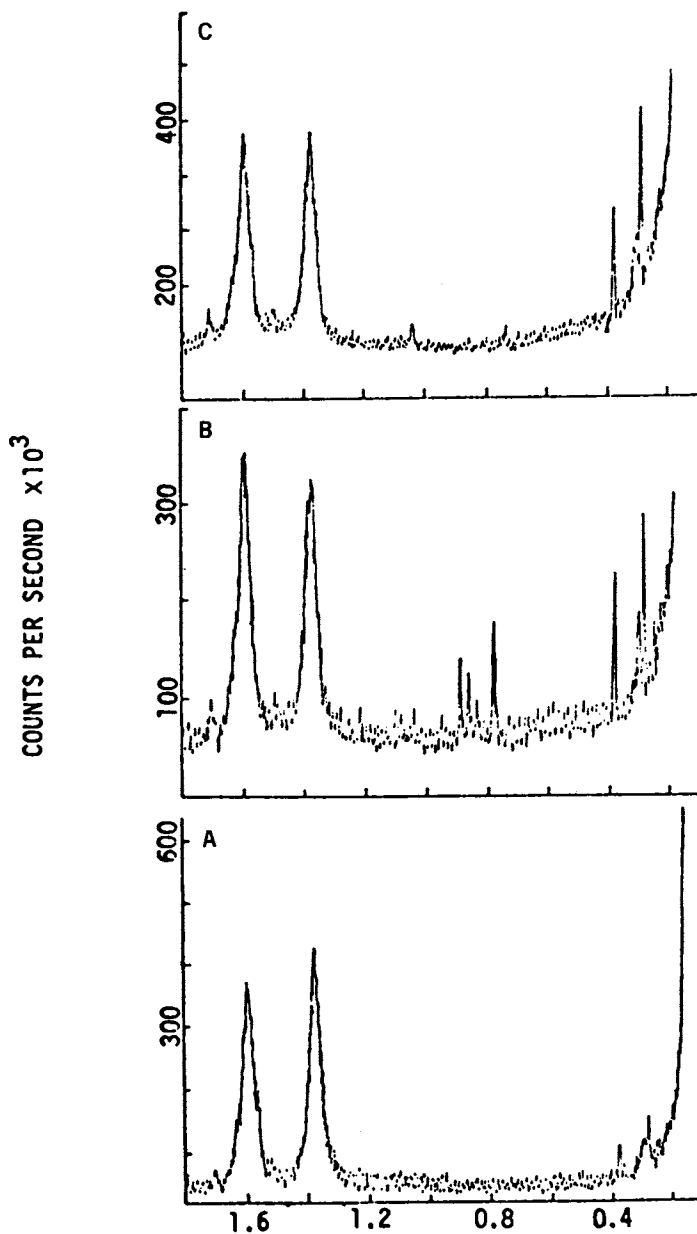


Figure 10. Laser Raman spectra of Tokai glassy carbon surfaces. Key: A, as polished; B, following a 3-min  $\text{O}_2$  rf plasma treatment; and C, following reduction with  $\text{LiAlH}_4$ . (Reproduced, with permission, from Ref. 132.)

with CME's, appear promising. Thermal desorption mass spectroscopy (TDMS) offers the potential for probing the strength of mediator/support bonds as well as for identifying stronger substrate/mediator interactions. This technique should provide the first method capable of rigorously differentiating between adsorption and covalent bonding of a mediator to an electrode surface. TDMS has been extensively used to investigate surfaces for heterogeneous catalysis (136,137, and references therein). However, its application to electrochemical systems has been limited to one report of the adsorption of HI on different faces of Pt single crystals (138). Extended X-ray absorption fine structure (EXAFS) will provide crystallographic details of nearest neighbor interactions without imposing the requirement of having long range order (139). Thus, it should be possible to study surface modifications ex situ and, in some cases, in situ to determine the bonding dimensions around the mediator active sites. Currently, only pioneering studies have been reported including the bonding of iodine adsorbed on the Ag [111] surface (140), the oxidation states and the geometries of electron transfer reactions of transition metal ions in solution (141,142,143) and the structure of oxidized surfaces (144,145). The application of EXAFS to CME's seems a logical next step.

A promising aspect of RS for probing surface chemistry involves its ability to evaluate the molecular orientation of monolayer coverages via polarization measurements (146). The orientation of a surface active dye, Suminol Milling Brilliant Red BS, has been studied at a water-carbon tetrachloride interface (147). As the surface area per molecule was reduced the spectra showed a transition which was interpreted as a change from a mixture of orientations to one predominantly perpendicular with respect to the surface. A thorough theoretical analysis of the use of depolarization ratios for the prediction of primary surface orientations of adsorbed molecules has also been reported (148). Similar developments are occurring in IR spectroscopy and a determination of the molecular orientations in a series of polymers has been reported (149).

### Summary

Presently, there appears to be two well-developed areas in the analysis of CME surface; the evaluation of surface topography by SEM and the determination of elemental composition by XPS. Methodology development now needs to be directed toward those techniques that will provide molecular description of surface, especially in situ measurements during electrolyses. Of the available spectroscopic methods such as IR and Raman, the sensitivity in a reflectance mode seems to be the major problem. There is a continuing need for better approaches to quantitation of the surface concentration, spatial distribution and orientation of immobilized molecular moieties. Carbonaceous

surfaces pose special problems that are currently being addressed. Finally, the use of ancillary methods should be considered. For example, x-ray fluorescence is available on most SEM instruments and could provide "total" concentration of mediator sites in polymeric films or on CME surfaces thus indicating the fraction of sites that possess electroactivity. This may also provide an alternative method for calibrating the XPS signal.

To reiterate, it is the molecular aspects of electrocatalysis that are presently not well understood. Research directed toward development of methods that will provide molecular descriptions of the interactions of the mediator with the support surface and the solution reactant needs to be emphasized. The fundamental knowledge gained from this research will direct the design and implementation of efficient electrocatalysts.

#### Acknowledgement

The authors gratefully acknowledge support from the Air Force Office of Scientific Research, the National Science Foundation, and the Koppers Company, Inc.

#### Literature Cited

1. Fujihira, M.; Ohishi, N.; Osa, T. *Nature*, 1977, 268, 226-8.
2. Fujihira, M.; Osa, T. "Progress in Batteries and Solar Cells", Kozowa, A.; et. al., eds., 1978, JEC Press (Cleveland, Ohio), 199-203.
3. Bolts, J.M.; Wrighton, M.S. *J. Am. Chem. Soc.*, 1978, 100, 5257-62.
4. Bolts, J.M.; Wrighton, M.S. *J. Am. Chem. Soc.*, 1979, 101, 5179-84.
5. Bocarsly, A.B.; Walton, E.G.; Bradley, M.G.; Wrighton, M.S. *J. Electroanal. Chem.*, 1979, 100, 283-306.
6. Finklea, H.D.; Murray, R.W. *J. Phys. Chem.*, 1979, 83, 353-8.
7. Hamnet, A.; Dare-Edwards, M.P.; Wright, R.D.; Seddon, K.R.; Goodenough, J.B. *J. Phys. Chem.*, 1979, 83, 3280-90.
8. Bocarsly, A.B.; Walton, E.G.; Wrighton, M.S. *J. Am. Chem. Soc.*, 1980, 102, 3390-8.
9. Kampas, F.J.; Yamashita, K.; Fajer, J. *Nature*, 1980, 284, 40-2.
10. Zagal, J.; Sen, R.K.; Yeager, E. *J. Electroanal. Chem.*, 1977, 83, 207-13.
11. Kuwana, T.; Fujihira, M.; Sunakawa, K.; Osa, T. *J. Electroanal. Chem.*, 1978, 88, 299-303.

12. Kobayashi, N.; Matsue, T.; Fujihira, M.; Osa, T. J. Electroanal. Chem., 1979, 103, 427-431.
13. Bettelheim, A.; Chan, R.J-H.; Kuwana, T. J. Electroanal. Chem., 1980, 110, 93-102.
14. Watkins, B.F.; Behling, J.R.; Kariv, E.; Miller, L.L. J. Am. Chem. Soc., 1975, 97, 549-50.
15. Kerr, J.B.; Miller, L.L. J. Electroanal. Chem., 1979, 101, 263-7.
16. Matsue, T.; Fujihira, M.; Osa, T. J. Electroanal. Chem., 1979, 126, 500-1.
17. Kerr, J.B.; Miller, L.L.; Van de Mark, M.R. J. Am. Chem. Soc., 1980, 102, 3383-90.
18. Dautartas, M.F.; Evans, J.F. J. Electroanal. Chem., 1980, 109, 301-12.
19. Dautartas, M.F.; Mann, K.R.; Evans, J.F. J. Electroanal. Chem., 1980, 110, 379-86.
20. Evans, J.F.; Kuwana, T.; Henne, M.T.; Royer, G.P. J. Electroanal. Chem., 1977, 80, 409-16.
21. Landrum, H.L.; Salmon, R.T.; Hawkrige, F.M. J. Am. Chem. Soc., 1977, 99, 3154-8.
22. Tse, D.C-S.; Kuwana, T. Anal. Chem., 1978, 50, 1315-8.
23. Stargardt, J.F.; Hawkrige, F.M.; Landrum, H.L. Anal. Chem., 1978, 50, 930-2.
24. Rickard, L.H.; Landrum, H.L.; Hawkrige, F.M. Bioelectrochem. Bioenerget., 1978, 5, 686-96.
25. Bowden, E.F.; Hawkrige, F.M.; Blount, H.N. Bioelectrochem. Bioenerget., Submitted.
26. Pearce, P.J.; Bard, A.J. J. Electroanal. Chem., 1980, 108, 121-5.
27. DeGrand, C.; Miller, L.L. J. Am. Chem. Soc., 1980, 102, 5728-32.
28. Kitani, A.; Miller, L.L. J. Am. Chem. Soc., 1981, 103, 3597-9.
29. Bolts, J.M.; Bocarsly, A.B.; Palazzotto, M.C.; Walton, E.G.; Lewis, N.S.; Wrighton, M.S. J. Am. Chem. Soc., 1979, 101, 1378-85.
30. Diaz, A.F.; Rosales, F.A.O.; Rosales, J.P.; Kanazawa, K.K. J. Electroanal. Chem., 1979, 103, 233.
31. Denisevich, P.; Willman, K.W.; Murray, R.W. J. Amer. Chem. Soc., 1981, 103, 4727-37.
32. Evans, J.F.; Kuwana, T. Anal. Chem., 1977, 49, 1632-1635.
33. Miller, C.W.; Karweik, D.H.; Kuwana, T. Anal. Chem., 1981, 53, 2319-23.
34. Haller, I. J. Am. Chem. Soc., 1978, 100, 8050.
35. Armstrong, N.R.; Cielinski, R. Anal. Chem., 1979, 51, 565-8.
36. Nowak, R.J.; Schultz, F.A.; Umana, M.; Lam, R.; Murray, R.W. Anal. Chem., 1980, 52, 315-21.
37. Diaz, A.F. J. Electroanal. Chem., 1980, 111, 111-4.

38. Kaufman, F.B.; Schroeder, A.H.; Engler, E.M.; Kramer, S.R.; Chambers, J.Q. J. Am. Chem. Soc., 1980, 102, 483-8.
39. Diaz, A.F.; Lee, W.Y.; Logan, A.; Green, D. J. Electroanal. Chem., 1980, 108, 377-80.
40. Tachikawa, H.; Faulkner, L.B. J. Am. Chem. Soc., 1978, 100, 4379.
41. Stargardt, J.F.; Hawkridge, F.M.; Landrum, H.L. Anal. Chem., 1979, 50, 930.
42. Landrum, H.L.; Salmon, R.T.; Hawkridge, F.H. J. Am. Chem. Soc., 1977, 99, 3154.
43. Pearce, P.J.; Bard, A.J. J. Electroanal. Chem., 1980, 112, 97.
44. Kaufman, F.B.; Schroeder, A.H. J. Electroanal. Chem., 1980, 113, 209-24.
45. Firth, B.E.; Miller, L.L.; Mitani, M.; Rogers, T.; Lennox, J.; Murray, R.W. J. Am. Chem. Soc., 1976, 98, 8271-2.
46. Lenhard, J.R.; Murray, R.W. J. Electroanal. Chem., 1977, 78, 195-201.
47. Moses, P.R.; Murray, R.W. J. Electroanal. Chem., 1977, 77, 393-9.
48. Anson, F.C.; Brown, A.P.; Oyama, N. J. Electroanal. Chem. 1978, 87, 435-41.
49. Lenhard, J.R.; Rocklin, R.; Abruna, H.; Willman, K.; Kuo, K.; Murray, R.W. J. Am. Chem. Soc., 1978, 100, 5213-5.
50. Rocklin, R.D.; Murray, R.W. J. Electroanal. Chem., 1979, 100, 271-82.
51. Kuo, K.; Moses, P.R.; Lenhard, J.R.; Green, D.C.; Murray, R.W. Anal. Chem., 1979, 51, 745-8.
52. Finklea, H.O.; Murray, R.W. J. Phys. Chem., 1979, 83, 353-8.
53. Armstrong, N.R.; Shepard, V.R. J. Phys. Chem., 1979, 83, 1268-76.
54. Smith, D.F.; Willman, K.; Kuo, K.; Murray, R.W. J. Electroanal. Chem., 1979, 95, 217-27.
55. Van der Mark, M.R.; Miller, L.L. J. Am. Chem. Soc., 1978, 100, 3223-5.
56. Ishikawa, R.M.; Hubbard, A.T. J. Electroanal. Chem., 1976, 69, 317-38.
57. Hubbard, A.T.; Ishikawa, R.M.; Katekaru, J. J. Electroanal. Chem., 1978, 86, 271-88.
58. Lennox, J.C.; Murray, R.W. J. Electroanal. Chem., 1977, 78, 395-401.
59. Davis, D.G.; Murray, R.W. Anal. Chem., 1977, 49, 194-8.
60. White, H.S.; Murray, R.W. Anal. Chem., 1979, 51, 236-9.
61. Tse, D.C-S.; Kuwana, T.; Royer, G. J. Electroanal. Chem., 1979, 98, 345-53.
62. Dautartas, M.F.; Evans, J.F.; Kuwana, T. Anal. Chem., 1979, 51, 104-10.
63. Lin, A.W-C.; Yeh, P.; Yacynych, A.M.; Kuwana, T. J. Electroanal. Chem., 1977, 84, 411-9.



64. Yacynych, A.M.; Kuwana, T. Anal. Chem., 1978, 50, 640-5.
65. Lenhard, J.R.; Murray, R.W. J. Am. Chem. Soc., 1978, 100, 7870-5.
66. Abruna, H.D.; Meyer, T.J.; Murray, R.W. Inorg. Chem., 1979, 11, 3233-40.
67. Allred, A.L.; Bradley, C.; Newman, T.H. J. Am. Chem. Soc., 1978, 100, 5081-4.
68. Albery, W.J.; Bowen, W.R.; Fisher, F.S.; Foulds, A.W.; Hall, K.J.; Hillman, A.R.; Edgell, R.G.; Orchard, A.F. J. Electroanal. Chem., 1980, 107, 37.
69. Armstrong, N.R.; Cielinski, R.C. J. Electroanal. Chem., 1980, 127, 2605-10.
70. Untereker, D.F.; Lennox, J.C.; Wier, L.M.; Moses, P.R.; Murray, R.W. J. Electroanal. Chem., 1977, 81, 309-18.
71. Itaya, K.; Bard, A.J. Anal. Chem., 1978, 50, 1467.
72. Hawn, D.D.; Armstrong, N.R. J. Phys. Chem., 1978, 82, 1288-95.
73. Fischer, A.B.; Wrighton, M.S.; Umana, M.; Murray, R.W. J. Am. Chem. Soc., 1979, 101, 3442-6.
74. Merz, A.; Bard, A.J. J. Am. Chem. Soc., 1978, 100, 3222-3.
75. Moses, P.R.; Wier, L.; Murray, R.W. Anal. Chem., 1975, 47, 1882-6.
76. Wier, L.M.; Murray, R.W. J. Electroanal. Chem., 1979, 126, 617-23.
77. Hill, J.M.; Royce, D.G.; Fadley, C.S.; Wagner, L.F.; Grunthaner, F.J. Chem. Phys. Lett., 1976, 44, 225.
78. Fadley, C.S. J. Electron Spectrosc., 1974, 5, 725.
79. Mehta, M.; Fadley, C.S. Chem. Phys. Lett., 1977, 46, 225.
80. Wagner, L.F.; Hussain, Z.; Fadley, C.S.; Baird, R.J. Solid State Commun., 1977, 21, 453.
81. Abruna, H.D.; Denisevich, P.; Umana, M.; Meyer, T.J.; Murray, R.W. J. Am. Chem. Soc., 1981, 103, 1-3.
82. Umana, M.; Denisevich, P.; Rolison, D.R.; Nakahama, S.; Murray, R.W. Anal. Chem., 1981, 53, 1170-5.
83. Czanderna, A.W., Ed., "Methods of Surface Analysis", Elsevier, New York, 1975, 114.
84. Dubois, J.E.; Lacaze, P.C.; Pham, M.C. J. Electroanal. Chem., 1981, 117, 233-41.
85. Umana, M.; Rolison, D.R.; Nowak, R.; Daum, P.; Murray, R.W. Surface Sci., 1980, 101, 295-309.
86. Moses, P.R.; Murray, R.W. J. Am. Chem. Soc., 1976, 98, 7435-6.
87. Moses, P.R.; Wier, L.M.; Lennox, J.C.; Finklea, H.O.; Lenhard, J.R.; Murray, R.W. Anal. Chem., 1978, 50, 576-85.
88. Elliot, M.C.; Murray, R.W. Anal. Chem., 1976, 48, 1247-54.
89. Everhart, P.S.; Reilley, C.N. Anal. Chem., 1981, 53, 665-76.
90. Knapp, D.R. "Handbook of Analytical Derivatization Reactions"; J. Wiley: New York, 1979.

91. Miller, C.W.; Fagan, J.R.; Karweik, D.H.; Kuwana, T. Appl. Surface Sci., In Press.
92. Miller, C.W.; Karweik, D.H.; Kuwana, T. "9TH International Conference On Atomic Spectroscopy: 22ND Colloquium Spectroscopicum Internationale, Tokyo, Japan, 4-8 August 1981, Symposium Proceedings", Pergamon Press: Oxford, England, In Press.
93. Savitzky, A.; Golay, M.J.E. Anal. Chem., 1964, 36, 1627.
94. Proctor, A.; Sherwood, P.M.A. Anal. Chem., 1980, 52, 2315.
95. Clarke, D.T.; Thomas, H.R. J. Polym. Sci. Polym. Chem. Ed., 1978, 16, 791.
96. Clarke, D.T.; Dilks, A. J. Polym. Sci. Polym. Chem. Ed., 1978, 17, 957.
97. Clarke, D.T. CRC Crit. Rev. Solid State Mater. Sci., 1978, 8, 1.
98. Facci, J.; Murray, R.W. J. Electroanal. Chem., 1980, 112, 221-9.
99. Miller, C.W.; Karweik, D.H.; Kuwana, T. Details to be published separately.
100. Carley, A.F.; Joyner, R.W. J. Electron Spectrosc., 1978, 13, 411-9.
101. Carley, A.F.; Joyner, R.W. J. Electron Spectrosc., 1979, 16, 1-23.
102. Van Duyne, R.P. in "Chemical and Biochemical Applications of Lasers", Vol. 4, Moore, C.B. ed., Academic Press: New York, 1979.
103. Jeanmaire, D.L.; Suchanski, M.R.; Van Duyne, R.P. J. Am. Chem. Soc., 1975, 97, 1699-1707.
104. Mimms, L.T.; McKnight, M.A.; Murray, R.W. Anal. Chim. Acta, 1977, 89, 355-61.
105. Pflug, J.S.; Faulkner, L.R. J. Am. Chem. Soc., 1980, 102, 6143.
106. Fox, M.A.; Nobs, F.J.; Voynick, T.A. J. Am. Chem. Soc., 1980, 102, 4029.
107. Kuwana, T.; Winograd, N. "Electroanalytical Chemistry", Vol. 7, A.J. Bard, ed., Marcell Dekker: New York, 1974.
108. Kuwana, T.; Heineman, W.R. Acc. Chem. Res., 1976, 9, 241-8.
109. Heineman, W.R. Anal. Chem., 1978, 50, 390A.
110. Ghosh, P.; Spiro, T. J. Am. Chem. Soc., 1980, 102, 5543-9.
111. Akahoshi, H.; Toshima, S.; Itaya, K. J. Phys. Chem., 1981, 85, 818.
112. Scott, N.S.; Oyama, N.; Anson, F. J. Electroanal. Chem., 1980, 110, 303-10.
113. Jester, C.P.; Rocklin, R.D.; Murray, R.W. J. Electrochem. Soc., 1980, 127, 1979-85.
114. Nikolic, B.Z.; Adzic, R.R.; Yeager, E.B. J. Electroanal. Chem., 1979, 103, 281.
115. Malpas, R.E.; Bard, A.J. Anal. Chem., 1980, 52, 109.

116. Delgass, W.N.; Haller, G.L.; Kellerman, R.I.; Lunsford, J.H. "Spectroscopy In Heterogeneous Catalysis", Academic Press: New York, 1979.
117. Bellamy, L. "The Infrared Spectra of Complex Molecules", J. Wiley and Sons: new York, 1954.
118. Szymanski, H.A. "IR - Theory And Practice of Infrared Spectroscopy", Plenum Press: New York, 1964.
119. Fleischmann, M.; Hendra, P.J.; McQuillan, A.J. Chem. Phys. Lett., 1974, 26, 163.
120. Creighton, J.A.; Albrecht, M.G.; Hester, R.E.; Mathew, J.A.D. Chem. Phys. Lett., 1978, 55, 55.
121. Pettinger, P.; Wenning, U.; Kolb, D.M. Ber. Bunsenges. Phys. Chem., 1978, 82, 1326.
122. Jeanmaire, D.L.; Van Duyne, R.P. J. Electroanal. Chem., 1977, 84, 1.
123. Fleischmann, M.; Hendra, P.J.; McQuillan, A.J. J. Chem. Soc., Chem. Comm., 1980, 193.
124. Van Duyne, R.P. in "Chemical and Biochemical Applications of Lasers", Vol. 4, Moore, C.B., ed., Academic Press: New York, 1979, 101-81.
125. Sequaris, J.M.; Koglin, E.; Valenta, P.; Nurnberg, H.W. Ber. Bunsenges. Phys. Chem., 1981, 85, 562.
126. Ervin, K.M.; Koglin, E.; Sequaris, J.M.; Nurnberg, H.W. J. Electroanal. Chem., 1980, 114, 179.
127. Cotton, T.M.; Schultz, S.G.; Van Duyne, R.P. J. Am. Chem. Soc., 1980, 102, 960.
128. Fujihira, M.; Osa, T. J. Am. Chem. Soc., 1976, 98, 7850.
129. Melendes, C.A.; Cafasso, F.A. J. Electrochem. Soc., 1981, 128, 755.
130. Nemanich, R.J.; Solin, S.A. Phys. Rev. B, 1979, 20, 392-401.
131. Tuinstra, F.; Koenig, J.L. J. Chem. Phys., 1970, 53, 1126.
132. Cotton, T.M.; Van Duyne, R.P.; Porter, M.D.; Kuwana, T. Unpublished Data.
133. Willman, K.W.; Rocklin, R.D.; Nowak, R. Kuo, K-N. J. Am. Chem. Soc., 1980, 102, 7629-34.
134. Lennox, J.C.; Murray, R.W. J. Am. Chem. Soc., 1978, 100, 3710-4.
135. Diaz, A.F.; Kanazawa, K.K. IBM J. Res. Dev., 1979, 23, 316-29.
136. Madix, R.J. in "Chemistry and Physics of Solid Surfaces", Vol. II, Vanselow, R., ed., CRC Press: Boca Ratan, Fla., 1979, 63-72.
137. Madix, R.J. Acc. Chem. Res., 1979, 12, 265.
138. Felter, T.E.; Hubbard, A.T. J. Electroanal. Chem., 1979, 100, 473-91.
139. Teo, B-K.; Acc. Chem. Res., 1980, 13, 412-9.
140. Citrin, P.H.; Eisenberger, P.; Hewitt, R.C. Phys. Rev. Lett., 1978, 41, 309-12.

141. Sham, T.K.; Hastings, J.B.; Perlman, M.L. J. Am. Chem. Soc., 1980, 102, 5904-6.
142. Sham, T.K.; Brunshwig, B.S. J. Am. Chem. Soc., 1981, 103, 1590-1.
143. Einstein, T.L.; den Boer, M.L.; Morar, J.F.; Park, R.L.; Larramore, G.E. J. Vac. Sci. Technol., 1981, 18, 4132.
144. Stohr, J.; Denley, D.; Perfetti, P. Phys. Rev. B, 1978, 18, 490-1.
145. Stohr, J.; Johansson, L.I. Phys. Rev. Lett., 1979, 43, 1882.
146. Richardson, N.V.; Sass, J.K. Chem. Phys. Lett., 1979, 62, 267-70.
147. Nakanaga, T.; Takenaga, J. J. Phys. Chem., 1977, 81, 645.
148. Hexter, R.M.; Albrecht, M.G. Spectrochim. Acta, Pt. A, 1979, 35A, 233.
149. Garton, A.; Carlsson, D.J.; Wiles, D.M. Appl. Spectrosc., 1981, 35, 432-5.

RECEIVED April 16, 1982

## Applications of Ion Beam Methods to Characterization of Adhesive Bonding Materials

W. L. BAUN

Wright-Patterson AFB, Materials Laboratory, OH 45433

Adhesive bonding technology brings the surfaces of both plastics and metals together to form an interface. Physical and chemical treatments change the morphology and the chemistry of these surfaces and govern whether bonding actually takes place at the interface of these materials. Therefore, there is an increasing need for sensitive analytical techniques to characterize such surfaces and interphases. Empirical bondability methods such as the water break test may indicate wettability and subsequent bondability but it tells us little of long time durability of the bond which may depend on surface chemistry. A number of analytical techniques have been developed for characterizing solid surfaces. Some of these techniques using electrons and photons as probes of the surface chemistry have been described in this symposium by other authors. In this paper methods of surface analyses using beams of ions will be described. Emphasis is placed on ion scattering spectrometry (ISS) and secondary ion mass spectrometry (SIMS). Examples are shown for adhesive bonding applications including determination of locus of failure, contamination, cleaning and thermal and chemical pretreatments.

In an effort to develop strong, light and corrosion resistant structures, the aerospace industry has gone more and more to adhesive bonding. The automotive industry is quickly following along using different structural alloys. In these fields, bonded structures must be strong and possess long-time durability. Both strength and durability depend on many factors of bond preparation and fundamental properties of the adhesive and adherend.

This chapter not subject to U.S. copyright.  
Published 1982 American Chemical Society.

One important influence in the formation of a good adhesive bond is surface or interfacial chemistry. In the broader sense, in which two substances are held together by interfacial forces, adhesion is of importance in many technologies such as in thin films and semiconductors. It is the purpose of this paper to discuss ion beam methods of surface characterization applicable to the broad area of adhesion with emphasis on adhesive bonding.

### Experimental Considerations

The question is often asked: "Which is the best surface chemistry tool for research on adhesive bonding?" This question is difficult to answer because it depends on the aspect of adhesion which is being studied. Often a combination of instruments must be used to take advantage of the strong points of each. Table I shows the facets of bonding and some of the characterization methods which are applicable in these areas. Ion beams either provide the primary interaction with the surface or are used with other methods to give information with depth as the surface is eroded away by the ion beam. Methods shown in Table I using an ion beam as an analytical probe are shown underlined, while techniques using an ion beam for elemental depth profiling with a different probe such as an electron or photon are shown underlined with a dashed line. The acronyms used here are the

Table I  
Aspects of Adhesive Bonding and Applicable  
Surface Characterization Methods

#### Adherend Chemistry

AEAPS, AEM, AES, APS, BIS, CIS, CL, EM, ES, EXAFS, IIRS, IIXS,  
IMMA, IS, ISS, LMP, PES, RBS, SIMS, SXAPS, SXES

#### Adherend Structure and Morphology

AEM, ELL, EM, HEED, IMMA, LEED, SEM, SIIMS, SRS, STEM, TEM, XEM,  
XRD

#### Adhesive Chemistry

AES, AIM, ASW, ATR, ESR, HA, IRS, ISS, LS, PES, SIMS, UPS, XPS,  
ISD

#### Adhesive Structure and Morphology

ATR, IR, UV, RAMAN, SEM

#### Interaction of Polymers with Metals

AES, AIM, AWS, CPD, ELL, EELS, ESDI, ESDN, FD, FDS, HA, IRS, IR,  
ISS, ISD, LS, PD, SC, SIMS, UPS, XPS, RAMAN, IIRS, IIXS

#### Failure Surfaces (locus of failure)

AES, ATR, ELL, ISS, SIMS, PES, XPS, SEM, SXES, SCAPS, SRS, UPS,

ones in current common usage and are defined by Powell (1). Many of these methods were described by Park (2), in a comprehensive review in which he categorized the techniques according to the kind of information they provide. This discussion included what is being probed, such as vibrational states, the probe itself, such as monoenergetic electrons, and what was actually being measured, such as the electron emission.

When an ion beam is used to interact with the surface, there are several phenomena which may be studied to characterize a solid surface as shown in Figure 1. Of the interactions shown, the use of scattered and sputtered ions (ISS and SIMS, respectively) provides the highest surface sensitivity. High energy ion methods in the MeV region (such as RBS) provide valuable quantitative information with depth. Since such high energy techniques are discussed elsewhere in this volume (3), the present work will concern only low energy methods (0.1 to 5KeV) and emphasize ion scattering spectrometry and secondary ion mass spectrometry. Also shown in Figure 1 is an ion beam which may be used with other surface techniques such as XPS and AES as described by Brundle (4) to produce an elemental depth profile analysis.

Ion Scattering Spectrometry (ISS) Use of low energy back-scattered ions to characterize a surface is a relatively recent development. The method has been reviewed by Buck (5). High energy ions had been used in the past to analyze surfaces but it was not until Smith (6) used low energy (1 KeV) noble gas ions to probe the surface of a variety of materials that the technique came into popular use. It was found from this work and others that when the energy of ions was lowered the scattered ion spectra became sharper and approached the behavior expected on the basis of a binary scattering event from a single surface atom. Therefore, the energy  $E_1$  retained by an ion of mass,  $M_{ion}$  with an incident energy  $E_0$  after scattering from an atom of mass  $M_{atom}$  through an angle  $\theta$  is given by equation (1) which is based on the conservation of kinetic energy and momentum (here  $M_{ion}$  is smaller than  $M_{atom}$ ).

$$\frac{E_1}{E_0} = \frac{M_{ion}^2}{(M_{ion} + M_{atom})^2} \left\{ \cos\theta + \left[ \frac{M_{atom}^2}{M_{ion}^2} - \sin^2\theta \right]^{1/2} \right\}^2 \quad (1)$$

For 90° scattering which is frequently used this reduces to a very simple relationship:

$$E_1/E_0 = (M_{atom} - M_{ion})/(M_{atom} + M_{ion}). \quad (2)$$

The original arrangement for 90° scattering in Figure 2a used an

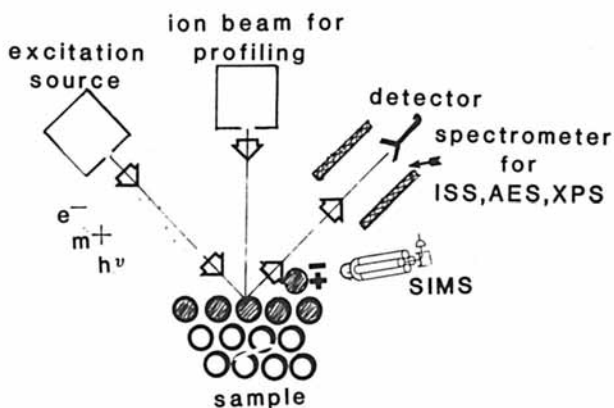


Figure 1. The use of ion beams for analysis of surfaces.

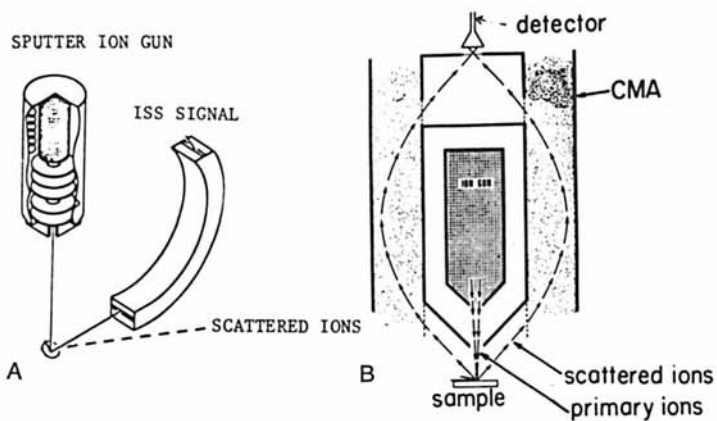


Figure 2. Equipment configurations for ion scattering. Key: A,  $90^\circ$  scattering using electrostatic analyzer; and B,  $138^\circ$  scattering using CMA.



electrostatic analyzer. Recently a great improvement in sensitivity was gained by the adaptation of a cylindrical mirror analyzer (CMA) substituted for the original electrostatic sector as shown in Figure 2b. The geometry of the CMA results in a scattering angle of  $138^\circ$ . The major advantage of low energy ion scattering is the extremely fine surface selectivity when low energy ions collide with the surface atom. The probability for neutralization is very high because of the long residence time ( $10^{-14}$  to  $10^{-16}$  sec.). Only about one in  $10^3$  of the scattered particles retain a positive charge even after one collision. Therefore, the probability that an ion is still in the charged state after two or more collisions is very small. Since the detector responds only to charged particles, contributions from particles which scatter more than once are almost certainly neutral and not counted by an ion detector. An inherent feature of ion scattering which may be considered an advantage or a disadvantage is the simultaneous sputtering of the surface as energy is transferred to the surface atoms from the ion beam. It is an advantage in that the concentration of the various atomic species may be followed with depth. On the other hand it is a disadvantage because damage is being produced by the sputtering. Once the atom sputters from the surface the sample is changed, and an exact experiment on that spot may not be repeated. One positive feature of ion scattering compared to most other spectroscopies is the simplicity of the spectra. Binary ion scattering gives one peak for each isotope of an element present. For instance, the scattering of helium from aluminum oxide results in the appearance of only two peaks in the spectrum, one for oxygen and one for aluminum. Each peak is sensitive to the amount present but absolute quantitative analyses can be difficult since the scattered yield depends on the scattering cross section and neutralization efficiency, neither of which is well known for most elements. During the ion scattering experiment atoms are sputtered from the surface, allowing depth profiling analysis from the removal of the surface layers by the probe ion during the analysis. Use of helium ions gives a very slow rate of surface removal and while neon and argon provide much higher sputtering rates, the ion beam may be focused and rastered on the surface to reduce sputtering while the signal is gated from the center of the crater to reduce crater edge effects. The signal may be collected from the surface using the rastered beam to give a lateral analysis of the surface. Therefore ion scattering provides a combination of indepth analyses and lateral analyses to give a three dimensional picture of the chemical makeup of the surface with depth.

Secondary Ion Mass Spectrometry (SIMS) When a low energy ion strikes the solid surface it undergoes and produces a number of interactions. The sputtered species which are removed from the surface are both positive and negative ions as well as

neutral particles. Neutral particles have much more abundance than ionic species and have also been used for surface analysis. Surface analysis by SIMS falls into two categories, low current density sputtering and high current density sputtering. Categories are determined by the characteristics of the primary ion beam. A low current density sputtering analysis results in a very small fraction of the surface being disturbed, a result that approaches a basic requirement of a true surface analysis method. This is generally known as the Static SIMS (SSIMS) method. The SSIMS method uses small current densities of  $10^{-9}$  A/cm<sup>2</sup> spread over an area of 0.1 cm<sup>2</sup> or more (7). High current density sputtering removes more material and is required for preparing elemental depth profiles. In the high current density method, changes are seen in the surface and near surface regions.

Equipment for SIMS may be as simple as that shown in Figure 3, or as complex as the ion microprobe (8). In a simple system a SIMS experiment requires a vacuum chamber to house the experiment, a sample holder, an ion source, an energy analyzer and a mass analyzer. In such simple systems the noble or reactive gas fills the system and the entire chamber including the ion gun and sample area are at approximately  $1-5 \times 10^{-5}$  torr. A more complicated type of instrument is one in which the performance is improved through the use of a differentially pumped vacuum system to produce ultra high vacuum in the vicinity of the sample. This also allows the entry of a reactive gas in the sample chamber area while sputtering with a noble ion for studying chemical changes or reactions on the surface. Still another improvement and added complexity may be made to the SIMS instrument by the mass analysis of the primary beam. The energy filter is generally made up of several elements whose function is to optimize collection of the secondary ions and to filter and focus the ions at the entrance to the mass analyzer. The mass analyzer in simple systems is usually a quadrupole filter.

It is recognized that SIMS has been used successfully as a stand-alone technique to solve many surface problems. However, it appears that the area of greatest use of SIMS is as a complement to other surface characterization methods. The extremely high sensitivity for some elements can be taken advantage of by using SIMS with other techniques in which these elements do not show high sensitivity. The SIMS technique is also ideal to use with fundamentally low resolution methods such as ion scattering, to separate and identify the adjacent masses which may be present at the sample surface. The most popular combination of instruments used thus far has been ISS-SIMS and AES-SIMS. SIMS has also been used on scanning electron microscopes, allowing high quality imaging along with lateral and depth analysis of the sample.

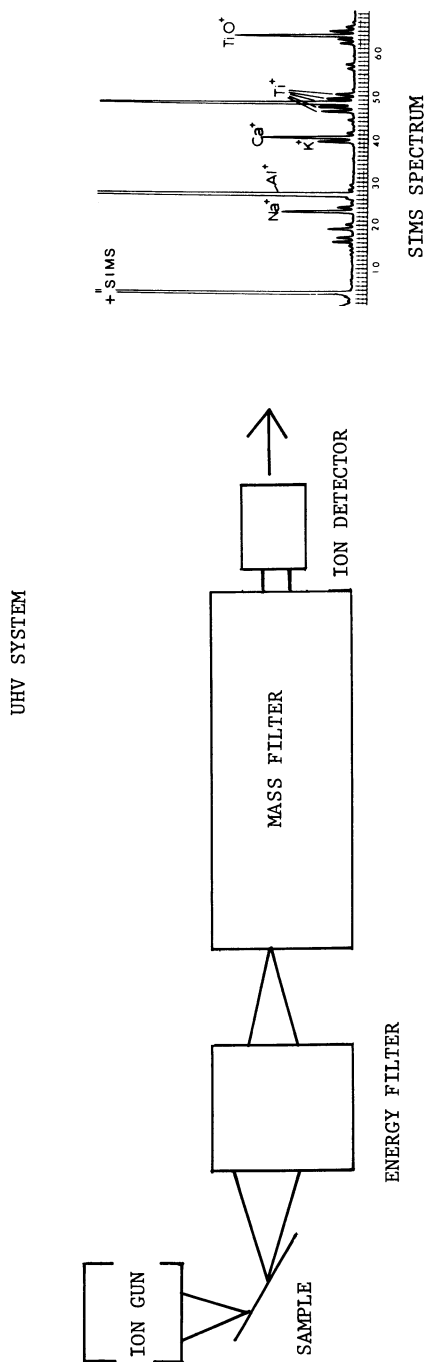


Figure 3. Equipment for a simple SIMS system.

A summary of the positive and negative aspects of ISS and SIMS analysis is given in Tables II and III.

Table II.  
Positive Aspects of Low Energy  
Ion Beam Analysis Methods

- ISS - Elemental Analysis  
Sensitivity to First Monolayer  
Profiling Capability with Depth  
Possible Operation in Near Static Mode
- SIMS - Elemental and Molecular Analysis  
Sensitivity to First Few Layers  
Profiling Capability with Depth  
Isotopic Analysis  
Extremely Sensitive to Many Elements  
Sensitivity to Hydrogen

Table III.  
Negative Aspects of Low Energy  
Ion Beam Analysis Methods

- ISS - Low Resolution  
Poor Sensitivity to Low Z Elements  
Specimen Charging (Insulators)  
Little Chemical Information
- SIMS - Extremely Variable Yields  
Specimen Charging (Insulators)  
Difficult Data Interpretation

These two techniques may be applied in a gentle manner using a near static ion beam to produce little change in the surface and also in a mode in which chemical profiling with depth is possible. ISS can detect all of the elements heavier than helium in the periodic table. The sensitivity variation across the periodic table is probably less than one order of magnitude. SIMS provides a distinct advantage of being able to analyze, in principle, all of the elements (including hydrogen) in the periodic table. Being able to identify isotopes is a definite advantage. The sensitivity of the SIMS technique can vary several orders of magnitude (perhaps up to  $10^4$ ) due to a rapidly changing secondary ion yield caused by matrix and chemical effects. The ability of ion scattering to resolve different elements in a complete unknown is at times somewhat limited. There are few intrinsic limitations or spectral interferences but the technique is fundamentally a low resolution technique in which there is some uncertainty as to the exact identity of

a given line. Specificity may be improved by going to a scattering ion closer to the mass of the unknown element, that is we would use helium for the light elements, neon for intermediate mass elements and argon for the heavy elements.

Ion scattering gives very little information on the chemical combination of the element detected in the sample, however, recently discovered yield variations (9) and the use of other fine features in the spectrum (10) give some possibility of using ion scattering to determine chemical species at the surface. The appearance of cluster ions in the secondary ion mass spectrum gives a good possibility of using SIMS to determine chemical combinations (11). The interpretation of such spectra is extremely complicated and has to be treated with a great deal of care. Molecular ions can be dislodged from the surface and give some idea of the chemical combination, but molecular complexes may also be synthesized at the sample surface in the gas phase above the sample surface. The presence of such ions in the mass spectrum does not unequivocally prove the presence of such species in or on the sample itself.

#### Application of ISS and SIMS

Changes in Chemistry Due to Surface Treatments. Many chemical etching and oxidizing treatments are used on metal and alloys to enhance a variety of properties. Numerous thermal pretreatments following fabrication improve strength, ductility, toughness or other properties. Each of these chemical or thermal treatments affect the composition of the surface either by introducing impurities, or by increasing or decreasing the concentration of alloying elements at the surface. Many impurities are present in the raw materials or are introduced during materials processing. Final fabrication of the materials into the desired shape for adhesive bonding may also introduce contaminants which are deleterious to adhesive bonding. Finally the environment and careless handling before and during the actual bonding can introduce contaminants or even physically alter the adherend surfaces. A summary of the sources of contaminants based upon preparation history which could affect adhesive bonding and bond properties is shown in Table IV.

Table IV  
Sources of Contaminants or Species Which Could Affect  
Adhesive Bonding and Bond Properties

1. Raw Materials Processing
  - a. Adherend
  - b. Adhesive
2. Prebonding Treatments
  - a. Chemical solution contributions
  - b. Alloy constituents

3. Bonding
  - a. Diffusion of impurities
4. Handling and Storage

Very often the mill scale that remains on a material following final processing or rolling has little relation to the concentrations of each element in the bulk. The ISS and SIMS spectra from such an initial 2024 aluminum alloy, as shown in Figure 4, indicate high magnesium concentration at the surface. Conventional alkaline cleaning treatments do not etch the surface appreciably, leaving the surface magnesium rich. Such a surface, when adhesively bonded, may exhibit good initial bondability but poor long time durability when compared with bonded structures in which formation of aluminum oxide has been assured. There is an ever increasing demand for materials which can be used at high temperatures with good corrosion resistance. Such requirements are satisfied in many cases by stainless steels or titanium alloys. Conventional methods of joining these materials such as welding, braxing and soldering may be used but reliable methods using adhesive bonding are also being developed. Stainless steel following final processing is normally covered with a surface layer containing processing aids and oxidation products. The surface must undergo an etch or pickle before it may be used for the final processing. It has been found that generally this surface layer in its original state has deleterious effect on adhesive bond strength. Unfortunately, after acid pickling the surface can be even more contaminated than it was originally. This contamination, as in aluminum, is called smut. The usual method for desmutting is to wipe the work piece after rinsing, while it is still wet or to brush mechanically with a stiff wire bristle brush. However, it has been found that only a portion of the smut is removed by these methods and chemical etches are required to remove all of the material. An example of smut on stainless steel is shown in Figure 5 (12), where a surface which had been treated in hot sulfuric acid is shown. The elements which are observed are silicon and oxygen with some carbon present on the surface and only a slight amount of the matrix stainless steel. The SIMS spectra were taken simultaneously with the ISS data and show primarily silicon and cluster peaks of silicon and oxygen together with a small amount of the matrix material. Even when the surface of the 304 stainless steel was wiped after rinsing the appeared visably clean some smut remained behind as detected by both positive SIMS and ISS. The smut was completely removed by dipping the work in hot caustic soda solution or in chromic acid solution conventionally used in the industry. The analysis of the smutted surface and the desmutted surface by a variety of techniques is shown in Table V. Each of the techniques has its strong points. In AES, for instance, both sulfur and chlorine are readily detected in

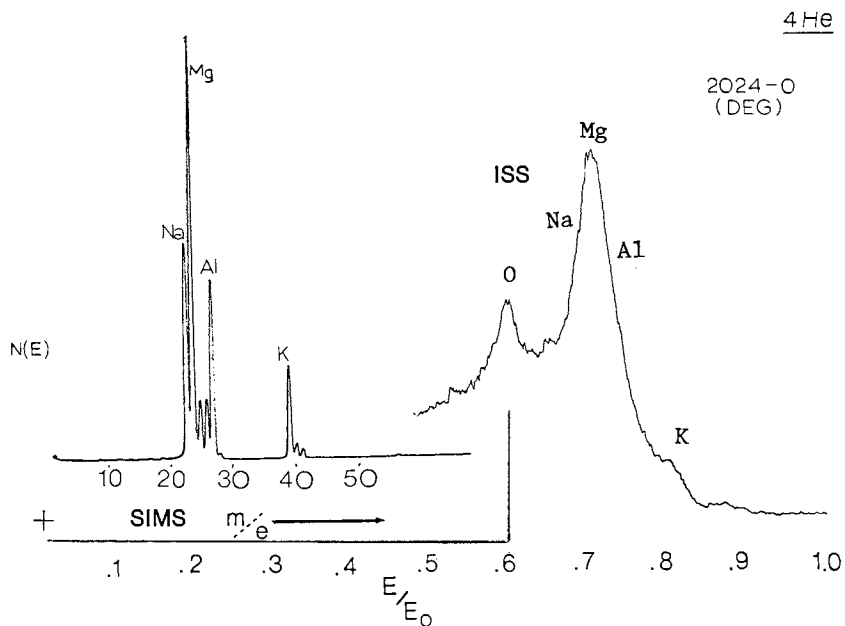


Figure 4. ISS/SIMS Data for as received 2024-aluminum alloy showing Mg-rich mill scale.

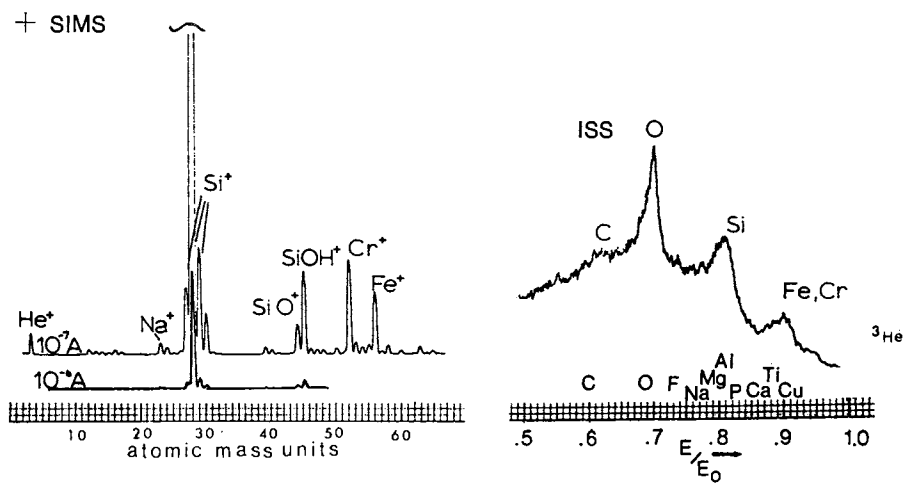


Figure 5. ISS/SIMS data for smut on 304-stainless steel.

the spectrum where as in the ISS spectrum neither of these elements was detected, probably because they occur in an area of high scattered ion background. The XPS data show definitely that silicon is in an oxidized state which would be expected from the formation in the highly oxidative medium of the acid etch.

Table V  
Species Found on 304 Stainless Steel  
by Surface Analysis Techniques

Technique	Smuttet in H <sub>2</sub> SO <sub>4</sub>	De-Smuttet in H <sub>2</sub> SO <sub>4</sub> -H <sub>2</sub> CrO <sub>4</sub>
AES	Si, O, S, Cl, C, Cu, Fe, Cr, Ni	O, C, S, Fe, Cr, Ni
ISS	Si, O, C, Cu(?), Fe, Cr	O, Na, Fe, Cr
+SIMS	Si <sup>+</sup> , Na <sup>+</sup> , SiO <sup>+</sup> , S, OH <sup>+</sup> , Cu <sup>+</sup> , CH <sub>n</sub> <sup>+</sup> , Fe <sup>+</sup> , Fe <sup>+</sup> , Cr <sup>+</sup> , Ni <sup>+</sup> , Cu <sup>+</sup>	Na <sup>+</sup> , K <sup>+</sup> , Si <sup>+</sup> , S <sup>+</sup> , OH <sup>+</sup> , CH <sub>n</sub> <sup>+</sup> , Cr <sup>+</sup> , Ni <sup>+</sup>
-SIMS	C <sub>n</sub> H <sub>n</sub> <sup>-</sup> , O <sup>-</sup> , OH <sup>-</sup> , Cl <sup>-</sup> , SiO <sup>-</sup> , SiO <sub>2</sub> <sup>-</sup> , SiO <sub>3</sub> <sup>-</sup> , SiF <sup>-</sup> , SiOF <sup>-</sup> , FeO <sub>2</sub>	C <sub>n</sub> H <sub>n</sub> <sup>+</sup> , O <sup>-</sup> , OH <sup>-</sup> , Cl <sup>-</sup> , SiO <sub>n</sub> <sup>-</sup> , (greatly reduced), CrO <sup>-</sup> , CrO <sub>2</sub> <sup>-</sup> , CrO <sub>3</sub> <sup>-</sup> , FeO <sub>2</sub> <sup>-</sup>
XPS	C <sup>a</sup> , O, S, Si <sup>b</sup> , N, Cu, Fe, Cr, Ni	C, O, Fe, Cr, Ni

<sup>a</sup>More than one form.

<sup>b</sup>Oxide form.

### Adhesives and Other Polymers

As mentioned earlier, ion beam methods have not been applied extensively to organic materials such as adhesives and other polymers. Ion scattering has been applied to adhesive bonding materials to determine the locus of failure and contamination effects. DiBenedetto and Scola (13) have used both ISS and SIMS to characterize surfaces of treated glass fibers and fiber/polymer interfaces. The results show how SIMS can be used to study the chemical surface and chemical changes on the surface and at interfaces. By working at low current levels with insulator surfaces, the SIMS analysis showed changes in the structure of a polymerized silane coating as a function of depth of penetration into the interface. The concentration of nitrogen and



hydrogen generated from the surface maintained a relatively constant level as the distance from the airtsilane interface increased; then within 160 Å into the surface, a dramatic increase in the nitrogen level was noted, to a depth of 240 Å. In this region, the simplicity of the SIMS spectra, with major peaks corresponding to the atomic constituents of  $\gamma$ -aminopropyltriethoxysilane, namely, H, C, N, O, and Si, suggested that low-molecular-weight oligomer was present in this region. This means that the silane coating was not sufficiently cured to provide a mechanically stable interface. Finally, from 240 Å to the silane-glass interface, the nitrogen and hydrogen generated from the surface reached a lower constant level but about three times higher than that generated from the air-silane domain. This suggests that the silane polymer coating adjacent to the glass interface is different from the silane polymer at the air interface. Thus, it is clear that the ISS/SIMS technique can be used to define the interface and interphase regions and also to follow changes at the interface due to a chemical reaction.

Gardella and Hercules (14) have shown SIMS data for poly (alkyl methacrylates) and also ISS data for Teflon. They found changes in molecular fragmentation patterns with only very slight changes in polymer processing. Careful examination of core level XPS data shows no identifiable changes in core level binding energies or intensity ratios. Side chain structure in the ester portion of the poly (alkyl methacrylates) dramatically influenced static SIMS data.

There have been few papers published concerned only with ISS of polymers except for Thomas, et al (15) and for abstracts of meeting presentations by Sparrow and Mishmash in 1977 (16) and Gardella and Hercules in 1979 (17). Both ISS and SIMS data appear in papers in which the emphasis is in another area, such as the cleaning of surfaces by ultraviolet light (17). Figure 6 shows ISS and SIMS data from polypropylene which has been exposed to ultraviolet light. Usually, following UV exposure, slightly more oxygen is observed in the ISS data. SIMS data show some changes in the fragmentation pattern and larger fragments are observed. Perhaps further study of such changes may be attributed to bond breakage and cross linking effects.

Thomas and co-workers found ion scattering data to be somewhat non individualistic, but they determined that it was very useful for determining segregation at the surface of a polymer. Table VI from Thomas, et al (15) shows the variation in the oxygen to carbon ratio at the surface compared to the bulk values.

Table VI

The C, H and O-containing polymers studied, with the theoretical O:C ratios derived from the formula of the repeating chemical unit. Also listed are the measured O:C ratios obtained by comparing the ISS peak, 2750eV He<sup>+</sup>) and the ratios after correction for the difference in sensitivities of the two elements based on the sensitivity ratio O:C = 18.1:1.

Polymer	Formula	O:C bulk	O:C measured	Corrected
PC	C <sub>16</sub> H <sub>14</sub> O <sub>3</sub>	0.19	1.9	0.10
PI	C <sub>22</sub> H <sub>10</sub> O <sub>5</sub> N <sub>2</sub>	0.23	0.76	0.04
PMMA-218	D <sub>5</sub> H <sub>8</sub> O <sub>2</sub>	0.4	0.34	0.02
PMMA-XT	C <sub>5</sub> H <sub>8</sub> O <sub>2</sub>	0.4	0.27	0.01
PBDDA	C <sub>10</sub> H <sub>14</sub> O <sub>4</sub>	0.4	0.32	0.02
PET	C <sub>10</sub> H <sub>8</sub> O <sub>4</sub>	0.4	1.1	0.06
PVA	C <sub>2</sub> H <sub>4</sub> O	0.5	0.77	0.04
POM	CH <sub>2</sub> O	1.0	2.8	0.15

An example of the non individualistic nature of ISS spectra from polymers is seen in Figure 7 where data are shown for a simple linear hydrocarbon, polyethylene, and compared to data obtained under identical conditions for graphite. As can be seen, one would be hard pressed to identify the polymer here. Naturally, it would be even more difficult to identify individual polymers.

#### Specimen Charging

A serious problem encountered in ion beam methods of analysis is that of specimen charging. Impact of energetic positive ions causes development of a positive charge on the surface of an insulator. This effect is especially prevalent in polymers, because they are usually excellent insulators. Table VII lists work functions for some typical polymers. It is questionable whether the term work function should be used for polymers, but the high value of these numbers shows the reason for the charging exhibited by polymers.

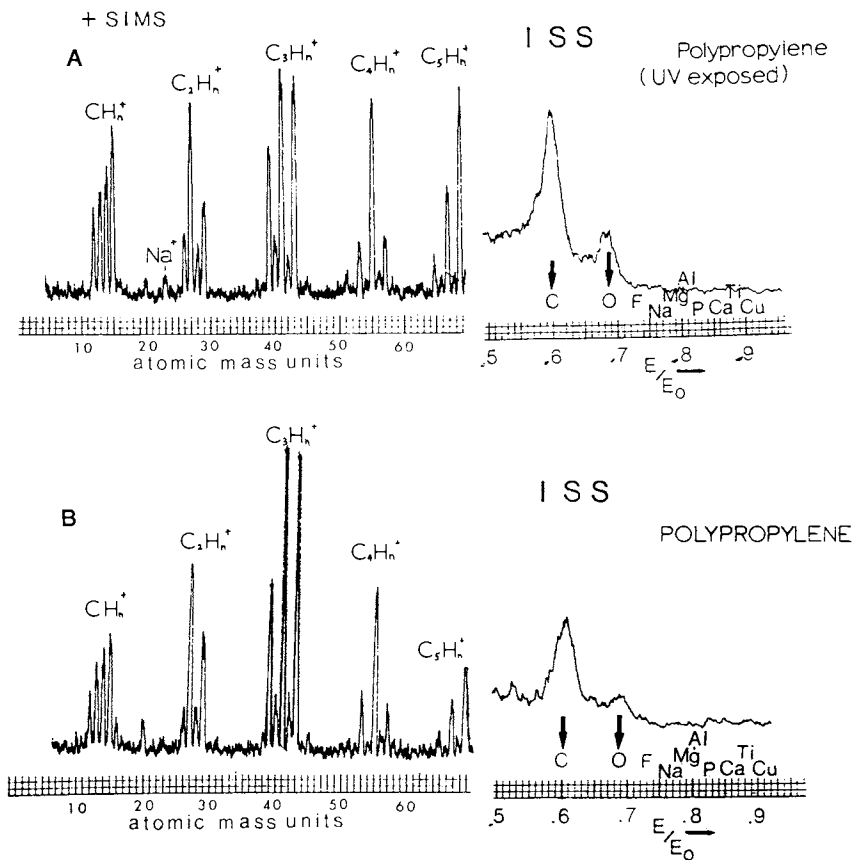


Figure 6. ISS/SIMS data for polypropylene UV exposed (A) and polypropylene, untreated (B).

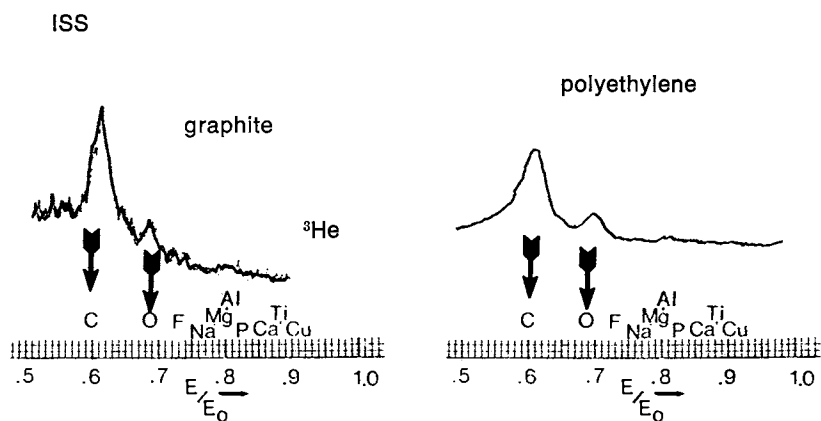


Figure 7. ISS data for graphite and polyethylene fiber under identical conditions.

Table VII  
Work function of polymers (Ref. 18)

<u>Polymer</u>	<u>Work Function, <math>\phi</math></u>
Teflon	5.75
Chlorotrifluoroethylene	5.30
Vinyl Chloride	5.13
Sulfone	4.95
Styrene	4.90
Methyl Methacrylate	4.68
Nylon 6.6	4.30

This charge will influence or even prevent the emission of secondary ions. To overcome this charging of insulators there have been numerous methods used, as seen in Table VIII.

Table VIII  
Methods of charge neutralization (Ref. 17)

- (1) Deposition of a conducting thin film or grid.
- (2) Use of  $\text{Cs}^+$  as primary ions, in this way a conducting layer is continuously deposited
- (3) Compensation of the charging by means of an extra electron beam
- (4) Use of neutral beams: the charging is reduced from the case of positive primary ions
- (5) Application of special electrodes for draining excessive negative charge
- (6) Shift of target holder potential  $V_H$  by  $\Delta V$  in a direction opposite to the previous charging of the insulator

#### Determining Locus of Failure

Frequently it is not simple using visual or even microscopic examination to determine after testing whether an apparent adhesive failure occurred at the interface due to improper wetting or at some new interface, leaving behind a thin layer of adhesive on the adherend or oxide on the adhesive. There is a resolution limitation of about 100 Å for most scanning electron microscopes (SEMs) which makes very thin organic films difficult to detect, especially when the adhesive is a pure polymer containing no fillers of higher atomic number than the polymer to increase contrast. Optical and staining methods have been reported to determine the presence of adhesive films. However, the optical techniques uses the interference phenomenon, which is applicable only to fairly thick films, certainly not to films only a few molecules thick or boundary layers containing both adhesive and adherend components. Staining techniques are sensitive only to specific compounds present in the usually complex adhesive systems. Several investigative techniques on both sides of a joint failure are necessary to determine the locus of failure conclusively.

It is also important to determine the locus of failure of thin films subjected to many mechanical tests depending on peel,

scratch, abrasion, and deceleration as reviewed by Mittal (18). Generally, thin polymer films on metals present the same problems as encountered in adhesive bonding. On the other hand, evaporated metal films, by nature of their simpler composition and more ideal interfaces, present fewer difficulties. There are usually differences in color between the evaporated film and the substrate which make it easier to determine the mode of failure. However, when both metals are the same or nearly the same color or when a metal is deposited on a thin oxide film or on a polymer, there can be problems of interpretation of visual results.

Just as in adhesive bonds, it is necessary to describe where a thin film failed following service or test as well as how well the film adhered to the substrate.

When we use spectrochemical tools to determine species on the surface, we probably use them slightly differently each time, especially in adhesive bonding. Even when chemical and morphological information has been collected, interpretation may be difficult. Just how do we decide where failure has occurred? In the typical complex adhesive bonded system, we have several interfacial regions as shown in Figure 8. Each of the materials coming together to form these interfaces has its own individual chemical signature. The substrate for instance usually contains alloying elements which vary in content between the surface and bulk. In addition to alloying elements, surface treatments leave behind elements characteristic of each treatment. For instance the popular FPL (Forest Products Laboratory) etch for aluminum alloys consist of sulfuric acid and sodium dichromate in distilled water and leaves a detectable amount of chromium on the alloy. Additives in the primer or adhesive may also be used to determine the location of a failure. Primers containing a corrosion inhibitor such as strontium chromate are examples of such materials. A pure polymeric adhesive with no additives can cause problems since the elements present may look just the same to some characterization methods as organic contamination. It is here that vibrational spectroscopy or XPS provides important information on molecular configuration. The capability of differentiating isotopes with the SIMS method allows doping of the adhesive with an isotope not normally found in the adhesive such as  $^{13}\text{C}$  or  $^{15}\text{N}$ .

Failure surfaces from the wedge test have proved to be interesting illustrations of the ISS-SIMS technique. The wedge test method provides information about adherend surface preparation. This configuration is sensitive to different surface preparation treatments and can discriminate between bonding processes that give good and poor service performance. The wedge specimen consists of two thin adherends with a wedge driven into the bondline. The position of the crack leading edge is deter-

mined microscopically and then the specimen is subjected to various external stimuli such as changes in temperature and relative humidity. The propagation of the crack tip is followed with time. Sometimes when the wedge is driven into the bondline, separation of the specimen occurs over a portion of the bondline as in the pictures shown in Figure 9. Here the wedge was driven in as shown first causing the cohesive failure in the adhesive at the left, then apparent adhesive failure between a and c during testing at 160°F and 95% R.H., followed at the right again by cohesive failure when the specimen is opened following the test. The adherend shows no indication of adhesive either visually or in the SEM, although there are slight reflectivity differences seen across the sample. Such specimens are usually examined in several areas of both failure surfaces. In the specimen shown in Figure 9 it appeared that the mode of failure had changed from primer/oxide to oxide/metal. The appearance of chromium in ISS/SIMS spectra in area c suggested failure at the original etched alloy surface. When the opposite side (the adhesive) was sampled in several areas it was even more evident that a mixed mode failure had occurred. The ISS/SIMS data from three areas on the adhesive corresponding to the same three areas on the adherend are shown in Figure 10. These spectra suggest strongly that the crack tip progresses initially from the adhesive into a boundary layer near the primer oxide interface. With time (under increased temperature and humidity) the crack tip continues to a weaker region which for this surface treatment appears to be near the oxide/alloy interface. Figure 11 summarizes the analysis of the bond failure for this particular surface treatment. The important aspect here is that under identical conditions, different surface preparations show different modes of failure. Weak boundary layers are not developed using some treatment/bonding combinations. Processes have been developed in which the locus of failure remains in the adhesive ("a cohesive failure") and it is necessary to use a mechanical test in which even more stress is placed on the interfacial region (19).

### Conclusions

Ion beams provide useful information either as a diagnostic tool or as a precision etching method in adhesion research. The combination ISS/SIMS method used along with other techniques such as SEM provides a powerful tool for elemental analysis of surface composition. These results, as well as earlier work in this laboratory, indicate that the surface composition can be significantly different from the bulk due to contamination, selective chemical etching and segregation. These same techniques also provide an analysis of the mode of failure in adhesive joints. Many failures classified as "adhesive" on the basis of visual inspection are frequently mixed mode failures or failures at a new interface containing elements of both adhesives and adherend.

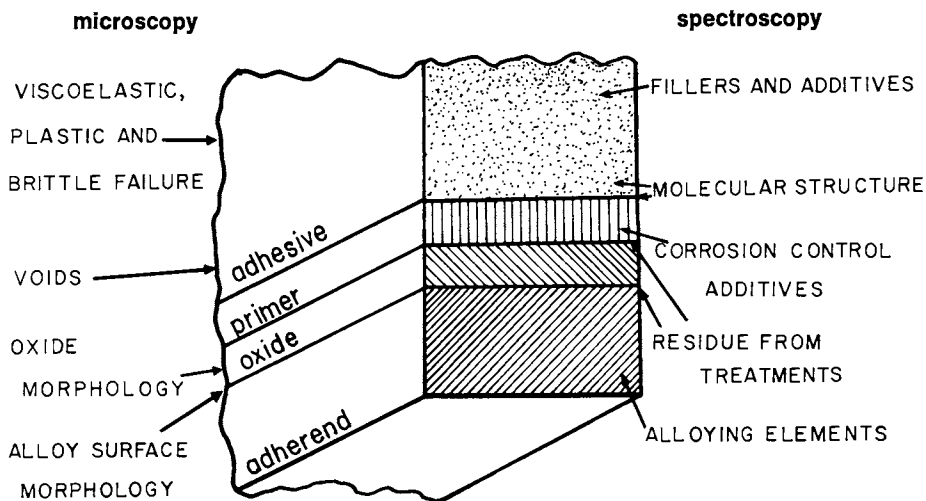


Figure 8. Model of adhesive bond showing applications of spectroscopy and microscopy.

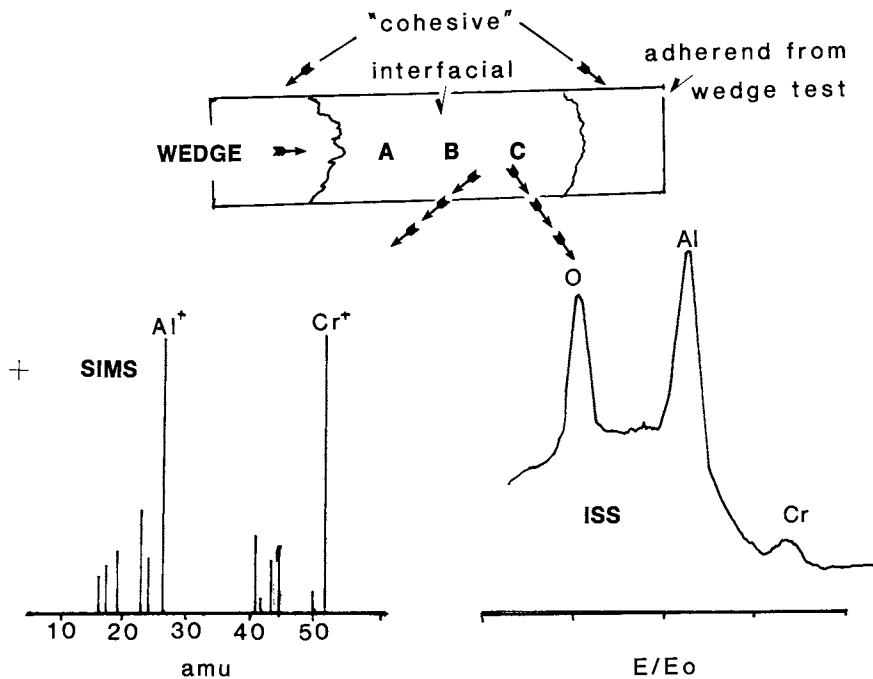


Figure 9. Wedge failure surface with ISS/SIMS data taken in area C on adherend.

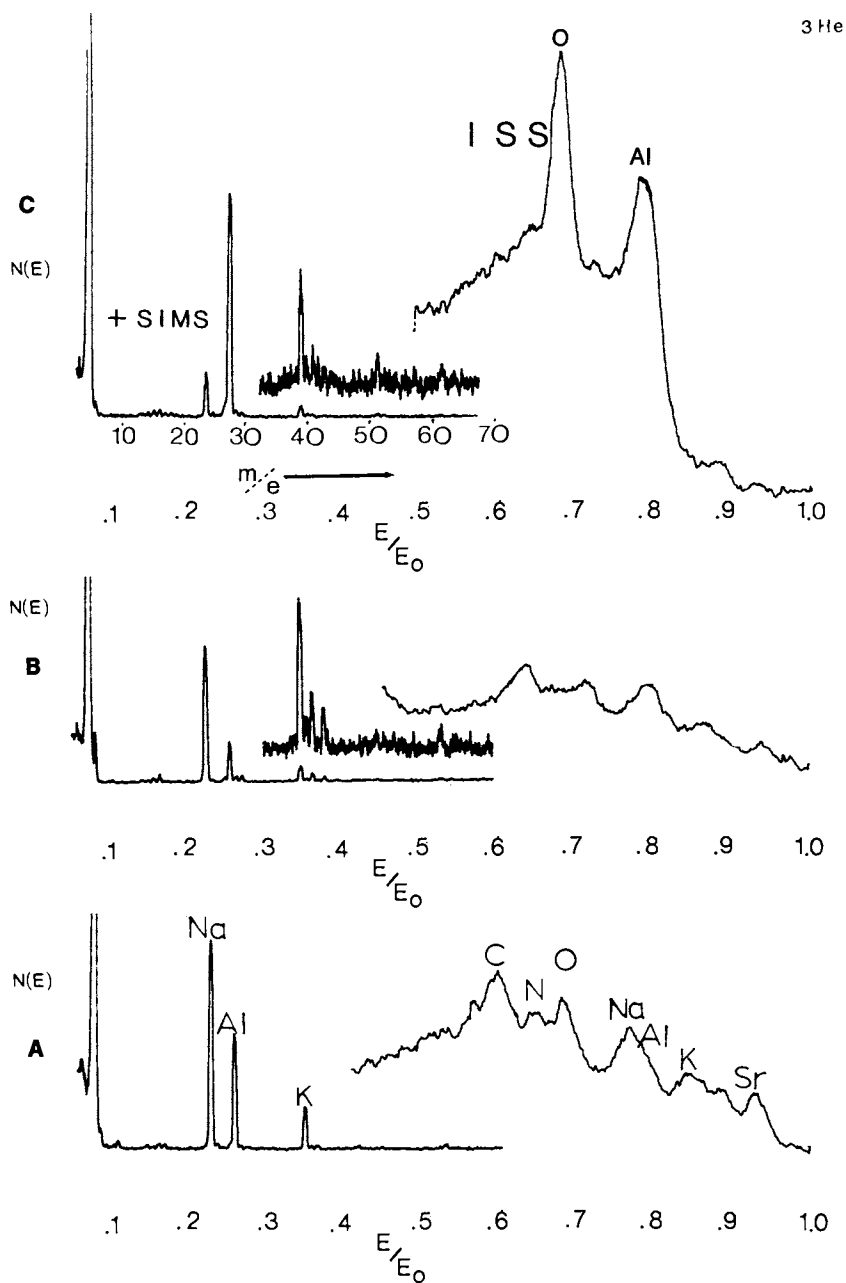


Figure 10. ISS/SIMS data from adhesive matching areas to adherend shown in Fig. 9.



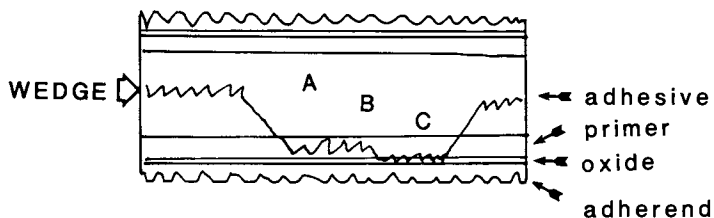


Figure 11. Summary of analysis of the mode of failure from data shown in Figs. 9 and 10.

#### Literature Cited

1. Powell, C. J., Appl. Surf. Sci. 1978, 1, 143.
2. Park, R. L. in Experimental Methods in Catalytic Research Vol. III, Academic Press, NY, 1976, p. 1.
3. Gossett, C. Robert, this volume.
4. Brundle, C., this volume.
5. Buck, T. M. in "Methods of Surface Analysis" A. W. Czanderna, Ed., Elsevier Amsterdam p. 75-102 (1975).
6. Smith, D. P. J. Appl. Phys. 1967, 38, 340.
7. Benninghoven, A., Surf. Sci. 1971, 28, 541.
8. McHugh, J. A. in "Methods of Surface Analysis", A. W. Czanderna, Ed., Elsevier Amsterdam p. 223, (1975).
9. Rusch, T. W. and Erickson, R., J. Vac. Sci. Technol. 1976, 13 374.
10. Baun, W. L. Appl. Surf. Sci. 1977, 1, 81.
11. Benninghoven, A., Surf. Sci. 1975, 53 596.
12. Baun, W. L. Surf. Technol. 1980 11. 385.
13. Dibenedeto, A. T. and Scola, D. A. J. Coll. Inter. Sci. 1978, 64, 480.
14. Gardella, J. A. and Hercules, D. M. Anal. Chem. 1980, 52, 226.
15. Thomas, G. E., van der Ligt, G., Lippits, G., van de Hei, G., Appl. Surf. Sci., 1980, 6, 204.
16. Sparrow, G. and Mishmash, E., Abstracts 28th Pittsburgh Conf., Cleveland, Ohio, 1977.
17. Gardella, J. A. and Hercules, D. M., Abstracts 30th Pittsburgh Conf., Cleveland, Ohio, 1979.
18. Mittal, J. Electrocomponent Science and Technology, 1976, 3, 21.
19. N. T. McDevitt and W. L. Baun J. Adhesion, in press.

RECEIVED June 25, 1982

# Surface Analysis of Fibers and Polymers by X-Ray Photoelectron Spectroscopy: Industrial Applications

MERLE M. MILLARD

U.S. Department of Agriculture Berkeley, CA 94710

Applications of surface analysis by X-ray photoelectron spectroscopy (XPS) are reviewed, emphasizing analysis of chemically modified fibers and polymers. The review is restricted to materials science applications involving non-metal-metal oxide systems. Results from the surface modification of fibers by low temperature plasmas, including oxidation treatments and application of coatings by deposition and plasma grafting, are reviewed. Examples emphasizing the ability of XPS to obtain results on non-uniform solids encountered in typical materials science applications, such as chemically modified polymer beads and granules, o-ring seals, wood and various intractable polymers, are presented. Recent results from the determination of inelastic mean free path lengths in organic solids are reviewed.

In this review the term X-ray photoelectron spectroscopy (XPS) will be used rather than the term adapted by Sieghahn, namely electron spectroscopy for chemical analysis (ESCA), to describe the surface sensitive electron spectroscopy under discussion. The fact that this symposium is taking place on the topic of industrial applications of surface analysis reflects the growth of the application of different areas of surface sciences in practical industrial and technological materials science areas. Initially, scientists working in XPS were concerned with establishing the fundamentals of the physics associated with the processes involved in the

This chapter not subject to U.S. copyright.  
Published 1982 American Chemical Society.

In Industrial Applications of Surface Analysis; Casper, L., et al.;  
ACS Symposium Series; American Chemical Society: Washington, DC, 1982.

technique and theory enabling understanding and prediction of behavior of the phenomena. It soon became apparent that a technique that allows determination of chemical composition and is sensitive to differences in chemical bonding within a region of several nanometers of the surface has great practical utility in areas where surface behavior was important such as catalysts and interfacial phenomena. The recent emphasis on new materials and advanced technology as reviewed in a recent volume of Science (1) has required the development of analytical techniques to characterize new materials and aid in the development of fabrication processes. Consideration of some of these technologies such as polymer development, conductive polymers, biopolymers, fiber reinforced composites, metallic glasses, heterogeneous catalysts, photovoltaic materials, integrated circuit processing, in light of the need to control and characterize not only bulk composition but especially interfaces makes it obvious why surface oriented analytical techniques are needed and used extensively in these areas. XPS has an advantage in that often materials as processed and used can be directly analyzed with little or no sample alteration prior to analysis.

This review will concentrate on non metallic and related areas such as organic fibers and various forms in which organic materials are used such as films, granules and small extruded geometries. Readers will be referred elsewhere for discussions of fundamentals of the technique and instrumentation. Applications of XPS to problems of industrial interest such as fiber modification and analysis carried out in our laboratory will be reviewed.

### Recent Reviews

A number of reviews can be consulted for an introduction to the fundamentals both theoretical and practical covering XPS. These include Riggs and Parker (2) and the book by Carlson (3). Electron spectroscopy is reviewed in alternate years in the Fundamental Reviews issue of Analytical Chemistry. The last literature review was published in 1980 (4) and this and previous reviews can be consulted for a coverage of all aspects of the literature of XPS. A number of recent symposia have been held on applications of surface analytical methods in various aspects of materials science such as the symposium on characterization of molecular structures of polymers by photon, electron, and ion probes at the March 1980 American Chemical Society meetings in Houston (5) and the International Symposium on Physicochemical Aspects of Polymer Surfaces at this meeting as well as the symposium on industrial applications of surface analysis of which this article is a part. Review articles on various applications of XPS in materials science are listed in Table I.

TABLE I

## Recent Reviews in Photoelectron Spectroscopy

XPS of Polymer Surfaces	(6 - 9)
Analytical Applications	(10, 11, 12)
Radiation Damage	(13)
Surface Modified Electrodes	(14)
Interfacial Chemistry and Adhesion	(15)
Surface Chemistry and Catalysis	(16, 17)
Mineralogy and Geochemistry	(18)
Microelectronics Processing	(19)

Instrumentation

The fundamentals of instrument design on an elementary level are discussed by Carlson (3). Discussions of instrumentation from a point of view of manufacturers' specifications is presented in two older articles (20, 21). Among the manufacturers listed in Evans' article (21), Hewlett-Packard and E.I. duPont no longer manufacture instruments. It is advisable to consult current manufacturers for up to date specifications of instrumentation. Development of instrumentation has not kept pace with recent activity in the field and hopefully instrument manufacturers currently manufacturing instruments will devote more effort to development in the future.

Introduction to Core Electron Spectra of Polymeric Materials

An excellent introduction to the common features observed in electron spectra of non metallic surfaces and a simple discussion of the physical processes giving rise to these features is included in the review article by Holm and Storp (7). A good discussion from a practical introductory viewpoint is included in a Handbook of XPS (22). More exotic effects that lead to secondary lines of lower intensity such as multicomponent structure are more often encountered in transition metals and metallic oxides or transition compounds. These effects are discussed in more detail in Carlson (3) and Wertheim (23). Shake up lines in addition to core lines are sometimes observed from polymers and result from processes involving transitions to states with energy above the ground state. These lines are usually less than a tenth or more of the intensity of the prominent core line. When first investigating a sample, it is useful to obtain a survey scan at lower resolution over regions that include elements thought to be present. Generally 550 to 50 eV is a window that contains strong lines from most of the elements encountered in polymer studies excluding exceptions such as fluorine. A survey scan will not only identify the

elements present but will aid in planning the regions to be investigated in detail and provide some idea of the number of scans to be collected for lines of lower sensitivity and intensity. Survey spectra in the region 550 eV to 50 eV (usually an accumulation of eight scans) are presented in Figure 1 for a number of surfaces illustrating the occurrence of various elements of interest in polymers and the fact that XPS survey spectra serve as a fingerprint enabling rapid identification of the components present in polymer samples. Tabulations of line positions for the elements and binding energies for compounds of the elements are available (22). Binding energies have been published for a number of polymers of common interest including commonly occurring elements such as oxygen, nitrogen, halogen, sulfur and silicon (24). Some of the older literature is still quite useful and can be consulted for binding energies of oxygen (25) and nitrogen compounds (26). A useful table of carbon binding energies for carbon substituted with fluorine has been published by Clark (27). Elemental composition can be estimated from electron spectra and tables of photoelectric cross sections have been compiled for various instruments and a procedure for obtaining elemental composition presented (22, 28). The author's experience has been with some precautions as to the nature of the sample under investigation using sensitivity factors determined in the instrument from known pure compounds of similar nature, reasonable composition data can be obtained with accuracy in the range of  $\pm 3 - 5\%$ .

### Electron Escape Depths

A parameter of fundamental importance in electron spectroscopy is the inelastic mean free path length (IMFP) for electrons of a given kinetic energy originating in solids. This parameter has to do with the fraction of observed electrons that originate from a given depth into the sample and is of critical importance in understanding XPS results.

The idealized escape of electrons from matter is illustrated diagrammatically in Figure 2a. An idealized curve approximating the relationship between the IMFP and the electron kinetic energy is shown in Figure 2b.

Carlson (3) summarizes the earlier data on IMFP's for electrons whose kinetic energy varies between 100 and 1500 eV through material in the elemental or oxide form. Inelastic mean free paths can be measured by determining the attenuation of a signal from a substrate with overlayers of varying known thickness. Experimentally this seems to be slightly less difficult for inorganic materials. Silicon dioxide grown or oxidized over silicon is an example. Overlayer films must be uniform and their thickness determined. Procedures have been developed in the microelectronics and thin film physics areas to

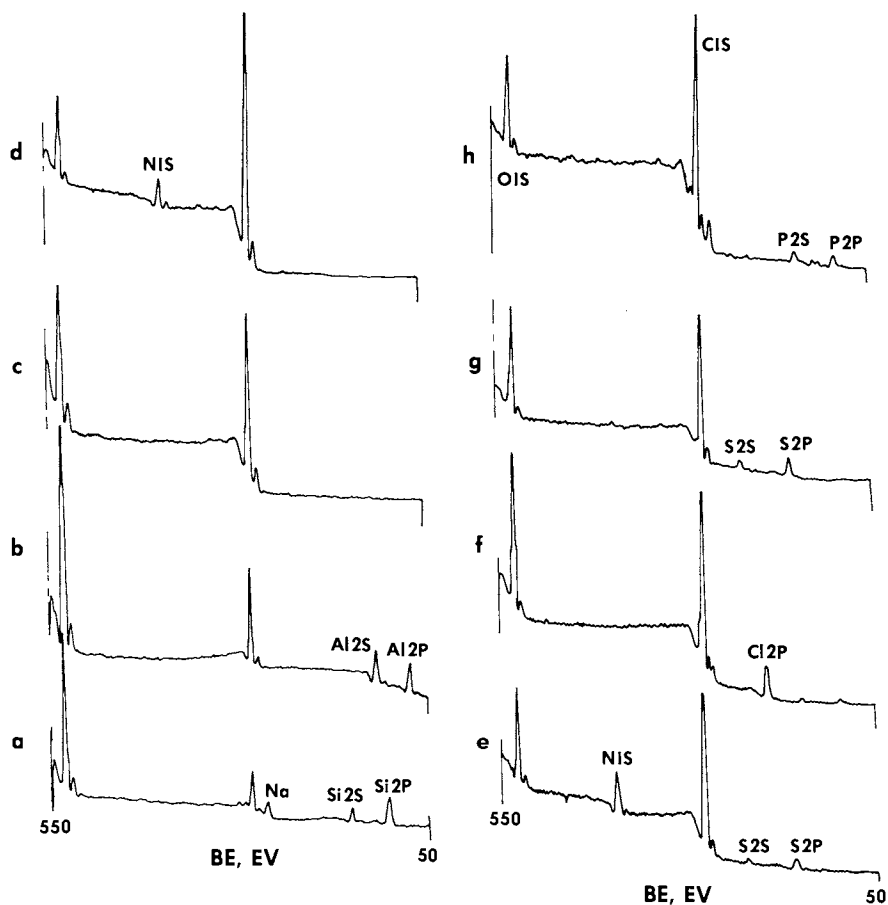


Figure 1. Wide scan spectra over the region 550–50 eV. Key: a, oxygen plasma cleaned glass; b, aluminum foil; c, solvent cleaned rayon fibers; d, solvent cleaned nylon fibers; e, solvent cleaned wool fiber; f, copolymer film (one monomer contains a chlorine substituted side chain); g, sulfonated 8% cross-linked styrene divinylbenzene copolymer beads; h, copolymer containing diphosphine chelating ligand.

grow oxides of known thickness over the respective element. The agreement among data for inorganic systems is fairly good, however, when one considers IMFP's for organic compounds and polymers, the agreement is fair. Little data existed for escape through organic overlayers until recently and a number of reports now exist reporting IMFP's for electrons with kinetic energies of interest escaping through organic overlayers. In addition, a compilation has recently been published of the data existing in the literature for IMFP's for various categories of materials and relationships between IMFP and kinetic energy derived (29). Earlier measurements reported by Cadman (30) and Clark (31) using different approaches were not in agreement concerning IMFP through organic materials. Cadman measured the intensity of core electrons escaping through organic polymers and organic compounds and related these intensities to IMFP's measured for C 1s electrons in graphite as a standard. Clark measured the attenuation of electrons escaping through poly-(p-xylene) using the overlayer approach. Clark's IMFP's were shorter at comparable kinetic energies than were Cadman's values. Brundle (32) deposited multilayers of cadmium arachidate over metalized glass substrates. The attenuation of the substrate signal was measured as a function of overlayer thickness. The derived IMFP's varied with the angle between the plane of the sample and a line normal to detector. This variation with grazing angle was interpreted in terms of incomplete substrate coverage and a patch correction was included. For electron kinetic energies between 1n 3d KE 1042 eV and Au<sub>4f</sub> 1402 eV the IMFP's varied between 4.5 nm and 5.1 nm. With the path correction these values became 3.6 nm to 4.1 nm. Hall (33) measured IMFP's from multilayers of barium stearate on germanium and copper. The values ranged between 2.7 to 5 nm at 230 eV to 6.5 + 0.5 nm at 1480 eV. Clark (34) used stearic acid, 9-n-butyl-10-anthryl propionic acid and diacetylene fatty acids to prepare cadmium salt multilayers. At 1170 eV IMFP's were 4.5 nm, 7.0 nm and 5.7 nm for the multilayers respectively. Roberts (35) coated silicon substrates with films of Poly(methylmethacrylate)(PMMA) and measured the thickness by ellipsometry. The IMFP's obtained were 2.9 + 0.4 nm for 1196 eV electrons and 3.3 + 0.5 nm for 1328 eV electrons. A plot of IMFP's vs. electron kinetic energy determined for organic material taken from Roberts (35) is given in Figure 3.

#### Plasma Oxidation of Fibers and Surface Grafting of Coatings to Wool Fibers

Plasma oxidation of fibers is an example of a treatment aimed at chemically modifying the surface to improve a surface property. These treatments have wide application in industry and are used to improve wettability and printability of plastics, the adhesion of materials to surfaces including tissue culture cells, and a variety of other applications (36).

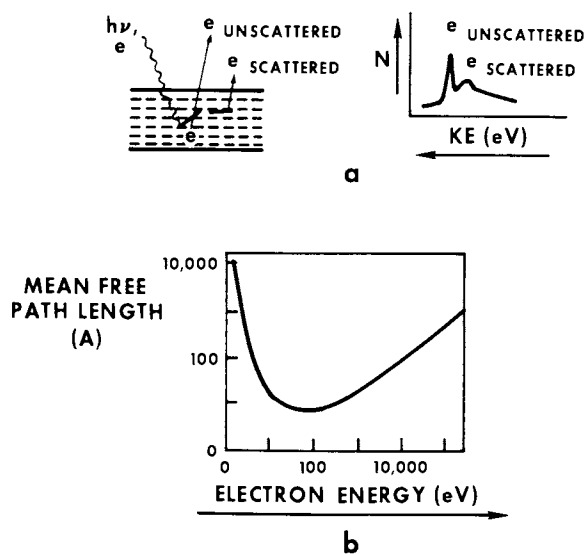


Figure 2. Electrons photoejected from a surface (a). Idealized graph of the mean free path length as a function of electron kinetic energy (b).

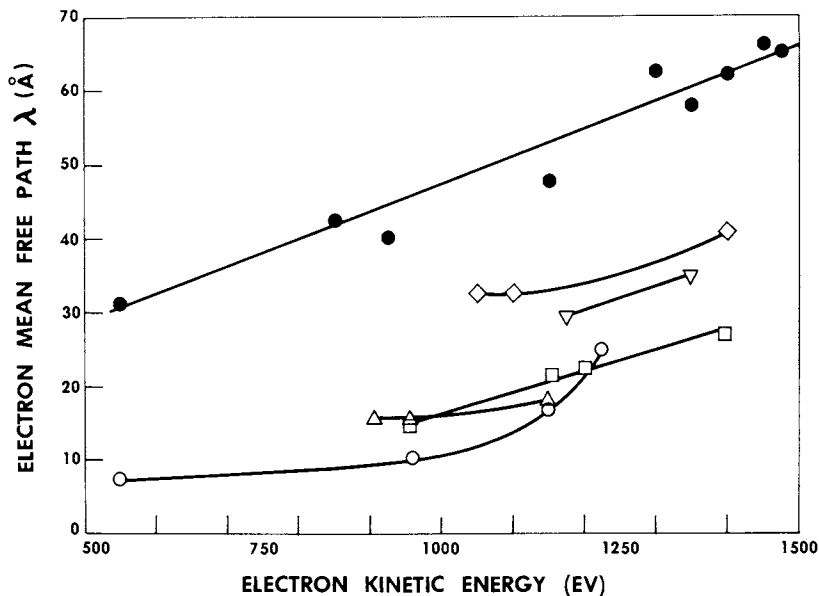


Figure 3. Electron mean free path as a function of electron kinetic energy through organic materials. Key:  $\nabla$ , PMMA;  $\square$ , poly(p-xylene);  $\circ$ , plasma polymerized fluorocarbon;  $\bullet$ , barium stearate;  $\diamond$ , cadmium arachidate; and  $\triangle$ , carbon. (Reproduced, with permission from Ref. 35.)



Oxidation of the surface of wool fibers is known to reduce felting shrinkage as well as improve other properties of wool fibers (37). Oxidation may be performed or effected in a number of ways including gas phase plasma treatment (38). Early attempts were made to detect changes on the surface of wool fibers using the magnetic deflection electron spectrometer at the University of California at Berkeley. The signal to noise ratio for spectra obtained was modest and run times amounted to several hours; however, interesting results were obtained allowing optimum development of the process. The plasma apparatus employed in these experiments is shown schematically in Figure 4. Wool yarn is continuously passed through the capillary inlet and outlet while the gas in which the plasma is maintained is introduced on either side of the reaction chamber. Electron spectra in the sulfur 2p region, obtained after exposure of wool yarn to an air plasma, are shown in Figure 5. The line at higher energy is due to oxidized sulfur species such as sulfate ion or cysteic acid. Sulfur 2p electron spectrum shown in Figure 6 are taken from wool yarn exposed to a plasma maintained in nitrogen (lower spectrum) and oxygen (top spectrum). As anticipated a higher level of oxidation is obtained in a pure oxygen plasma. The sulfur 2p electron spectrum obtained from corona discharge treated wool top is shown in Figure 7a while the spectrum taken from untreated control is shown in Figure 7b. Coatings of organic substances could be permanently attached to the surface of fibers by adsorbing the substance on the wool fiber and then exposing the coated yarn to a discharge in air or argon (39). Electron spectra were taken after various changes in the process to follow the amount of material attached to the surface and its loss after solvent extraction and cleaning. The change in the area of the various electron lines characteristic of the coatings was taken as an estimation of the relative loss of coating after solvent extraction. Figure 8 illustrates typical spectra taken from discharge grafted fluoro-carbon coatings and a couple of flame retardant coatings containing phosphorus and halogen are illustrated in Figure 9. These spectra were obtained from individual fibers or woven wool yarn attached to double backed tape (40).

#### Analysis of Plasma Deposited Fluorocarbon Coatings on Polymer Films and Wool Fibers

A variety of organic monomers may be polymerized in a plasma and deposited onto substrates 41,42. This process was investigated for a variety of fluoro-carbon monomers and substrates including polymer films and fabrics of woven wool fibers. Spectra were obtained using a Varian IEE-15 spectrometer. Typical electron line widths encountered from these

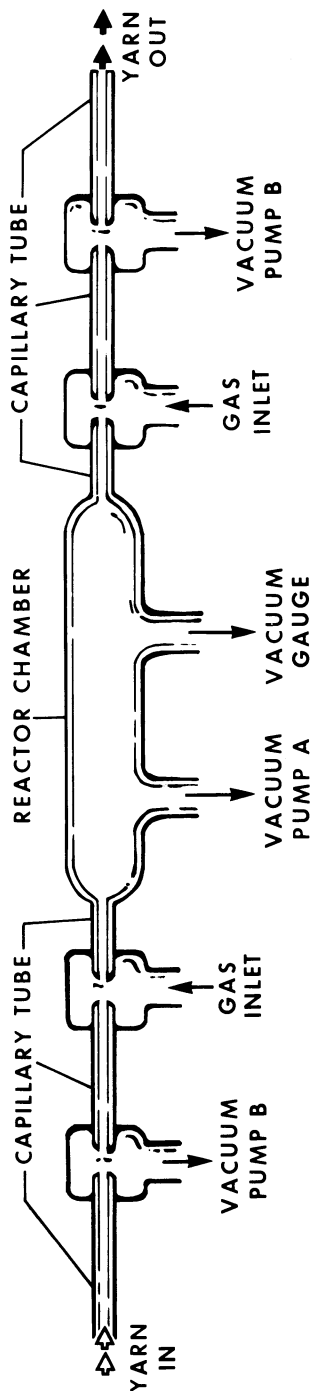


Figure 4. Plasma reactor for continuous treatment of yarn.

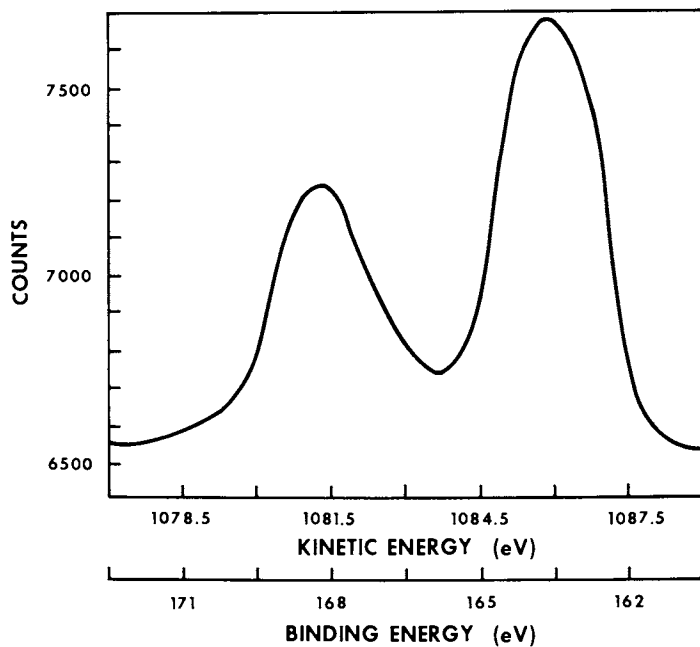


Figure 5. Sulfur 2p electron spectrum from plasma treated wool yarn. (Reproduced from Ref. 38. Copyright 1972, American Chemical Society.)

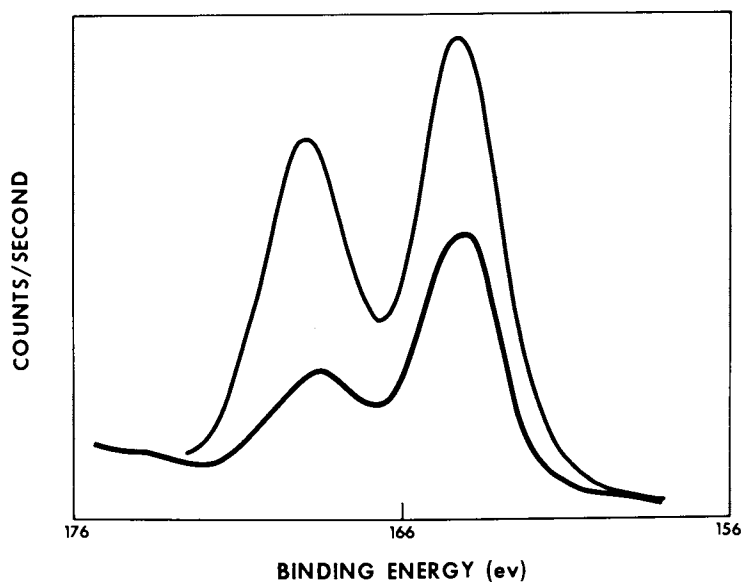


Figure 6. Sulfur 2p electron spectrum from wool yarn exposed to oxygen plasma (top) and to a nitrogen plasma (bottom).

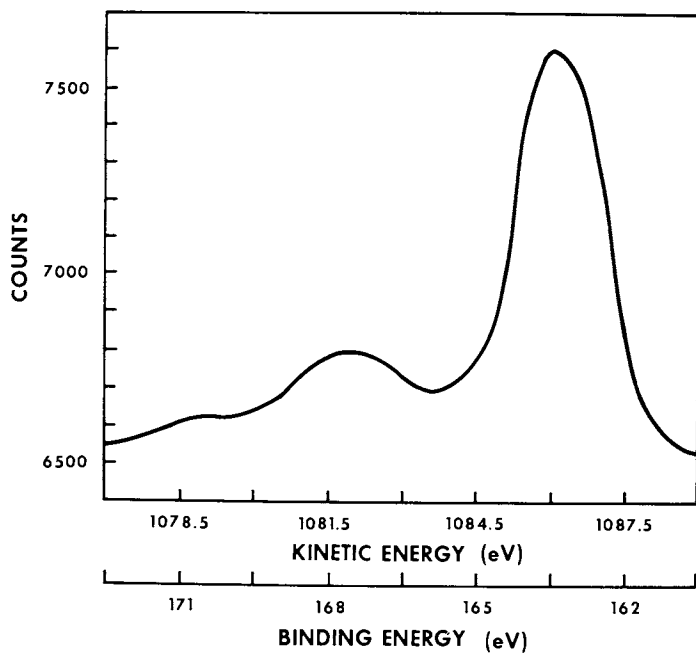


Figure 7a. Sulfur 2p electron spectrum obtained from untreated wool. (Reproduced from Ref. 38. Copyright 1972, American Chemical Society.)

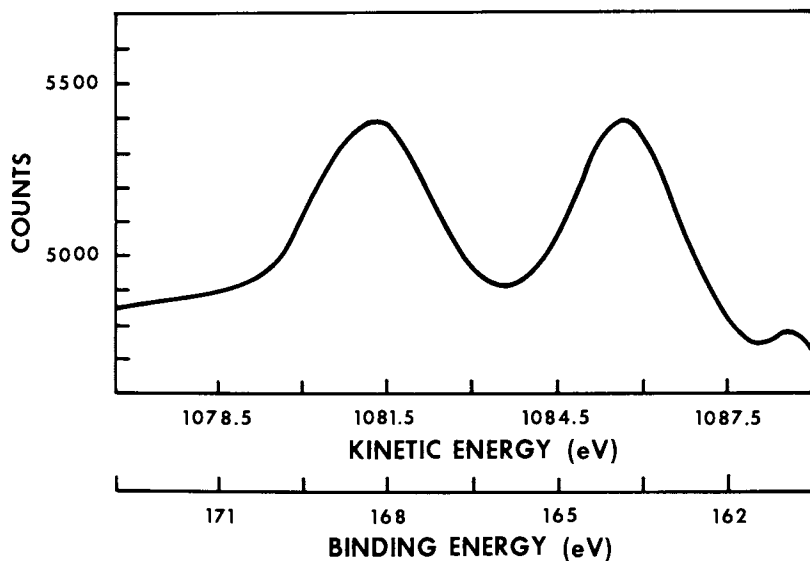


Figure 7b. Sulfur 2p electron spectrum obtained from plasma treated wool. (Reproduced from Ref. 38. Copyright 1972, American Chemical Society.)

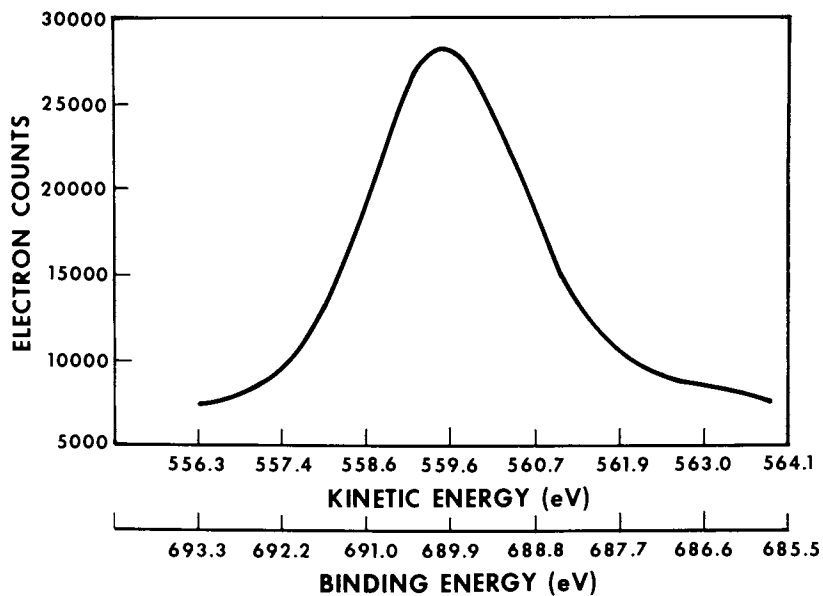


Figure 8. Fluorine 1s spectrum from fluorocarbon coating plasma grafted to wool yarn.

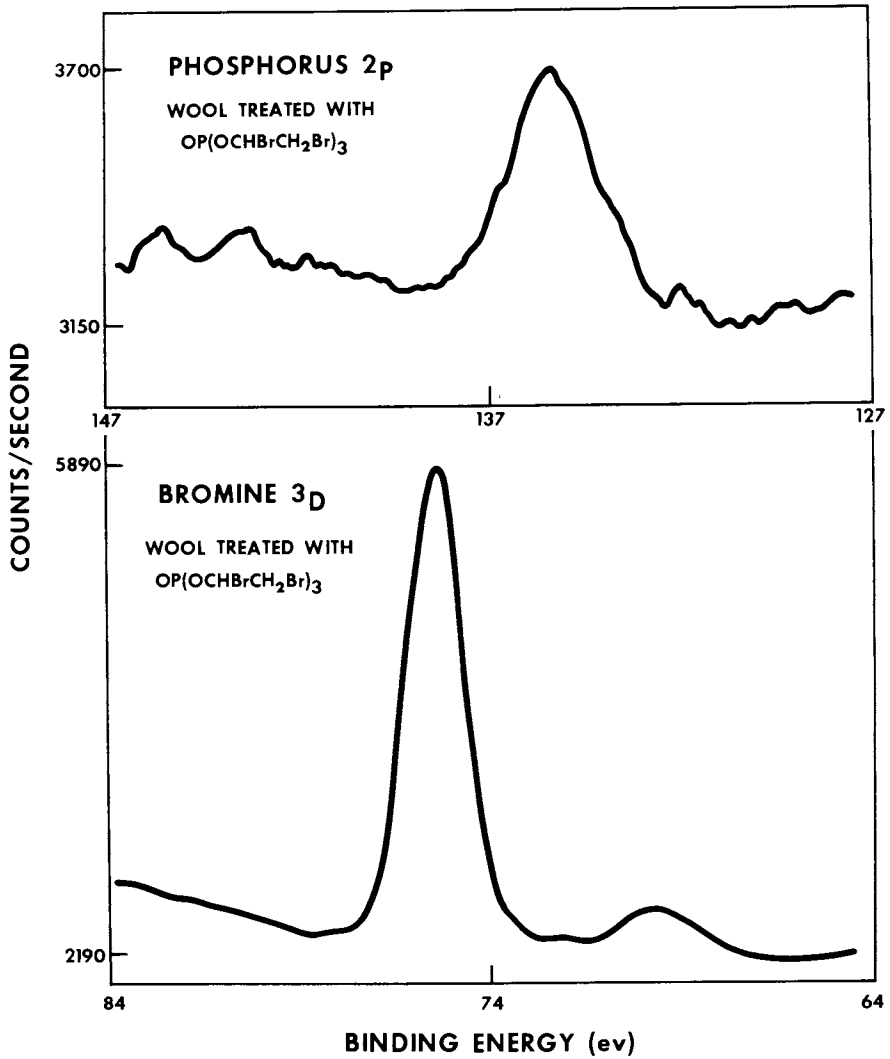


Figure 9a. Electron spectra from flame retardant coatings plasma grafted to fabric.

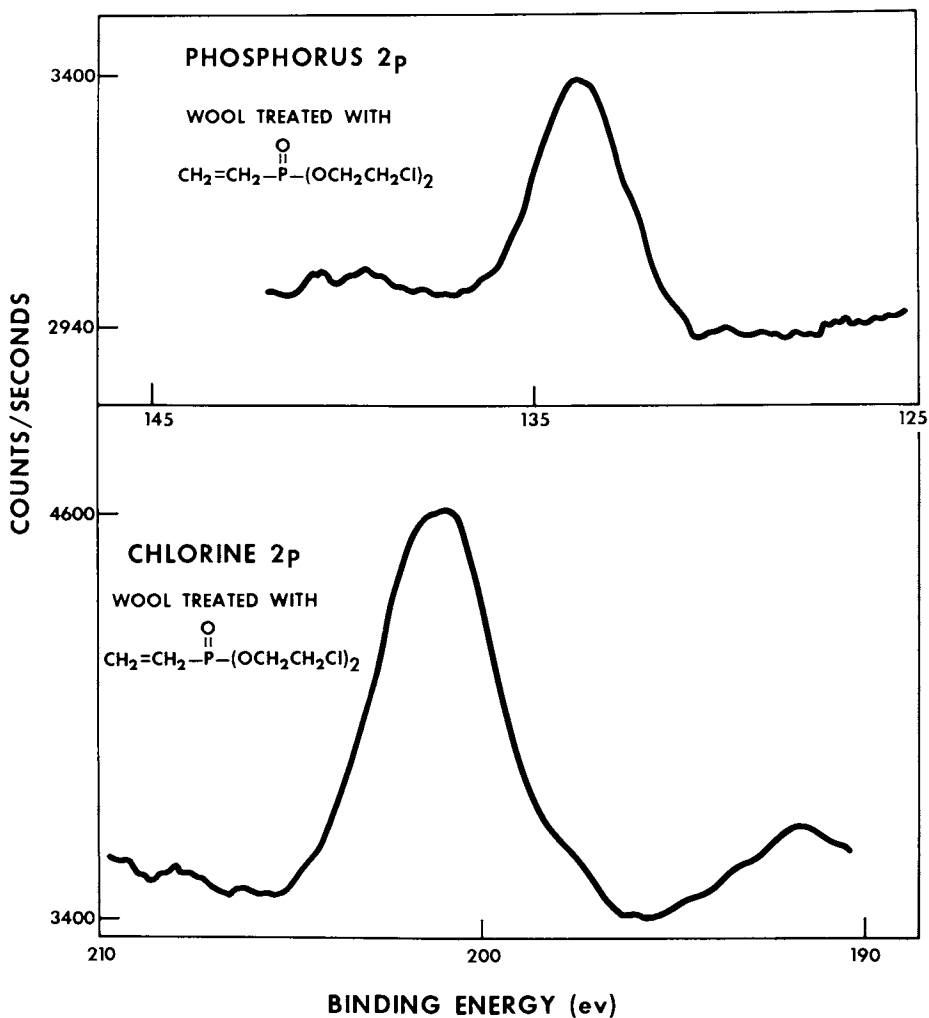


Figure 9b. Electron spectra from flame retardant coatings plasma grafted to fabric.

surfaces in this instrument were of the order of magnitude of  $2.6 \pm 0.2$  eV. At this resolution, a curve deconvolution procedure was necessary to extract the position of overlapping electron lines. We used a non-linear least squares curve fitting program written at the University of California at Berkeley (43). This program uses Lorentzian and Gaussian functions that are described by four independent parameters and a convergence with reasonable values for the parameters is usually obtained after several trials. The quality of fit of the spectra was judged in part by values of the weighted variance. Acceptable deconvolutions usually had values of the weighted variance below 10. Examples of deconvoluted spectra in the C 1s region obtained from plasma polymerized tetrafluoroethylene and hexafluoroethane deposited on plastic substrates are shown in Figure 10a and b top and bottom respectively. The carbon 1s spectrum from the fluorocarbon film deposited using hexafluoroethane (Figure 11a) and tetrafluoroethylene (Figure 11b) on wool fabric is shown. The parameters derived from these spectra are shown in Table VI. Examples of the oxygen 1s spectra obtained from polymerized hexafluoroethane on polypropylene and wool textile are shown in Figure 12a and b. Interestingly, the fluorine 1s spectra obtained from fluorocarbon films on wool contained two components. The higher binding energy component corresponded to fluorine covalently bonded to carbon while the lower binding energy component was in the region reported for ionic fluoride. The latter were presumably associated with cationic sites on wool such as protonated amines. An example of the deconvoluted fluorine 1s spectra is shown in Figure 13 taken from hexafluoroethane film on wool. Parameters derived from the oxygen and fluorine spectra are included in Table II.

#### Plasma Treated Wool Fibers

The spectra from plasma treated wool fibers was re-examined using the Varian IEE spectrometer and changes in the carbon, oxygen and nitrogen 1s levels could be analyzed (44). Lines at higher binding energy representing oxidized carbon species could be readily observed. As expected, the intensity of higher binding energy lines were maximum using an oxygen plasma and least using a nitrogen plasma. Of interest in the development of efficient process scale equipment was the discovery that active oxidizing species were present at considerable distances beyond the region of plasma activation and spectra obtained from wool fibers in the air afterglow region revealed levels of oxidation only slightly below those obtained near the source of the plasma. Deconvoluted carbon 1s electron spectra obtained from oxygen plasma and air plasma afterglow treated fibers are shown in Figure 14 a and b. These spectra were fitted with Lorentzian functions with a leading constant tail whose FWHM value was



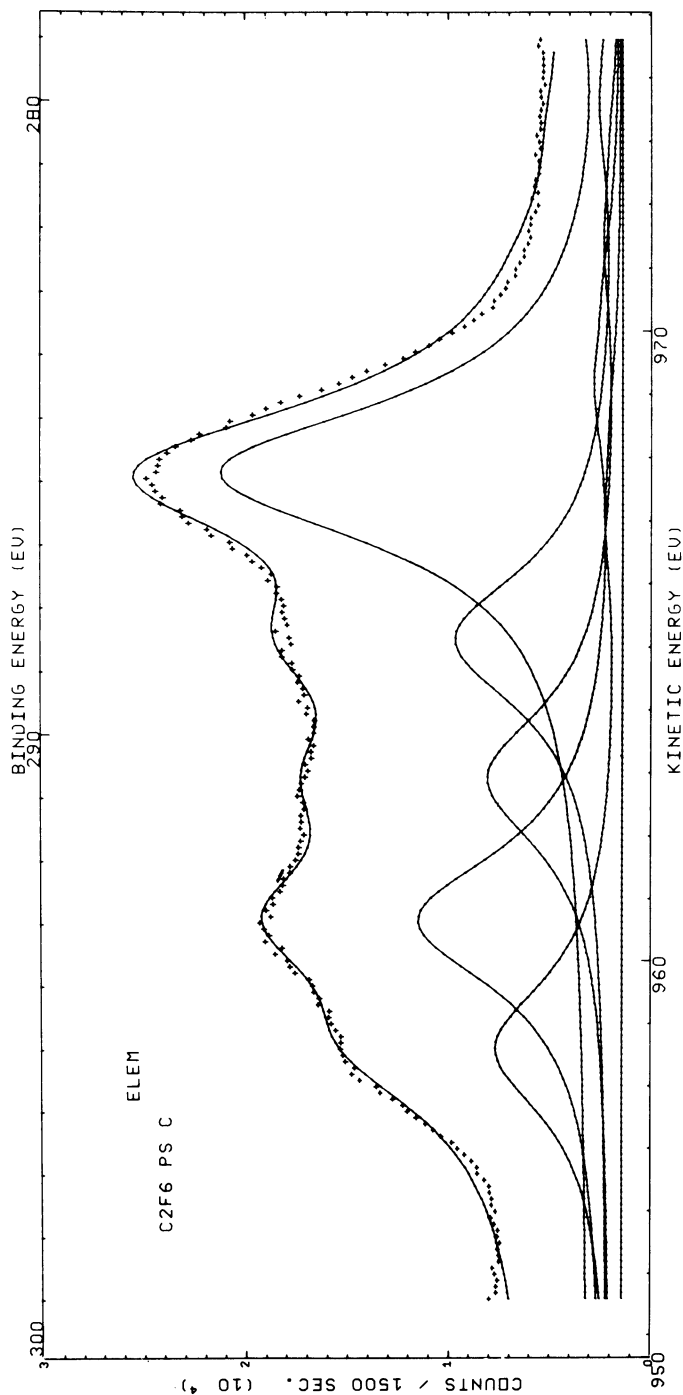


Figure 10. Carbon 1s spectrum from hexafluoroethane plasma polymerized onto polystyrene.

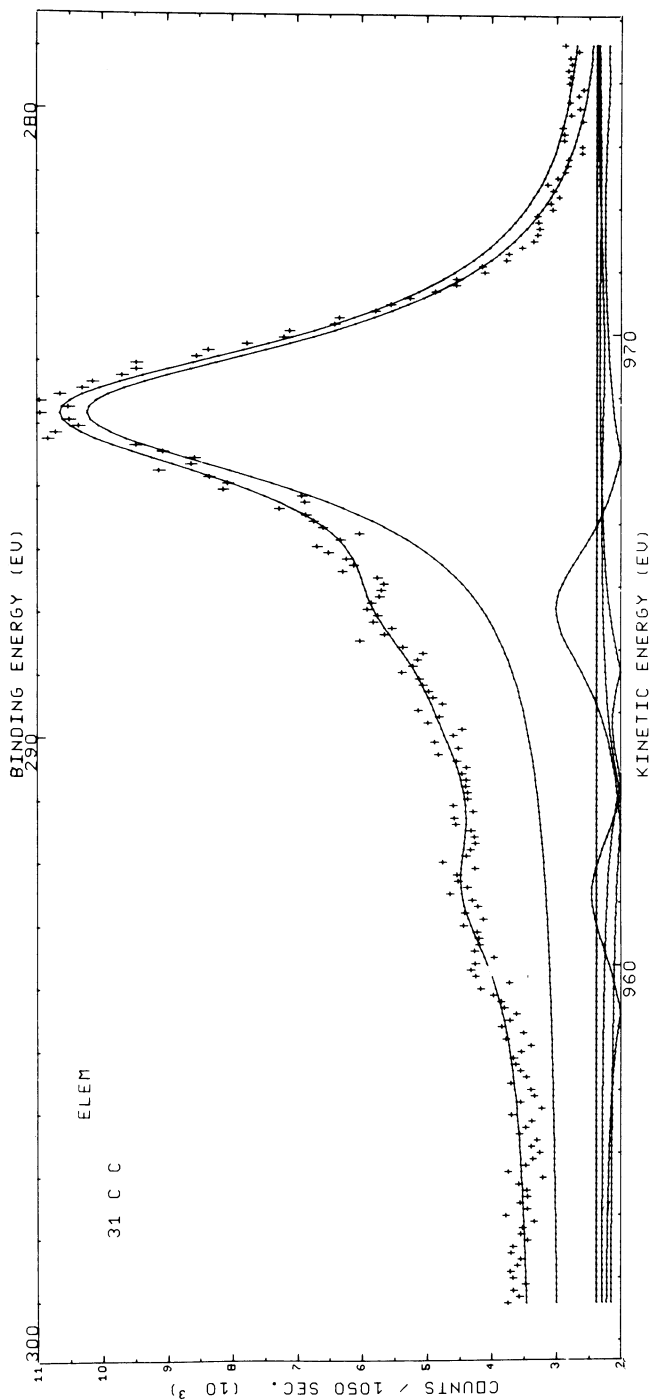


Figure 11a. Carbon 1s spectrum from hexafluoroethane plasma polymerized on wool fabric. (Reproduced, with permission, from Ref. 42. Copyright 1976, Dekker.)

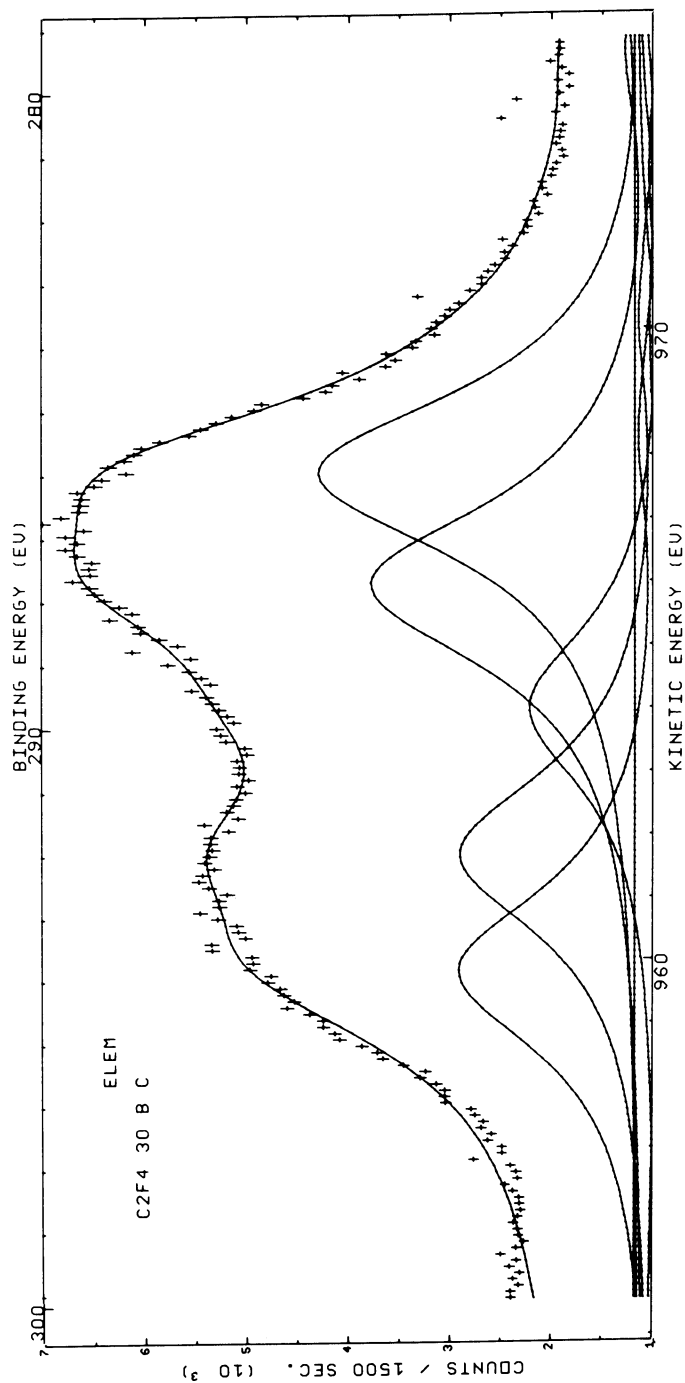


Figure 11b. Carbon 1s spectrum of tetrafluoroethylene plasma polymerized onto wool. (Reproduced, with permission, from Ref. 42. Copyright 1976, Dekker.)

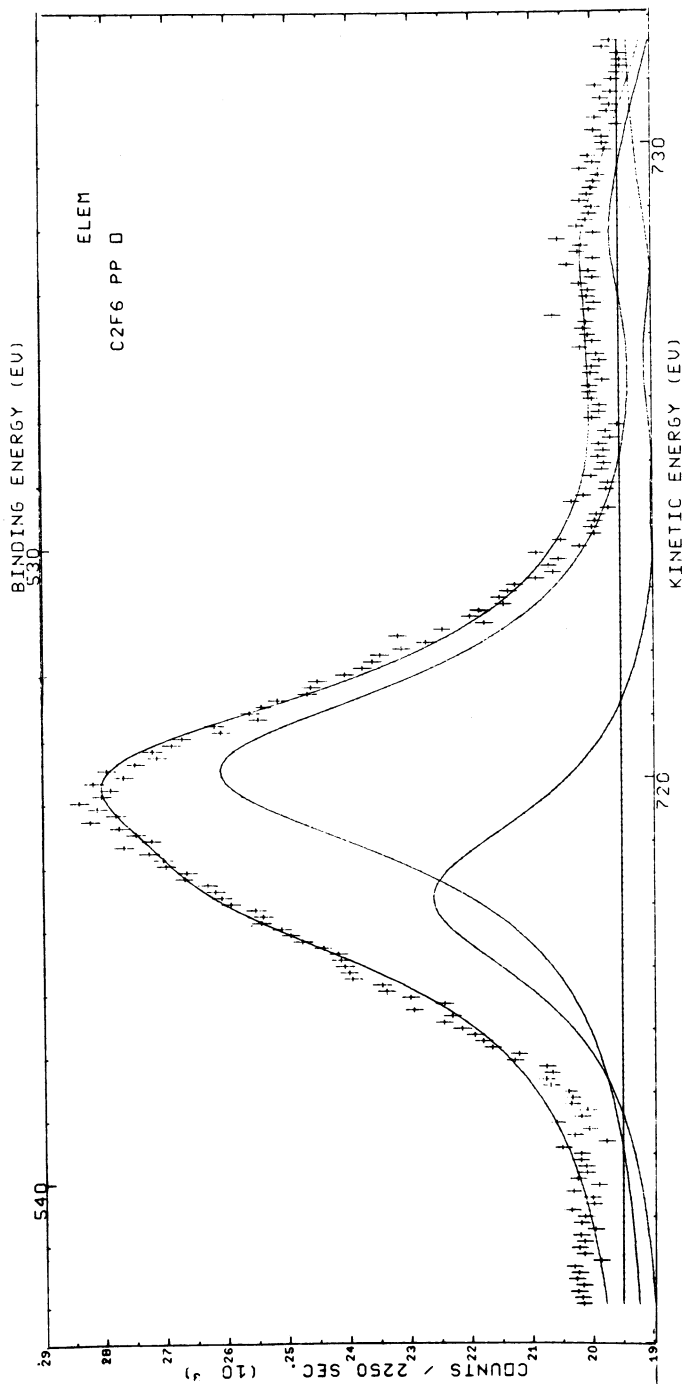


Figure 12a. Oxygen 1s spectra obtained from hexafluoroethane plasma polymerized on polystyrene.

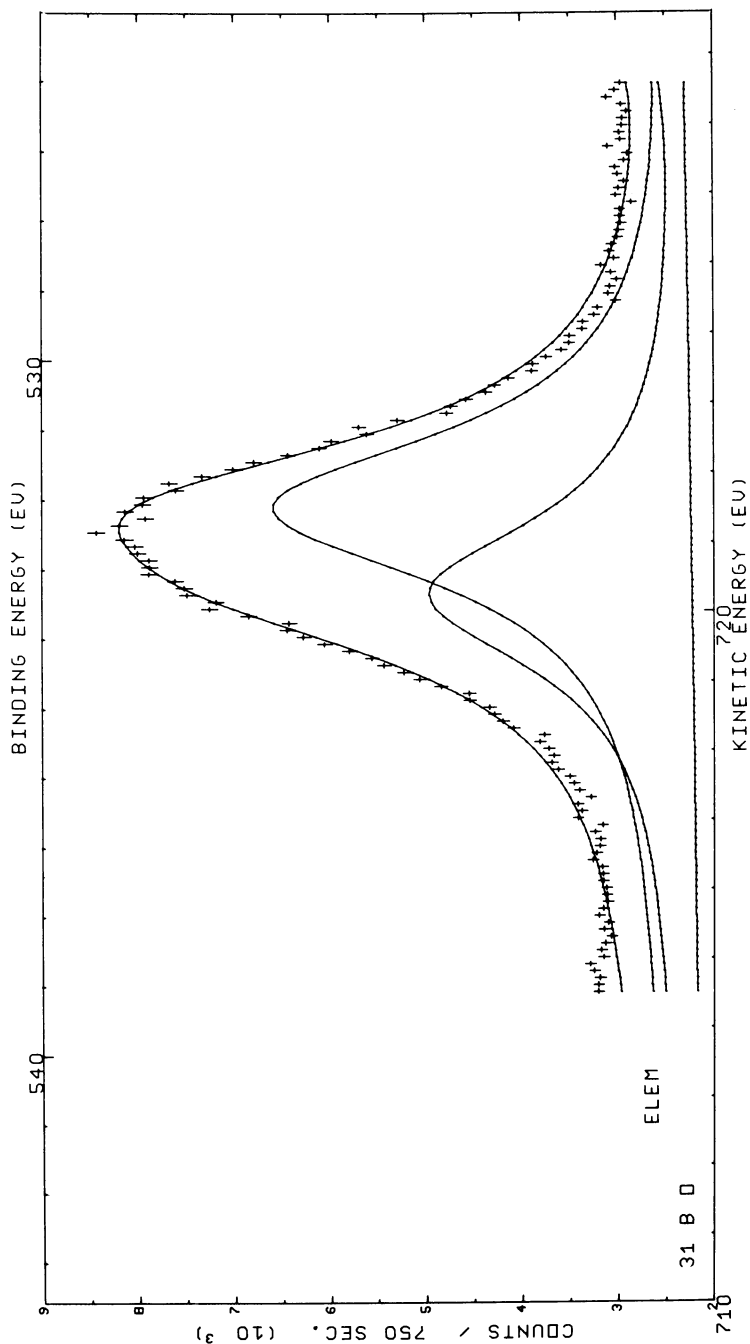


Figure 12b. Oxygen 1s spectra obtained from hexafluoroethane plasma polymerized on wool fiber. Reproduced, with permission, from Ref. 42. Copyright 1976, Dekker.

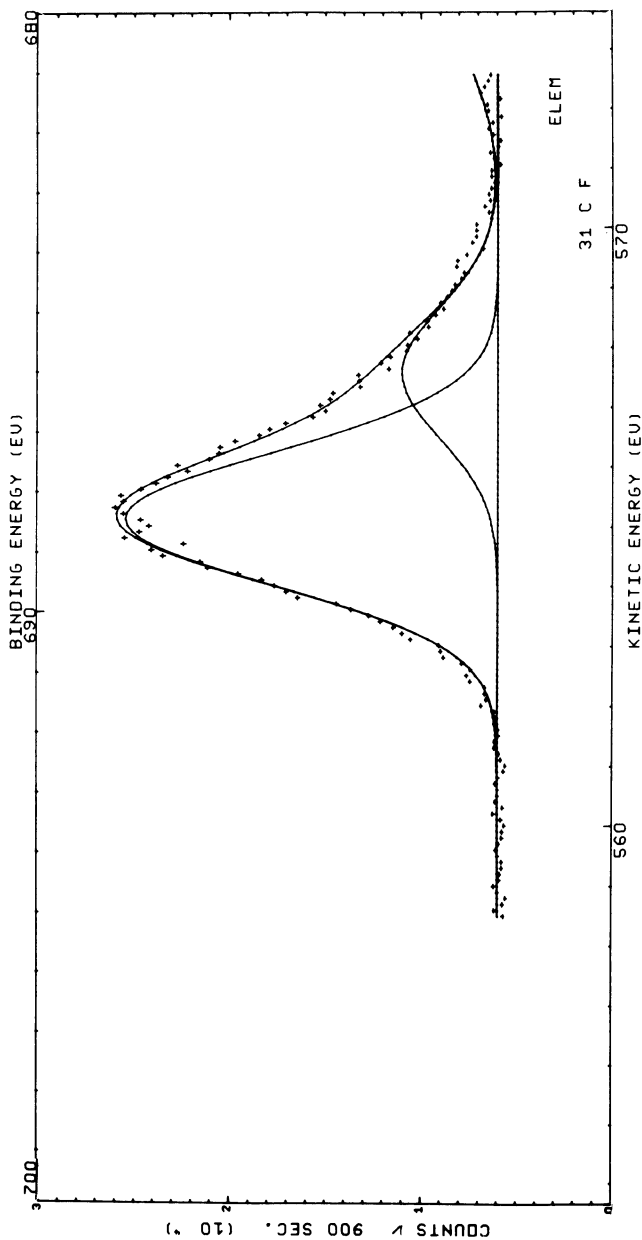


Figure 13. Fluorine 1s spectrum from hexafluoroethane plasma polymerized on wool fabric. (Reproduced, with permission, from Ref. 42. Copyright 1976, Dekker).

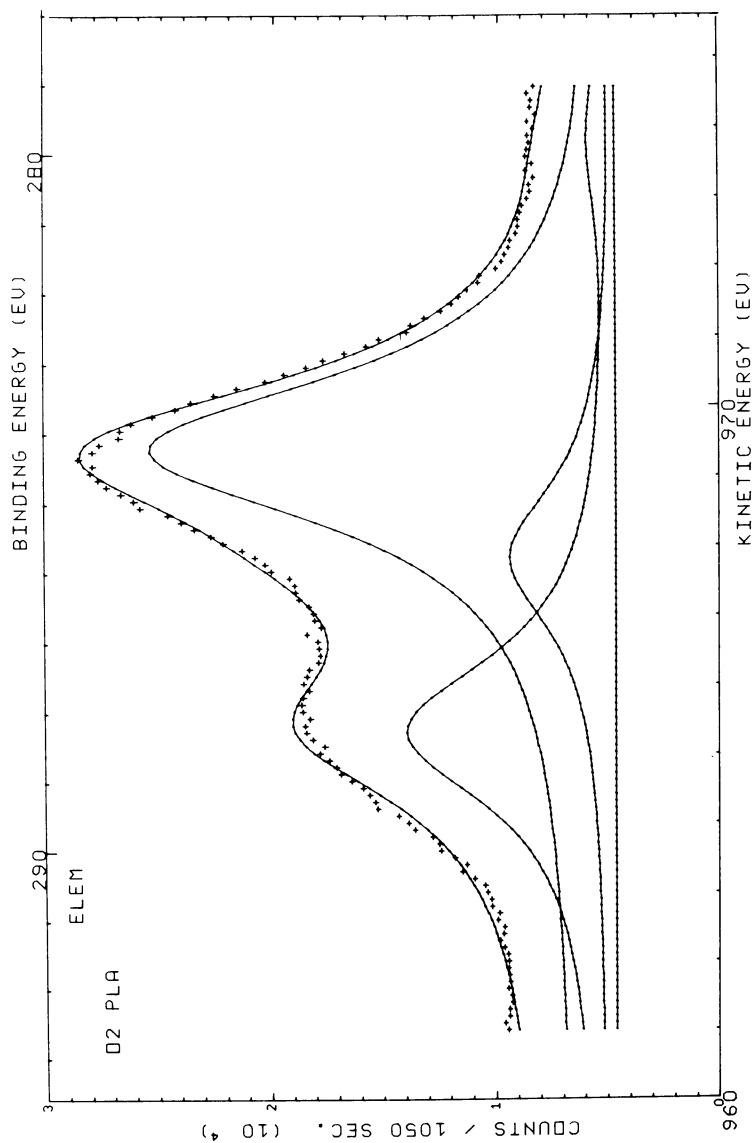


Figure 14a. Carbon 1s spectra from wool fibers oxidized in oxygen plasma. (Reproduced, with permission, from Ref. 44. Copyright 1977, Academic Press.)

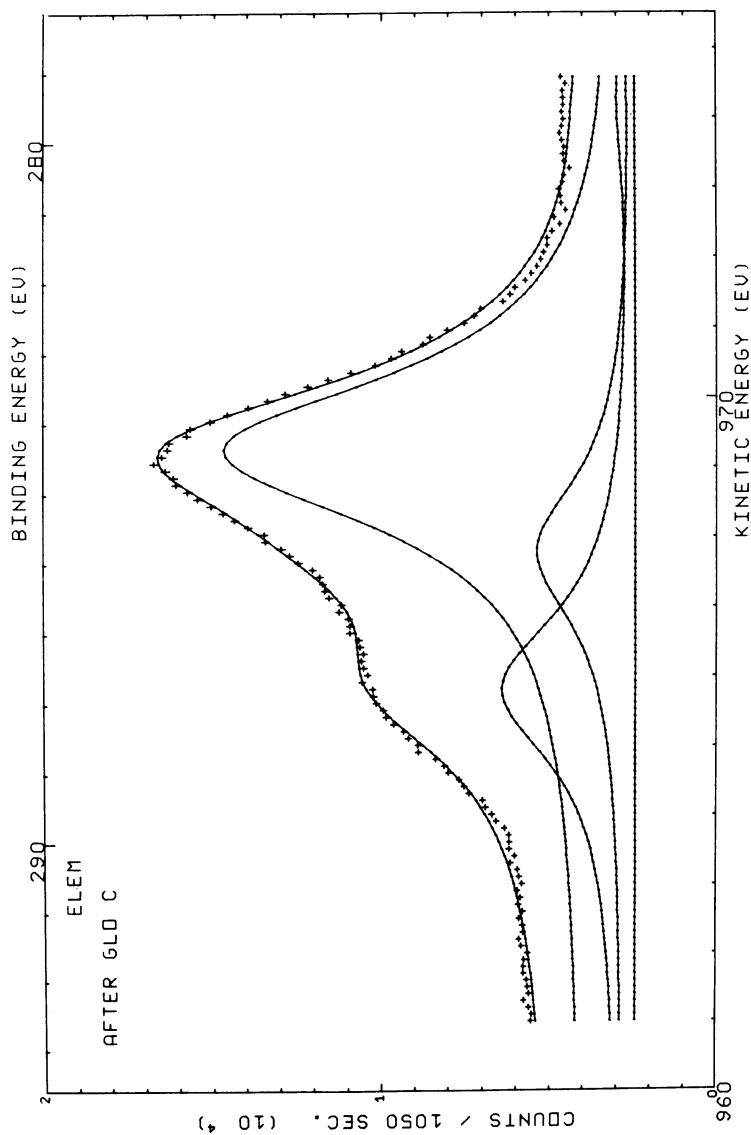


Figure 14b. Carbon 1s spectra from wool fibers oxidized beyond the excitation region. (Reproduced, with permission, from Ref. 44. Copyright 1977, Academic Press.)



TABLE II.  
X-ray Photoelectron Spectral Data Obtained from Plasma-Polymerized Fluorocarbon Surfaces

Sample	C 1s Intensity		Carbon 1s B.E. eV(ratio)		FWHM (eV)	0 1s Intensity (counts/sec)
	1000 (Counts/Sec)					
1. C <sub>2</sub> F <sub>6</sub> on polypropylene	8.0	285.0 (1)	287.6 (0.402)	290.0 (0.415) 292.1 (0.648)	2.69	2,373
2. C <sub>2</sub> F <sub>6</sub> on polystyrene	7.2	285.0 (1)	287.6 (0.426)	289.8 (0.336) 292.1 (0.508)	2.72	3,730
3. C <sub>2</sub> F <sub>6</sub> on wool 31C	4.779	285.0 (1)	286.0 (0.37)	288.3 (0.22) 290.1 (0.105)	2.26	7,230
4. C <sub>2</sub> F <sub>6</sub> on wool 31B	4.124	285.0 (1)	286.4 (2.5)	287.7 (0.0008) 289.0 (0.505)	1.7	4,467
5. C <sub>2</sub> F <sub>4</sub> on polypropylene with argon, C	18.231	285.0 (1)	287.2 (2.2)	289.3 (1.42) 291.6 (2.62) 293.5 (1.41)	2.66	4,905
6. C <sub>2</sub> F <sub>4</sub> on wool 30B	2.06	285.0 (1)	286.8 (0.85)	289.7 (0.40) 291.0 (0.6)	3.19	1,580

Sample	F 1s		FWHM (eV)	Surface atom ratio
	Total intensity (counts/sec)	Corrected intensity (counts/sec)		
1.	3,660	7,000	2.8	16.6 F/O
2.	6,830	13,600	2.67	7 F/O
3.		27.2	2.6	2 F/O
4.	7,240	13,900	2.6	0.35 F/O

2.6 eV. The oxygen and nitrogen spectra were deconvoluted into two components. The result of plasma treatment was to increase the relative intensity of the lower binding energy line in each case. The higher binding energy oxygen line was in the region normally reported for oxygen bound to carbon and sulfur while the lower binding energy line is in the region reported for oxides and may represent reduced oxygen species containing a negative charge. The two nitrogen 1s lines differed by 1.6 to 1.9 eV for the various plasma treatments. The unique structural interpretation for these two lines is difficult due to uncertainty in the interpretation of simple protein spectra. Possibilities include polypeptide chain nitrogen and side chain nitrogen and protonated basic nitrogen groups and the unprotonated group. The oxygen and nitrogen spectra were fitted with gaussian functions with an exponential tail. Full width at half maximum was set at 2.6 eV for oxygen and 2.4 eV for nitrogen. Examples of deconvoluted oxygen and nitrogen spectra from oxygen plasma treated wool fiber as well as untreated control are shown in Figures 15 and 16. Parameters derived from the various spectra are included in Table III.

Table III

Carbon 1s Electron Line Parameters  
Spectra From Plasma Treated Wool Fiber

Sample	Binding energy (eV)	Relative line area	Shift in (eV)
Untreated Wool fiber	285.0	1.0	0.0
	286.07	0.092	1.07
	287.77	0.043	2.77
Nitrogen plasma treated wool fiber	285.0	1.0	0.0
	286.43	0.28	1.43
	288.46	0.31	3.46
Afterglow plasma treated wool fiber	285.0	1.0	0.0
	286.56	0.24	1.56
	288.42	0.33	3.4
Oxygen plasma treated wool fiber	285.0	1.0	0.0
	286.55	0.23	1.55
	289.04	0.45	4.04

Table III (Continued)  
 Oxygen 1s Electron Line Parameters  
 Spectra From Plasma Treated Wool Fiber

Sample	Binding energy (eV)	Relative line area	Shift in (eV)
Untreated Wool fiber	530.4	1.0	0.0
	532.06	9.19	2.02
Nitrogen plasma treated wool fiber	530.73	1.0	0.0
	532.25	2.89	1.52
Afterglow plasma treated wool fiber	530.87	1.0	0.0
	532.41	3.1	1.53
Oxygen plasma treated wool fiber	530.61	1.0	0.0
	532.29	3.62	1.68

Nitrogen 1s Electron Line Parameters  
 Spectra From Plasma Treated Wool Fiber

Untreated Wool fiber	398.03	1.0	0.0
	399.94	8.9	1.9
Nitrogen plasma treated wool fiber	398.6	1.0	0.0
	400.3	3.0	1.67
Oxygen plasma treated wool fiber	398.95	1.0	0.0
	400.54	2.74	1.59

The electron spectra discussed were taken on woven pieces or fibers attached to double backed tape in a manner such that minimal tape was exposed. The effect of surface uniformity and density was investigated by comparing the spectra taken from wool fibers and from wool fibers compressed into thin continuous transparent films. Wool fiber or woven textile can be pressed into thin transparent films by applying pressure to moist samples between heated plates in a hydraulic press (45).

The nitrogen and sulfur electron spectra obtained from individual fibers attached to double backed tape and pressed into a film are shown in Figure 17. The electron line intensities of the spectra obtained from these two samples are given in Table IV. In general, the electron lines from the smooth dense film were three times as intense and thirty percent narrower than the electron lines obtained from fibers. The position of the lines were identical.

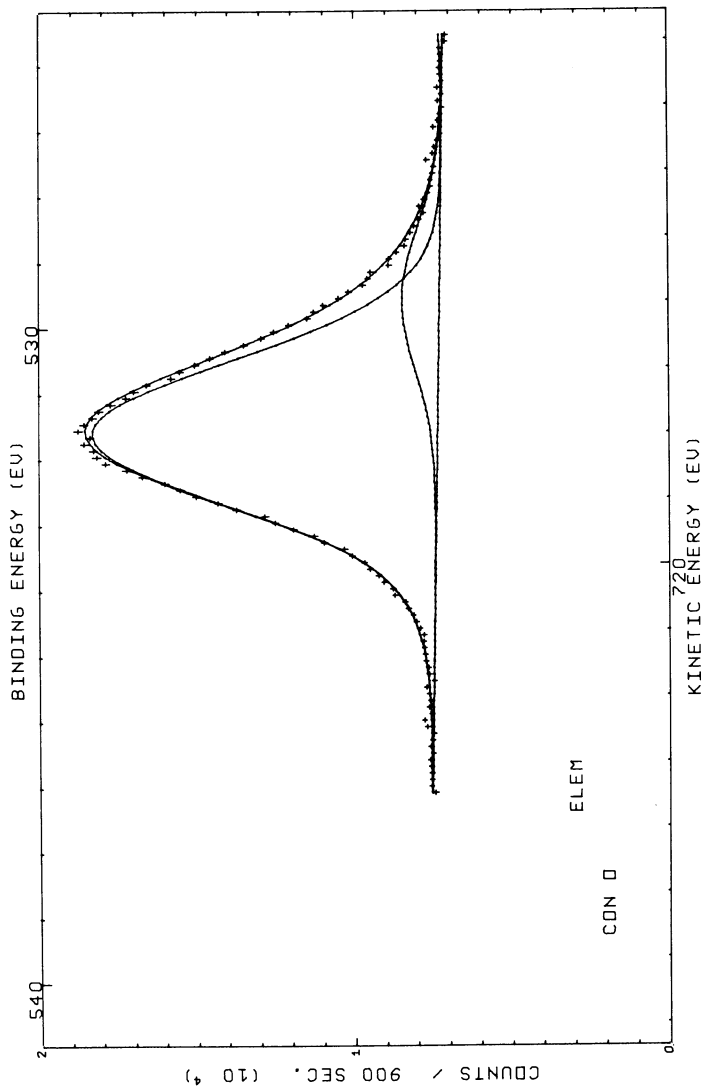


Figure 15. Oxygen 1s spectra from control and oxygen plasma treated wool fabric. (Reproduced, with permission, from Ref. 44. Copyright 1977, Academic Press.)

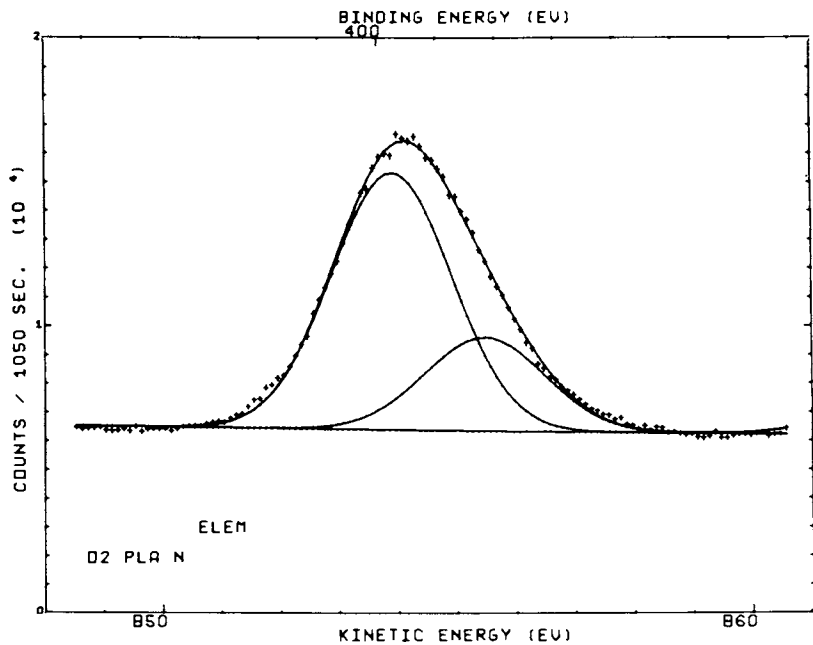


Figure 16a. Nitrogen 1s spectra from control and oxygen plasma treated wool yarn. (Reproduced, with permission, from Ref. 44. Copyright 1977, Academic Press.)

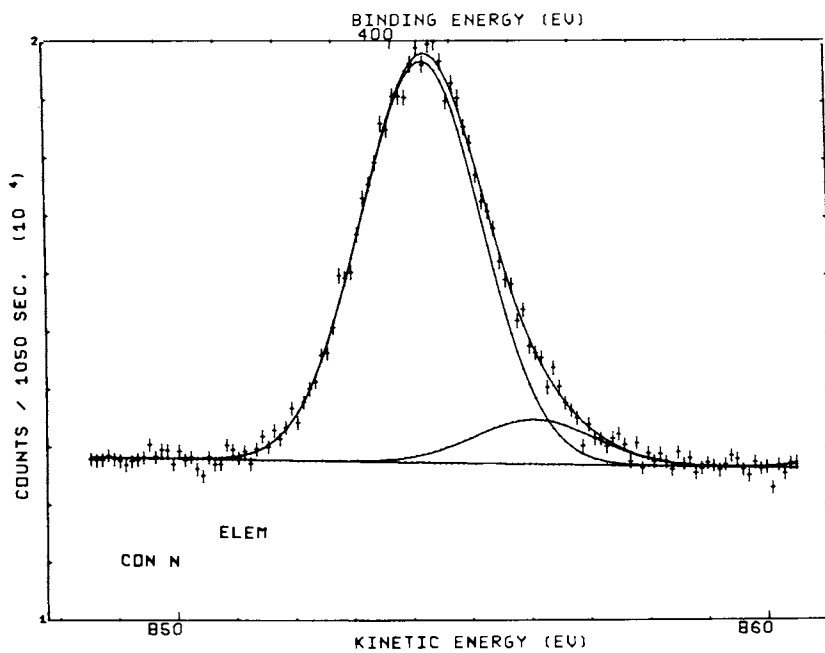


Figure 16b. Nitrogen 1s spectra from control and oxygen plasma treated wool yarn. (Reproduced, with permission, from Ref. 44. Copyright 1977, Academic Press.)

TABLE IV

Electron Line Intensities from Isolated Wool Top Fibers and Thin Transparent Film Pressed from Wool Fibers

Sample	Electron line intensities ( $10^3$ cps)			
	C 1s	O 1s	N 1s	S 2p
Unoxidized wool top fibers	30.6	12	5	1.4
Unoxidized wool top fibers pressed into a thin film	100	36.6	15.5	3.2

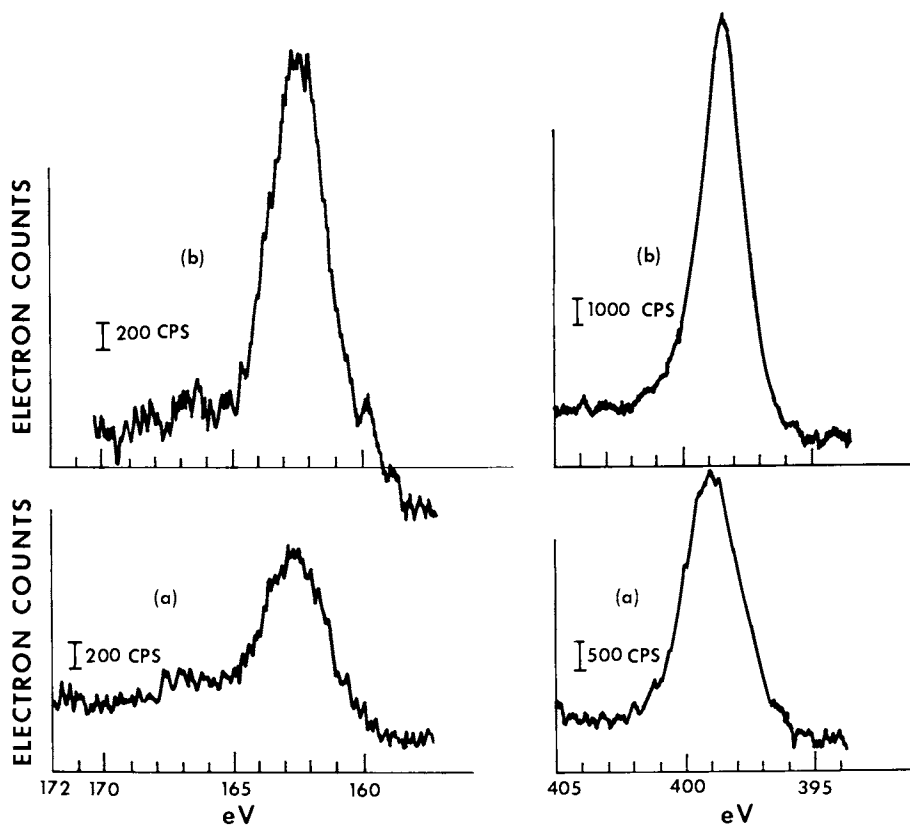


Figure 17. Electron lines from wool fibers (a) and wool film (b).

Chemical Modifications of Surface Functional Groups with Elements Having High Photoelectric Cross Sections

The surface sensitivity of XPS can be enhanced by chemically modifying surface functional groups with reagents that contain elements with higher detection sensitivity. If the derivation reaction is quantitative or reproducible, the enhanced surface signal can be used to determine the surface concentration of functional groups not normally detectable due to lack of sufficient binding energy shift or low sensitivity (46).

We explored the detection and quantification of specific functional groups in proteins using quantitative specific chemical modifications that contain elements with high detection sensitivity. Fluorine was introduced specifically into Bovine Serum Albumin (BSA) by N-trifluoroacetylation of the  $\epsilon$ -amino group of lysine using ethyl thiotrifluoroacetate (47). The fluorine electron spectrum from N-trifluoroacetylated BSA is shown in Figure 18.

Wool fiber surfaces could be efficiently trifluoroacetylated using this reagent and spectra obtained from wool fibers modified in this way is shown in Figure 19. Ethyl vinyl sulfone was also used to derivatize lysine in casein and BSA (48). The active hydrogen in lysine will add across the double bond resulting in the introduction of the sulfone group into the protein. The protein contains no sulfur line higher in binding energy than 163 eV and the sulfone sulfur line is readily identifiable. The sulfur 2p spectrum from ethyl vinyl sulfone (EVS) modified casein is shown in Figure 20. A series of spectra obtained from EVS modified BSA is shown in Figure 21. Initially only a low binding energy line is present in BSA and as the level of sulfone modification increases the intensity of the higher binding energy line increases. These spectra were obtained by rapidly scanning the S 2p region at low anode intensity due to the rapid loss of the sulfone line in the spectra as a result of radiation exposure in the instrument. A series of spectra obtained as a function of time of X-ray exposure in the instrument revealed the intensity of the sulfone sulfur rapidly decreases with time. This example illustrates the potential of XPS to detect and study radiation sensitive materials (48).

The sulfhydryl group in papain was modified using mercury containing reagents and the spectrum in the mercury region is illustrated in Figure 22a obtained from mercury papain. The spectrum obtained from PCMB modified ovalbumin is shown in Figure 22b. The mercury 4f electron line can be detected in fairly low concentration and is an interesting case of detection of specifically chemically modified functional groups. These principals can be applied to study and estimate the presence of functional groups on the surface of a variety of materials that would not normally be detectable.



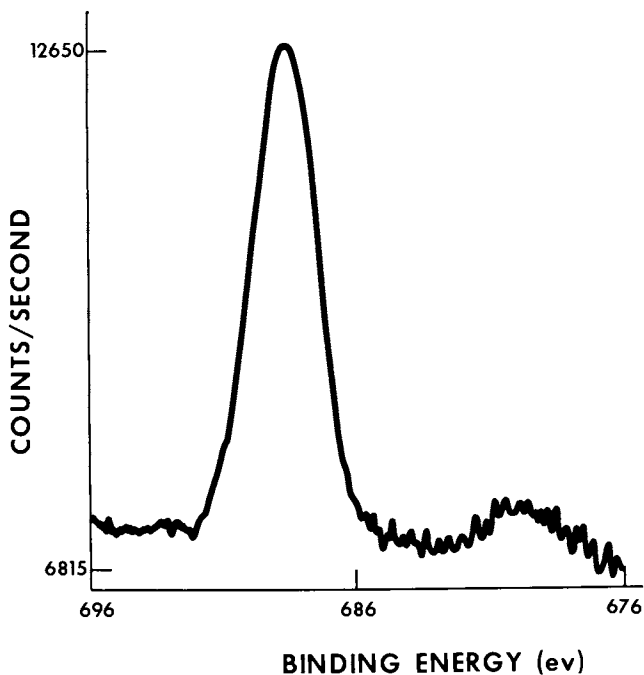


Figure 18. Fluorine 1s spectrum from bovine serum albumin trifluoroacetylated with ethyl thiotrifluoroacetate. (Reproduced from Ref. 47. Copyright 1974, American Chemical Society.)

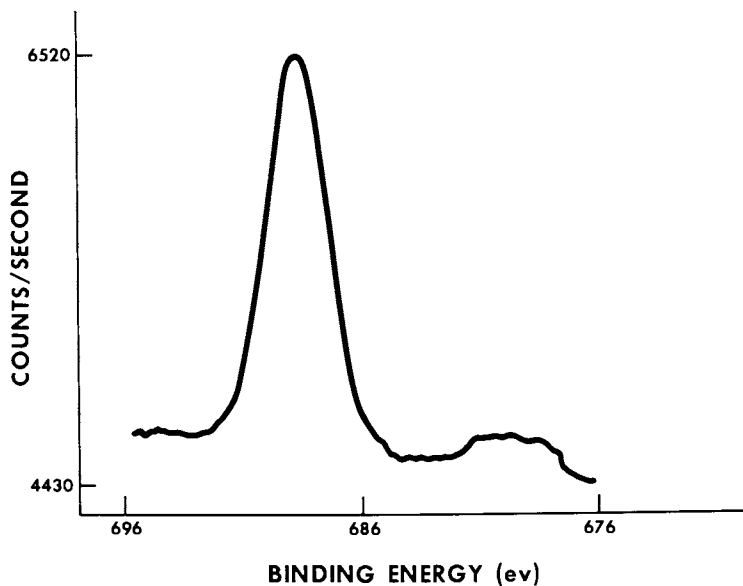


Figure 19. Fluorine 1s spectrum of wool trifluoroacetylated with ethyl thiotrifluoroacetate.

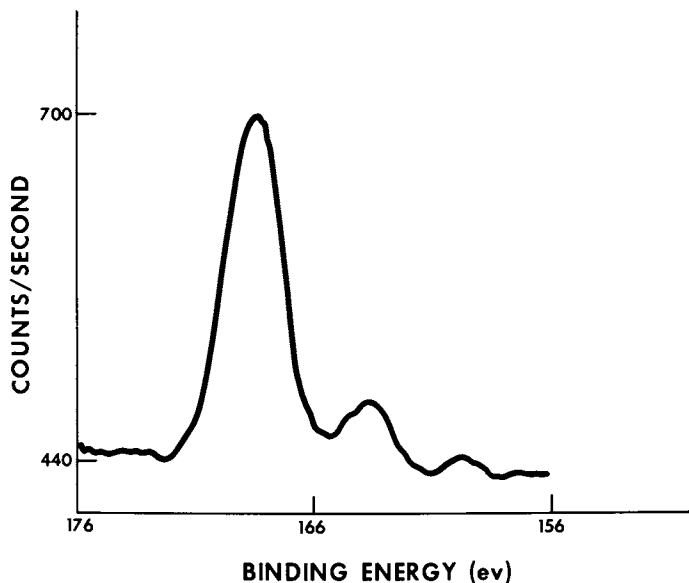


Figure 20. Sulfur 2p spectrum from casein modified with ethyl vinyl sulfone. (Reproduced, with permission, from Ref. 48. Copyright 1976, North-Holland Publishing Co.)

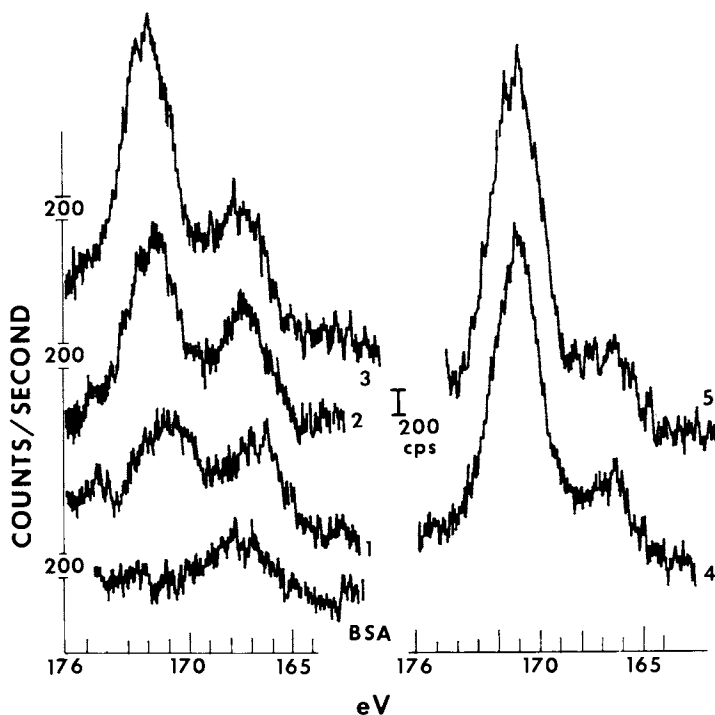


Figure 21. Sulfur 2p spectra contained from a series of ethyl vinyl sulfur modified samples of BSA. (Reproduced, with permission, from Ref. 48. Copyright 1976, North-Holland Publishing Co.)

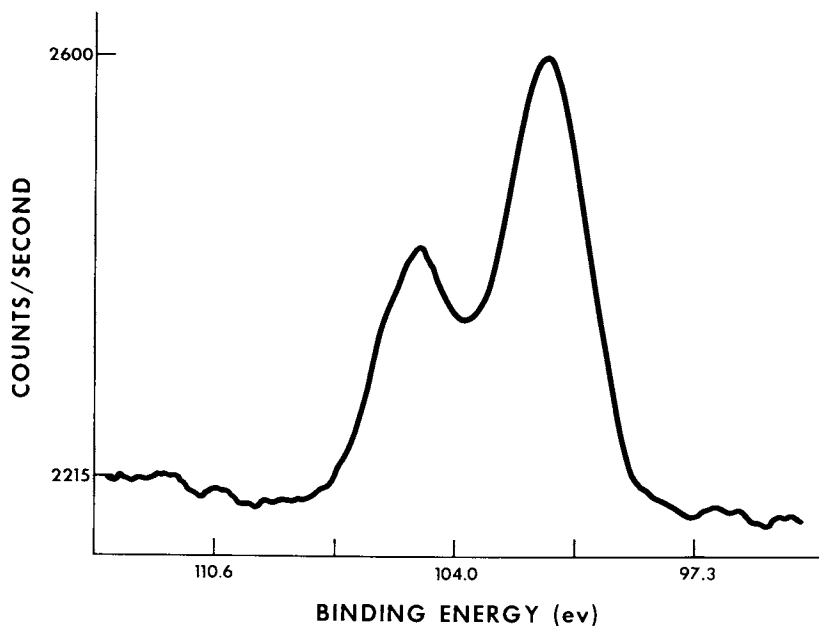


Figure 22a. Mercury 4f spectrum from mercury papain.

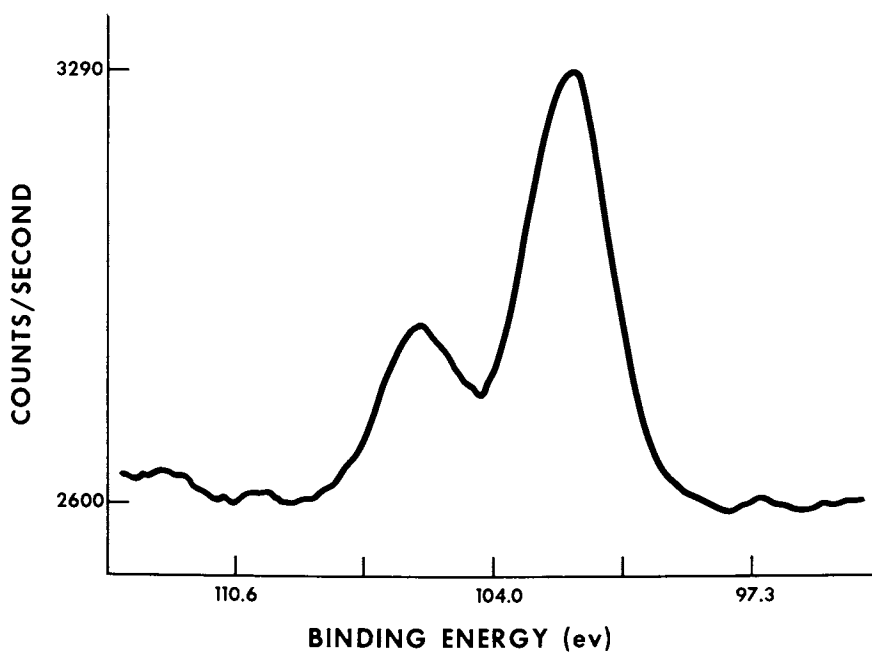


Figure 22b. Mercury 4f spectrum from PCMB modified ovalbumin.

### Examples of Recent Materials Science Applications of XPS

XPS is particularly suited to analyze solid materials in various materials science applications of polymeric materials. Several examples of the use of XPS to analyze the surface of solids in irregular forms such as fibers, powders, films, beads, and various extruded shapes such as o-rings will be presented. XPS can provide a rapid survey analysis as well as quantitative analysis within several percent depending on the sensitivity for the element in question. Unique structural information can often be obtained on solids that, due to their intractability and lack of solubility would present problems for investigation by other spectroscopic methods.

### Growth Regulators Encapsulated in Natural Polymers

Controlled release of various physiologically active substances into organisms or the environment has received considerable attention in recent years. Controlled release from matrices that are naturally biodegradable is desirable from a standpoint of minimizing additional contamination of the environment by materials that are degraded slowly. The analysis of various formulations of plant growth regulators in biodegradable matrices such as chitosan, feather keratin and cellulose represents an interesting example of the use of XPS for analytical and structural studies on solid materials.

A variety of approaches to controlled release of physically active substances from solid formulations has been proposed and studied. Some of these approaches are schematically diagrammed in Figure 23 where R is some active substance to be released into the environment. Chitosan was chosen as a possible material to encapsulate plant growth regulators as many regulators are organic acids and chitosan is readily available from chitin and has an amino group that would be a site for acid base or ion exchange type entrapment. The structural formula of chitin and the deacetylated product chitosan is represented in Figure 24. Chitosan can be dissolved in acids and can be crosslinked with gluteraldehyde as well (49). We equilibrated crosslinked chitosan with various organic acid type growth regulators containing chlorine such as 2,4-D and p-chlorophenoxy acetic acid. A wide scan spectrum of gluteraldehyde crosslinked chitosan in the form of granules is presented in Figure 25. The inset contains accumulated scans over the N 1s and Cl 2p region. The N 1s spectrum has a line around 399 eV due to the neutral amine nitrogen with a shoulder at the higher energy side of the line due to some protonated amine groups. The chlorine line is due to the chloride ion resulting from some neutralization of the amine by HCl. Figure 26 contains accumulated spectra over these regions for chitosan equilibrated with 2,4 D. The nitrogen spectra contains a low binding energy

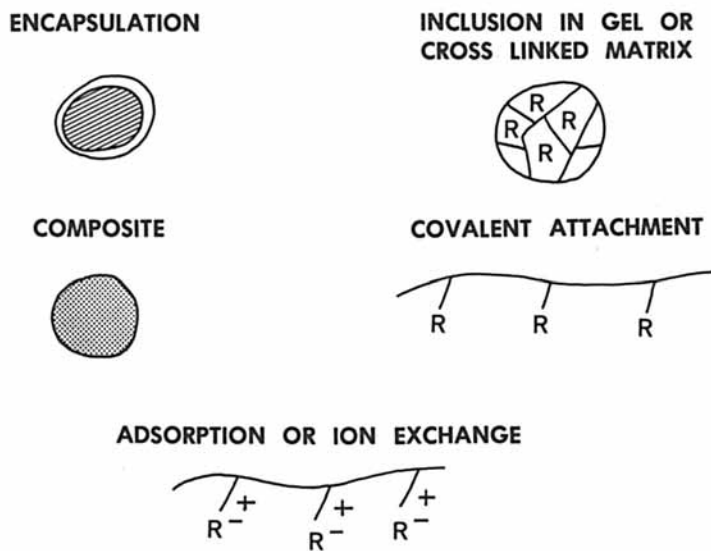


Figure 23. Scheme of biodegradable controlled release approaches.

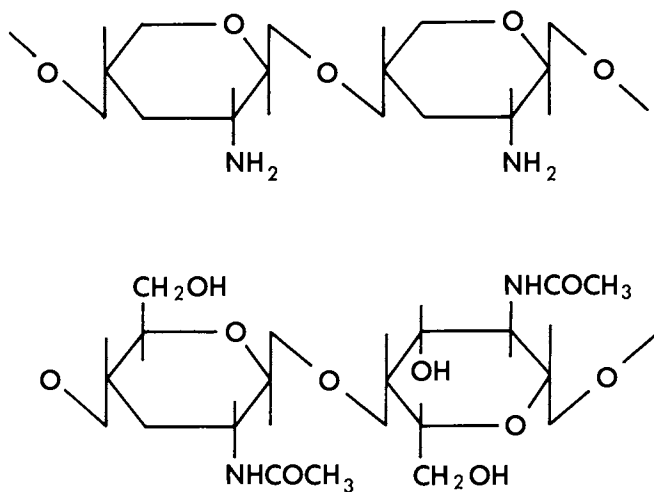


Figure 24. Structure of chitosan (top) and chitin (bottom).

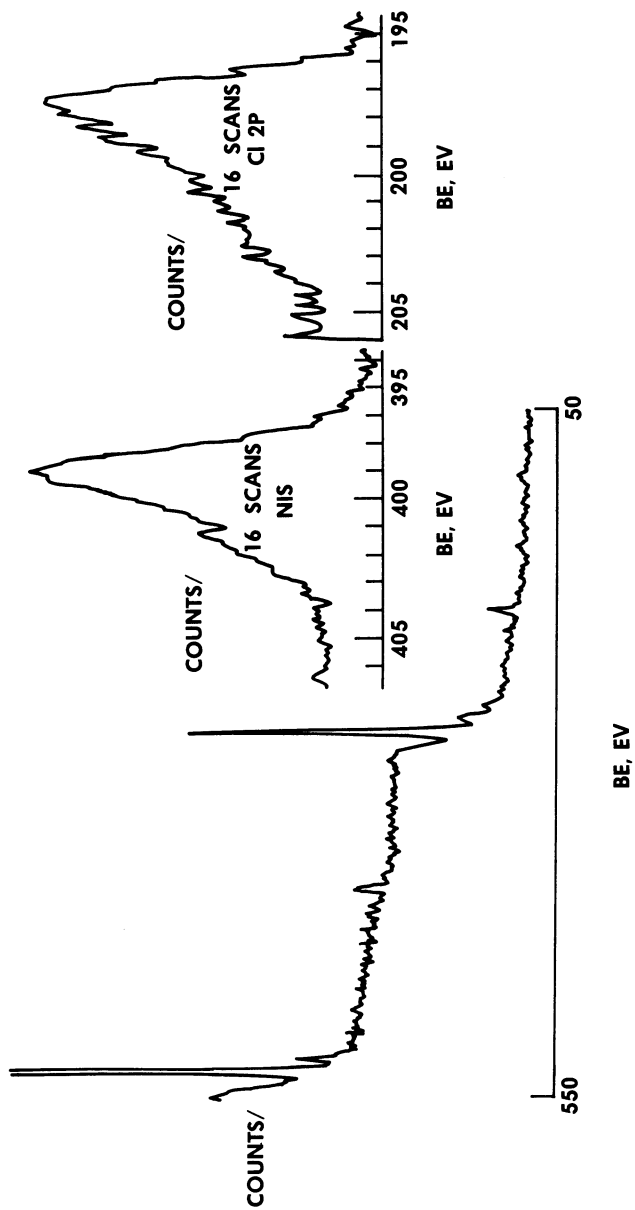


Figure 25. Electron spectra from glutaraldehyde cross-linked chitosan.

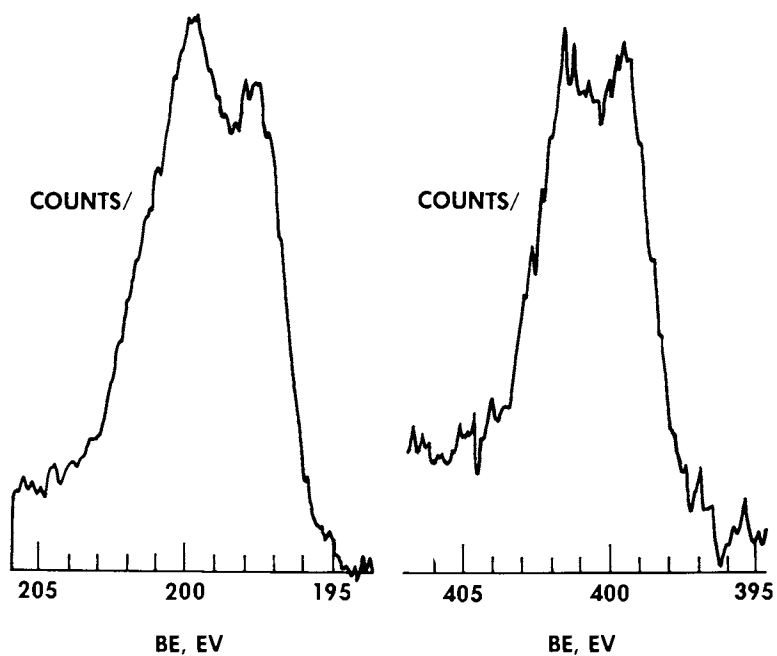


Figure 26. Chlorine 2p and nitrogen 1s region from 2,4-D in chitosan.

line  $\nu$  399 due to free amine and a higher binding energy line at  $\nu$  401 due to the protonated amine group. The chlorine 2p spectrum contains two unresolved chlorine lines, one presumably due to the chloride ion present in the matrix as well as chlorine covalently bound to carbon from the 2,4-D. Spectra obtained from granules of chitosan containing p-chlorophenoxyacetic acid is shown in Figure 27. The higher binding energy nitrogen line predominates due to protonated amine and the chlorine 2p region contains two unresolved lines due to ionic and covalent chlorine. The presence of 2,3,5-triiodobenzoic acid in chitosan could be readily detected due to a strong line due to iodine.

Feather keratin was an interesting material that lended itself to controlled release formulations. Feather keratin can be solubilized by solution into boiling ethanol in the presence of bisulfite to reduce the disulfide linkage. Varying amounts of the growth regulator is added at this stage and the solution allowed to cool to a gel. This gel can be pressed into a film at 100° C and 20,000 lbs per square inch. This process partially reforms disulfide crosslinks resulting in a crosslinked matrix with entrapped growth regulator. Electron spectra obtained from feather keratin films containing 2,4-D is shown in Figure 28. A survey scan indicates the presence of chlorine and individual accumulated scans indicate the presence of organic covalently bound chlorine due to the presence of 2,4-D. Growth regulators containing functional groups capable of complexing or interacting with metal halides were attached to cellulose by a procedure involving bridging by metal halides such as  $TiCl_4$  (50). Cellulose powder was treated with  $TiCl_4$  in an indifferent solvent complexing the  $TiCl_4$  to the cellulose. The electron spectrum obtained from the  $TiCl_4$  cellulose complex is shown in Figure 29. A wide scan spectrum reveals the presence of the titanium 2p lines as well as chlorine 2p lines. Indole acetic acid was added to the cellulose  $TiCl_4$  complex and the spectrum obtained from the cellulose  $TiCl_4$  indoleacetic acid complex is shown in Figure 30. In addition to lines present before, the nitrogen 1s line indicates the presence of indoleacetic acid. The titanium presumably acts as a bridge complexing the nitrogen and oxygen from cellulose to attach the indoleacetic acid to cellulose.

### Siloxane Urethane Interpenetrating Network

There has been considerable recent interest in the determination by XPS of the surface composition of co-polymers whose components differ considerably in their surface free energy (51). When the individual components of block co-polymers or interpenetrating networks can be detected and individually identified by XPS, a fairly rapid co-polymer composition determination is possible as well as the determination of the composition of



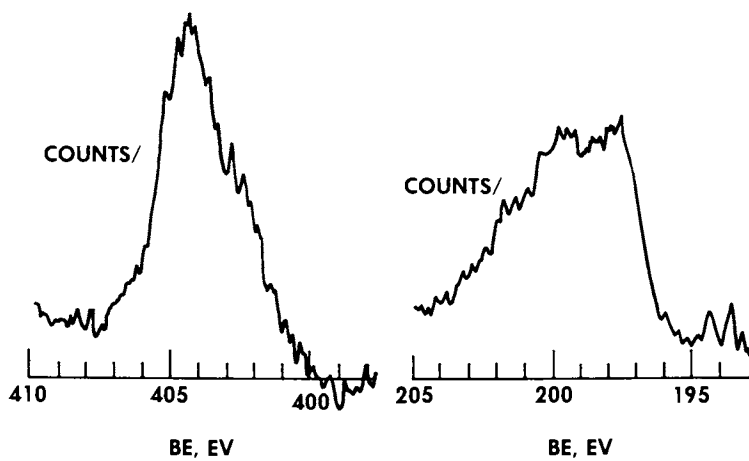


Figure 27. Nitrogen 1s spectrum and chlorine 2p spectrum from p-chlorophenoxy-acetic acid in chitosan.

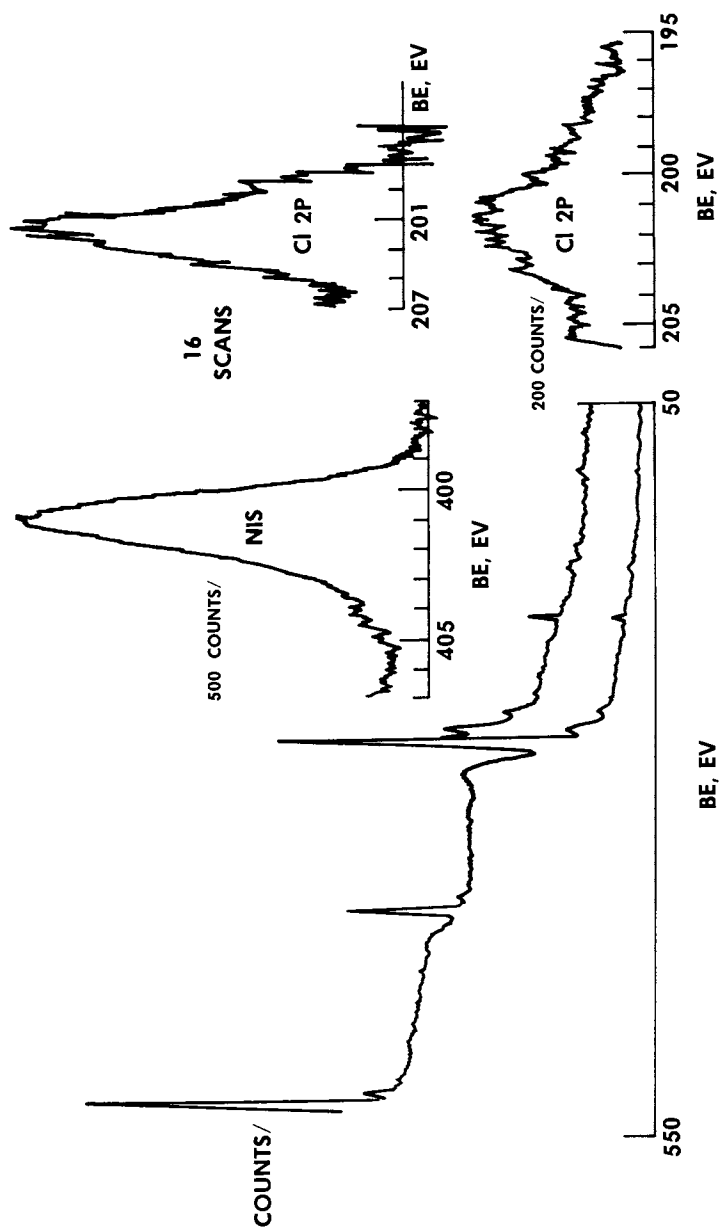


Figure 28. Electron spectra from 2,4-D entrapped in feather keratin.

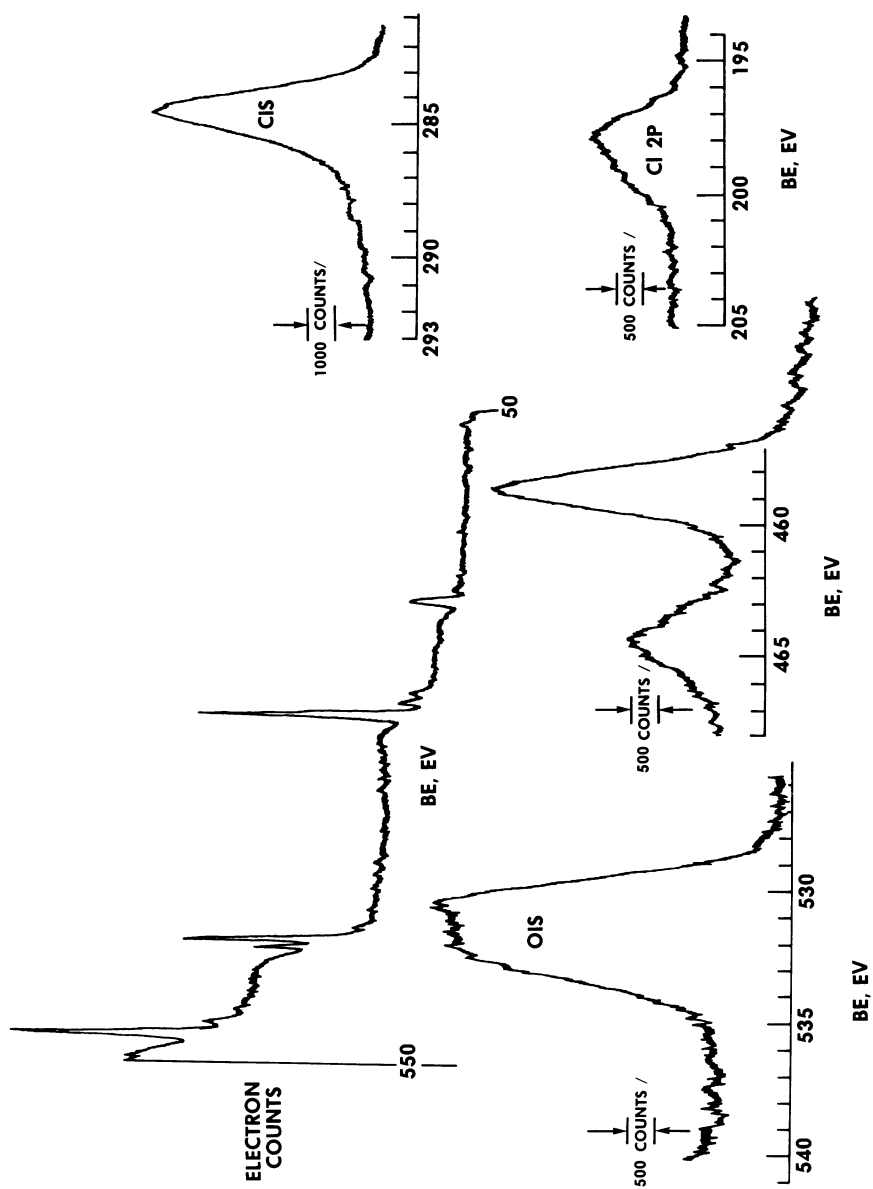


Figure 29. Electron spectra from cellulose powder treated with  $\text{TiCl}_4$ .

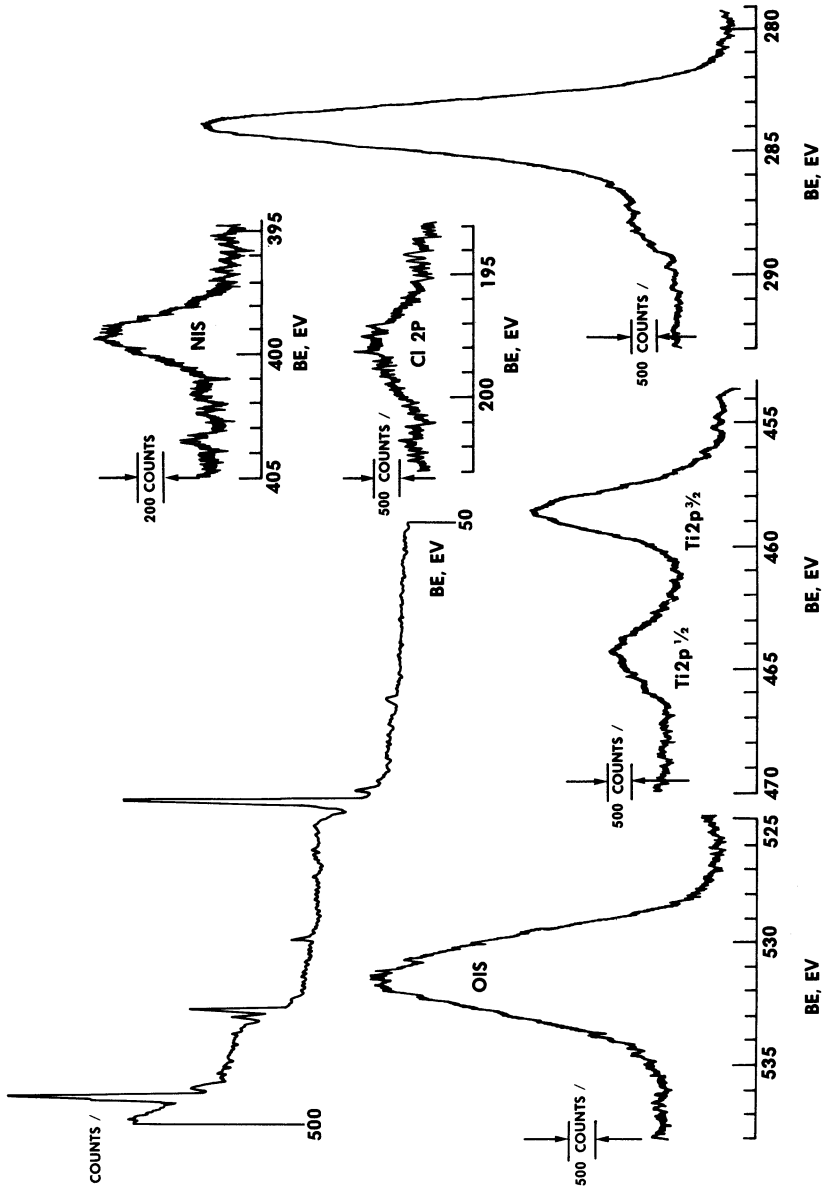


Figure 30. Electron spectra from TiCl<sub>4</sub> bridged indoleacetic acid complex anchored to cellulose.

the copolymer system at various interfaces and throughout the bulk.

An investigation of the composition of a urethane fluoroalkyl siloxane interpenetrating network illustrates these possibilities (52). A fluoroalkyl siloxane of modest degree of polymerization was obtained by hydrolysis under mild conditions of 3-(heptafluoroisopropoxy)propyltrichlorosilane  $[(CF_3)_2CFO(CH_2)_3SiCl_3]$ . A commercially available urethane such as Adiprene L315 described as a fully saturated liquid polymer with  $9.45 \pm 0.20$  available isocyanate and the fluoroalkyl siloxane described above were combined in equal proportions by weight in the presence of 1,4-diaza(2,2,2)bicyclooctane (Pabco) and dibutyltindilaurate in catalytic amounts and allowed to stand for one week. A solid insoluble rubber-like material cream in color resulted after this period of time. The polymer was extracted with toluene and Freon 113 for eight hours. Toluene was a solvent for the urethane and Freon 113 for the siloxane prior to treatment with the catalyst. A 12% weight loss resulted after this extraction. This solid interpenetrating network polymer was analyzed by XPS using thin sections obtained from various locations in the polymer sample including the air and reaction flask interface. The spectrum taken from the sample is illustrated in Figure 31. A nitrogen 1s line characteristic of the urethane and the fluorine 1s, silicon 2p and C 1s lines are all characteristic of the fluoroalkylsiloxane. The composition of the samples obtained from locations throughout the polymer is given in Table V. The analysis was calculated by correcting the electron line intensities using Wagner's sensitivity factors and summing the corrected intensities. Elemental composition was calculated by dividing each elemental electron line intensity by the sum of all electron line intensities. Several samples were analyzed for fluorine by combustion analysis and the fluorine content so determined agreed with that calculated by XPS measurements within less than 5%. The variation in composition was considerable in going from the air interface at the top to the glass interface at the bottom. The silicon content varied between 5.3 and 6.7%. The fluorine content varied between 34.5 and 25.3% while the nitrogen content varied between 1.2% and a trace.

#### Penetration of a Vacuum Pump Fluid Into O-Ring Seals

The next surface analysis example has to do with the question of penetration of a vacuum pump fluid into O-ring seals (53). A Buna-N O-ring was operated in the presence of Fomblin vacuum pump fluid. The point of interest was to find if the pump fluid had penetrated to O-ring material. A Buna-N O-ring was operated in the presence of hydrocarbon non fluorinated fluid and the spectrum obtained from the surface of this O-ring is shown in figure 32. Electron lines from fluorine and silicon are present and are probably due to a fluorosiloxane lubricant

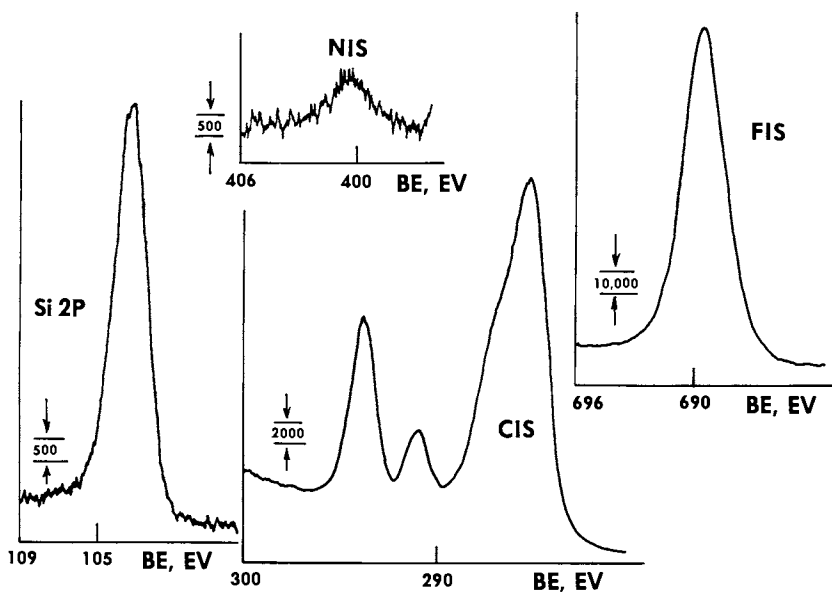


Figure 31. Electron spectra from fluoroalkylsiloxane urethane interpenetrating network.

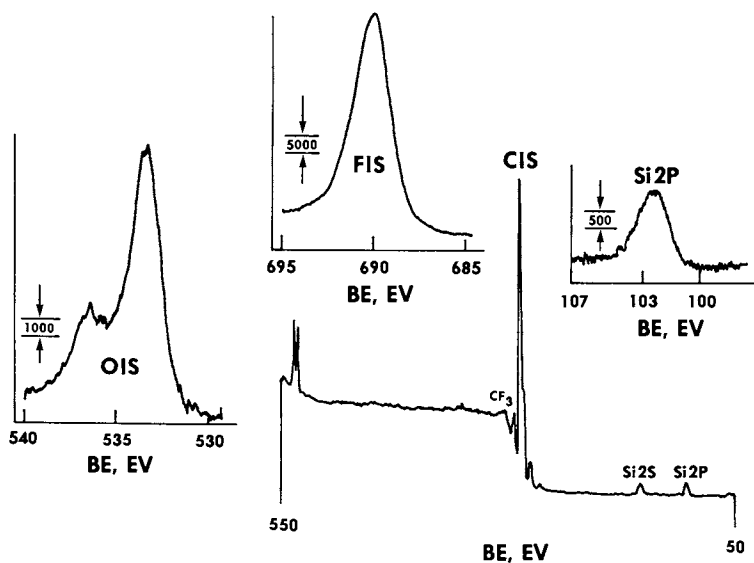
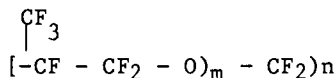


Figure 32. Electron spectra from buna-N seal exposed to hydrocarbon fluid.

TABLE V  
Composition of Siloxane Urethane Interpenetrating Network from  
 Various Regions of the Sample

Sample	Corrected Intensities and Percentages in parentheses				
	Si 2p	F 1s	O 1s	C 1s	N 1s
Fluorosiloxane polymer	48.8(6.24)	300(38.4)	135.0(17.2)	298.5(38.1)	
Adiprene L315 urthane			33.2(28)	77.4(65.4)	7.76(6.55)
Air Interface	25.7(6.7)	120(31.5)	70.0(18.4)	165.0(43.3)	trace
Below Air Interface	15.9(6.5)	85(34.6)	43.8(17.9)	100.0(40.7)	0.95(.4)
Center Cut	13.6(64)	73.5(34.5)	38.4(18)	86.5(40.6)	0.95(.45)
Near Glass Interface	13.6(5.27)	81(31.4)	62.3(24.1)	100.0(38.7)	1.2(.46)
Glass Interface	38.2(5.34)	181(25.3)	186.0(26)	307.0(43)	2.97(.41)

occurs at about 533.1 eV. Figure 33 illustrates the electron spectra taken from the Buna-N O-ring operated in the presence of Fomblin. Fomblin is a fluorocarbon ether with the following formula:



In addition to fluorine and electron lines due to carbon bonded to three and two fluorine atoms, an intense oxygen electron line at 535.1 eV is present. This is higher than the values reported for oxygen in non-fluorinated organic compounds but is in the range plausible for a fluorocarbon ether where oxygen is bonded to carbon with electron withdrawing fluorine groups attached. This fluorocarbon ether oxygen identifies the material present on the surface as Fomblin and indicates that this fluid has penetrated to the extent of at least 10 nm into the surface.

#### Sulfonation of 8% Crosslinked Styrene Divinylbenzene Copolymer Beads

The extent of sulfonation of 8% crosslinked styrene divinylbenzene co-polymer beads (Biorad Bio Bead SX 8) was investigated by comparing the surface composition after sulfonation of the beads using chlorosulfonic acid, sulfuric acid and fuming sulfuric (54). Each reagent was refluxed in methylene chloride for a similar period of time. A wide-scan spectrum indicates the presence of sulfur 2p and 2s electrons, indicative of sulfonation. The surface sulfur content was fairly similar in the surface region analyzed by XPS. The composition determined from beads sulfonated by the three methods is indicated in Table VI.

Electron spectra taken from a sample of beads sulfonated in sulfuric acid is illustrated in Figure 34. The sulfur 2p line is fairly intense and more than adequate for analytical purposes. Another feature of interest was the determination of the barium ion to sulfur atom ratio in the resins when they were converted to the barium ion form. A single scan over the barium 3s region is shown in Figure 34 for a sample in the hydrogen ion form and after conversion to the barium ion form. The sulfur to barium ratio varied between 1.3 to 2.4 for a number of samples analyzed indicating considerable variation in the extent of sharing barium ions among the sulfur atoms.

The distribution of sulfate groups on the surface and into the interior of beads sulfonated under conditions to yield surface modification and surface plus interior modification was investigated by oxygen plasma etching (OPE)(55) of beads that were sulfonated in refluxing sulfuric and in cold sulfuric for the same time interval. The cold sulfonation yielded beads sulfonated so minimally that the sulfate group could not be detected by titration while the capacity of the beads sulfonated hot could be titrated as usual. The beads sulfonated cold are labelled surface while the other are labelled normal. The



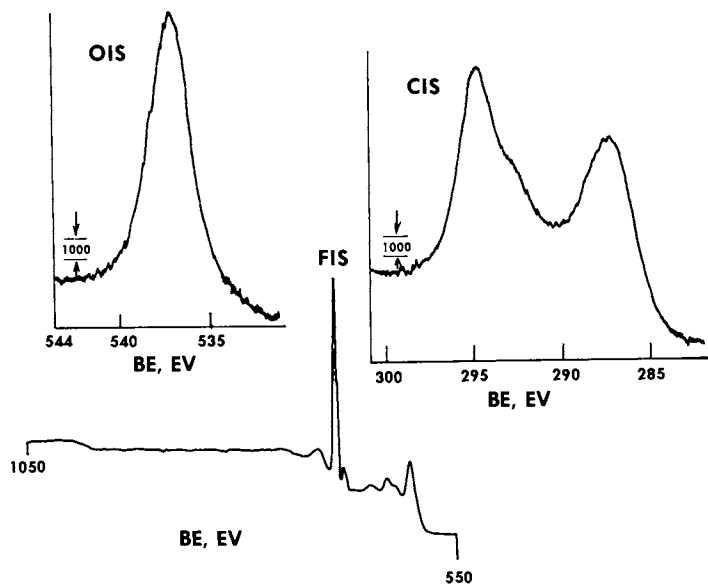


Figure 33. Electron spectra from buna-N seal exposed to the fluorocarbon ether fomblin.

TABLE VI

Corrected Intensities and Composition Calculated for Sulfonated Styrene Divinylbenzene Crosslinked Beads

	C 1s	O 1s	S 2p
Chlorosulfonic* acid	42.6	12.5	3.5
%	76.6	21.3	5.9
Fuming Sulfuric acid	42.6	14.4	3.5
%	70.0	24.0	5.7
Sulfuric acid	44.4	12.5	3.0
%	74.0	20.8	5.0

\*Intensity in 1000 counts/sec.

intensity of the barium and sulfur electron lines were more intense by a factor of 4 for the normal compared to the surface sulfonated. The surface sulfur-to-barium rate was 2.1 for the surface compared to 1.6 for the normal. The distribution of the sulfur and barium into the interior of the beads was determined by oxygen plasma etching the beads for varying periods of time and determination of the surface composition after etching by XPS. Under the etching conditions used, the rate of etching into the interior of polystyrene spheres has been determined to be  $\sim 10.0$  nm per minute. When a coating is present only on the surface, the concentration of the elements in the coating slowly decreases as the surface is oxidized away. The elements forming nonvolatile oxides remain as an ash on the surface and become diluted as etching proceeds. If the modification penetrates into the interior, the concentration of the elements in the coating increases until the unmodified interior material is reacted.

This behavior is illustrated by the data shown in Table VII. The intensity of the barium and sulfur lines decreases with OPE while the intensities of these elemental lines increases up to fifteen minute etching and then begins to decrease in the case of surface sulfonation. This further substantiates the external surface nature of the mild sulfonation as compared to the presence of sulfonic acid sites much deeper into the interior of the bead in the case of sulfonation under more vigorous conditions.

The surface electron lines as a function of etch time are illustrated in Figure 35 for the two sets of samples.

#### Wood Surface Treatment

An XPS study of the oxidative surface treatment of white pine represents an interesting example of the ability of the technique to obtain surface structural information on a sample that would present problems for many analytical methods (56). A survey and carbon 1s spectrum from untreated white pine is shown in Figure 36. Survey spectra and chlorine 2p as well as carbon 1s spectra are shown in Figure 37 taken from white pine treated with hydrogen peroxide, HCL, and acetic acid with heating. This oxidative treatment has oxidized carbon as evidenced by shoulders in the C 1s spectra at higher binding energies and introduced carbon chlorine bonds on the surface as evidenced by the chlorine 2p line around 200 eV.

#### Polymer Anchored Catalysts

The determination of structure and bonding of polymer anchored catalysts is another area where the insolubility of the materials often precludes solution spectroscopic studies and one is limited to techniques that can be applied to irregular solids (57). In addition, combining oxygen plasma etching and surface analysis allows investigation of the depth of penetration of the metal into the polymer and allows detection of components that require concentration to allow detection.

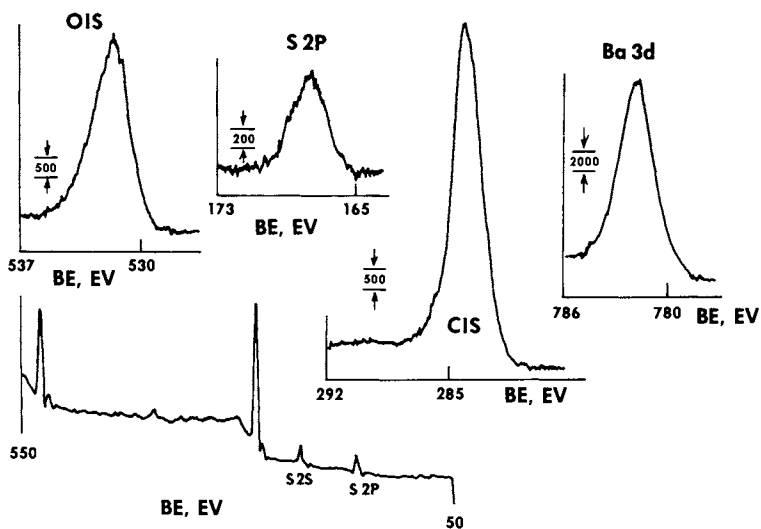


Figure 34. Electron spectra taken from sulfonated styrene divinylbenzene beads.

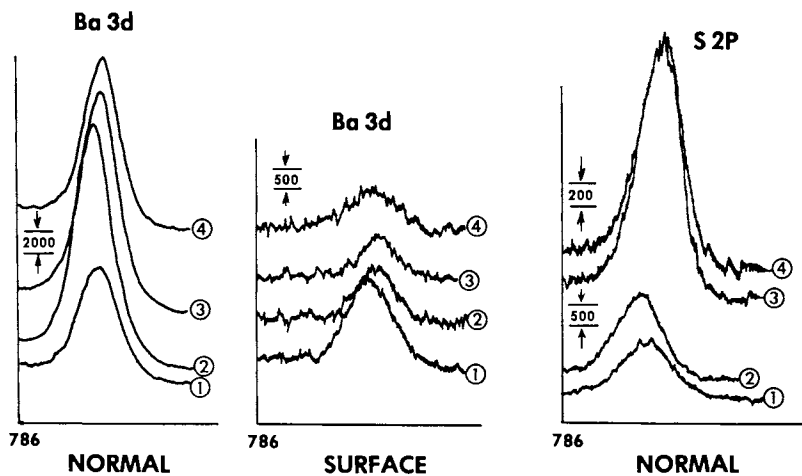


Figure 35. Electron spectra as a function of oxygen plasma etching exposure from normally sulfonated beads and surface only sulfonated beads.

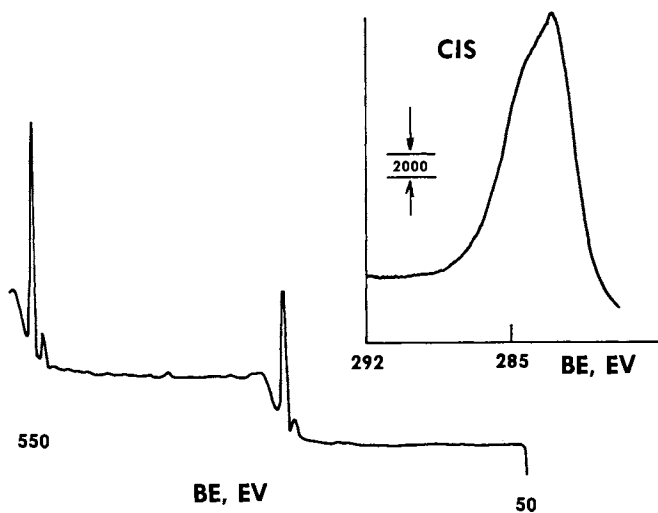


Figure 36. *Electron spectrum from untreated white pine.*

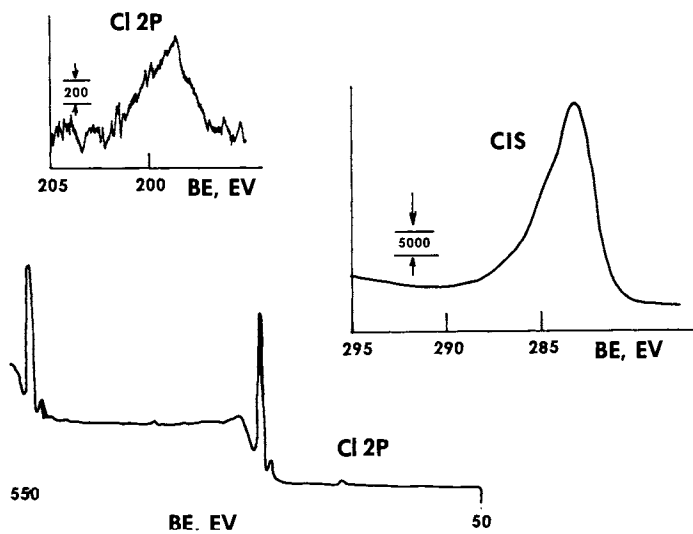


Figure 37. *Electron spectrum from surface oxidized white pine.*

TABLE VII

Intensities of Electron Lines from Surface Sulfonated and Normal Sulfonated Beads as a Function of Oxygen Plasma Etching

Etch time (min)	Ba 3s Intensity 1000 cps		Sulfur 2p Intensity 1000 cps	
	Surface	Normal	Surface	Normal
0	2.4	11.0	0.35	1.4
5	1.25	23.0	0.30	2.0
15	1.1	20.6	0.25	2.5
25	1.0	16.0	0.20	2.3

An example of such an analysis of rhodium phosphine ligand anchored catalysts is presented (58). A survey scan of a copolymer containing a diphosphine ligand prior to introduction of the metal is shown in Figure 1, spectrum h. The presence of phosphorus in the polymer is evident from this spectrum. Figure 38 illustrates accumulated surface scans in the rhodium 3d and phosphorus 2p region taken from granules of the rhodium anchored catalyst. The surface concentration is low enough that scan accumulation was necessary to detect these elements. These particles were oxygen plasma etched for thirty minutes and Figure 39 includes a survey spectrum as well as Rh 3d and P 2p spectra taken from the sample after OPE. The intensity of the rhodium and phosphorus lines is enhanced considerably as a result of etching. To investigate the depth of penetration of the anchored metal into the surface of the particles, surface spectra were obtained as a function of OPE times. This data is given in Table VIII and the phosphorus and rhodium spectra as a function of etch time in minutes is shown in Figure 40. The intensity of the rhodium and phosphorus lines increases up to twenty minutes of etching or equivalent to penetration of 160 nm into the surface of the particles. This analysis indicates that rhodium is fairly uniformly distributed into the particles at least 160 nm into the interior.

TABLE VIII

Intensities from oxygen Plasma Etched (OPE) Polymer Anchored Rhodium Catalyst Beads

OPE Etching (min.)	Rh 3d Intensity (1000 counts/sec.)	P 2p Intensity (1000 counts/sec.)
0	0.40	0.10
5	1.25	0.80
10	1.75	1.00
20	2.40	1.60

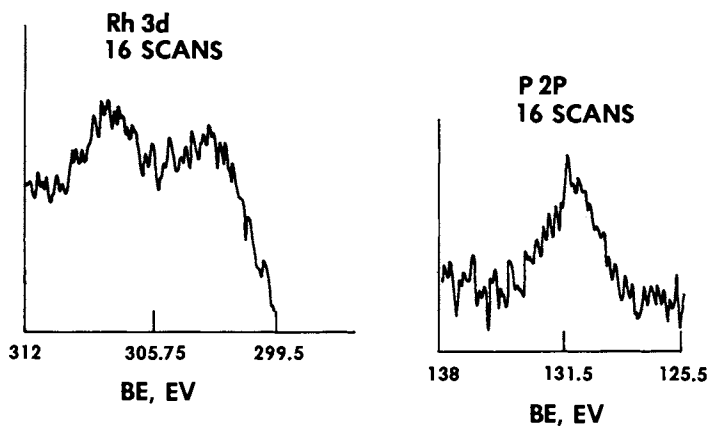


Figure 38. Accumulated surface scans from phosphine anchored rhodium catalyst.

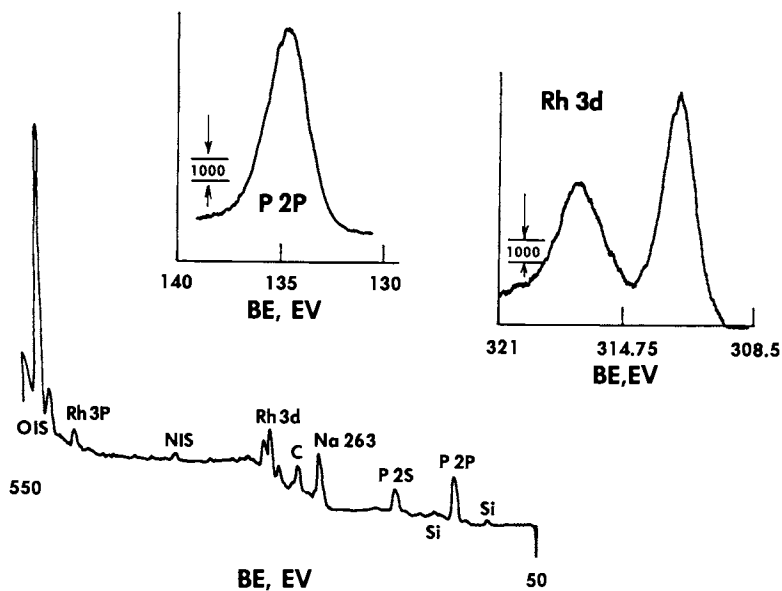


Figure 39. Electron spectrum from phosphine anchored rhodium containing catalyst after 30-min exposure to oxygen plasma etching.

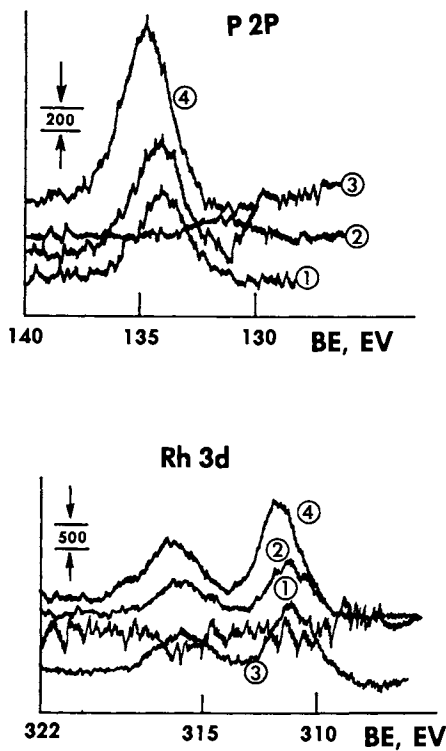


Figure 40. Electron lines from phosphine anchored catalyst as a function of oxygen plasma etching exposure.

Sulfone Polymer Radiation Chemistry

Often during the study of substances by XPS, one observes changes in the spectra such as line broadening, changes in intensity and less frequently appearance of new lines that are indicative of chemical changes as a result of radiation damage in the instrument. Initially these observations were usually considered to be annoying and various measures such as reduction of the intensity, lower temperatures or faster scan rates were taken in an attempt to obtain spectra free from radiation damage alterations. More recently, it has been recognized that XPS is a sensitive and useful technique with which to study radiation chemistry of solids (13).

Materials can be subjected to radiation treatment and these effects analyzed by XPS (59). Alternately, one can observe changes due to X-ray irradiation in XPS spectrometers and investigate structural changes accompanying this process.

Sulfones seem to be particularly susceptible to radiation damage and we observed the decrease in the intensity of the sulfone sulfur electron line during studies on proteins chemically modified with ethyl vinyl sulfone (48). This observation correlated with the known radiation chemistry of polysulfones where radiolysis leads to carbon sulfur bond cleavage and loss of  $\text{SO}_2$  (60). Sulfone polymers are used as positive resists as a result of their radiation chemistry (61). As an example of the type of observations that can be made by observing the spectra of radiation sensitive materials as a function of time of irradiation, spectra of polysulfones after various times of irradiation in a Dupont 650B are shown in Figure 41b. These spectra are novel in that initially a single line is present due to the sulfone sulfur in the S 2p region and upon irradiation in the instrument a lower binding energy line appears at 166 eV which represents one of the products of the radiation induced decomposition reaction. This line increases in intensity with time. The relative intensity of these lines observed at increasing X-ray exposure time is given in Table IX. Another more common type of behavior is illustrated in Figure 41a, spectrum a. X-ray radiation exposure of a polysulfone resulted in the decrease of the sulfone sulfur line with no other lines appearing. The decrease in intensity of this line is given as a function of radiation time in Table IX.



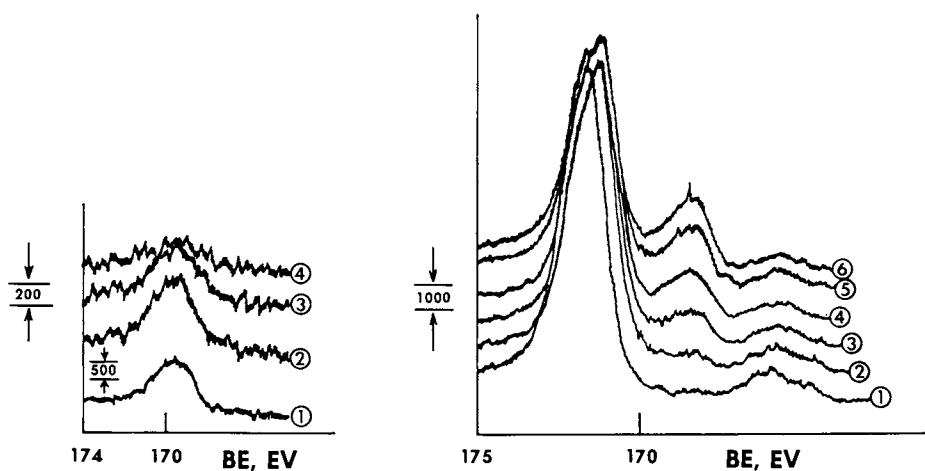


Figure 41. Sulfur 2p spectrum as a function of irradiation time of a polysulfone illustrating decrease in intensity of one line (left). Sulfur 2p spectrum of a polysulfone as a function of irradiation time illustrating the decrease in intensity of the original sulfone line and the appearance of a sulfur containing product (right).

TABLE IXSulfur Intensities as a Function of Radiation Exposure

	S 2p Intensity 168.6 eV 1000 counts/sec.	S 2p Intensity 166 eV 1000 counts/sec.	S 2p Intensity 168.7 eV 1000 counts/sec.	Irradiation Time min.
1.	15.3	0.0	1.2	0.0
2.	14.1	0.7	0.7	1.0
3.	13.0	1.4	0.6	2.0
4.	11.8	2.0	0.3	6.0
5.	11.2	2.6		
6.	10.4	3.1		
7.	9.0			
8.	8.3			
11.	7.6			

Surface Analysis of Modified Polyester Fibers  
Utilizing a Variety of Spectroscopic Methods.

Up to this point this review has concerned the use of X-ray photoelectron spectroscopy to analyze surfaces of fibers and irregular solids. This is so because the author believes that XPS is unique in its surface sensitivity and ability to differentiate among various chemical forms of elements on the surface as well. Problems can arise as a result of radiation damage to organic substrates due to X-ray radiation. However, this problem is much less severe than the damage problems resulting from other techniques utilizing electrons or ions such as Auger, SIMS and the electron microprobe. A recent paper has appeared utilizing a number of surface analysis techniques to study chemically modified polyester fibers (63). The methods employed included scanning electron microscopy (SEM), wettability, fourier transform infrared spectroscopy (FTIR) in combination with attenuated total reflectance spectroscopy (ATR), raman microscopy (MOLE), laser microprobe mass analysis (LAMMA), secondary ion mass spectrometry (SIMS) and XPS. The effect of a surface treatment to improve the adhesion of a tire cord adhesive to poly (ethylene terephthalate) (PET) fibers consisting of a commercial formulation comprising a phenol blocked methylene bisphenylene diisocyanate and a

glycerol epoxy resin was studied. The limitations of several of these methods became apparent when applied to organic substrates combined with the fact that the modification was confined to the outer few nanometers of the surface and represented much less than one percent of the total. FTIR and MOLE failed to detect signals characteristic of the modification in the presence of the fiber. Only products from the decomposition of the substrate fiber were detected by LAMMA and SIMS. The technique most able to detect the surface to the chemical modification was XPS. The isocyanate and the glycerol epoxy component of the modification contain nitrogen and chlorine which are unique to the modification. Nitrogen and chlorine core electron lines were detected and the nitrogen to chlorine atom ratio was sensitive to cleaning treatments applied to the modified yarn.

#### Literature Cited

1. Science, 1980, 208, 775-966.
2. Riggs, W.M.; Parker, M.J. in "Methods of Surface Analysis", A.W. Czauderna, ed. Elsevier Scientific Publishing: New York, 1975, pp 103-157.
3. Carlson, T.A. "Photoelectron and Auger Spectroscopy:", Plenum Press, New York, 1975.
4. Baker, A.D.; Brisk, M.A.; Liotta, D.C. Anal. Chem. 1980, 52, 161R-174R.
5. Dwight, D.W.; Fabish, T.J.; Thomas, H.R., Photon, Electron, and Ion Probes of Polymer Structure and Properties," ACS Symposium Series 162, American Chemical Society, Washington, D.C., 1981, pp. 1-442.
6. Dilks, A. "Electron Spectroscopy". Vol. 4 Brundle, C.R.; Baker, A.D., Eds. Academic Press, London, 1981, pp 277-359.
7. Holm, R.; Storp, S. Surf. and Interface Anal., 1980, 2(3), 96-106.
8. Clark, D.T. CRC Crit. Rev. Solid State Matter Sci., 1978, 8, p 1.
9. Clark, D.T. "Polymer Surfaces". Clark, T.D.; Feast, W.J. eds. John Wiley, New York, 1978, pp 305-358.
10. Briggs, D. "Electron Spectroscopy". Baker, A.D.; Brundle, C.R., eds. Academic Press, London, 1978 Vol. 2, 305-358.
11. Seah, M.P. Surf. and Interface Anal., 1980, 2(6), 222-239.
12. Hoffmann, S. Surf. and Interface Anal., 1980, 2, 148-160.
13. Coppertwaite, R.G. Surf. and Interface Anal., 1980, 2(1), 17-25.
14. Snell, K.D.; Keenan, A.G. Chem. Soc. Quart. Rev., 1979, 8, 259-282.
15. Mittal, K.L. Pure and Appl Chem., 1980, 52, 1295-1305.
16. Roberts, M.W. Chem. Soc. Quart. Rev., 1977, 6(4), 373-391.
17. Barr, T.L. Am. Lab., 1978, 10, 40-51.

18. Bancroft, G.M.; Brown, J.R.; Fyfe, W.S. Chem. Geol., 1979, 25, 227-43.
19. McGuire, G.E.; Holloway, P.H. Scanning Electron Microscopy, Vol. 1, 1979, Johari, Om. ed. SEM Inc., AMF O'Hare, Chicago, 173-182.
20. Lucchesi, C.A.; Lester, J.E. J. Chem., Ed. 1973, 50, A205-269
21. Evans, Jr. C.A. Anal. Chem., 1975, 47, 855A-866A.
22. Wagner, C.D.; Riggs, W.M.; Davis, L.E.; Moulder, J.F.; Muilenberg, J.E. "Handbook of XPS"; 1979, Perkin Elmer, Physical Electronics, Eden Prairie, Minn., 12-28.
23. Wertheim, G.K. "Electron and Ion Spectroscopy of Solids"; Fiermans, L.; Vennik, J.; Dekeyser, W.; ed., 1977, Plenum Press, New York; pp. 192-229.
24. Clark, D.T.; Thomas, H.R. J. Poly Sci. Poly Chem ed., 1978, 16, 791-820.
25. Lindberg, B.J.; Hamrin, K.; Johansson, G.; Gelius, U.; Fahlman, A.; Nordling, C.; Siegbahn, K. Phys. Sci., 1970, 1, 268.
26. Nordberg, R.; Albridge, R.G.; Bergmark, T.; Erickson, U.; Hedman, J.; Nordling, C.; Seigbahn, K.; Lindberg, B.J. Ark. Kemi., 1968, 28, 257.
27. Clark, D.T.; Shuttleworth, D. J. Poly. Sci. Polym. Chem. ed. 1980, 18, 27-46.
28. Anand, M.; Cohen, R.E.; Baddour, R.F. Polymer, 1981, 22, 370.
29. Seah, M.P.; Dench, W.A. Surface and Interface Analysis, 1979, 1, 2-11.
30. Caldman, P.; Gossedge, G.; Scott, J.D.; J. Electron Spec. and Rel. Phenom., 1978, 13, 1-6.
31. Clark, D.T.; Thomas, H.R.; J. Polym. Sci. Polym. Chem. ed., 1977, 15, 2843-67.
32. Brundle, C.R.; Hopster, H.; Swalen, J.D. J. Chem. Phys., 1979, 70, 5190-96.
33. Hall, S.M.; Andrade, J.D.; Ma, S.M.; King, R.N; J. Electron Spec. and Rel. Phenom., 1979, 17, 181-89.
34. Clark, D.T.; Fok, Y.C.T.; Roberts, G.G. J. Elec. Spec. Rel. Phenom., 1981, 22, 173-185.
35. Roberts, R.F.; Allara, D.L.; Pryde, C.A.; Buchanan, D.N.E.; Hobbins, N.D. Surf. and Interface Anal., 1980, 2, 5-9.
36. Hudis, M. in "Techniques and Applications of Plasma Chemistry" Hollahan, J.R.; Bell, A.T., ed., 1974, John Wiley, New York, pp. 113-145.
37. Asquith, R.S. "The Chemistry of Natural Protein Fibers." Plenum Press, New York, NY, 1977.
38. Millard, M.M. Anal. Chem., 1972, 44, 828.
39. Millard, M.M.; Lee, K.S.; Pavlath, A.E. Text. Res. J., 1972, 42, 307-313.
40. Millard, M.M.; Pavlath, A.E.; Text. Res. J., 1972, 82, 460.
41. Millard, M.M. in "Techniques and Applications of Plasma Chemistry". Hollahan, J.R.; Bell, A.T., ed., 1974, John Wiley, New York, pp. 177-213.

42. Millard, M.M.; Pavlath, A.E. J. Macromol. Sci-Chem., 1976, A10(3), 579-97
43. Fadley, C.S. "Core and Valence Electronic States Studied With XPS". Lawrence Radiation Laboratory Report, 1970, UCRL 19535.
44. Millard, M.M. "Characterization of Metal and Polymer Surfaces". Vol. 2, Lee, Lieng-Huang, ed., 1977, Academic Press, New York, pp. 85-100.
45. Ward, W.M., 1976, Western Regional Research Center, USDA, Berkeley, CA, unpublished data.
46. Batich, C.D; Wendt, R.C. in ref 5 pg. 221.
47. Millard, M.M.; Masri, M.S. Anal. Chem., 1974, 46, 1820.
48. Millard, M.M.; Friedman, M; Biochem. Biophys. Res. Commun., 1976, 70, 445-51.
49. Masri, M.S.; Randall, V.G.; "Proceedings of the First International Conference on Chitin/Chitosan". Muzzarelli, R.A.A.; Pariser, E.R., ed., 1978, MIT, Cambridge, MA, pp. 277-87
50. Messing, R.A. Methods in Enzymology, Vol. 29, Immobilized Enzymes, 1976. Mosbach, K., ed., Academic Press, New York, 166-169.
51. Dwight, D.W.; Thomas, H.R. Polymer Preprints Division of Polymer Chemistry, ACS, 1981, 22(1), 300-304.
52. Pittman, A.G.; Millard, M.M. "Interaction of Urethanes with Fluoroalkyl Siloxanes" submitted to J. App. Polym. Sci.
53. Raby, B.A., 1976. UTHE Technology Int., Sunnyvale, CA, unpublished data.
54. Wood, R.D., 1978. Biorad Laboratories, Inc., Richmond, CA, unpublished data.
55. Millard, M.M.; Bartholomew, J.C. Anal. Chem., 1977, 49, 1290-1296.
56. Johns, Wm., 1976. Forest Products Laboratory, Richmond, CA, unpublished data.
57. Kaneko, M.; Tsuchida, E. J. Polym. Sci. Macromol. Rev., 1981, 16, 397-522.
58. Stille, J.K., 1979. Colorado State University Chemistry Dept., Fort Collins, Colo., personal communication.
59. Sasaki, T.; Williams, R.S.; Wong, J.S.; Shirley, D.A. J. Chem. Phys., 1979, 71, 4601-10.
60. Brown, J.R.; O'Donnell, J.H. J. Applied Polym Sci, 1975, 19, 405-417.
61. Bowden, M.J. CRC Critical Reviews in Solid State and Materials Science, 1979, 8(3), 223-65.
62. Wall, L.A. "Fluoropolymers". 1972, John Wiley, New York.
63. Gillberg, G.; Kemp, D. J. App. Polym. Sci., 1981, 26, 2023-51.

RECEIVED April 19, 1982

## Surface Analysis of Glasses

L. L. HENCH and D. E. CLARK

University of Florida, Department of Materials Science and Engineering,  
Gainesville, FL 32611

Understanding and controlling glass corrosion is important since many products that directly influence the quality of our lives already are or eventually will be manufactured from glass. Only recently have the analytical tools for surface and solution analyses been developed to the point where they can be used for characterizing glass surface reactions. This paper reviews our present understanding of glass surfaces-environmental reactions. Practical examples are used to illustrate the present utility and future promise of surface analyses in solving scientific and industrial problems.

Glass is one of our primary industrial materials. A high resistance to a variety of chemical environments has made glass the material of choice in such diverse applications as laboratory chemical ware, windows, linings of large chemical tanks, pH electrodes, pharmaceutical and food containers, fiber optic communications, electronics, and more recently nuclear waste disposal. Because of the large investment of energy and raw materials in these large tonnages of glass objects it is important to improve the long term reliability and performance of this class of materials. However, in order to design glasses that will show improvements in chemical resistance it is first necessary to understand the interactions between a glass surface and its chemical environment. This understanding has been achieved as a result of the development of a variety of surface analysis tools during the last decade. Recent reviews summarize the operational features of most of these surface analytical methods.(1-5) The objective of this paper is to describe the general features of glass surfaces as a function of chemical environment as deduced from various types of surface analyses.

0097-6156/82/0199-0203\$07.25/0  
© 1982 American Chemical Society

### Theory

When exposed to a liquid or gas environment a heterogeneous reaction takes place at or near the surface of the glass. The central point in understanding the chemical behavior of glasses is to recognize that nearly all glass surfaces consist of compositional gradients. Ultra high purity vitreous silica is a noteworthy exception. All other silicate based glasses rapidly develop surface reaction layers when exposed to the atmosphere immediately after production.(1) Storage of an object before use continually alters the surface gradients. Thus, when a glass article is put into service the chemical environment either dissolves the initial reaction film and forms a new layer or extends the initial film.

Numerous experiments on simple and complex glasses have shown that a glass interacts with its environment such that a continuum of surface compositions is possible; however, a silicate glass can generally be described(2) as one of 5 surface types at any particular instant in its processing and environmental history (Figure 1). The ordinate in Figure 1 represents the relative concentration of  $\text{SiO}_2$  (silica) in the glass and the abscissa corresponds to the depth into the glass surface. If species are selectively dissolved from the glass surface the relative  $\text{SiO}_2$  concentration will increase producing a  $\text{SiO}_2$ -rich surface layer. If all species in the glass are dissolved simultaneously the relative concentration of  $\text{SiO}_2$  will remain the same as in the original glass. When combinations of selective dissolution, congruent dissolution and precipitation from solution occurs then anyone of the 5 types of surfaces shown in Figure 1 is possible.

Type I glasses have undergone a surface reaction that is only a monolayer thick and no compositional profile is measurable. Exchange of alkali and alkaline earth ions with hydrogen and/or hydronium ions (i.e., selective dissolution) result in Type II glass surfaces if there is sufficient concentration of network formers in the surface film to stabilize it. If network formers are not sufficient, or the environment is rich in  $\text{OH}^-$  or other species which can break Si-O-Si network bonds, the surface layer is unstable and a Type IV surface is produced. Additives in the glass or the environment can interact with the  $\text{SiO}_2$ -rich (silica-rich) layer that forms first on the glass and produce a second film isolating the glass from its environment. Such dual protective barriers result in Type III surfaces. Finally, a glass that is undergoing total network dissolution (also referred to as congruent dissolution) is described as having a Type V surface. Often from the perspective of average surface composition there is little distinction between Type I and Type V surfaces. However, large quantities of ions are being lost from a Type V surface during corrosion and consequently

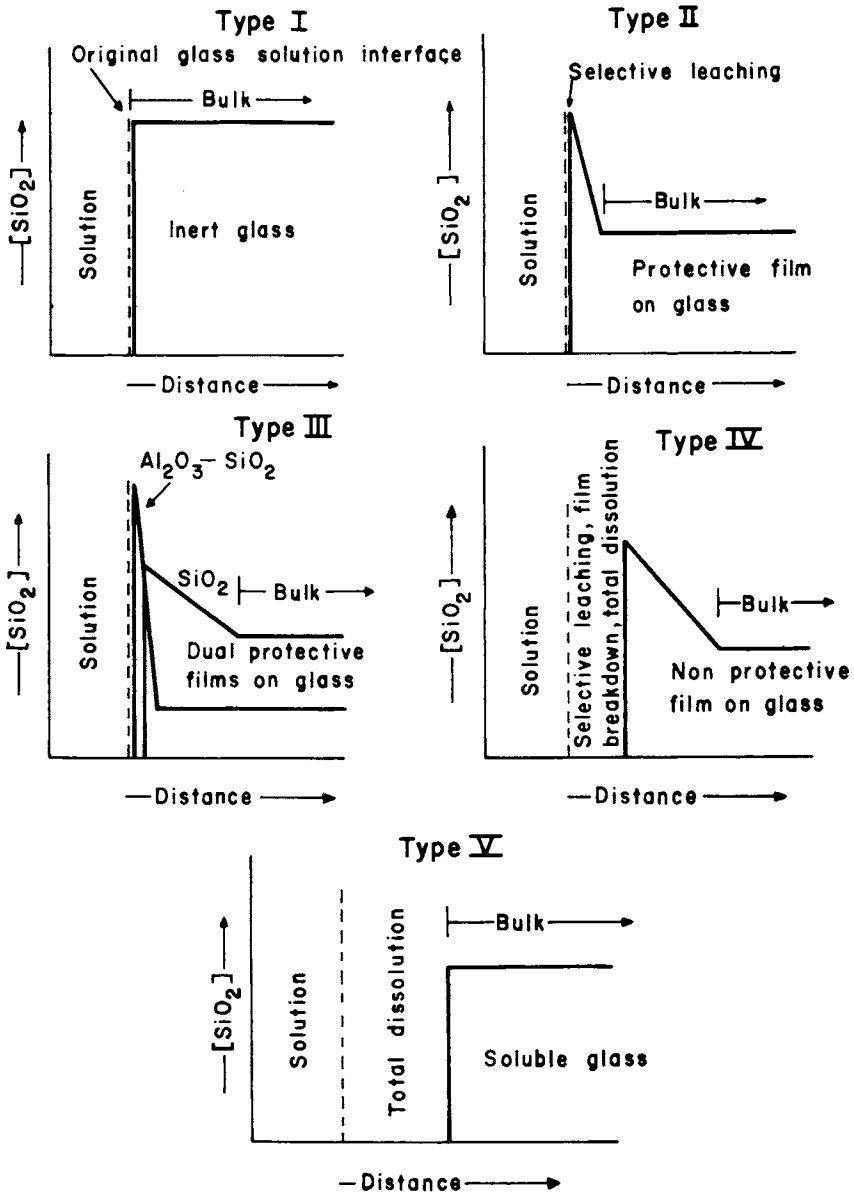


Figure 1. Five types of glass surfaces produced during corrosion. (Reproduced, with permission, from Ref. 2. Copyright 1977, North-Holland Publishing Co.)



extensive surface pitting can result due to localized heterogeneous attack. Additionally, large dimensional changes usually accompany corrosion of glasses with Type V surfaces.

Studies of the kinetics of the above processes show that Type II surfaces are present when

$$C_1 = k_1 t^{1/2} \quad (1)$$

where  $C_1$  is the concentration of species in solution,  $t$  is reaction time and  $k_1$  is the rate constant for the diffusion controlled process. Type V surfaces correspond to a regime of kinetics where

$$C_2 = k_2 t \quad (2)$$

where  $C_2$  and  $t$  have the same meaning as in Equation 1 and  $k_2$  is the rate constant for the interface controlled network dissolution process. Type IV surfaces result when both processes occur together, and,

$$C_3 = k_1 t^{1/2} + k_2 t \quad (3)$$

Formation of Type III surfaces requires a third kinetics term to describe the solution precipitation and/or surface condensation reactions, usually with an unknown time dependence,  $t^x$ , that are taking place along with ion exchange and some small amount of network dissolution, and,

$$C_4 = k_1 t^{1/2} + k_2 t - k_3 t^x \quad (4)$$

Although it may be possible to specify some limited conditions where the rate constants in Equations 1 and 2 can be measured, these conditions seldom correspond to the range of compositions and environments of general interest. The complexity of Equations 3 and 4 more often describe the relevant problems of understanding and controlling glass surfaces.

Continued exposure of a glass to many chemical environments leads to progressive changes in both composition and thickness of the surface films. Figure 2 describes such a change under static corrosion where the ions from the glass are permitted to build up in solution and increase the pH. Selective leaching (dissolution) and a Type II surface behavior results in formation of a surface film. With time, dissolution of the surface film network occurs due to buildup of  $\text{OH}^-$  in the solution leading to a Type IV surface. Eventually at high pH's the surface film network is totally destroyed and the glass is corroding congruently (i.e., Type V behavior). Congruent dissolution proceeds until complete dissolution of the glass occurs or until the solution in contact with the glass becomes saturated with respect to the individual species.

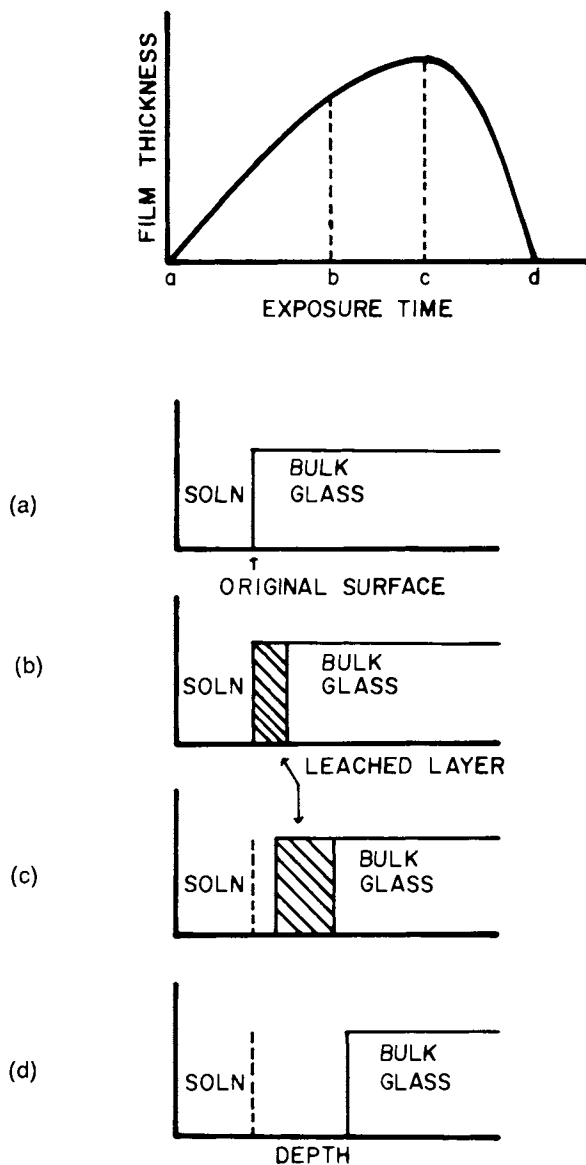


Figure 2. Effect of various stages of corrosion on changes of glass surfaces. Conditions: (b) type 2,  $\alpha = 0$ , selective leaching; (c) type 4,  $0 < \alpha < 1$ , selective leaching and network dissolution; and (d) type 5,  $\alpha = 1$ , network dissolution. (Reproduced, with permission, from Ref. 7. Copyright 1980, North-Holland Publishing Co.)

### Experimental Procedures

In order to generalize the results of the surface analyses of a glass it is essential to identify a number of variables in the use environment. These variables include: time, temperature, pH, ratio of surface areas (SA) exposed to volume (V) of reactant solution ( $SA/V = \text{cm}^{-1}$ ), static, flow, or replenished reactant solutions, partial pressure of  $\text{H}_2\text{O}$  in gaseous environments or organic reactant solutions, etc. It is often difficult to quantify all of the above variables in actual use environments. Consequently, various laboratory tests have been advocated to simulate use environments, with the above variables more or less under control, as shown in Figure 3.

The ASTM tests for glass durability, Figures 3a and 3b, evolved as a comparative method using glass containers with a specific volume of solution (3a), or powders crushed to a specified grain size (3b) and heated for short times in an autoclave at  $121^\circ\text{C}$ . The concentration of alkali ions in solution is used as a comparative index of durability with higher concentrations indicating poorer performances. Since the reaction time is short,  $SA/V$  is not controlled, and surface analyses of the glass after reaction is difficult, this type of test should not be used for quantitative studies of reaction kinetics. Additionally the autoclave conditions tend to bypass diffusional processes which dominate at lower temperature. Similar limitations exist for the IAEA (International Atomic Energy Agency) and Soxhlet tests (3c, 3d) and they should generally be used only for the purpose of comparing glass corrosion performance.(6)

The ISO (International Standards Organization) suspended sample test (3d), now adopted as MCC-1 by the U.S. Dept. of Energy Materials Characterization Center,(7) and the Sanders static cell test (8,9)(3f) make it possible to control the critical variables needed for kinetics analysis. Addition of tubing to and from the chambers in 3d and 3f is straightforward and enables corrosion to be studied as a function of flow rate.

Studying attack by a gaseous atmosphere, termed weathering,(1,10) also requires two differing configurations, as shown in Figure 4. Static weathering (4a) results in trapped reactant solution, often water, very high  $SA/V$  values, and predominantly network dissolution (Equation 2). The most frequently encountered weathering condition is that shown in Figure 4b. A reaction occurs between the glass surface and the various gases in the atmosphere with the reaction product remaining on the surface. Insufficient water is available for dissolution of the reaction products and removal by runoff. Diffusion tends to dominate the reaction kinetics when an ample supply of water vapor and reactive gases are present.

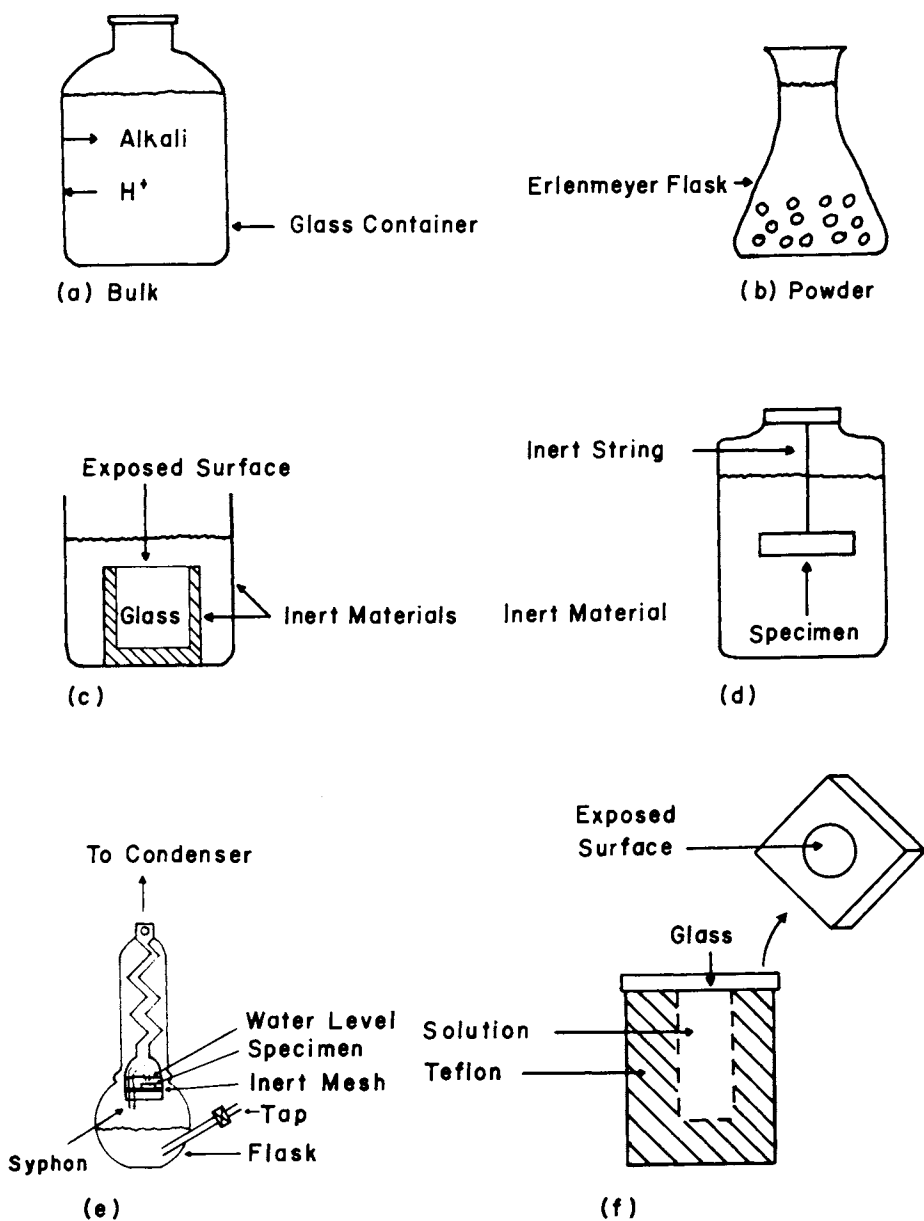


Figure 3. Experimental arrangements for studying glass corrosion. Conditions: (a,b) ASTM,  $T = 121^\circ\text{C}$ —autoclave,  $t = 1\text{ h}$ ; (c) IAEA,  $T = 25^\circ\text{C}$ ,  $t = \text{variable}$ ; (d) ISO,  $T = \text{variable}$ ,  $t = \text{variable}$ ; (e) Soxhlet,  $T \approx 100^\circ\text{C}$ ,  $t = \text{variable}$ ; and (f)  $T = 25\text{--}95^\circ\text{C}$ ,  $t = \text{variable}$ . (Reproduced, with permission, from Ref. 7. Copyright 1980, North-Holland Publishing Co.)

Generally, theoretical analysis and experimental interpretation of surface compositional data assume a homogeneous glass. At times this assumption is not valid. Phase separation, compositional segregation, devitrification, bubbles (seeds) or unreacted batch or refractory particles (stones) may be present and lead to accelerated attack at interfaces. Surface abrasion, polishing relics, scratches, and pits also can cause accelerated attack if the features are larger than approximately 0.5  $\mu$ m.<sup>(11)</sup> When the glass is formed as a coating as in enameling or glazing, pinholes may be left. Figure 5 is a series of scanning electron micrographs illustrating preferential attack of pinholes in an experimental commercial porcelain enamel used for lining large chemical reaction vessels. The presence of the pinholes and mill additions greatly increase the rate of attack of the heterogeneous enamel compared to a homogeneous glass of the same composition.<sup>(12)</sup>

#### Auger Electron Spectroscopy (AES) Profiles

AES analysis requires that the surface be irradiated with low energy (3KeV) electrons which produces characteristic Auger electrons. The energy of these Auger electrons are unique for each element and the number of these electrons is related to the concentration of that element in the material. Numerous analyses of glass surfaces have been performed using AES.<sup>(1,2,7,12-16)</sup> Used in combination with Ar ion-milling (a means of removing thin layers from the surface) compositional profiles of the glass surface can be obtained in which the concentration of each element is plotted as a function of depth into the surface.

Figure 6 is the surface compositional profile of the glass enamel shown in Figure 5 after 8 days of exposure to a boiling solution containing 20% HCl. Previous analysis of this corrosion environment using infrared reflection spectroscopy (IRRS), weight loss, and scanning electron microscopy (SEM) indicated that a SiO<sub>2</sub>-rich film formed on the enamel during liquid phase corrosion.<sup>(12)</sup> The SiO<sub>2</sub>-rich film controls the diffusion rates of the more mobile alkali and alkaline earth cations and therefore the chemical durability of the enamel. The surface compositional profile of Figure 6 confirms this interpretation. Sodium, calcium, and barium are depleted from the enamel surface to a depth of 0.4  $\mu$ m. Even zirconium is lost from the surface layer. The SiO<sub>2</sub> network shows little change with milling which indicates that the surface has developed a predominately SiO<sub>2</sub>-rich film during corrosion.

Figure 7 shows similar results for a commercial soda-lime-silica container glass corroded for only one hour in 37°C water.<sup>(1)</sup> Figures 7a and 7b show the AES spectra of the outer, unmilled surface before and after corrosion. The decrease of

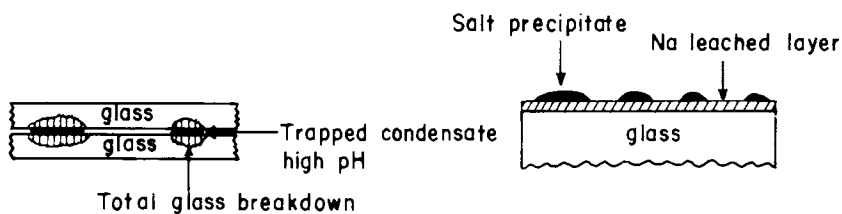


Figure 4. Weathering conditions for glass: static weathering (left); time, long;  $SA/V$ , extremely high; reaction (2)  $\gg$  reaction (1); and dynamic weathering (right); atmospheric reactions significant; reaction (1)  $\gg$  reaction (2).

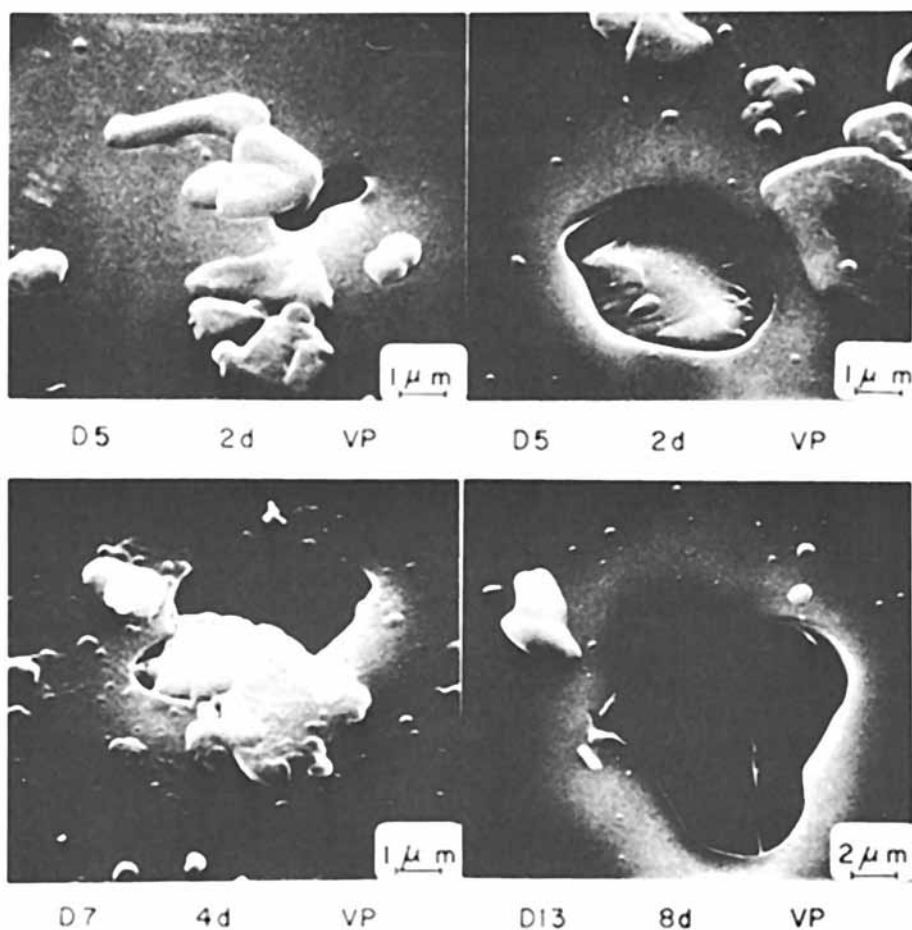


Figure 5. SEM photographs of pinholes on a glass enamel.

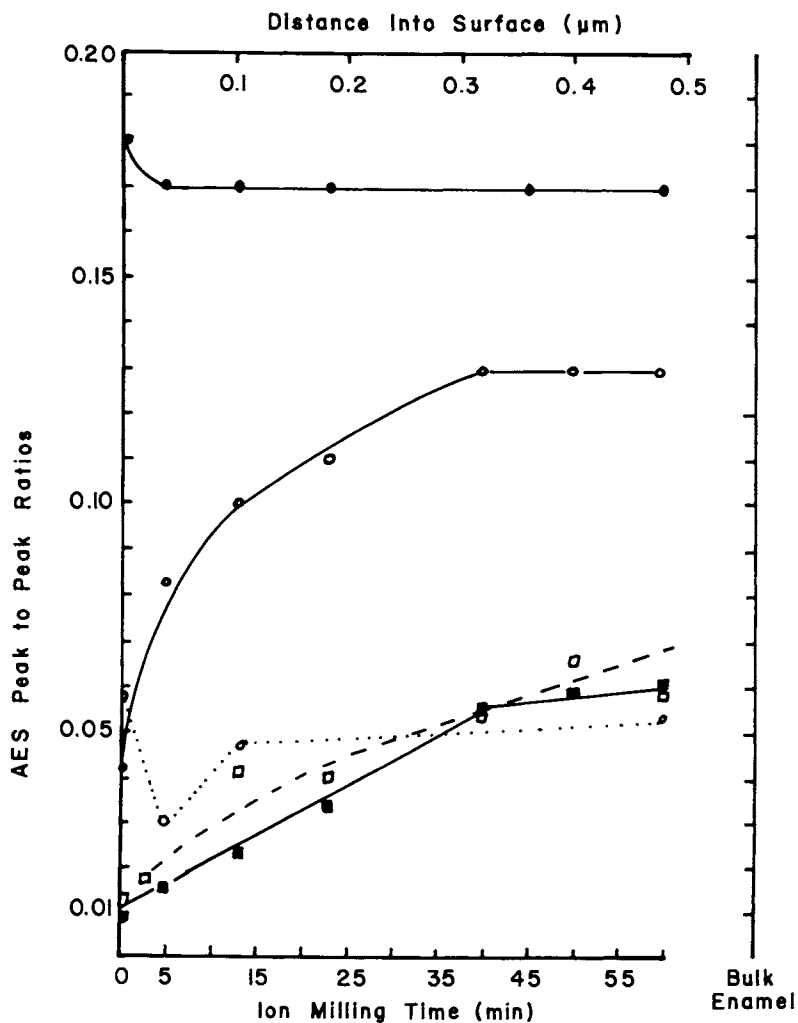


Figure 6. AES profile of a glass enamel. Key: —●—, Si; —○—, Zr; ···○···, Na; —□—, Ba; and —■—, Ca.

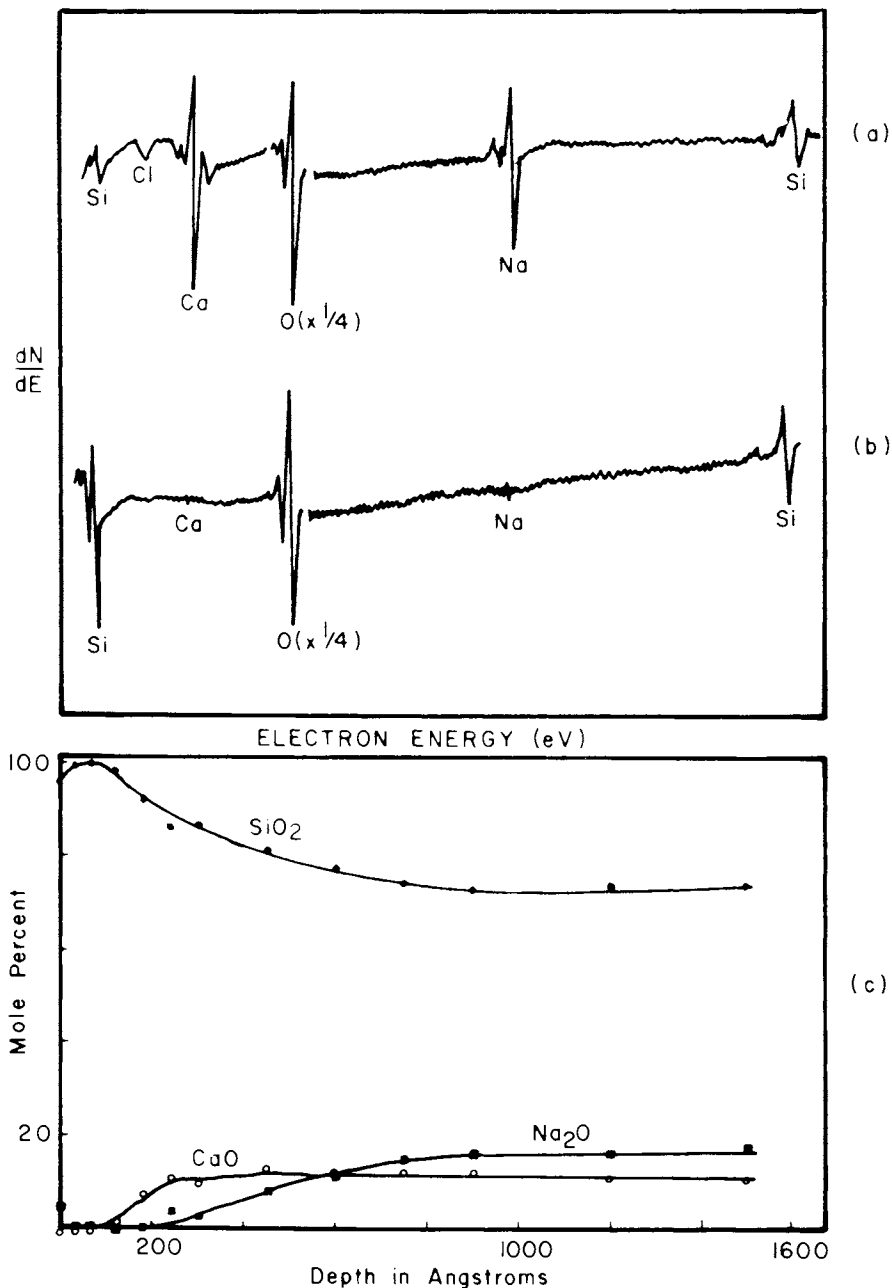


Figure 7. Auger surface spectrum of a commercial soda-lime-silica glass before corrosion (a); after corrosion, for 1 h (b), 37°C; and compositional profile obtained by AES-Ar ion milling of the corroded glass in (b) and spectra obtained at various depths for 1 h, 37°C (c). (Reproduced, with permission, from Ref. 1. Copyright 1979, Books for Industry.)



the sodium and calcium signals is accompanied by a simultaneous increase in the silicon signal. Removal of successive layers of the corroded surface by Ar ion milling shows that the loss of sodium is to a depth of 800 Å thick. Thus, even mild aqueous environments are sufficient to produce compositional gradients.(1,13) This experiment, as well as that of Figure 6, also shows that ions with multiple valence as well as monovalent alkali ions exchange with components of the corrosion environment. Other AES studies show similar results.(14,15)

However, certain cations with multiple valence states are capable of forming a second, stable reaction film in conjunction with and on top of a SiO<sub>2</sub>-rich layer. This Type III surface (see Figure 1) is especially important for complex multicomponent nuclear waste glasses. Figure 8 (top) shows an AES spectrum of a reference borosilicate nuclear waste glass, PNL 76-68 (Battelle Pacific Northwest Laboratories, see Ref. 7 for specifics on corrosion variables of these materials), after 3 days exposure to static 90°C deionized water.(16) Figure 8 (bottom) shows the compositional profile for this corroded glass. Iron has concentrated in the surface layer along with zinc. Other recent studies(17) have shown that critical concentrations of silica, iron, and zinc are necessary for the Type III surface to be stable and provide an effective barrier to diffusion of more mobile species.

### Secondary Ion Mass Spectroscopy (SIMS) Profiles

In SIMS the surface of the solid is bombarded with a primary beam of ions and this produces secondary ions from the surface which can be detected and quantified with a Mass Spectrometer. The very process by which SIMS analysis is obtained produces its own milling of the surface and consequently no additional Ar-ion milling is required as with AES and ESCA.

Aqueous corrosion profiles have also been measured on soda-lime-silica glasses using SIMS.(18) Both negative and positive oxygen primary ions were used for sputtering in combination with a metal diaphragm to minimize charging. Figure 9 shows the surface compositional profile for a 20 mol % Na<sub>2</sub>O - 10% CaO - 70% SiO<sub>2</sub> glass reacted for 30 minutes in 75°C H<sub>2</sub>O. Depletion of sodium (as Na<sub>2</sub>O) extends to a depth of 1000 Å whereas the Ca (as CaO) loss was approximately one-half this depth. The surface of the glass was enriched in SiO<sub>2</sub> to a value of nearly 95%. These results are very close to those shown in Figure 7 for AES ion-milling of a water corroded glass of similar composition.

A limitation of the above analyses is the absence of hydrogen profiles. Figure 10 shows schematically the importance of hydrogen ions in both the selective dissolution

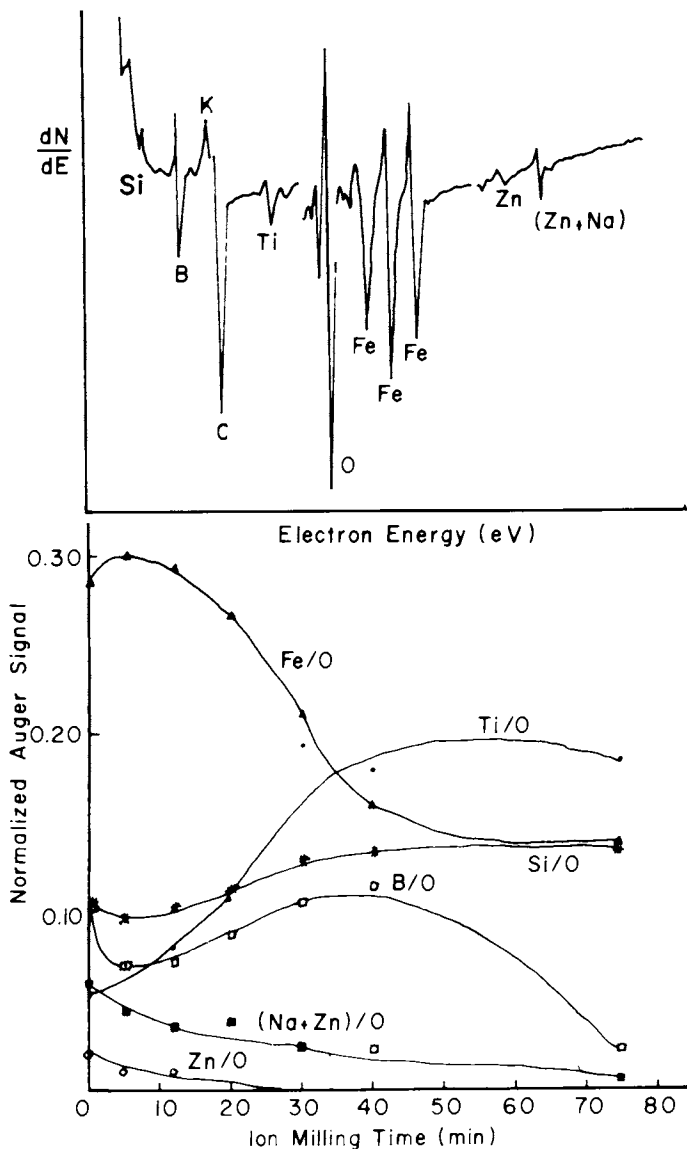


Figure 8. Auger surface spectrum of a corroded nuclear waste glass together with its compositional profile. Conditions: (top and bottom) PNL glass composition 76-68, 90°C for 3 d in  $H_2O$ ,  $SA/V = 0.1 \text{ cm}^{-1}$ . Key: (top) Si = 75 eV, B = 179 eV, K = 252 eV, C = 272 eV, Ti = 418 eV, O = 510 eV, Fe = 651 eV, Zn = 906 eV, (Zn + Na) = 994 eV + 990 eV; and (bottom) Fe/O = 651 eV, Ti/O = 418 eV, Si/O = 75 eV, B/O = 179 eV, (Na + Zn)/O = 990 + 994 eV, Zn/O = 906 eV. (Reproduced, with permission, from Ref. 7. Copyright 1980, North-Holland Publishing Co.)

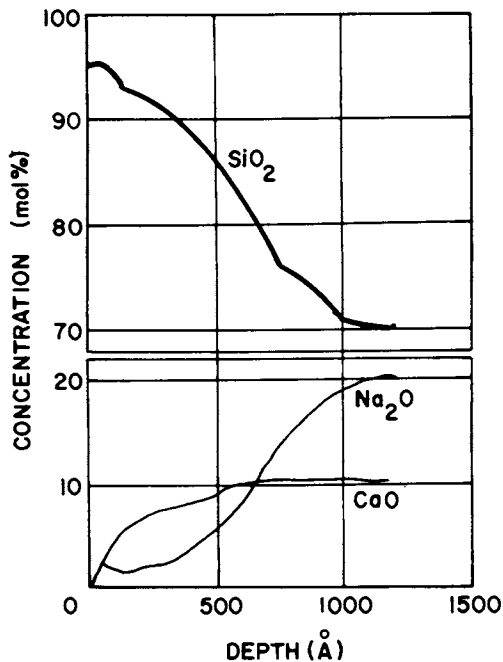


Figure 9. Compositional concentration profiles of a soda-lime-silica glass corroded for 30 min at 75°C in water. Obtained with SIMS. (Reproduced from Ref. 18. Copyright 1979, American Chemical Society.)

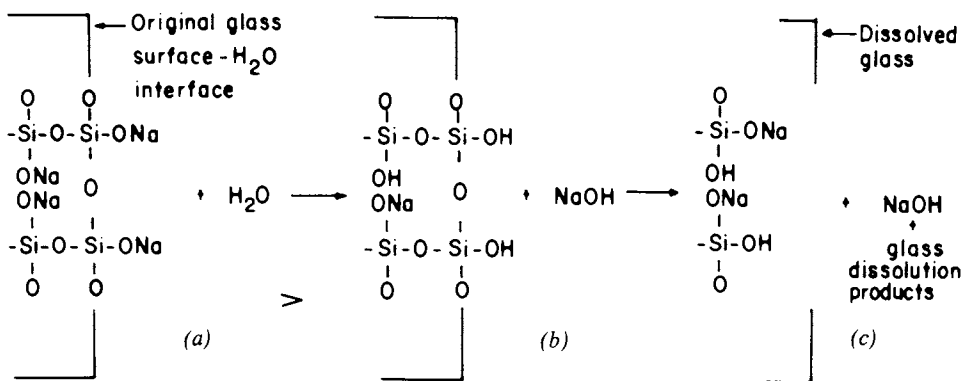


Figure 10. Mechanisms of glass corrosion for a soda-silica glass. Conditions: a,  $t = 0$ ,  $pH = 7$ ; b (stage 1),  $t > 0$ ,  $pH \leq 9$ , selective Na dissolution; and c (stage 2),  $t \gg 0$ ,  $pH \geq 9$  total dissolution. (Reproduced, with permission, from Ref. 1. Copyright 1979, Books for Industry.)

of alkali ions and the total network dissolution of a silicate glass.(1) It is not possible to analyze for the contribution of hydrogen using AES because hydrogen atoms and ions do not produce Auger electrons. However, SIMS can be used since all mass numbers that leave the surface during ion bombardment can be analyzed in the mass spectrometer. Figure 11 shows the profile resulting from SIMS analysis, using a 1.5 KV He/Ne ion beam, of a soda-lime-silica glass with only ambient atmospheric weathering.(1) There is sodium depletion to a depth of approximately 2000 A and hydrogen ion enrichment to about the same depth or more. A thinner layer of calcium ion exchange is observed with both the sodium and calcium ions remaining on the surface as mixed carbonate-hydroxide salts comprising a weathered reaction layer.

#### Resonant Nuclear Reaction (RNR) Profiles

A technique which can yield hydrogen concentration profiles of a glass surface(19) without the complications of ion milling involves using the resonant nuclear reaction between hydrogen ( $^1\text{H}$ ) and ( $^{15}\text{N}$ ). At precisely 6,385 MeV (lab) there is a resonance in the reaction  $^{15}\text{N} + ^1\text{H} = ^{12}\text{C} + ^4\text{He} + 4.43 \text{ MeV gamma rays}$ . Consequently, for a given  $^{15}\text{N}$  energy the yield of characteristic gamma rays from this reaction is proportional to the hydrogen present. So by imposing a beam of  $^{15}\text{N}$  particles with controlled energy on a glass surface and measuring the gamma ray yield vs  $^{15}\text{N}$  energy, the hydrogen concentration can be determined. A similar method has been used to measure the sodium concentration profile on the same glass using the characteristic 1.32 MeV gamma ray released from the reaction of  $^{23}\text{Na}$  with a high energy beam of hydrogen ions.(19) The resulting compositional profiles for both hydrogen and sodium of a commercial soda-lime-silica window glass reacted with water for 540 hours at 90°C are shown in Figure 12. Sodium exchange with hydrogen was detected to a depth of 0.6 m. The shape of the profiles fit a diffusion model for the exchange process.(19) It was suggested by Lanford, et al.(19) that the 3 for 1 replacement of hydrogen ions for sodium ions in the measured profiles indicates that hydronium ions ( $\text{H}_3\text{O}^+$ ) are the exchanging species in the surface reaction. However, there are several significant differences between the RNR profiles (Figure 12) and profiles obtained by AES and SIMS that make such a conclusion premature. First, the RNR profile does not include information on the concentration gradient of calcium and aluminum ions. Both species have been shown to participate in surface exchange reactions and must be accounted for in understanding the interaction of  $\text{H}^+$  or  $\text{H}_3\text{O}^+$  with the surface. Secondly, the depth of the hydrogen and sodium profiles obtained with the RNR technique (Figure 12) is significantly less than observed for AES and SIMS ion milling

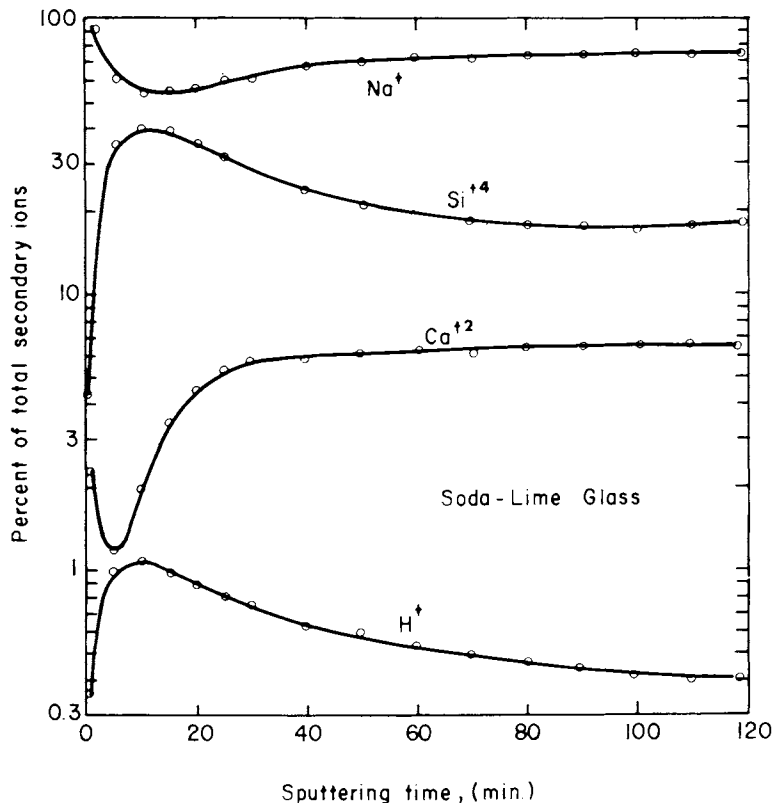


Figure 11. SIMS compositional profile of an ordinary glass slide. (Reproduced, with permission, from Ref. 1. Copyright 1979, Books for Industry.)

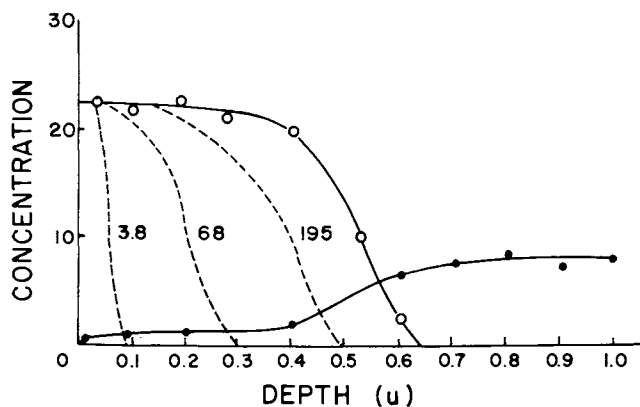


Figure 12. Compositional profile for both hydrogen and sodium obtained from a commercial soda-lime-silica window glass reacted with water for up to 540 h at  $90^{\circ}\text{C}$ . Obtained with RNR. Key: -O-, hydrogen; and -●-, sodium. (Reproduced, with permission, from Ref. 19. Copyright 1979, North-Holland Publishing Co.)

methods, as shown in Figures 6-11. The dashed curves in Figure 12 are for reaction times ranging from 3.8 hrs to 540 hrs in 90°C water resulting in reported exchange depths from 0.1 to 0.6  $\mu\text{m}$ . Figures 7 and 9 show that depths of 0.1  $\mu\text{m}$  were detected in a similar glass after just minutes of reaction in 37°-70°C water using AES and SIMS. Therefore, it is concluded that additional work is required before the profiles and reaction mechanisms of multicomponent glasses can be interpreted quantitatively.

#### Electron Spectroscopy for Chemical Analysis (ESCA) Profiles

In ESCA the surface of the material is irradiated with low energy monochromatic x-rays ejecting electrons. The energies of the ejected electrons can be correlated to the species as well as the shell from which the electron was ejected. Thus compositional as well as information concerning the chemical state of the species in the material can be obtained. ESCA also appears to do less damage to the surface during analysis than does AES. In order to perform a compositional profile Ar ion-milling is required.

A recent study has been conducted using ESCA in conjunction with ion milling in an effort to resolve the issue of  $\text{H}_3\text{O}^+$  vs  $\text{H}^+$  involvement in surface corrosion.<sup>(20)</sup> A simple  $\text{Na}_2\text{O}\cdot 0.3\text{SiO}_2$  glass was corroded in static 25°C deionized water with  $\text{SA/V} = 10 \text{ m}^{-1}$ . Figure 13 shows the profile of the leached surface. Sodium is depleted to a depth of approximately 0.4  $\mu\text{m}$  with a concurrent increase in both silicon and oxygen. If  $\text{H}^+$  is replacing the  $\text{Na}^+$  then the O/Si ratio should remain constant; however, if  $\text{H}_3\text{O}^+$  is exchanging with  $\text{Na}^+$ , then the O/Si ratio will increase proportionally to the  $\text{Na}^+$  depletion. Figure 14 is a plot of the O/Si ratio obtained experimentally, compared with the ratio required if  $\text{Na}^+$  were replaced by  $\text{H}_3\text{O}^+$  (14). This result favors a mechanism of  $\text{H}^+$  rather than  $\text{H}_3\text{O}^+$  exchanging with  $\text{Na}^+$ . ESCA has also been shown to be an excellent means for investigating coatings on glasses (21).

#### Secondary Ion Photoemission Spectroscopy (SIPS) Profiles

As in SIMS a primary beam of monoenergetic ions is impinged on the surface of the material ejecting both secondary ions as well as excited neutral atoms. The deexcitation of the excited or metastable atoms produces luminescence which is measured in SIPS. When a glass surface is bombarded with ions of several keV energy, luminescence occurs consisting of photon emission from excited single atoms. Since the spectral intensity is proportional to the concentration of the luminescent components involved in the sputtering process it is possible to obtain a compositional profile of the surface.<sup>(22,23)</sup> Figure 15 is a plot of lithium concentration profiles in the surface region of

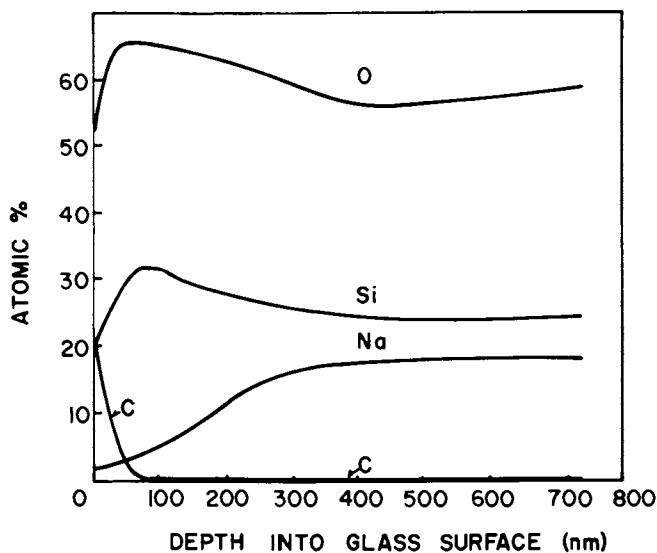


Figure 13. Compositional profiles for a soda-silica glass leached in water for 15 min at 25°C in deionized water,  $SA/V = 10 \text{ m}^{-1}$ . Obtained with ESCA. (Reproduced, with permission, from Ref. 20. Copyright 1980, PNL Report 3465.)

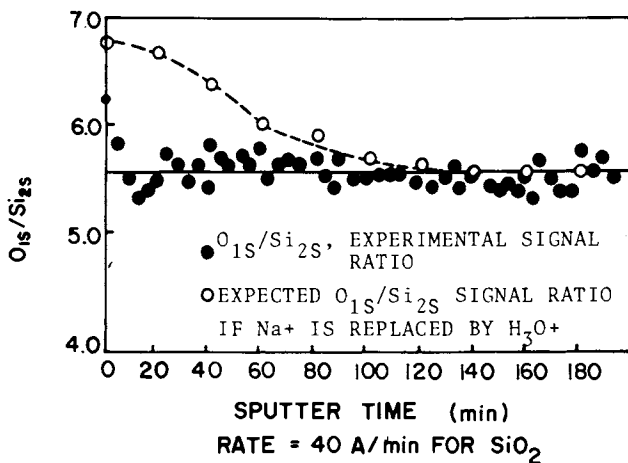


Figure 14. Oxygen-to-silicon ratio profile for the data presented in Fig. 13. (Reproduced, with permission, from Ref. 20. Copyright 1980, PNL Report 3465.)

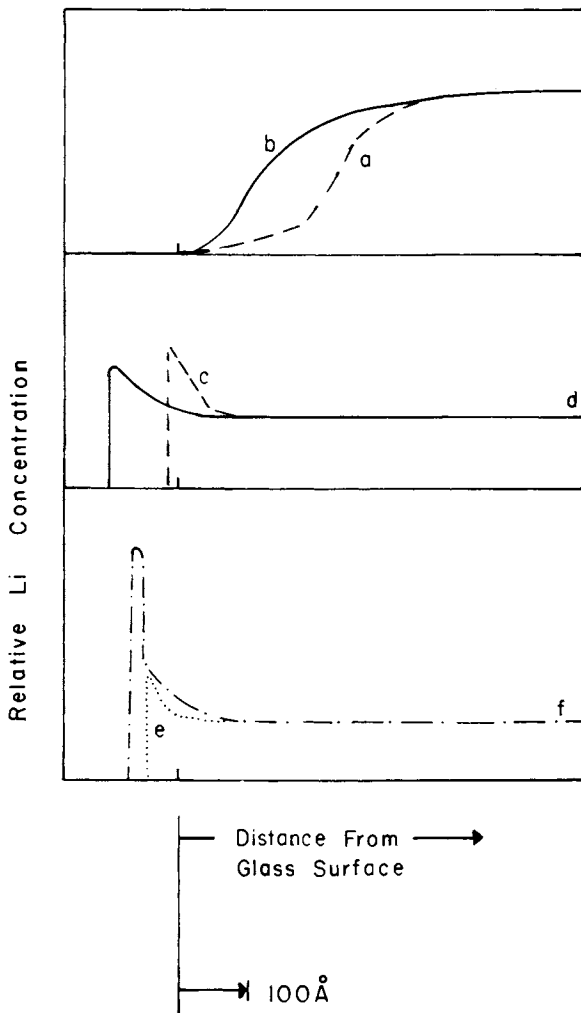


Figure 15. Lithium concentration profiles for a pH glass electrode.



a pH electrode membrane after exposure to various gaseous atmospheres at 120°C for 64 hours.(23) The lithium migrates to the surface by an ion exchange process even though the partial pressure of H<sub>2</sub>O is very low in the gases studied. Addition of CO<sub>2</sub> to the gaseous atmosphere increases the thickness of the lithium reaction layer formed on the surface, presumably due to formation of Li<sub>2</sub>CO<sub>3</sub>. The carbonate provides a sink for the collection of lithium at the glass surface, thus encouraging the diffusion of more lithium from the interior to the surface.

The SIPS technique is equally useful for measuring concentration of alkali depleted layers due to aqueous corrosion,(22) also shown in Figure 15. The pH electrode glass was leached in 0.1N H<sub>2</sub>SO<sub>4</sub> at 25°C resulting in an outer region adjacent to the reacting solution of low lithium concentration. This layer is about 100-150 Å thick for a glass annealed and controlled cooled at 40/min. A quenched glass membrane forms a thinner leached layer. The transition layer between lithium depleted surface and bulk lithium concentration is about 200-250 Å.

This technique is also suitable for obtaining compositional profiles of various cationic species in glass, as shown in a study of hydrated obsidian, a naturally occurring vitreous silicate.(24) Figure 16 shows the relative concentration of several elements as a function of depth for a typical obsidian artifact from Kaminaljuyu, Guatemala reported by Tsong, et al.(24) Hydrogen extends throughout the surface reaction zone to a depth of nearly 40 μm. Sodium and calcium are depleted to almost the same depth, as is potassium and lithium (not shown). The aluminum and silicon concentration are constant throughout the thick hydrated layer.

#### Infrared Reflection Spectroscopy (IRRS) Profiles

The IRRS technique involves irradiating the sample surface with infrared radiation and measuring the specularly beam intensity. Strong reflection for most glass occurs between 1400 cm<sup>-1</sup> and 400 cm<sup>-1</sup> corresponding to the Si-O vibrations. Since IRRS samples to a depth of 0.3 - 0.5 μm it can be used to follow the formation of the outer reaction layer during corrosion. When used together with fine mechanical polishing, it is ideal for profiling very thick reaction layers (i.e., several μm).(25,26,27)

Figure 17 shows typical spectra of vitreous silica, containing no alkali ions, and a binary 33 mole % Li<sub>2</sub>O-67 mole % SiO<sub>2</sub> glass (33L). Corrosion of the high alkali glass for 240 minutes in 100°C static water, SA/V = 1.0 cm<sup>-1</sup>, results in the leaching of lithium ions from the glass surface as shown by the loss of the NS peak at 850 cm<sup>-1</sup>. A SiO<sub>2</sub>-rich layer forms on the glass, as is shown by the shift of the LS peak in the corroded glass from 975 cm<sup>-1</sup> to a value of 1090 cm<sup>-1</sup>, close to

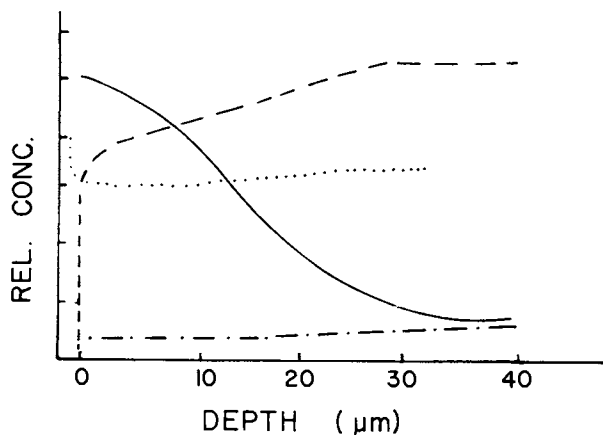


Figure 16. Compositional profile of an obsidian artifact (natural glass). Obtained with SIPS. Key: ---, Na; ····, Ca; —, H; and — · —, Al. (Reproduced, with permission, from Ref. 24. Copyright 1978, Science.)

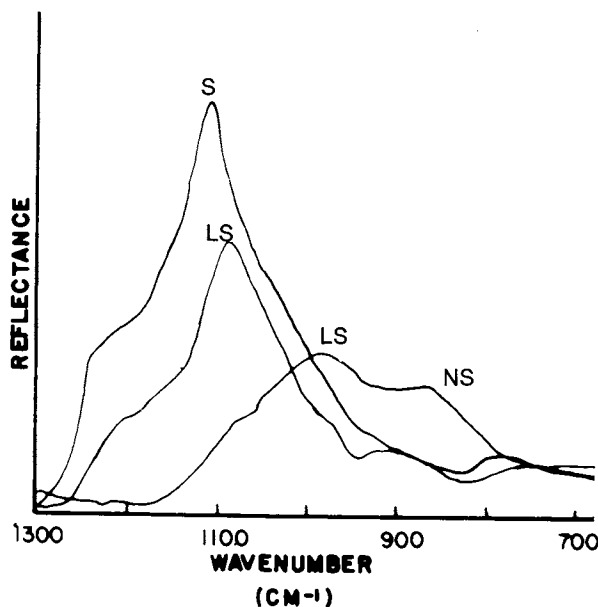


Figure 17. IR reflection spectra of a  $\text{Li}_2\text{O-SiO}_2$  (33:67 mol %) glass after corroding for 240 min at  $100^\circ\text{C}$  in deionized water. Obtained with IRRS. Conditions: 33 L nucleated 3 h at  $475^\circ\text{C}$ , uncrystallized, and  $SA/V = 1$ .

that of vitreous silica. This peak is due to -Si-O-Si- stretching vibrations in the material. As alkali is leached from the surface the concentration of SiO<sub>2</sub> and consequently of bridging Si-O-Si bonds increases, as shown by the previous AES, SIMS, ESCA, and SIPS profiles.

Sequential polishing of the sample surface, with weighing and IRRS analysis between layers removed, can be used to produce a compositional profile for samples with large depletion zones. Figure 18 shows infrared reflection spectra for a nuclear waste glass reacted in a simulated repository environment at 90°C. Figure 19 shows the compositional profile obtained from the spectra in Figure 18. Such IRRS profiles provide a good estimation of the thickness of the leached layers on the glass. The thickness of the leached layers can be used together with rates of ion release to produce plots useful for predicting the long range corrosion performance of these materials. Because of the ease of operation of the IRRS method it is possible to use it in hot cell or remote operations to monitor leaching behavior of radioactive glasses.

### Conclusions

Various surface analysis techniques show that silicate glasses rapidly develop surface compositional profiles when exposed to water. When water is present as a vapor an alkali-rich layer (presumably a hydrated alkali carbonate) forms over the SiO<sub>2</sub>-rich layer. Water as a liquid dissolves the alkali and leaves the silica-rich film. As long as this SiO<sub>2</sub>-rich film is stable the rate of corrosion due to diffusion is reduced with exposure time. Addition of multi-valent species to the glass or reactant results in formation of a complex protective surface layer in the glass which may be stable over a wide range of environmental conditions.

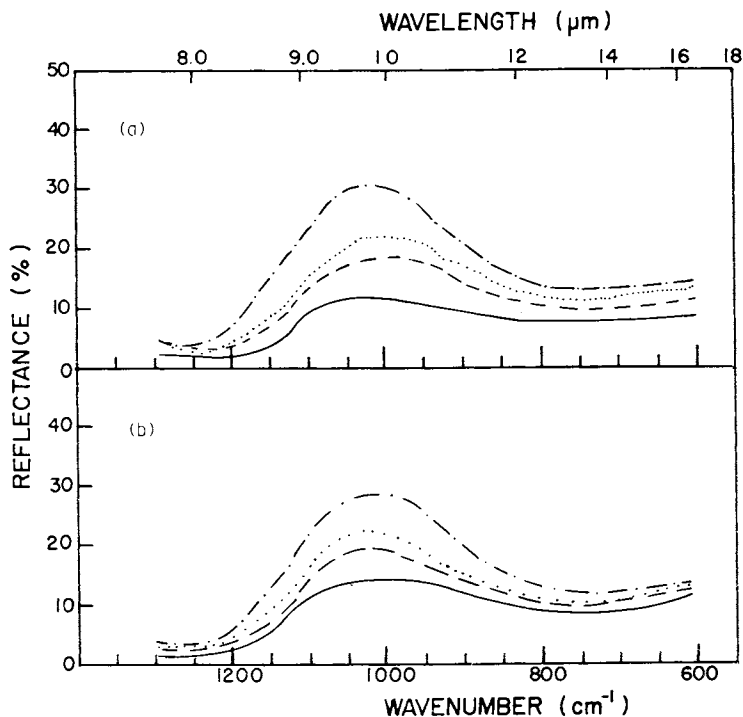


Figure 18. IR reflection spectra of a simulated nuclear waste glass buried in a granite repository for 28 d at 90°C with  $SA/V = 1.0$ . Each spectrum corresponds to a different depth within the surface. The percent reflectance is obtained when all of the corroded surface layer is removed by polishing. Key to a (IRRA-polish of corrosion layer glass #3): —, 0.002; ---, 0.008; ···, 0.010; and — · —, 0.012 cm removed thicknesses, respectively. Key to b (IRRA-polish of corrosion layer glass #3): —, 0.002; ---, 0.005; ···, 0.009; and — · —, 0.010 cm removed thicknesses, respectively.

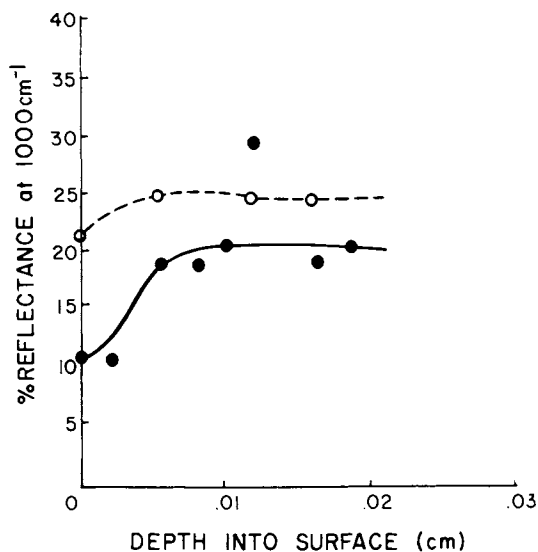


Figure 19. Compositional profile of the leached layers for the two different glasses. The curves flatten and become contrast at a depth corresponding to the thickness of the leached layer. Key: —●—, glass #3, 28 d, 90°C, SA/V = 0.1; and —○—, glass #5, 28 d, 90°C, SA/V = 0.1.

Acknowledgements

The authors gratefully acknowledge research support of AFOSR Contract F49620-80-C-0047.

Literature Cited

1. Clark, D. E.; Pantano, Jr., C. G.; Hench, L. L. "Corrosion of Glass," Books for Industry: New York, 1979.
2. Hench, L. L.; Clark, D. E. J. Non-Crystal. Solids, 1978, 28, 83-105.
3. Gottardi, V. ed. "The Chemical Durability of Glass--A Bibliographic Review of Literature;" International Commission on Glass, Institut de Verre: Paris, 1965; p. 76, 1973; p. 109.
4. R. A. Huggins, ed. "Annual Review of Materials Science;" Annual Reviews, Inc.: Palo Alto, Calif., 1976, Vol. 2, pp. 529-572.
5. V. Weiss and J. J. Burke, eds. "Characterization of Materials in Research, Ceramics and Polymers;" Syracuse Univ. Press: Syracuse, NY, 1975; 211-251.
6. MCC-1 Static Leach Test, Materials Characterization Center, submitted to the Materials Review Board, by Pacific Northwest Laboratory, Operated for the U.S. Department of Energy by Battelle Memorial Institute, August 1980 (no PNL # as of this date, 8/26/81).
7. Clark D. E.; Lue Yen-Bower, E. Surface Science, 1980 100, 53-70.
8. Sanders D. M.; Hench, L. L. J. Amer. Ceram. Soc., 1973, 56(7), 373-377.
9. Sanders, D. M.; Hench, L. L. Amer. Ceram. Soc. Bull., 1973 52(9), 662-665.
10. Simpson, H. E. Glass Ind., 1965 46(5), 272.
11. Sanders, D. M.; Hench, L. L. Amer. Ceram. Soc. Bull., 1973 59(9), 666-669.
12. Clark, D. E.; and Ethridge, E. C. Amer. Ceram. Soc. Bull., 1981 60(6), 646-649.
13. Pantano, Jr., G. C.; Dove, D. B.; Onoda, Jr., G. Y. J. Non-Crystal. Solids, 1975, 19, 41-53.

14. Rynd, J. P.; Rastogi, A. K. Amer. Ceram. Soc. Bull., 1974, 53(9), 631-634, 637.
15. Chappell, R. A.; Stoddart, C. T. H. Phys. Chem. Glasses, 1974, 15(5), 130-135.
16. Hench, L. L.; Clark, D. E.; Lue Yen-Bower, E. Nuclear and Chemical Waste Management, 1980, 1, 59-75.
17. Nogues, J. L.; Hench, L. L.; Zarzycki, J. J. Nuclear Materials (to be published).
18. Gossink, R.; de Grefte, H. A. M.; Werner, H. W. J. Amer. Ceram. Soc., 1979, 52(1-2), 4-9.
19. Lanford, W. A.; Davis, K.; Lamarche, P.; Laursen, T.; Groleau, R.; Doremus, R. H. J. Non-Crystal. Solids, 1979, 33, 249-266.
20. Chick, L. A.; McVay, G. L.; Mellinger, G. B.; Roberts, F. P. "Annual Report on the Development and Characterization of Solidified Forms for Nuclear Wastes, 1979," Battelle Memorial Inst., PNL Report 3465, Dec. 1980.
21. Budd, S. M. "ESCA Examination of Tin Oxide Coatings on Glass Surfaces," in Glass Surfaces, D. E. Day, ed., pp. 55-64, North Holland Publishing CO., Amsterdam (1975).
22. Bach, H.; Bauke, F. K. Phys. & Chem. of Glasses, 1974, 15(5), 123-129.
23. Baucke, F. K. J. Non-Crystal. Solids, 14, 1974, 13-31.
24. Tsong, I. S. T.; Houser, C. A.; Yusef, N. A.; Messier, R. F.; W. B. White. Science, 1978, 201 339-341.
25. Sanders, D. M.; Person, W. B.; Hench, L. L. Appl. Spectrosc., 1972, 26(5), 530-536.
26. Sanders, D. M.; Person, W. B.; Hench, L. L. Appl. Spectrosc., 28(3), 247-255.
27. Clark, D. E.; Ethridge, E. C.; Dilmore, M. F.; Hench, L. L. Glass Tech., 1977, 18(4), 121-124.

RECEIVED May 20, 1982

## Problems and Prospects of Instrumental Surface Analysis of Electronic Materials and Processes

MARY A. RYAN and GARY E. McGUIRE

Tektronix Inc., Beaverton, OR 97077

During the past decade, characterization and mass production of small electronic devices has shown significant advances in all areas of device processing. Increasing emphasis is being placed on uniformity, quality and cost. Process characterization and quality control have led to the widespread use of surface analysis techniques. This is because most IC structures are composed of thin layers,  $\leq 1\mu\text{m}$ , of semiconductors, insulators and metals. Surface analysis techniques provide elemental and chemical state information that has also been used in the development of emerging device processing technologies. Examples of the application of instrumental surface analysis in quality control and process development will be reviewed along with a summary of the materials problems that do not lend themselves to the available analytical techniques.

Characterization and mass production of small electronic devices has shown significant advances in the areas of crystal growth, slicing, polishing, cleaning, oxidation, patterning, implantation, diffusion, metallization and packaging. In addition to considerations for mass production, there has been increasing emphasis on uniformity, quality and cost. The need for process characterization and quality control has led to the widespread use of instrumental surface analysis in the IC industry. Because of the extensive use of films that are  $1\mu\text{m}$  or less in thickness, instrumental techniques for characterizing thin films and surfaces are utilized in all areas of IC processing. Surface analysis has become essential in the development and monitoring of cleaning processes while thin film profiling has been invaluable in the study of the composition of dielectric films, dopant profiles, inter-metallic diffusion and other thin film interactions. Surface analysis techniques provide elemental and chemical state information that has been used in the development of plasma and chemical vapor deposition techniques, thermal oxidation, plasma oxidation and plasma etching.

0097-6156/82/0199-0229\$06.25/0

© 1982 American Chemical Society



In this review, the process steps in IC fabrication and the major new technologies utilized are discussed. Numerous examples of the application of instrumental surface analysis in the study of electronic materials and processing are given.

However, this article is not intended to provide an exhaustive review of the voluminous literature on the application of surface analytical techniques to semiconductor problems. Numerous reviews have been published which have treated various aspects of these applications (1-5). This article is intended to give an overview, drawing from more recent publications, of the ways in which surface analysis continues to play a vital role in the development and application of the numerous material technologies involved in semiconductor processes. In addition, the need for further development of surface techniques and a summary of the materials problem that do not lend themselves to the available analytical techniques are described.

### Semiconductor Processing

A brief introduction to the process steps involved in fabricating a semiconductor device will provide a framework for discussing the major semiconductor process technologies which are to follow. Excellent and more comprehensive treatments of this topic are available (6, 7). The semiconducting substrate on which the device is fabricated is a wafer of single crystal material. The most common method used to grow large single crystals is the Czochralski Technique. Crystals are grown by this technique by inserting a perfect single crystal into a crucible containing molten ultra-high purity material. Specific impurities called dopants may be introduced to the molten solution in very small amounts to produce a specific type of conductivity. In the case of silicon, boron, aluminum or gallium may be used as dopants for positive (p-type) charge carriers while phosphorus, arsenic or antimony may be used for negative (n-type) carriers. As the seed crystal is slowly withdrawn from the melt, the molten material adheres to the seed crystal and forms a single crystal growth zone as it cools. Single crystal boules may be 100-125 mm in diameter and over 200 cm long. Wafers less than a millimeter thick are sawed from the boule at precise crystallographic orientations. The wafers are ground smooth on both sides and highly polished on one side. Each wafer can now be processed into many integrated circuits, each composed of numerous individual devices.

To fabricate the integrated circuit (IC), layers with various electrical properties must be introduced into or deposited onto the substrate. These layers may consist of insulating, semiconducting, and conducting films. The construction of the layers in only the desired areas relies on a series of patterning steps which is briefly illustrated in Figure 1. Light sensitive

positive photoresist which depolymerizes where it is exposed to actinic radiation or negative photoresist which polymerizes upon exposure is used to define the basic IC features. Currently resists sensitive to UV radiation make up the bulk of the resist used in manufacturing; however, resist sensitive to x-ray and electron beam exposure are undergoing rapid development.

The layers in a simple transistor requiring a separate patterning sequence are listed in Table I. Each mask listed in Table I requires the patterning sequence of Figure 1. In addition, process steps such as numbers 1, 3, 4 and 5 in Table I may require the growth or deposition of a dielectric before the patterning step. The resist, and often the dielectric, is removed in the exposed areas leaving a pattern on the substrate. Sometimes all of the photoresist is removed and the dielectric alone provides the pattern. A dopant is implanted or allowed to dif fuse into the surface over the whole wafer. However, the dielectric and/or resist act as a protective layer permitting the dopant to reach the substrate only in the areas previously exposed to light in the patterning process. Different technologies or devices will incorporate variations in the process steps and may require a different number or sequence of patterning steps.

After the fabrication steps outlined above, each wafer will now contain many integrated circuits. Each circuit is tested to determine that it functions correctly before the wafer is sawed into individual die each containing one integrated circuit. The die is mounted on a heat dissipating and mechanically supporting substrate. Electrical contacts are made from the small conductive bonding pads on the die to large metal leads. To provide further protection, the die and substrate are enclosed in a plastic or metal case with only the electrical leads protruding.

#### Semiconductor Processing Technologies and the Application of Surface Analysis Techniques

In this section the individual technologies utilized in the process steps listed in Table I will be discussed. A brief description of the technology and its application and importance in semiconductor processing is presented. Examples of the contribution made by surface analytical techniques in developing and utilizing these technologies are given. Due to their importance in semiconductor applications, the following surface techniques will be emphasized: Auger electron spectroscopy (AES), x-ray photoelectron spectroscopy (XPS, also known as ESCA), secondary ion mass spectrometry (SIMS), and Rutherford Backscattering Spectroscopy (RBS). A complete treatment of phenomena involved in these surface analytical techniques is given in references 8, 9, 10, and 11. A brief summary of the four major techniques is given in Table II.

TABLE I  
TYPICAL STEPS IN PROCESSING A BIPOLAR DEVICE

<u>MASK</u>	<u>PROCESS STEP</u>	
1	1	Buried Layer - heavily doped n <sup>+</sup> region
	2	Epitaxy - deposition of n-type layer
2	3	Isolation - p-type diffused region to provide electrical isolation between adjacent devices.
3	4	Base - p-type diffusion
4	5	Emitter - n <sup>+</sup> diffusion
5	6	Contacts to the various active regions
6	7	Metallization - conductive paths to electrically connect devices to form a circuit.
7	8	Protective layer to shield the device chemically and mechanically.

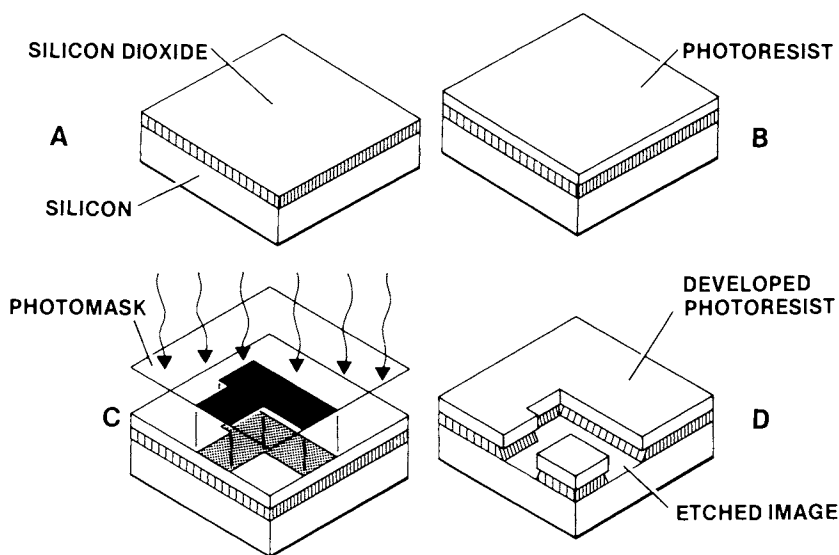


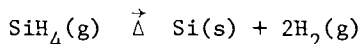
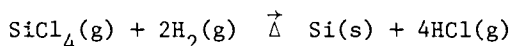
Figure 1. Typical photolithographic processing steps necessary to pattern SiO<sub>2</sub> layer on a Si substrate. Key: A, thermal oxidation; B, photoresist deposition; C, resist exposure through photomask; and D, develop photoresist.

TABLE II  
SUMMARY OF ANALYTICAL TECHNIQUES:  
CAPABILITIES AND LIMITATIONS

CHARACTERISTIC	AES	XPS	SIMS	RBS
Excitation Source	e <sup>-</sup>	X-Ray	Ion	Ion
Detected Emission	e <sup>-</sup>	e <sup>-</sup>	Ion	Ion
Elemental Detection	Z>3	Z>1	Z>1	Z>2
Elemental Identification	Excellent	Excellent	Good	Good
Sensitivity Variation	50	50	10 <sup>4</sup>	10 <sup>3</sup>
Detection Limits	0.1%	0.1%	10 <sup>-4</sup> %	10 <sup>-3</sup> %
Chemical Information	Yes	Yes	No	No
Lateral Resolution	50nm	2mm	1μm	1mm
Depth Resolution	5Å	5Å	10Å	100Å
Depth Probed		Sputter Depth		10 <sup>4</sup> Å
Depth Analysis		Destructive		Non-Destructive
Beam Induced Decomposition	High	Low	Low	Low
Sample Charging	Yes	Minor	Yes	No
Standards Required	Yes	Yes	Yes	No
Matrix Effects	Minor	Minor	Major	No
Special Feature	Spatial Resolution	Chemical Information	High Sensitivity	Non-Destructive Depth Analysis

Epitaxial Layers. Epitaxial deposition produces a single crystal layer on a substrate for device fabrication or a layer for multilevel conductive interconnects which may be of much higher quality than the substrate. The epitaxial layer may have a different dopant concentration as a result of introducing the dopant during the epitaxial growth process or may have a different composition than the substrate as in silicon on sapphire. Methods used for epitaxial growth include chemical vapor deposition (CVD), vapor phase epitaxy (VPE), liquid phase epitaxy (LPE), molecular beam epitaxy (MBE) and solid phase epitaxy (SPE).

Epitaxial deposition of Si may be achieved by CVD in any of a number of gas phase reactions similar to the ones listed below:



The use of surface analytical techniques in the study of epitaxial growth of Si has been primarily restricted to studies of the factors which affect the growth of a single crystalline layer: substrate cleaning, contamination and crystal quality.

Current research interest is in the solid phase epitaxial regrowth of amorphous Si using laser processing. RBS has been used to follow the melting and recrystallization of the crystal-amorphous interface (12). This is accomplished by monitoring the backscattered spectrum with the substrate oriented in a direction that will allow the  $\text{He}^+$  to channel along the crystal planes.

In another example of SPE, a single crystal Si substrate with a 1000Å thick Pd layer covered with 1µm of amorphous Si was heated to produce  $\text{Pd}_2\text{Si}$  (13). As the  $\text{Pd}_2\text{Si}$  reaction proceeds the thickness of the amorphous layer decreases and epitaxial Si is grown under the silicide layer. RBS, SIMS and AES were used to study the kinetics of the reaction. Substrate orientation and the concentration of carbon in the amorphous layer were found to be important factors in the rate of SPE growth.

Since amorphous Si is used in SPE and since some devices may be constructed using amorphous Si instead of epitaxial Si, it is pertinent to mention work in that area here. Amorphous Si exhibits electronic properties that are similar to those of crystalline semiconductors. These films contain considerable amounts of bonded hydrogen. For example, the hydrogen content of amorphous silicon films prepared from the glow discharge decomposition of silane ( $\text{SiH}_4$ ) has been found to vary between ~5 to 50 percent atomic (14). Without the hydrogen, the dangling Si bonds would create a high surface state density at the amorphous-crystalline interface. The importance of understanding the role of hydrogen in the electrical properties of amorphous Si has prompted the use of SIMS and nuclear reaction analysis (NRA) to determine the distribution of hydrogen in these films (15). For accurate results

by SIMS, it was found to be essential to perform the analysis in a chamber with a base pressure of  $10^{-10}$  torr to prevent deposition of hydrogen containing species on the sample surface.

Both the ability to detect hydrogen and the ability of SIMS to differentiate between isotopes were exploited in a study of deuterium diffusion in hydrogenated amorphous Si (14). Layered samples of hydrogenated and deuterated films were depth profiled before and after various heat treatments. The diffusion coefficient for deuterium obtained from these experiments implied that degradation of these films due to hydrogen out-diffusion at  $100^{\circ}\text{C}$  would not be significant until after more than  $10^4$  years.

Surface and thin film analysis has been used more extensively in the study of epitaxial growth of compound semiconductors where there is the additional requirement to monitor stoichiometry. Epitaxial deposition of GaAs is most frequently achieved by VPE or LPE, however, the area of most active research is MBE of GaAs and  $\text{Ga}_{1-x}\text{Al}_x\text{As}$ . In MBE, a molecular beam of elements like Ga or As are generated from thermal ovens in an ultrahigh vacuum system. After expanding into the vacuum space, the constituents condense and grow on the substrate under kinetically controlled conditions. The ovens are equipped with shutters which allow the beams to be interrupted to change doping levels, or for the growth of GaAs- $\text{Ga}_{1-x}\text{Al}_x\text{As}$  superlattices (16). The incorporation of both molecular beam and surface analytical equipment in a single UHV system was responsible for much of the early progress in defining and understanding MBE growth mechanisms (17). Reflection High Energy Electron Diffraction (RHEED), SIMS and AES are most applicable to MBE. Since growth by MBE is a kinetic process, the ability to examine the surface during growth is very valuable. SIMS can provide information on contamination and dopants to very low levels. AES is used to monitor surface contamination and stoichiometry while RHEED is used to monitor the crystal structure during epitaxial growth. Once a specific growth process is well developed the incorporation of much of the analytical equipment in an MBE system is not essential.

The MBE growth of semiconductor systems other than GaAs have also been reported. Partin used AES to determine substrate surface contamination in the growth of PbTe films by MBE (18). The surface chemical composition of InP as a function of thermal cleaning temperature was studied by Cheng, et al. (19), also using AES. They used an arsenic molecular beam and temperature of about  $500^{\circ}\text{C}$  to clean a freshly oxide passivated InP. The surface oxides are replaced by arsenic oxides which then vaporize at these temperatures. An atomically flat and carbon contamination free surface was obtained, as monitored in situ with AES and RHEED (19).

The Dielectric. Depending on the substrate, various dielectrics are used as diffusion and ion implantation masks, field and

gate dielectric for MOS devices, insulating layers for multilayer connections, capping layers for doped oxides, surface passivation and oxidation masks (7). The popularity of silicon as the material for microelectronic circuits is due to a large extent to the properties of silicon dioxide. When the silicon wafer is heated in an atmosphere of oxygen or water vapor, a hard, adherent, highly insulating film of silicon dioxide forms. Since the  $\text{SiO}_2$  layer is so intimately involved in the fabrication process, any contamination of this layer can ultimately affect device performance. During the oxide growth process whether thermal, plasma or other, conditions are maintained to give a sharp interface between the oxide and Si substrate. Unsatisfied bonds produce surface states which act as electrical traps in MOS devices. AES (20), XPS and SIMS (21) have been used to determine the chemical nature of the transitional region at the  $\text{SiO}_2$ -Si interface. A number of discrete chemical species are observed in the 3-7Å interface layer in thermal oxides, including silicon bonds to C, OH and H and a range of silicon oxidation states from 0 to +4. Ionic contaminants from the oxidation process or dopants from the substrate may become incorporated into the oxide film. Since these species migrate through the oxide under electrical bias they produce an electrical hysteresis in operating devices. Most surface analytical techniques probe the surface with a charged species (ions or electrons) which induces a positive charge on the insulating oxide surface. This also causes the mobile ionic contaminants including sodium to migrate to the  $\text{SiO}_2$ -Si interface and to change the concentration depth profile. One recent study successfully used SIMS to depth profile sodium in  $\text{SiO}_2$  films by neutralizing the surface charging caused by the probing primary ion, with a focused beam of electrons (22). In another study AES with sputter profiling, and SIMS were used to show that there is also a pile-up of phosphorus at the Si- $\text{SiO}_2$  interface during thermal oxidation of heavily doped Si (23). The vacancies in the interfacial region act as a sink for phosphorus. Subsequent high temperature annealing failed to reverse the pile-up.

Passivating films of  $\text{SiO}_2$  are deliberately doped with P, As and B to produce a protective glassy layer over the surface of a device. This layer acts as a barrier to ionic contamination that may be inadvertently introduced after device fabrication. AES with sputter profiling has been used to determine the concentration and distribution while XPS has been used to determine the chemical bonding of the dopant species (24). During the past few years there has been a shift away from the exclusive use of oxide passivating layers to nitride or mixed oxide-nitride films because of their resistance to ionic contamination and moisture penetration. Device structures with mixed oxide-nitride layers are becoming increasingly popular for non-volatile memories. Films deposited by CVD from gaseous mixtures of silane and ammonia at elevated temperatures provide the most consistently pure nitride films. However, the use of low temperature glow

discharge plasma deposition of nitrides from  $\text{SiH}_4$  and  $\text{NH}_3$  or  $\text{N}_2$  mixtures has been the major technology resulting in the increased use of nitride films in the semiconductor industry.

Although CVD and plasma deposited films offer excellent properties as a passivation layer, the inability to reproduce chemical and physical properties has been a problem. Depending on gas flow rates and deposition conditions, free Si, H, C and O may be incorporated into the films. Characterization of these films has been restricted almost exclusively to surface analytical techniques and ellipsometry. AES and XPS have been used to determine the C, N, O, and Si content of CVD silicon nitride. The composition is then related to refractive index which is a measurement easily made in a process lab (25). The ability of XPS to distinguish chemical oxidation states was used to show that there was less than 3 at.% free silicon in CVD silicon nitride on silicon when the refractive index was less than 2.08. AES data indicated that as the refractive index increased the percent  $\text{SiO}_2$  decreased. Recently Kapoor, et al. (26), also used AES to determine O, N and Si in  $\text{Si}_3\text{N}_4$  films intended for MNOS structures. Variations in the oxygen content of the films were correlated with variations in the trapped electron density and are believed to be due to nonbridging oxygen atoms acting as electron acceptors. The structural features of AES signals in the N(E) mode were used to provide information on Si-H and elemental Si in plasma deposited Si nitride films since the H content could not be measured directly by AES (27). The hydrogen content could be measured by SIMS except quantification is difficult. Nuclear reaction analysis using the  $^1\text{H}(^{19}\text{F}, \alpha \gamma)^{16}\text{O}$  reaction is the only technique used in studies of nitride films that quantitatively measures the depth distribution of the hydrogen (28).

Oxides of Ga and As also play an important role in the fabrication of GaAs devices. Achieving an adequate passivating film with a low density of interface states on GaAs or other compound semiconductors is as desirable as it is for silicon devices. The fact that the oxides of Ga and As are not stable, unlike  $\text{SiO}_2$ , during high temperature thermal oxidation or subsequent high temperature processing steps makes them less than ideal as passivating films. In spite of their instability there has been considerable interest in the preparation of these oxides using low temperature processing techniques and in their characterization with surface analysis techniques.

The growth mechanism of anodically grown oxides of GaAs was studied using SIMS (29). This study sought to determine whether oxygen or Ga and As were the mobile species during oxide growth by using isotopically labeled  $\text{H}_2\text{O}$ . SIMS was used to profile through the anodic oxide to determine the  $^{16}\text{O}$  and  $^{18}\text{O}$  distribution. Figure 2 shows that oxygen is incorporated into the film at the oxide-electrolyte interface. This suggests that Ga and As are the mobile species and that mass transport occurs through the interstices of the growing oxide.



Similar experiments were performed by Koshiga et al in a study of the oxidation of GaAs in an oxygen plasma generated by a DC electrical discharge (30). Using  $^{18}\text{O}_2$  and  $^{16}\text{O}_2$  plasmas in subsequent steps it was shown, again by SIMS, that oxygen is incorporated into the film at the plasma-oxide interface in agreement with the mechanism found by Coleman et al. (29) for anodic oxides. SIMS is the only common surface technique that can readily distinguish isotopes of the lighter elements.

RBS is capable of distinguishing the isotopes of heavier elements, however the more common use of RBS is for the determination of stoichiometric ratios and composition as a function of depth. RBS was used in another study of plasma grown oxide films on GaAs to determine the ratio of O to Ga and As (31). Based on the well known ion scattering cross-sections, a ratio approaching 1.5 was found for films greater than 1000Å thick. The composition of the oxide inferred from this result is a mixture of  $\text{Ga}_2\text{O}_3$  and  $\text{As}_2\text{O}_3$ .

Complementary data was obtained by other surface analysis techniques. In one study sputter profiling of Ga, As and O by AES and XPS showed a deficiency of As in plasma grown oxides (32). In another study a comparison of thermal, anodic and plasma oxidation layers on GaAs was made using SIMS, AES, and XPS (33). AES depth profiles showed that the oxide layers were very similar for anodic and plasma oxidation. The O, Ga and As concentration levels were nearly constant with depth until the interface with the substrate was reached. However, the thermally grown oxide was depleted in As, and the substrate near the oxide-substrate interface was enriched in As and depleted in Ga. Annealing the plasma oxide produced a profile similar to the thermal oxide. XPS studies of thermal oxides (32, 34) complement the results obtained by Watanabe (33). The shift in the 3d photoelectron binding energies of As and Ga as shown in Figure 3 indicate the surface of the oxide is predominately  $\text{Ga}_2\text{O}_3$ , a mixture of  $\text{Ga}_2\text{O}_3$  and  $\text{As}_2\text{O}_3$  in the bulk and Ga and As in the GaAs substrate. Other experiments determined that a water rinse of the surface had caused the surface depletion of  $\text{As}_2\text{O}_3$  and that the low binding energy As satellite resulted from the  $\text{Ar}^+$  sputter beam reduction of  $\text{As}_2\text{O}_3$ . Changes in the structural features of Auger transitions that appear in XPS spectra due to x-ray excitation of Auger electrons were also used to provide information on the chemical states of Ga and As (34). These structural features are the result of coupling of the core electron hole with the valence electrons. Similar changes could be observed in electron excited Auger transitions. However, XPS spectra are taken with better energy resolution so that the combined information in photoelectron and Auger transitions provides the most definitive information on the chemical states of the surface species. SIMS analysis of thermal oxides on GaAs,  $_{1-x}P_x$  also shows a depletion of As in the oxide (35). The oxide was found to be composed of Ga

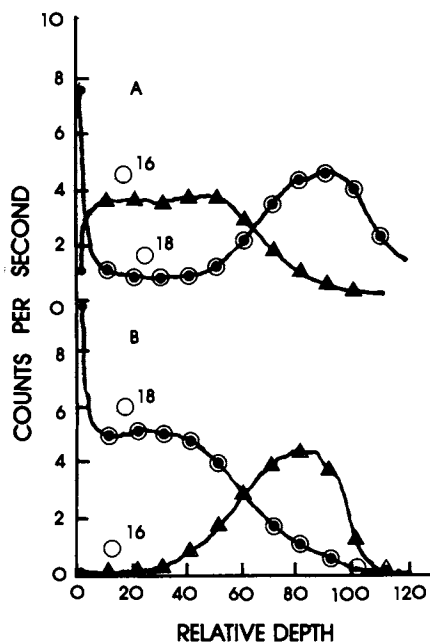


Figure 2. SIMS depth profiles of the isotopic oxygen distribution for GaAs. Key to (A):  $\Delta$ , anodically oxidized in  $H_2^{18}O$ ;  $\circ$ , anodically oxidized in  $H_2^{16}O$ . Key to (B):  $\circ$ , anodically oxidized in  $H_2^{18}O$ ; and  $\Delta$ , anodically oxidized in  $H_2^{16}O$ . (Reproduced, with permission, from Ref. 29. Copyright 1979, Electrochemical Society.)

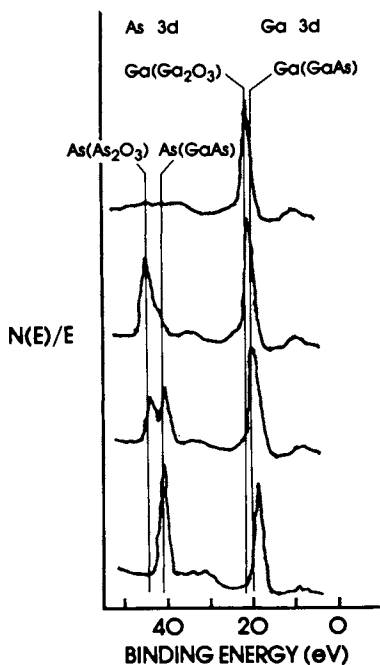


Figure 3. Progression of Ga 3d and As 3d photoelectron transitions as a function of depth in an anodically grown oxide on GaAs. The change in binding energy transitions for the As 3d in  $As_2O_3$  and GaAs, and for the Ga 3d in  $Ga_2O_3$  and GaAs, reflect a changing chemical composition as a function of depth. Key from top to bottom: anodized surface, 325–1415 Å, 1580 Å, and GaAs substrate. (Reproduced, with permission, from Ref. 34. Copyright 1979, Electrochemical Society.)

and P compounds with As rich regions at the oxide surface and at the oxide-semiconductor interface. Incorporation of P into the grown oxide shows somewhat improved electrical behavior of these oxides compared with the behavior of thermal oxides grown on GaAs.

Patterning. The patterning process shown in Figure 1 requires some means to etch or react with the exposed wafer areas. Historically wet chemical etchants of various acids and bases have been the most common means of removing material. Analytical techniques with high spatial resolution, such as AES and SIMS, are used to detect unremoved material in a window that might prevent proper operation of the device. The need for this type of analysis has increased with the decrease in the size of IC features. A simple extrapolation of etch rates and times is no longer possible because the small geometries retard the flow of etchant into the window.

The preparation or etching of compound semiconductors is more complex due to the potential of altering the surface stoichiometry. Shiota et al. (36) used AES to show that the final As/Ga at the surface of GaAs was very dependent on the chemical activity of wet chemical etchants. Bertrand was able to follow the changes in the chemical bonding of Ga and As on p-type GaAs etched in HCl or Br<sub>2</sub> in methanol and relate this to Schottky barrier heights of similarly prepared surfaces with Pb contacts (37).

During the past several years there has been a dramatic shift away from wet chemical etching to plasma etching, ion milling, and other gas phase techniques. These techniques have advantages over wet chemical etching in terms of chemical disposal, edge definition and undercutting. However, they have disadvantages that prevent their universal application in the IC industry. In plasma etching the material to be removed must form a volatile species. Figure 4 shows the residue left after plasma etching an Al film that contained 4% atomic Cu. The Al is successfully volatilized in the CCl<sub>4</sub> plasma. The Cu does not form a volatile product and is left behind as a surface contaminant. Impurities may not only form non-volatile residues but also inhibit the plasma etching characteristics of the film to be etched. For example, Nakata et al. (38) used AES to show that trace impurities of Fe and Cu significantly inhibit the plasma etching characteristics of Cr and Cr oxide films used in photo-mask production.

Ion milling is a more widely applicable etching technique in that all materials may be sputtered away anisotropically. The ion milling rate typically does not vary more than a factor of 100. Redeposition of material from the substrate or surrounding fixtures can lead to undesirable cross-contamination. Hosaka et al. (39) used SIMS to show that redeposition of ionic impurities can occur during ion etching of SiO<sub>2</sub> layers on Si when using a

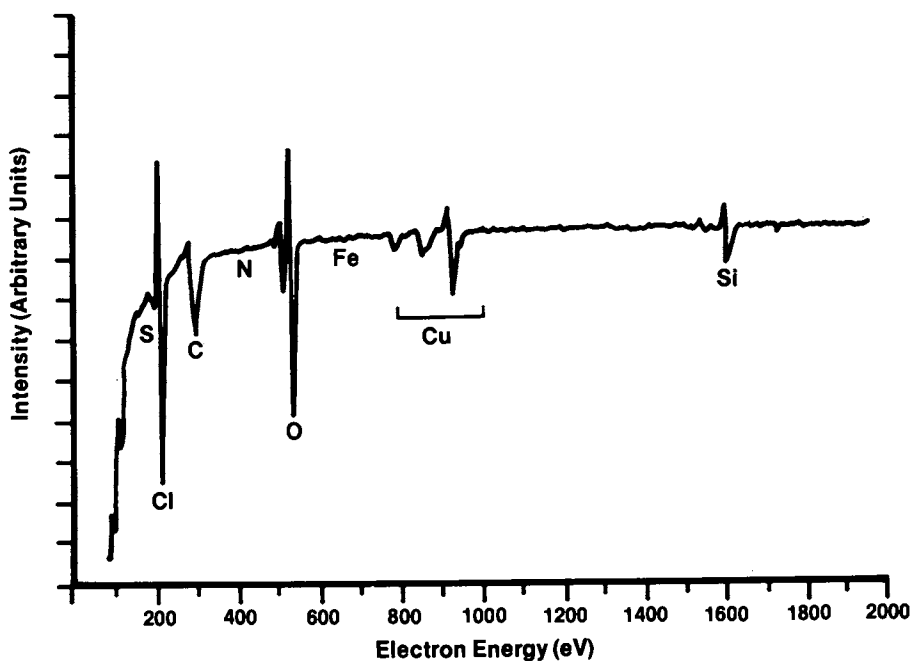


Figure 4. AES spectrum of nonvolatile Cu residue from 4% Cu-doped Al metalization on Si after plasma etching in  $\text{CCl}_4$  (55).

large diameter Kaufman type ion source. Shielding the surrounding support fixtures with a material with no ionic impurities was shown to be an effective means of reducing contamination.

Dopant. Dopant species may be introduced into the semiconducting substrate at various points in the process and by different means. As mentioned above, some dopant may be added to the molten solution as the single crystal is being grown. Dopant introduced in subsequent steps (see steps 1, 3, 4, and 5, Table I) may be introduced by means of diffusion or ion implantation. In diffusion the dopant is introduced as a gas or liquid onto the surface of the wafer and allowed to diffuse into the substrate. In ion implantation the gaseous dopant is ionized and accelerated into the wafer. SIMS has been used extensively to obtain dopant concentration depth profiles because it is the most sensitive of the surface analytical techniques and because sputtering is an intrinsic part of the dynamic SIMS process (40). AES, combined with ion sputtering, has also been used to obtain depth profiles for high dose implants (41).

Sophisticated theoretical models now exist that are able to predict very accurately the implant concentration profiles that result for a particular ion implant dose, ion energy and substrate (42, 43). These models have been refined to the state where they may be able to predict the implant profile more accurately than the profile can be determined experimentally, due to the low implant doses, spectral interferences or artifacts of the sputtering process. It is becoming accepted practice to use ion implantation to create standards for SIMS analysis (41). Nevertheless, the use of analytical techniques to experimentally determine depth profiles remains essential because subsequent processing steps may result in redistribution of the dopant species. In addition, depth analyses may be necessary for more complicated implant profiles where theoretical models are inadequate. For example, SIMS was used to profile the Si concentration in an Si implanted GaAs wafer (44). By varying the accelerating voltage for multiple implants, a nearly constant doping level was achieved to a depth of  $1\mu\text{m}$ .

Subsequent to ion implantation, the wafer must be annealed to remove the damage to the crystal lattice caused by the implantation process and to electrically activate the dopant species. The dopant must occupy a substitutional site before it becomes electrically active. Of the surface analysis techniques only RBS can provide information on the location of the dopant in the lattice. When the high energy ion beam used in RBS is oriented parallel to the crystal planes of a semiconducting substrate, the ions will channel along the crystal planes. Very few scattering events result unless those planes are occupied by interstitial atoms. By observing the RBS signal as a function of angle between the incoming ion beam and the crystal planes, RBS can be used to determine both the extent of crystal damage and the quantity of substitutional and interstitial dopant atoms.

Redistribution of the dopant species occurs as a result of the annealing process. Lidow et al. (40) studied the effects of thermal annealing on Se implanted GaAs. The implanted Se profiles closely matched theoretical predictions. However, the change in the depth profile as a result of annealing at 1000°C for 15 minutes, 3 hours and 12 hours was less than predicted based on previously determined diffusion constants. To explain these results, the authors suggest that the diffusion process is complicated by the recrystallization and annealing of the ion damage in the crystal lattice.

Historically thermal annealing has been the method of removing implantation damage. Recently however, laser annealing has been pursued as an attractive alternative. Tsien, et al. (45) compared annealing boron implanted silicon using a continuous wave (CW) carbon dioxide laser to thermal furnace annealing at 1000°C for 30 minutes. SIMS, RBS and electrical measurements were used to determine crystal damage recovery, B concentration profiles and electrical activation. The CO<sub>2</sub> laser irradiation produced better results than furnace annealing with virtually no redistribution of the implanted species.

RBS has been used in the study of pulsed laser annealing of As implanted Si. Williams et al. (46) found that if a dose dependent threshold power level were exceeded, the melt regime produced essentially perfect recrystallization of the implanted amorphous Si. Figure 5 shows RBS spectra obtained from near random and aligned orientations for a high As dose implant annealed with above threshold conditions. The low signal level between peaks in the aligned spectrum indicates excellent crystal regrowth and high As substitutionality. Segregation of As near the surface is suggested since the As signal for the aligned and random crystal orientations are equally intense. In addition, the As concentration in the crystal lattice is approximately a factor of two greater than the accepted solid solubility of As in Si. The fact that laser annealing can be used to form metastable phases or systems in which the solubility limit is exceeded is considered an advantage over thermal annealing.

White and Christie used SIMS and RBS to measure dopant profile broadening caused by pulsed laser annealing (47). They also observed the incorporation of Group III-V dopants in Si at levels exceeding previously accepted solid solubility limits. Non-substitutional species, like Fe, were not incorporated in the Si but were segregated to the surface.

Metallization. In the fabrication sequence described in Table I, metal layers are used as conductive paths between points on the same integrated circuit or as contact points between the IC and its package. The metal layers may be single component, multi-component alloys or multilayered thin films depending on the application. The methods used for depositing the metal are

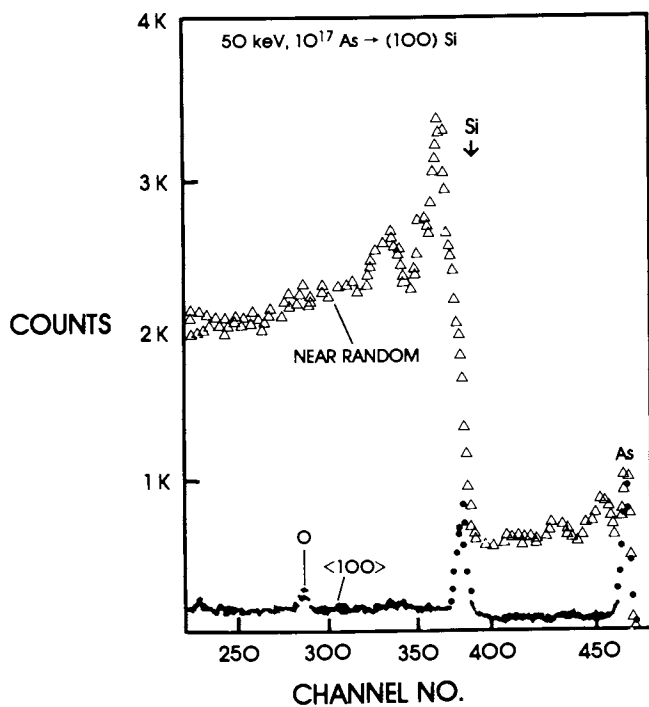


Figure 5. RBS spectra obtained from near random and aligned orientations for pulsed-laser annealed, As ion-implanted Si. (Reproduced, with permission, from Ref. 46. Copyright 1981, Journal of Applied Physics.)

quite diverse and depend to a large extent on the melting point of the metal and the requirements of the contact. These methods include thermal and electron beam evaporation, chemical vapor deposition, sputtering and electroplating.

Common concerns involving metal contacts include adhesion to the substrate, degradation due to corrosion, electromigration etc. and the tendency for some multilayered metallization schemes to undergo rapid interdiffusion. Surface analysis has been used to address a number of these problems.

Ohmic contacts to GaAs are frequently made by AuGeNi or AgInGe. In this system, the Ni or In acts as a wetting agent to promote adhesion to the substrate. AES has been used to profile through these films in order to study the role of the Ni and In in promoting adhesion during high temperature alloying and device operation (48).

Denison and Hartsough (49) also used AES to study the Cu distribution in 2-4% Cu doped Al films. The Cu is introduced to prevent electromigration in this system when used as an ohmic contact to Si. Their results showed Cu segregation to the film substrate interface for both DC magnetron sputtered and evaporated films. The segregation was partially reversible upon subsequent annealing.

Barrier metals, as opposed to alloys like AuGeNi, are employed in many thin film metallization systems to promote adhesion and prevent interdiffusion. Gold is an excellent conductor, however, it has very poor adhesion to both Si and GaAs. Gold also shortens the device lifetime when it diffuses into an active region of the device. For this reason it is used in multilayered structures such as Ta/Pt/Ta/Au (50), W/Au (50) and Cr/Au (51). SIMS, AES and RBS have all been used effectively in studying metal-metal interdiffusion, to extract diffusion coefficients, and to estimate device lifetimes.

Finally, surface analysis has been used in the investigation of metal silicides used to form rectifying Schottky barrier contacts to semiconductors. These silicides are formed by thermal or laser sintering of the metal after deposition onto the substrate. Excess unreacted metal is removed by chemical etching. XPS has been used to show that the metal has been oxidized if the excess metal cannot be removed (52).

Recently, RBS has been used to study the metal-silicon reactions induced by both a CW laser and an electron beam (53). Uniform, large area, single phase silicides were formed by adjusting the beam power level to induce a solid state reaction. Under certain conditions metastable mixed-phase systems were also obtained. RBS could non-destructively determine the stoichiometry of the phases formed without additional standards. AES and SIMS have also been used in the study of metal silicides. These applications and other points of interest in the fabrication, characterization and application of metal-semiconductor Schottky barrier junctions have been reviewed recently by Sharma and Gupta (54).



### Conclusion

The use of surface analysis to investigate semiconductor materials and processes has grown at a surprising rate since the first commercial introduction of these techniques. Almost all areas of device processing have been studied by one or more of the techniques discussed in this review. Many of the current problems in semiconductor processing present a challenge to the state of the art in surface analysis. The doping levels and bulk impurities of high purity semiconductors are often below the detection limits of most surface analysis techniques. Contamination of the sample during sampling and/or analysis with carbon, hydrogen or oxygen containing species makes quantitation of low levels of these elements difficult. The whole area of quantitative analysis by surface analysis techniques has received a great deal of attention but requires even further development. Well characterized standards similar to the sample are necessary for accurate quantitative results with most techniques. Appropriate standards are often not available and are frequently difficult to prepare.

It is expected that the geometrical dimensions of IC devices will continue to decrease through the use of electron beam and x-ray lithography. Analysis of these small geometries presents additional challenges since a tradeoff exists between analysis area, and detection limits for the microbeam analysis techniques, AES and SIMS. The other surface analysis techniques of XPS and RBS already have very limited spatial resolution with respect to the current geometrical dimensions of IC's. The fabrication of denser and more complicated IC's also increases the value of each wafer which increases the need for additional process characterization and control. The increased application of surface analysis to semiconductor problems will provide a better understanding of these processes and will stimulate the further development of instrumental surface analysis techniques.

### Literature Cited

1. Holloway, P.H.; McGuire, G. E. Appl. Surface Sci. 1980, 4, 410-444.
2. Morabito, J. M.; Lewis, R. K. "Methods of Surface Analysis"; Czanderna, A. W., Ed.; Elsevier Scientific Publishing Company: New York, NY, 1975; pp. 279-328.
3. Holloway, P. H. "Applied Surface Analysis, ASTM STP 699"; Barr, T. L.; Davis, L. E., Eds.; American Society for Testing and Materials: Philadelphia, PA, 1980; pp. 5-23.
4. Zinner, E.; Scanning 1980, 3 (2), 57-78.
5. Yin, S. Y. Proc. 16th Nat. Conf. Microbeam Analysis Society; Vail, CO, July 1981; 342-378.
6. Gise, Peter G.; Blanchard, Richard "Semiconductor and Integrated Circuit Fabrication Techniques"; Reston Publishing Company: Reston, VA; 1979.

7. Oldham, W. G. Sci. Am. 1977, 237 (3), 111-128.
8. McHugh, J. A. "Methods of Surface Analysis"; Czanderna, A. W., Ed.; Elsevier Publishing Company: New York, NY, 1975; pp. 223-278.
9. Chu, W. K.; Mayer, J. W.; Nicolet, M. -A. "Backscattering Spectrometry"; Academic Press: New York, NY, 1978.
10. Carlson, T. A. "Photoelectron and Auger Spectroscopy"; Plenum Press: New York, NY, 1975.
11. Joshi, A.; Davis, L. E.; Palmberg, P. W. "Methods of Surface Analysis"; Elsevier Publishing Company: New York, NY, 1975; pp. 159-222.
12. Williams, J. S.; Brown, W. L.; Celler, G. K.; Leamy, H. J.; Poate, J. M.; Rozgonyi, G. A.; Sheng, T. T. J. Appl. Phys. 1981, 52 (2), 1038-1049.
13. Liao, Z. L.; Lau, S. S.; Nicolet, M. A.; Mayer, J. W.; Blattner, R. J.; Williams, P.; Evans, Jr., C. A. Nucl. Inst. and Meth. 1978, 149, 623-627.
14. Carlson, D. E.; Magee, C. W. Appl. Phys. Lett. 1978, 33 (1), 81-83.
15. Clark, G. J.; White, C. W.; Allred, D. D.; Appleton, B. R.; Magee, C. W.; Carlson, D. E. Appl. Phys. Lett. 1977, 31, 582-585.
16. Chang, L. L.; Esaki, L. "Molecular Beam Epitaxy"; Pamplin, B., Ed.; Pergamon Press: New York, NY, 1980; pp. 3-14.
17. Luscher, P. E.; Collins, D. M. "Molecular Beam Epitaxy"; Pamplin, B., Ed.; Pergamon Press: New York, NY, 1980; pp. 15-31.
18. Partin, D. L. J. Electron Mater. 1981, 10, 313-325.
19. Cheng, K. Y.; Cho, A. Y.; Wagner, W. R.; Bonner, W. A. J. Appl. Phys. 1981, 52 (2), 1015-1021.
20. Helms, C. R.; Spicer, W. E.; Johnson, N. M. Solid State Commun. 1978, 25 (9), 673-676.
21. Grunthaner, F. J.; Maserjian, J. "Physics of SiO<sub>2</sub> and Its Interfaces"; Pantelides, S., Ed.; Pergamon Press: New York, NY, 1978; pp. 389-395.
22. Magee, C. W.; Harrington, W. L. Appl. Phys. Lett. 1978, 33 (2), 193-196.
23. Schwarz, S. A.; Barton, R. W.; Ho, C. P.; Helms, C. R. J. Electrochem. Soc. 1981, 128 (5), 1101-1106.
24. Zeller, M. V., Application Note, Physical Electronics Division, Perkin-Elmer Corporation, Eden Prairie, Minnesota.
25. Wittberg, T. N.; Hoenigman, J. R.; Moddeman, W. E.; Cothorn, C. R.; Gullett, M. R. J. Vac. Sci. Technol. 1978, 15, 348-352.
26. Kapoor, V. J.; Bailey, R. S.; Smith, S. R. J. Vac. Sci. Technol. 1981, 18 (2), 305-308.
27. Madden, H. H. J. Electrochem. Soc. 1981, 128 (3), 625-629.
28. Stein, H. J.; Wells, V. A.; Hampy, R. E. J. Electrochem. Soc. 1979, 126 (10), 1750-1754.

29. Coleman, Jr., D. J.; Shaw, D. W.; Dobrott, R. D. J. Electrochem. Soc. 1977, 124, 239-241.
30. Koshiga, F.; Sugano, T. Thin Solid Films 1979, 56, 39-49.
31. Kauffman, R. L.; Feldman, L. C.; Poate, J. M.; Chang, R. P. H. Appl. Phys. Lett. 1977, 30, 319-321.
32. Mizokawa, Y.; Iwasaki, H.; Nishitani, R.; Nakamura, S. J. Electrochem. Soc. 1979, 126, 1370-1374.
33. Watanabe, K.; Hashiba, M.; Hirohata, Y.; Nishino, M.; Yamashina, T. Thin Solid Films 1979, 56, 63-73.
34. Schwartz, G. P.; Gualtieri, G. J.; Kammlott, G. W.; Schwartz, B. J. Electrochem. Soc. 1979, 126, 1737-1749.
35. Kuhlman, G. J.; Pancholy, R. K.; Phillips, D. H. Thin Solid Films 1979, 56, 129-142.
36. Shiota, I.; Motoya, K.; Ohmi, T.; Miyamota, N.; Nishizawa, J. J. Electrochem. Soc. 1977, 124 (1), 155-157.
37. Bertrand, P. A. J. Vac. Sci. Technol. 1981, 18 (1), 28-33.
38. Nakata, H.; Nishioka, K.; Abe, H. J. Vac. Sci. Technol. 1980, 17 (6), 1351-1357.
39. Hosaka, S.; Kawamota, Y.; Hashimoto, S. J. Vac. Sci. Technol. 1981, 18 (1), 17-22.
40. Lidow, A.; Gibbons, J. F.; Deline, V. R.; Evans, Jr., C. A. Appl. Phys. Lett. 1978, 32, 15-17.
41. Leta, D. P.; Morrison, G. H. Anal. Chem. 1980, 52, 514-519.
42. Gibbons, J. F.; Johnson, W. S.; Mylroie, S. W. "Projected Range Statistics"; 2nd ed., Dowden, Hutchinson, and Ross, Stroudsburg, PA, 1975.
43. Hofker, W. K.; Oosthoek, D. P.; Koeman, N. J.; DeGrefte, H. A. M. Radiat. Eff. 1975, 24, 223.
44. Liu, S. G.; Douglas, E. C.; Wu, C. P.; Magee, C. W.; Narayan, S. Y.; Jolly, S. T.; Kolondra, F.; Jain, S. RCA Review 1980, 41, 227-262.
45. Tsien, P. H.; Tsou, S. C.; Takai, M.; Roeschenthaler, D.; Ramin, M.; Ryssel, H.; Ruge, I.; Wittmaack, K. Phys. Status Solidi A 1981, 63, 547-555.
46. Williams, J. S.; Brown, W. L.; Celler, G. K.; Leamy, H. J.; Poate, J. M.; Rozgonyi, G. A.; Sheng, T. T. J. Appl. Phys. 1981, 52 (2), 1038-1049.
47. White, C. W.; Christie, W. H. Solid State Technol. 1980, 23 (9), 109-116.
48. McGuire, G. E.; Holloway, P. H. Scanning Electron Microscopy 1979, 1, 173-202.
49. Denison, D. R.; Hartsough, L. D. J. Vac. Sci. Technol. 1980, 17 (6), 1326-1331.
50. Christou, A. Scanning Electron Microscopy 1979, 1, 191-202.
51. Holloway, P. H. Solid State Technol. 1980, 23 (2), 109-115.
52. Lowry, R. K.; Hogrefe, A. W. Solid State Technol. 1980, 23 (1), 71-75.

53. Shibata, T.; Sigmon, T. W.; Regolini, J. L.; Gibbons, J. F. J. Electrochem. Soc. 1981, 128 (3), 637-644.
54. Sharma, B. L.; Gupta, S. C. Solid State Technol. 1980, 23 (5), 97-101.
55. McGuire, G. E.; Holloway, P. H. "Electron Spectroscopy: Theory Techniques and Applications"; Brundle, C. R.; Baker, A. D., Eds.; Academic Press: London, 1981; pp. 1-84.

RECEIVED May 21, 1982

# Use of Surface Analytical Techniques to Examine Metal Corrosion Problems

D. R. BAER and M. T. THOMAS

Pacific Northwest Laboratory, Richland, WA 99352

The applications of several surface analytical techniques to the solution of corrosion problems are reviewed in this paper. The use of surface techniques in corrosion work is increasing both because the methods are more widely available than previously and because the techniques themselves are being refined. However, the application of these methods to particular corrosion problems is not always straightforward and care must be taken to match the use of any method to the specific problem. Some general guidelines concerning the applicability of surface tools are discussed before several examples of their application are given. Techniques discussed include: X-ray photoelectron spectroscopy (XPS), Auger electron spectroscopy (AES), Rutherford backscattering (RBS) and nuclear reaction spectroscopy.

Corrosion affects our lives in many different ways and has been termed the "silent scourge" and a "cancer of materials" (1). Although these terms may seem overly dramatic, a 1976 study found that metallic corrosion cost the United States \$70 billion a year or roughly 4.2% of the gross national product (2). If corrosion of paints, plastics, wood, glasses and other materials were included, the cost would be over \$1 trillion a year (3). Either amount is considerably larger than the \$45 billion expense for importing foreign crude oil in 1977.

Corrosion is simply the destruction or deterioration of a material because of a chemical reaction with its environment (4). Types of corrosion range from rust on an automobile to intergranular cracking of a pipe in a gas well. In addition to its economic impact, corrosion affects our health and safety, the development of new technology, the existence of ancient works of art and even, through material availability, national security (2).

0097-6156/82/0199-0251\$08.75/0  
© 1982 American Chemical Society

The enormous economic and other costs of corrosion have motivated considerable research toward minimizing corrosion and understanding its causes. During the past five years, analytical tools sensitive to the surface (or the outer 10 to 500Å of a material) have been increasingly applied to the study of corrosion. This paper outlines general criteria to help determine the usefulness of surface techniques for the study of specific corrosion problems and gives several examples showing how the techniques have been applied.

### TYPES OF CORROSION AND THEIR RELATIONSHIP TO SURFACE AND INTERFACE ANALYSES

Corrosion necessarily involves a reaction of a material with its environment at a solid-gas, solid-liquid or solid-solid interface. One might think, therefore, that corrosion scientists would be among the most enthusiastic users of surface analytical techniques, which by their nature examine such interfaces (5). However, as McIntyre (5) notes about XPS, "the impact on corrosion science has been rather modest," and according to an editorial in Corrosion (6), any significance of surface science in solving corrosion problems is not obvious to many corrosion professionals and plant operators. Recent advances in surface science techniques have increased the usefulness of these methods in applied areas such as corrosion. To understand the current role of surface analysis in corrosion research and problem solving, it is necessary to know about the many forms of corrosion and the advantages and limitations of surface techniques in each area.

#### Types of Corrosion

There are many types of corrosion, as would be expected from its general definition. It has been traditional (4) to divide the study of corrosion into two areas: the study of low temperature corrosion by aqueous or other solutions, controlled by electrochemical processes (wet); and the study of gaseous corrosion at high temperatures, controlled by thermodynamics and diffusion processes (dry). In addition to the obvious differences, the two areas have many phenomena in common.

Nearly all metals are thermodynamically unstable in most environments and the result of this instability is corrosion, such as oxidation or some other reaction with the environment. In both "wet" and "dry" corrosion three general phenomena occur. First, material from the metal can dissolve in the environment. This takes forms such as evaporation and volatile compound formation at high temperatures and material dissolution in aqueous solutions. Material loss by such processes may weaken a structure or cause loss of a protective layer. Second, a reaction layer may form on the surface of the metal. Frequently, these layers reduce the rate of a reaction and thus protect the material (passivate a

metal). However, not all films are protective and in some corrosion environments normally protective films are themselves attacked. The conditions for which passive protective films are formed and attacked are subjects of active investigation in corrosion research. Several common types of corrosion involve the attack of these protective films and replacement by faster growing non-protective layers. This attack may be uniform (general corrosion), localized at discrete points (pitting) or induced by stress (stress corrosion). Third, material from the environment may be incorporated into the metal. Oxides may precipitate within the metal or hydrogen may be adsorbed and in either case the material can be embrittled and unable to withstand design loads. Hydrogen-induced embrittlement occurs in both aqueous and gaseous environments.

The nature of corrosion depends critically on both the environment and the material. Often corrosion is localized in particular areas because of non-uniformities in the material (near welds or corners) or non-uniformities in the environment such as shielded areas near gaskets (crevice corrosion).

It is important to realize that corrosion rates may be controlled by any of several thermodynamic or kinetic properties of the alloy-scale-environment system and not just by surface or interface reactions. The three stages of high temperature oxidation of a metal, shown schematically in Fig. 1, serve as an example (7). The first or transient stage includes initial gas adsorption, two-dimensional oxide nucleation, initial three-dimensional oxide formation and finally, formation of the dominant oxide that will control the oxidation rate in Stage II. Various portions of Stage I have been widely studied using surface analytical techniques, but its duration can be very short and it is usually assumed (not always correctly) that Stage I has little impact on ultimate corrosion properties of the material. In the second or steady-state stage of oxidation, scale growth is often determined by diffusion parameters and thermodynamics of the oxide-metal system. This stage has been widely studied by standard corrosion methods and has been modeled by many oxidation theories. The final stage involves oxide scale failure and often the onset of damaging corrosion. Stage III is frequently induced by accumulated stress at the oxide metal interface or by weakening of the interface due to a compositional change.

Although surface and interface reactions play a major role in Stage I, any of several processes may be the slowest or rate controlling step in Stages II or III. Surface and interface methods may not be very helpful when surface and interface reactions are not controlling the corrosion rate.

#### Relationship to Surface Analysis Techniques

Although some stages of corrosion are not controlled by the rate of surface or interface reactions, surface reactions must

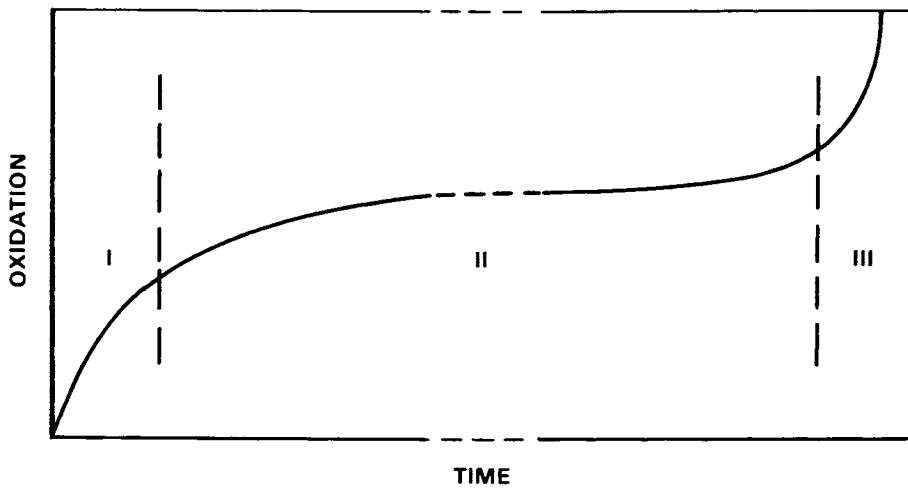


*Figure 1. Scheme of three stages of high temperature gaseous oxidation (7). Key: I, transient; II, steady state; and III, breakaway.*



occur in corrosion and surface analytical methods are the principal tools that exist to study these processes. The wide range of surface analytical techniques provide chemical and compositional information at surfaces and interfaces that is not usually available to other methods. These techniques are continually being developed and applied in sophisticated ways to corrosion work. It is impossible, therefore, to provide more than a general overview in this review.

The specific natures of surface techniques and, in some cases, their applications to corrosion have been discussed by a number of authors. General use of surface tools in Corrosion has been discussed by Larson (8), Joshi (9, 10) and in the PHI Interface Volume 3 #2 (1980). There has been considerable application of surface methods to electrochemical corrosion (11-15) including use of various types of vacuum compatible corrosion cells (16, 17). Castle (11, 12) and McIntyre (5) have shown how X-ray photoelectron spectroscopy (XPS or ESCA) can be applied to corrosion problems and uses of Auger electron spectroscopy (AES) in corrosion have been given by Clough (18, 19) and Thomas et al (20). Possible uses of ion beams in corrosion studies were presented by Dearnaley (21). Raman spectroscopy (22, 23) and ellipsometry (19) are not discussed in detail in this paper, but they offer the advantage of allowing in situ measurements in a wide variety of corrosive environments.

A series of criteria that should be met before XPS can be fully applied to corrosion studies of thin films has been established by Castle (11, 12). These criteria, when generalized to other surface science techniques, suggest four general areas or concerns (Table I) that should be addressed before a surface technique (or in fact any experimental technique) is applied to a corrosion problem. Although these concerns or questions seem very elementary, the specific problem and solutions they imply may be very difficult to sort out. In fact, in some cases, answers can not be obtained without testing or trying the method in similar or known conditions.

Technique Selection. The design of an experiment is dictated by the nature of the analytical techniques available. The "alphabet soup" of surface methods provide many alternatives to the researcher, but they also add confusion because few workers have a complete array of methods at their laboratory nor do they have a working knowledge of the many possible techniques. Comparison charts, such as Table II (also see ref. 25) can help in selection of appropriate techniques, but operator experience, equipment style and accessories, and availability all make important differences. Frequently it is useful to apply two or more complementary methods to solve a problem. The different types of data can be used to confirm or rule out any particular model or theory.

Table I  
QUESTIONS TO ASK WHEN APPLYING A SURFACE TECHNIQUE TO A CORROSION PROBLEM

General Questions	Specific Examples
1. Is the technique appropriate?	What is the best technique for this problem? Can several techniques combine to provide a more definitive answer? What techniques are readily available? Will I be able to compare my data to other types of measurements?
2. Are there potential problems in the use of the selected techniques?	Do the experimental requirements of the technique and the appropriate corrosion conditions combine to give information that is not altered by sample handling or the measurement process itself? Is the sample stable under vacuum? Is the chemistry or surface composition altered by electron, ion or X-ray beam excitation? Does the corrosion layer change upon cooling or removal from solution?
3. Can the required data be acquired?	Can the desired areas of interest (appropriate interface or corrosion area) be identified for analysis? Is data acquisition fast enough to generate desired data in reasonable time for allowable cost? Can contamination mask the desired signals? Is the appropriate type of data being taken?
4. Can the data be usefully analyzed?	Is there a sufficient data base for the technique to apply to my needs or must it be generated? Can I analyze the data to pull out the information I need? Can surface compounds be differentiated from alloy components? Can atomic composition be obtained from the data? Can different structures (island or layer) be distinguished from the data? Does data relate to corrosion process of interest?

Table II  
 CHARACTERISTICS OF SOME SURFACE TECHNIQUES

Technique	Corrosion Use	Probing Particle and Energy	Analyzed Particle	Elements Detected	Sensitivity
Auger Electron Spectroscopy	Atomic composition, elemental mapping	Electrons 1-10keV	Electrons 1-2200eV	Li-U	10 <sup>-3</sup>
X-ray Photoelectron Spectroscopy	Surface composition, bonding and chemical information	X-rays	Photo and other electrons	Li-U	10 <sup>-3</sup>
Secondary Ion Mass Spectrometry	Surface composition, isotope identification	Ar <sup>+</sup> Ar <sup>+</sup> O <sup>+</sup> 0.5-10keV	Secondary ions	H-U	10 <sup>-4</sup> -10 <sup>-8</sup>
Rutherford Back-scattering Spectroscopy	Elemental analysis, profiling	He <sup>+</sup> 2meV	Backscattered ion	He-U	10 <sup>-1</sup> -10 <sup>-4</sup>
Nuclear Reaction Spectroscopy	Light element, isotope analysis	H <sup>+</sup> D <sup>+</sup> He <sup>+</sup> 0.2-2MeV	Reaction products	Selected elements isotopes	1-10 <sup>-4</sup>
RAMAN Scattering	Compound identification on surfaces	Monochromatic light	Scattered light	RAMAN active molecules	Needs ~1 mono-layer or more
Ellipsometry	Thickness, density, defect structure, interface width	Monochromatic polarized light	Polarization state of polarized light	---	Fraction of monolayer

Continued on next page.

Table II (contd)

Technique	Analysis Depth	Volume Width	Sample Restrictions	Advantages	Concerns	Handbook or General Reference
Auger Electron Spectroscopy	~5-20 $\text{\AA}$	30 $\mu\text{m}$ -500 $\text{\AA}$	Vacuum compatible	Specific element identification. High sensitivity to low Z material. Fast-easy. Semi-quantitative. Good spatial resolution.	Needs standards to quantify, possible beam damage to surfaces.	26
X-ray Photoelectron Spectroscopy	~5-20 $\text{\AA}$	~mm	Vacuum compatible	Minimum surface damage. Chemical information. Specific elemental identification. Semi-quantitative.	Poor lateral resolution, slow profiling	27
Secondary Ion Mass Spectrometry	5 $\text{\AA}$	3mm-1 $\mu\text{m}$	Vacuum compatible	High sensitivity. Hydrogen detection.	Difficult to quantify. Wide variation in sensitivity.	28
Rutherford Backscattering Spectroscopy	~10,000 $\text{\AA}$	~mm	Vacuum compatible	Fast-quantitative. Non-destructive depth profiling.	Low sensitivity to low Z. Needs accelerators.	29
Nuclear Reaction Spectroscopy	~10,000 $\text{\AA}$	~mm	Vacuum compatible	Fast, isotope selection, can detect H, D, T.	Limited elements detectable.	29

Table II (contd)

Technique	Analysis Depth	Volume Width	Sample Restrictions	Advantages	Concerns	Handbook or General Reference
RAMAN Scattering	$\sim 1,000\text{\AA}$	down to $1\mu\text{m}$	None	Can be done in situ at temperature in complex gaseous or liquid environments.	Need comparative standards for compound recognition, difficult to see thin layers, limited data base.	22 23
Ellipsometry	Light penetrable layers	$\sim \text{mm}$	Reflecting surface	Can be done in situ in aqueous or gaseous environments.	No elemental identification, need model to understand.	24

Many complex problems using two or more methods require a coordinated effort among several researchers with everyone involved knowing as much about the problem and existing results as possible.

Potential Problems. Most, but not all, of the surface sensitive techniques require measurements to be made in a vacuum, frequently near room temperature. Because these conditions are usually different from the corrosion conditions, the possibility that the desired information will be lost in the transfer from the corrosion chamber to surface analysis chamber is a major concern. There is also a possibility that the measurement itself will alter the composition or chemistry of interest. Various aspects of those problems may apply to any method for which analysis occurs under conditions different from those in which the sample is generated, but they are of particular concern for surface methods that examine the very outer layers of the material.

Each of the problems mentioned occur on some specimens, but many examples exist where useful information was not obscured by dehydration in the vacuum, beam damage, or oxidation during handling. For example, XPS measurements by Castle (11), Asami et al (30), Baer and Thomas (31), and others contain results that would not have been possible if the vacuum, sample transfer or X-ray beam were altering the measurements. In some situations, special sample handling and modes of data acquisition are necessary to obtain reliable results (14, 31). Most experiments should include some method to check for specimen damage during handling and data acquisition.

Data Acquisition. Frequently, data analysis takes as much or more time than data acquisition, and appropriate analysis can be done only if adequate data were taken initially. Because choosing an appropriate surface technique does not adequately define what is to be done, considerable thought needs to go towards determining the types of data to be taken and into possible control samples or other checks to insure that the data are meaningful.

The null or non-informative result is a particular problem in surface analysis because it can occur for many reasons. For example, if a contaminant, such as Cl, is suspected of causing a corrosion problem and it is searched for and not found, there are several possible reasons. It may not be the problem and thus should not be found. However, there are several other less desirable possibilities including: it was washed off as the samples were being prepared; it caused the corrosion, but is not present in the corrosion layer being examined (the sample is being examined in wrong condition); it is present at concentrations below the sensitivity level of the technique; it is removed by the analysis conditions (probe effect); it is at a location other than that being examined (in a different area of the sample or at an

interface not being measured). Because there are many possible reasons for a null measurement, it is often important to have various types of control samples in "known" conditions.

Data Analysis. Data analysis is, of course, directly related to data acquisition. However, not all good data is or can be completely analyzed. For example, McIntyre (5) has observed that "a broad base in chemical shift data has been slow in developing" for XPS data. Until such a data base existed, it was difficult for both expert and non-expert to interpret spectra from corrosion products, particularly on complex alloys. The Handbook of X-Ray Photoelectron Spectroscopy (27) and collections of Auger parameter data (32) are examples of data compilations very useful to a researcher trying to interpret measurements of corrosion products.

Refinements in the use of any techniques often involve advances in the method of data analysis. One of the major concerns in using XPS, for example, is a lack of lateral spatial resolution. However, work by Castle (11, 12) shows how this weakness is turned into an advantage. Often films formed in aqueous solution are less than 50 Å thick and distinct photopeaks from both the base material and the oxidized film can be simultaneously measured. For uniform films, the oxide-to-metal peak ratios will depend upon the electron escape depth and thus the incident photon energy. By determining the change in the peak ratio for different photon energies, the film thickness can be determined. If the peak ratio does not change with photon energy, the presence of an island-like surface phase is indicated (12). Thus XPS can determine the general structure of a thin layer in spite of very limited spatial resolution. It is interesting to note that the presence of the island-like distribution could be detected by XPS even if it were of too small a scale to be resolved with a high spatial resolution (<1000Å) method.

As the preceding example suggests, considerable information can be obtained by sophisticated data analyses. Often proper data analysis takes more time than data acquisition and it is easy to take more data than can be reasonably analyzed. A distinction should be made concerning controlled or semi-controlled measurements and exploratory searching. Frequently, the presence or absence of a particular element provides all the necessary information and analysis is simple and immediate. However, further quantification of such an analysis can be difficult and time consuming.

Quantitative analysis depends upon the availability of various parameters such as cross sections, sensitivity factors, and penetration or escape depths. Tables of these quantities are useful although not always reliable or readily found. The ability of any technique to solve a particular problem will depend upon both the accessibility and accuracy of supporting data.

## EXAMPLES

The purpose of this section is to show, by example, how the concerns of technique selection, potential problems, data acquisition and analysis have been applied for several different corrosion problems and techniques. Examples of fundamental research work and industrial problem solving have been included to show the range of applicability of the techniques. In most cases, more than one technique was used to solve the problem. Frequently, a surface analysis technique was used in combination with one or more other types of analysis method. These examples are not comprehensive; it is hoped that sufficient references have been supplied to enable the reader to find other work of relevant interest.

### Relationship of Grain Boundary Chemistry and Fracture in an Aqueous Environment (AES)

Intergranular embrittlement of iron and nickel base alloys is a serious problem for many technological applications of these materials. It is generally accepted that grain boundary impurities and/or hydrogen absorbed from either aqueous or gaseous environments are important embrittling agents, but it is not known whether the impurities and hydrogen act independently or synergistically. Considerable work has been reported (33) relating impurity segregation to grain boundaries and embrittlement in steels. Other interdisciplinary studies, combining surface science investigation and materials science measurements, were undertaken to help gain an understanding of the impurity-hydrogen mechanisms for embrittlement of simple Ni and Fe alloys in an aqueous environment (20, 34, 35, 36). Specific objectives of these experiments were to determine fracture properties of the materials as a function of both grain boundary chemistry and hydrogen potential.

Consideration of Surface Tool Concerns. Direct measurements of grain boundary chemistry usually require analysis of fracture surfaces. AES was selected for use in determination of grain boundary composition because the size of the electron beam allows measurements on individual grains and the SEM image allows non-intergranular fracture areas of the sample to be excluded from analysis. Some workers have preferred analysis over large areas in order to obtain an "average" grain boundary composition. Individual grain analysis allows the distribution of impurities to different boundaries to be measured. A numerical average of grain boundary composition was used in this study, although McMahon (33) and co-workers now use a "probable Maximum Grain Boundary Concentration".

Identification of impurities at grain boundaries is one of the most straightforward uses of AES. However, analysis of fractured surfaces does have three potential problem areas. First, it



is not always possible to obtain an intergranular fracture, particularly with a standard low-temperature impact-fracture device. Materials such as nickel must be charged with hydrogen to facilitate the fracture and this treatment is not always successful. Second, there is a possibility that impact or other fracture methods may selectively open certain grain boundaries and give results that are not representative of true average grain boundary composition. Third, absolute measurements of grain boundary coverages require careful calibrations for the material systems of interest. Calculations using sensitivity factors and electron escape depths provide useful estimates of coverages, but calibrations should be made when absolute coverages are important (37, 38).

Experimental. Iron and nickel alloys were produced from vacuum melted and zone refined materials. Specimens of appropriate shapes and sizes were machined from the material and heat treated in different ways to set grain size and to induce different levels of grain boundary segregation. One set of specimens was designed for Auger analysis of impact fracture surfaces using Physical Electronics 545 and 590 scanning Auger microprobe (SAM) systems. A second set of samples was designed to fit a straining electrode apparatus where tensile properties of the materials were measured as a function of cathodic hydrogen potential. AES measurements on a fracture surface were taken to represent the grain boundary composition of straining electrode samples that had undergone identical heat treatments. After AES impact fracture and straining electrode fracture, surfaces were examined with a conventional scanning electron microscope.

Results. AES analysis of impact fracture surfaces on nickel showed considerable spread in sulfur composition at grain boundaries as shown in Fig. 2. The composition varied from approximately 0.04 to 0.20 monolayers on the sample heated to 1100°C for one hour and 0.15 to 0.25 monolayers on a sample that had received additional heating at 600°C for 240 hours. The additional heat treatment shifted the average grain boundary composition by nearly 0.1 monolayer of coverage.

A direct relationship between sulfur content at grain boundaries and fracture mode in hydrogen was found for both iron and nickel. The fracture mode as a function of grain boundary sulfur in nickel is shown at three different hydrogen potentials (39) in Fig. 3. At a given hydrogen potential, the mode changes from ductile to intergranular as the sulfur concentration changes. For a particular grain boundary composition, the fracture mode can change as the potential is changed. If the critical concentration of sulfur is defined as that causing 50% intergranular fracture, it is observed that this critical concentration decreases as the amount of hydrogen in the material (increased negative potential) increases. It has also been possible to compare effects of various segregated elements for embrittling both iron and nickel (40).

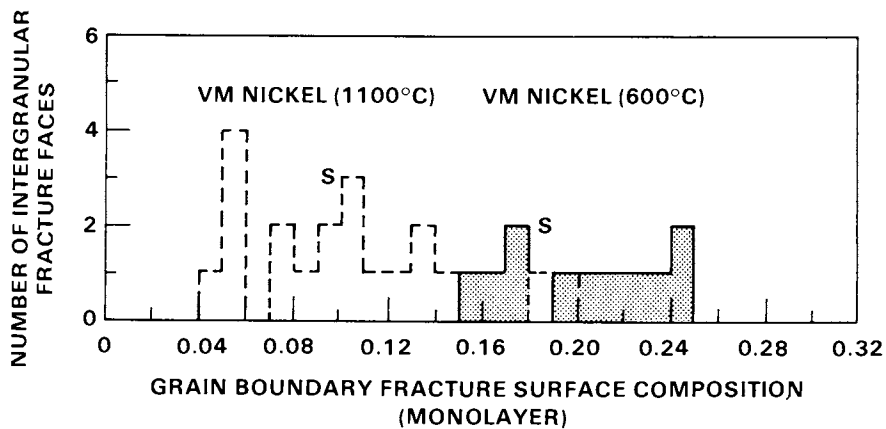


Figure 2. Histogram of sulfur coverages at grain boundaries of vacuum-melted nickel after two different heat treatments (39).

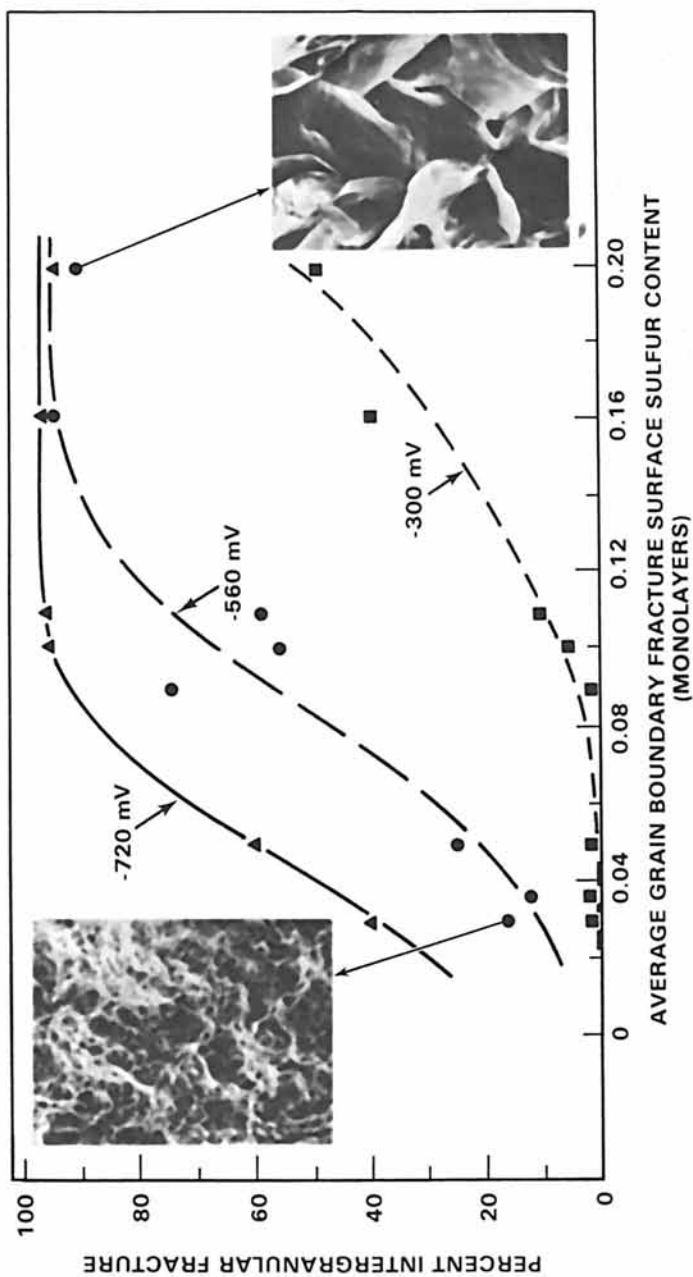


Figure 3. Fracture mode of nickel as a function of sulfur at grain boundaries at three different hydrogen potentials (39).

These results imply that some elements weaken the material by decreasing critical intergranular fracture stress, some enhance hydrogen permeation and some affect both processes.

Results of these on-going experiments are helping to clarify the mechanisms acting to produce environmentally induced embrittlement of Fe and Ni and suggest different roles for various segregated impurities. It is expected that understanding of the important mechanisms will help the designing of new alloys which are more durable in particular environments.

### Electrochemical Reactions at $UO_2$ Surfaces (XPS)

The reactions of  $UO_2$  in aqueous solutions are of importance to the long-term storage of fission reactor spent-fuel. In particular, the leaching and dissolution mechanisms of  $UO_2$  in water will determine nuclide release rates in cases where fuel cladding fails (41). In order to determine the reactivity of  $UO_2$ , a number of studies have been done including XPS work by McIntyre et al (14). Part of the objective of their work was to determine the variations in surface oxidation state of  $UO_2$  upon exposure to aqueous solution in an effort to understand how the reactivity of  $UO_2$  would change.

Surface Tool Concerns. Because surface chemistry was of prime interest in the McIntyre study, XPS was chosen as the technique to use. Often AES can provide chemical information, but previous XPS work had shown easily identifiable oxidation states of  $U_2O_5$  and  $U_2O_8$  suggesting that XPS was a good choice and avoiding possible electron beam effects that AES might induce.

In order to avoid surface contamination upon removal of samples from the electrochemical corrosion cell, samples were transferred from the solution to the vacuum entry system in an inert gas chamber. Previous work had shown a tendency of the X-ray beam to slowly reduce  $U^{6+}$  states on  $UO_2$ . McIntyre et al, therefore, checked for such a decomposition and found none within the first 30 minutes of exposure to X-rays.

In order to determine relative amounts of various oxidation states on  $UO_2$ , a peak fitting routine was needed. Effort was required to ensure that the desired information could be obtained from the fits and that sufficient data was taken in order to have good statistics for the fitting routine.

Experimental. Uranium oxide electrodes were prepared from sintered  $UO_2$  and reduced to the correct stoichiometry in a vacuum furnace. After cleaning, samples were exposed to a 0.5 M  $Na_2SO_4$  solution of pH 7 and electrochemically oxidized at a potential of +300 mV<sub>SCE</sub>. After various times, samples were removed from the solution within the inert gas chamber. They were rinsed in deoxygenated water and transferred into the UHV chamber within 60 seconds. XPS peaks were taken using an Al  $K_{\alpha}$  X-ray source.

**Results.** It was found that XPS spectra of mixed oxides could be interpreted using only the  $U^{4+}$  and  $U^{6+}$  oxidation states. A  $1.3 \pm 0.2$  eV shift existed between these two states which was maintained for mixed valence oxides. The  $U(4f_{7/2})$  photoelectron spectra for  $UO_2$  is shown in Fig. 4a while the spectra for a surface oxidized at +300 mV is shown in Fig. 4b. The peak fits obtained, maintaining the 1.3 eV separation between  $UO_2$  (+4) and  $UO_3$  (+6), show good fits to the data and were used to determine the ratio of  $U^{6+}/U^{4+}$  in the surface oxide. Angle resolved XPS measurements indicated that the surface oxide was sufficiently thick after two minutes of oxidation to prevent any  $U^{4+}(UO_2)$  contribution to the spectrum from the  $UO_2$  substrate.

Oxidations for varying times showed systematic variations in the  $U^{6+}/U^{4+}$  ratios that fell into three values stable for significant periods of time (Fig. 5). These ratios of  $U^{6+}/U^{4+} = 0.5, 1.0$  and  $2.0$  are believed to correspond to the presence of  $U_3O_7$  ( $UO_2 \cdot UO_2 \cdot UO_3$ ),  $U_2O_5$  ( $UO_2 \cdot UO_3$ ), and  $U_3O_8$  ( $UO_2 \cdot UO_3 \cdot UO_3$ ), respectively. The surface film composition is controlled by various rates of surface dissolution, oxygen diffusion into the  $UO_2$  and precipitation. Film dissolution is believed to occur upon oxidation to  $UO_3$ . Because no appreciable layer of  $UO_3$  was found on the surface, it is concluded that dissolution of  $UO_3$  occurs at a rate faster than solid-state oxidation.

#### Electrochemical Behavior of Titanium Implanted with Platinum (RBS)

For this study by Thompson et al (42), ion implantation and RBS were combined with more traditional electrochemical measurements to help establish the corrosion mechanisms of alloys in which a noble metal (Pt) was combined with an active/passive base metal (Ti). The alloys were created by ion implantation of Pt into pure Ti and were not of uniform bulk composition. Such surface alloys offer the possibilities of using a very small amount of a noble material to create a corrosion resistant coating on an otherwise chemically unstable but inexpensive metal or alloy.

The Ti-Pt system was chosen for study because it may relate to practical applications of such alloys, it represents a limiting case of active element/noble element alloys and therefore provides information relevant to several systems and the high mass number of Pt ( $M=195$  amu) compared to that of Ti ( $M=48$  amu) allows use of RBS to determine atomic distributions.

The specific objectives of the experiment were to determine critical concentrations of Pt necessary for stable passivity of the surface alloy in 1N  $H_2SO_4$  and to aid understanding of the mechanisms of noble metal redistribution.

Consideration of Surface Tool Concerns. RBS was chosen as the analysis tool for several reasons; it works well on the Ti-Pt system, it provides non-destructive information about Pt distribution after implantation and after electrochemical analysis and

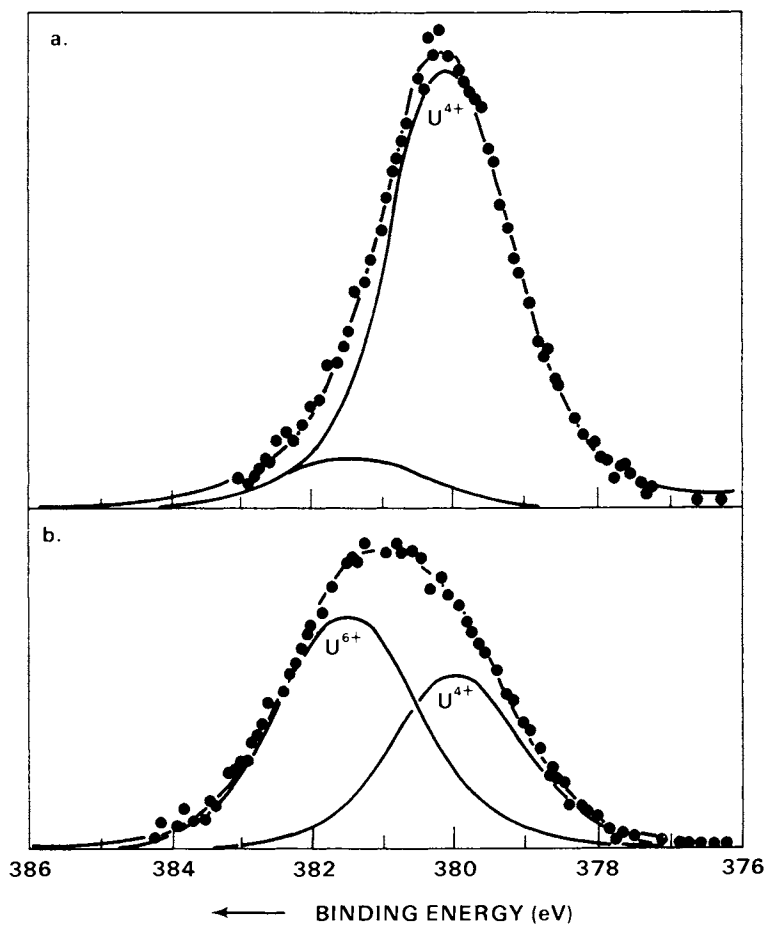


Figure 4.  $U(4f_{7/2})$  XPS spectra from a uranium oxide electrode. Key: a, reduced  $UO_2$ ;  $U^{6+}/U^{4+} = 0$ ; and b, anodic oxidation at  $+300 \text{ mV}_{SCE}$  in  $0.5 \text{ M Na}_2\text{SO}_4$  for 6 h;  $U^{6+}/U^{4+} = 1.3$ . (Reproduced, with permission, from Ref. 14. Copyright 1981, AIP.)

it can be done in the same system as the ion implantation. Sample vacuum compatibility was no problem, but oxidation of the sample during handling did require attention during data analysis. The specific objective concerning distribution of Pt made RBS data acquisition and analysis reasonably straightforward.

Experimental. Pure Ti electrodes were ion implanted with Pt and the distribution of Pt was determined using RBS. Samples were then inserted into a 1N H<sub>2</sub>SO<sub>4</sub> electrolyte for electrochemical studies. After electrochemical analysis, some samples were again analyzed to determine the Pt distribution.

Results. The presence of Pt reduces the corrosion rate of Ti by shifting the free corrosion potential to more noble values (Fig. 6) where the Ti dissolution rate is slower. This shift is produced by the catalytic effect of Pt on hydrogen recombination which alters the cathodic reactions at the alloy surface. At the corrosion potential, the cathodic and anodic currents are equal. Although the shift in corrosion potential reduces the anodic current, anodic dissolution of Ti still occurs. The long-term corrosion rate of a surface alloy depends upon what happens to the Pt as the Ti is being dissolved. If Pt is removed from the surface, the corrosion rate will increase as the implanted volume of the alloy is dissolved. If Pt builds up on the surface, the corrosion rate should remain low.

One means of testing the nature of the Pt distribution during corrosion, involves holding the sample at one electrochemical potential and observing the current as a function of time. Such current versus time plots are shown in Fig. 7 for two samples containing different amounts of Pt. For the specimen containing a peak concentration of 0.086% Pt, the corrosion current varied with time as would be expected if Pt was dissolved with the Ti. By knowing the Ti dissolution rate (anodic current), it was possible to directly compare the Pt distribution measured by RBS with the corrosion current. As indicated in the figure, they correspond very well. At long times, the corrosion rate reverted to that of pure Ti. A different pattern was observed, however, when 0.83% Pt was deposited in the sample. In this case, the corrosion current remained cathodic for a considerable period of time, even when the original implanted alloy layer had been dissolved. In this case, a Pt layer built up and passivity was maintained. The unstable drop-off of current at long times appeared to be caused by clusters of Pt atoms detaching from the surface in an irregular manner. However, the current was still predominantly cathodic and some passivity was maintained.

Analysis of samples after electrochemical measurements produced a surprise. Samples that displayed the pure Ti-like corrosion behavior after long times, showed an increased concentration of Pt on the surface. Pt was not "lost" to the solution as

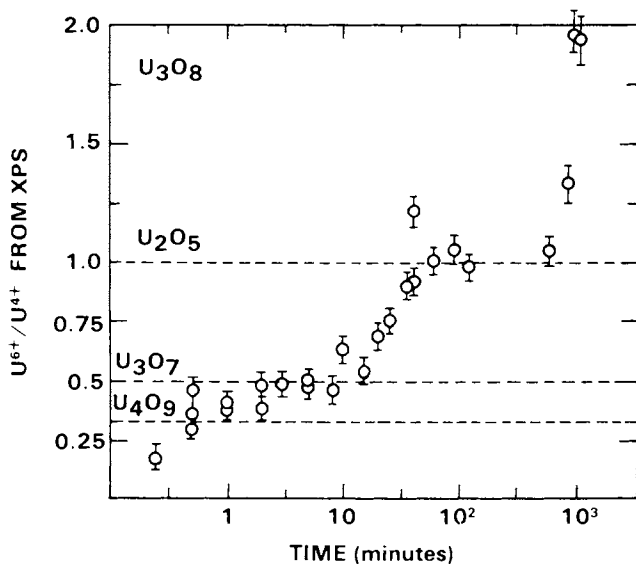


Figure 5. Changes in  $UO_2$  surface oxide as a function of time at  $300 \text{ mV}_{\text{SCE}}$  in  $0.5 \text{ M Na}_2\text{SO}_4$ ,  $\text{pH} = 7$ . (Reproduced, with permission, from Ref. 14. Copyright 1981, AIP.)

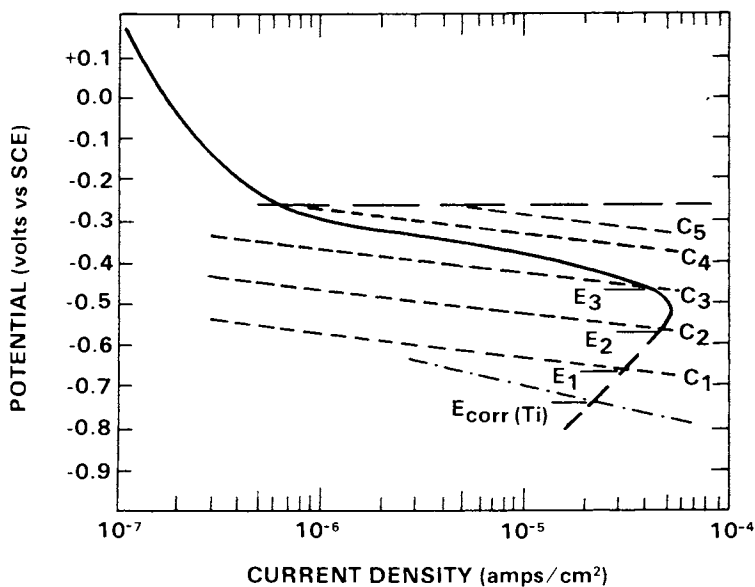


Figure 6. Anodic polarization curve for titanium with superimposed schematic curves for hydrogen discharge. Key: — · —, cathodic current (Ti); ---, cathodic current (Pt); —, anodic current (pure Ti); and Pt concentration,  $C_1 < C_2 < C_3 < C_4 < C_5$ . (Reproduced, with permission, from Ref. 42. Copyright 1979, AIME.)



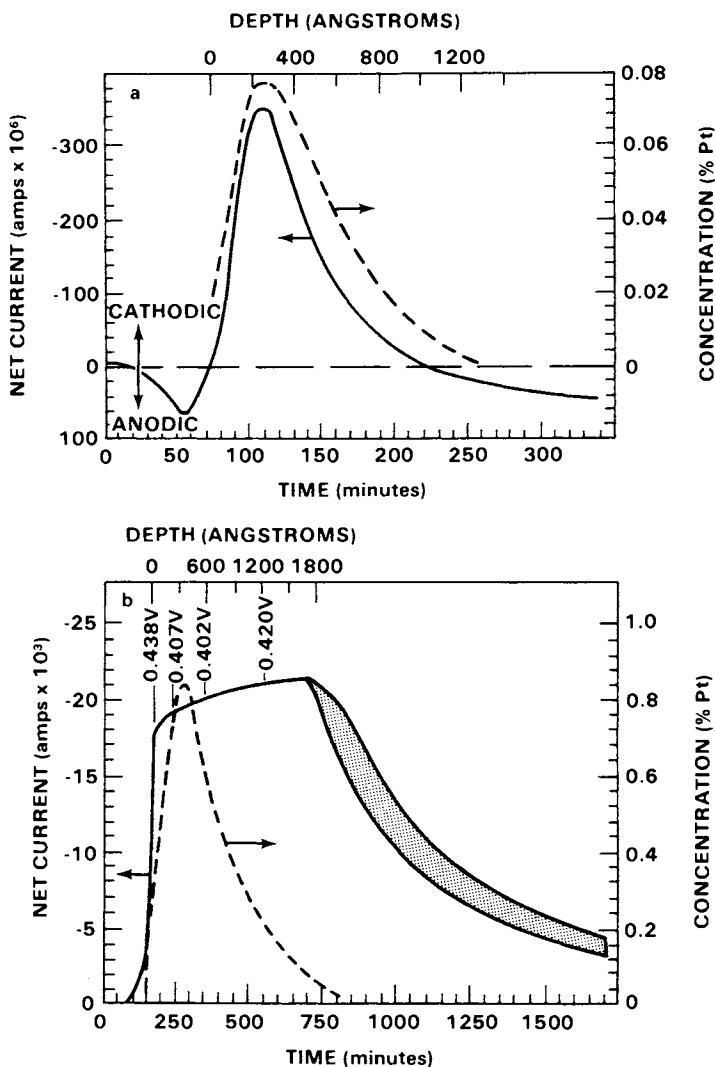


Figure 7. Net current as a function of time and concentration profile for Ti implanted with 0.086 at % Pt (a), and 0.83 at % Pt (b) Key: ---, concentration vs. depth; and —, current vs. time. (Reproduced, with permission, from Ref. 42. Copyright 1979, AIME.)

presumed, but was on the surface in an electrochemically "inactive" form.

In this study, ion implantation and RBS analyses were important tools used to complement electrochemical measurements. Without the combination of both types of measurements, important information would have been lost. Electrochemical analysis alone would not show the inactive Pt while RBS analysis alone would have made determination of corrosion rates much more tedious.

#### Pretreatments of Stainless Steels - Crevice Corrosion and High Temperature Oxidation (AES)

Stainless steel alloys are in wide use in many technological applications where corrosion resistance is a concern. Because the corrosion properties of these steels are very important, they have been widely studied by many methods, including considerable use of surface analytical tools. The nature of the protective films formed on these alloys in different environments is of great interest.

Two recent studies have used surface techniques to examine the protective layers formed in various oxidation conditions and related the nature of the oxide to the corrosion rates in specific environments. Hultquist and Leygraf (43, 44) have examined crevice corrosion resistance in a NaCl solution at room temperatures while Baer (45) has looked at higher temperature (800°C) air oxidation. Oxygen potential, or partial pressure, is an important parameter in both studies where it was found that controlled oxidation can tailor the Cr profile in the alloy and surface oxide for maximum corrosion protection. Specific goals in each experiment were oxide characterization and comparison to corrosion rates.

Consideration of Surface Tool Concerns. Reasonably fast data acquisition, small probing beam size (allowing both faster sputter profiling and spatial resolution) and semiquantitative data analysis, give AES a primary role in each of these two experiments. The low oxygen potential anneals were done in a UHV chamber so that the anneal and analysis could be performed in the same system. Possible concerns include: sample charging during the analysis, electron beam or ion beam induced oxide reduction (46) and differential sputtering during profiles. Many of the concerns can be minimized by using low electron currents and low sputtering voltages. Considerable experience by many researchers shows that these problems can be minimized or do not appreciably complicate data analysis.

Experimental. For the crevice corrosion study, samples were pretreated in three different ways similar to industrial polishing (SiC paper), pickling (acid cleaning) and bright annealing (short vacuum anneal). The high temperature samples were vacuum annealed

at 1000°C for two hours. In both experiments, alloys were oxidized at low oxygen pressures by annealing in a UHV chamber with a controlled oxygen environment. After the anneals, AES analysis was made to determine the nature of the oxides obtained. Crevice corrosion samples were then examined in a 1/2 M NaCl solution pH 8, where a stepwise ramp in applied voltage was used to determine the pitting potential. The high temperature samples were oxidized in air at 800°C.

Results--Crevice Corrosion. The ability of a two-hour anneal in  $10^{-6}$  Pa oxygen at 700K to slow dissolution rates of various steels in tap water is shown in Fig. 8. For every alloy except the 5% Cr material, the treatment decreased the long-term dissolution rates. This controlled or modified anneal altered the corrosion rate by changing the chromium content in the passive film as shown in Fig. 9. Oxidation in a controlled way optimizes the amount and depth distribution of the chromium and enhances its protective qualities. This increased protection showed up as an increased pitting potential in Table III. When materials received the oxidation annealing surface treatment, the potential at which pitting starts was increased by at least 150 mV<sub>SCE</sub>. Thus the conditions of use for these alloys can be extended with an appropriate surface treatment.

Results--High Temperature Oxidation. Two studies have shown that oxidation of annealed wrought 40  $\mu$ m grain sized 304 stainless steel in air at 800°C produced a rapidly growing iron-rich oxide (47, 48). Oxidation of the same material in  $10^{-3}$  Pa oxygen allowed the equilibrium Cr-rich oxide to form as shown in Fig. 10a. Additional oxidation in air at 800°C caused very little change in this protective layer (Fig. 10b), while other parts of the sample without the preoxidation treatment grew a thick Fe-rich oxide layer.

Results from both studies indicate that various pretreatments of alloys can enhance the corrosion resistance of the materials. In addition, alloys without the optimum levels of chromium can be treated to produce good corrosion behavior, thereby allowing the use of lower Cr material in some applications. New materials, possibly without any Cr, may well require careful pretreatment before placed in service (49).

#### Corrosion Control on Gold-Coated Contacts Used in Submarine Navigational Computers (AES, XPS, RBS)

Electrical intermittents caused by poor contacts of printed circuit boards (PCBs) is a major source of problems for navigational computers used on nuclear submarines. The cause of the intermittencies has been traced to the presence of dirt, tarnish, corrosion products and organic contaminants accumulating at the pin connector junctions (50).

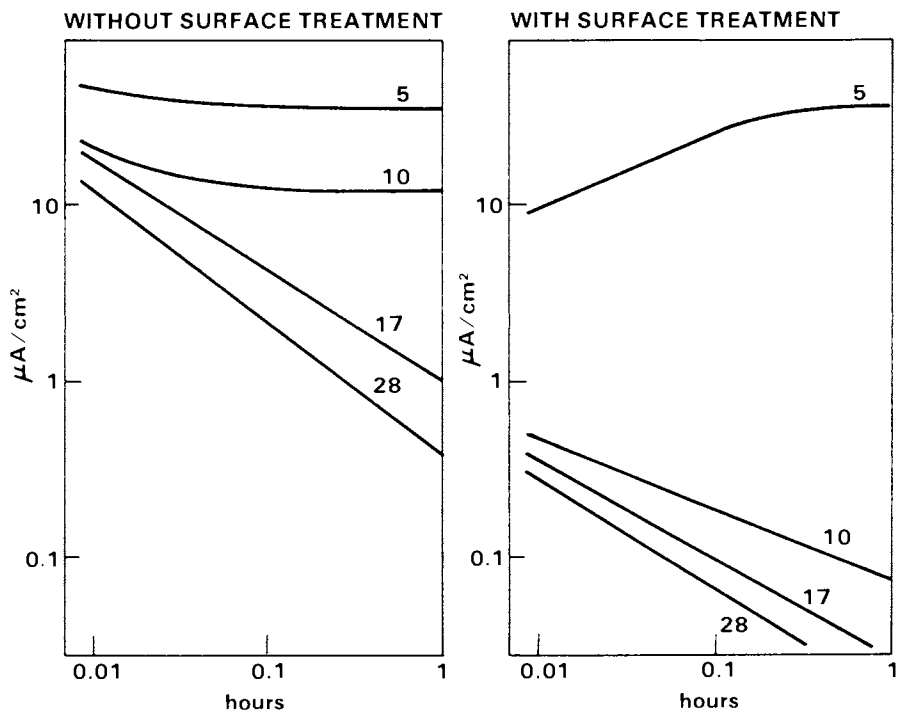


Figure 8. Dissolution current vs. time for Fe5Cr, Fe10Cr, Fe17Cr, and Fe28Cr with and without surface treatment. (Reproduced, with permission, from Ref. 43. Copyright 1980, Elsevier Sequoia.)

Table III

Critical potential for crevice corrosion in 0.5 M NaCl,  
pH = 8, at room temperature

Composition	SIS	ASTM	After mechanical	After surface
			polishing (800 mesh) mV (SCE)	treatment mV (SCE)
Fe13Cr	2302	410	-200 <sub>+25</sub>	-50 <sub>+50</sub>
Fe17Cr	2320	430	-125	+50
Fe25Cr5Ni1.5Mo	2324	329	+50	+250
Fe18Cr2MoTi	2326		+75	+600
Fe18Cr9Ni	2333	304	-25	+250
Fe18Cr11Ni2.7Mo	2343	316	+50	+300
Fe20Cr25Ni4.4MoCu	2562		+150	≥1000

Adapted from Ref. 43.

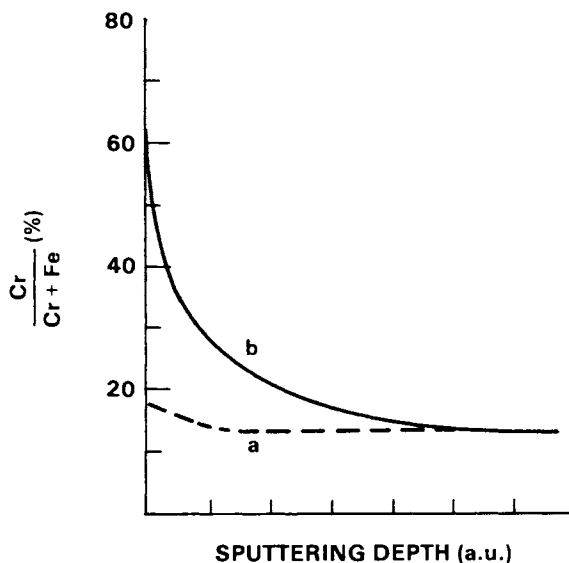


Figure 9. Chromium depth profile in Fe13Cr after normal (a) and controlled or modified annealing (b). (Reproduced, with permission, from Ref. 43. Copyright 1980, Elsevier Sequoia.)

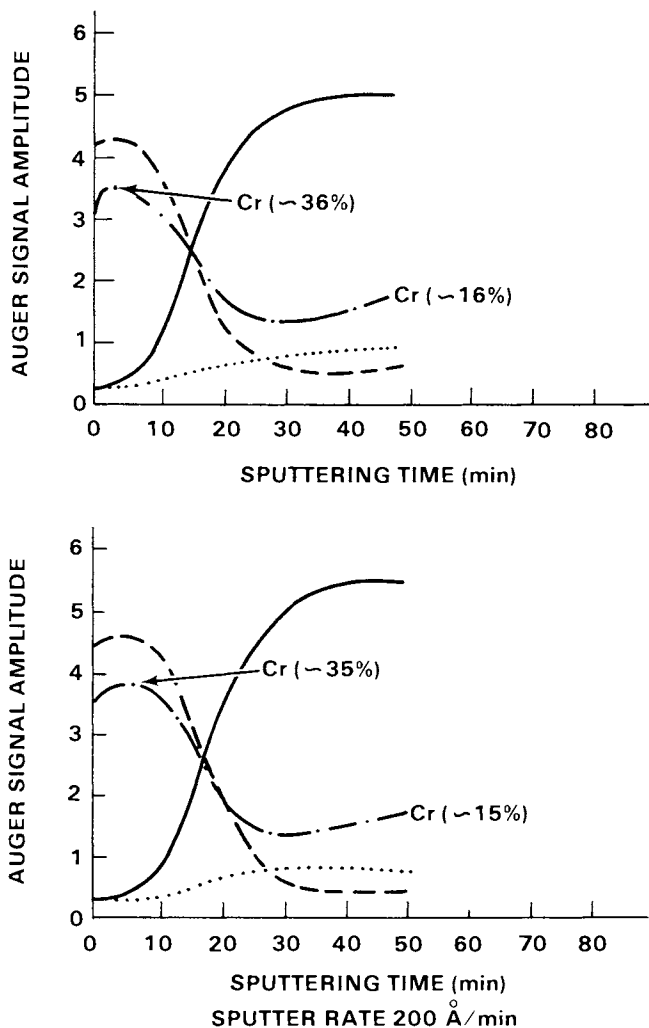


Figure 10. Sputter depth profile of oxide formed at  $10^{-3}$  Pa oxygen pressures (top) as formed (bottom) after additional oxidation in air. Key to top plot: —, Fe (~77%); ---, O (~64%); - · - ·, Cr (as indicated); · · ·, Ni (~7%); and O(LT 1%). Key to bottom plot: —, Fe (~78%); ---, O (~65%); - · - ·, Cr (as indicated); · · ·, Ni (~7%); and O (LT 1%). (Reproduced, with permission, from Ref. 45. Copyright 1981, North-Holland Publishing Co.)

The bellow-form spring female pins were fabricated primarily from a beryllium-copper alloy, but rely on thin film coatings for corrosion resistance. The pin was coated with a 15  $\mu\text{m}$  layer of silver and then  $\sim 0.8 \mu\text{m}$  of gold. A tarnish layer formed on the gold when silver sulfide formed at defects in the gold film and migrated across the gold surface. This tarnish, plus accumulated organic material from sources such as galley greases, caused the electrical problems.

Although replacing the contacts with silver-free connectors was the long-range solution in submarines and in all other circuit board applications, some short-term preventative measures were desirable in the effort to avoid expensive retrofits. A modified chromate coating process was found to extend useful life of the connectors. Because the nature of the chromate film growth is influenced by the electrochemical behavior of the contacts and impurities, the exact nature of the films formed on real and model contacts was examined as well as effects of impurities.

The specific goals of the experiment were to characterize the passive film and determine if it was primarily protective with chromium in the +3 state or if some chromium was in the +6 state indicating the possibility of a self-healing film. The effects of various impurities on chromate film growth were also examined.

Consideration of Surface Analysis Concerns. The researchers in this study used a wide range of surface and other tools, taking appropriate advantage of the strengths of the various methods. Previous work had shown that AES and XPS could be used to study chromate films without unreasonable problems and provided a basis for the current study. XPS was used to obtain specific chemical information while AES was used whenever spatial resolution and electron imaging were desired. RBS and electron microprobe work was used to analyze composition structures of thicker layers. This study is a good example of multitechnique use.

Experimental. Much of the XPS and AES work was done on coupons made of a BeCu alloy which had been electroplated with Ag or Au or both. The chromate films were grown in a manner consistent with specifications for refurbishing contacts on submarine navigational computers.

Results. XPS spectra of the chromate films on the bimetallic strips, on pure silver and on pure gold showed no indication of a  $\text{Cr}^{+6}$  state (Fig. 11) suggesting that flaws in the chromate film would not heal and therefore would be susceptible to corrosive attack. This non-healing aspect of the chromate films on the Ag/Au contacts differs from the effect of chromate films on Al (51) and was confirmed in field studies. Therefore, the chromate films formed on the Au/Ag/Be-Cu contact are protective, but will not heal over scrapes and other damage caused by usage.

Field applications of the chromating procedure occasionally produced large deposits of insulating films. Although these films could be cleaned off by repeated cleaning and detarnishing steps, such deposits were sufficiently troublesome to warrant learning the cause and taking steps to eliminate the problem. AES profiles (Fig. 12) of the deposits showed them to be low in Cr and high in Cu. Empirical studies showed that the presence of  $\text{CuCl}_2$  would stimulate excess film growth in the chromate process. The presence of Cu in the contacts themselves (uncovered at the edge of male connectors) and the presence of Cl in salts in the submarine atmosphere lead to favorable conditions for the formation of  $\text{CuCl}_2$  and therefore, the film growth problems. RBS and electron microprobe analysis of good connectors and insulation films suggested that damage to the gold film was not the problem. There was no evidence of Cu diffusion in pores or scratches in the gold contact. Thus, the likely cause is submarine atmospheric attack of Cu exposed at edges of contacts.

This study showed that the chromating process would not provide long-term protection of PCB connectors if use produced damage to the film and that careful cleaning was necessary in order to avoid insulating film buildup during the chromating process.

## CONCLUSIONS

Corrosion processes can be very complex and, as the above examples show, surface analytical techniques can often provide unique information important for the understanding of these processes and to the solution of corrosion problems. By their basic nature, surface sensitive methods excel at examining thin layers at surfaces and interfaces that are difficult to detect and analyze by other methods but which can have a large influence in corrosion. The higher spatial resolution surface techniques are particularly useful for analysis of small area corrosion problems such as pitting and corrosion of electronic components and integrated circuits.

The use of surface tools need not be limited only to thin layers or small dimension corrosion. Creative application of surface methods to larger scale corrosion products, more characteristic of industrial problems, has provided useful information not previously available. More sophisticated uses of surface methods that are being developed and tested continually will provide even more information for corrosion research.

Although surface tools can provide a large amount of important data, their application to corrosion problems is not always straightforward. Considerable care must be taken to ensure that the information obtained is both correct and related to the problem under investigation. Because the methods are usually applied outside of the corrosion environment, it is often necessary to



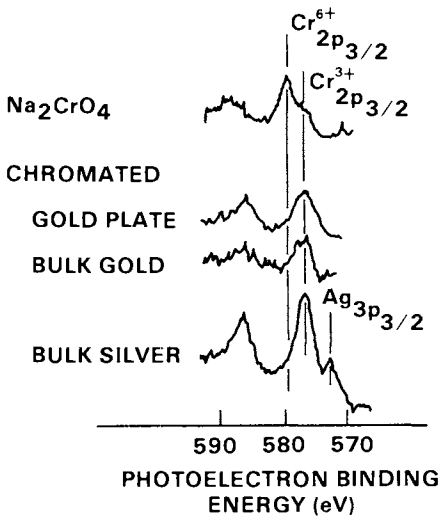


Figure 11. Chromium 2p XPS peaks of Na<sub>2</sub>CrO<sub>4</sub>.

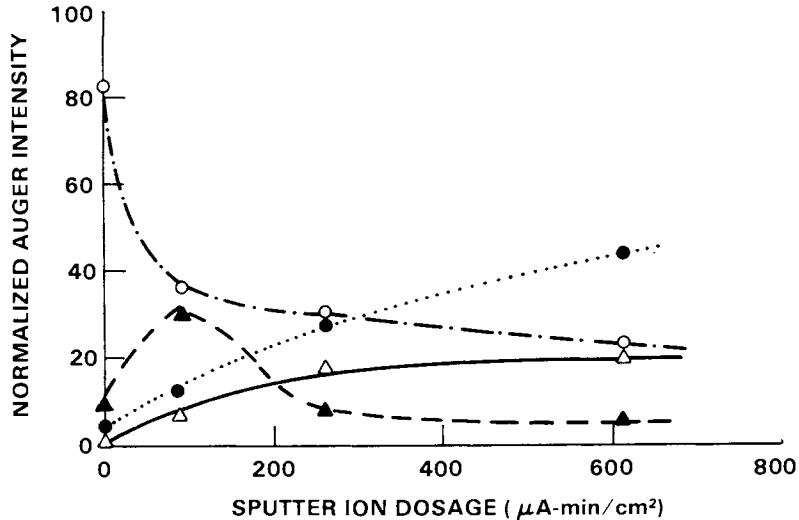


Figure 12. Auger sputter profile of insulating film formed during chromating of male PCB connector. Key:  $\Delta$ , chromium;  $\blacktriangle$ , copper;  $\bullet$ , oxygen; and  $\circ$ , carbon. (Reproduced, with permission, from Ref. 50. Copyright 1980, North-Holland Publishing Co.)

design tests to determine data consistency and relevance. Analysis by more than one surface method can often clarify ambiguous results.

The information obtained using surface techniques can be rather different than that gathered by more traditional methods of corrosion research. The greatest understanding of corrosion processes is likely to involve a thorough knowledge of both types of results and much information may be gained by the effort to relate the different types of measurements. As observed by Egon Matijevic (6), "Only a collaboration of workers in different disciplines, including colloid and surface science, can bring about advances in exploring and combating various corrosion phenomena."

#### ACKNOWLEDGMENTS

The authors would like to thank S. M. Bruemmer, R. H. Jones, and J. T. Prater for critical reading of the manuscript.

This work was supported by the Materials Science Division of the Office of Basic Energy Sciences, U.S. Department of Energy under contract DE-AC06-76RLO-1830.

#### LITERATURE CITED

1. Kruger, J. "1980 Yearbook of Science and the Future;" Encyclopedia Britannica: 1980; pp. 134-145.
2. Kruger, J. ASTM Standardization News May 1981, 9(5):21.
3. "Costly Corrosion Not Licked--Yet," News article Department of Energy Insider, February 2, 1981.
4. Fontana, M.G.; Greene, N.D. "Corrosion Engineering--2nd ed.," McGraw-Hill, New York, NY, 1978.
5. McIntrye, N.S. The PHI Interface 1980, 3(2):3, Physical Electronics, Eden Prairie, MN.
6. Matijevic, E. Corrosion 1979, 35:229.
7. Whittel, D.P. "Proceedings of the International Conference on High Temperature Corrosion--San Diego;" NACE: Houston, March 1981.
8. Larson, D.T. Corrosion Science 1979, 19, pp. 657-673.
9. Joshi, A. "Fractography in Failure Analysis," ASTM STP645, ed. by B.M. Straus and W.H. Cullen, Jr. Am. Soc. Test Mat. 1978, pp. 275-293.
10. Joshi, A. "Reviews on Coatings and Corrosion"; ed. J. Yahalom, Freund Publishing House, Tel-Aviv, Israel, 1979, pp. 51-77.
11. Castle, J.E. Surface Science 1977, 68, pp. 583-602.
12. Castle, J.E. "Applied Surface Analysis ASTM STP699"; ed. T.L. Barr and L.E. Davis, Am. Soc. Test. Mat. 1980, pp. 182-198.
13. Sherwood, P.M.A. Surf. Sci. 1980, 101, pp. 619-623.

14. McIntyre, N.S.; Sunder, S.; Shoesmith, D.W.; Stanchell, F.W. J. Vac. Sci. Tech. 1981, 18, pp. 714-721.
15. Burstein, G.T. Corrosion 1981, 37, pp. 549-556.
16. O'Grady, W.E.; Yang, C.Y. J. Vac. Sci. Tech. 1982, 20.
17. Stout, D.A.; Gavelli, G.; Lumsden, J.B.; Staehle, R.W. "Applied Surface Analysis ASTM STP699"; ed. T.L. Barr and L.E. Davis, Am. Soc. Test Mat. 1980, pp. 42-53.
18. Clough, S.P. "The PHI Interface"; Physical Electronics, Eden Prairie, MN, 1980, 3(2):4.
19. Clough, S.P. "Modern Surface Analysis: Metallurgical Applications of AES and XPS"; Metallurgical Soc. of AIME, New York, NY, 1979.
20. Thomas, M.T.; Jones, R.H.; Baer, D.R.; Bruemmer, S.M. "The PHI Interface"; Physical Electronics, Eden Prairie, MN, 1980, 3(2):3.
21. Dearnaley, G. "Ion Irradiation for Materials Analysis"; ed. S.T. Picraux, Plenum Press, New York, NY, 1974.
22. Thibau, R.H.; Brown, C.W.; Heidersbach, R.H. Applied Spectroscopy 1978, 32, pp. 532-535.
23. Farrow, R.L.; Mattern, P.L.; Nagelberg, A.S. Appl. Phys. Lett. 1980, 36, p. 212.
24. Aspnes, D.E. J. Vac. Sci. Tech. 1981, 18, pp. 289-295.
25. Evans, C.A. Jr. "ARPA/NBS Workshop IV, Surface Analysis for Silicon Devices"; National Bureau of Standards Special Publication 400-23, 1976.
26. Davis, L.E.; MacDonald, N.C.; Palmberg, P.W.; Riach, G.E.; Weber, R.E. "Handbook of Auger Electron Spectroscopy--2nd ed."; Physical Electronics, Eden Prairie, MN, 1976.
27. Wagner, C.D.; Riggs, W.M.; Davis, L.E.; Moulder, J.F.; Muilonberg, G.E. "Handbook of X-ray Photoelectron Spectroscopy"; Perkin-Elmer, Eden Prairie, MN, 1979.
28. Benninghoben, A.; Evans, C.A. Jr.; Powell, R.A.; Shimizu, R.; Storms, H.A. "Secondary Ion Mass Spectrometry-SIMS II"; Springer-Verlag, New York, NY, 1979.
29. Mayer, J.W.; Rimini, E., Eds. "Ion Beam Handbook for Material Analysis"; Academic Press, New York, NY, 1977.
30. Asami, K.; Hashimoto, K.; Shimodaira, S. Corrosion Science 1978, 18, pp. 125-137.
31. Baer, D.R.; Thomas, M.T. J. Vac. Sci. Tech. 1981, 18, pp. 125-137.
32. Wagner, C.D.; Zatko, D.A.; Raymond, R.H. Anal. Chem. 1980, 52, pp. 1445-1451.
33. McMahon, C.J. J. Mat. Sci. Eng. 1980, 42, pp. 215-226.
34. Bruemmer, S.M.; Jones, R.H.; Thomas, M.T.; Baer, D.R. Scripta Metallurgica 1980, 14, pp. 1233-1237.
35. Bruemmer, S.M.; Jones, R.H.; Thomas, M.T.; Baer, D.R. Scripta Metallurgica 1980, 14, pp. 137-141.
36. Jones, R.H.; Bruemmer, S.M.; Thomas, M.T.; Baer, D. R. Met. Trans. Aug. 1981, 12A.
37. Seah, M.P. J. Vac. Sci. Tech. 1980, 17, pp. 16-24.

38. Marchut, L.; McMahon, C.J. Jr. "Applications of Electron and Position Spectroscopies in Materials Science and Engineering"; ed. O. Buck, Academic Press, New York, NY.
39. Bruemmer, S.M.; Jones, R.H.; Baer, D.R.; Thomas, M.T. "Influence of S, P and Sb on the Intergranular Hydrogen Embrittlement of Nickel"; Pacific Northwest Laboratory, Richland, WA. Submitted to Met. Trans.
40. Jones, R.H.; Bruemmer, S.M.; Thomas, M.T., Baer, D.R. Proceedings of NATO Institute on Atomistics of Fracture, 1981.
41. Wang, R. "Spent Fuel Special Studies Progress Report: Probable Mechanisms for Oxidation and Dissolution of Single-Crystal UO<sub>2</sub>" PNL-3566, Pacific Northwest Laboratory, Richland, WA., 1981.
42. Thompson, N.G.; Lichter, B.D.; Appleton, B.R.; Kelly, E.J.; White, C.W. "Ion Implantation Metallurgy"; ed. C.M. Price and J.K. Hirvonen, AIME, 1979.
43. Hultquist, G.; Leygraf, C. Mat. Sci. Eng. 1980, 42, p. 199.
44. Hultquist, G.; Leygraf, C. J. Vac. Sci. Tech. 1980, 17, pp. 85-88.
45. Baer, D.R. Appl. Sur. Sci. 1981, 7, pp. 69-82.
46. Mitchell, D.F.; Sproule, G.I.; Graham, M.J. J. Vac. Sci. Tech. 1981, 18, pp. 690-694.
47. Merz, M.D. Met. Trans. 1979, 10A, p. 71.
48. Baer, D.R.; Merz, M.D. Met. Trans. 1980, 11A, pp. 1973-1980.
49. Wallwork, G.R. "Proceedings of the International Conference on High Temperature Corrosion-San Diego"; NACE, Houston, 1981.
50. Shafrin, E.G.; Murday, J.S.; Guttenplan, J.D.; Hashimoto, L.N. Appl. Sur. Sci. 1980, 4, pp. 456-465.
51. Katzman, H.A.; Malot, G.M.; Bauer, R.; Stupian, G.W. Appl. Sur. Sci. 1979, 2, pp. 416-432.

RECEIVED May 4, 1982

## Surface Characterization in Mineral Processing

D. W. FUERSTENAU and S. CHANDER

University of California, Department of Materials Science and Mineral Engineering,  
Berkeley, CA 94720

Surface and interfacial phenomena of importance in mineral processing are reviewed. Examples of a fundamental and an applied nature are taken from the recent literature to illustrate how the use of several different surface characterization techniques makes it possible to delineate a detailed molecular-scale picture of interfaces. Lack of techniques to study solid/liquid interfaces *in-situ* has led to the development of many *ex-situ* and indirect methods for surface characterization.

The results of such measurements are often interpreted through use of models requiring various underlying assumptions. It has been often necessary to use a combination of two or more techniques to delineate the physico-chemical interfacial phenomena. Mineral processing research has extensively involved determination of electrokinetic behavior, voltammetry, gas adsorption, aqueous-phase adsorption, infrared and UV-VIS spectroscopy, measurement of contact angles, and, more recently, ESCA analysis to delineate surface composition. Correlations between processing behavior and surface chemical characteristics are demonstrated.

The recovery of valuable minerals and metals requires several stages of sequential processing operations. The mined ore must be crushed and ground to fine sizes prior to treatment by such beneficiation processes as heavy-medium separation, tabling, magnetic separation, electrostatic separation, flotation, selective flocculation, etc. Since most of these processes are carried out in aqueous media, solid-liquid separations by such operations as thickening and filtration are an integral part of the benefici-

0097-6156/82/0199-0283\$08.25/0

© 1982 American Chemical Society

ation flowsheet. Sometimes, the beneficiated minerals are too fine to be used directly and must undergo size enlargement by agglomeration and/or sintering before subsequent utilization.

The above processes involve separation based either on bulk properties (for example, size, density, shape, etc.) directly or by subtle control of the chemistry of the narrow interfacial region between the mineral particle and the aqueous solution in which it is suspended. In the processing of certain ores, such as those of uranium, gold or oxidized copper, chemical alteration of the minerals may be required to recover the valuable metals. These techniques are not discussed here, except to include those aspects which are directly related to surfaces and interfaces.

Because mineral separations are generally made at fine particle sizes, properties of surfaces and interfaces play a dominant role in the performance of many of the mineral processing unit operations. The various types of interfaces involved in mineral processing operations are summarized in Table I. Alteration of surfaces by surface chemical methods is often used to modify mineral properties in order to affect their response to such separation techniques as flotation or selective flocculation. By control of interfacial chemistry and physics, it is possible to control ore breakage, sequential separations of valuable minerals, and, when necessary, re-agglomeration to recover solid or liquid products. In this review more emphasis has been given to the solid/liquid interface because of its greater importance in understanding the response of specific minerals to a processing stage. There are very few techniques for *in-situ* analysis of solid/liquid interfaces and it is therefore, often necessary to obtain indirect information through several different types of measurements. For example, solid/liquid interfaces have been

Table I: Interfacial Interactions of Importance in Mineral Processing

Two Phase Interactions

L/V	Foam separation
S/L	Wet comminution, leaching, filtration
S/V	Dry comminution, electrostatic separation, photometric sorting

Three Phase Interactions

S/L <sub>1</sub> /L <sub>2</sub>	Liquid-phase agglomeration
S/L/V	Flotation, agglomeration, filtration
S <sub>1</sub> /S <sub>2</sub> /L	Flocculation, selective flocculation, slime coatings, thickening

Four Phase Interactions

S <sub>1</sub> /S <sub>2</sub> /L/V	Floc flotation
S/L <sub>1</sub> /L <sub>2</sub> /V	Oil flotation, liquid-phase agglomeration, carrier flotation

Table II: Surface or Interfacial Properties which are Considered Directly Responsible for Performance of Various Unit Operations in Mineral Processing

SURFACE OR INTERFACIAL PROPERTY	PROPERTIES IN GAS OR VACUUM				PROPERTIES OF MINERAL - SOLUTION INTERFACES				PROPERTIES OF THREE PHASE SYSTEM					
	Specific surface area or particle size	Elemental	Phase	Surface species*	Surface energy	Surface charge or potential	Point-of-zero-charge	Surface charge	Surface potential	Zeta potential	Structure of adsorbed layer of ions or molecules	Contact angle	Film thickness	Film viscosity
UNIT OPERATION														
Comminution			X		X									
Photometric sorting				X		X								
Electrostatic separation							X							
Flotation and its modifications	X			X			X	X	X	X	X	X	X	X
Selective flocculation	X			X			X	X	X	X	X	X	X	X
Electrophoretic separation								X		X	X	X	X	X
Thickening, filtration	X							X	X	X	X	X	X	X
Agglomeration	X							X	X	X	X	X	X	X
Leaching	X	X	X	X										

\* Includes surface functional groups, adsorbed ions and molecules.

studied by investigating the solid after it has been separated from the liquid. The study of the solid/vacuum (or gas) interface in such cases is primarily an *ex-situ* method to characterize solid/liquid interfaces and for completeness several *ex-situ* techniques have been included in this review.

### Surface Properties of Importance in Mineral Processing

The mineral processing unit operations in which surfaces or interfaces play an important role are listed in Table II. Also given in the table are the more important interfacial properties on which the performance of particular unit operation depends. In order to acquire a detailed picture of the chemical and physical processes on a molecular scale at various interfaces, it is necessary to ascertain the following: (i) the physical and chemical nature of the mineral surface, (ii) the surface concentration of atomic, ionic or molecular species and their identity, (iii) the geometric or structural arrangement of these surface species including their mobility, and (iv) the charge distribution and the energy level distribution of valence electrons in the adsorbate and the surface. This information is not easy to obtain and frequently a combination of several measuring techniques is needed.

Techniques for the measurement of surface properties of minerals in gas or vacuum are summarized in Table III. As stated in the previous section, many of these techniques are used indirectly to study processes occurring at mineral/solution interfaces. Methods to study solid/solution interfaces are listed

Table III. Techniques for Measurement of Surface Properties of Mineral Particles

Surface Property	Technique of Measurement
Specific surface area	Gas adsorption
Pore size distribution	Mercury porosimeter, gas adsorption/desorption
Surface topography	Optical microscopy, SEM
Surface chemical analysis (including surface region)	Auger spectroscopy, ESCA, Moessbauer spectroscopy, electron microprobe, EDS
Surface chemical micro-distribution	SEM with energy dispersive spectroscopy (EDS)
Phase analysis of surface or surface region	LEED, SEM-electron diffraction
Surface functional groups	IR spectroscopy, chemical methods
Surface energy	Direct measurement of energy required to create a new surface



in Table IV, and properties of mineral particle/fluid/fluid systems are listed in Table V. Since the unit operation of flotation has been most widely investigated as far as interfacial behavior is concerned, several examples in this review are taken from fundamental and applied studies of various aspects of flotation.

### The Electrical Double Layer at Mineral/Water Interfaces

Since the electrical double layer at mineral/water interfaces is known to control the adsorption of ions, on which depend the response of several unit operations, its characterization is of utmost importance. The most important parameter that describes the electrical double layer in mineral/water systems is the point-of-zero-charge (PZC). This is the condition in the aqueous solution at which the surface charge is zero. For semi-soluble salt-type minerals (such as barite,  $\text{BaSO}_4$ , or iodyrorite,  $\text{AgI}$ ) in which ions are free to pass between the two phases, the surface charge arises from the preference of the lattice ions for the solid relative to the aqueous phase. Equilibrium is attained when the electrochemical potential of the ions constituting the crystal lattice is constant throughout the system. Those particular ions which are free to pass between both phases and therefore establish the electrical double layer are called potential-determining ions. The surface charge,  $\sigma_0$ , is expressed in terms of the adsorption density of potential-determining cations,  $(\Gamma_+)$  and anions,  $(\Gamma_-)$ , as

$$\sigma_0 = zF (\Gamma_+ - \Gamma_-)$$

where  $F$  is the Faraday constant and  $z$  the valence for a symmetrical (1-1 or 2-2) salt. For oxides, in which the metal cations and oxygen ions are not free to move from solid to solution and vice versa,  $\text{H}^+$  and  $\text{OH}^-$  have long been considered to be potential-determining (1). These ions interact with the oxides to establish the various equilibria.

The surface potential,  $\psi_0$ , of the mineral (measured with reference to the solution) is usually considered to be zero at the PZC. The value of the surface potential at any activity of the potential-determining cation,  $a_+$ , is given by

$$\psi_0 = \frac{RT}{z^+F} \ln a_+/a_+(PZC)$$

where  $a_+(PZC)$  is the activity of the potential-determining electrolyte at the PZC,  $R$  is the gas constant,  $T$  is the absolute temperature and  $z^+$  is the valence of the potential-determining cation in the electrolyte.

Ions in solution adsorb at mineral/solution interfaces to balance the surface charge and maintain electroneutrality. These ions are known as the counter ions. In contrast to the situation

Table IV: Techniques for Measurement of Properties of Mineral/Particle Solution Interfaces

Surface Property	Technique of Measurement
Interfacial area	Adsorption or negative adsorption of ions or molecules of known size
Point-of-zero-charge	Adsorption of potential-determining ions, many indirect methods based on a characteristic response to mineral processing operation
Surface charge	Adsorption of ions
Zeta potential	Electrophoretic mobility, streaming potential, etc.
Electrode potential	Direct measurement with a standard electrode
Surface functional groups	Specific adsorption of ions or molecules, <i>in-situ</i> spectroscopic techniques
Adsorption of surfactants	"Loss from solution" method, direct measurement using radioactive tracers, ellipsometry, nephelometry
Concentration of oxidizable/reducible species at surface	Voltammetry
Surface energy	Solubility, heat of solution

Table V: Techniques for Measurement of Properties of Mineral Particle/Fluid/Fluid Systems

Interfacial Properties	Technique for Measurement
Wettability	Contact angles, displacement of a fluid by another on the solid surface
Wetting film thickness	Equilibrium thickness measured by optical methods (interference fringes, and reflectance techniques)
Film viscosity	Contact time, drainage and rupture of liquid film

in which the potential-determining ions are special for each system, any ions present in the solution can function as counter ions. As has been well established, the counter ions occur in a diffuse layer that extends from the interface out into the solution. The closest distance of approach of counter ions to the surface is one hydrated ionic radius away, shown as the distance  $\delta$  in Figure 1. This first layer of adsorbed counter ions is called the Stern plane. Depending on the ionic strength of the solution, there is a considerable drop in potential between the solid surface and the plane  $\delta$ , this potential drop being  $\psi_0 - \psi_\delta$ .

If counter ions are adsorbed only by electrostatic attraction, they are called indifferent electrolytes. On the other hand, some ions exhibit surface activity in addition to electrostatic attraction because of such phenomena as covalent bond formation, hydrogen bonding, hydrophobic and solvation effects, etc. Because of their surface activity, such counter ions may be able to reverse the sign of  $\psi_\delta$  because the charge of such ions adsorbed exceeds the surface charge.

Although it is difficult to measure  $\psi_\delta$ , the conditions where the sign of  $\psi_\delta$  may be reversed can be determined through measurements of the zeta potential or electrokinetic potential,  $\zeta$ . Electrokinetic phenomena, which involve the interrelation between mechanical and electrical effects at a moving interface, have found widespread use in colloid and surface chemistry. The two electrokinetic effects that have been most widely used are electrophoresis and streaming potential. Since  $\zeta$  is the potential at the slipping plane when liquid moves relative to the solid, only ions in the diffuse layer outside the slipping plane are involved in the electrokinetic process. All sorts of charge compositions on the surface and in the inner ( $\beta$ ) and outer ( $\delta$ ) Stern planes can give the same zeta potential (see Figure 1). Thus, while knowledge of the zeta potential at some single condition may be of certain value, determination of the change in zeta potentials as solution conditions are varied may be extremely useful. From these changes, modes of adsorption of various kinds of ions can be ascertained if one makes the useful assumption that the slipping plane and the Stern plane coincide. This approximation seems permissible because the potential difference between the plane and the slipping plane is small compared to the total potential difference across the double layer. The condition under which there may be no ambiguity is when  $\psi_\delta = 0$ , for then  $\zeta$  must be zero. The condition where  $\zeta$  reverses sign has been termed the iso-electric point or simply the point of zeta potential reversal (PZR).

### Surface Characterization in Flotation

Separation of minerals by flotation developed as an art about seventy years ago, but the need for separating increasingly complex mixtures of minerals necessitated that scientific research be di-

rected towards understanding the basic surface chemistry of this important process. Since most minerals are hydrophilic, organic surfactants must be added to make desired minerals hydrophobic through selective adsorption. Such reagents are called collectors. Perhaps a summary of the different methods that can be utilized for the flotation separation of iron ores will illustrate the complexity of the chemistry of flotation systems. Six different procedures have been developed for the flotation of hematite ( $\text{Fe}_2\text{O}_3$ ) from quartz ( $\text{SiO}_2$ ) or vice versa:

1. Flotation of hematite using a sulfonate as the collector at pH 2 to 4.
2. Flotation of hematite with a fatty acid as the collector at pH 6 to 7.
3. Flotation of quartz with an amine as collector at pH 6 to 7.
4. Flotation of quartz activated with calcium ions at pH 11 to 12, using a soap as the collector together with starch to depress the hematite.
5. Flotation of hematite with an amine as collector at pH 1.5 in the presence of hydrochloric acid or sulfuric acid.
6. Flotation of hematite with hydroxamate as collector at pH 8 to 9.

To fully understand the physical-chemical basis of flotation in these systems so that new flotation procedures might be developed to make other appropriate mineral separations, extensive research in applied surface chemistry is required.

One of the earliest research tools used for such flotation investigations was the determination of factors that affect contact angles, a technique used with great success by Wark and his co-workers in Australia (2). Since most flotation separations are based on the selective adsorption of collectors at mineral/water interfaces, direct measurement of the amount of the reagent adsorbed permits physical-chemical analysis of adsorption phenomena as it relates to wettability. Gaudin and his co-workers (3) determined adsorption isotherms of a number of collectors on a variety of minerals, leading the way in this important approach to flotation chemistry. Another significant step in delineating the physical chemistry of flotation systems was the bringing of the concepts of the electrical double layer into widespread use in the interpretation of flotation phenomena (4). Figure 2 shows how the results of all these methods of experimentation can be correlated with the flotation of quartz using dodecylammonium acetate (DAA) as collector. This figure illustrates how measurements that reflect conditions at the solid/liquid interface (adsorption density and zeta potential) can be correlated directly with surface phenomena that reflect complex conditions at solid/-liquid/gas interfaces (contact angle and flotation behavior).

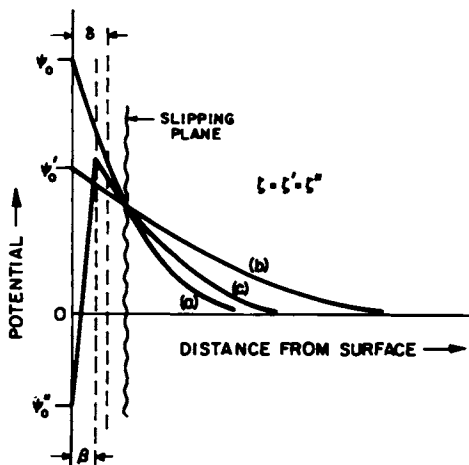


Figure 1. Potential variation through the electrical double layer for a higher concentration of potential-determining ion (a), a lower concentration of potential-determining ion (b), and in the presence of a specifically adsorbed counter ion with a potential-determining ion below the point-of-zero charge (c). Note that the  $\zeta$  potential in all three instances could be identical. (Reproduced, with permission, from Ref. 1. Copyright 1970, International Union of Pure and Applied Chemists.)

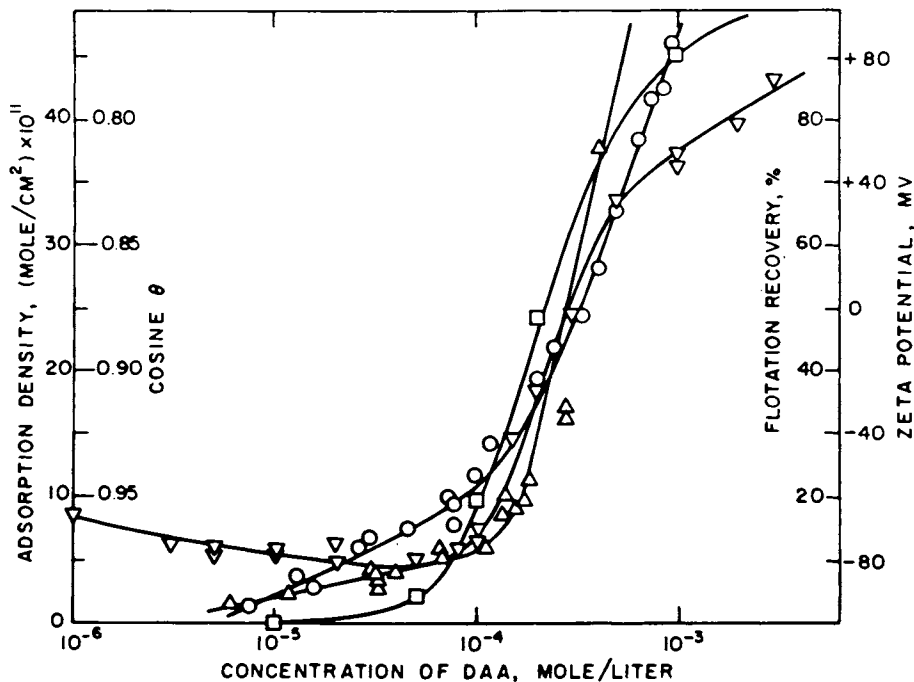


Figure 2. Correlation among contact angle. Key:  $\circ$ , adsorption density;  $\Delta$ , flotation response;  $\square$ ,  $\zeta$  potential; and  $\nabla$ , quartz as a function of dodecylammonium acetate (DAA) concentration at pH 6-7.

Flotation of Naturally Hydrophobic Minerals. Flotation response of naturally hydrophobic minerals correlates very well with electrokinetic measurements. Figure 3 shows that the flotation of coal correlates well with zeta potential of demineralized coal (5). The flotation rate is maximum where the zeta potential is zero and it decreases with increase in the magnitude of the zeta potential. Similar observations were made earlier by Chander and Fuerstenau (6) for the flotation of molybdenite. The decrease in flotation rate with increase in zeta potential is because of the electrical double layer repulsion between the charged particle and the air bubble.

Contact Angles and Flotation as a Function of Electrode Potential. Contact angles have successfully been used to delineate the wettability and floatability of minerals for a long time. Also, electrochemical methods have been in use to study mineral-solution interactions for minerals with conducting or semiconducting properties (7, 8). Voltammetry is one such technique which can be used to estimate the concentration of oxidizable (or reducible) species at the surface. From the oxidation (or reduction) potential of the species, its nature can be inferred. Frequently voltammetric measurements must be supplemented with other techniques to characterize the surface species. Although such techniques as ellipsometry (for in-situ studies) and various spectroscopic techniques (for ex-situ studies) are being used by electrochemists, in general they have not been very extensively utilized by researchers in mineral processing. However, one such study involved combining contact angle measurements with voltammetry to delineate the interfacial phenomena with reference to the flotation of sulfide minerals (7). The investigation combined electrochemical phenomena at the electrode/solution interface with three phase phenomena involving solid/liquid/gas phases. Contact angle measurements for a copper electrode (which were similar for cuprous sulfide) in solutions of potassium diethyldithiophosphate are superimposed on a voltammogram in Figure 4. The voltammogram consists of an oxidation cycle shown by the solid line, and a reduction cycle shown by the broken line, and the three-phase contact between the mineral surface and the bubble is shown as inserts at several electrode potentials. The arrows on the curves indicate the direction of polarization of the mineral surface. The oxidation peak corresponds to the oxidation of the collector ions and the reduction peak to reduction of the oxidation product. The oxidation product makes the surface hydrophobic, as indicated by the large contact angle. The surface remains hydrophobic until the electrode potential is sufficiently low so as to reduce the oxidation product. These results correlated well with flotation behavior as a function of applied potential (9).

The Space Charge Layer of Galena and the Kinetics of the Oxygen Reduction Reaction. The reduction of oxygen on the surface

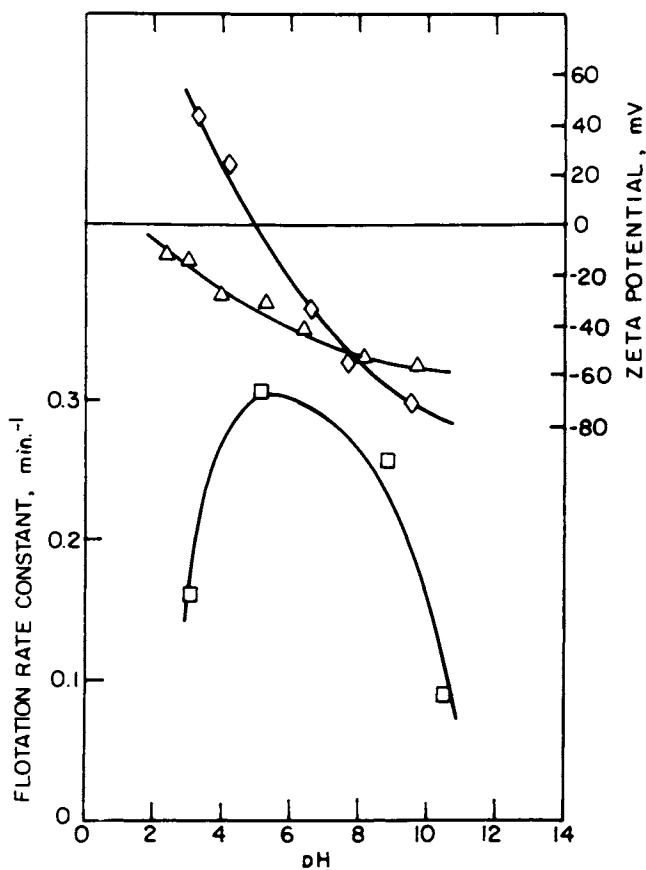


Figure 3.  $\zeta$  potential ( $\Delta$ ) and flotation rate constant ( $\square$ ) of Somereset coal as a function of pH in  $2 \times 10^{-3}$  M KCl. The  $\zeta$  potential ( $\diamond$ ) for demineralized coal (0.3% ash) is also shown. (Reproduced, with permission, from Ref. 5.)

of sulfide minerals is known to be important in the adsorption of collectors used for their flotation. Richardson and Edelstein (10) studied the effect of space charge of galena on the kinetics of oxygen reduction using combined electrochemical, interfacial capacitance and surface photovoltage (SPV) techniques. The current density, interfacial capacitance and the SPV for a typical galena sample is given as a function of the electrode potential in Figure 5. The top portion of the figure shows characteristic anodic and cathodic polarization curves corresponding to the electrochemical processes at the galena electrode. Although it is not possible to include a complete analysis of the interfacial capacitance and surface voltage measurements, it can be seen that a minimum in the interfacial capacitance occurs at the same potential where the SPV changes sign. Both techniques reflect the interfacial characteristics of the galena/solution interface. From their studies, Richardson and Edelstein concluded that because of the large limiting current density for diffusion of electrons or holes to the surface, it is unlikely that the rate of supply of either electrons or holes to the surface is rate determining in the reduction of oxygen and oxidation of sulfhydryl flotation collectors. Potentials of different samples and the corresponding charge at the interface resulted from variation in bulk carrier densities, illumination or adsorption. These variations explain the differences in collector adsorption behavior of natural sulfides and the electrochemical behavior of collector/sulfide mineral interactions.

Surface Functional Groups on Minerals and Ores: Coal as an Example. A knowledge of the nature and concentration of functional groups on the surfaces of minerals is vital for understanding the response of these minerals to various mineral processing techniques. These functional groups play an important role in adsorption of surfactants used in mineral processing. In recent years, significant research efforts have been made to develop processes to beneficiate coal for recovery at fine sizes. The most attractive technique is flotation because conventional heavy-media separators and cyclones are ineffective to recover coal at fine sizes.

Coals have generally been analyzed either for their moisture, ash and volatile matter contents or elemental (C, H, N, S, and O) content. Sometimes they have been analyzed for ash compositions. Only in recent years, since it has become necessary to beneficiate coals more effectively, the need to characterize the surfaces of coals is being fully recognized. Fortunately, coals and activated carbons have been the subject of investigation of scientists working in areas other than mineral processing, and sufficiently developed techniques are available for the characterization of these materials. Of major importance to mineral processing is the nature and concentration of functional groups on coal surfaces. Particular stress has been laid on substituent groups containing



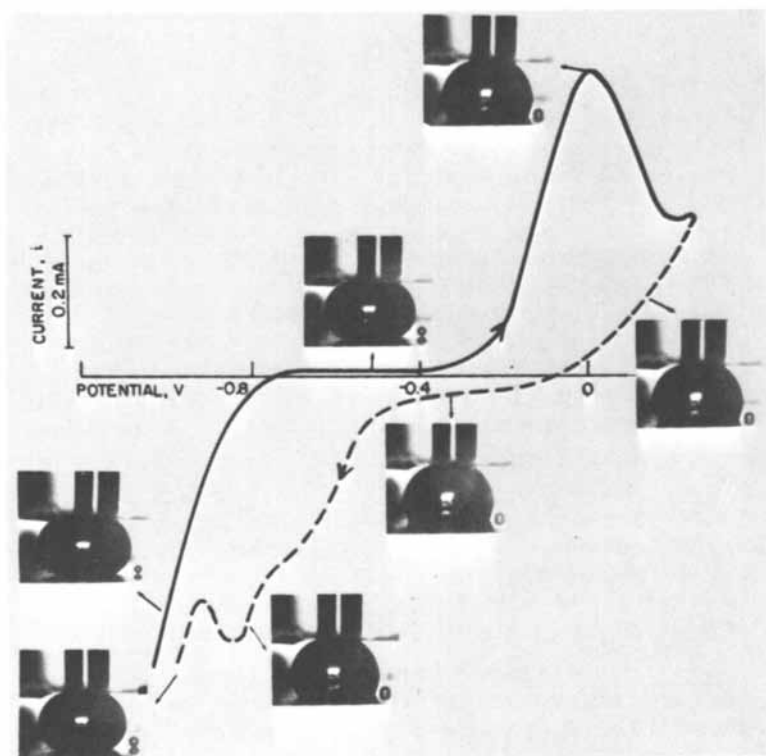


Figure 4. Photographs of bubble profiles superimposed on a voltammogram showing change in contact angle with electrode potential of copper in the presence of  $2 \times 10^{-3}$  M potassium diethyldithiophosphate as flotation collector. Conditions: sweep rate, 50 mV/s; pH 9.3 (0.25 M sodium borate). (Reproduced, with permission, from Ref. 7. Copyright 1975, Universita Degli Studi.)

"reactive" oxygen, that is on groups which in peats and lignites, include alcoholic and phenolic -OH, -COOH, =CO and -OCH<sub>3</sub>, but among bituminous coals are restricted to =CO and phenolic/alcoholic -OH (11). There is evidence for peroxide and esteroxygen as well as, with respect to more mature coals, ether and heterocyclic oxygen. The methods employed to determine these functional groups may be divided into two groups: i) chemical methods and ii) spectroscopic methods which are briefly described in the paragraphs that follow.

The concentration of acidic groups can be determined by neutralization with a base, using solutions of sodium bicarbonate, sodium carbonate, sodium hydroxide or sodium ethoxide as titrants. Only those acidic groups which are much more strongly dissociated than the conjugate acids of the bases are completely neutralized. Thus, the differences in the amount of base required may be used to characterize the acidity of surface groups. Boehm (12) identified four different type of surface groups by this technique.

To gain additional information about the chemical nature of surface groups several methods involving the formation of derivatives of surface groups have been developed:

1. Nitration - Nitro groups are introduced onto the carbon surface by the sulfonitric mixture or nitronium tetrafluoroborate and their concentration is determined.
2. Methylation - Carboxylic groups are determined by their methylether derivatives. Methylation may be carried out by diazomethane in the presence of a Broensted acid, such as HCl or in the presence of a Lewis acid such as BF<sub>3</sub>, or in methanol. Phenolic-OH may also be estimated by this method if methylation in ether is followed by saponification to eliminate interference from -COOH.
3. Formation of Oximes - Carbonyl functional groups can be transformed into an oxime derivative by alcoholic hydroxylamine chlorohydrate and monitored by the liberation of HCl.
4. Acetylation - Phenolic and hydroxyls can be measured most accurately by acetylation and subsequent hydrolysis of the acetylated sample with barium hydroxide.
5. Reduction - Carbon dioxide evolved when coal is heated with a suitable catalyst (such as copper carbonate or copper sulfate) is a measure of carboxyl groups. Other reducing agents such as amalgamated Zn with HCl, LiAlH<sub>4</sub> and NaBO<sub>2</sub> attack different groups differently and may be used for characterization.

Infrared Spectroscopy can be used to gain important information about functional groups on surfaces of minerals, but quantitative determinations have been difficult. For complex materials, like coal, the spectra are still not resolved fully; for example, there is great deal of uncertainty about the  $1600\text{cm}^{-1}$  band which is the dominant feature of all coal spectra. Fourier-transform infrared spectroscopy, which is a considerable improvement in this technique, has recently been used to investigate low-temperature oxidation of coal (13).

The dependency of maximum rate constants for the flotation of coal on the concentration of carboxyl and phenol surface groups is shown in Figure 6. Each data point corresponds to a different coal sample (5). At low concentration of the surface oxygen groups, the surface of coal is quite hydrophobic and the flotation rate is high. Increase in these surface groups makes the surface hydrophilic with resultant decrease in flotation rate.

#### Application of Raman Spectroscopy to the Study of Interfaces in Mineral Processing.

Raman spectroscopy appears to offer great promise for *in-situ* studies of solid/liquid interfaces of interest in mineral processing. Until recently, infrared spectroscopy was the only technique available to investigate the vibrational spectra of adsorbed species, but this technique could not be used for *in-situ* studies because water is a strong absorber of IR radiation. (In special cases, it may be possible to use Fourier Transform IR Spectroscopy in the presence of water because of its higher sensitivity.) It has been applied as an *ex-situ* technique, however (when the mineral particles are removed from the aqueous phase, dried and prepared into a suitable sample). Conventional Raman spectroscopy is, in general, much too insensitive for spectrochemical studies because of the low level of adsorbed scatterers normally present in the electrical double layer. A new approach, however, is the application of Laser Raman Spectroscopy. The recent developments of continuous wave lasers has made it possible to effectively enhance the Raman scattering cross-section of a species of interest by factors up to  $10^5$  (14). As a result, it becomes possible to detect species with excitation coefficients of  $10^3\text{ M}^{-1}\text{ cm}^{-1}$  at millimolar concentration levels. Since the exciting line is in the visible region, there is only low-level interference from water. Some aspects of infrared and Raman spectroscopies are compared in Table VI.

In mineral processing, there are numerous systems in which postulates have been made to suggest adsorption of surface active molecules on specific surface sites. Most of the postulates are based on inference from a variety of observations and direct evidence has been lacking. It should now be possible to use Raman spectroscopy to characterize solid/aqueous solution interfaces. A few studies exist in which adsorption at metal and metal oxide

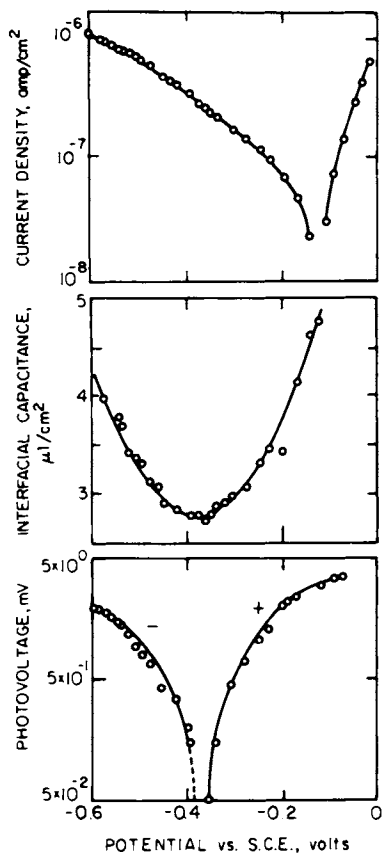


Figure 5. Current, capacitance, and surface photovoltage vs. potential for galena. (Reproduced from Ref. 10.)

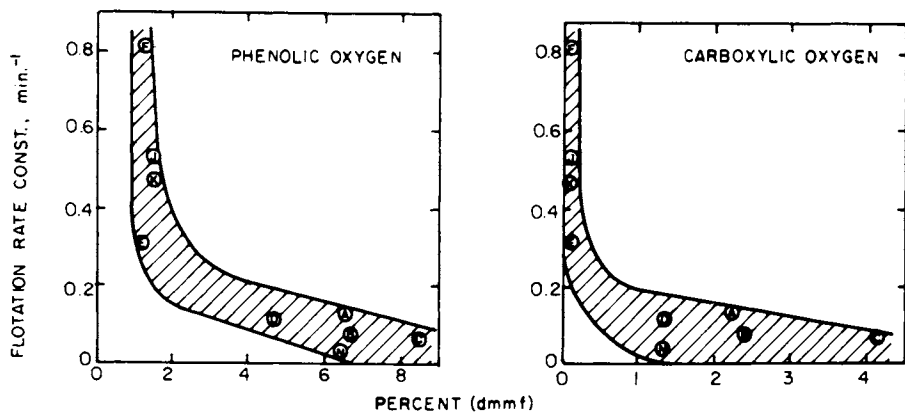


Figure 6. Flotation rate constant of several coals as a function of their phenolic-OH and carboxylic surface groups.

Table VI: A comparison of Infrared and Laser Raman Spectroscopy for the Characterization of solid/liquid Interfaces

Infrared Spectroscopy	Raman Spectroscopy
Adsorption process	Light-scattering process
Spectra dominated by adsorbent	Spectra dominated by surface atoms
Strong interference from adsorbed water	No interference from colorless solvents
Sample preparation more difficult for transmission mode	Flat sample for high signal/noise ratio
<i>ex-situ</i> technique	<i>in-situ</i> technique

surfaces has been studied by this method. Investigations til 1979 have been reviewed by Takenaka (15). Three different sites for the adsorption of pyridine on oxides have been distinguished using Raman spectroscopy. The sites identified are: Lewis sites, Bronsted sites and hydrogen-bonded sites. The increase in peak areas of four Raman bands for the adsorption of pyridine on alumina is shown in Figure 7 (16). With increase in coverage, the adsorption first occurs at Lewis sites, as observed by the band at  $1019\text{ cm}^{-1}$ . Pyridine molecules adsorb by coordination bond formation between nitrogen in the pyridine molecule and aluminum in the oxide. This is followed by an increase in intensity of the band at  $999\text{ cm}^{-1}$  which corresponds to hydrogen bonding between the pyridine molecule and hydroxyls on the surface of alumina. The adsorption phenomena leading to an increase in bands at  $991$  and  $1031\text{ cm}^{-1}$  are for physisorption. When the alumina was activated at high temperature ( $950^{\circ}\text{C}$ ), the intensity of the  $1019\text{ cm}^{-1}$  band increased and that of  $999\text{ cm}^{-1}$  band decreased, which is to be expected because of the loss of surface hydroxyls from the alumina surface on heating.

### Ore Mineralogy

Ore mineralogy is the dominant factor in the selection of mineral processing methodology. For many years, optical microscopy, X-ray diffraction, and the electron microprobe have been used to determine locking, grain size, composition, etc. Locking patterns (that is, the grain size and manner in which different minerals are intergrown in an ore sample) have a profound influence not only on the surface properties of particles but also on their behavior in various mineral processing operations. Some typical locking patterns found in ores are schematically shown in Figure 8. Consider each of the grains to be about  $0.1\text{ mm}$  in diameter. On the left of Figure 8, (i) shows a simple locked grain that can be separated if the particle size is reduced below the size of the two components. Locking exhibited by (ii) is the

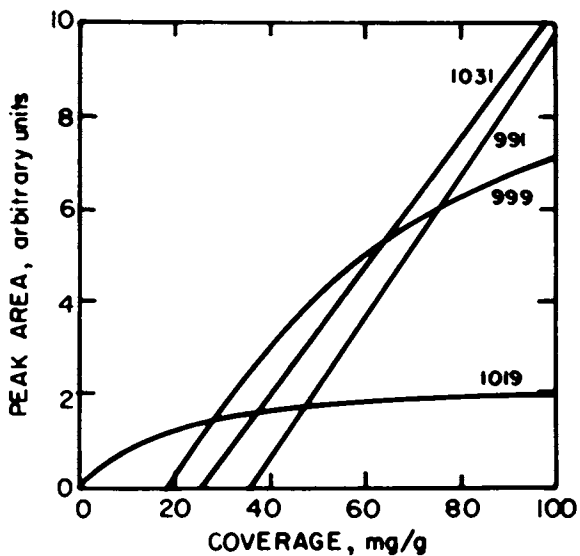


Figure 7. Peak areas of Raman bands for the adsorption of pyridine on alumina. (Reproduced from Ref. 16. Copyright 1974, American Chemical Society.)

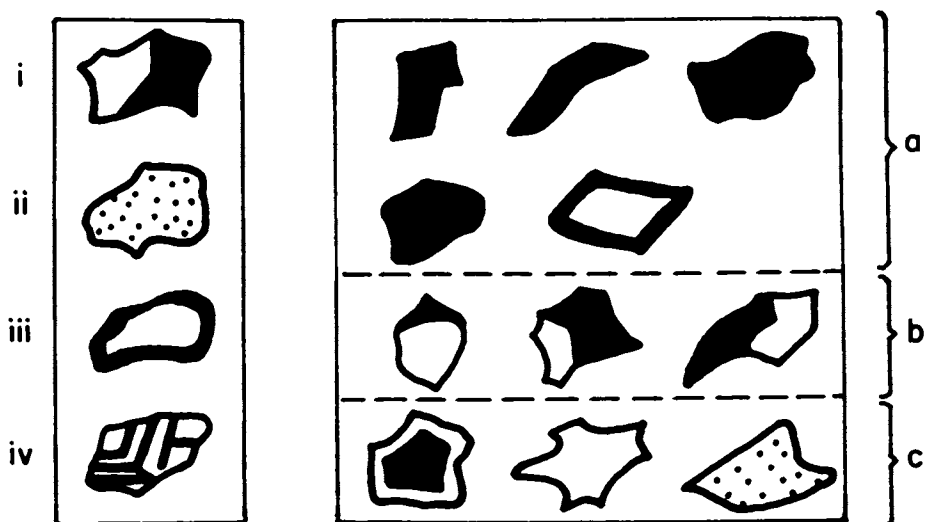


Figure 8. A scheme of locked mineral particles.

type that would require extremely fine grinding and therefore separation may not be possible. Surface chemical measurements on such particles may not be very meaningful. For example, if a particle of coal (low energy surface) contains clay particles (high energy surface) as exemplified by (ii), then electrokinetic, measurements or heat of wetting measurements may be dominated by contribution of the high-energy clay particles. Particles of type (iii) are particularly troublesome in flotation because the surface may be a coating of one mineral on the surface of another. As a further illustration of flotation response, where particles respond to the nature of the surface, the ore particle reporting to the concentrate may be those shown in (a) and those reporting to the tailings in (c). The middlings, particles having somewhat equal probability to go into the concentrate or tailings, are shown in (b). The conventional analytical techniques have limited usage in assessing finely disseminated and complex ores, but new techniques are now available which respond to the need for specific, detailed analysis of mineral distribution. For example, scanning electron microscopy, with greater depth of field and higher resolution than optical microscopy, provides excellent means to study locking patterns of minerals, grain size, and topography of mineral and ore particles. In addition, an energy dispersive analyzer used either with scanning or transmission electron microscopes, can provide chemical information about the area being analyzed. Micro-X-ray diffraction can be obtained from individual particles or grains to provide crystallographic information. X-ray photoelectron spectroscopy (or electron spectroscopy for chemical analysis) can be used to obtain information regarding composition, bonding and oxidation state in surface layers. As the ores become more complex, these new techniques will find greater role in helping solve mineral processing problems.

#### Characterization of Ores After Various Treatments

In mineral processing, surface characterization techniques are used primarily to study mechanisms of various subprocesses. These studies are carried out mostly in research laboratories using model systems so as to keep the system simple and amenable to interpretation by known laws of physics and chemistry. For these very reasons, some of the newer surface characterization techniques have been used to investigate pure solids, often single crystals. In mineral processing operations, one necessarily deals with particles of complex ores with an objective to recover the valuable minerals contained in the ore. Experience, both in industry and laboratory, shows that complex ore particles behave differently from simple solids in many ways. In process evaluation and in optimization of operating plants, it is necessary to characterize the ore particles as they undergo various treatments. In recent years ESCA has been found to be a useful technique for

this purpose. The benefits of this technique are illustrated with the help of two examples. The first is in the flotation separations of complex sulfide ores and the second is in the hydro-metallurgical treatment of lateritic ores for the recovery of nickel.

Complex sulfide ores represent an important part of world's reserves of Cu, Pb and Zn. Because of the highly disseminated nature of these ores, very fine grinding is often necessary to liberate valuable minerals. Flotation separations of such ores is often difficult. Recently, Predali et al. (17) used ESCA to study the surface of an ore as it passes through various stages of the processing operation. The surface concentration of species in the ore at different stages of the operation are compared with the bulk concentration in Table VII. The surface concentration of galena is consistently high in each ore sample. It was concluded that galena, being the most fragile mineral, coats the surface of the other particles. Higher surface concentrations of Pb, Zn, and Cu in the tailings indicate that these metals are lost from the surfaces of mineral grains in the tailings. Since the tailings from complex sulfide treatment plants usually have high surface areas and large tonnages are involved, the losses of valuable metals in the adsorbed state could be quite significant. It may be possible to reduce these losses through a better understanding of the mechanism of the adsorption of metal ions on gangue particles. One such study is described in a subsequent section of this paper.

The ESCA technique was also used by Clifford et al. (18) to study pyrite surfaces in an attempt to establish a mechanism for the interaction of pyrite with various reagents. Pyrite was found to be heavily oxidized throughout the flotation stage. An important observation of Predali et al. (17) is that the oxidation behavior of pyrite during wet-grinding differs from that during aging in air. In wet grinding, the surface is covered with oxy-hydroxides and hydroxides of iron with a significant decrease in the surface concentration of sulfur; the results are tabulated in Table VIII and can also be seen in the ESCA spectra given in Figure 9. No significant formation of sulfur or oxidized sulfur was observed. In contrast to this, aging in air leads to formation of basic iron sulfate, preserving the ratio of sulfur-to-iron atoms in the bulk. Aging in distilled water did not result in any modification of the pyrite surface. The effect of collectors and depressors was more difficult to see, however. It was not possible to discern appreciable changes in the C or S peaks after adsorption of the collector. Similarly, C and N could not be detected when NaCN adsorbs on the surface. Adsorption of copper and zinc ions could be measured by ESCA but these ions did not influence the flotation of pyrite. These ions are known, respectively, to activate and deactivate sphalerite. Perhaps, because of the heavily oxidized surface of pyrite the activation of adsorbed copper ions is inadequate to affect its floatability.



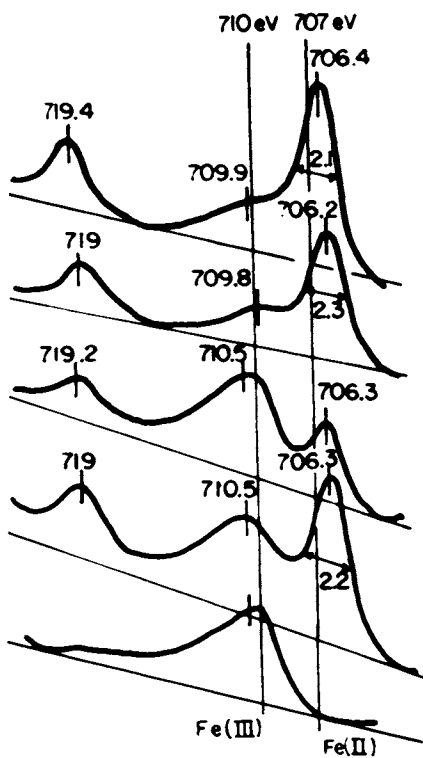


Figure 9. ESCA spectra of pyrite after several aging and aeration treatments, reading from top to bottom: dry ground, 20 d in distilled water, crusher outlet, floated at pH 4.5, and goethite FeO-OH. (Reproduced, with permission, from Ref. 17. Copyright 1981, Elsevier Sequoia.)

Table VII: Atom Content (percent) in the Bulk (B) and on the Surface (S) of the Ore at Various Operating Stages (17).

Material		Pb	Zn	Cu	Fe
Feed	S	3.8	2.9	2.4	91.1
	B	0.5	3.4	2.1	96.0
Rougher copper concentrate	S	9.0	4.6	11.6	74.8
	B	0.8	2.9	12.9	83.5
Twice-cleaned copper concentrate	S	13.4	4.7	37.1	44.8
	B	0.9	2.4	31.8	64.9
Rougher zinc concentrate	S	7.7	13.4	5.6	73.3
	B	1.3	18.4	2.2	78.1
Twice-cleaned zinc concentrate	S	10.7	32.6	8.2	48.4
	B	2.3	58.9	4.7	44.1
Tailings	S	5.9	5.2	3.4	85.4
	B	0.3	0.7	0.3	98.6

Table VIII: Surface Composition by ESCA in Aging and Aeration of Pyrite (17).

Sample	Fe(II)/Fe(III)*	S/Fe	% SO <sub>4</sub>
Freshly ground	0.58	2.00	3
30 days in air	3.08	2.60	38
20 hours in distilled water	0.66	1.80	5
At the crusher outlet	2.64	1.32	12
6 hours of wet grinding	2.20	1.45	14
1 hours of aeratin in the flotation cell	3.44	0.91	16
5 min of aeration in the flotation cell at pH 12	6.15	0.77	18

\* Fe(III) = 710 ev, Fe(II) = 706 ev

Hydrometallurgical treatment of lateritic ores, by the reduction roast/ammonia leach process is one of the methods used for the recovery of nickel from low grade lateritic ores. In a recent study Chander and his associates (19, 20) used such techniques as X-ray and electron diffraction, surface area measurement, ESCA, and Moessbauer spectroscopy to characterize the ore and to study how the ore changes as it undergoes various

processing stages. Although the results are too detailed to be presented here, it was possible to show a number of different phenomena: For example, ESCA indicates that ferrous and ferric ions are present in almost equal proportions on the surface of the ore. Since Moessbauer spectroscopy, and X-ray and electron diffraction showed only the presence of ferric ions, it was concluded that ferrous ions are present in surface layers, perhaps as a ferrous silicate. ESCA also suggests that reoxidation of the reduced ore is limited to the surface layers, particularly at 600°C, and is not detectable by conventional methods of analysis. (The extraction of nickel is very sensitive to the extent of reoxidation.) Finally, ESCA, X-ray and Moessbauer spectroscopy demonstrate how the cooling rate and environment affect the leachability of nickel from the reduced ore.

### Grinding Aids for Comminution

The unit operation of comminution, which is used extensively in a variety of industries, such as mineral processing, cement, ceramics, chemicals, pharmaceuticals, etc., has long been recognized to be energy-inefficient. One way to improve the energy efficiency of the size reduction operation has been the use of certain additives, known as grinding aids. Table IX demonstrates the effectiveness of some industrial grinding aids for dry and wet grinding processes. Most of the research on grinding aids has been directed towards finding specific additives that will improve the efficiency of grinding specific materials. However, even though additives have been found to be industrially successful in some instances, the rational development and application of grinding aids requires a clear understanding of their mode of action. Although the mechanism of their action is poorly understood at present, it is well recognized that surface chemical interactions play an important role.

Adsorbed surfactants can influence the comminution process in several ways:

- 1) Since comminution involves new surfaces, the energy required to produce a given amount of surface can be decreased by reducing the solid surface energy through the adsorption of surfactants.
- 2) Adsorption of surfactants can reduce the strength of materials by blocking the motion of dislocations near the surface, rendering their motion under stress gradients very difficult.
- 3) Surfactant molecules might penetrate deep into the tips of preexisting cracks and exert pressure on the crack tips, aiding the fracture process.
- 4) Adsorbed surfactants may reduce agglomeration (or recombination) of broken particles aiding the comminution process.

Table IX: Examples of the Effect of Grinding Aids in Dry and Wet Grinding Systems (21).

Materials Ground	Grinding Media	Grinding Aid	Effect
Cement clinker	Air	Di- or triethanol-amine (0.1%)	22-29% increase in grinding rate
Cement clinker	Air	Organosilicon (0.01-0.05%)	70% reduction in grinding time
Quartzite	Water	Flotigam P (0.03%)	120% increase in surface area
Alumina	Water	Organosilicon	75% reduction in grinding time
Limestone	Water	Flotigam P (0.03%)	70% increase in surface area
Taconite	Water	XF-4272 (0.06%)	18% increase in amount -325-mesh
Zircon	Water	Triethanolamine	75% reduction in grinding time
Quartz	Water	AlCl <sub>3</sub> (0.75 molar)	25% increase in relative new surface

The first three mechanisms of surfactant adsorption have been criticized mainly because crack propagation velocities in comminution devices are often much more than the rate of adsorption of the surfactants normally used as grinding aids (20). There is considerable evidence and concurrence of opinion on the prevention of agglomeration as the mechanism of grinding aid action (21). It is believed, therefore, that grinding aids that chemisorb on solid particles would most effectively reduce adhesive tendencies between particles and thereby improve grinding efficiency. Grinding aids may also affect the viscosity of the suspension and this may be the main influence on wet ball milling. As mentioned before, most of the existing work on the development of grinding aids has been oriented towards finding suitable reagents for the comminution of specific minerals and much needs to be done towards understanding the mechanism of action of such grinding aids. These types of studies will necessarily require characterization of the solid/gas interface in dry grinding and the solid/liquid interface in wet grinding.

#### Adsorption of Metal Ions in Leaching

The loss of dissolved metals during the leaching of ores was studied by Osseo-Asare and Fuerstenau (22). These investigators

showed that metal losses can occur by the adsorption of metal ions onto gangue particles. Adsorption isotherms and electrophoretic mobilities were measured to characterize several interfaces: rutile, alumina, quartz and hematite in ammoniacal solutions of copper, nickel and cobalt. The percentage of copper adsorbed is shown in Figure 10. Since the point-of-zero-charge of rutile, alumina, quartz and hematite occur at pH 6.2, 9.1, 2.0 and 8.1, respectively, it is clear that these ions do not adsorb by a simple electrostatic mechanism. For nickel and cobalt, the adsorption densities also decreased in the order  $TiO_2 > Fe_2O_3 > Al_2O_3 > SiO_2$ . The electrophoretic mobility behavior of the oxide in the presence of hydrolyzable metal ions can be represented in a generalized manner, as shown in Figure 11. Simple curves were obtained for a number of systems by James and Healy (23) who used ammonia-free solutions, and more complex curves by Osseo-Asare and Fuerstenau who used ammoniacal solutions. James and Healy explained the zeta-potential reversal ( $PZR_1$ ) by surface enhanced precipitation of the metal hydroxide at the surface. The broken curve in ammoniacal solutions has two other zeta-potential reversals,  $PZR_2$  and  $PZR_3$ . They occur because the metal-ammine complexes in ammoniacal solutions prevent precipitation of hydroxide at the surface. Osseo-Asare and Fuerstenau developed a model to explain the uptake of metal ions (24). Their model combines electrical double layer theory with properties of the substrate (PZC, dielectric constant), the solvent medium (dielectric constant), and the aqueous ionic and non-ionic species (stability constants). These investigators concluded that the presence of hydroxyl groups in the aqueous complex and solvation effects due to the dielectric constant of the solid play a dominant role in the uptake of metal by oxide colloids in aqueous ammoniacal solutions.

#### Discrepancies in Observed Surface Properties of Minerals

A review on mineral/water interfacial phenomena could not be complete without referring to apparent discrepancies in the measured surface properties of minerals. For example, various researchers have reported quite different values of the points-of-zero-charge of various minerals (1); as shown in Table X, which summarizes published results on the measurement of the PZC's of ferric oxide, both synthetic and natural hematite. Several attempts have been made to delineate factors that might be responsible for observed variations in the PZC's: Parks (36) has considered the effect of impurities; Healy, Herring and Fuerstenau (37) have considered crystal structure; Lyklema has examined the role of micropores (38); O'Connor, Johansen and Buchanan (39) have looked at surface dehydration, Pravidic and Sotman (40) have considered the effect of stoichiometry; Kulkarni and Somasundaran (41) have considered the effect of mineralogical heterogeneities and storing or aging of minerals; Smolik, Harmon and Fuerstenau (42)

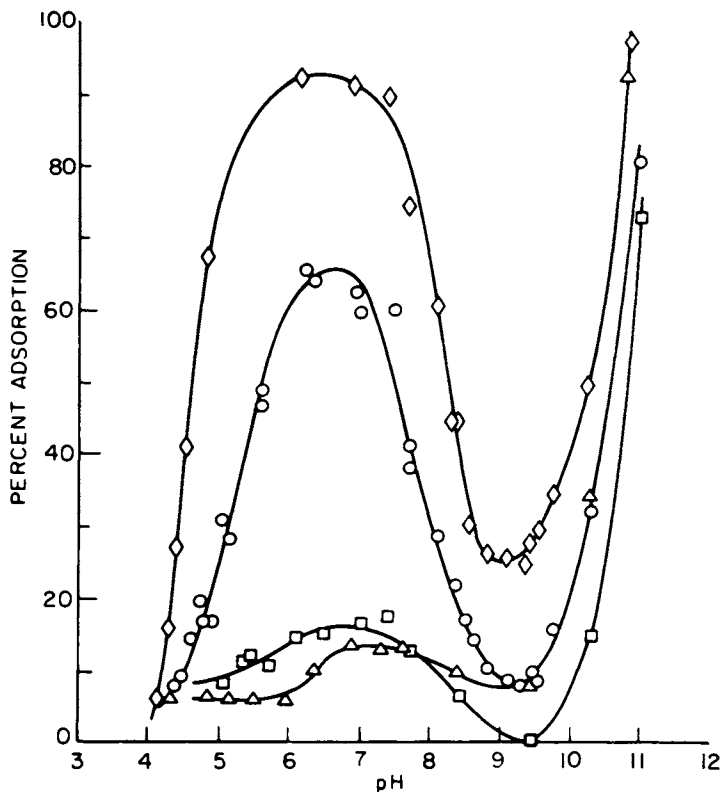


Figure 10. Percent adsorption of copper ions as a function of pH in solutions containing  $10^{-3}$  M  $\text{Cu}^{2+}$  and  $5 \times 10^{-1}$  M total ammonia, on: titania ( $\diamond$ ), hematite ( $\circ$ ), alumina ( $\square$ ), and quartz ( $\triangle$ ). (Reproduced, with permission, from Ref. 22. Copyright 1981, Academic Press.)

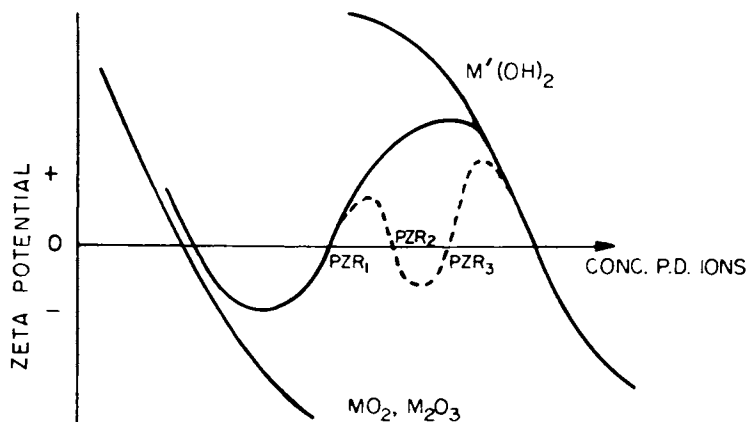


Figure 11. Generalized electrophoretic curves for the adsorption of hydrolyzable metal ions on oxides in ammonia and ammonia-free solutions (23, 24). PZR are various  $\zeta$  potential reversals.

Table X: Points-of-Zero-Charge of Natural and Synthetic Hematite.

Materials	PZC	Method	Reference
Synth. hematite	pH 9.0	Titration	Atkinson et al.(25)
Synth. hematite	pH 9.0	Titration	Peck et al.(26)
Synth. hematite	pH 8.5	Electrophoresis	Han et al.(27)
Synth. hematite	pH 8.4	Titration	Parks et al.(28)
Synth. hematite	pH 8.3	Electrophoresis	Troelstra et al.(29)
Synth. hematite	pH 8.2	Electrophoresis	Yap et al.(30)
Synth. hematite	pH 8.1	Electrophoresis	Raghavan et al.(31)
Hematite (Quebec)	pH 5.4	Titration	Ahmed et al.(32)
Hematite (Brazil)	pH 5.4	Stream. pot.	Joy et al.(33)
Hematite (Brazil)	pH 5.7	Titration	Joy et al.(33)
Hematite (Minn.)	pH 6.7	Electrophoresis	Iwasaki et al.(34)
Hematite	pH 6.7	Electrophoresis	Johansen et al.(35)
Hematite, specular	pH 7.7	Titration	Peck et al. (26)
Hematite, red	pH 8.6	Titration	Peck et al. (26)

have studied the effect of chemical pretreatment. Smolik et al. (42) clearly showed that surface composition and the change in surface composition by selective leaching can affect the observed surface properties. By carrying out streaming potential experiments with a bed of andalusite ( $Al_2O_3 \cdot SiO_2$ ) particles they were able to systematically study the effect of dissolution with the same particles. By cycling between acidic and basic conditions that systematically change the Si/Al ratio in the surface, they observed a shift in PZC as shown in Figure 12. These investigations clearly suggest that careful control of procedures for the preparation of samples for surface characterization studies is needed. It also indicates the necessity for careful characterization of minerals for research in mineral processing.

### Summary

Amongst the various interfaces present in different mineral processing unit operations, solid/liquid interfaces play a dominant role. Selected examples of a fundamental and applied nature have been given to illustrate the various surface characterization techniques that have been utilized by researchers in the field of mineral processing. Because of the complex nature of the interfacial region between the solid and liquid and the lack of many *in-situ* techniques, information about the molecular nature of interfacial processes is obtained through indirect measurements. The results of such measurements are often interpreted through use of models with various underlying assumptions. It has been necessary, because of the limitation of each of the techniques with regard to the information that they can provide, to use a combination of several techniques to acquire a detailed molecular-scale picture of interfacial physico-chemical phenomena in

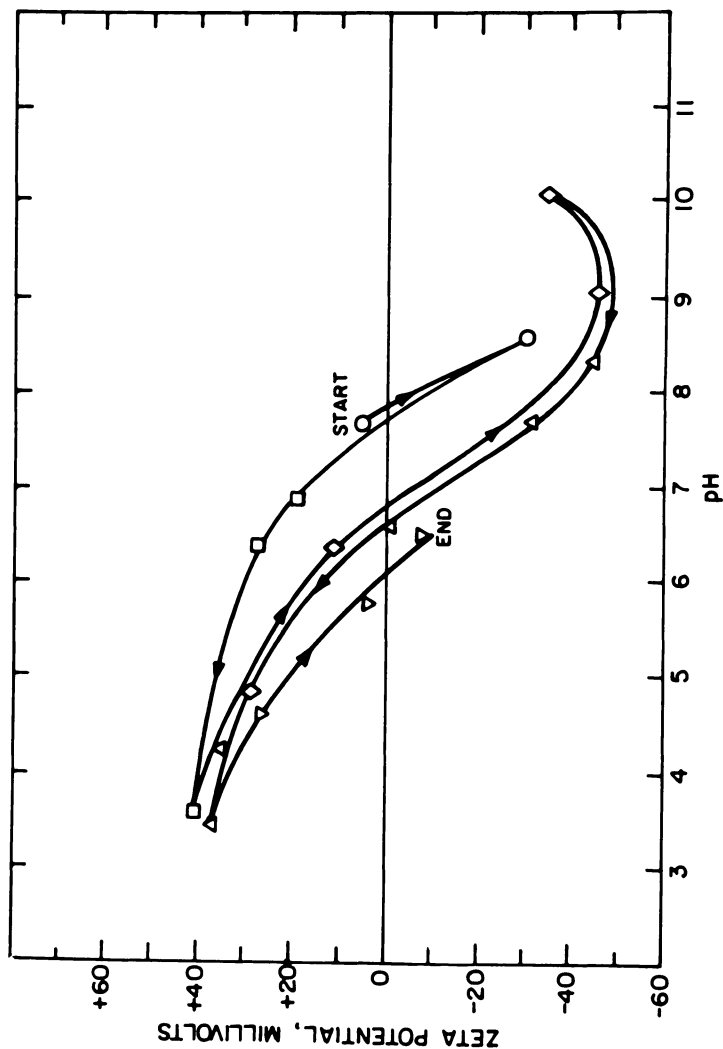


Figure 12. Shift in point-of-zero charge of andalusite through acid-base cycling in a streaming potential apparatus. Key:  $\circ$ , cycle 1;  $\square$ , cycle 2;  $\triangle$ , cycle 3;  $\Delta$ , cycle 4; and  $\nabla$ , cycle 5. (Reproduced, with permission, from Ref. 42. Copyright 1966, AIME.)



mineral/water systems. The need to develop *in-situ* measurement techniques for surface characterization has been emphasized. Raman spectroscopy does show promise for study of solid/liquid interfaces. It has been employed with some success in allied areas but has not been utilized by scientists working in the area of mineral processing.

### Acknowledgements

In preparing this review, the authors wish to acknowledge the financial support of the National Science Foundation and the Office of Surface Mining, U.S. Department of the Interior for a grant to the California Institute of Mining and Mineral Resources, University of California, Berkeley. Discussions with Professor T.W. Healy are acknowledged.

### Literature Cited

1. Fuerstenau, D. W., Pure and Applied Chemistry, 1970, 24, 135.
2. Sutherland, K. L.; Wark, I. W., Principles of Flotation, Australian Inst. of Mining and Metallurgy, Melbourne, 1955.
3. Gaudin, A. M., Flotation, McGraw Hill, New York, 1957.
4. Aplan, F. F.; Fuerstenau, D. W., Chapter 7, in Froth Flotation -- 50th Anniv. Vol., D. W. Fuerstenau, Ed., AIME, New York (1961).
5. Rosenbaum, J. M.; Fuerstenau D. W., unpublished results.
6. Chander, S.; Fuerstenau, D. W., Trans. AIME, 1972, 252, 62.
7. Chander, S.; Fuerstenau, D. W., International Journal of Mineral Processing, 1975, 2, 333.
8. Woods, R., J. Phys. Chem., 1971, 75(3), 354.
9. Chander S.; Fuerstenau, D. W., Trans. AIME, 1975, 258, 284.
10. Richardson, P. E.; Edelstein, D. L., "The Physical Chemistry of Mineral-Reagent-Interactions in Sulfide Flotation," USBM Information Circular 8819, 1978, p. 72.
11. Ignasiak, B. S.; Ignasiak, T. M.; Berkowitz, N., Reviews in Analytical Chemistry, 1975, 2(3), 278.
12. Boehm, H. P., Adv. Cat., 1966, 16, 179.
13. Bouwman, R.; Freriks, Ivo L.C., Fuel, 1980, 59, 315.
14. Paul, R. L.; Hendra, P. J., Minerals Sci. Engg., 1976, 8, 171.
15. Takenaka, T., Adv. Colloid and Interface Sci., 1979, 11, 291.
16. Hendra, P. J.; Turner, I. D. M.; Loader, E. J.; Stacey, M., J. Phys. Chem., 1974, 78, 300.
17. Predali, J. J.; Brion, D.; Hayer, J.; Pelletier, B., "Proc. XIII International Mineral Processing Congress," Elsevier, 1981, 136.
18. Clifford, R. K.; Purdy, K. L.; Miller, J. D., AIChE Symposium, 1975, 71, (150), 138.
19. Sharma, V.N.; Chander, S., Hydrometallurgy, 1981, 7, 315.
20. Anila, V.; Singru, R. M.; Sharma, V. N.; Chander, S., Hydrometallurgy, 1981, 7, 329.

21. "Comminution and Energy Consumption," Publication NMAB-364, National Academy Press, Washington, D.C., 1981, 206.
22. Osseo-Asare, K.; Fuerstenau, D.W., International Journal of Mineral Processing, 1980, 7, 117.
23. James, R.O.; Healy, T.W., J. Colloid Interface Sci., 1972, 40, 42.
24. Osseo-Asare, K.; Fuerstenau, D. W., International J. of Mineral Processing, 1980, 7, 219.
25. Atkinson, R.J.; Posner, A.M.; Quirk, J.P.; J. Phys. Chem., 1967, 71, 550.
26. Peck, A. S.; Raby, L.H.; Wadsworth, M.E., Trans. AIME, 1966 235, 301.
27. Han, K.N.; Healy, T.W.; Fuerstenau, D.W., J. Colloid Interface Sci., 1973, 44, 407.
28. Parks, G.A.; deBruyn, P.L., J. Phys. Chem., 1962, 66, 967.
29. Troelstra, S.A.; Kruyt, H.R., Kolloidzshr., 1942, 101, 182.
30. Yap, S.N.; Mishra, R.K.; Raghavan, S.; Fuerstenau, D.W., Adsorption from Aqueous Solutions, (Ed. P.H. Tewari), Plenum, 1981, 119.
31. Raghavan, S; Fuerstenau, D.W., J. Colloid Interface Sci., 1975, 50, 319.
32. Ahmed, S.M.; Maksimov, D., Canadian J. Chem., 1968, 46, 3841.
33. Joy, A.S.; Watson, D.; Cropton, R.W.G., Trans. AIME, 1964, 229, 5.
34. Iwasaki, I.; Cooke, S.R.B.; Choi, H.S., Trans. AIME, 1960, 217, 237.
35. Johansen, P.G.; Buchanan, A.S., Australian J. Chem., 1957, 10, 398.
36. Park, G. A.; Chem. Rev., 1965, 65, 177.
37. Healy, T. W.; Herring, A. P.; Fuerstenau, D. W.; J. Colloid Interface Sci., 1966, 21, 435.
38. Lyklema, J., J. Electroanal. Chem., 1968, 18, 341.
39. O'Connor, D. J.; Johansen, P. G.; Buchanan, A. S., Trans. Faraday Soc., 1956, 52, 229.
40. Pravdic, V.; Sotman, S.; Croat. Chem. Acta, 1963, 35, 247.
41. Kulkarni, R. D.; Somasundaran, P.; Powder Tech., 1976, 14, 279.
42. Smolik, T. J.; Harman; Fuerstenau, D. W., Trans. AIME, 1966, 235, 367.

RECEIVED May 3, 1982

## Particle Charge in Nonaqueous Dispersions

M. L. HAIR

Xerox Research Centre of Canada, Mississauga, Canada L5L 1J9

D. LANDHEER

Delphax Systems, Mississauga, Canada L5L 1J9

Recent advances made in measuring particle charge and mobility in nonaqueous suspensions are reviewed. Microelectrophoretic techniques have been used to determine zeta potential and the measurements related to particle stability. Recently, great strides have been made in developing electrical and optical transient methods for measuring particle charge and mobility in these nonaqueous dispersions. It has been possible to obtain particle charge/mass ratios as well as the field dependence of particle mobility.

One of the most important parameters in pigment dispersion technology is the charge which exists on the surface of the particles. This charge contributes to particle-particle stability (i.e., shelf life, film formation) and, particularly in insulating fluids, the movement of the particles in an applied electric field (i.e., electrophoresis) can be used to develop latent electrostatic images. Technological applications are thus found in paint technology, lubrication, and electro-photography.

Nearly all surfaces in contact with a fluid have a surface charge  $q$  and thus a potential  $\psi$  which falls off as we move away from the surface. The surface charge may be caused either by ionization of the surface groups, by adsorption of ions on to the surface or by direct charge exchange with the fluid. In order to maintain electrical neutrality, this surface charge must be balanced by an equal number of counter ions in the surrounding fluid and thus we are left with a picture of the electrical double layer as shown in Figure 1. In this representation the initial surface potential  $\psi$  is reversed due to strong absorption in the so-called Stern layer and then slowly drops to zero. When an electric field  $E$  is applied to the particle, the particle migrates relative to the fluid and the potential at the slippage plane can be measured. This is known

0097-6156/82/0199-0313\$06.00/0

© 1982 American Chemical Society

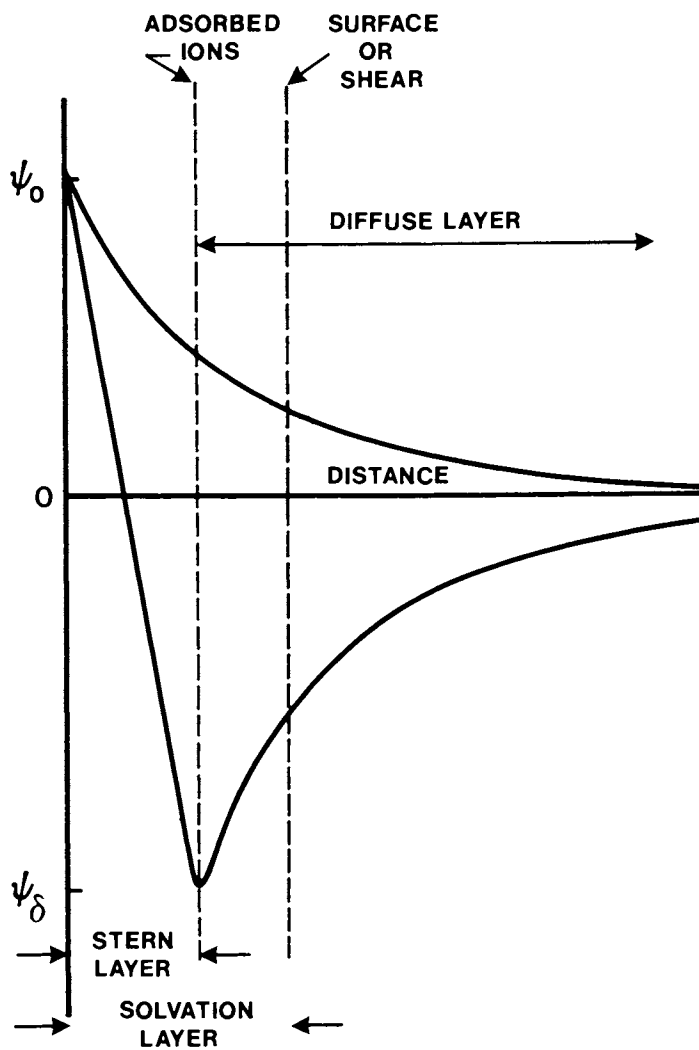


Figure 1. The electrical double layer.

as the zeta potential. Three general equations describing the migration velocity  $v$  or the mobility  $u$  have been derived.

$$qE = 6\pi\eta va \quad \text{or} \quad u = \frac{\epsilon \zeta}{6\pi\eta} \quad (1)$$

$$u = \frac{\epsilon \zeta}{4\pi\eta} \quad (2)$$

$$u = \frac{\epsilon \zeta f(\kappa a)}{6\pi\eta} \quad (3)$$

The first equation simply considers the effect of an applied field  $E$  on a point charge  $q$  balanced by the Stokes viscous drag and applies when  $\kappa a \ll 1$ .  $\eta$  is the viscosity of the fluid,  $v$  the particle velocity and  $a$  the particle diameter. The second equation, due to Smoluchowski is restricted in its applicability to cases where the radius of the particle is much greater than the thickness of the double layer (i.e.,  $\kappa a \gg 1$ ). The third incorporates cases 1 and 2 in an approach due to Henry(1). The reciprocal thickness of the double layer is given by

$$\kappa = \left[ \frac{8\pi e^2 N_A I}{1000 \epsilon kT} \right]^{1/2}$$

where  $I$  is the ionic strength of the electrolyte,  $N_A$  is Avogadro's number,  $k$  is the Boltzmann constant and  $e$  is the charge of an electron. Units are defined in the Legend of Symbols.

### Measurement of Zeta Potential

The measurement of zeta potential in aqueous systems by microelectrophoretic techniques is well established and there are many pieces of equipment commercially available. In principle, the method is very simple. The suspension under investigation is placed in a cell and a known electric field is applied. The particles undergo migration in the field and their velocity is measured directly using an optical microscope and a timing device. Either cylindrical or rectangular cells may be used. The rectangular cells are easier to use and usually consist of optical flats (40x25x0.5 mm) which are separated by 0.5 mm spacer to give a width/depth ratio  $\sim 50$ . Clearly only low fields can be applied to such a cell. In insulating fluids the applied fields are non-uniform, surface conduction along the cell walls becomes a problem and the information abstracted is of limited value. Also insulating fluids can sustain large local potential drops at the electrodes in contradistinction to the case in water where electrochemical reactions limited the voltage drop at the electrodes to a few volts. For further details, the

interested reader is referred to the many articles in the colloid literature(2).

### Surface Potential and Particle Stability

Despite its limitations, the simple microelectrophoresis cell has been used successfully by several workers to study the behavior of particles in low conductivity fluids. A series of experiments demonstrating the role of the zeta potential in determining particle-particle stability in xylene and hydrocarbon suspensions were described by Parfitt and his co-workers(3, 4, 5) in the 1960's. The purpose behind the measurements was to explore the extension of DLVO theory (as developed for aqueous systems) into the nonaqueous fluids. It is well accepted that stability against flocculation arises when the attractive van der Waal's force between two particles is overpowered by the electrostatic repulsion which arises when the particles become sufficiently close that the electrical double layers surrounding the particles become intermixed.

The potential at some distance  $x$  away from a flat surface is given by equation

$$\frac{d^2\psi}{dx^2} = \frac{8\pi\eta ze}{\epsilon} \sinh\left(\frac{ze\psi}{\kappa T}\right) \quad (4)$$

For interacting double layers and spherical particles the repulsive potential  $V(r)$  at a distance  $r$  from the particle centre can be approximated as,

$$V(r) \approx \frac{\epsilon a^2 \psi_0^2}{r} \exp(-\kappa r) \quad (5)$$

In insulating fluids, the ionic concentration is extremely small ( $\sim 10^{-10}M$ ) and thus the thickness of the double layer ( $1/\kappa$ ) can be about of 10  $\mu m$ . Under these conditions, equation 5 simplifies to

$$V(r) \approx \frac{\epsilon a^2 \psi_0^2}{r} \quad (6)$$

and thus the repulsive force is directly proportional to the product of the surface potentials. Moreover, because the double layer is so large, it seems reasonable to assume that the measured zeta potential closely approximates the surface potential. Thus, the stability of a particulate system in an insulating fluid should be directly related to the square of the measured zeta potential. By measuring both stability ratios and zeta potentials for a series of particulate suspensions, Parfitt

and his co-workers were able to demonstrate that the general qualitative trend between zeta potential and stability was in agreement with the predictions of the theory.

One aspect of their experimental observations, however, was of great importance: The authors clearly recognized the role that small quantities of water could play in altering the charge on a surface. Special care was taken in their experiments to alter and control the amount of water in their system. In fact, by altering the amount of water on the surface of their particles those workers were able to prepare both positive and negative particles using the same basic chemical system. Clearly, given this type of experimental result, it is imperative that surface water must be controlled for charge measurements in low conductivity fluids to be meaningful.

#### Transient Measurements

Most of the practical applications of electrophoresis in insulating fluids employ fields as high as  $10^6$  V/m. Traditional microelectrophoresis experiments are limited to approximately 100 V/cm and a question arises as to the effect of these high fields on the charge on the particles under investigation. In order to measure electrophoretic mobility under high field conditions recent workers have resorted to transient measurements using either photographic or light scattering techniques to detect particle motion. Early work in this area (6, 7) was plagued by instabilities and the first genuinely successful measurement was by Stotz (8) in 1978. In this method Stotz allowed well-controlled, charged particles to sediment between plain vertical electrodes spaced 1 mm apart. The particles undergo normal gravitational sedimentation but can be deflected horizontally by short field pulses of alternating polarity. The particle tracks are then photographed. Using this method, electric fields up to  $10^5$  V/m were applied and the particle mobilities determined. The mobility  $u$  is related to the electrophoretic displacement  $S$  by equation 7.  $t$  is the pulse duration and  $E$  the applied electric field. The radius of the particles may be obtained by observing the sedimentation velocity,  $V_{\text{sed}}$ . For full practical details the reader is referred to the original publication.

$$u = S / tE \quad (7)$$

$$r_p = \left[ 9\eta V_{\text{sed}} / 2g(\gamma_p - \gamma) \right]^{1/2} \quad (8)$$

Most technological suspensions consist of very polydisperse particles. In order to simplify his experimental system Stotz employed monodispersed latex suspensions (particle diameter = 6 or  $30\mu$ ). In an interesting comparative experiment, he also measured the particle mobilities using the simple

microelectrophoresis equipment of the type described above. Good agreement was observed under low field condition (i.e.,  $E < 10^4$  V/m). However, at high fields ( $E \sim 10^6$  V/m) the particle mobilities had increased by an order of magnitude. This effect of field on particle charge is confirmed by subsequent workers and will be discussed in Section 5.

### Electrical and Optical Transients

The use of an optical transient measurement to determine particle mobility under varying field conditions was described by Novotny (9) in 1979. This method is based on the observation of the time dependent changes in the intensity of light scattered from the particles during electrophoretic motion and is applicable to any system in which there is sufficient contrast between the liquids and the particles. The basis for the experiment is shown in Figure 2. In principle the measurement is very simple. A thin, capacitor-like cell is prepared by separating two transparent electrodes using a Teflon gasket. A dilute suspension of the particles under study is placed in the capacitor. Monochromatic light is directed onto the cell and the scattered light detected by a photomultiplier. Two modes of operation can be employed. In the first mode ("sweepout experiment"), the particles are initially distributed uniformly throughout the cell. When the electric field is applied, the particles are swept to the detector electrode and the intensity change is observed as a function of time (Figure 2a). Provided that monochromatic light is used, the scattering function can be easily analyzed and the particle mobilities thus determined. In the second form of the experiment ("transit method") all the particles are initially driven to the top electrode. In this mode the scattering function is shown in Figure 2b. Again, provided that the incident radiation is monochromatic, the physics may be defined and the particle mobilities may be calculated. Mobilities were determined using fields of  $10^2 - 2.5 \times 10^3$  V/m and are reproduced in Figure 3. It is clear that the mobilities increase dramatically as the field increases thus confirming Stotz' data and encouraging good agreement is obtained between the sweep-out and transit experiments.

A later paper by Novotny (10) describes the use of a similar cell in which sufficient additional electronics were added so that the electrical transient accompanying the particle motion could be measured in combination with the optical transient. The experimental system is shown diagrammatically in Figure 4. This experiment is carried out in the sweepout mode. A voltage is applied and the particles are driven to one electrode. A short time at rest allows the excess ions to redistribute throughout the cell, at which time a second pulse of the same polarity and magnitude as the first is applied. In this second transient the particles do not move and thus are not contributing to the current



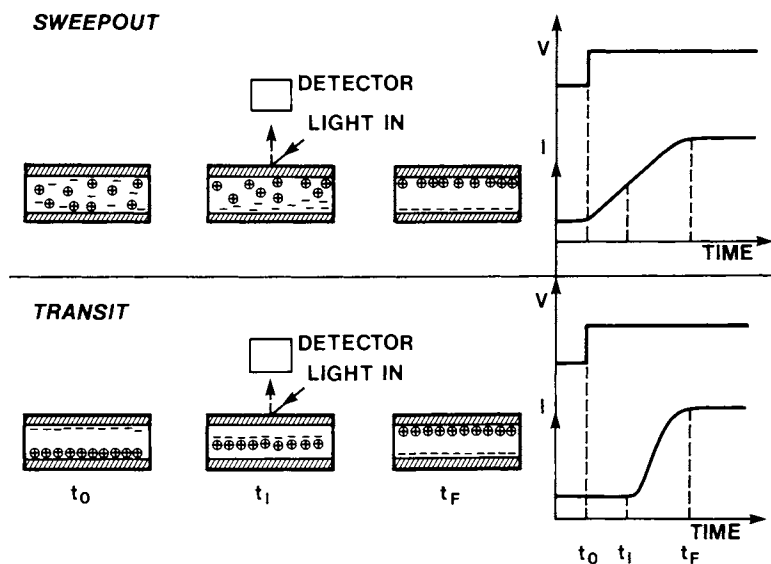


Figure 2. Sweepout and transit light scattering measurements (9).

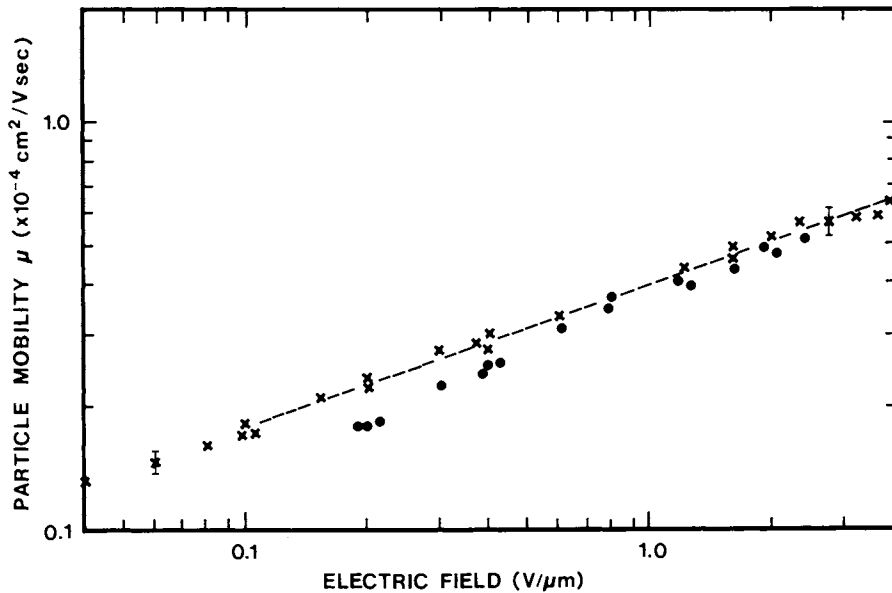


Figure 3. Field dependence of mobility (9). Key:  $\times$ , sweepout expansion; and  $\bullet$ , transit expansion.

i.e., only the current associated with excess ion sweep-out is detected. The difference between these two sweep-out measurements should represent the charge associated with the movement of the particles. In many cases this simple picture is not true and this is easily seen in the results reproduced in Figure 5. In this experiment the optical and electrical transients were recorded simultaneously for a dispersion containing relatively high particle concentration. The current-time curve reveals that in the initial movement, two species transit the cell at different times. Clearly both cannot be due to the movement of the particles across the cell; the simultaneous optical measurement demonstrates that the motion of the charged particles is contributing only to the second maximum. The first peak is due to excess ions in the suspension, presumably the charge control agent which is put in specifically to assure proper charging of the suspended particles.

#### Field Dependence on Mobility

Although it is convenient in elementary texts to consider electrophoresis in terms of only the driving Coulomb force and the Stokes frictional resistance (equation 1) it has long been recognized that two additional forces can play an important role. These are the electrophoretic retardation and the relaxation effect. Both of these have their origin in the electric double layer. The retardation effect is caused by a local movement of liquid induced by the charge of the diffuse double layer. This has been calculated by Stotz who shows that for the extended electrical double layer which would be anticipated in highly resistive fluids the main influence of liquid flow occurs within a distance of  $2a$  from the particle surface and may be disregarded.

The effect of field variations on measured mobility are considerable and discussion of this in terms of double layer relaxations provides the major thrust of Stotz' paper. When the field is applied to a particle and its double layer, the particle moves in one direction relative to the double layer and there is, therefore, an induced asymmetry. The relaxation time required to restore the original symmetry can be defined as

$$\tau_r = \frac{\epsilon}{4\pi\sigma} \quad (9)$$

where  $\sigma$  is the conductivity of the suspension. Clearly, as the field is increased and higher particle velocities are achieved this displacement of the double layer becomes aggravated to a point at which a complete separation occurs. At this point a critical velocity can be defined,

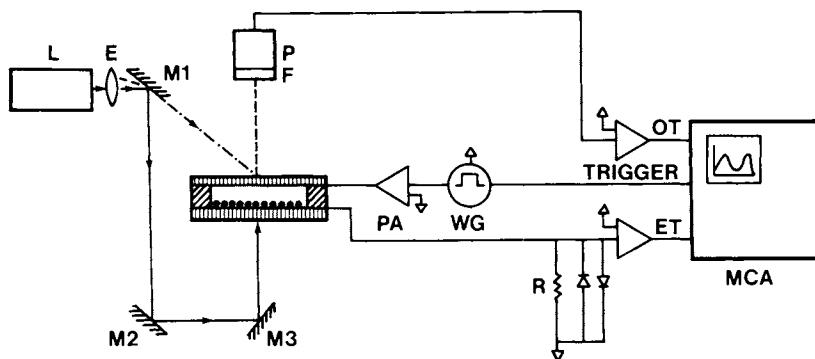


Figure 4. Experimental setup for determination of particle mobility using both optical and electrical transients (10).

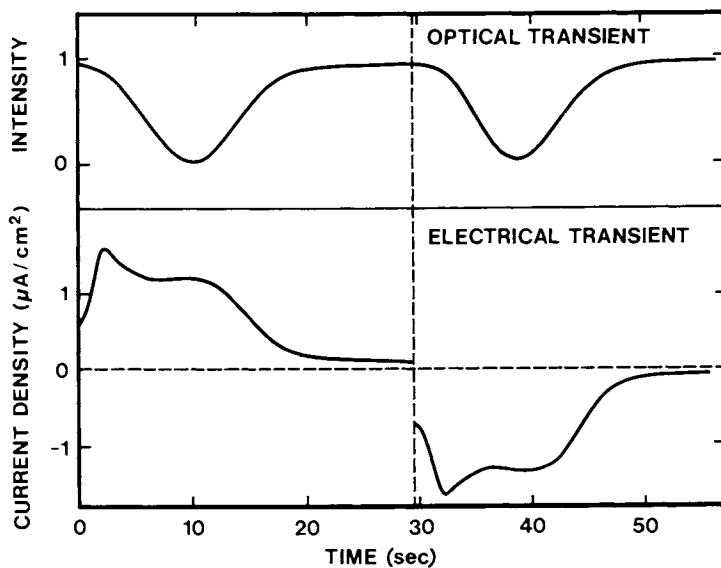


Figure 5. Simultaneous recording of both optical and electrical transients with high particle concentration (10).

$$V_c = 1/\kappa\tau_r \quad (10)$$

Estimated values of this critical velocity are surprisingly low (about 31m per second) and can easily be exceeded in practical systems. Thus, a picture of the physical system emerges: At low fields the particles are surrounded by their double layer and migrate with a mobility controlled by the zeta potential. The mobility is thus essentially independent of the applied field. However, as the field is increased the double layer is gradually ripped away from the particle and the mobility increases. A point is eventually reached at which the double layer is effectively removed from the particle which then migrates in accord with equation 1. At this point the mobility is once again independent of field strength. This general trend is evident in the results shown in Figure 3. The levelling out at both high and low fields is apparent in Stotz's data and, in this respect, the coincidence of the microelectrophoretic results with the transient results at low field strength is very gratifying.

#### Determination of Q/M

Although the optical and transient methods described above give the most fundamental data regarding the charge and mobility of the particles in insulating fluids there is, from a practical point of view, the need for a relatively simple measurement of particle charge which can be used in screening experiments. Charge/mass (Q/M) measurements of particles suspended in nonaqueous fluids have been previously described (11, 12). Essentially, the methods involve application of a constant voltage across the charged colloidal dispersion, measurement of the charge collected on the electrode of opposite polarity, and then determination of the mass deposited on the electrode. A recent version of this measurement has been published by Novotny and Hair (13). The experimental device and results are shown in Figure 6. The charged colloidal suspension under study is placed in a well defined planar capacitor cell having at least one transparent electrode. The cell diameter is much greater than its thickness (~1 cm), thus simplifying the interpretation. Because the cell is relatively thick, the plate-out of particles is a relatively slow process. This is an advantage in that conventional electronics can be employed and expensive equipment is avoided. In making the measurement, a constant voltage is applied to the cell and the current is recorded. The plate-out of the particles can be observed either visually or using optical detection and thus a transit time is also recorded. After transport of the particles is complete the cell is opened and the particle mass is determined by weight change. (If this is not convenient, the mass collected can also be determined from the

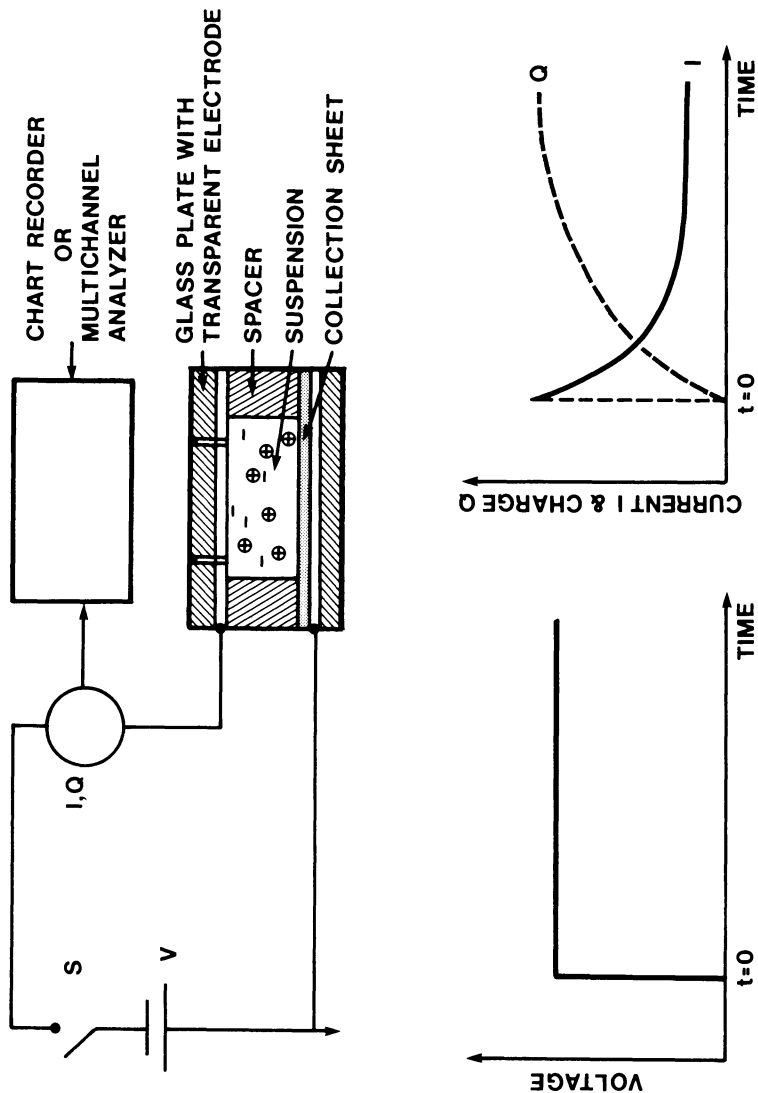


Figure 6. Apparatus for determination of  $Q/M$  (13).

optical measurements provided a mass-optical density calibration has been previously established.)

After the constant voltage is applied the observed current is recorded as a function of time (Figure 6). If the dispersion contains only charged particles and counter ions then the charge  $Q$  measured at the time of observation of total plate-out represents the total charge on the particles. However, as can be seen from Figure 5 and the discussion in Section 4, there is a considerable contribution due to excess ions in the system. This contribution, or excess charge, must be subtracted from the measured  $Q$ .

The excess charge can be estimated by continuing to monitor the current after plate-out is completed. If it is assumed that the charge transported in a time equal to the plate-out time is representative of the excess charge initially present in the system, then this may be simply subtracted from the measured  $Q$ . Alternatively, the particles may be centrifuged and the sweep-out experiment repeated with the supernatant fluid. A third method of estimating the excess charge is to carry out the plate-out experiment and then allow the system a short time at short circuit. The excess ions will redistribute in the cell (the particles adhering to the electrodes). On application of the original voltage, it can be assumed that the charge now collected  $Q_E$  is representative of the contribution of the excess ions:  $Q_E = Q_T - Q$ .

This method has the advantage of simplicity. It is very difficult to provide a complete description of the charge transient because it involves the transport of at least two charged species of opposite polarity. Moreover, many of the measurements are done under conditions where space charge limitations apply, thus further complicating any detailed interpretations. (Note, however, that recent computer calculations have been moderately successful in explaining the shape of the transient which is observed under space charge limited conditions (14, 15)). However, provided the interpretation is restricted to the determination of total particle charge, the analysis is simple and can be based on electrostatic arguments only. Thus, although the mobility of the particle may vary with field due to changes in the effective zeta potential, this  $Q/M$  measurement determines only the total charge transported.  $Q/M$  is constant and is thus independent of the field.

The purpose of this paper has been to present a short overview of the recent advances that have been made in determining particle charge and mobility in nonaqueous suspensions. Clearly the nature of the charge on the particles plays a major role in determining the strength of the adhesion of these particles to an electrode and the electrical transient methods described here may be used to determine the force of that adhesion. In this respect the reader is referred to three recent papers by Vincett (15, 16, 17). This work was oriented towards

an electrophotographic imaging process in which the particles were charged electrostatically by contact with metal electrodes rather than the chemical charging usually encountered in technological application. However, the work again confirms the effect of field on particle mobility and provides a useful discussion of mobility under space charge limited conditions.

#### LEGEND OF SYMBOLS

All equations are in Gaussian units where charge is measured in esu, potential in statvolts and distance in centimetres.

<u>SYMBOL</u>	<u>NAME</u>	<u>UNITS</u>
$\epsilon$	dielectric constant	80.4 for water at STP
$E$	electric field	statvolt / cm
$\sigma$	conductivity	esu /cm <sup>2</sup> -sec
$\eta$	viscosity	gm/ cm-sec = poise
$u$	mobility	cm <sup>2</sup> /statvolt -sec

#### Literature Cited

- Henry, D.C. Proc. Roy. Soc. Ser. A 1931, 133, 106.
- James, A.M. "Surface and Colloid Science" (Eds. R.J. Good, R.R. Shomberg) Plenum Press, 121, Vol. 11, 1979.
- McGown, D.N.L.; Parfitt, G.D.; Willis, E.J. Colloid Sci. 1965, 20, 650.
- Lewis, K.E.; Parfitt, G.D. Trans. Faraday Soc. 1966, 62, 652.
- McGown, D.N.L.; Parfitt, G.D. Discuss. Faraday Soc. 1966, 42, 225.
- Kuo, S.; Osterle, F.J. Colloid Interface Sci. 1967, 25, 421.
- Harris, L.B. Rev. Sci. Instrum. 1969, 40, 905.
- Stotz, S. Colloid and Interface Science 1978, 65, 118.
- Novotny, V.J. Appl. Phys. 1979, 50, 324.
- Novotny, V.J. Appl. Phys. 1979, 50, 2787.
- Dahlquist, J.A.; Brodie, I. J. Appl. Phys. 1969, 40, 3020.
- Mohn, E. Phot. Sci. Eng. 1971, 15, 451.
- Novotny, V.; Hair, M.L. J. Colloid and Interface Science, 1979, 71, 273.
- Roselman, I.C.; Tait, W. Third International Conference on Electrophotography 1977.
- Vincett, P.S. J. Colloid and Interface Science 1979, 69, 354.
- Vincett, P.S. J. Colloid and Interface Science 1980, 76, 95.
- Vincett, P.S. J. Colloid and Interface Science 1980, 76, 83.

RECEIVED April 5, 1982

# Surface Analysis and Solar Energy Materials

A. W. CZANDERNA

Solar Energy Research Institute, Materials Branch, Golden, CO 80401

This paper is a summary of various methods that are important for studying the stability of interfaces in solar energy materials and for studying the interfaces themselves. An overview is given that explains why interfaces are crucially important for developing long-life, cost-effective, multilayer, polycrystalline, thin-film stacks for solar energy conversion systems (SECS). Second, broad categories of characterization methods, approaches, and processes in interface science are reviewed and related to studies required for components in SECS, in which the importance of compositional analysis of interfaces is emphasized. Surface characterization methods include surface area, real and clean surfaces, structure and topography, interface composition or purity, surface thermodynamics, diffusion, amount adsorbed, and nature of adsorbate/solid interactions. Third, an overview is given of the solar-related research needs and opportunities in various topical areas in interface science. These topics include thin films; grain, phase, and interface boundaries; oxidation and corrosion; adhesion; chemisorption, catalysis, and surface processes; abrasion and erosion; photon-assisted surface reactions and photoelectrochemistry; and interface characterization methods. A brief review is given concerning the current status of interfacial characterization. The paper mentions typical interface problems currently being encountered with reflectors, polymers, absorbers, and photovoltaic cells, and it briefly discusses the ways that interface methods can or are being applied to solar materials research.

The purpose of this paper is to provide a broad overview of why interfacial stability is crucially important in materials used for the direct conversion of solar radiation to useful end-products in man-made collection/conversion systems. The importance of interfacial stability and studies of interfacial phenomena has been addressed in considerable detail in previous review articles (1-3) and in the proceedings of a workshop (4).

0097-6156/82/0199-0327\$06.00/0  
© 1982 American Chemical Society



Hence, the focus of this summary will primarily be to highlight why solar energy conversion systems (SECS) require long-life, high-performance, inexpensive components with extensive interfaces. Then, a brief discussion will be given about the broad categories of interfacial characterization techniques that are expected to be important for studying interfaces in SECS components. After the interfacial topics of importance for solar materials research are mentioned, some specific problems of interest will be indicated, especially those involving surface analysis for elemental composition at an interface.

### Solar Radiation and Man-Made Collection Devices

The conversion of solar energy into heat, fuels, or electricity is accomplished by a wide range of technologies. The sunlight first interacts with the biosphere producing winds, ocean currents, thermal gradients, salinity gradients, moving water, and plants, which can be harnessed by turbines, low-temperature heat engines, or biomass processing systems. These are generally considered indirect conversion processes in which solar photons result in biological processes or in an indirect use in a thermal conversion system. Alternatively, the solar radiation is constrained to interact with systems designed and constructed to convert solar energy directly into electricity, heat, fuels, chemicals, or mechanical work.

Fuels and chemicals from solar energy may be obtained from the processing of biomass residues or energy plantation products, from the synthesis of materials using solar thermal or solar electric energy, and from direct conversion using photochemical or photobiological systems. The systems to convert sunlight to electricity (or mechanical work) include photovoltaic, photoelectrochemical, solar thermal, wind energy, and ocean thermal gradient systems. Solar energy conversion systems that can provide heat directly include passive buildings, solar ponds, flat-plate collectors, evacuated tube collectors, nonimaging low concentration ratio collectors, single-axis tracking concentrators (Fresnel, parabolic, and hemispherical) and two-axis tracking concentrators (parabolic dishes, spherical dishes, and central receivers) (5). Many of the technological concepts are illustrated in Fig. 2 of Ref. 5 from which it can be inferred that the reflective, absorptive, and photovoltaic collection processes require large areas of exposure to the sun. In fact, all solar energy collection and/or conversion technologies are area-intensive because solar radiation at the earth's surface has a low energy density, typically  $10^7$  kcal/km<sup>2</sup>-min (3). At this value, today's national energy consumption (85 quads) would require intercepting about  $1.17 \times 10^5$  km<sup>2</sup> (45,000 square miles) of sunlight by using SECS operating at 10% efficiency for 500 min/day. Obviously, the area of SECS will increase if the collecting surface of the device is not always normal to the solar radiation and decrease if system conversion efficiencies can be increased, as is now the case in concentrating thermal systems. However, the interfacial area may be increased up to ten times by the design of collector components.

### Importance of Interfaces in SECS

The interfaces of importance in SECS are the solid/solid (S/S), solid/gas (S/G), and solid/ liquid (S/L) (4). The area-intensive nature of SECS components was established in the previous section. The major problem is collecting solar energy at a cost that is competitive with other energy forms. Thus, low initial cost is required for the materials, support structures, and production processes in the SECS of interest in Fig. 1 (6). This requires, for example, using thin films in mirrors, in photovoltaic systems, for antireflection coatings on windows, for passive collection, etc.; in addition, these films must be made from inexpensive, durable, and easily processed materials (5). Inexpensive long-life materials in flat-plate collectors and durable, stable absorber coatings are also necessary.

Solar systems are subjected to a unique set of conditions that may alter their stability and, hence, their performance and life-cycle costs. These conditions include UV radiation, temperature, atmospheric gases and pollutants, the diurnal and annual thermal cycles, and, in concentrating systems, a high-intensity solar flux. In addition, condensation and evaporation of water, rain, hail, dust, wind, thermal expansion mismatches, etc., may impose additional problems for the performance of a solar system. These conditions and problems must be considered not only individually, but also for synergistic degradative effects that may result from their collective action on any part of the system. Since these degradative effects may also reduce the system or component performance, protective encapsulation of sensitive materials from the hostile terrestrial environment is required to provide component durability.

The constraints imposed on design by initial cost, performance, and durability dictate using some form of polycrystalline, thin-film, multilayer stack for SECS employing reflectors, transmitters, thermal absorbers, and photovoltaic absorbers (PV cells) (5). Several generic multilayer stacks for solar applications are shown in Fig. 1. For transmitters, the design has fewer interfaces. Extensive illustrations of multilayer, thin-film stacks for specific solar thermal and PV collector systems are given in recent publications (1-10). The design illustrated by Fig. 1 emerges from considerations mentioned above. As can be deduced from Fig. 1, interface areas will range from two (simple transmitter) to several times (PV cell) the area of the solar flux being collected.

Now, consider stability. If a satisfactory initial system or component performance and cost are assumed, then in many cases the critical issue is to maintain the physical behavior of materials adjoining an interface for up to 30 years. The physical behavior may include properties that directly influence solar device performance, such as reflectance, transmittance, absorptance, emittance, and photovoltaic efficiency; or solar device performance may be indirectly affected by properties such as adhesion, permeability, photo-oxidative stability, or interdiffusion. The required stability of interfaces in SECS components is counter to basic physics and chemistry, because atoms at interfaces must be more reactive and thermodynamically less stable than when in the bulk of materials (2). Yet, the density of solar energy requires deploying systems with large interfacial

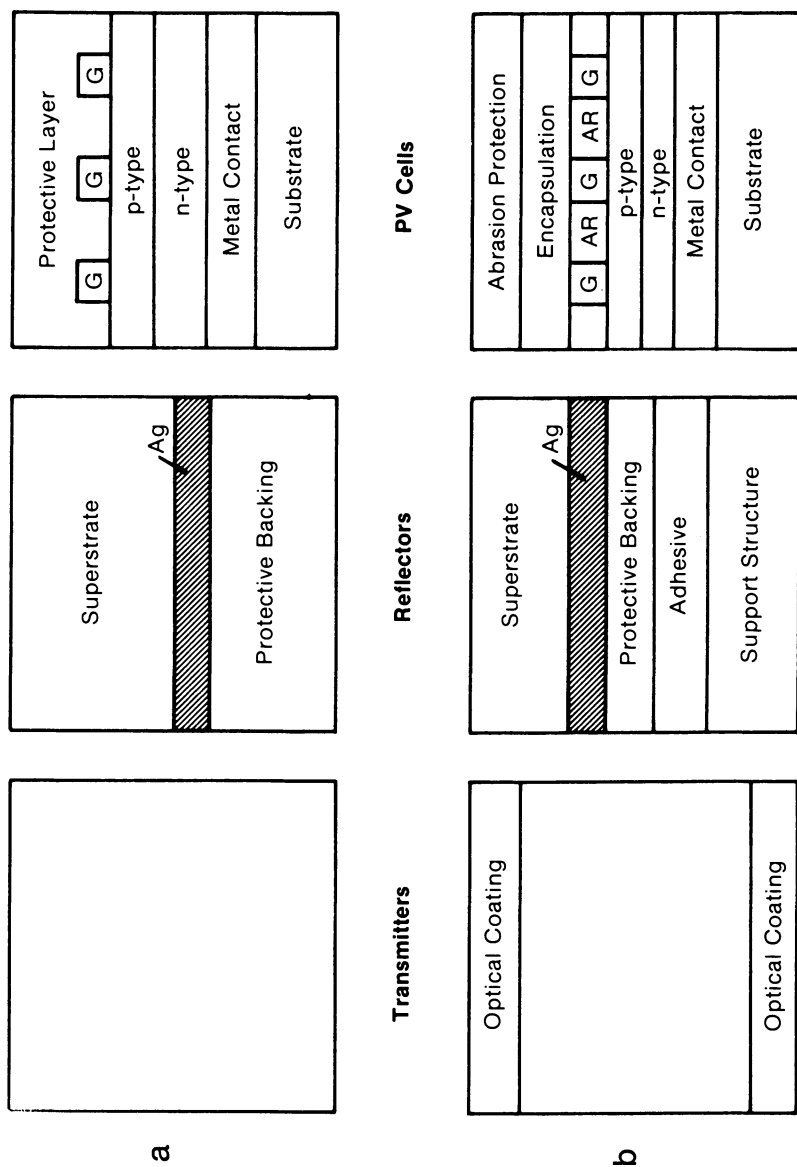


Figure 1. Simple (a) and more complex (b) stack designs for solar transmitters, reflectors, or thin film PV cells showing the multilayer, multiphase, and multicomponent contributions to S/S and S/G interfaces. G is a grid and AR an antireflection coating in the PV cells.

areas! Fortunately, kinetic limitations frequently retard the effects of a thermodynamic driving force. Therefore, systems with large areas of different kinds of polycrystalline materials can remain stable if they are chosen and fabricated correctly.

In Table 1, the consequences of requiring large areas for collection, the cost because of competition with currently available energy forms, materials specificity for performance, and durability (to reduce life-cycle costs) are summarized. These criteria dictate a multilayer stack collector design in which polycrystalline thin film(s) of the active material must be protected from a hostile terrestrial environment.

**Table 1. Cost, Performance, Durability, and Design Requirements in Multilayer Stacks for Collecting Solar Energy**

<u>Parameter/Issue(s)</u>	<u>Requirement(s)</u>
Area Intensive	~1 kW/m <sup>2</sup>
Polycrystalline Films/Coatings	Cost
Materials Specific	Performance
Multilayer Stacks	Design/Cost
Extensive Interfaces	Durability
Interfacial Stability	Durability/Cost
UV, Cyclic T, T, Atmospheric Conditions	Durability

There is little question that one of the most active research areas in materials science is studying interfaces. In the past, emphasis in materials science has been placed on relating the bulk properties to the structure and composition of the solid. Today, efforts are in progress that relate surface reactivity and stability to the crystallographic orientation and composition, primarily at the S/G interface. Since a fundamental understanding of interfacial behavior and degradation mechanisms at an atomistic level is necessary if short-time test data are to be extrapolated to 30-year lifetimes, careful studies at the S/S, S/G, and S/L interfaces are required (4).

### Interface Studies Applicable to Solar Materials

An overview of the most important phenomena in interface science related to studying solar materials is presented in this section. The methods for characterizing interfaces and those deemed likely to have the largest near-term impact on solving the problems of interface degradation are then mentioned.

The three phases of interest are the solid (S), liquid (L), and gas (G) phases, none of which is infinite. The boundary region between the S, L, and G phases has fundamentally different properties from the bulk. The S/S, S/G, and S/L surfaces, in that order, are of greatest interest to the solar materials scientist (4). Some of the broad topical areas of study at the interfaces of SECS are listed in Table 2. An understanding of these topics is enhanced by applying the methodologies of interface science.

**Table 2. Topical Study Areas at Different Interfaces Between the Solid (S) Liquid (L), and Gas (G) Phases**

Interface		Topical Area of Study
<u>Solid A</u> <u>Solid B</u>	S/S	Corrosion, grain boundary passivation, adhesion, delamination, epitaxial growth, nucleation and growth abrasion, wear, friction, diffusion, boundary structure thin films, solid state devices, mechanical stability, creep.
<u>Liquid</u> <u>Solid</u>	S/L	Wetting, spreading, lubrication, friction, surface tension, capillarity, electrochemistry, galvanic effects, corrosion, adsorption, nucleation and growth, ion electromigration, optical properties, cleaning techniques.
<u>Gas</u> <u>Solid</u>	S/G	Adsorption, catalysis, corrosion, oxidation, diffusion, surface states, thin films, condensation and nucleation, permeation, energy transfer.

The experimental effort for studying the S/S, S/L, and S/G interfaces is now very extensive; the theoretical treatments are difficult (11). A realistic view of the boundary at a solid surface is not the ideal plane of infinite dimensions, but of different crystal planes with composition, structure, orientation, and extent that are fixed by the pretreatment of the solid. As shown by Fig. 6 in Ref. 2, imperfections such as an isolated atom, a vacancy, a kink, or a ledge all coexist with a terrace as well as crevices and dislocations. During pretreatment of a solid, impurities may accumulate at or in the boundary in trace and larger quantities, and drastically alter the behavior of the boundary. Wide variations in the microscopic topography, which may be observed with SEM, may also adversely influence the stability of the surface. Following controlled use of the solid, reexamining the interface permits one to evaluate the influence of the use on the measured properties of the interface. Characterization of the interface before, after, and, if possible, during use of the material is clearly required.

As an overview of characterizing a solid interface, the following concerns are addressed: interfacial area and location; the composition of the interface; the form of the solid interface; the topography; the crystallographic structure of the interfacial region; the type of thermodynamic processes that may occur; the mechanism by which species migrate over or along the interface; the thickness of the interface phase; for solid surfaces, the amount and location of gas or liquid adsorbed; and the nature of the adsorbate-solid interaction. For studying all these phenomena, the history of addressing these concerns in gas adsorption on solid surfaces alone leads us to recognize that careful experimentation is the primary necessity in interface science.

The experimental methods deemed most appropriate for studying solar materials have been considered in some detail (1-4). Briefly, these include using polycrystalline materials and methods that permit direct examination.

Real surfaces, which can be obtained by ordinary laboratory procedures such as mechanical polishing or chemical etching, have been studied extensively because they are easily prepared, readily handled, and amenable to many types of measurements. Real surfaces generally consist of an oxide with a variable coverage of chemisorbed and physically adsorbed species. It is the real surface that is encountered in most practical applications, and this in particular will be the case for solar materials. These will generally consist of polycrystalline thin films, coatings, or solids. Except for materials that can withstand solar concentration factors of about 1000, the large areas required for solar collectors mitigate against using single crystalline materials in devices.

The cost-effective deployment of large areas of solar collectors will most probably be polycrystalline materials, with all index planes emerging at the surface. Therefore, it is not expected that the structural determination of solar materials surfaces will be applied except for a few special cases. However, determining S/S interfacial structures is important, as shown by Figs. 6-9 in Ref. 2. The challenge in solar interface research will be to understand the changes in surface activity of heterogeneous real surfaces and interfaces. Here, SEM and possibly STEM techniques should be used extensively.

Concerning the elemental composition of interfaces, the useful properties of real interfaces often depend on the presence of chemical impurities. These impurities tend to prevent the self-minimization of the surface energy of the solid, and influence the growth kinetics, topography, surface and interface diffusion coefficients, and residence time of adsorbed species. Depending on the surface energy, impurities may concentrate at the interface or incorporate themselves into the bulk. These processes involve mass transport to, from, and along the interface, and may produce significant time-dependent changes in the properties of the material. Therefore, it is extremely important to be able to identify the elemental composition of interfaces at various stages of using solar materials. The techniques of XPS, AES, EELS, SIMS, ISS, and RBS seem especially important in solar materials research (1,3,4).

All small particles and all large flat polycrystalline surfaces, which are characteristic of the type planned for solar applications, possess a relatively large excess surface energy and are thermodynamically unstable. The interface atoms are restrained from interatomic motion by nearest neighbor bonding, but these bonds are weaker than for a corresponding position in the bulk. The potential barriers for interface diffusion are lower than for bulk diffusion, so less activation energy is required to produce interface diffusion processes. Diffusion along grain boundaries and across S/S interfaces in multilayer stacks clearly require using surface spectroscopies for detecting compositional changes.

Studying the amount adsorbed and the nature of adsorbate/solid interactions applies primarily to the S/G and S/L interfaces. Adsorption is the

accumulation of a surface excess of two immiscible phases. Most of the measuring techniques used to study chemisorption require UHV. This is unfortunate for the solar surface materials scientist, because solar systems are required to operate in real environments at atmospheric pressure, and sometimes immersed in electrolytes. Chemisorptive phenomena of interest are those that lead to degradation of solar materials interfaces. Thus, an understanding of the weak cochemisorption processes (40-150 kJ/mol) on a surface with a prior adsorbed layer, carried out at sub- to superatmospheric pressures, will require pushing to the limit the currently available techniques such as IR, LASER Raman, ellipsometric, microgravimetric, and magnetic measurements. At the same time, innovative methods of detection need to be developed (1). The problems of studying real surfaces of solar materials are similar to those encountered in studies of corrosion and catalysis.

In studying interfaces of solar materials, one must compromise the pure scientific objective of gaining an understanding by severely limiting the variables that need to be controlled. As indicated (6), detailed study of particular solar materials is best undertaken when the selections can be made as a result of other research. The selection of the solid form, the specific S/S, S/L, or S/G surface, and the preparation technique (e.g., thin-film deposition) will be dictated by the cost and the performance properties of the components. Once the options have been narrowed, it is clear that in-depth, fundamental investigations of the interfaces between the materials need to be carried out. However, the proper long-term applied research must be carried out to gain the required understanding so the cause of degradative failure can be corrected or anticipated. Interface characterization seems most important. The interfaces that should be studied are addressed in the next section.

Broad philosophical guidelines are needed to narrow the choices of surface analytical facilities required for the general study of solar materials interfaces. The choices should be guided by their value for (a) studying the interfaces of long-term interest to solar energy conversion systems; (b) studying interfaces under (actual and simulated) conditions as close as possible to those encountered when operating the system; (c) studying the fundamental processes at the S/S, S/G, and S/L surfaces that impact (a) and (b); and (d) having optimum impact on problems encountered in thermal, photovoltaic, photoconversion, and ocean thermal energy conversion systems. Since solar materials must remain stable for long periods, the interface properties that provide input data on their reactivity and/or degradation must be specifically studied. These properties are the surface composition or purity, topography, structure, area, interaction with ambient gases or vapors at various pressures and radiation exposures, and electron energy distribution. The leading experimental methods for characterizing these properties are listed in Table 3. A number of these methods, notably ELEED, ILEED, FEM, and FIM, are not applicable to the study of polycrystalline materials in mass-produced solar systems. Thus, the initial characterization should not attempt to relate reactivity to structural sensitivity per se, but only to the average structural distribution on a polycrystalline surface. As the number of problems at the S/L surface increases, some of the methodologies discussed at the recent conference on

nontraditional approaches for studying the solid/electrolyte interface will have to be considered (12).

**Table 3. Tabulation of Some Common Methods for Measuring Important Properties of Interfaces<sup>a</sup>**

Composition/purity; elemental identification	AES, XPS, SIMS, ISS, RBS, EELS (Core level), APFIM, NRA, PIXE, GDMS, GDOS, SCANIR, EDX, laser microprobe, and electron microprobe
Chemical state characterization	IR and Raman Spectroscopy, FT-IR, EELS, XPS, SIMS, ESDIAD, ellipsometry, and laser fluorescence
Structural characterization	LEED, HEED, RHEED, FIM, FEM, TED, XRD, HVEM, AEM, EXAFS, ISS, ion channeling, ESDIAD, UPS, electron channeling, SEXAFS, vibrational EELS, and Raman spectroscopy
Topography	SEM, EM, optical microscopy, and interferometry
Amount adsorbed and film growth	Microgravimetric, ellipsometric, and radiotracer are direct techniques. There are numerous indirect techniques.
Surface area	Microgravimetric and volumetric adsorption, EM
Inclusions	SAM, SIMS
Microdefects	EM, TED, STEM
Electron density of states	UPS

<sup>a</sup>All techniques are not applicable to all interfaces of interest. Some provide information near the interface rather than at the interface. Recent review articles should be consulted about the applicability of any particular method to specific characterization needs.

### Surface Science and Solar Materials Interfaces

In this section, an overview will be provided of the topical areas of surface science research that are especially important to solar energy technologies. These comments are based in part on a report from a workshop held in July 1980 (4). Broad areas of surface science that affect solar materials research are indicated.

It is clear that interface phenomena will play a widespread and dominant role in many solar energy conversion technologies. Preparing stable



interfaces with the desired performance properties will be critical in the reliable deployment of those technologies. Most of the problems are long range in nature; understanding of interfacial phenomena is needed to correlate the molecular properties of interfaces with their behavior in corrosion, grain boundary fracture, adhesion, catalysis, and embrittlement. Studies that have been concentrated on the S/G interface must be broadened to the S/L and S/S interfaces. New techniques need to be developed and, when necessary, national centers of surface science research need to be established.

Table 1 of a paper by Murr (2) lists problems and/or concerns related to specific interface materials and specific components of SECS. In Table 2 of the same work, he related topical study areas and/or research problems to S/S, S/L, S/G, L/L, and L/G interfaces. It is also useful to divide interface science into specific topical areas of study and consider how these will apply to interfaces in solar materials. These study areas are thin films; grain, phase, and interfacial boundaries; oxidation and corrosion; adhesion; semiconductors; surface processes, chemisorption, and catalysis; abrasion and erosion; photon-assisted surface reactions and photoelectrochemistry; and interface characterization methods. The actual or potential solar applications, research issues and/or concerns, and needs and opportunities are presented in the proceedings of a recent Workshop (4) and summarized in a recent review (3).

In principle, it would seem that enough interfacial characterization capabilities are now available (see Table 3) to determine the information required to understand interfacial behavior. In practice, there are severe limitations to the various experimental approaches as outlined in a recent document (14). For example, AES detection sensitivity is limited to about 0.1% of the surface atom density, XPS requires a long time to gather data and has poor lateral resolution, and both ISS and SIMS destroy the surface with ion bombardment. Then, there are problems associated with the effect of the power density from electron beams, sample or substrate destruction, valence identification, and theoretical interpretation for S/S interfacial analysis; ion etching techniques also have serious limitations (13). Presently, particle probe beams require a vacuum environment that obviously requires vacuum compatibility for specimens. The correlation between interfacial characterization in vacuum with that under real ambient conditions is extremely difficult, especially for S/G and S/L interfaces. In ion etching, artifacts may degrade spatial resolution such as surface roughness, zones of mixing, bulk and surface diffusion, residual gas adsorption, matrix effects, and other consequences of sputtering the sample. Various remedies and improvements have been proposed such as using reactive ion beams, multiple ion beams, sample rotation and special mounting, variable ion energies and angles of incidence, and data deconvolution methods, but it may be necessary to invent a new way for probing S/S interfaces.

Progress in all interfacial science is limited by both the availability and the effective application of analytical techniques. In the vicinity of an interface, information is sought ideally with the best possible spatial resolution concerning the absolute value and three-dimensional distribution of the chemical identity, crystal structure, the nature of bonding, and electri-

cal characteristics. In some cases, there is concern for rapid information acquisition and feedback to the control system environment as, for example, in the manufacture of large-area thin-film devices (14).

S/S, S/L, and S/G interfaces of many types occur in most solar devices, often with several in close proximity. To extrapolate from short-term laboratory behavior to 30-year lifetimes requires an atomic-level mechanistic understanding of the degradation processes occurring at interfaces. The latter, in turn, require using state-of-the-art methods of microcharacterization that yield structural, chemical, or electronic information with a lateral spatial resolution approaching atomic dimensions (14).

For characterizing interfacial microstructure and microchemistry, further research is needed to extend photon and ion analytical techniques for in situ characterization of S/L and S/G interfaces (e.g., laser, Raman, IR, and related techniques); to improve techniques for S/S interfacial analysis such as depth profiling, RBS, and NRA; to devise AEM experiments and techniques appropriate to studies involving diffusion, corrosion, oxidation, grain boundary recombination processes, and defect structures; to use HVEM in conjunction with in situ environmental stages with analytical capabilities for S/S, S/L, and S/G interfaces; to pinpoint methods for quantitative surface analysis; to understand better beam artifacts and to improve methods of data analysis for AES, XPS, ISS, and SIMS; to invent new or improve existing techniques for interfacial analysis, including polymers; and to correlate in situ S/L interfacial measurements with results of parallel experiments obtained after removal of the fluid. An ultimate goal is to relate the mechanical (adhesion, delamination, abrasion resistance, etc.), chemical (oxidation, phase change, diffusion, etc.), and electrical (resistivity, barriers, etc.) behavior of interfaces to their atomic, defect, and chemical state and configuration (14).

### Interface Science Applied to Solar Energy Materials

Major research efforts should be carried out on interfaces to elucidate mechanisms of degradation in solar-stressed environments to guide modifications of materials to minimize the effect of the detrimental processes on the performance of the system; to understand the influences of structure, bonding, and composition that provide interfacial stability; to devise materials preparation and fabrication processes that yield the desired chemical, electronic, physical, or mechanical properties; and to devise new experimental techniques to study and/or measure the important properties of interfaces. In the initial work, the most promising polycrystalline materials should be selected, and enhanced stability/reactivity should be studied when those materials are exposed to a solar-stressed environment and interfacial contact. Research goals should include elucidating mechanisms of degradation and reactions at S/S, S/L, and S/G interfaces, of photoenhanced degradation of polymers, and of photoenhanced ion transport in transmitting materials. S/G reactions and cochemisorption processes need to be studied at atmospheric pressure. Diffusion in coatings and films, including atom transport and accumulation at grain boundaries, needs to be understood. Studying the structural, bonding, and composi-

tional influences on adhesion, including the interactions between polymer/metal (oxide) surfaces and between dust and transmitting materials, is important. Influences of interfacial effects on the optical properties and on the nucleation and growth of new phases at interfaces, as both relate to system performance, need to be assessed.

In Table 4, the current problem with several components in SECS are listed. These are only a few of the solar problems of interest. They were selected because of my own association with them or with the authors and are not intended to indicate particular priorities for study. These problems have been discussed in detail or reviewed in previous work (1,3). However, a few comments on the mirror degradation problem are appropriate.

**Table 4. Some Current Problems with Solar Materials**

System or Component	Material(s)	Problem
Reflectors	Silver/glass	Degradation
Encapsulants/coatings	Polymers/metal (oxides)	Photodegradation, interface degradation
Solar cell material	Cu <sub>2</sub> S	Degradation in O <sub>2</sub> and H <sub>2</sub> O
Absorbers	Black chrome, black cobalt	Degrade at elevated temperatures
Thin-film solar cells	Numerous	Interdiffusion at junction

Silver has the highest solar reflectance of any element (~97%) and will therefore require the least concentrator area to collect a given amount of solar radiation. Although silver itself is relatively unreactive, a fractional monolayer of adsorbed oxygen enhances its reactivity to atmospheric gases such as water, carbon dioxide, sulfur dioxide, nitric oxide, etc. (15). At room temperature and atmospheric pressure, nearly one monolayer of oxygen always can be expected on silver. Therefore, chemisorption of atmospheric gases initiates corrosive reactions and a degradation of the reflectance. The results of these reactions have yielded visually transparent areas in mirrors used in demonstration heliostat fields in time spans ranging from several months to a few years.

The state-of-the-art mirror system now in use is a glass second-surface silver mirror backed with copper and paint, as shown in Fig. 2. For this system, the characterization and study of the glass/silver, silver/copper, and copper/paint interfaces before and after various stages of use are clearly required to understand the multilayer mirror stack. The methods of characterization outlined in Sec. 2.4 of Ref. 3, especially those of ISS, XPS, AES, and SIMS, are clearly applicable to this problem. Interfacial degradation reactions may begin at the silver/glass interface

because of impurities at the interface. These may be residual impurities resulting from the method of preparation, or the impurities may accumulate there because of radiation-induced transport processes of various ions in the glass. To illustrate the presence of residual impurities, a mirror was fabricated through the silvering step, i.e., float glass, application of a  $\text{SnCl}_2$  sensitizer, and electroless deposition of 70 nm of silver. This mirror was ion etched with  $^{20}\text{Ne}^+$  to the silver glass interface where the XPS spectra shown in Fig. 3 were taken (16). The elements anticipated were identified, i.e., Ca, Na, O, and Si from the glass and Ag. In addition, the  $3d_{3/2}$  and  $3d_{5/2}$  Sn lines were identified and, in more detailed work (16), shown to have core level shifts of 2.7 to 2.8 eV. Based on this shift, the most probable species trapped at the Ag/glass interface is  $\text{SnCl}_3^-$ . The Cl is not detectable in the spectrum of Fig. 3, presumably because of ion stimulated desorption. (On unbombarded glass sensitized only with  $\text{SnCl}_2$ , both Sn and Cl are detectable with XPS, but even using 250 eV electron beams for AES precludes detection of Cl.) From elements detected at the Ag/glass and Cu/paint interfaces, Thomas, et al. (16) have shown that the electrochemical potentials, which exist in the presence of  $\text{H}_2\text{O}$ , are sufficient to render the mirror system in Fig. 2 thermodynamically unstable.

Deterioration of the mirror may also result from interdiffusion of Cu and Ag, and reaction of the copper and silver with atmospheric gases. To secure evidence for these potential reactions, a mirror similar to that in Fig. 2 was prepared and stored at room temperature for a year. The lacquer backing, used instead of paint, was removed with acetone and an AES depth profile obtained. For the profile in Fig. 4,  $1 \times 1$  mm raster of  $\text{Ar}^+$  bombardment was used along with a  $30 \mu\text{m}$  FWHM electron beam. The three principal conclusions drawn from analysis of the profile in Fig. 4 are: no impurities segregate at the Ag/Cu interface; Fe, trapped in the 30 nm thick Cu layer during electroless deposition, results in formation of some iron oxide at the Cu/paint interface; and Cu diffuses into Ag to the Ag/glass interface, as shown from AES spectra taken after continuing the profile in Fig. 4 to the Ag/glass interface. More details of our surface analytical studies of silver mirrors will be available (16,17).

Space limitations preclude illustrating some of the other problems given in Table 4. ISS has been used to show that the copper oxide/polypropylene interface participates in the catalyzed thermal oxidative degradation of the polymer (18). ISS profiles were also used to demonstrate the purity of  $\text{Cu}_2\text{S}$  formed by reacting Cu films in  $\text{H}_2\text{S}/\text{H}_2$  mixtures (19). A reflection-absorption FT-IR approach for studying the photochemical, interfacially catalytic, thermal, and environmental degradation of polymer coated metal (oxide) films has been developed and now is in use (20). For surface analysis of absorber coatings, extensive literature citations have been summarized for SEM, AES, XPS, SIMS, RBS, and IR (3). ISS, SIMS, and XPS have also been used to characterize black cobalt absorber coatings (21). Kazmerski and his collaborators [see Refs. 84-93 in (3)] have used XPS, SIMS, and high resolution (160 nm diam. beam) SAM to resolve some of the grain boundary and interdiffusion issues in various PV materials such as Si, GaAs,  $\text{CuInSe}_2$ , and InP.

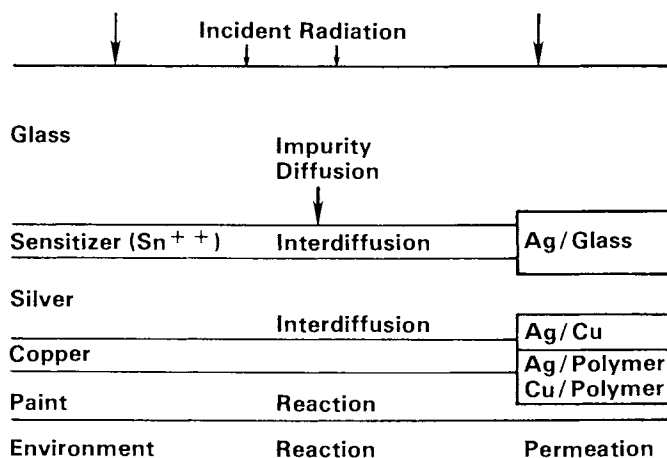


Figure 2. Potential modes of degradation at interfaces in a typical mirror system.

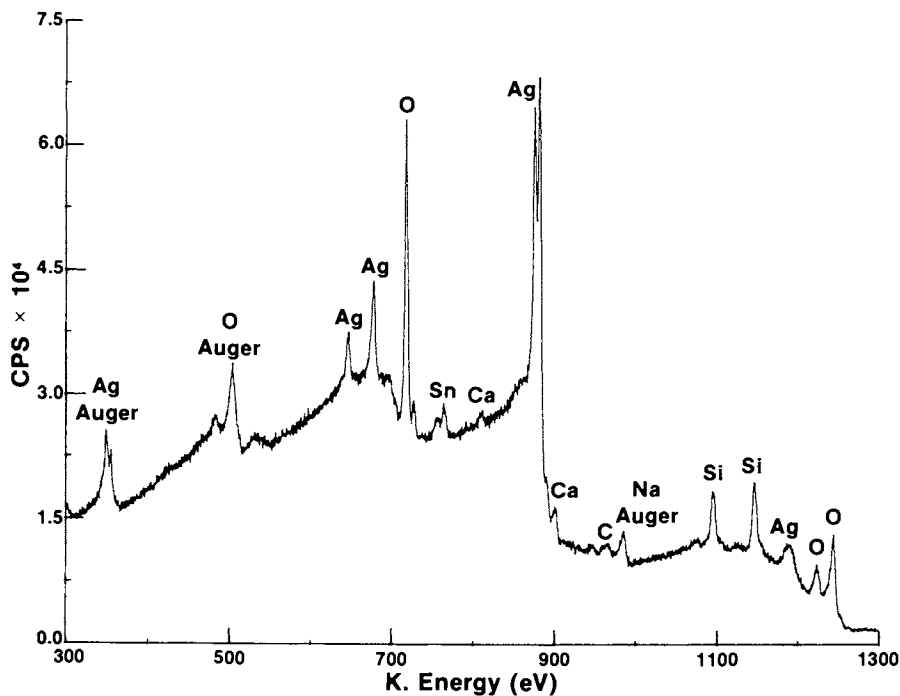


Figure 3. XPS spectrum at the Ag/glass interface after ion etching with  $^{20}\text{Ne}^+$  through  $\sim 70$  nm of Ag. The partially completed mirror was made by sensitizing float glass with a  $\text{SnCl}_2$  solution and then depositing only the silver.

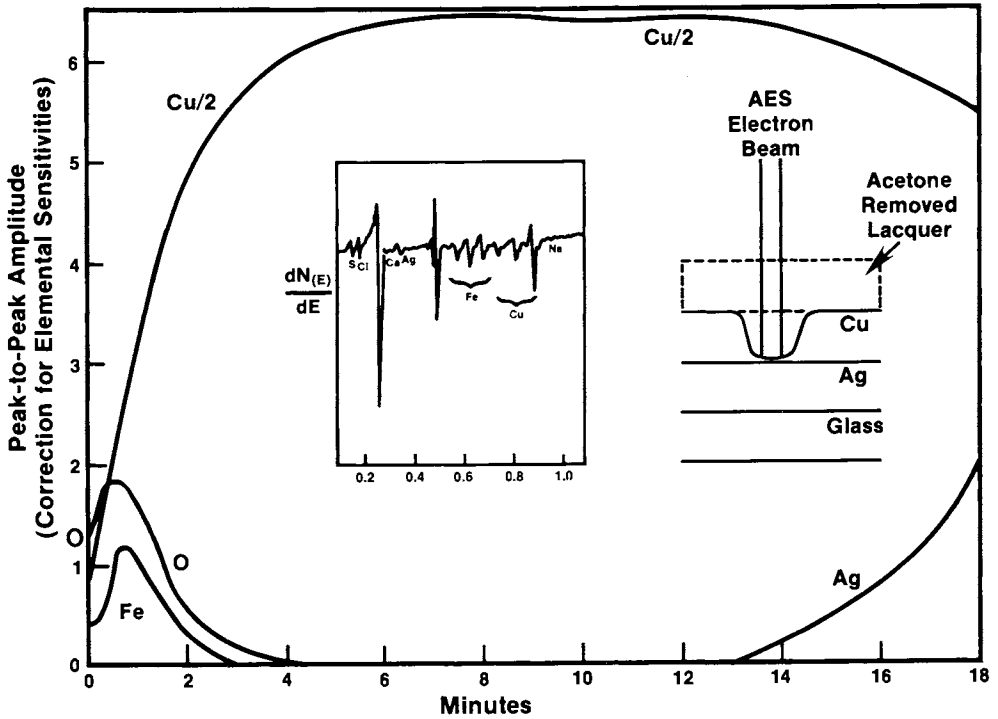


Figure 4. AES depth profile of a mirror of the type shown in Fig. 2 after storage at room temperature for 1 year. The lacquer layer was removed with acetone prior to profiling with  $^{40}\text{Ar}^+$ .

## Conclusions

Extensive interface research is crucially essential for developing long-life, cost-effective, multilayer, polycrystalline, thin-film stacks for SECS. Microchemical analysis and other interface measuring techniques must be employed to solve the interfacial stability problems in the stacks. Important topical areas in solar materials interface science include thin films; grain, phase, and interfacial boundaries; corrosion and oxidation; adhesion; chemisorption, catalysis, and surface processes; abrasion and erosion; photon-assisted surface reactions and photoelectrochemistry; and interface characterization methods.

## Glossary of Acronyms

AEM	analytical electron microscopy
AES	Auger electron spectroscopy
APFIM	atom probe field ion microscopy
EDX	energy dispersive x-ray analysis
EELS	electron energy loss spectroscopy
ELEED	elastic low energy electron diffraction
EM	electron microscopy
ESCA	electron spectroscopy for chemical analysis (see also XPS)
ESDIAD	electron stimulated desorption ion angular distribution
EXAFS	extended x-ray fine structure spectroscopy
FEM	field emission microscopy
FIM	field ion microscopy
FT-IR	Fourier transform infrared spectroscopy
GDMS	glow discharge mass spectrometry
GDOS	glow discharge optical spectrometry
HEED	high energy electron diffraction
HV	high vacuum
HVEM	high voltage electron microscopy
ILEED	inelastic low energy electron diffraction
IR	infrared
ISS	ion scattering spectroscopy
LEED	low energy electron diffraction
NRA	nuclear reaction analysis
PIXE	proton induced x-ray emission
PV	photovoltaic
RBS	Rutherford backscattering spectroscopy
RHEED	reflected high energy electron diffraction
SAM	scanning Auger microscopy
SCANIR	surface compositional analysis by neutral and ion impact radiation
SECS	solar energy conversion systems
SEM	scanning electron microscopy
SEXAFS	surface extended x-ray fine structure spectroscopy
S/G	solid/gas interface
SIMS	secondary ion mass spectroscopy

S/L	solid/liquid interface
S/S	solid/solid interface
STEM	scanning transmission electron microscopy
TED	transmission electron diffraction
TEM	transmission electron microscopy
UHV	ultrahigh vacuum
UPS	ultraviolet photoelectron spectroscopy
UV	ultraviolet
XPS	X-ray photoelectron spectroscopy (see also ESCA)
XRD	X-ray diffraction

### Acknowledgments

The author is deeply grateful for the many stimulating discussions with Dr. R. J. Gottschall that sharpened the focus of the third and fifth sections. The technical and/or editorial input from B. L. Butler, P. J. Call, L. E. Murr, J. O'M. Bockris, H. F. Helbig, P. Schissel, and G. Gross helped improve the manuscript. Similar assistance from L. L. Kazmerski on applications of interface studies to PV devices is gratefully acknowledged. Finally, the author appreciates the input from the 55 participants who not only made Ref. 4 possible but also helped in updating the section entitled "Surface Science and Solar Materials Interfaces." This work was performed under U.S. DOE Contract No. EG-77-C-01-4042.

### Literature Cited

1. Czanderna, A. W. "Solar Materials Science"; Murr, L. E., Ed.; Academic: New York, 1980, 93-151.
2. Murr, L. E. *Solar Energy Materials* 1981, 5, 1-16.
3. Czanderna, A. W. *Solar Energy Materials* 1981, 5, 349-377.
4. Czanderna, A. W.; Gottschall, R. J., Eds.; Basic Research Needs and Opportunities on Interfaces in Solar Materials. DOE Document No. CONF 8006156, April 1981; *Mat. Sci. Engr.* 1982, 53, 1-170.
5. Call, P. J. *Mat. Sci. Engr.* 1982, 53, 7-16.
6. Butler, B. L. *Mat. Sci. Engr.* 1982, 53, 17-24.
7. Johnston, W. D. Jr. "Solar Voltaic Cells"; Dekker: New York, 1980; Green, M. A. "Solar Cells: Operating Principles, Technology and Systems Applications"; Prentice-Hall: Englewood Cliffs, NJ, 1981.
8. Murr, L. E., Ed.; "Solar Materials Science"; Academic: New York, 1980.
9. Seraphin, B. O., Ed.; *Solar Energy Materials*, 1980, 3, 1-346.
10. Kazmerski, L. L., Ed.; "Properties of Polycrystalline and Amorphous Thin Films and Devices"; Academic: New York, 1980.
11. For example, see Refs. 11 to 30 in Ref. 3.
12. Special issue; *Surf. Sci.* 1980, 101, 1-646.
13. Holloway, P. H.; Bhattacharya, R. S. *Mat. Sci. Engr.* 1982, 53, 81-92.
14. Silcox, J., et al. *Mat. Sci. Engr.* 1982, 53, 149-162.



15. Czanderna, A. W. "Microweighing in Vacuum and Controlled Environments"; Czanderna, A. W.; Wolsky, S. P., Eds.; Elsevier: Amsterdam, 1980, 175-233.
16. Thomas, T. M.; Pitts, J. R.; Czanderna, A. W.; SERI Technical Memorandum; to be published in 1982.
17. Pitts, J. R.; Thomas, T. M.; Czanderna, A. W.; SERI Technical Memorandum; to be published in 1982.
18. Miller, A. C.; Czanderna, A. W.; Jellinak, H. H. G.; Kachi, H.; J. Colloid Interface Sci. 1982, 85, 244-255.
19. Prince, E. T.; Ph.D. Thesis, Clarkson College, Potsdam, NY, May, 1981.
20. Webb, J. D.; Smith, D. M.; Chughtai, A. R.; Schissel, P.; Czanderna, A. W.; SPIE, 1981, 289, 190-195.
21. Parks, J.; M.S. thesis, Colorado School of Mines, Golden, CO, June, 1981.

RECEIVED June 1, 1982

# Applications of Surface Analysis in the Nuclear Industry

N. S. McINTYRE

University of Western Ontario, Center for Interdisciplinary Studies in Chemical Physics,  
London, Ontario N6A 3K7, Canada

In the past ten years the number of chemistry-related research problems in the nuclear industry has increased dramatically. Many of these are related to surface or interfacial chemistry. Some applications are reviewed in the areas of waste management, activity transport in coolants, fuel fabrication, component development, reactor safety studies, and fuel reprocessing. Three recent studies in surface analysis are discussed in further detail in this paper. The first concerns the initial corrosion mechanisms of borosilicate glass used in high level waste encapsulation. The second deals with the effects of residual chloride contamination on nuclear reactor contaminants. Finally, some surface studies of the high temperature oxidation of Alloys 600 and 800 are outlined; such characterizations are part of the effort to develop more protective surface films for nuclear reactor applications.

In the past ten years, the nature of the research and development tasks facing the nuclear power industry has changed markedly. Many of these tasks represent the finishing stages of developments which began two decades before with the first commercialization of nuclear energy. In contrast to early research and development, many of the new tasks have been chemistry-related, rather than more directly associated with physics or engineering topics, as in the past. Much nuclear reactor related chemistry of interest in the past 10-15 years has involved reactions at interfaces; thus the introduction of surface analysis techniques, around 1970, has coincided with the undertaking of a number of research projects in the nuclear industry where surface analysis has been of much value.

In Table 1, some examples of actual surface analysis studies are given, along with the particular area of nuclear energy

0097-6156/82/0199-0345\$06.00/0  
© 1982 American Chemical Society

**Table 1**

---

<b>Some Applications of Surface Analysis in the Nuclear Industry</b>	
<b>1. Radionuclide Waste Management</b>	<b>– Waste form leaching – Ion absorption on minerals and backfill – Container corrosion</b>
<b>2. Transport of Radioactivity in Reactor Coolants</b>	<b>– Chemical decontamination of reactor circuits – Corrosion of heat-transport tubing</b>
<b>3. Reactor Component Development</b>	<b>– Growth of passive oxides – Hydrogen embrittlement – Surface chloride contamination</b>
<b>4. Fuel and Cladding Fabrication</b>	<b>– Uranium precipitation in mixed fuels – Acid cleaning of fuel cladding</b>
<b>5. Reactor Safety</b>	<b>– Iodine surface reactions – High temperature cladding reactions</b>
<b>6. Fuel Reprocessing</b>	<b>– Fuel dissolution mechanisms – Corrosion of vessels</b>

research to which they were relevant. A number of aspects of high level radioactive waste management involve the study of interfaces and material transfer across them: leaching studies of the glass or ceramic waste form require a detailed characterization of the surface film formed, in order to determine the mechanisms of radionuclide movement. XPS<sup>(1,2)</sup> AES,<sup>(3)</sup> and SIMS<sup>(4)</sup> studies of waste glass have already been reported. Typical nuclear waste repository mineral surfaces have been reacted with water and their transformations studied by XPS.<sup>(5)</sup> The adsorption of some fission product iodides on copper has been investigated by XPS<sup>(6)</sup> in a preliminary study of waste container corrosion.

Radioactivity transport in reactor coolant circuits involves both surface corrosion and deposition. Several XPS studies<sup>(8,9)</sup> of reactor boiler alloys have been reported which show the very strong effect of coolant chemistry on the films deposited. The chemistry of corrosion products precipitated on  $ZrO_2$  and  $Al_2O_3$  surfaces has been studied using XPS.<sup>(9)</sup> More recently, chemical decontamination of radioactive boiler circuits has been assisted by XPS analysis of the surface-active decontaminating agent.<sup>(10)</sup> Surface oxidation in gas-cooled reactor circuits has also been investigated. AES has been used to follow the  $CO_2$  oxidation of a chromium steel<sup>(11)</sup> and some pure metals.<sup>(12)</sup>

The development of improved structural materials for reactor components has sometimes relied on the growth of thin oxide films to passivate the surface and these can be monitored by several surface techniques. The nature of protective films grown on nuclear boiler alloy during gas phase oxidation has been studied using SIMS.<sup>(13)</sup> Hydrogen embrittlement, particularly of zirconium alloys, is a major concern because of the increased susceptibility to delayed failure of the hydrides. Surface analysis of zirconium hydrides using SIMS has been shown to be relatively quantitative and has allowed the distribution of hydrogen to be monitored on a  $+5 \mu m$  scale.<sup>(14)</sup> AES has been used to relate grain boundary chemistry to fracture behavior of iron and nickel alloys.<sup>(15)</sup>

Research directed to new methods of uranium/plutonium/thorium fuel production has benefitted from surface analysis. The air oxidation of plutonium metal has been studied by XPS.<sup>(16)</sup> Research into sol-gel production of  $UO_2$ - $ThO_2$  fuel pellets has used XPS to identify  $UO_2$  complexes of differing stoichiometries which are recovered during centrifugation.<sup>(17)</sup> The chemical processes involved in cleaning of zirconium-niobium fuel cladding has been investigated using XPS.<sup>(18)</sup> Discoloration of the surface was associated with  $Nb_2O_5$  product which resulted from the hydrolysis of a niobium fluoride. AES<sup>(19)</sup> and SIMS<sup>(20)</sup> for surface analysis of highly radioactive fuel have been described recently. Irradiated High Temperature Reactor fuel particles have been analyzed by XPS, without recourse to a highly-shielded facility.<sup>(21)</sup>

Recently begun reactor safety studies will require surface studies to determine the nature of the reaction products fission

gases, such as iodides, with containment surfaces. Also, during possible thermal excursions in a reactor, chemical reactions within the fuel elements themselves are of great importance--particularly those involving interphase relationships. Within zirconium alloy cladding, the local oxygen concentrations have been investigated by AES,<sup>(22)</sup> following thermal cycling of the cladding to represent accident conditions. This work has shown that and phases of zirconium can be distinguished on a micron lateral scale, based on the measure of local oxygen concentration.

In the chemical reprocessing of spent reactor fuel, there are a number of possible applications of surface analysis techniques. Quite recently, XPS studies of dissolution mechanisms of  $UO_2$  fuel have begun.<sup>(23)</sup> Studies in support of surface protection of dissolution vessel and off-gas handling systems have required extensive work using AES.<sup>(24)</sup>

This present paper discusses in more detail three separate nuclear-related studies where surface analysis has been used extensively: borosilicate glass leaching, surface chloride contamination, and gas phase oxidation of some nickel alloys.

#### Analysis of Borosilicate Glass Leaching Using Secondary Ion Mass Spectrometry (SIMS)

This study has involved the reaction of a simple sodium borosilicate glass with water at room temperature. This followed previous SIMS investigations of a much more complex glass containing elements simulating the composition of a high level nuclear waste.<sup>(4)</sup> Some typical SIMS depth profiles for some elements in this simulated waste glass are shown in Figure 1. Profiles shown followed aqueous leaching at 25°C for periods of 2d and 50d. An important benefit of such profiles is the capability for following concentration changes of minor, but important elements such as cesium and strontium (typically 100-500  $\mu\text{g/g}$  in the bulk phase).

The shape of the very reproducible boron elemental profiles suggested a diffusion-related phenomenon might be responsible for the concentration change. This present paper reports further investigation of the boron concentration profiles at a very early stage in the water-glass reaction. For this purpose, a much simpler glass formulation was used: 1:1:4  $B_2O_3:Na_2O:SiO_2$ , containing trace concentrations (1000  $\mu\text{g/g}$  of  $VO_2$ ). The  $v$  ion was used as an intensity reference since it was not noticeably affected by leaching.

Fresh glass sample surfaces were produced immediately prior to leaching by fracture. These were exposed to static aqueous leaching at 25°C in a Teflon vessel for periods of 1 minute to 3 days. At several reaction times, samples were also leached in an ice-water mixture (0°C). Blank specimens were fractured at the same time and left in contact with the ambient atmosphere. All samples were analyzed with a Physical Electronics Industries SIMS-3500 spectrometer using a 5 KeV  $Ar^+$  primary ion beam and a 5 KeV rastered electron beam to reduce charging of the insulating glass surface.

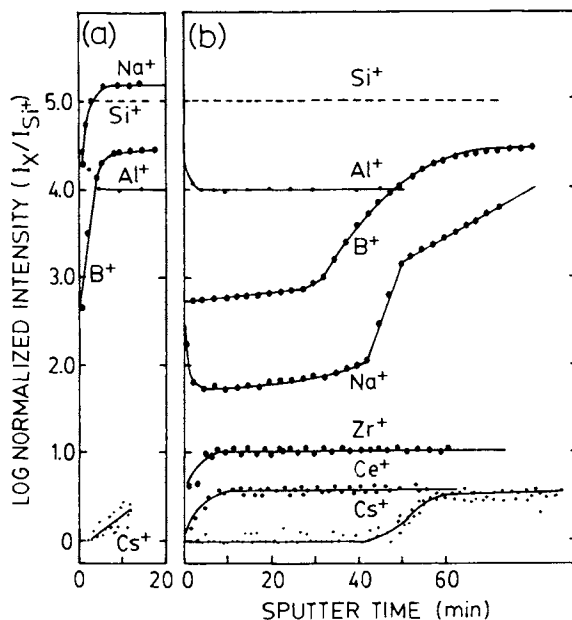


Figure 1. SIMS depth profiles in a simulated nuclear waste glass. Major and minor elemental profiles are shown for fractured surfaces exposed to 25°C aqueous leaching for 2 d (a) and 50 d (b). (Reproduced, with permission, from Ref. 4. Copyright 1980, North-Holland Publishing Co.)

In Figure 2 the positive ion intensities are plotted as a function of time for several major elements in the glass. These depth-composition profiles are compared for unleached and 30 minute aqueous leaching conditions. For each case, the results of profiles on two separate samples have been shown (solid and dashed lines), so that the reproducibility of the method can be judged.

The profiles of the unleached glass surface showed essentially no change in intensity of the sodium and potassium ions as a function of depth. However,  $\text{Si}^+$  and  $\text{B}^+$  ion intensities were found to be consistently lower at the outer surface than within the bulk of the glass. Depth profiles for both ions have a similar shape. This effect is believed to result from surface hydration which alters the yield of ions from the borosilicate network. Unhydrated glass surfaces, introduced into the spectrometer immediately after fracturing, showed little or no depression of either  $\text{Si}^+$  or  $\text{B}^+$  signals, and hydrate clusters, such as  $\text{Si}(\text{OH})^+$  were much reduced in intensity.

Following a thirty minute leaching reaction, the intensity of  $\text{Na}^+$  ions at the outer surface was reduced by a factor of ten; the surface region so affected was found to be altered to a minimum depth of 2.0 nm (based on a sputtering rate of 0.5 nm/min for  $\text{SiO}_2$ ). Unlike the boron and silicon behavior, the depression of sodium at this particular surface is believed to result from an actual migration of  $\text{Na}^+$  ions into the leach solution. A certain quantity of boron may be leaching concurrently, since the depth profile of boron no longer is parallel to that of the  $\text{Si}^+$ , but is reduced in intensity relative to that observed for a non-leached sample.

Temperature changes are expected to affect both solid dissolution rates and diffusion coefficients during the initial stages of leaching. In Figure 3(a), the depth profiles of surfaces leached for 30 minutes at 24°C and 0°C are compared. From a comparison of the attenuation of the boron and silicon intensities at each temperature, the depth of penetration of surface hydration was judged to be twice as great for a 25°C leach solution than a 0°C solution. In addition, the surface region depletion of sodium was interpreted to be substantially greater in depth and magnitude for the sample leached at 24°C than for 0°C. In Figure 3(b) an attempt is made to determine how well the shapes of the boron depth profiles conform to simple Fickian diffusion model. The error function plots obtained suggest that a single diffusion-controlled mechanism is more appropriate for the reactions at 0°C than at 24°C. The diffusion-controlled limiting reaction is likely the inward movement of hydrogen or hydronium ion to react with the borosilicate network, producing the hydration species which are detected by SIMS. (25)

In Figure 4, the changes in ion intensity for two different reaction times are plotted for 0°C aqueous leaching. The ion

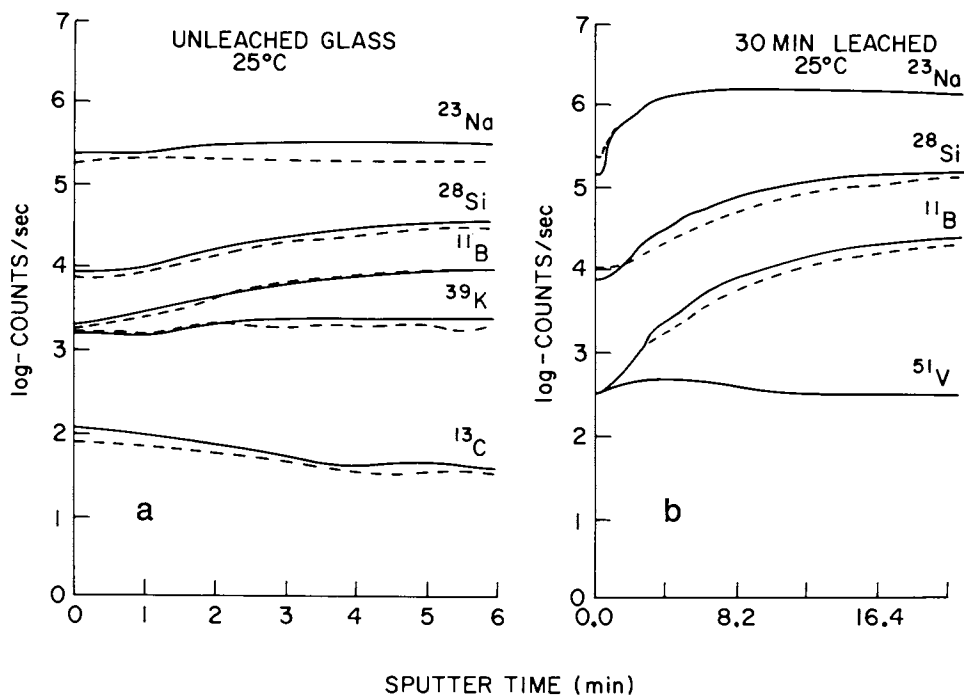


Figure 2. SIMS depth profiles for a sodium borosilicate glass blank sample, air-exposed only (a), and sample exposed to aqueous leaching at 25°C for 30 min (b).



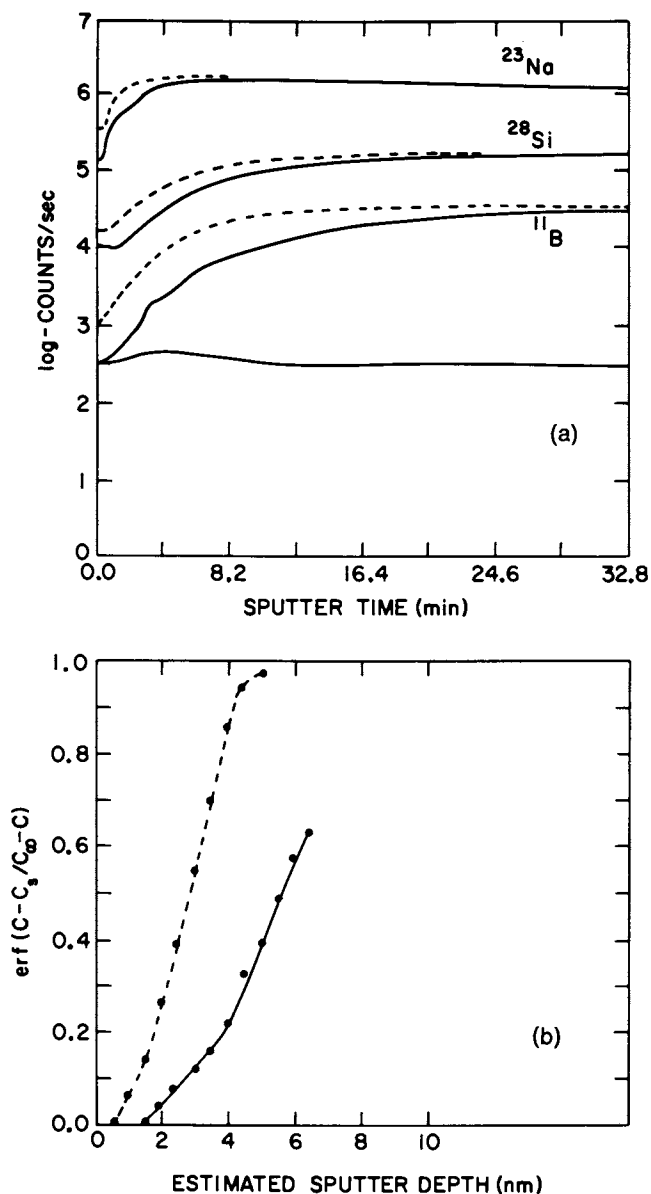


Figure 3. Comparison of SIMS depth profiles of aqueous leaching of a sodium borosilicate glass, for 30 min (a). Key: ---,  $0^\circ\text{C}$ ; and —,  $25^\circ\text{C}$ . Error function plot for boron ion intensities in a (b). Key: — · —,  $0^\circ\text{C}$ ; and —●—,  $25^\circ\text{C}$ .

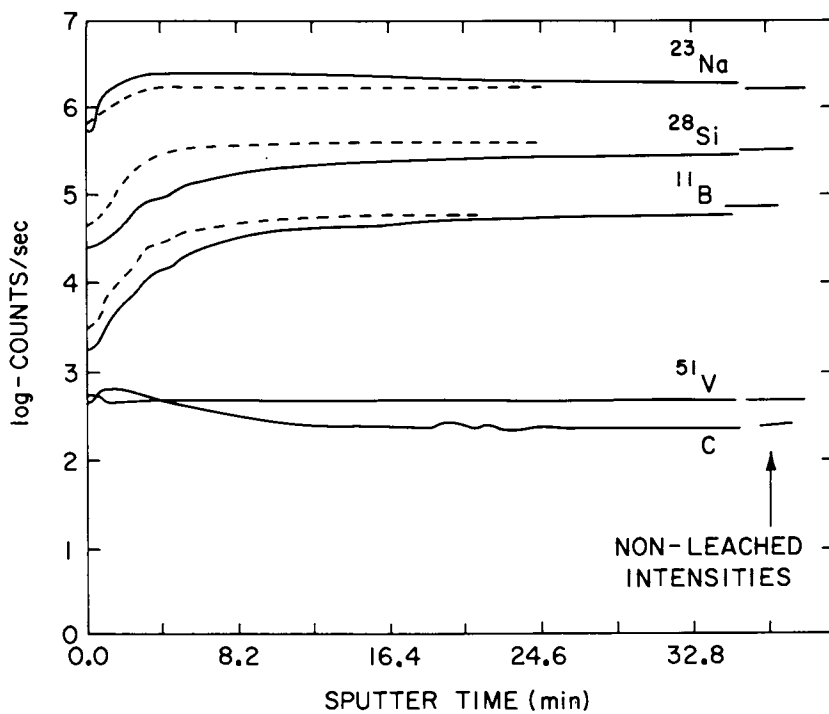


Figure 4. SIMS depth profiles for a borosilicate glass exposed to 0°C aqueous leaching for periods of 5 (---) and 30 (—) min.

intensities measured after sputtering 15-20 nm into the leached glass surfaces agree very well with the relative ion intensities for unleached glass surface. The major changes observed as the leaching period increases from 5 to 30 nm is an increased depth to which the apparent hydration occurs. In addition, there is some evidence that, with increased leaching, sodium accumulates within the zone directly below the sodium depleted region.

In summary, these SIMS studies have shown that reproducible measurements of some surface chemistry changes are possible following very early attack of glass surfaces by water. Early depletions of sodium and more surprisingly, boron, are indicated even after a few minutes of leaching time. The apparent effects of surface hydration on the SIMS relative ion yields also warrants further investigation.

#### Reaction of Chlorinated Hydrocarbons with Nuclear Component Surfaces

It is well known that chloride ions in aqueous or humid systems promote pitting corrosion of stainless steel surfaces. This is generally believed to result from the substitution of chloride ions into the surface oxide lattice with subsequent breakdown of the passification of the underlying alloy. The elimination of inorganic chloride contamination from stainless steel components used in nuclear applications has been a goal of designers for many years.

The effect of organic-chloride compounds on these alloy surfaces is much less understood, although many chlorinated hydrocarbons are used in their manufacture. For example, drawing fluids often contain chlorocarbons, as do inspection chemicals which are sprayed or brushed on surfaces in a search for incipient cracks. For a long time, it has been argued by users that volatile chlorocarbons would not remain long in contact with the exposed surface, and that any residue could be removed by rinsing with another solvent. However, entrapment of chlorinated hydrocarbons in microscopic fissures or surface features could lead to their retention as a hydrolyzed product. This present study has used surface analysis to detect any chemical changes which occur when stainless steel surfaces are contacted with a chlorinated hydrocarbon, trichloroethane.

Coupons of Type 304 stainless steel were prepared by mechanical abrasion and rinsed with methanol. Each sample was analyzed by XPS prior to treatment to ensure that no detectable casually-introduced chlorine was present. Two separate series of laboratory experiments were done: one series (a) followed the effects of short-term contact between chlorocarbon and the alloy surface, a second series (b) investigated the effects of prolonged vapor and liquid contact with the alloy in a glass refluxer. In series (a) the clean alloy surface was swabbed using trichloroethane-soaked tissue and immediately inserted into the vacuum chamber of an XPS spectrometer for analysis. After analysis, the same coupon was exposed to the atmosphere for periods of 72 and 336 hours

(14 days). After each exposure, an identical surface region of the coupon was analyzed by XPS. In series (b) individual coupons were suspended in trichloroethane liquid at 25°C and 65°C for periods up to 60 hours. The chlorocarbon liquid was contained in a refluxing column and additional coupons were suspended in the vapor in a manner ensuring good degreasing action. Following exposure, all samples were left in the laboratory atmosphere for approximately 1500 hours (2 months). The samples were then analyzed by XPS and/or by Scanning Auger Microscopy (SAM).

Stainless steel surfaces swabbed with trichloroethane immediately before insertion in the XPS spectrometer, consistently showed evidence of chloride retention in their Cl(2p) spectra, even after exposure to a spectrometer vacuum of  $10^{-7}$  Pa for 24 hours at 34-40°C. Figure 5(a) shows such a spectrum. From the Cl(2p) spectral envelope, two sets of Cl(2p  $3/2-1/2$ ) doublets were derived by deconvolution. The more intense doublet "1" is assigned to organically-bound chlorine, being close in energy to chlorine bound in some aliphatic hydrocarbons.<sup>(26)</sup> The Cl(2p  $3/2$ ) line labelled "2" corresponds closely to the binding energies observed for ionic metal chlorides such as in FeCl<sub>2</sub> and FeCl<sub>3</sub>.<sup>(26)</sup> Exposure of the same area of the alloy surface to the atmosphere for 72 hours resulted in a large relative increase in the amount of ionic chloride in the spectrum (Figure 5(b)), although the total quantity of chlorine relative to iron decreased somewhat (Cl/Fe = 0.04). Thus, chemical alteration of the surface chloride is evident during ambient exposure.

Longer-term exposures of the alloy to trichloroethane vapor and liquid were made in a glass refluxing column. Some specimens exposed for 50 hours at 25°C were analyzed by XPS immediately afterwards, and some were left in the laboratory for a further 1500 hours (2 months) before analysis. In both cases the surface C/Fe ratio was 0.08-0.10, i.e., about twice the concentration of chlorine in the preceding short-term exposure. These surfaces had visibly darkened, indicating the growth of a film of significant thickness, i.e., 10-100 nm. The Cl(2p) spectrum showed that a substantial portion was bound as ionic chloride (Figure 5(c)). Significantly, the surface oxide composition differed considerably from that of specimens analyzed immediately after exposure to vapor. Chromium (III) oxide, Cr<sub>2</sub>O<sub>3</sub>, rather than Fe<sub>2</sub>O<sub>3</sub>, was the dominant oxide, (see Figure 6(b)). Figure 6(a) is, for comparison, the spectrum of the near normal surface, that of the specimen exposed briefly by swabbing with trichloroethane just before analysis. On the chromium-rich surface (Figure 6(b)) produced by chloride contamination, the iron is not entirely bonded as oxide. The Fe(2p) spectrum in Figure 7(a) differs from that for Fe<sub>2</sub>O<sub>3</sub> in Figure 7(b), the normal surface iron oxide on the alloy. The satellite line on the high binding energy side of the line (see arrow) occurs at the same energy as the prominent satellite in the spectrum of FeCl<sub>2</sub>.<sup>(27)</sup>

The surfaces of stainless steel coupons were also exposed

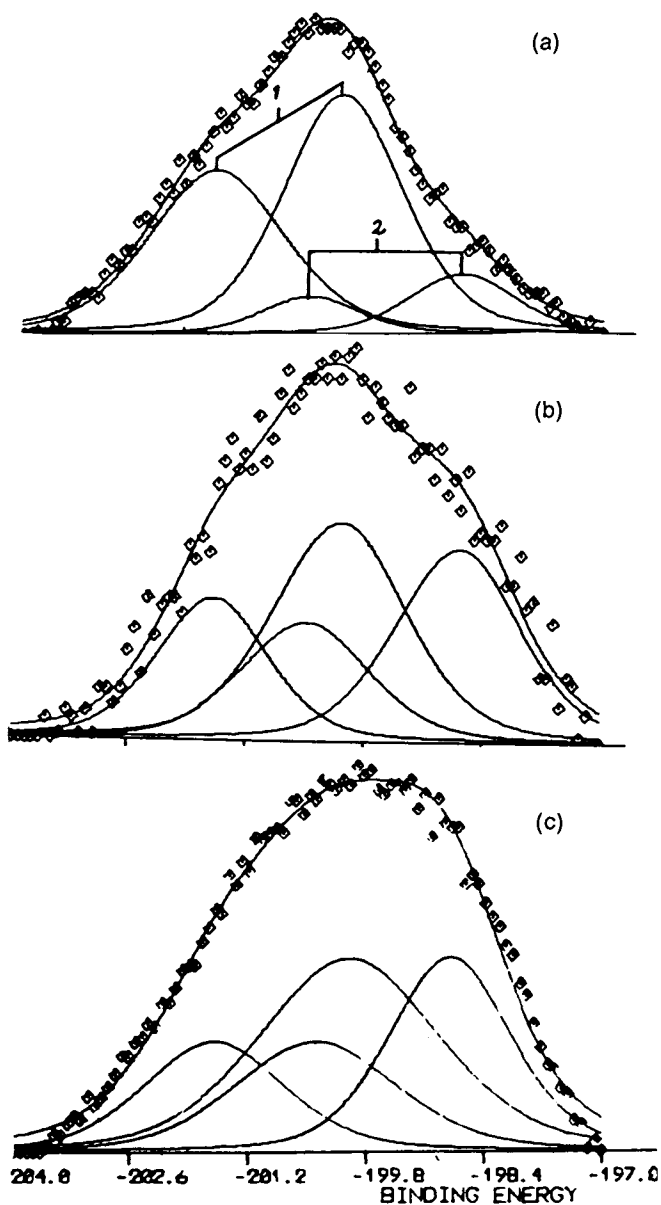


Figure 5. Three Cl 2p photoelectron spectra for a 304 stainless steel surface immediately after rinsing with trichloroethane (a), the same surface after atmospheric exposure for 50 h (b), and the surface of 304 stainless steel exposed to trichloroethane vapor for 50 h and to atmosphere for 3000 h (c).

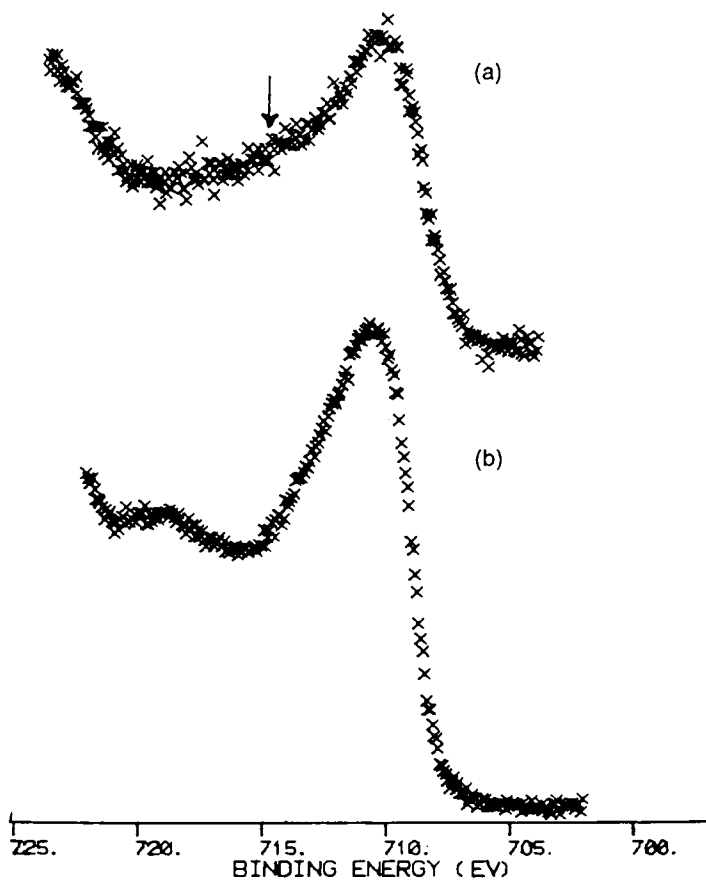


Figure 6. Two x-ray photoelectron spectra of the Fe 2p photoelectron line for a 304 stainless steel surface exposed to trichlorethane vapor for 50 h and atmosphere for 1500 h (a) and a 304 stainless steel surface as received (b).

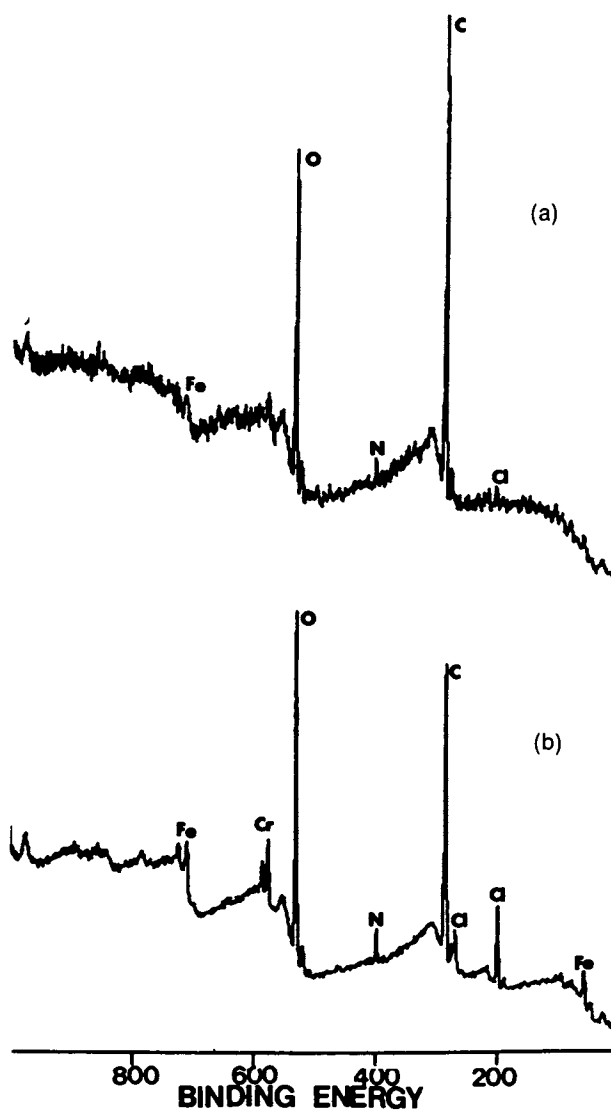


Figure 7. Two total energy range x-ray photoelectron spectra for a 304 stainless steel surface exposed to trichlorethane vapor for 50 h and atmosphere for 1500 h (a), and a 304 stainless steel surface as received (b).

in a commercial chlorocarbon vapor degreaser. These were analyzed subsequently by XPS and SAM, along with appropriate "blank" specimens, which had not been exposed to the solvent. Both surface techniques detected small chloride concentrations on the "blank" specimens, as sodium chloride ( $\text{Cl/Fe} = 0.02$ ). However, there was a significantly higher chloride level on the commercially-degreased surfaces ( $\text{Cl/Fe} = 0.04$ ). No sodium accompanied the chloride on these samples.

The Auger depth-composition profiles vapor-degreased surfaces and a "blank" surface are compared in Figures 8(a) and (b). Figure 8(b) shows that the small amount of chloride on the "blank" surface is a maximum at the outer surface and drops to undetectable as the film is penetrated 2 nm. By contrast, on the specimens exposed to vapor degreasing, the chloride concentration consistently reached a maximum 2 to 4 nm within the film. This increased level of chlorine in the film appeared to be related to a decrease in the ratio of iron to chromium oxides, particularly at the depth where the chlorine concentration was a maximum.

The shorter-term exposure experiments show that some portion of the organically-bound chlorine, such as trichlorethane or its decomposition products, remains absorbed on a 304 stainless steel surface, even after heating at 35-40°C in a high vacuum. Conversion to an ionic species begins after a short contact period and can be detected using XPS. Formation of the ionic chloride is likely the result of hydrolysis by water also absorbed on the surface, and is perhaps catalyzed by the surface metal oxides. Further atmospheric exposure up to a few months increases the relative amount of the ionic form of chlorine. The composition of the surface oxide layer was altered, with chromium oxide replacing iron oxide as the major species. There was further evidence that chlorine was present as iron chloride, perhaps up to 5% of the surface film. The conditions under which oxidation of such surfaces occurred are quite comparable to those which could occur on steel surfaces in industrial usage.

#### Surface Studies of Boiler Tubing Oxidation

The initial surface composition of boiler tubing, prior to its installation will have an important impact on the amount and type of activated corrosion products in an aqueous reactor coolant. Consequently, the type of thermal pre-treatment the tubing undergoes, for example, for mechanical stress release, will affect the surface oxide film, and ultimately, the corrosion behavior. This particular work has been directed toward characterization of surface oxide films which form on Inconel 600 (nominal composition: 77% Ni, 16% Cr, 7% Fe, — a tradename of Inco Metals Ltd., Toronto, Canada) and Incoloy 800 (nominal composition: 31% Ni, 19% Cr, 48% Fe 2% other, — a tradename of Inco Metals Ltd., Toronto, Canada) heated to temperatures of 500-600°C for periods of up to 1 minute in flowing argon. These are conditions equivalent to those experienced by CANDU (CANadian Deuterium Uranium) reactor boiler hairpins during in situ stress relief.



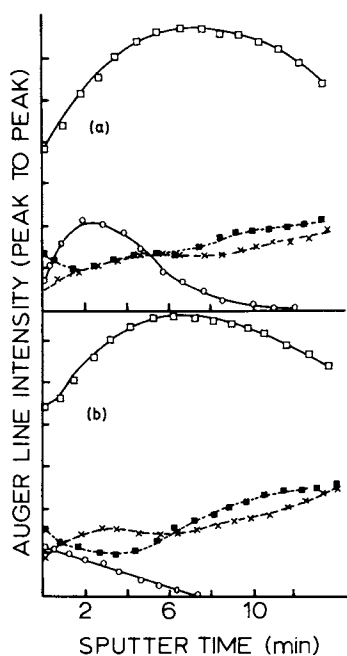


Figure 8. Two depth composition profiles obtained by AES: a 304 stainless steel surface exposed to commercial vapor degreasing, then exposed to atmosphere for 1500 h (a), and a stainless steel surface as received (b). Key:  $\square$ , O ( $\times 1$ );  $\blacksquare$ , Cr ( $\times 2$ );  $\circ$ , Cl ( $\times 10$ ); and  $\times$ , Fe ( $\times 1$ ).

Samples of Inconel 600 and Incoloy 800 coupons were exposed to heating in a flow cell for periods up to 60 seconds at 550-550° C. The reactive gas used was argon containing 0.01% oxygen.

XPS depth profiles are particularly useful for following the evolution of film composition, since different oxide and metal phases can often be distinguished.<sup>(7)</sup> In Figure 9(a)-(d), XPS depth profiles are shown for films grown on an abraded Inconel 600 surface following exposures of 1 minute; 2 minutes, 5 minutes, and 60 minutes at 500°C. The concentration and composition of the main alloy constituents: chromium, nickel and iron are plotted cumulatively showing both metallic and oxide concentrations as a function of depth into the oxide film. Thus, the relative oxide phase areas should correspond roughly to the total amounts of these oxides present. Throughout the first 60 minutes, the oxidation process is dominated by the outward movement of chromium and its preferential oxidation. Initially, this process virtually prevents significant oxidation of nickel; eventually the rate of replenishment of chromium ion is slowed by the growing complexity of the film and the nickel phase near the surface becomes oxidized. Iron also exhibits strong tendencies to migrate to the outer surface, which is subsequently restricted by the thickening oxide film. After 1 minute of oxidation the surface film composition chromium and iron oxides, is significantly less complex than at longer oxidation times.

In the case of Incoloy 800 oxidation, chromium and iron surface--enriched oxides were found in equivalent XPS depth profiles' surprisingly large concentrations of the minor (<1%) matrix elements, titanium and manganese were however also detected. Figure 10 shows the enrichment of titanium elements at the outer surface of the 550°C oxidized alloy, as well as profiles of the major matrix elements. The mobility of both titanium and manganese at this temperature is considerably higher than for the major elements. Oxidation at 450°C also resulted in manganese enrichment in the surface oxide layer, but, in this case, no titanium was detected.

In the study of complex oxide films, the determination of phase distribution becomes of prime importance. In these cases, element distributions along one direction on the surface are particularly useful. Figure 11 shows chromium, manganese and titanium distributions. Manganese and titanium distributions are highly localized and probably affected by the grain boundary intersections with the surface. The distribution of titanium is, moreover, a strong function of the temperature which is altered with distance along the surface because of the flow of gas in one direction. The strong temperature dependence of titanium may, in fact, be useful as an indicator of the temperature history of the surface.

#### Conclusions

The examples described are those of work presently in progress which will be reported in more detail at a later date.

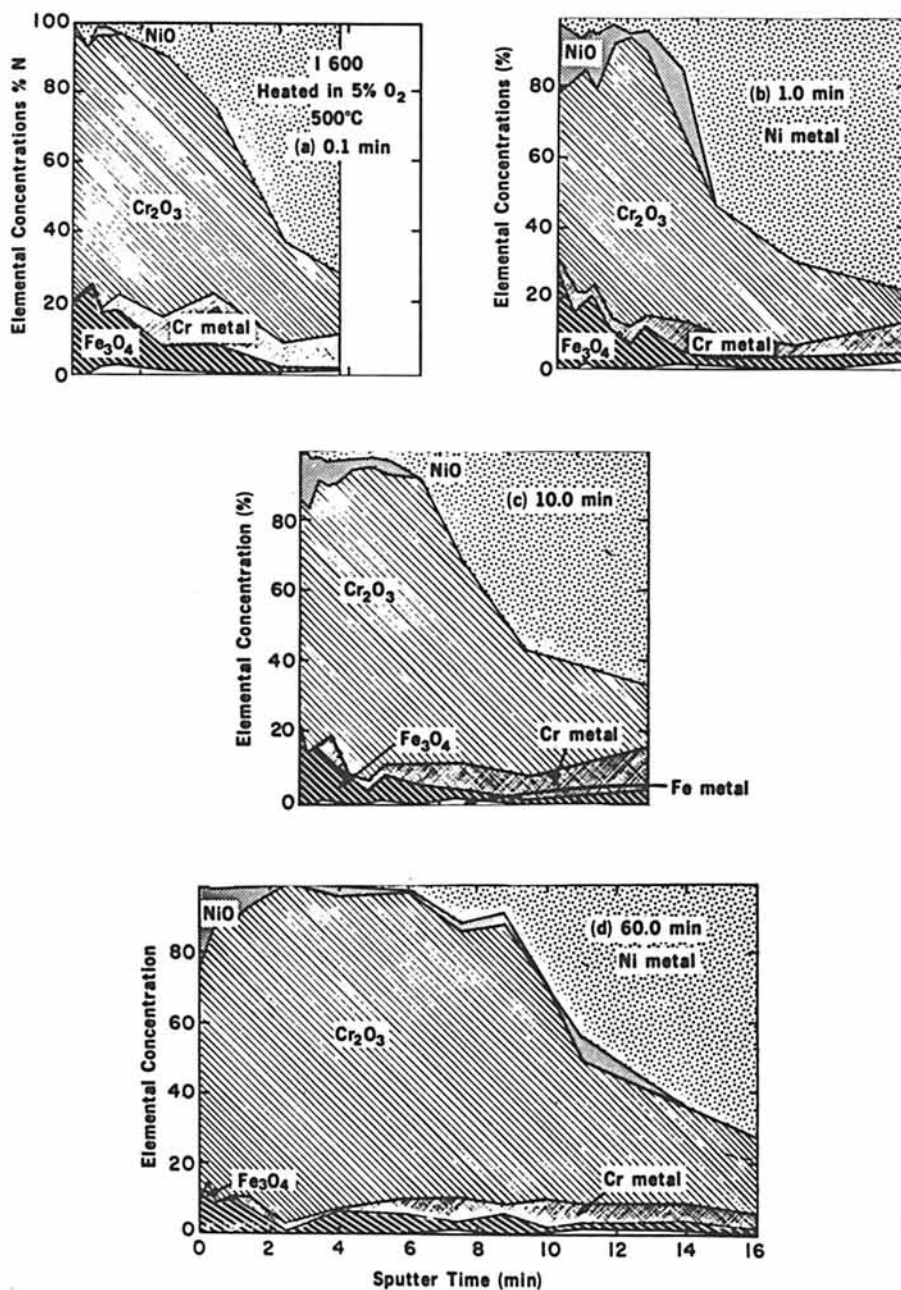


Figure 9. XPS depth composition of an Inconel 600 alloy surface exposed to 550°C air oxidation.

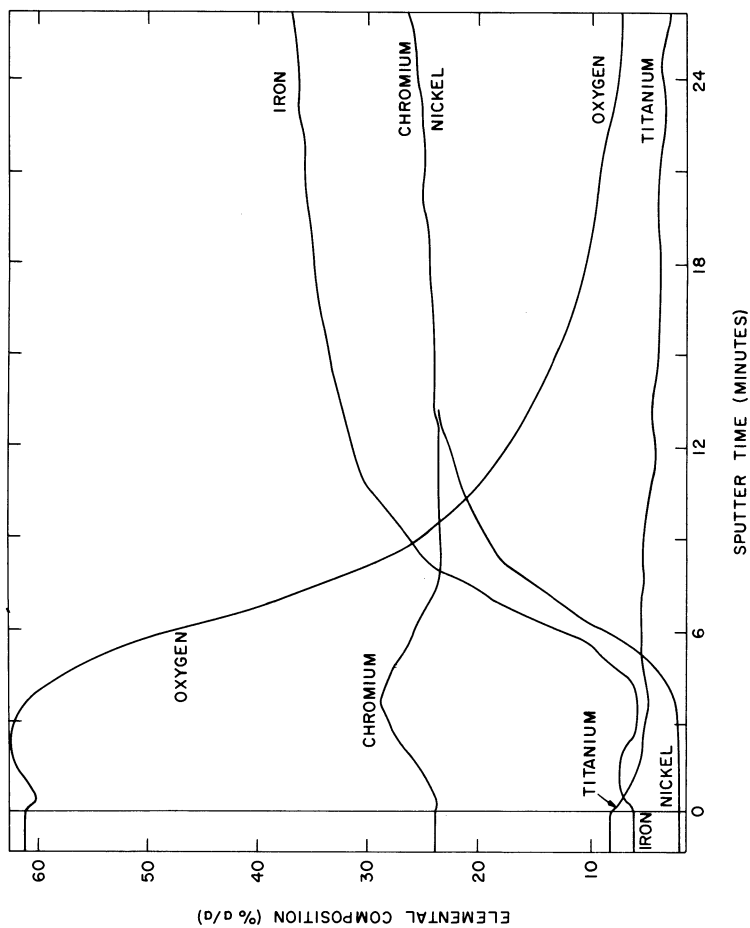


Figure 10. AES depth composition profile of an Incoloy 800 alloy surface oxidized at 550°C for 1 min. Air heated to 800°C for 10 s.

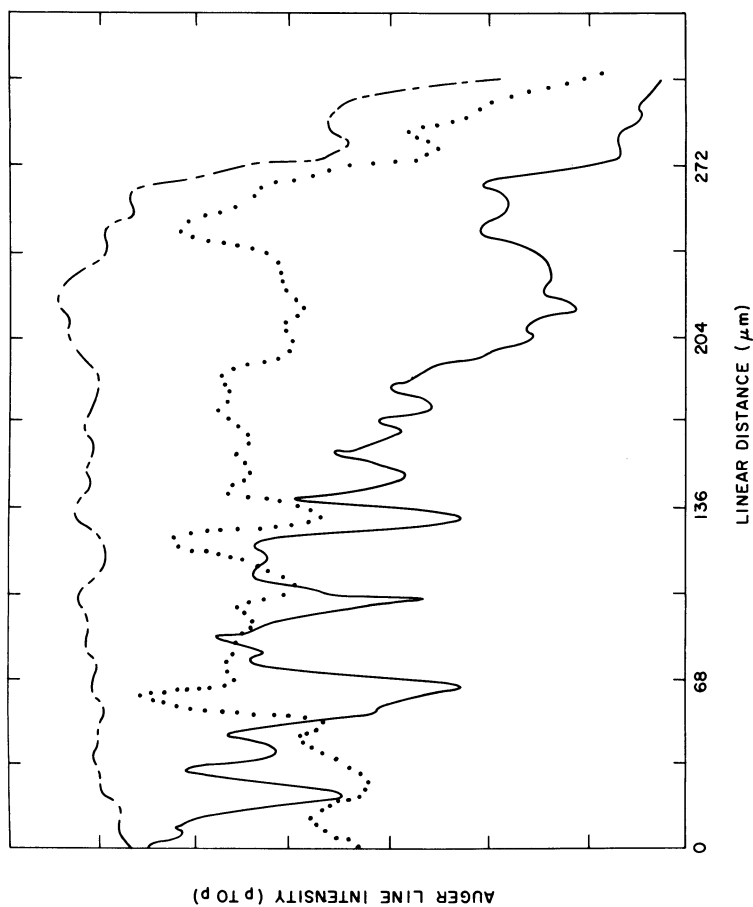


Figure 11. AES line scan of element distributions on an Incoloy 550 surface oxidized at 600°C for 1 min. Key: ---, Cr; ···, Mn (X3); and —, Ti (X3).

Because of the applied nature of much of the work in the nuclear power industry, there are many good examples of surface analysis which will unfortunately, never appear in the open literature. It is entirely likely that many studies similar to those reported here have been undertaken in laboratories other than those familiar to the author. In any case, there are still many challenging research projects within the industry for a surface scientist with a fertile imagination.

#### Acknowledgement

The author acknowledges the experimental assistance of F.W. Stanchell and the advice and encouragement of R.B. Stewart, both of Whiteshell Nuclear Research Establishment, Pinawa, Canada.

#### Literature Cited

1. B.W. Veal, D.J. Lam, A.P. Paulikas, and D. P. Karim, Nucl. Technol., (1980) 51, 136.
2. L.R. Pederson, M.T. Thomas, and G. L. McVay, J. Vac. Sci. Technol. (1981) 18, 732.
3. D.E. Clark and E. Lue Yen-Bower, Surface Science (1980) 100, 71.
4. N. S. McIntyre, B.F. Phillips, and G. G. Strathdee, Surface Science (1980), 100, 71.
5. P.C. Fung, G.W. Bird, N.S. McIntyre, G.G. Sanipelli, and V. J. Lopata Nucl. Technol. (1980), 51, 188.
6. Z. Haq., G.M. Bancroft, W.S. Fyfe, G. Bird, and V. J. Lopata Environmental Sc. Technol. (1980) 14, 1106.
7. N.S. McIntyre, D. G. Zetaruk, and D. Owen, J. Electrochem.Soc (1979) 126, 750.
8. N.S. McIntyre, D.G. Zetaruk, and E.V. Murphy, (1979) 2, 151
9. P.H. Tewari and N.S. McIntyre, Prog. Chem. Eng(1975) 71,134
10. D.W. Shoesmith and N.S. McIntyre, WNRE, unpublished results.
11. G.C. Allen, I.T. Brown, and R.K. Wild, J. Nucl. Mater. (1977) 68, 179.
12. G.C. Allen, I.T. Brown, and R.K. Wild, Oxid. Met. (1978) 12, 83.
13. H.F. Bittner, J.T. Bell, J.D. Redman, W.H. Christie and R.E. Eby, Met. Trans. (AIME) (1980) 11A, 783.
14. C.D. Cann, K. Nuttal, V.R. Deline, and N.S. McIntyre, abstract, Microscopical Society of Canada, Montreal (1981).
15. S.M. Bruemmer, R.H. Jones, M.T. Thomas, and D.R. Baer, Scripta Met. (1980) 14, 137.
16. G.F. Larson, J. Vac. Sci. Technol. (1979) 17, 000.
17. N.S. McIntyre and P.H. Tewari, WNRE, unpublished results.
18. N.S. McIntyre, WNRE, unpublished results.
19. M.W. Urie, N.F. Panayotou, and J.E. Robinson, Hanford Engineering Development Laboratory Report, (1980) HEDL-SA-2027
20. G. Bart, T. Aerne, U. Flukiger, and E. Sprunger, EIR (Switzerland) Report No. 390 (1980)
21. G.C. Allen, P.M. Tucker, and R.K. Wild, J. Nucl. Mater. (1978) 71, 345

22. H. Schneider, Mikrochimica Acta, (1979) Suppl. 8, 149.
23. N.S. McIntyre, S. Sunder, D.W. Shoesmith, and F.W. Stanchell, J. Vac. Sci. Technol. (1981) 18, 714.
24. S.P. Clough and T.R. Pinchback, J. Materials for Eng.Systs. (1979) 1, 55
25. E.H. Doremus in Treatise on Materials Science and Technology, (Academic Press, N.Y, 1979) Vol 17, M. Tornoza and R.H. Doremus, Eds.
26. C.D. Wagner, W.M. Riggs, L.E. Davis, J.F. Moulder, and G.E. Muilenburg, Handbook of X-Ray Photoelectron Spectroscopy, (1979) Perkin-Elmer Corporation, Eden Prairie, MN
27. G.A. Vernon, G. Stuckey, and T.A. Carlson, Inorganic Chemistry (1976), 15, 278.

RECEIVED April 5, 1982

# The Surface Chemistry of First-Wall Materials in Magnetic Fusion Devices

H. F. DYLLA

Princeton University, Plasma Physics Laboratory, Princeton, NJ 08544

The understanding of plasma-materials interactions in magnetic fusion devices has progressed over the last six years with the application of surface analytic techniques to in-situ experiments in tokamaks. A review is given of the surface studies of first-wall materials which have enabled optimization of surface conditioning techniques to minimize plasma impurity levels in presently operating devices. As the power and discharge duration are increased for the next generation of large D-T fueled plasma devices, thermal effects due to the increased power loading on first-wall structures become the dominant materials problem. Specifically, the development and testing of materials for the high heat-load structures and gettering system within the vacuum vessel of the Tokamak Fusion Test Reactor (TFTR) are described. These studies have produced data on the surface chemistry and vacuum behavior of a variety of technological materials (e.g., stainless steel, titanium, Inconel, graphite, refractory coatings, and bulk getters) that have wide application in many technologies, in addition to fusion reactor design.

This paper reviews the surface chemistry of the materials in use for first-wall structures in magnetic fusion devices. For the present generation of magnetic fusion devices, hydrogen-induced desorption and decomposition of first-wall surfaces are primarily responsible for the observed surface chemistry of first-wall materials. As the power and discharge duration increases for the next-generation of large D-T burning devices, the power-loading on first-wall surfaces will increase substantially. This progression will shift the emphasis of important plasma-wall interactions from hydrogen-induced surface chemistry to high-power thermal

0097-6156/82/0199-0367\$08.75/0

© 1982 American Chemical Society

In Industrial Applications of Surface Analysis; Casper, L., et al.;  
ACS Symposium Series; American Chemical Society: Washington, DC, 1982.



effects. This paper traces this progression from the observed surface chemistry of the primary first-wall materials (stainless steel, Inconel, and titanium) in the present-generation devices to the development of specialized materials for gettering systems and high heat-load structures in the next-generation devices. In the first section of the paper the relevant plasma-wall interactions are reviewed, followed by a description of the primary detrimental effect of plasma-wall interactions: the generation of plasma impurities. The next section reviews the surface chemistry, and in particular, the changes in surface chemistry affected by the various conditioning techniques that are applied in present generation devices. In the final section, the materials development necessary for the next-generation of D-T burning tokamaks is described.

### Survey of Plasma-Wall Interactions

The design of first-wall components in a magnetic fusion device involves the selection of materials for the vacuum vessel and all plasma-contacting hardware, and the specification of surface treatments for this hardware which minimizes the contamination of high temperature plasmas. The optimal design of first-wall hardware requires an understanding of the nature and severity of plasma-wall interactions (1) which result in impurity influx; these can include the processes of desorption (electron, ion, photon, and thermally-induced), sputtering, arcing, ablation, and evaporation. The expected flux of plasma particles incident upon a first-wall component represents a convenient classification parameter to categorize the materials problems. Figure 1 shows a diagram of a present-generation tokamak-type fusion device. In a typical device most of the inner surface area of the vacuum vessel will not be exposed to direct contact with the plasma and is thus classified as a low-flux surface. Those surfaces specifically designed to intercept plasma, either for the purpose of defining the plasma boundary or for affecting the plasma boundary by removing power or particles from the plasma-edge (such as a neutralizer plate or limiter), can be classified as high-flux surfaces. In the present generation of devices, the distinction between the two types of surfaces is quite evident, although there may exist some fraction of the vacuum vessel surface area or separate, interposed plasma liner that is subjected to a locally higher flux, such as those areas directly behind a localized limiter or within line-of-sight of high power neutral beam injectors. With the next generation of large tokamaks (TFTR, JET, JT-60), the distinction between high-flux and low-flux surfaces blurs as a larger fraction of the internal surface area is devoted to hardware to handle the increased power-loading.

In addition to a spatial variation, the expected plasma flux and consequent plasma-wall interactions on first-wall components

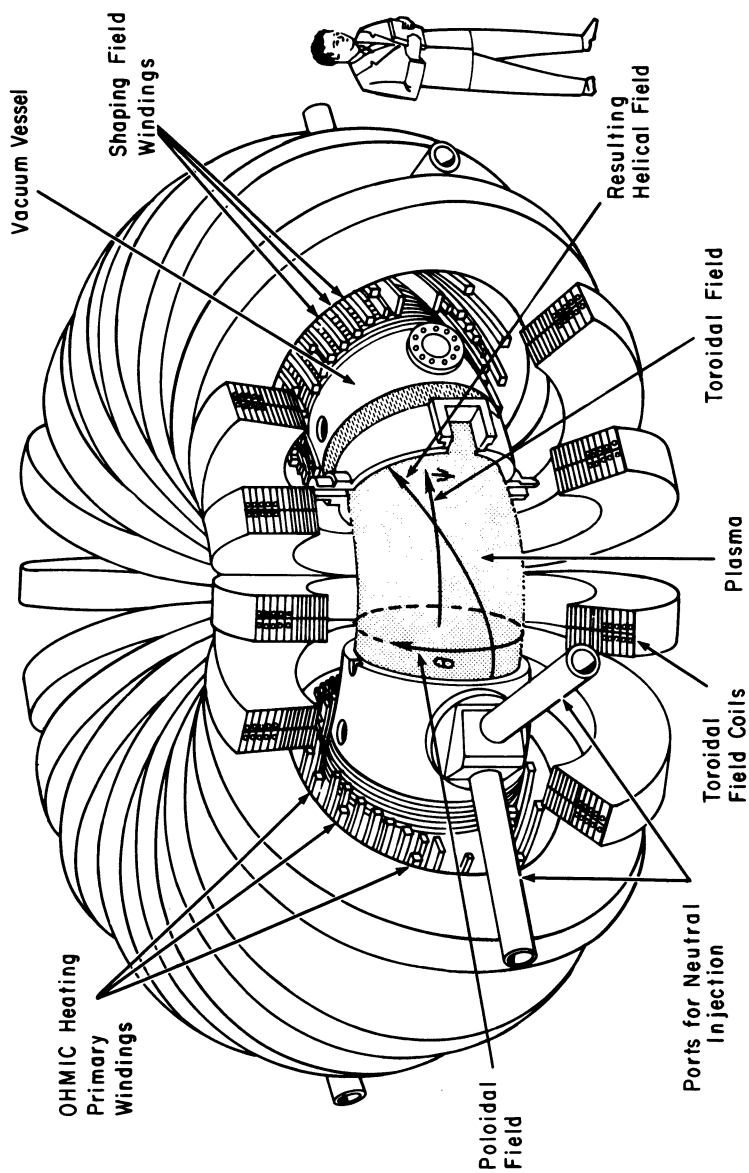


*Figure 1. Diagram of a Tokamak-type fusion device showing the major structural components.*

have a temporal variation dependent on the evolution of the plasma discharge. During the start-up or initiation phase of a tokamak discharge, plasma confinement and positioning is poor thus subjecting much of the internal surface area to bombardment by low energy ( $kT = 2-50$  eV) plasma particles. Desorption of loosely-bound adsorbates by ion, neutral, and electron impact is a dominant process during this phase. The desorbed species are hydrogenic atoms or the primary low Z surface contaminants: O, C, and to lesser extent Cl, S, and N. The source of these species is obvious; any of the typically-applied vacuum vessel conditioning procedures cannot remove all desorbable species from a large device, and the pulsed nature of the present generation of devices allows time for recontamination of surfaces between discharge cycles.

Time-resolved studies with probes (2) and motion-picture studies of tokamak discharges (3) have shown that unipolar arcing is also an important process during the start-up phase. The arcing can be driven by transient high fluxes incident on unconditioned surfaces during the poorly confined state of the discharge start-up, or they can be driven by the large ( $\sim 100$  V) vacuum vessel potentials developed by the plasma current transformer to ionize the fill-gas for initiation of the discharge.

It is unclear from present spectroscopic and surface-probe evidence of impurity flux measurements whether or not the threshold energy for sputtering processes is exceeded during the start-up phase (2,4). During the start-up phase, the plasma current distribution is established and basic plasma confinement is achieved. The plasma density can rise depending on the gas input and density limit imposed by a variety of conditions (5) (among them plasma current, magnetic field, and plasma impurity levels), and the plasma temperature and confinement will rise with the density. If no additional energy is introduced into the plasma other than through the plasma current transformer, steady-state or quiescent conditions can be established depending only on the stability of control systems for the plasma current, position, and density. With only ohmic heating of the plasma from the current transformer, plasma ion and electron temperatures reach  $kT_0 \approx 1$  keV at the center of the discharge for a pure hydrogenic discharge. Measured spatial profiles of plasma temperatures during the quiescent phase show distributions  $T(r)$  which vary from parabolic  $T_0(1 - r^2/r_a^2)$  to fairly flat profiles (where  $r_a$  is the plasma minor radius). There is less experimental data on the important boundary layer within the vicinity of the plasma limiter or a divertor neutralizer plate, but the existing measurements (6-10) show plasma ion temperatures of the order of 50 eV at the limiter scrape-off (or divertor separatrix), with decay lengths of the order of (1-2 cm) for the plasma temperature and density within the boundary plasma.

With the above background information, the important plasma-wall interactions during the quiescent phase can be defined: desorption and unipolar arcing are expected to be only transient processes occurring on unconditioned surfaces. With proper conditioning, and after the discharge initiation phase, sputtering effects should dominate. Charge-exchange sputtering can affect all first-wall components with line-of-sight (or first-bounce line-of-sight) to the plasma. In a tenuous plasma, the higher energy charge-exchange particles born at the center of the discharge can reach the wall unattenuated. However, as the plasma density is raised to the levels desired for reactor operation ( $\geq 10^{14} \text{ cm}^{-3}$ ), the charge-exchange flux arising at the first-wall is dominated by particles born in the outer (cooler) region of the plasma. Typical measured charge-exchange neutral fluxes for medium density, ohmically-heated discharges (4,12) are in the range of  $10^{14} \text{ cm}^{-2} \text{ s}^{-1}$  with average particle energies of 100-200 eV.

Ion sputtering dominates on those surfaces which intercept magnetic field lines (limiters and neutralizer plates). Ion sputtering effects will be localized depending on the magnetic field geometry and on the rather short decay lengths (1-2 cm) of the plasma parameters within a boundary plasma. An important difference between charge-exchange neutral and ion sputtering is the presence of the electrostatic sheath which envelops any surface bounding a plasma, and affects incident charged-particle energies and trajectories. Insufficient data are available from surface probe measurements to elucidate the effect of sheath formation on hydrogenic ion sputtering; however, in the case of multiply-charged impurity ions which are known to exist in the edge-plasma (13,14,15) (CIII, OII, etc.), any reasonable edge potential is sufficient to accelerate these ions to energies substantially above sputtering thresholds.

For a well-behaved, ohmically-heated discharge, (i.e., no pathogenic magnetohydrodynamic behavior), in a tokamak with properly-sized limiters or neutralizer plates, particle fluxes during the quiescent phase to the latter surfaces are below the level where mass transport by evaporation is significant. As both the total energy and energy density rise with auxiliary heating of tokamak plasmas, thermal effects in first-wall hardware become more important. Auxiliary heating is necessary to raise the central plasma temperature from the ohmic-heating plateau of  $kT \approx 1 \text{ keV}$  to the level required for reactor operation of  $kT \approx 10 \text{ keV}$ . The auxiliary heating schemes presently under development involve either the injection of high power neutral beams or radio frequency waves at various resonant frequencies. With either heating scheme, increased sputtering of all first-wall components is expected as the average temperature of the plasma rises, and increased thermal effects (enhanced desorption and evaporation) are expected on all high flux surfaces as the energy density of

the plasma rises. In addition, there are localized plasma-wall interactions that are indigenous to a particular heating scheme: 1) with neutral beam heating, higher thermal loads ( $> 1 \text{ kw/cm}^2$ ) can be incident on surfaces directly behind injection ports in the case of injection into tenuous plasmas (16); 2) with RF heating the antennae structures designed for launching RF waves into the plasma suffer arcing problems due to the high electric fields across the structure (17). The solution to the neutral beam "shine-through" problem involves the development of vacuum vessel protective plates specifically designed for high flux hydrogenic loading. The design constraints for such a first-wall element include the ability to withstand and conduct high heat loads, and minimal erosion under the expected incident plasma and particle fluxes. The materials problems affecting the design of RF antennae structures have only recently been addressed in several studies (18,19) where specific low secondary-electron emission coatings were developed to increase the resistance to arc formation.

#### Plasma Impurity Effects

Much of the concern for understanding and controlling plasma-wall interactions in magnetic fusion devices is related to the control of impurities in high temperature plasmas. Eventual important concerns of magnetic fusion reactor technology are those processes which will affect the structural integrity of the first-wall: net erosion (20) and bulk neutron and alpha particle radiation damage (21). However, the first-order concern for the present and TFTR-generation devices is the control of impurities that are introduced by plasma-wall interactions.

Impurities (i.e., all species except hydrogenic ions and helium) can affect many aspects of plasma behavior and, indeed, considerable experimental and theoretical effort has been expended on studies of impurity effects and impurity transport. The most serious effect of impurities is radiation loss due to line-radiation and Bremstrahlung of the partially or fully electron-stripped impurity ions (22). Depending on the atomic charge ( $Z$ ) of the impurity ion and the average temperature of the plasma, relatively small impurity concentrations can dominate the energy transport of the plasma and ultimately prevent the attainment of ignition conditions in high temperature D-T plasmas. Figure 2 shows the maximum allowed impurity concentration of several common impurity elements as a function of plasma temperature. It is evident from Figure 2 that tolerable impurity concentrations of low  $Z$  elements like O are  $\leq 10^{-2}$ , whereas for the constituent metals of stainless steel (e.g., Fe), the concentration should be  $\leq 10^{-3}$ . The tolerable concentrations of higher  $Z$  elements like W are so low ( $\leq 10^{-4}$ ) that use of such materials is impractical for most first-wall applications. In addition to radiation losses,

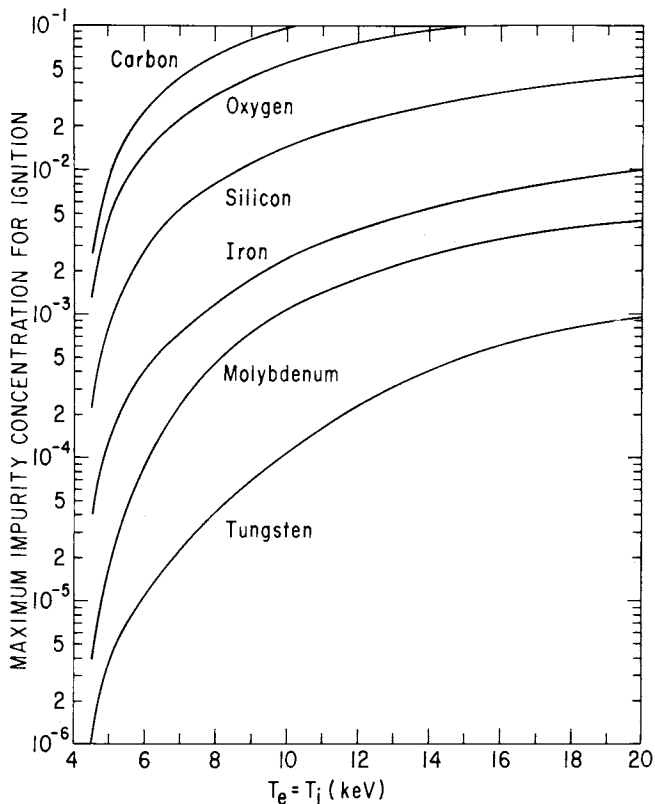


Figure 2. Maximum allowed impurity concentration for ignition of D-T plasma as a function of plasma temperature assuming radiative losses only. (Reproduced, with permission, from Ref. 22. Copyright 1978, American Nuclear Society.)

impurities can: 1) affect particle transport by modifying the plasma current profile and magnetohydrodynamic activity; 2) affect the efficiency of auxiliary heating by modifying the absorption of neutral beam or RF energy; and 3) lower the plasma reactivity by diluting the hydrogenic ion concentration. Not all the effects of impurities are deleterious to plasma performance. It has been demonstrated (23) that the radiation caused by moderate concentrations (~ 0.5-1.0%) of low Z impurities is useful for cooling the edge plasma. This technique decreases the power-loading on limiter surfaces by radiation of power over the entire plasma surface area.

### Conditioning Studies

Comparison of Techniques. A figure-of-merit for the impurity concentration that exists in a plasma is a parameter based on the classical resistivity of the plasma (24), the "effective Z":

$$Z_{\text{eff}} = \sum_i \frac{n_i Z_i^2}{n_e}$$

where  $n_i$  is the concentration of the  $i^{\text{th}}$  ion species and  $n_e$  is the electron concentration (density). Thus, for a pure hydrogenic plasma  $Z_{\text{eff}} = 1$ .

Previous to 1976 most tokamaks operated with consistently high  $Z_{\text{eff}}$  (> 5) plasmas, primarily attributed to oxygen contamination due to ineffective conditioning of first-wall surfaces. Over the period 1975-1980, a basic understanding of the first-wall problem related to low Z contaminants has been achieved and various conditioning procedures have been developed which effectively eliminate the problem. This work is based on the application of surface analysis and residual gas analysis techniques to studies in a variety of tokamaks: ALCATOR (25), PULSATOR (26), ORMAK (27), TFR (28, 29), PLT (30), MACROTOR (31) JFT-2 (32), ISX (33), PDX (34, 35) and ASDEX (36). A review of the subject has been published by the author (37). The net result of these studies is that all operating tokamaks have achieved low  $Z_{\text{eff}}$  (1-2) operation with several primary first-wall materials (stainless steel, Inconel, titanium) after proper wall-conditioning.

The conditioning techniques which have been applied to first-wall materials, either as pre-treatment procedures previous to installation of the material in the device or as in-situ treatments applied within the completed device, include one or more of the following: 1) a chemical or physical surface pretreatment; 2) vacuum baking at moderate (100-250 C) to high-temperatures (> 500 C); 3) discharge cleaning; and 4) deposition of a coating with specific properties (such as a gettering or

passivation material). The most successful techniques have involved a chemical pretreatment applied for removal of the macroscopic surface contamination, (e.g., particulates and hydrocarbon films) followed by a combination in-situ treatment of vacuum baking and discharge cleaning, or discharge cleaning and titanium gettering.

It is worthwhile to consider the effect of each of these conditioning procedures on the surface chemistry of the commonly used first-wall materials. The chemical pretreatments which have been applied involve the use of solvent and/or alkaline washes. The physical pretreatments applied usually involve an abrasive removal or modification of the surface layer (e.g., sanding, polishing, and glass-bead honing). The benefit of pretreatment procedures is the removal of the macroscopic surface contamination that results from the manufacture, machining and handling of the material. For example, excessive surface oxide layers can be removed by acid etching, or abrasive treatments; and hydrocarbon contamination due to machining operation and handling can be minimized by a number of successful chemical-degreasing procedures. None of these techniques results in complete removal of the oxide layer on structural material. Upon subsequent exposure of stainless steels, Inconels, and titanium to air, a minimal (30-100 Å) passivation oxide layer will form at ambient (300 K, 760 Torr) conditions (37, 38). On top of the passivation layer, exposure to atmosphere will result in multilayer absorption of H<sub>2</sub>O and simple hydrocarbons (39). Some pretreatment procedures (e.g., electropolishing) can reduce the effective surface area of a material, (typically by a factor of two). The result of any of these pretreatment procedures is insufficient for these techniques to serve as stand-alone conditioning for first-wall materials. Further in-situ conditioning is required in order to prevent excessive low Z contamination of plasmas.

One commonly applied in-situ treatment is vacuum-baking of the complete vacuum vessel. The baking of vacuum vessels to moderate temperatures (150-350 C) is a standard technique for the achievement of ultra-high vacuum conditions by reducing the intrinsic outgassing rates of the vessel materials. The dominant residual gas in a vacuum system previous to baking is H<sub>2</sub>O. H<sub>2</sub>O outgassing is most affected by moderate baking, which removes H<sub>2</sub>O that is adsorbed on and absorbed in the passivation oxide layer. The outgassing of other residual gases, H<sub>2</sub>, CH<sub>4</sub>, CO, and CO<sub>2</sub>, is also reduced and, in situations requiring the lowest obtainable pressure with minimal pumping speed, a pre-bake at high temperature (400-600 C) is applied to all vessel components to minimize the bulk inventory of dissolved gases. Baking at such temperatures will not produce a surface free of carbon or oxygen, nor will it produce a surface suitable for first-wall materials. Baking will reduce the equilibrium vapor pressure of residual gas species such that the thermal outgassing of these species is a



negligible source of plasma contamination, but it will not significantly reduce the particle desorption coefficients which are a more significant source of plasma contamination from first-wall materials. Baking at moderate temperatures will not reduce the surface oxides on the commonly used technical materials because of their stability against thermal decomposition (see Figure 8), nor is there a mechanism for significant removal of surface carbon. For temperatures up to 800 C, adsorbed hydrocarbon will pyrolyze; some carbon will desorb as CO, CO<sub>2</sub>, and CH<sub>4</sub>, but in the absence of a supply of O or H, the primary decomposition product is adsorbed carbon. This surface carbon will disappear under vacuum conditions only when sufficiently high temperatures are reached ( $\geq 800$  C) that diffusion into the bulk metal is significant. This would be an impractical procedure to apply to fusion devices because of the large size and mechanical complexity of the vacuum vessels.

A conditioning method which is very effective for reducing particle desorption coefficients without resorting to high temperature bake-out is discharge cleaning (1, 31, 37). The method, as generally defined, is the application of a pulsed or dc discharge within the device vacuum vessel, with the discharge conditions specifically tailored to clean exposed material surfaces by particle bombardment. The cleaning mechanism can be purely physical sputtering if a rare gas is employed as the discharge gas, or chemical effects can be exploited, if a chemically active gas is used. Over the last three decades of experience with magnetic fusion devices, numerous discharge cleaning "recipes" have been invented which include variations in the discharge gas mixture, discharge parameters and wall conditions. With the relatively recent (since 1975) studies specific to discharge cleaning, the methodology has been reduced to two techniques, both using pure hydrogen as the discharge gas. One technique (31) uses the plasma current transformer circuit to produce a rapid ( $\sim 1$  pps) series of low-current discharges in a relatively high H<sub>2</sub> pressure ( $1-2 \times 10^{-4}$  Torr). The second technique (34) employs one or more separate electrodes which are introduced into the vacuum vessel to serve as anodes for a glow discharge. All first-wall components which are to be cleaned are electrically grounded and, thus, as the cathode in the discharge, are subjected to hydrogen ion bombardment. For both the pulse discharge cleaning (PDC) and the glow discharge cleaning (GDC) method, the discharge conditions (usually the current and pressure) are adjusted to maximize the production of residual gases (usually H<sub>2</sub>O and CH<sub>4</sub>) that can be removed from the device through the vacuum pumping system. The experimental evidence indicates that the cleaning mechanism is the same for both techniques: the removal of surface carbon and the partial reduction of oxides in the near-surface region by low energy hydrogen ion bombardment. Since surface chemical reactivity is

crucial,  $H_2$  discharge cleaning is quite sensitive to the temperature of the bombarded material. Simultaneous  $H_2$  discharge cleaning and vessel-bakeout at moderate temperatures ( $150^{\circ}$ - $350^{\circ}C$ ) has proven to be a very effective tokamak conditioning procedure. Particle induced desorption rates and the surface concentration of "accessible" C and O can be reduced within a device to the extent that low Z contamination of resulting high temperature plasmas is negligible.

Surface Chemistry of Discharge Cleaning. The results of recent studies of hydrogen discharge cleaning have generated a reasonable understanding of the surface chemistry involved with this conditioning technique. The rationale for these studies was the need to develop effective conditioning procedures for the large tokamaks which are presently operating or nearing completion, such as PDX, ASDEX, JET, JT-60, and TFTR. The glow discharge cleaning technique has been used to condition the large divertor tokamaks PDX (34), and ASDEX (36); both vacuum vessels contain complicated internal hardware. Figure 3 shows the time-dependence of the primary residual gases produced during  $H_2$  glow discharge conditioning of the  $38\text{ m}^3$  stainless steel vacuum vessel of the PDX tokamak (34, 37). The initial partial pressures of  $CH_4$ , CO, and  $C_2H_4$ , shown in Figure 3a correspond to an impurity removal rate of  $\sim 10^{19}$  molecules  $s^{-1}$  when multiplied by the vacuum system pumping speeds. This rate subsequently decays as  $1/t$ ; however, after 100 hours of discharge cleaning approximately 100 equivalent monolayers of carbon and oxygen have been removed from the vessel as estimated from the integral of the curve in Figure 3a averaged over the internal surface area ( $200\text{ m}^2$ ). At two specific times during the conditioning period shown in Figure 3a, the discharge was turned off and the vessel was vented to atmospheric pressure for several hours. Recovery of the vacuum vessel to pre-existent surface conditions occurs in a relatively short time following continuation of the glow discharge process, as shown in the expansion of the residual gas curve in Figure 3b. Such a brief exposure to atmosphere appears to saturate only the first monolayer of the vessel surface: the integral of the exponential portion of the curve in Figure 3b represents  $\approx 2 \times 10^{15}$  carbon atoms/ $cm^2$ . The total cross section,  $q$ , for the hydrogen-ion-induced removal process can be estimated from the observed time constant ( $\tau_0 = 26\text{ min}$ ) and the hydrogen ion flux ( $\Gamma \approx 10^{13}\text{ cm}^{-2}\text{ s}^{-1}$ ):

$$q = \frac{1}{\Gamma\tau_0} \approx 5 \times 10^{-17}\text{ cm}^2 \quad (1)$$

yielding a value which is consistent with ion-induced desorption cross sections measured for simple adsorbate molecules on stainless steel surfaces (40, 41).

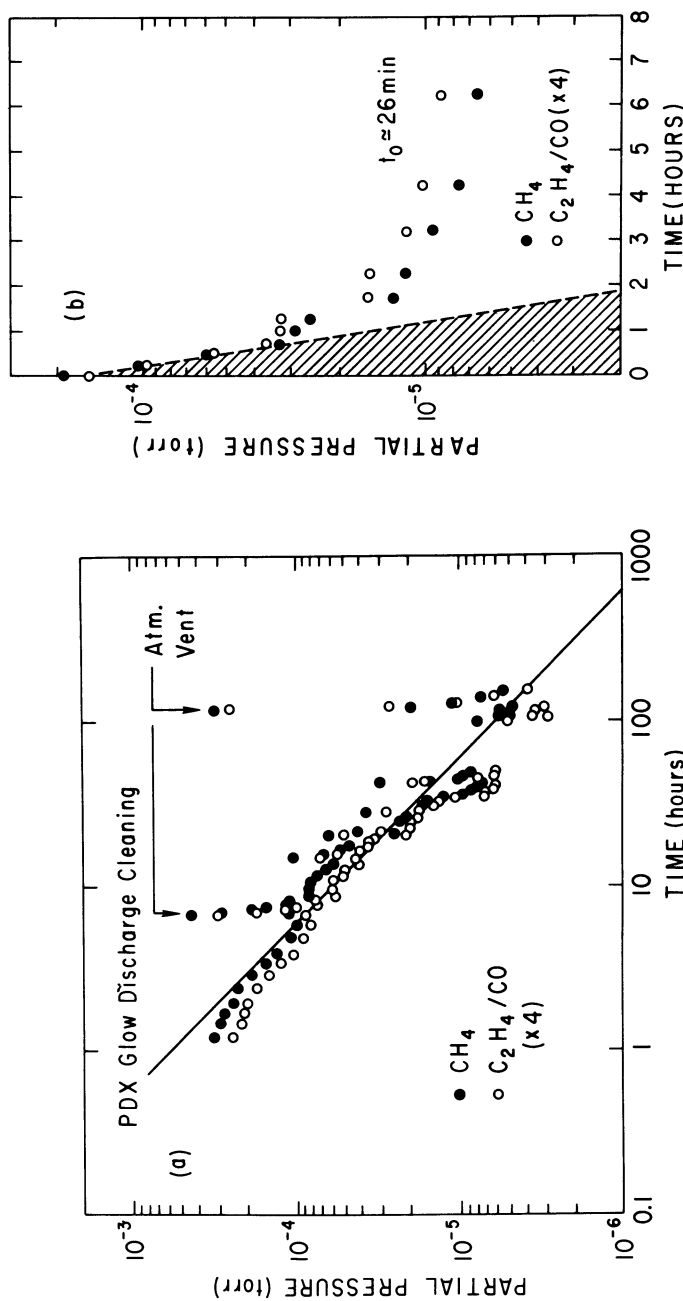


Figure 3. Partial pressures of the residual gases  $\text{CH}_4$  (16 amu) and  $\text{CO}/\text{C}_2\text{H}_4$  (28 amu) (a) produced during  $\text{H}_2$  glow discharge conditioning (GDC) of the PDX vessel. At the indicated arrows, the torus was exposed to atmospheric pressure for several hours. Residual gas production (b) during GDC immediately after atmospheric exposure. (Reproduced, with permission, from Ref. 37. Copyright 1980, North-Holland Publishing Co.)

While residual gas measurements are useful for optimizing discharge cleaning processes, concomitant surface analysis measurements have been necessary to elucidate the mechanisms involved in the surface chemistry. A number of *in-situ* surface studies (26-30, 32-35) have been performed on tokamaks where sample wall materials were exposed to discharge cleaning and transported under vacuum to multi-technique analysis chambers.

A schematic diagram of the surface analysis diagnostic (42) used to characterize wall conditioning processes in the PDX tokamak is shown in Figure 4. This diagnostic contains a 6 m long, 1 cm wide, stainless steel tape-loop which serves as the sample directly, or as a substrate for evaporated coatings of other materials. In operation, a portion of the tape surface is exposed to discharge cleaning (or any conditioning procedure) within the tokamak vacuum vessel. Following exposure, the exposed portion of tape is transported to the analysis chamber where the techniques of Auger electron spectroscopy (AES), x-ray photoelectron spectroscopy (XPS), and secondary ion mass spectroscopy (SIMS) are used to characterize the surface of the sample.

Data gathered from surface analysis on PDX (and from similar diagnostics on other devices) (26-33) have indicated interesting differences between the carbon and oxygen chemistry which occur on technological metals under low-energy hydrogenic bombardment. Figure 5 shows AES measurements of the change in elemental composition of the surface of stainless steel and Inconel samples as a function of exposure to H<sub>2</sub> discharge cleaning (37, 43). Both samples are initially covered with the usual carbonaceous contamination that is characteristic of little or no surface-pretreatment. Discharge cleaning effectively removes the layer, reducing the surface carbon concentrations to  $\approx 30$  at.%, with exposure times of the order of an hour. The initial rate of carbon removal is  $\approx 3 \times 10^{12}$  C atoms cm<sup>-2</sup> s<sup>-1</sup>; whereas, only after exposure of the underlying passivation oxide layer (after 1 hour) is there a noticeable rate of oxygen removal of  $\approx 3 \times 10^{10}$  atoms cm<sup>-1</sup> s<sup>-1</sup>.

Analysis by XPS and SIMS techniques of stainless steel samples exposed to H<sub>2</sub> discharge cleaning (35, 44) has provided insight into the processes involved in the reduction of the oxide layer. The evidence indicates that only a partial reduction of the oxide layer occurs during hydrogen discharge cleaning and the remainder is stable under low-energy hydrogen bombardment. Figure 6 shows XPS spectra of the Fe and Cr 2p<sub>3/2</sub> photoelectron emission from a stainless steel sample. The top spectra (6a, d) show the characteristic mixed oxides of untreated stainless steel: two oxidation states of Fe (FeO and Fe<sub>2</sub>O<sub>3</sub>) and Cr (CrO and Cr<sub>2</sub>O<sub>3</sub>), with no reduced metallic state visible in the near-surface region. After exposure of the sample to H<sub>2</sub> glow discharge cleaning (Figure 6b, e), the Fe<sup>III</sup> state disappears, leaving a

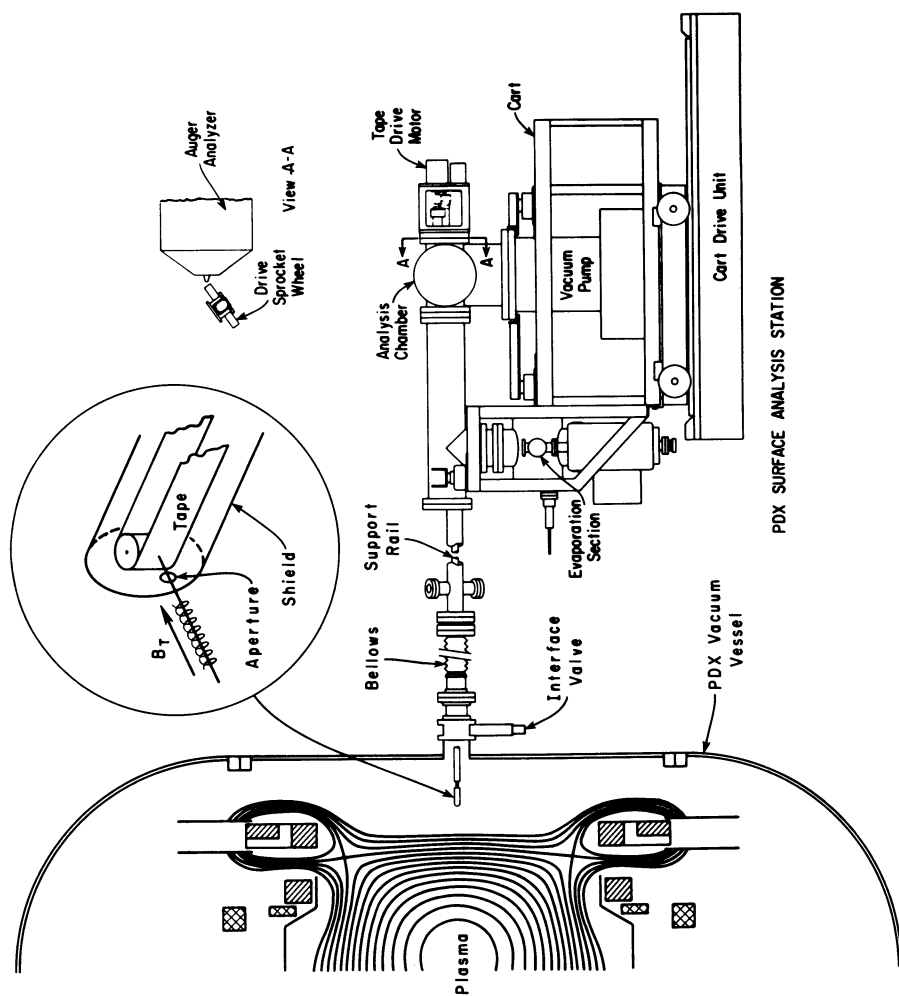


Figure 4. Scheme of the surface analysis diagnostic for materials studies on PDX Tokamak. (Reproduced, with permission, from Ref. 42. Copyright 1980, American Institute of Physics.)

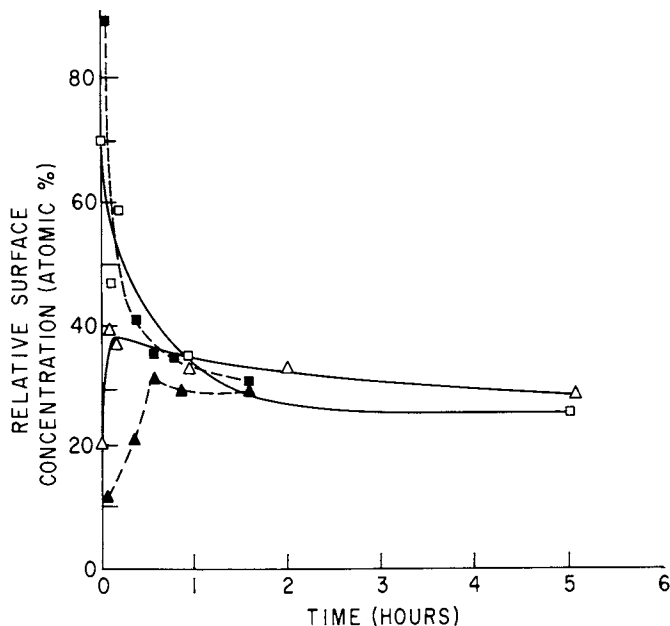


Figure 5. Observed change in the elemental surface composition of hydrocarbon-covered 304 stainless steel and Inconel as a function of exposure to hydrogen discharge cleaning. The stainless steel sample was exposed to glow discharge cleaning in the PDX Tokamak (Ref. 37) and the Inconel sample was exposed to pulse discharge cleaning in the TFR Tokamak. Key: □, C SS substrate; △, O SS substrate; ■, C Inconel substrate; and ▲, O Inconel substrate. (Reproduced, with permission, from Ref. 43. Copyright, 1981, NHPC.)

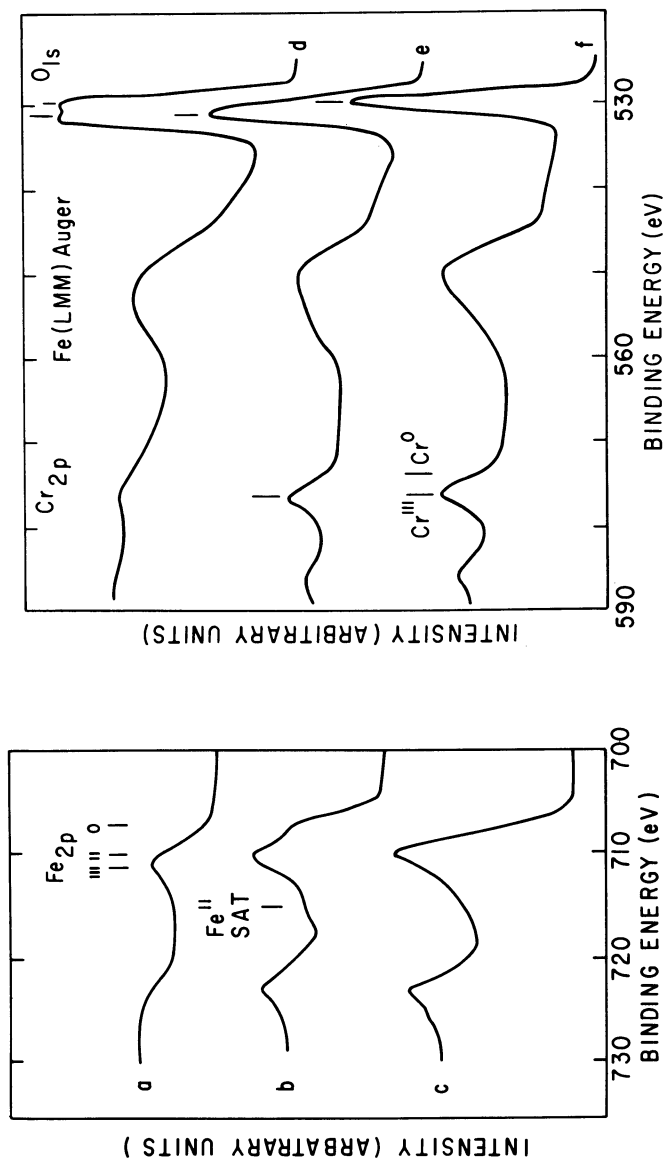


Figure 6. X-ray photoelectron spectra of type 304 stainless steel. Key: (a,d) initial surface; (b,e) after exposure to  $H_2$  glow discharge cleaning; and (c,f) after  $A^+$  ion bombardment. (Reproduced, with permission, from Ref. 35. Copyright 1980, American Institute of Physics.)

strong Fe<sup>II</sup> state with a well-developed satellite, and reduced Fe<sup>0</sup> is observed; however, no change is observed in the Cr 2p<sub>3/2</sub> line (except for increased intensity due to removal of the overlying carbon layer) and, in contrast to Fe, no metallic Cr<sup>0</sup> is observed. After exposure to the H<sub>2</sub> glow discharge the appearance of Fe<sup>0</sup> in the XPS spectra is a result of H-induced reduction of the Fe-oxides and not the detection of bulk Fe<sup>0</sup> below the oxide layer, nor the result of differential sputtering of the oxide. This conclusion is based on the bottom spectra in (Figure 6e, f) which were observed after gentle A<sup>+</sup> ion bombardment of a stainless steel surface at a fluence of 6 x 10<sup>-4</sup> C cm<sup>-2</sup>. This dose is sufficient to remove only the carbon contamination layer and not remove the oxide layer, (approximately a 10<sup>-</sup> larger dose would be required to completely sputter the oxide layer). After A<sup>+</sup> sputtering no metallic Fe<sup>0</sup> is observed (although a conversion of Fe<sup>III</sup> to Fe<sup>II</sup> is seen).

Additional information on the nature of the reduction reaction is available in the O1s photoelectron spectra and SIMS spectra of the steel surface. The unexposed surface shows a two-component O1s line (Figure 6d). The lower binding-energy peak (at 529.8 eV) is attributed to the metal-oxide and the higher energy peak (at 531.5 eV) is attributed to the hydroxide (45, 46). After exposure to the H<sub>2</sub> glow discharge, the O1s line consists only of the hydroxide line (Figure 6e), whereas after A<sup>+</sup> sputtering (Figure 6f) only the oxide component is visible. Secondary ion spectra of the exposed stainless steel show enhancement of the molecular ions FeOH and CrOH following glow discharge exposure (Figure 7).

The appearance of the FeOH in the XPS and SIMS spectra supports a reaction mechanism for H<sub>2</sub>O formation from stainless steel surfaces exposed to low-energy hydrogen proposed by Dietz, et al. (47): the hydrolysis of the metal oxide,



and the subsequent reduction of the hydroxide to a free metal with the liberation of H<sub>2</sub>O,



Assuming quasi-equilibrium for the forward and the reverse reactions of Eq. (2) the rate equation for reaction of Eq. (3) can be written as:

$$\frac{d}{dt} P(\text{H}_2\text{O}) = k [\text{MO}] [\text{H}]^2 \quad (4)$$

where [MO] and [H] represent the concentration of metal-oxide and hydrogen in the near surface region.

The temperature dependence of Eq. (4), the production of H<sub>2</sub>O from



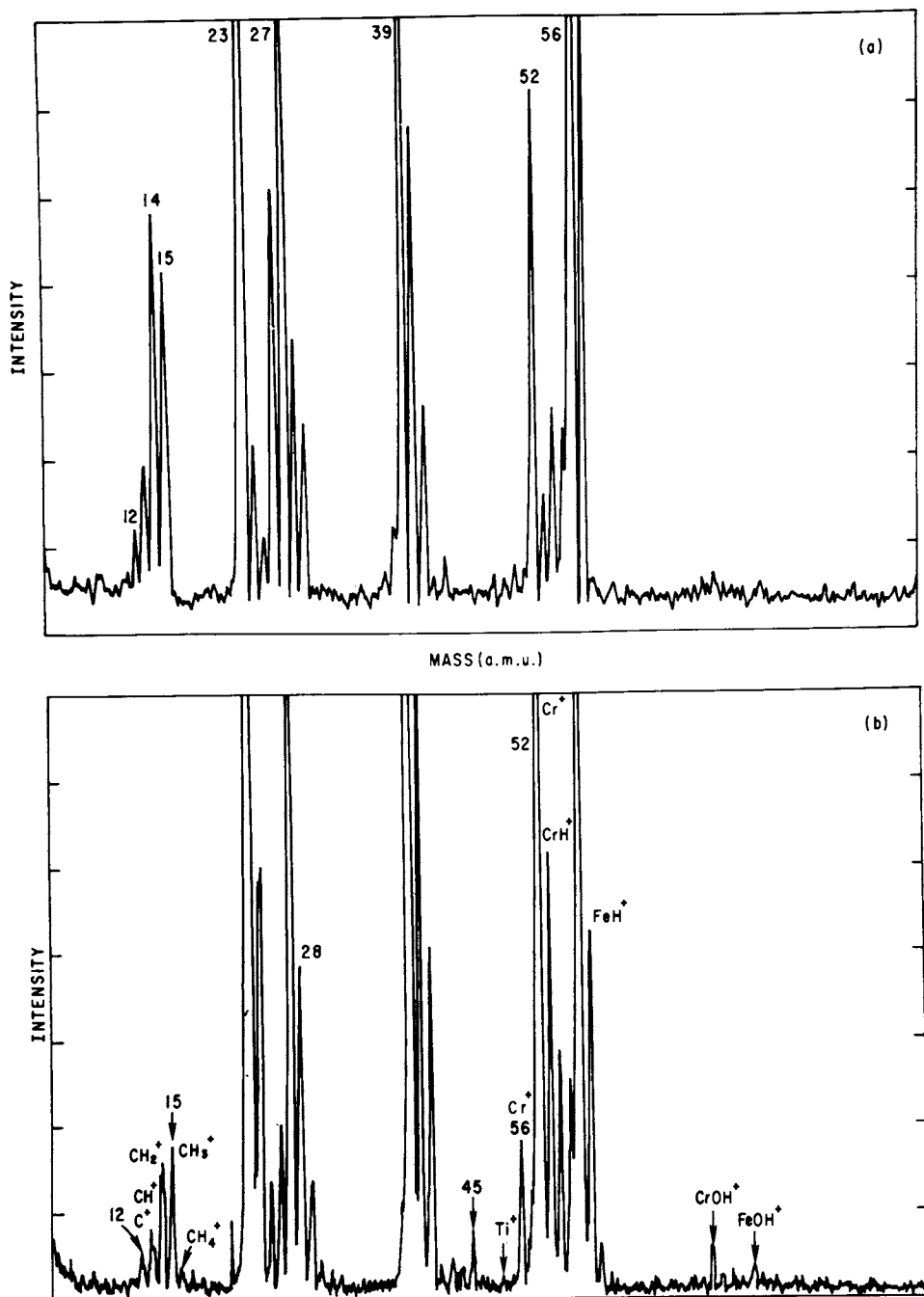


Figure 7. Secondary ion mass spectra of type 304 before (a) and after (b) exposure to  $H_2$  discharge cleaning. (Reproduced, with permission from Ref. 44. Copyright 1980, NHPC.)

stainless steel bombarded with low-energy (0.2 eV)  $H^0$ , has been measured by Dietz, et al. (48, 49). The reaction rate was found to increase by almost two orders of magnitude as the steel temperature was raised from ambient to 350 C. The reaction rate saturates at 350 C which is consistent with the recombinative release of surface hydrogen being the rate-limiting step. The result of this experiment has an important implication to wall conditioning by  $H_2$  discharge cleaning: there is a distinct advantage for discharge cleaning at moderate wall temperatures (150-350 C) where the  $H_2O$  production rate is enhanced. The presence of surface carbon will enhance the probability of other surface reactions generating volatile oxidation products (such as CO and  $CO_2$ ) that will compete with the reaction in Eq. (3). In fact, the carbon oxides are generally present at roughly the same concentration as  $H_2O$  in the discharge effluent of devices that are discharge cleaned with vacuum vessels at room temperature (36, 50).

The rate constants,  $k$ , of Eq. (4) for the reduction of metal oxides of interest to fusion device wall materials ( $FeO$ ,  $Cr_2O_3$ ,  $TiO$ , etc.) have not been measured. However, the equilibrium constants,  $K_p = p(H_2O)/p(H_2)$ , for the reduction of these oxides with molecular hydrogen are derived from the measured standard free energies ( $\Delta G^0 = -kT \ln K_p$ ) of the oxides (51). The temperature dependence of  $K_p$  for several metal oxides with respect to reduction by hydrogen, shown in Figure 8, is consistent with XPS results described previously:  $FeO$  was reduced by the glow discharge treatment but  $Cr_2O_3$  was stable. Moreover, no reduction of the most stable oxides ( $TiO$  and  $Al_2O_3$ ) has been seen for similar low energy hydrogen exposures.

### Coating Technologies

Gettering Materials. An alternative to in-situ discharge cleaning as a conditioning technique is the deposition of coatings with specific surface properties on first-wall structures. A commonly applied coating technique in tokamaks is the sublimation of titanium onto all or a fraction of the vacuum vessel surface area (37, 52). The use of titanium coatings in such a manner has beneficial effects on the operation of tokamaks that can be related to two basic properties of freshly-evaporated Ti films: the ability to getter oxygen and hydrogen, and the stability of the resulting titanium oxide and hydride. Much of the improvement noted in tokamak plasma performance after the use of titanium gettering can be traced to a significant drop in the plasma concentration of oxygen (typically by more than a factor of two). This result is consistent with the surface chemistry presented in the previous section: the titanium oxides, which are formed as the Ti-coating chemisorbs oxygen emitted from the plasma, are more stable with respect to hydrogen reduction than

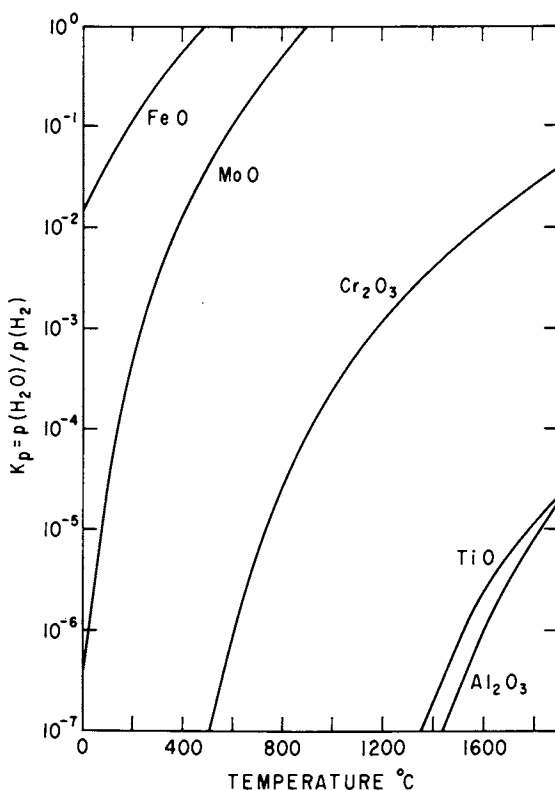


Figure 8. Temperature dependence of the equilibrium constant,  $K_p = \frac{p(\text{H}_2\text{O})}{p(\text{H}_2)}$  for the reduction of several metal oxides often present in Tokamak walls. The  $K_p$  values are calculated from thermochemical data listed in Ref. 51. The reduction curve for NiO, the most prevalent metal oxide on Inconel alloys, lies above the FeO curve, and thus is more easily reduced in hydrogen than the oxides shown. (Reproduced, with permission, from Ref. 37. Copyright 1980, North-Holland Publishing Co.)

the FeO, Cr<sub>2</sub>O<sub>3</sub> oxides on the underlying stainless steel vessel wall (or NiO and Cr<sub>2</sub>O<sub>3</sub> on an Inconel vessel wall). In addition, a Ti coating can minimize the hydrogen-induced decomposition of the underlying metal oxides by two mechanisms. If the deposited Ti layer is thick compared to the implantation range of plasma particles, the layer will shield the underlying oxide from decomposition. Alternatively, a thin Ti layer may reduce the metal oxidation rate by decreasing the hydrogen concentration in the oxide by accelerating the hydrogen atom recombination rate (48).

The hydrogen gettering properties of evaporated titanium also have a beneficial effect on the performance of magnetic fusion devices. Because of the high diffusivity and low retention of hydrogen isotopes in stainless steel and Inconel-type alloys (53), a substantial fraction of the implanted hydrogen flux will be re-emitted, "recycled" (54). The use of titanium (or any hydride-forming metal) on the first-wall can substantially reduce the recycled hydrogen. The control of recycling hydrogen isotopes is an essential requirement for the success of auxiliary plasma heating schemes such as neutral beam injection and RF resonance heating techniques. Both heating schemes require control of the plasma density to optimize the power input. Control of the plasma density is difficult when the wall-averaged recycling coefficient (the ratio of recycled-to-incident particle flux) approaches or exceeds a value of unity. In this case the plasma density can rise rapidly without input from the gas injection system because of the increased efficiency of ion-induced desorption processes.

The hydrogen-isotope retention and recycling properties of first-wall materials are also the determinant of the isotopic ratio in a multi-component plasma. Maximization of the reactivity of D-T plasmas (16) and the efficiency of minority-specie RF heating schemes require precise control of the isotopic mixtures, a task which is considerably easier in low recycling situations. Titanium sublimation over 20-40% of the vacuum vessel of the PLT tokamak was sufficient for density and isotopic mixture control for both the high power neutral beam (55) and ion cyclotron resonance heating experiments (56), which have generated record ion temperatures for these heating techniques. Notwithstanding the practical success of titanium gettering for tokamak operation, the recycling process is poorly understood in detail because it depends on the hydrogen emission spectrum of the plasma and the hydrogen retention characteristics of the first-wall materials; both properties are poorly characterized in actual fusion devices and difficult to simulate in laboratory tests.

For the next generation of D-T tokamaks (JET and TFTR), titanium gettering cannot be used as a wall conditioning or a density control technique because of the problems of hydrogen embrittlement and tritium-inventory control. The present plans for the JET device call for the use of high-temperature first-wall

components (400-600 C) for the control of plasma impurities and hydrogen recycling (57). For TFTR an active gettering system (16) is under development that is based on the use of an array of Zr-Al alloy, non-evaporative getters that are distributed along the top and bottom of the vacuum vessel (Figure 9). The Zr-Al getters absorb hydrogen isotopes reversibly and impurities (oxygen and carbon) irreversibly (58). By in-situ heating of the getter material to 700 C, the absorbed hydrogen isotopes desorb and can be removed by the primary vacuum system before hydrogen embrittlement problems or tritium inventory limits are reached.

Since Zr-Al getters are a new technology for fusion device applications, a number of studies have been performed concurrent with the design of the TFTR system to provide information on the kinetics of the absorption-desorption processes (59, 60, 61). Of particular importance have been the measurement of the effects of discharge cleaning and the development of a simple in-situ technique for quantifying the actual hydrogenic loading. Excessive hydrogenic loading would normally be expected when active Zr-Al getters are exposed to the high H<sub>2</sub> pressures associated with discharge cleaning of the vacuum vessel. Fortunately, when the getters are maintained at room temperature during discharge cleaning, the amount of oxygen-containing residual gas typically released during the wall bombardment is sufficient to make the getter surface inert with respect to hydrogen absorption (see Figure 10). In addition to such studies on the particular Zr-Al alloy (0.84 Zr, 0.16 Al) tentatively chosen for the TFTR getter system, several laboratories are pursuing related studies on alternative non-evaporative getter materials (62, 63).

High-Heat Load Materials. The primary first-wall materials problem for the next generation of magnetic fusion devices is the choice of material for the high heat-load structures. In the present generation of operating tokamaks, most of the first-wall surface area receives a relatively low power flux (1-10 watts cm<sup>-2</sup>) for the duration of the plasma discharge (~ 1s), and only the relatively small area limiters receive a high power (0.1 - 1 kW cm<sup>-2</sup>) flux. As the discharge duration and circulating power are raised by more than an order of magnitude in the TFTR-generation devices, a substantially increased fraction (to approximately 50%) of the first-wall structures will be required to withstand high flux power-loading (16). This progression is changing the emphasis of materials studies and development of first-wall components. The emphasis is shifting from a concern with plasma-wall interactions that are dominated by hydrogen-induced changes in surface chemistry, to plasma-wall interactions that are dominated by high flux effects, e.g., sputtering, evaporation, and melting.

Figure 9 shows a cut-away drawing of the TFTR vacuum vessel

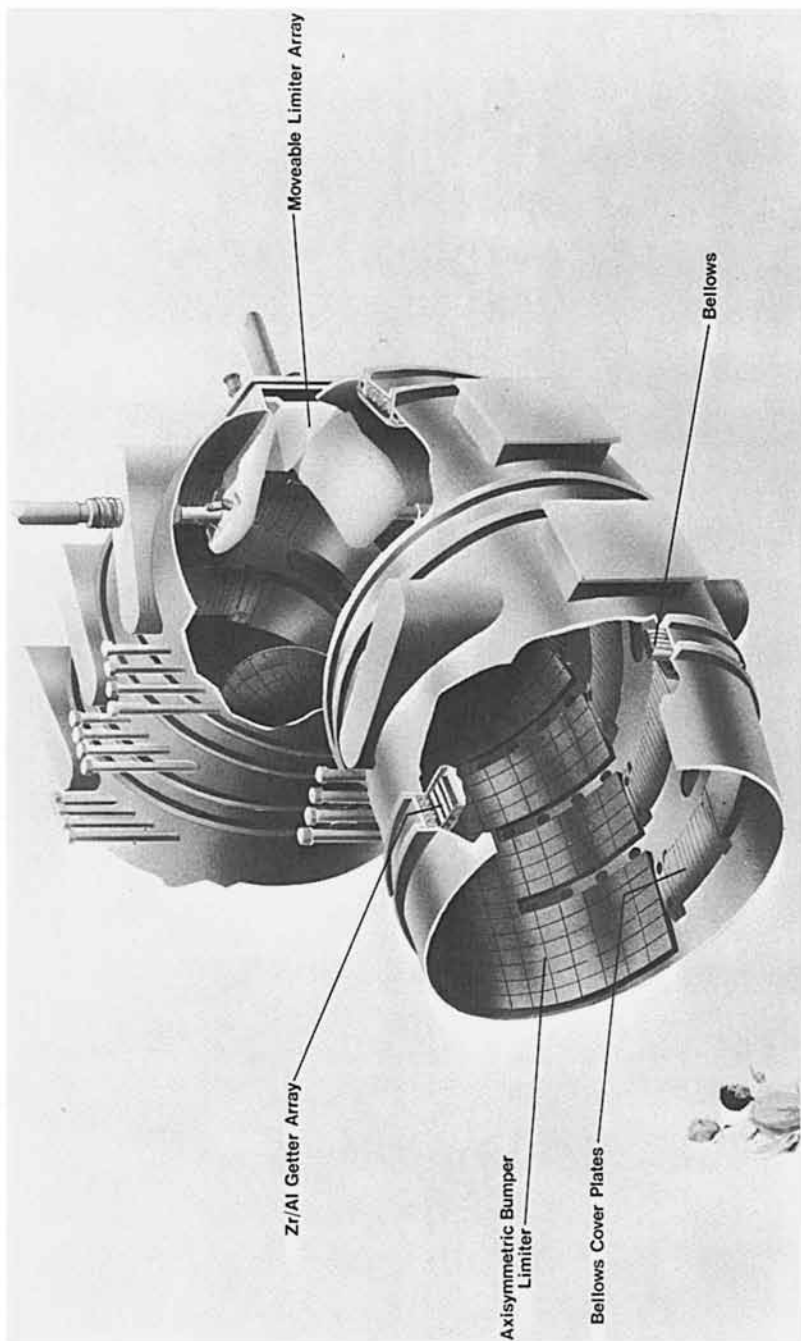


*Figure 9. Cut-away drawing of the vacuum vessel for the TFTR showing the location of high heat-load structures (bumper limiter, moveable limiter, and bellows covers) and one of 36 Zr-Al getter modules for impurity and density control.*

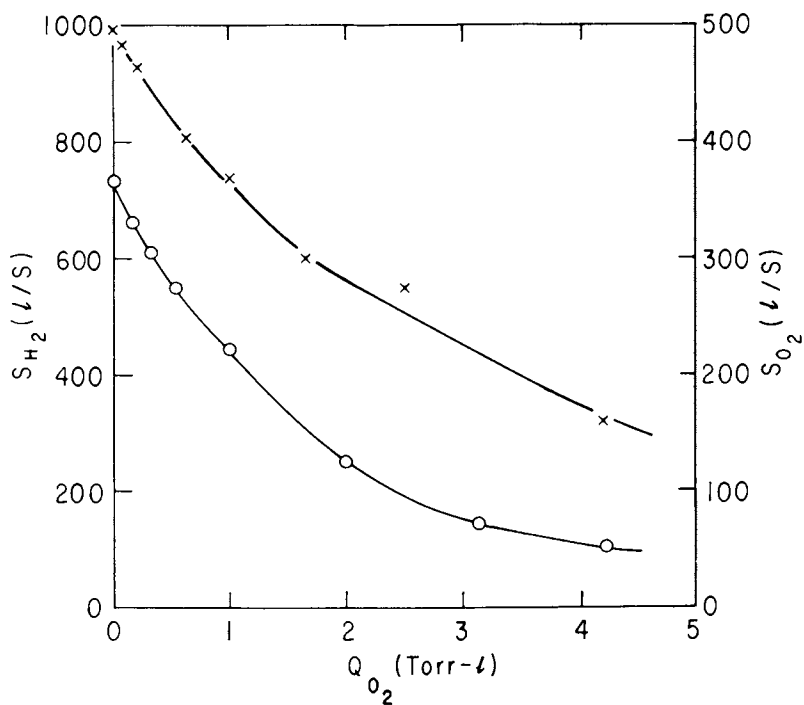


Figure 10. Hydrogen and oxygen pumping speeds for the 0.84 Zr, 0.16 Al alloy getter as a function of the oxygen surface loading. Key:  $\times$ —,  $S_{H_2}$ ; and  $\circ$ —,  $S_{O_2}$ . (Reproduced, with permission, from Ref. 60. Copyright North-Holland Publishing Co.)

that indicates the high heat-load first-wall structures that are being designed for this device (16); 1) large area, toroidal bumper-limiter which protects the entire inner wall of the vacuum vessel; 2) bellows cover-plates which protect the poloidally-directed vacuum vessel bellows; and 3) a massive, moveable-limiter for plasma-shaping. The high heat loads that these structures will experience ( $1-10 \text{ kW cm}^{-2}$ ) require new criteria to be considered in the materials selection process. The primary criteria are: 1) the ability to withstand high power loading with minimal material release by evaporation, sputtering, desorption, or arcing, and 2) the ability to withstand high thermal stress. Additional desirable properties include low hydrogen isotope retention to minimize tritium inventory problems and low atomic number constituent elements to minimize the effect on plasma contamination and neutron activation.

For the TFTR heat load structures, more than twenty different materials were surveyed for thermal conductivity and thermal shock resistance (64). As a result of these tests several grades of graphite and OFHC copper were chosen as the basic structural materials, and a number of candidate coating materials were identified. This selection involved a collaborative materials research program at several laboratories (64-68) to develop and test particular low-Z refractory coatings to minimize the chemical erosion and sputtering of the base materials. For any of the proposed coating materials it was important to characterize the sputtering behavior, hydrogen chemistry and hydrogen retention properties in comparison with the properties of the base materials.

As an example of the supporting data from the coating development program, Figure 11 shows the measured hydrogen ion erosion yields as a function of ion energy for several candidate low-Z coating materials (e.g.,  $\text{TiB}_2$ ,  $\text{TiC}$ ,  $\text{SiC}$ ) and several base materials (304 SS, C and Mo). The carbide coatings exhibit less erosion with hydrogen ion bombardment than pure graphite, and thus are useful for coating graphite based structure. On the basis of these laboratory tests, limiter configurations using  $\text{TiC}$ -coated graphite for the high heat-load surfaces have been designed and are presently being tested in the ISX (69), PDX (70), and DIII (71) tokamaks. The ultra-high vacuum compatibility, chemical inertness, and high thermal-shock resistance make the carbide/graphite composites useful for any vacuum process where the ability to handle high power loading is required.

### Summary

The studies reviewed in this paper have produced data on the surface chemistry and vacuum behavior of a variety of technological materials, including the effects of hydrogen discharge cleaning on structural metals such as stainless steel



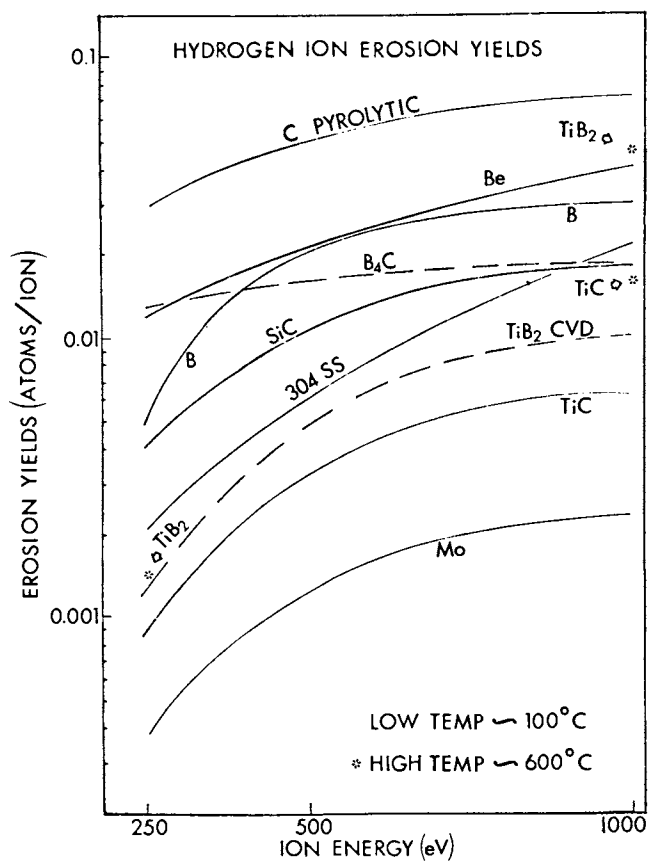


Figure 11. Comparative hydrogen ion erosion yields for several materials considered for first-wall structures. (Reproduced, with permission, from Ref. 66. Copyright 1979, North-Holland Publishing Co.)

and titanium, the application of Zr-Al alloys for bulk-gettering of active gases in large vacuum systems, and the development of UHV compatible materials and structures for absorbing high-heat loads. These studies were instigated by problems arising in the design and operation of magnetic fusion devices; however, the results have wide application in other technologies which require vacuum processing or a vacuum environment.

#### Acknowledgements

The author gratefully acknowledges the contributions and assistance of numerous colleagues in the preparation of this manuscript, particularly J. Cecchi, S. Cohen, R. Knize, D. Manos, D. Mattox, P. Staib, M. Achard, K. Wilson, W. Wampler, and M. Ulrickson. This work was supported by U.S. Department of Energy Contract No. DE-AC02-76-CHO-3073.

#### Literature Cited

1. McCracken G.M.; P.E. Stott, Nucl. Fusion 1979, 19, 889.
2. McCracken, G.M., J. Nucl. Mater. 1980, 93 & 94, 3.
3. Goodall, D.H.J., Proc. of the 5th Int. Conf. on Plasma Surface on Plasma Surface Interactions, (Gatlinburg, TN, May 1982), to be published by J. Nucl. Mater.
4. Voss, D.E.; Cohen, S.A., J. Nucl. Mater. 1980 93 & 94, 405.
5. Hawryluk, R.J.; Schmidt, J.A. Nucl. Fusion 1976, 16, 775.
6. McCracken, G.M.; Cohen, S.A.; Dylla, H.F.; Magee, C.W.; Picraux, S.T.; Rossnagel, S.M.; Wampler, W.R. Proc. 9th European Conference on Controlled Fusion and Plasma Physics, Oxford, England, Sept. 1979.
7. Staudenmaier, G.; Staib, P.; Behrisch, R. Nucl. Fusion 1980, 20, 96.
8. Erents, S.K.; Hotston, E.S.; McCracken, G.M.; Sofield, S.J.; Shea, J. J. Nucl. Mater. 1980, 92 & 93.
9. Zuhr, R.A.; Withrow, S.P.; Roberto, J.B. J. Nucl. Mater. 1980, 93 & 94, 127.
10. Wampler, W.R.; Picraux, S.T.; Cohen, S.A.; Dylla, H.F.; McCracken, G.M.; Rossnagel, S.M.; Magee, C.W.; J. Nucl. Mater. 1979, 85 & 86, 983.
11. Cohen, S.A.; Dylla, H.F.; Wampler, W.R.; Magee, C.W.; J. Nucl. Mater. 1980, 93 & 94, 109.
12. Wagner, F. J. Vac. Sci. Technol. 1982, 20, 1211.
13. Wampler, W.R.; Picraux, S.T.; Cohen, S.A.; Dylla, H.F.; Rossnagel, S.M.; McCracken, G.M. J. Nucl. Mater. 1980, 93 & 94, 139.
14. Staudenmaier, G.; Staib, P.; Poschenrieder, W. J. Nucl. Mater. 1980, 93 & 94, 121.
15. Staib, P.; Dylla, H.F.; Rossnagel, S.M. J. Nucl. Mater. 1980, 93 & 94, 166.

16. Cecchi, J.L. J. Nucl. Mater. 1980, 93 & 94, 28.
17. Hwang, D.Q.; Grotz, G.; Hosea, J.C. J. Vac. Sci. Technol. 1982 20, 1273.
18. Ruzic, D.; Moore, R.; D. Manos; Cohen S. J. Vac. Sci. Technol. 1982 20, 1313.
19. Timberlake, J.; Cohen, S.; Crider, C.; Estepp, G.; Hooke, W. J. Vac. Sci. Technol. 1982, 20, 1309.
20. Nygren, R.E. Proc. of the 2nd Int. Conf. on Fusion Reactor Materials, (Seattle, Aug. 1981), to be published in J. Nucl. Mater.
21. Straalsund, J.L.; Bloom, E.E., *ibid.*
22. Jensen, R.V.; Post, D.E.; Jassby, D.L. Nucl. Fusion 1977, 17, 1187.
23. Bol, K.; Arunasalam, V.; Bitter, M.; Boyd, D.; Brau, K.; Bretz, N.L.; Bussac, J.; Cohen, S.A.; Colestock, P.; Davis, S.L.; Dimock, D.L.; Dylla, H.F.; Eames, D.R.; Efthimion, P.C.; Eubank, H.P.; Goldston, R.J.; Hawryluk, R.J.; Hill, K.W.; Hinnov, E.; Hosea, J.C. Hsuan, H.; Jobs, F.C.; Johnson, D.W.; Mazzucato, E.; Medley, S.S.; Meservey, E.B.; Sauthoff, N.R.; Schmidt, G.L.; Stauffer, F.; Stodiek, W.; Strachan, J.D.; Suckewer, S.; Tait, G.D.; Ulrickson, M.; von Goeler, S. in Proc. 7th Int. Conf. on Plasma Physics and Controlled Nuclear Fusion Research Innsbruck, 1978, (IAEA, Vienna, 1979), Vol. 1, p. 11.
24. Spitzer, L.; Harm, R. Phys. Rev. 1953, 89, 977.
25. Parker, R.R.; Pappas, D.S.; Apgar, E. Bull. Am. Phys. Soc. 1976, 21, 1141.
26. Staib, Ph.; Staudenmaier, G. J. Nucl. Mater. 1976, 63 37.
27. Clausing, R.E.; Emerson, L.C.; Heatherly, L.; Colchín, R.J. J. Nucl. Mater. 1976, 63, 495.
28. Staib, Ph.; Staudenmaier, G. J. Nucl. Mater. 1978, 76 & 77, 78.
29. Staudenmaier, G.; Staib, Ph.; Venus, G. J. Nucl. Mater. 1978, 76 & 77, 445.
30. Dylla, H.F.; Bol, K.; Cohen, S.A.; Hawryluk, R.J.; Meservey, E.B.; Rossnagel, S.M.; J. Vac. Sci. Technol. 1978, 16, 752.
31. Oren, L.; Taylor, R.J.; Nucl. Fusion 1977, 17, 1143.
32. Gomay, Y.; Tazima, T.; Fujisawa, N.; J. Vac. Sci. Technol. 1979, 15, 103.
33. Y. Gomay, Clausing, R.E., Colchín, R.J., Emerson, L.C., Heatherly, L., Namkung, W., Simpkins, J.E., J. Vac. Sci. Technol. 1979, 16, 918.
34. Dylla, H.F.; Cohen, S.A.; Rossnagel, McCracken, G.M.; Staib, Ph. J. Vac. Sci. Technol. 1980, 17, 286.
35. Staib, Ph.; Dylla, H.F.; Rossnagel, S.M. J. Vac. Sci. Technol. 1980, 17, 291.
36. Poschenrieder, W.; Staudenmaier, G.; Staib, P. J. Nucl. Mater 1980, 93 & 94, 322.
37. Dylla, H.F.; J. Nucl. Mater. 1980, 93 & 94, 61.

38. Mathewson, A.; Achard, M.H. in Proc. 7th Int. Vacuum Congress and 3rd Int. Conf. on Solid Surfaces, Vienna, 1977, Eds. R. Dobrozemsky; Rudenauer, F.; Fiehböck, F.P.; Breth, A., (Vienna 1977) Vol. 2, p. 1217.
39. "Surface Contamination, Genesis, Detection, and Control," Ed. K.L. Mittal (Plenum, N.Y. 1979).
40. Taglauer, E.; Heiland, W. J. Nucl. Mater. 1980, 93 & 94, 823.
41. Bastaz, R.; J. Nucl. Mater. 1980, 93 & 94, 830.
42. Rossnagel, S.M.; Cohen, S.A.; Dylla, H.F.; Staib, Ph. J. Vac. Sci. Technol. 1980, 17, 301.
43. Equipe TFR, J. Nucl. Mater. 1981, 99 334.
44. Staib, P.; Dylla, H.F.; Rossnagel, S.M.; J. Nucl. Mater. 1980, 93 & 94, 315.
45. Brundle, C.R.; Chuang, T.J.; Wandelt, K. Surf. Sci. 1977, 68, 459.
46. McIntyre, N.S.; Zetaruk, D.G. Anal. Chem. 1977, 49, 1521.
47. Dietz, K.J.; Waelbroeck, F.; Wienhold, P. KFA-Jülich, 1977, Rep. No. Jul-pp-1448.
48. Dietz, K.J.; Ali-Khan, I.; Waelbroeck, F.; Wienhold, P. Proc. 4th Intern. Symp. on Plasma Chemistry, Zürich 1979, (IUPAC Communications, 1981).
49. Winter, J.F.; Waelbroeck, F.; Brandt, B.; Dietz, K.J.; Ali-Khan, I.; Wienhold, P.; J. Nucl. Mater. 1980, 93 & 94, 812.
50. Waelbroeck, F.; Winter, J.; Ali-Khan, I.; Wienhold, P. KFA-Jülich, 1980, Rep. No. Jul-pp-1692.
51. Kubaschewski, O.; Evans, E.L. Evans; Alcock, C.B., 4th ed. Eds.; "Metallurgical Thermochemistry"; (Pergamon Oxford, 1967).
52. Stott, P.E.; Daughney, C.C.; Ellis, R.A. Nucl. Fusion 1975, 15, 431.
53. Wilson, K.L. in Proc. of the 2nd Topical Conference on Fusion Reactor Materials, Seattle, August 1981 to be published to J. Nucl. Mater.
54. Marmor, E.S. J. Nucl. Mater. 1978, 76 & 77, 59.
55. Eubank, H.P.; Goldston, R.J.; Arunasalam, V.; Bitter, M.; Bol, K.; Boyd, D.; Bretz, N.L.; Bussac, J.P.; Cohen, S.A.; Colestock, P.; Davis, S.L.; Dimock, D.L.; Dylla, H.F.; Efthimion, P.C.; Grisham, L.R.; Hawryluk, R.J.; Hill, K.W.; Hinov, E.; Hosea, J.C.; Hsuan, H.; Johnson, D.W.; Martin, G.; Medley, S.S.; Meservey, B.; Sauthoff, N.R.; Schilling, G.; Schivell, J.F.; Schmidt, G.L.; Stauffer, F.; Stewart, L.D.; Stodiek, W.; R. Stooksberry, R.; Strachan, J.D.; Suckewer, S.; Takahasi, H.; Tait, G.D., Ulrickson, M.; von Goeler, S.; Yamada, M. "PLT Neutral Beam Heating Results"; in Proc. of the 7th Intern. Conf. on Plasma Physics and Controlled Nuclear Fusion Research, Innsbruck, Austria, 1979, (IAEA, Vienna, 1979) Vol. 1, p. 167.
56. Hosea, J.C.; Arunasalam, V.; Bernabei, S.; Bitter, M.; Boyd, D.; Bretz, N.L.; Crien, R.; Cohen, S.A.; Colestock, P.;

- Davis, S.L.; Dimock, D.L.; Dylla, H.F.; Eames, D.R.; Efthimion, P.C.; Eubank, H.P.; Goldston, R.J.; Grisham, L.R.; Hinnov, E.; Hsuan, H.; Hwang, D.; Jobes, F.C.; Johnson, D.W.; Kaita, R.; Lawson, J.; Mazzucato, E.; McNeill, D.H.; Medley, S.S.; Meservey, E.B.; Mueller, D.; Sauthoff, N.R.; Schilling, G.; Schivell, J.F.; Schmidt, G.L.; Sivo, A.; Stauffer, F.; Stodiek, W.; Stooksberry, R.; Strachan, J.D.; Suckewer, S.; Tait, G.D.; Thompson, H.; von Goeler, S. "Fast Wave Heating in the Princeton Large Torus, Princeton University, Plasma Physics Laboratory Report PPPL-1588, 1979 pp 14.; "Course on Physics of Plasma Close to Thermonuclear Conditions, Varenna, Italy, 1979; in Proc. of the Course on Physics of Plasmas Close to Thermonuclear Conditions (Commision of the European Communities, Brussels, 1980) Report EUR FU BRU/XII/476/80 Vol. II, p 571.
57. Usselmann, E.; Venus, G; Proc. 11th Sym. on Fusion Technol. Oxford, 1980, (Pergamon, Oxford, 1981) p. 343.
58. Ferrario, B.; Rosai, L; in Proc. 7th Int. Vacuum Congress and 3rd Int. Conf. on Solid Surfaces, Vienna, 1977, Eds. Dobrozemsky, R; Rudenauer, F.; Fiehbock, F.P.; Berth, A.; (Vienna, 1977) Vol. 1, p. 359.
59. Dylla, H.F.; Cecchi, J.L.; Ulrickson, M.; J. Vac. Sci. Technol. 1981 18, 1111.
60. Knize, R.J.; Cecchi, J.L.; Dylla, H.F. in Proc. of the 2nd Topical Conference on Fusion Reactor Materials, Seattle, 1981, to be published in J. Nucl. Mater.
61. Knize, R.J.; Cecchi, J.L.; Dylla, H.F.; J. Vac. Sci. Technol. 1982, 20, 1135.
62. Mendelsohn, M.H.; Gruen, D.M. J. Less Comm. Met. 1980, 74, 449.
63. Ferrario, B., SAES Getters S.P.A., private communication.
64. Ulrickson, M. J. Vac. Sci. Technol. 1981 18, 1037.
65. Mattox, D.M. Thin Solid Films 1979 63, 213 .
66. Mattox, D.M.; Mullendore, A.W.; Pierson, H.O.; Sharp, D.J. J. Nucl. Mater. 1979, 85 & 86, 1127.
67. Kaminsky, M. Thin Solid Films 1980, 73, 91 *ibid*; 73, 117.
68. K.L. Wilson and A.E. Pontau, J. Nucl. Mater. 1980 93 & 94, 569.
69. Clausing, R.E.; Emerson, L.C; Heatherly, L.; in Proc. of the 2nd Topical Conference on Fusion Reactor Materials, Seattle, 1981, to be published in J. Nucl. Mater.
70. Cecchi, J.L. Proc. Ninth Symp. on Engineering Problems of Fusion Research Chicago, 1981. (IEEE, New York, 1981) p. 1378.
71. Sevier, D.L.; Trester, P.W; Hopkins, E., in Proc. of the 2nd Topical Convergence on Fusion Reactor Materials, Seattle, 1981, to be published J. Nucl. Mater.

RECEIVED April 15, 1982

# Application of Thermal Analysis and Photoelectron Spectroscopy for the Characterization of Particulate Matter

R. L. DOD and T. NOVAKOV

University of California, Lawrence Berkeley Laboratory, Berkeley, CA 94720

Photoelectron spectroscopy (ESCA) and thermal evolved gas analysis (EGA) have been applied to characterize sulfur- and nitrogen-containing species in atmospheric particulate matter. Particulate amines and amides previously identified only by ESCA have been detected by EGA, a bulk method, for the first time. EGA and ESCA results suggest the existence of a sulfate similar to ammonium sulfate but with some of the ammonium ions replaced by a charged organic nitrogen complex.

Carbon-, nitrogen-, and sulfur-containing species account for most of the mass of aerosol particles. In spite of years of effort by many investigators, the exact chemical forms of carbon, sulfur, and nitrogen in these particles are not known; nor are the formation mechanisms of these species known with certainty. There are many reasons for this situation, including the complexity of the system and the dependence of the apparent chemical composition on the analytical methods used. For example, wet chemical analyses of sulfur and nitrogen species report only ions in solution. These ions, however, may be originally water soluble (e.g., sulfate and ammonium from ammonium sulfate), or they may be ionic products of hydrolyzable species such as amides (1). Of course, insoluble species will not be detected by wet chemical techniques.

In contrast, methods such as photoelectron spectroscopy (ESCA) analyze the entire sample content without sample preparation. However, ESCA is a surface technique, and the sample is exposed to vacuum and X-ray bombardment during analysis. ESCA results therefore may not be representative of the bulk composition; some volatile species may be lost because of the vacuum, and in principle the X-ray bombardment may cause chemical changes of some species.

Because of these possible problems, it seemed desirable to employ a technique that will analyze the bulk properties of

particles without chemical treatment or pre-separation of the sample and to compare these results with ESCA results. Thermal analysis in the evolved gas analysis (EGA) mode is one such technique. We will present some results of the application of ESCA and EGA to the characterization of sulfur and nitrogen species in atmospheric particulate matter.

### Methods and Procedures

The ESCA method (2) and its application to aerosol particles (3) have been extensively discussed in the literature and will not be described here. The instrument used in these experiments is a modified AEI ES-200 electron spectrometer which has been updated by the installation of a Surface Science Laboratories Model 239G position-sensitive photoelectron detector. The modifications also included replacement of all lens and analyzer power supplies, as well as changing to a modern microprocessor-based data system. Data collection with the modified spectrometer is approximately 10 times as rapid as with the original, thus substantially decreasing sample degradation during analysis.

In EGA the sample is heated at a predetermined rate in an oxidizing or neutral atmosphere. The evolved gases resulting from volatilization, decomposition, and combustion of the sample are monitored as a function of temperature by one or more gas-specific detectors. The carrier gas is usually oxygen or nitrogen. For analysis of carbonaceous materials, the gas detected in the oxygen mode is  $\text{CO}_2$ . For analysis of nitrogenous species, we use oxygen as the carrier gas and detect total nitrogen oxides,  $\text{NO}_x$ .

A schematic representation of the EGA apparatus used in our analysis of aerosol particles is shown in Figure 1. The sample, collected on a pre-fired quartz filter, is placed in the quartz combustion tube so that its surface is perpendicular to the tube axis. The tube is supplied with purified oxygen, with excess oxygen escaping through an axial opening at the end of the tube.

The remainder of the oxygen (together with gases produced during analysis) is drawn at a constant rate determined by a critical orifice through a nondispersive infrared  $\text{CO}_2$  analyzer (MSA LIRA 202S) and then through a chemiluminescent  $\text{NO}_x$  analyzer (Thermo-Electron Model 14D). Material may be evolved from the sample by volatilization, pyrolysis, oxidation, or decomposition. To ensure complete conversion of all carbon to  $\text{CO}_2$ , a section of the quartz tube immediately outside the programmed furnace is filled with a  $\text{CuO}$  catalyst bed which is kept at a constant  $900^\circ\text{C}$  by a second furnace. This is especially necessary at relatively low temperatures ( $< 250^\circ\text{C}$ ) where volatilization and incomplete combustion are the dominant processes occurring in the carbonaceous component.

Analyte gas concentrations are monitored as a function of temperature, and the resultant "thermogram" is a plot of

concentration vs. temperature with the integrated area of the curves being proportional to the carbon or nitrogen content of the sample. Quantitation is effected by calibration with gases of known concentration and by measuring the gas flow rate through the system. This calibration is verified by analyzing samples of quantitatively known elemental content.

The thermograms of ambient and source aerosol samples reveal distinct features in the form of peaks or groups of peaks. One important component of the carbonaceous aerosol is graphitic carbon, which is known to cause the black or grey coloration of ambient and source particulate samples (4). To determine which of the thermogram peaks corresponds to this graphitic carbon, we monitor the intensity of a He-Ne laser beam which passes through the filter. This provides simultaneous measurement of sample absorptivity and CO<sub>2</sub> evolution. The light penetrating the filter is collected by a quartz light guide and filtered by a narrow band interference filter to minimize the effect of the glow of the furnaces. An examination of the CO<sub>2</sub> and light intensity traces enables the assignment of the peak or peaks in the thermograms corresponding to the black carbon because they appear concurrently with the decrease in sample absorptivity.

The potential of this method (in the CO<sub>2</sub> mode) (5) is illustrated in Figure 2, where the complete thermogram of an ambient sample is shown. The lower trace represents the CO<sub>2</sub> concentration, while the upper curve corresponds to the light intensity of the laser light beam that reaches the detector during the temperature scan. Inspection of the thermogram shows that a sudden change in the light intensity occurs concomitantly with the evolution of the CO<sub>2</sub> peak at about 470°C. The light intensity I<sub>0</sub>, after the 470°C peak has evolved, corresponds to that of a blank filter. This demonstrates that the light-absorbing species in the sample are combustible and carbonaceous — the graphitic carbon referred to above. The carbonate peak evolves at about 600°C; and as carbonate is not light absorbing, it does not change the optical density of the sample. In addition to black carbon and carbonate, the thermogram in Figure 2 shows several distinct groups of peaks at temperatures below ~ 400°C that correspond to various organics.

The potential for applications of EGA to the characterization of nitrogenous species is illustrated in Figure 3, where NO<sub>x</sub> thermograms of NH<sub>4</sub>NO<sub>3</sub>, (NH<sub>4</sub>)<sub>2</sub>SO<sub>4</sub>, NH<sub>4</sub>HSO<sub>4</sub>, and NaNO<sub>3</sub> are shown. It is obvious from the figure that distinguishing the principal nitrogen species is feasible by this technique.

## Results and Discussion

The analytical results of our previous ESCA work (3) can be summarized as follows:

Sulfur is found to be predominantly in a +6 oxidation state, i.e., sulfate. Other chemical states of sulfur have also been



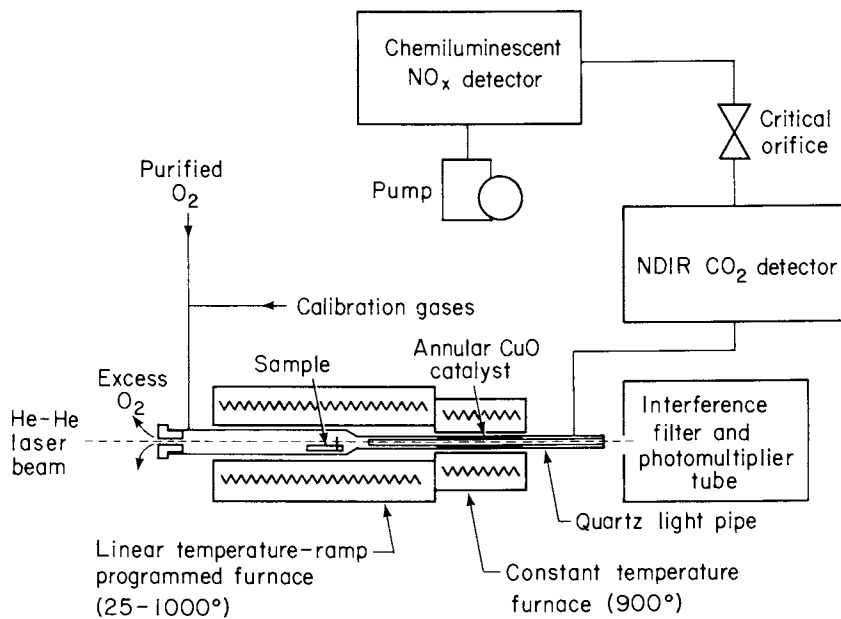


Figure 1. Scheme of thermal analysis (EGA) apparatus.

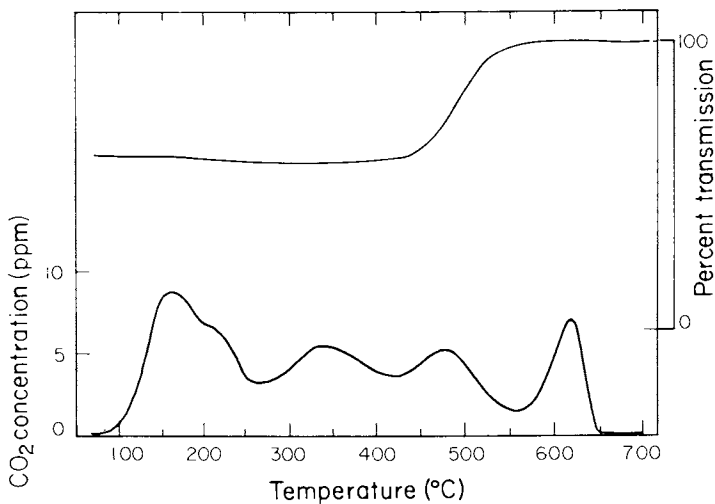


Figure 2. Carbon and optical thermogram of a Berkeley, CA, ambient particulate sample.

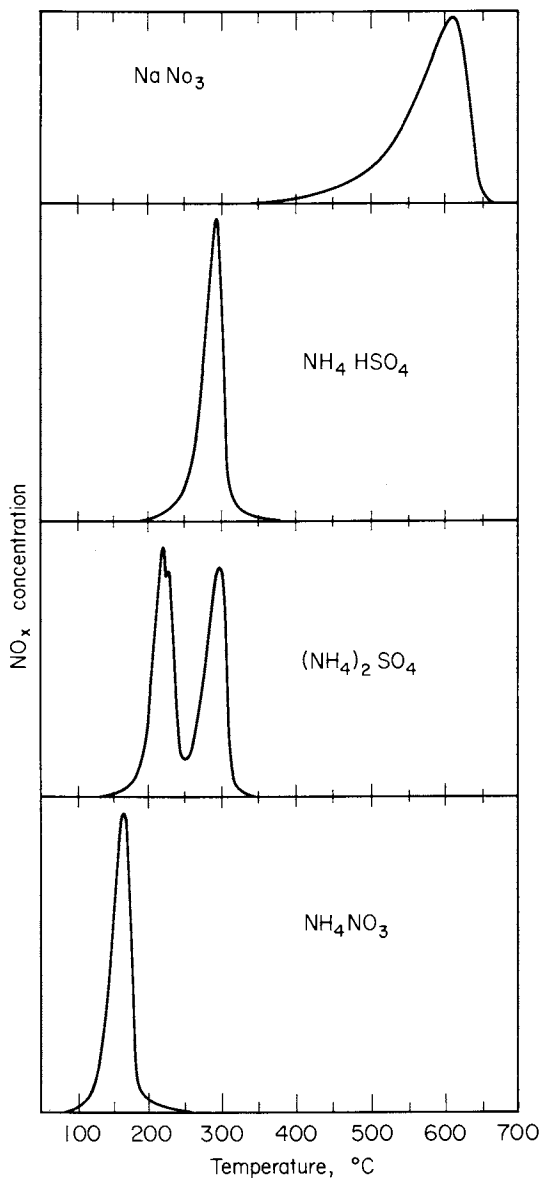


Figure 3.  $\text{NO}_x$  EGA thermograms of nitrogen standard compounds.

observed, although these seldom approach sulfate concentrations. Generally, at high pollutant concentrations sulfate is practically the only sulfur species present. Nitrogen can be present in an oxidized and a reduced form. The oxidized form has been identified as nitrate, while the reduced form consists of ammonium and a group of species consisting of particulate amines and amides,  $N_x$ . These  $N_x$  species were first discovered by ESCA (6) and are easily distinguished from ammonium by a  $\sim 2$  eV chemical shift of the N(1s) peak.

Attempts were made to prove the existence of the particulate amines by other techniques with only limited success. At best, indirect evidence (7) was obtained from the fact that nitrate and ammonium cannot account for total particulate nitrogen as determined by combustion. However, the observed nitrogen deficiency was much less than indicated by ESCA. An attempt to detect  $N_x$  by infrared spectroscopy (8) failed because of interfering absorption bands.

In order to detect  $N_x$  species by EGA, we used the results of our earlier ESCA analyses (6), which demonstrated that exposing a sample to vacuum and x-ray bombardment or heat results in the volatilization of most of the nitrate and ammonium salts. Sample volatility is seen on exposure to vacuum only but is greatly enhanced by simultaneous exposure to x-rays. Since the x-rays are sufficiently energetic (Al  $K\alpha$  - 1486 eV) to penetrate the particles, and assuming a high degree of porosity, this volatility enhancement should be a bulk rather than a surface effect. Thus, in a sample exposed to vacuum and x-ray, the only major nitrogenous species will be  $N_x$ . This is illustrated in Figures 4a and b. The  $NO_x$  thermograms of the original and ESCA-exposed samples are shown in Figures 4c and d. The ESCA spectra show that the principal species are volatile nitrate and ammonium, probably present as ammonium nitrate and ammonium sulfate, and nonvolatile  $N_x$ . The corresponding thermograms show a reduction in intensity in the triplet located between 150-300°C, assigned to ammonium nitrate and ammonium sulfate. Peaks at  $\sim 350$  and 450°C and the peak at  $\sim 550$ °C are unchanged, however. The first two probably correspond to  $N_x$ , while the last peak is most likely due to a metal nitrate.

We have used the ESCA results to provide empirical information about the apparent stoichiometry of sulfate, ammonium, and nitrate ions and other elements and species. Wet chemical analyses performed at several laboratories seemed to contradict some of the conclusions reached from ESCA studies. For example, total reduced nitrogen as determined by ESCA often agrees with the determination of ammonium by wet chemical methods. A consequence of this discrepancy is that in analyses where wet analysis would indicate ammonium sulfate, ESCA would suggest ammonium bisulfate, based on the assumption that particulate  $N_x$  species are not associated with sulfate. This assumption may not be valid, because it has been demonstrated (1) that a large fraction of  $N_x$  present

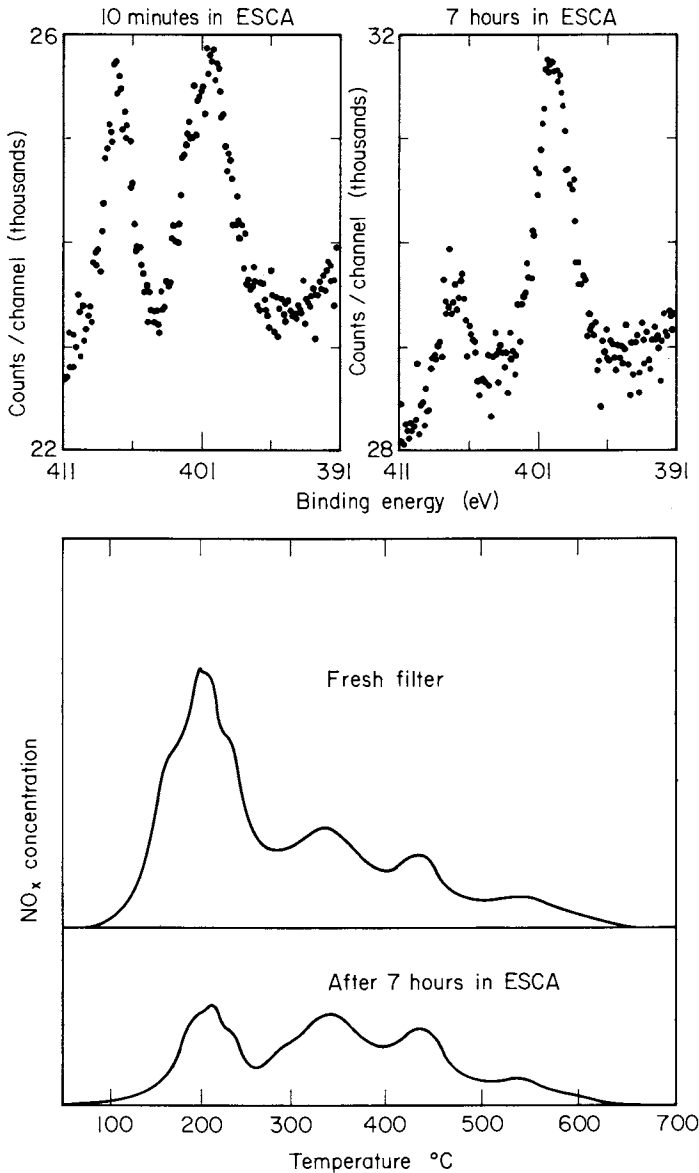


Figure 4. ESCA spectra and NO<sub>x</sub> thermograms from an ambient particulate sample from Riverside, CA; before and after exposure to ESCA conditions. Spectrum of fresh filter shows NO<sub>3</sub><sup>-</sup>(407 eV), NH<sub>4</sub><sup>+</sup>(402 eV), and N<sub>2</sub>(400 eV). NO<sub>3</sub><sup>-</sup> and NH<sub>4</sub><sup>+</sup> components are largely missing after 7 h.

in the original sample may be hydrolyzed to ammonium and removed by water extraction.

An insight into this apparent inconsistency may be achieved by combined ESCA and EGA analysis. Figure 5 shows the ESCA spectrum of the N(1s) region of a sample collected in Gaithersburg, Maryland. In addition to a small nitrate peak, a pronounced ammonium peak is also seen. This sample contains a very small concentration of  $N_x$  that is evidenced only by a slight asymmetry of the ammonium peak. This sample contains enough ammonium to almost completely neutralize the sulfate as determined by ESCA. The conclusion is that here the sulfate is in the form of ammonium sulfate. The  $NO_x$  thermogram of the same sample is shown in Figure 6. The positions of  $NH_4NO_3$  and  $(NH_4)_2SO_4$  thermogram peaks are indicated in the figure. This thermogram suggests that the principal counterion for sulfate is ammonium, not  $N_x$ , and that the sulfate is present as  $(NH_4)_2SO_4$ . This is consistent with the ESCA observations.

This situation is quite different for an Anaheim sample whose N(1s) ESCA spectrum is shown in Figure 7. Here in addition to  $NO_3^-$  and  $NH_4^+$ , the  $N_x$  peak is clearly seen. Volatility in ESCA vacuum indicates that the nitrate in this sample is present as  $NH_4NO_3$ , and therefore a significant portion of the ammonium is associated with the nitrate. The remainder of the ammonium is insufficient to provide counterions for the sulfate. This ESCA result suggests an ammonium-deficient sulfate compound such as ammonium bisulfate. We note that if the entire reduced nitrogen were hydrolyzed, there would be sufficient ammonium to conclude that the sulfate is present as ammonium sulfate.

The thermogram of this sample is shown in Figure 8. The ammonium nitrate peak and the first peak of ammonium sulfate match closely the positions of standard compounds. However, the peak at  $270^\circ C$  is noticeably shifted from the second ammonium sulfate peak, although the overall appearance of the doublet is similar to that of ammonium sulfate. A tentative explanation of this observation is that the sample does not contain pure ammonium sulfate, but rather that some of the ammonium ions are replaced by a charged organic nitrogen complex. This complex should produce the right chemical shift (relative to ammonium) in the ESCA spectrum, decompose at a lower temperature than ammonium bisulfate, and hydrolyze to ammonium in water solution.

### Summary

Addition of EGA to the analysis of atmospheric aerosol particles has permitted an independent speciation and determination of the nitrogenous component for samples which have not had chemical or physical pretreatment. The discovery from ESCA analyses that a substantial fraction of the particulate nitrogen exists chemically bound to the carbonaceous fraction has been confirmed by EGA. The indication from ESCA and EGA that inorganic sulfate

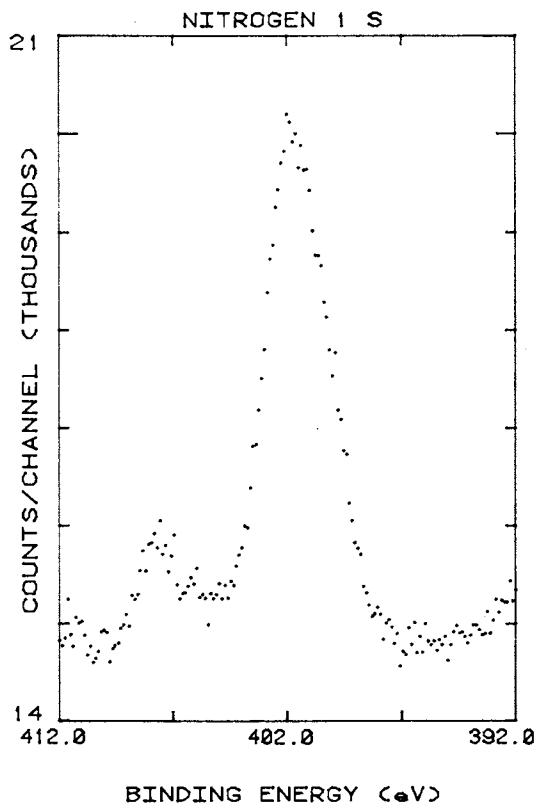


Figure 5. N 1s ESCA spectrum of April 24, 1979 ambient particulate sample from Gaithersburg, MD. Dominant nitrogen specie is  $\text{NH}_4^+$  (402 eV) with small components of  $\text{NO}_3^-$  (407 eV) and  $\text{N}_x$  (400 eV).

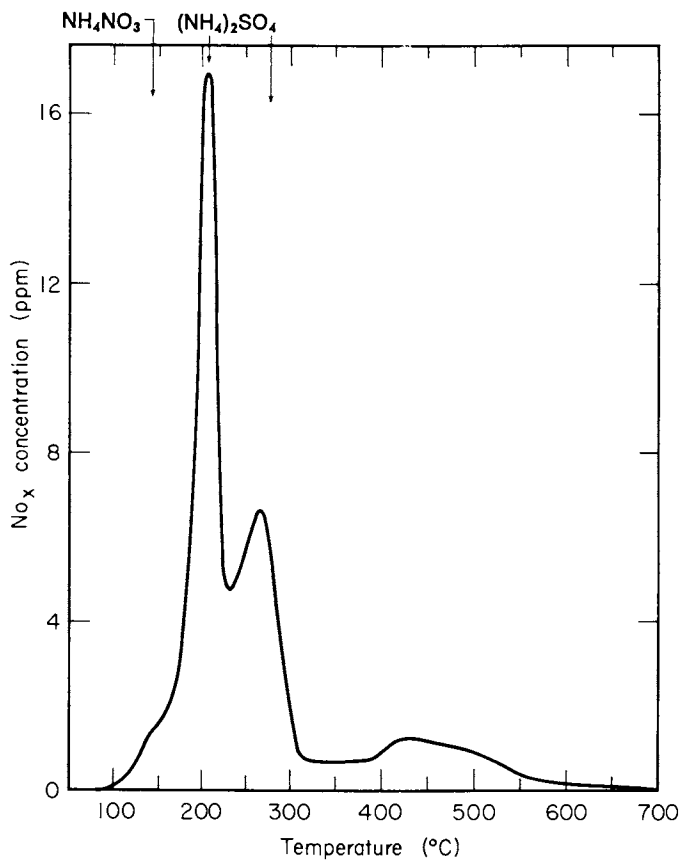


Figure 6. NO<sub>x</sub> thermogram of April 24, 1979 ambient particulate sample from Gaithersburg, MD.

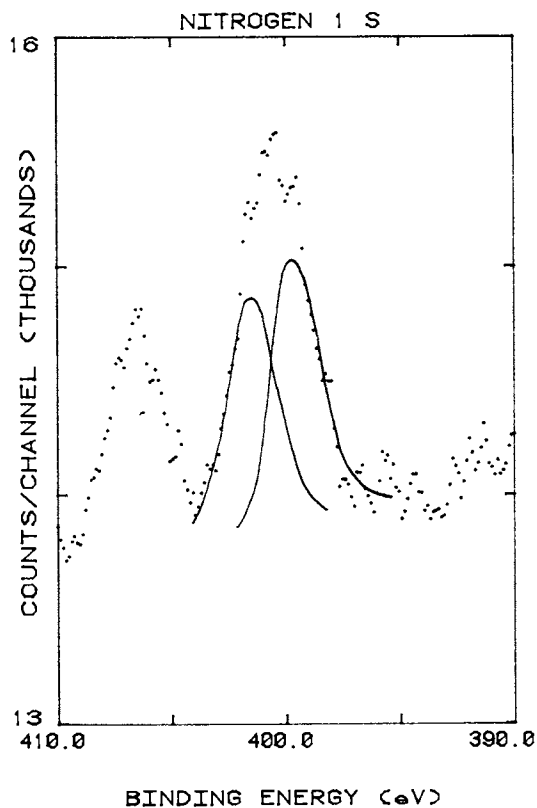


Figure 7.  $N 1s$  ESCA spectrum of July 27, 1979 ambient particulate sample from Anaheim, CA. Nitrogen evenly divided among  $NO_3^-$  (407 eV),  $NH_4^+$  (402 eV), and  $N_2$  (400 eV). Solid line shows deconvoluted  $NH_4^+$  and  $N_x$  components.



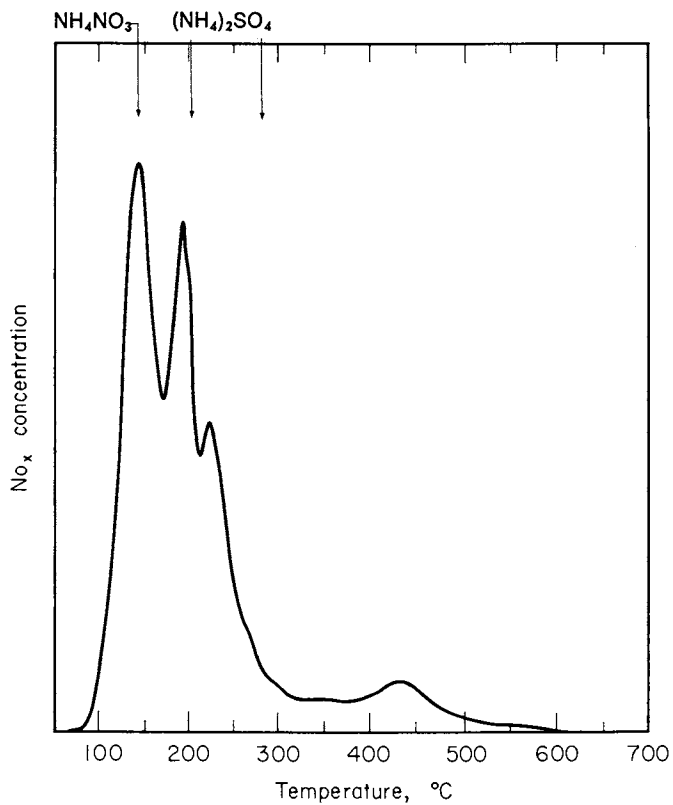


Figure 8. *NO<sub>x</sub> thermogram of July 27, 1979 ambient particulate sample from Anaheim, CA.*

may be linked to the carbon matrix through charged nitrogenous functional groups is unique and unconfirmed. We are currently modifying our EGA apparatus to permit determination of evolved sulfur to further study this problem.

The study described here demonstrates that ESCA provides information regarding the chemical nature of the surface of an unperturbed sample which would be difficult to acquire by other methods. A major weakness of ESCA, the necessity of exposing the sample to vacuum, together with its attendant problem of sample volatilization, can also be one of its strengths. The volatility of some nitrogenous species in atmospheric aerosol particles can be used to provide strong evidence for chemical identity of ionic compounds (e.g., ammonium nitrate) rather than simply ionic identities as provided by wet chemical methods. This volatility is accelerated by x-ray irradiation, so that similar results could be achieved only by extended vacuum exposure alone if another analytical technique were used. Also, with ESCA, volatile losses can be conveniently monitored since the sample remains in the spectrometer throughout the process.

#### Acknowledgments

This work was supported by the Assistant Secretary for the Environment, Office of Health and Environmental Research, Pollutant Characterization and Safety Research Division of the U.S. Department of Energy under Contract No. DE-AC 03-76SF00098 and by the National Science Foundation.

#### Literature Cited

1. Gundel, L.A.; Chang, S.G.; Clemenson, M.S.; Markowitz, S.S.; and Novakov, T. *in* "Nitrogenous Air Pollutants"; Grosjean, D., Ed.; Ann Arbor Science, Ann Arbor, 1979; p. 211.
2. Siegbahn, K.; Nordling, C.; Fahlman, A.; Nordberg, R.; Hamrin, K.; Hedman, J.; Johansson, G.; Bergmark, T.; Karlsson, S.E.; Lindgren, I.; and Lindberg, B.J. Nova Acta Regiae Soc. Sci. Ups., Ser. IV 1967, 20.
3. Novakov, T. *in* "Analysis of Airborne Particles by Physical Methods"; Malissa, H., Ed.; CRC Press, West Palm Beach, 1978, p. 191.
4. Rosen, H.; Hansen, A.D.A.; Dod, R.L.; and Novakov, T. Science 1980, 208, 741.
5. Dod, R.L.; Rosen, H.; and Novakov, T. *in* "Atmospheric Aerosol Research Annual Report 1977-78"; Lawrence Berkeley Laboratory Report LBL-8696, 1980; p. 2.
6. Chang, S.G.; and Novakov, T. Atmos. Environ. 1975, 9, 495.
7. Spicer, C.W. Atmos. Environ. 1977, 11, 1089.
8. Chang, S.G.; and Novakov, T. *in* "Atmospheric Aerosol Research Annual Report 1976-77"; Lawrence Berkeley Laboratory Report LBL-6819, 1977; p. 57.

RECEIVED May 24, 1982

# INDEX

- A**
- Absolute sensitivities of elements, ISS 23  
 Absolute sensitivity, XPS 18  
 Acid-base  
   adsorption, iron oxides 82-85  
   complexes on metals, spectral measurement 79-80  
   interaction at interfaces, wet chemical analysis 71-72  
 Acid-base interactions  
   adsorption inorganic surface 82  
   FTIR 79  
   hydrogen bonds 71  
   laser Raman IR, spectroscopy 79  
   solute and inorganic surface 80  
 Acid pickling, surface contamination 130  
 Acid site concentration, conductometric titrations 79  
 Acid strength 73  
 Acid strength vs. butylamine titration for clays 74f  
 Acidic sites  
   iron oxides 83  
   pigments 83f  
   silica adsorption 85-86  
 Acidity of indicators 73  
 Acids and bases on inorganic surfaces, heats of adsorption 80-82  
 Adhesion bonding, surface characterization  
   ISS 123  
   SIMS 125  
 Adhesive bond model 139f  
 Adhesive bonding  
   contaminants 129  
   experimental considerations 122-129  
   locus of failure determination 136-138  
   low energy method, characterization 123  
   materials, characterization 121-141  
   properties, contaminants 129f  
   surface characterization methods 122f  
   surface sensitivity, ISS and SIMS 123  
 Adhesive interactions, adsorption processes 70  
 Adhesives, ion beam applications 132-134  
 Adsorption  
   on Cab-O-Sil, Langmuir plot 86  
   of Cu ions 308f  
   data, Langmuir isotherms, pyridine onto ferric oxides 83  
 Adsorption—Continued  
   on glass surfaces, basic sites 86  
   interactions, external reflection IR spectroscopy 37  
   Langmuir isotherms for pyridine 84f  
   metal ions in leaching 306-307  
   from organic solvents onto inorganic surfaces 82  
   phenomena, wettability, minerals 290  
   polymethyl methacrylate onto silica gel 81f  
   processes adhesive interactions 70  
   of silica, acidic sites 85-86  
   of test acids and bases, aluminum oxide 86  
   triethylamine onto iron oxide 85  
 Aerosol particles, ESCA and EGA analysis 398  
 Alloys, dissolution current 274f  
 Alloys, pretreatment, corrosion resistance 273  
 Alpha particles resulting from  $^{12}\text{C}(3\text{He}\alpha\text{O})^{11}\text{C}$  reaction, spectrum 66f  
 Alumina, Raman bands for pyridine adsorption 300f  
 Aluminum alloy  
   ISS spectra 130  
   ISS/SIMS data 131f  
   SIMS spectra 130  
 Aluminum oxide, adsorption of test acids and bases 86  
 Aluminum oxide, basic sites 86  
 Andalusite, point-of-zero charge 310f  
 Anthraquinone, Hammett acidity indicators 73f  
 Applications, ion beam method, characterization of adhesive bonding materials 121-141  
 Applications, surface analysis, nuclear industry 345  
 Aqueous corrosion profiles soda-lime-silica glasses, SIMS 214  
 Aqueous titrations, phenolic and carboxylic surface acids 75  
 Area-intensive nature, solar energy conversion systems 328  
 ASTM tests, glass durability 208  
 Atomic composition depth profile, SIMS 20



- Bonding materials, adhesive, characterization, application of ion beam methods ..... 121-141
- Boron concentration, water-glass reaction ..... 348
- Boron and silicon behavior, glass leaching ..... 350
- Borosilicate glass, SIMS depth profiles ..... 353f
- Borosilicate glass leaching, SIMS analysis ..... 348-354
- Bovine serum albumin, spectra of ethyl vinyl sulfur modified samples ..... 176f
- Bovine serum albumin trifluoroacetylated with ethyl thio-trifluoroacetate, spectra ..... 174f
- Broadband capabilities, surface electromagnetic wave propagation IR spectroscopy ..... 41
- Buna-N seal exposed to fluorocarbon ether fomblin, electron spectra .. 189f
- Buna-N seal exposed to hydrocarbon fluid, electron spectra ..... 186f
- Butter yellow, Hammett acidity indicators ..... 73t
- Butylamine titration vs. acid strength for clays ..... 74f
- C**
- C implantation example, nonresonant reactions ..... 63
- Carbon black  
analysis of chemically reactive sites 78f  
chemical properties ..... 75  
surface acidity ..... 75  
surface analyses ..... 75  
titration of surface sites ..... 75
- Carbon black surface acids on black pearls, neutralization ..... 76f
- Carbon difference spectra ..... 107f
- Carbon and optical thermogram of particulate sample ..... 400f
- Carbon spectra, high resolution ..... 105f
- Carbon surfaces, SEM examination .. 91
- Carboxylic surface groups and phenolic-OH, flotation rate constant ..... 298f
- Casein modified with ethyl vinyl sulfone, spectra ..... 175f
- Catalysis and corrosion, photon spectroscopy ..... 35
- Catalyst, polymer anchored, XPS analysis ..... 193
- Cellulose, growth regulators, XPS analysis ..... 180
- Cellulose powder, electron spectra .... 183f
- Channelling and blocking experiments, instrumental requirements 27
- Channelling experiments, RBS ..... 25, 27
- Characterization of treated ores ..... 301-305
- Charge neutralization, methods, analysis of polymers ..... 136t
- Charge transient, nonaqueous dispersions ..... 324
- Charge/mass measurements, nonaqueous fluids ..... 322
- Chemical behavior, glasses ..... 204
- Chemical bonding insensitivity, energetic ion beam analysis ..... 50
- Chemical bonding, XPS ..... 144
- Chemical composition, XPS ..... 144
- Chemical environment of atom, XPS .. 18
- Chemical identities, compositional analysis ..... 2
- Chemical impurities, interfaces, elemental composition ..... 333
- Chemical profiling with depth, ISS and SIMS ..... 128
- Chemical properties of carbon blacks 75
- Chemical reaction surface analysis methods ..... 4
- Chemical reactivity, surface groups .. 69
- Chemical shift, shake-up and multiple splitting information, Auger electron spectroscopy ..... 20
- Chemical shift phenomenon, XPS .... 18
- Chemical vapor deposition, films ..... 237
- Chemically modified electrode(s) analysis ..... 89-113
- extended x-ray absorption fine structure, (EXAFS) ..... 112
- inelastic electron tunneling spectroscopy (IETS) ..... 110
- Raman spectroscopy ..... 112
- thermal desorption mass spectroscopy (TDMS) ..... 112
- atomic speciation, analysis ..... 93-99
- bonding, analysis ..... 110-112
- elemental composition, XPS ..... 112
- molecular speciation, analysis ..... 99-110
- problems ..... 90
- spectral studies ..... 109
- structure, analysis ..... 110-112
- surface topography, analysis ..... 91-93
- surface topography, SEM ..... 112
- Chemically modified electrode surfaces, surface analysis ..... 90
- Chemically modified electrode thickness, analysis ..... 99
- Chemically modified polyester fibers, surface analysis techniques ..... 198
- Chemisorptive phenomena, degradation of solar materials interfaces 334
- Chitan and chitosin, structure ..... 178f
- Chitosan  
*p*-chlorophenoxyacetic acid, spectra ..... 181f  
electron spectra ..... 179f

Chitosan— <i>Continued</i>		Contact angles, minerals, flotation investigations	290
containing 2,4-D, spectra	179f	Contact angles and flotation and electrode potential	292
encapsulation of plant growth regulators, XPS analysis	177	Contact angles and voltammetry, sulfide minerals, flotation	292
Chitosin and chitan, structure	178f	Contaminants, adhesive bonding	129
Chlorinated hydrocarbon reaction, nuclear component surfaces	354	Controlled release approaches	178f
<i>p</i> -Chlorophenoxyacetic acid in chitosan, spectra	181f	Controlled release formulations, feather keratin, XPS analysis	180
Chromate films, AES and XPS	277	Conversion, solar energy	328
Chromium depth profile in Fe <sub>13</sub> Cr	275f	Copolymer composition, XPS analysis	180
Clays, butylamine titration vs. acid strength	74f	Copolymers, surface composition, XPS	180
Coal, oxidation, Fourier transform IR spectroscopy	296	Copper ions, adsorption	308f
Coal, surface functional groups	294	Copper, bubble profiles and voltammogram, contact angle and electrode potential	293f
Coating technologies, first-wall materials	386–391	Core electron spectra, polymeric materials	145–146
Collection processes, solar energy	328	Core level shake-up process in XPS	15f
Comminution process, minerals, surfactants	305	Core lines, XPS	145
Composition semiconductor interfaces, surface structure	9	Core-electron removal, XPS, final states	16
Composition and structure, process history	5	Core-hole level, AES	20
Composition of surfaces	4	Core-hole state, AES	16
Compositional analysis	2	Core -level binding energies, XPS	18
ion scattering spectroscopy	23	Core-level photoionization cross-sections, XPS	18
Compositional gradients, glass surfaces, AES analysis	214	Core-level photoionization, AES	20
Compositional profiles of leached glasses	226f	Corrosion	
for samples with large depletion zones, IRRS analysis	224	crevice, critical potential	275t
of the surface, SIPS analysis	219	glass, performance, IAEA and Soxhlet tests	208
Computer simulation		glasses	206
elastic backscattering analysis	55	passive protective films	253
of the partial spectrum of lubricant	57f	stainless steel surfaces	354
of the partial spectrum of steel sample	58f	surface analysis	
steel sample	56	data acquisition	259
Concept of a surface	1	data analysis	261
Conditioning, first-wall surfaces	374	technique selection	255
Conditioning method, discharge cleaning, first-wall materials	376	techniques	253–262
Conditioning procedures, effect on surface chemistry, first-wall materials	375	surface oxidation state, UO <sub>2</sub>	266
Conditioning procedures, Tokamaks	377	types, wet and dry	252–253
Conditioning studies, magnetic fusion devices	374–386	Corrosion behavior, boiler tubing	359
Conductometric titrations, acid site concentration	79	Corrosion control, gold-coated contacts, AES, XPS, RBS	273–278
Conductometric titrations, acid sites	77	Corrosion mechanisms of alloys, RBS and ion implantation	267
Conductometric titration of polystyrene latex	81f	Corrosion problem approach	256t
Configuration, experimental, of surface electromagnentic wave propagation spectroscopy	43f	Corrosion problems, analytical conditions	259
		Corrosion rates	253
		Corrosion reactions	252
		Corrosion resistance, pretreatments of alloys	273
		Corrosion resistance, stainless steel alloys	272



Elastic backscattering analysis— <i>Continued</i>		Electron lines	
overlapping distributions .....	55	phosphine anchored catalyst .....	194f
thick film example .....	53	sulfonated beads and oxygen plasma etching .....	190t
thin film example .....	52	wool fibers and film .....	172f
Elastic electron or ion scattering cross sections, measurement .....	4	Electron mean free path and electron kinetic energy through organic materials .....	149f
Electric field amplitude in ellipsometry .....	43f	Electron-solid scattering models .....	4
Electrical double layer .....	313, 314f	Electron spectroscopy for chemical analysis	
flotation systems .....	290	characterization of sulfur and nitrogen in atmospheric particulates .....	398
highly resistive fluids, retardation effect .....	320	coatings on glasses .....	219
mineral/water interfaces .....	287	composition bonding, and oxidation state in mineral surface layers .....	301
potential-determining ions .....	287	flotation separations of complex sulfide ores .....	302
potential variation .....	291f	hydrometallurgical treatment of lateritic ores for nickel .....	302
Electrical and optical transients, particle mobility .....	320f	lateritic ores, hydrometallurgy .....	304
Electrical and optical transients with high particle concentration .....	321f	lateritic ores, nickel .....	304
Electroactive surface mediator .....	109	ore particles, various treatments .....	301
Electrocatalysis systems, design .....	90	particulate amines and amide .....	397
Electrochemical reactions at $\text{UO}_2$ surfaces, XPS .....	266	profiles, glass surface .....	219
Electrochemical systems, external reflectance .....	42	pyrite surface .....	302
Electrochemically determined coverage, XPS signal .....	95	spectra, nitrate and ammonium .....	402
Electrode		spectra and Nox thermograms, particulate sample .....	403f
<i>See also</i> —Chemically modified electrodes		spectra of pyrite .....	303f
chemically modified analysis .....	89–113	spectrum of particulate sample .....	405f
untreated pyrolytic graphite, SEM .....	94f	stoichiometry of sulfate, ammo- nium, and nitrate ions .....	402
Electrode analysis .....	104t	surface characterization .....	13
Electrode potentials, contact angles and flotation .....	292	surface composition of pyrite .....	304t
Electrode sample handling system .....	103	surface corrosion .....	219
Electrokinetic effects, mineral inter- faces, electrophoresis and streaming potential .....	289	Electron spectrum	
Electrokinetic measurements, flotation response, hydrophobic response .....	292	from Buna-N seal exposed to fluorocarbon ether fomblin .....	189f
Electron energy loss spectroscopy, solar materials research .....	333	from Buna-N seal exposed to hydrocarbon fluid .....	186f
Electron escape depths, electron spectroscopy .....	146–148	from cellulose powder .....	183f
Electron impact cross-section, AES .....	20	chitosan .....	179f
Electron kinetic energy, and mean free path length .....	149f	from 2,4-D in feather keratin .....	182f
Electron kinetic energy, relation- ship, inelastic mean free path length .....	146	from flame retardant coatings plasma grafted to fabric .....	155f
Electron kinetic energy through organic materials, electron mean free path .....	149f	from fluoroalkylsiloxane urethane interpenetrating network .....	186f
Electron line intensities from wool fibers .....	172t	from phosphine anchored rhodium containing catalyst .....	194
		from sulfonated styrene divinyl- benzene .....	191f
		from $\text{TiCl}_4$ bridged indoleacetic acid anchored to cellulose .....	184f
		from treated wool .....	153f



- Electron spectrum—*Continued*
- from treated wool yarn ..... 152f
  - from untreated wool ..... 153f
  - from wool yarn ..... 152f
- Electronic characteristics of thin films and/or UV-visible reflection spectroscopy ..... 41
- Electronic devices
- dopant, SIMS, RBS, and AES ..... 242
  - epitaxial layer, analysis ..... 234
  - metallization ..... 243
  - AES, SIMS, XPS, and RBS ..... 245
  - patterning, AES and SIMS ..... 240
- Electronic devices and transitional region of SiO<sub>2</sub>-Si interface, AES, XPS, and SIMS ..... 236
- Electronic energy level diagram, XPS process ..... 14
- Electronic materials
- analytical techniques, capabilities and limitations ..... 233t
  - process characterization, instrumental surface analysis ..... 229
  - quality control, instrumental surface analysis ..... 229
- Electronic materials and processes, instrumental surface analysis ..... 229
- Electronic properties, amorphous Si ..... 234
- Electronic spectroscopy, surface analysis ..... 106
- Electronic structure and atomic dynamics, surfaces ..... 3
- Electrons, AES ..... 16
- Electrons photoejected from a surface ..... 149f
- Electrophoresis, electrokinetic effects, mineral interface ..... 289
- Electrophoresis, insulating fluids ..... 317
- Electrophoretic curves for adsorption of metal ions on oxides ..... 308f
- Electrophoretic methods and surface acidity and basicity ..... 86-87
- Electrophoretic retardation and relaxation effect ..... 320
- Electrostatic detectors, RBS ..... 27
- Electrostatic repulsive forces, backscattering ..... 53
- Electrostatic scattering, RBS ..... 53
- Element profile, nuclear reaction analysis ..... 60-68
- Elemental composition, interfaces, solar materials ..... 333
- Elemental composition, XPS, chemically modified electrode ..... 112
- Elemental identity, compositional analysis ..... 2
- Elemental resolution, ion scattering spectroscopy ..... 23
- Elemental surface composition of stainless steel and Inconel ..... 381f
- Ellipsometric spectra, optical properties and film thickness ..... 42
- Ellipsometry
- characteristics ..... 257t
  - electric field amplitude ..... 43f
  - external reflection spectroscopy ..... 42
  - UV-visible reflection spectroscopy ..... 41
- Embrittlement, Fe and Ni ..... 266
- Embrittlement, hydrogen induced, corrosion ..... 253
- Emission IR spectroscopy ..... 40
- Energetic ion beam
- elastic backscattering analysis ..... 51-60
  - materials analysis ..... 49
  - near surface analysis with ..... 49-68
- Energetic ion beam analysis, ..... 50
- Energy equations, ISS ..... 123
- Energy loss considerations, backscattering analysis ..... 52
- Energy range, energetic ion beam analysis ..... 50
- Energy scale, energetic ion beam analysis ..... 50
- Energy spectra, backscattering analysis ..... 52
- Energy spectrum, nonresonant reactions ..... 63
- Energy transfer from probe to sample, side effects ..... 35
- Enthalpies of acid-base interaction, heats of adsorption ..... 82
- Enthalpy of hydrogen bonding, Drago correlation ..... 72
- Environment, ambient, surface ..... 35
- Epitaxial growth
- chemical vapor depositon ..... 234
  - liquid phase epitaxy ..... 234
  - molecular beam epitaxy ..... 234
  - molecular phase epitaxy of Si, surface analytical techniques ..... 234
  - solid phase epitaxy ..... 234
- Epitaxial layers, electronic devices, analysis ..... 234
- Equipment configurations for ion scattering ..... 124f
- Equipment for SIMS system ..... 126, 127f
- Erosion, first-wall, magnetic fusion devices ..... 372
- Estimation of the thickness of leached layers, IRRS profiles ..... 224
- Evolved gas analysis thermograms of nitrogen standard compounds ..... 401f
- characterization of nitrogenous species ..... 399

Evolved gas analysis— <i>Continued</i>	
characterization of sulfur and nitrogen in atmospheric particulates .....	398
particulate amines and amide .....	397
thermograms of nitrogen standard compounds .....	401f
Experimental configuration of surface electromagnetic wave propagation spectroscopy .....	43f
Experimental considerations, adhesive bonding .....	122–129
Experimental procedures, glass surface analysis .....	208–210
Extended vacuum transfer system, electrode sample handling system .....	103
External reflectance, electrochemical systems .....	42
External reflectance spectroscopy .....	41
External reflection experiment for oxide coated metal .....	38f
External reflection IR spectroscopy applications to surface analysis .....	37
description of technique .....	37
surface and thin film analysis .....	36, 40
External reflection IR spectrum of poly(acrylic acid) on aluminum .....	39f
External reflection, spectroscopy, ellipsometry .....	42
<b>F</b>	
Failure mode, analysis .....	140f
Failure surfaces from the wedge test, ISS-SIMS technique .....	137
Feather keratin, controlled release formulations, XPS analysis .....	180
Feather keratin, 2,4-D, electron spectra .....	182f
Fiber modification and analysis, XPS .....	144
Fibers, plasma oxidation, surface properties .....	148
Fibers, surface analysis, XPS industrial application .....	143–199
Field dependence, mobility .....	319f, 320
Field emission and ionization experiments .....	4
Field variations, measured mobility .....	320
Film thickness .....	99
Final state relaxation, XPS .....	14
Final states, core-electron removal, XPS .....	16
First-wall, impurities, effects .....	374
First-wall components, magnetic fusion device, design considerations .....	368
First-wall materials coating technologies .....	386–391
conditioning method .....	375, 376
First-wall materials— <i>Continued</i>	
conditioning techniques .....	374
glow discharge cleaning .....	376
hydrogen-isotope retention and recycling properties .....	388
low Zeff operation .....	374
magnetic fusion devices, high-heat load materials .....	389
magnetic fusion devices, surface chemistry .....	367
pulse discharge cleaning .....	376
vacuum-baking .....	375
First-wall structures, high heat-load ..	391
First-wall structures, hydrogen ion erosion yields .....	392f
First-wall surfaces, conditioning .....	374
Flame retardant coatings, wool fibers, spectra .....	150
Flotation	
hydrophobic minerals .....	292
separation, minerals .....	289
sulfide minerals, contact angles and voltammetry .....	292
surface characterization .....	289–297
Flotation and contact angles and electrode potential .....	292
Flotation investigations, contact angles, minerals .....	290
Flotation rate constant, phenolic-OH and carboxylic surface groups .....	298f
Flotation rate constant of Somerset coal, zeta potential .....	293f
Flotation response, hydrophobic minerals, electrokinetic measurement .....	292
Flotation separation, iron ores .....	290
Flotation separations of complex sulfide ores, ESCA .....	302
Flotation systems, electrical double layer .....	290
Fluoroalkylsiloxane, XPS analysis .....	185
Fluorocarbon coatings, plasma deposited, analysis .....	150–157, 154f
Fluorocarbon surfaces, plasma-polymerized, XPS data .....	166t
Four phase interactions, mineral processing .....	284t
Fourier transform IR spectroscopy	
<i>See also</i> —FTIR	
acid-base interactions .....	79
oxidation of coal .....	297
Fracture in aqueous environment and grain boundary chemistry .....	262
Fracture mode of nickel at grain boundaries .....	265f
Fracture mode, grain boundary composition .....	263
FTIR, spectra of stearic acid on iron .....	80
FTIR reflection, interaction of oxide film on aluminum .....	80

- FTIR reflection spectroscopic studies, organic acids oxide films on aluminum ..... 79
- Functional groups, mineral surfaces, IR spectroscopy ..... 297
- Fusion device applications, Zr-Al getters ..... 389
- Fusion device, Tokamak-type ..... 369f
- Fusion devices, magnetic, first-wall materials, surface chemistry ..... 367
- Fusion wall materials, metal oxides ..... 386
- G**
- Ga and As 3d photoelectron transitions ..... 239f
- GaAs growth mechanism, electronic devices, SIMS ..... 237
- Galena, current, capacitance, and surface photovoltage vs. potential ..... 295f
- Galena, space charge layer, oxygen reduction reaction kinetics ..... 292
- Gas-solid interface, solar entry materials ..... 332t
- General stress corrosion ..... 253
- Gettering materials, first-wall materials ..... 386
- Glass  
borosilicate, SIMS depth profiles ..... 353f  
chemical behavior ..... 204  
composition and thickness ..... 206  
corroded, IR reflection spectra ..... 223f  
corrosion ..... 206  
leached, compositional profile ..... 226f  
positive ion intensities ..... 350  
sodium borosilicate, leaching, SIMS depth profiles ..... 352f  
sodium borosilicate, SIMS depth profiles ..... 351f
- Glass coatings, ESCA analysis ..... 219
- Glass corrosion performance, IAEA and Soxhlet tests ..... 208
- Glass durability, ASTM tests ..... 208
- Glass enamel, surface compositional profile ..... 210
- Glass leaching, boron and silicon behavior ..... 350
- Glass surface  
adsorption, basic sites ..... 86  
AES profiles ..... 210-214  
analysis ..... 203  
compositions ..... 204  
electron spectroscopy for chemical analysis profiles ..... 219  
general features, surface analysis .. 203  
hydrogen concentration profile, resonant nuclear reaction ..... 217  
IR reflection spectroscopy profiles ..... 222-224
- Glass surface—*Continued*  
resonant nuclear reaction profiles ..... 217-219  
SIMS profiles ..... 214-217  
SIMS studies, surface chemistry changes ..... 354  
SIPS profiles ..... 219-222  
sodium concentration profile, resonant nuclear reaction ..... 217
- Glass surface analysis, experimental procedues ..... 208-210
- Glassy carbon, analysis of spectra ..... 106
- Glassy carbon, surface pits ..... 93
- Glassy carbon and pyrolytic graphite  
Glassy carbon electrodes, SEM of treated ..... 94f
- Glassy carbon electrodes, surface composition ..... 103
- Glassy carbon surface, radio frequency (rf) plasma treatments ..... 93
- Glassy carbon surfaces, Tokai, laser Raman spectra ..... 111f
- Glow discharge cleaning, first-wall materials ..... 376
- Glow discharge cleaning technique ..... 377
- Glow discharge condition (GDC) of PDX vessel ..... 378f
- Gold-coated contacts, surface analysis, AES and XPS ..... 277
- Grain boundaries, sulfur composition, AES ..... 263
- Grain boundaries of nickel, sulfur coverages ..... 264f
- Grain boundaries of nickel at fracture mode ..... 265f
- Grain boundary composition, AES ..... 262
- Grain boundary composition, fracture mode ..... 263
- Grain boundary chemistry and fracture in aqueous environment, AES ..... 262
- Graphite electrode, modified, differential pulse polarogram ..... 98f
- Graphite and polyethylene fiber, ISS data ..... 135f
- Grinding aids, effects ..... 306t
- Grinding aids for comminution, mineral processing ..... 305-306
- Growth regulators, cellulose, XPS analysis ..... 180
- Growth regulators, encapsulated in natural polymers, XPS analysis ..... 177-181
- H**
- Hammett acidity scale, equation ..... 73
- Heats of adsorption, enthalpies of acid-base interaction ..... 82



- Intensity to concentration conversion, SIMS ..... 20
- Intensity ratios, XPS spectra ..... 99
- Interaction(s)
- of oxide film on aluminum, FTIR reflection ..... 80
  - mediator with electrode and solution substrate ..... 90
  - in mineral processing, interfacial plasma-wall, magnetic fusion devices ..... 368-372
- Interface(s)
- acid-base interactions ..... 71
  - elemental composition, chemical impurities ..... 333
  - elemental composition, solar materials ..... 333
  - materials science research ..... 331
  - mineral processing, Raman spectroscopy ..... 297
  - mineral/particle, properties ..... 288*t*
  - mineral/water, electric double layer plastics and metals bonding, characterization ..... 121
  - solar energy conversion systems ..... 329-331
    - properties ..... 335*t*
    - research goals ..... 337
  - solar materials ..... 334
  - surface science ..... 335-337
- Interface(s) and material transfer, radioactive waste management .. 346
- Interface analysis, corrosion ..... 252
- Interface analysis, photon based techniques ..... 10
- Interface degradation, solar materials ..... 331
- Interface phenomena, solar energy conversion technologies ..... 335
- Interface science, solar energy materials ..... 331, 337-339
- Interface structure ..... 5
- Interface studies, solar materials ..... 331-335
- Interfacial behavior, solar materials, limitations of methods ..... 336
- Interfacial chemistry, adhesive bond formation ..... 122
- Interfacial degradation models, mirror system ..... 340*f*
- Interfacial degradation reactions, silver/silver interface, solar materials ..... 338
- Interfacial interactions in mineral processing ..... 284*t*
- Interfacial microstructure and microchemistry, solar materials, research needs ..... 337
- Interfacial properties, mineral processing ..... 286
- Interfacial stability, solar energy materials ..... 327
- Interferences in backscattering spectra, nuclear reaction analysis ..... 60
- Internal or external reflection-absorption techniques, UV-visible reflection spectroscopy ..... 41
- Internal reflectance spectroscopy ..... 41
- Internal reflection experimental set up ..... 38*f*
- Internal reflection IR spectroscopy, applications ..... 36
- Internal reflection IR spectroscopy, surface analysis ..... 36
- Internal reflection Raman spectroscopy, enhance of electromagnetic field strength ..... 45
- Interpenetrating network polymer, XPS analysis ..... 180, 185
- Ion and electron spectroscopy, requirements and problems ..... 34
- Ion beam applications, adhesives and other polymers ..... 132
- Ion beam method, specimen charging ..... 134-136
- Ion beams for surface analysis ..... 124*f*
- Ion enhanced diffusion, sputtering process artifacts ..... 28
- Ion implantation, modifying the surface-sensitive properties of metals ..... 56
- Ion implantation, semiconductor industry ..... 56
- Ion implantation and RBS, corrosion mechanisms of alloys ..... 267
- Ion induced x-ray analysis, instrumentation, applications ..... 59
- Ion induced x-ray spectrum for solid lubricant sample ..... 60, 61*f*
- Ion microprobe, SIMS ..... 126
- Ion milling, depth profiling ..... 27
- Ion neutralization, models ..... 4
- Ion scattering
- adhesive bonding materials, locus of failure and contamination effects ..... 132
  - basic process ..... 16
  - equipment configurations ..... 124*f*
  - simplicity of spectra ..... 125
  - simultaneous sputtering of surface .. 125
  - surface characterization ..... 13
- Ion scattering data, polymer surface .. 133
- Ion scattering process, description .... 16
- Ion scattering spectrometry, description ..... 16, 18
- Ion scattering spectroscopy
- advantages and disadvantages ..... 28, 30 128*t*
  - application ..... 129-132
  - depth profiling ..... 27
  - energy equations ..... 123

Ion scattering spectroscopy— <i>Continued</i>		Iron oxide(s)— <i>Continued</i>	
information content .....	23	acidic sites .....	83
sensitivity .....	128	heats of adsorption .....	85
solar materials research .....	333	IRRS analysis, compositional profile for samples with large depletion zones .....	224
surface characterization, adhesion bonding .....	123	IRRS profile, estimate of the thick- ness of leached layers .....	224
surface sensitivities .....	24		
adhesive bonding .....	123	<b>K</b>	
Ion scattering spectroscopy data		Kaolinite, attapulgite, and bentonite, surface acidity .....	73
for graphite and polyethylene fiber	135f	Kinetic analysis, glass surfaces .....	208
polymer surfaces, O:C ratios .....	134t	Kinetics, Pd <sub>2</sub> Si reaction, studies .....	234
Ion scattering spectroscopy process ..	17f	Knock-on effects, sputtering process artifacts .....	28
Ion scattering spectroscopy surface analysis, cylindrical mirror analyzer .....	125		
Ion scattering spectroscopy/SIMS data from adhesive matching areas to adherend .....	140f	<b>L</b>	
for aluminum alloy .....	127f	Labeling, chemical, identification, chemically modified electrodes ..	102
for polypropylene .....	135f	Langmuir isotherm, pyridine onto ferric oxide, equations .....	83
for stainless steel .....	131f	Langmuir isotherms for pyridine adsorption .....	84f
surface analysis .....	126	Langmuir plot, adsorption on Cab-O-Sil .....	86
wedge failure surface with .....	139f	Langmuir plot, pyridine adsorption onto Hi-Sil .....	86
wedge test, bond failure .....	138	Laser Raman IR spectroscopy, acid- base interactions .....	79
Ion scattering spectroscopy spectra		Laser Raman spectroscopy, minerals	297
aluminum alloy .....	130	Laser Raman spectra of Tokai glassy carbon surfaces .....	111f
application, adhesives and other polymers .....	133	Lateritic ores, ESCA hydrometal- lurgical treatment .....	304
polymers, nonindividualistic nature	134	Lateritic ores, nickel, ESCA .....	304
Ion sputtering effects, plasma-wall interactions, magnetic fusion devices .....	371	Latex particles, titration of ionic groups .....	77-79
Ion-neutralization probability, ion scattering spectroscopy .....	23	Latexes, strong and weak acid sites ....	77
Ion-solid interaction, theory .....	4	Leaching	
Ionic groups on latex particles, titration .....	77-79	borosilicate glass, SIMS .....	348
IR and laser Raman spectroscopy, solid/liquid interfaces .....	299t	glass, profiles of ions .....	350
IR reflection spectroscopy		ion intensity .....	350
<i>See also</i> —IRRS		of sodium borosilicate glass, SIMS depth profiles .....	352f
profiles, glass surfaces .....	222-224	Leaching rates, glass, temperature effect .....	350
of simulated nuclear waste .....	225f	Light scattering measurements, sweepout and transit .....	319f
IR spectra, vibrational properties of molecular structures .....	36	Liquid-solid interface, solar energy materials .....	332t
IR spectroscopy		Local atomic structure, analysis of photoelectron-induced diffrac- tion effects .....	2
analysis of surfaces and thin films	33-48		
application of chemically modified electrode surfaces .....	109		
functional groups, mineral surfaces	297		
reflection, surface analysis .....	36		
surface information .....	35-41		
IR spectrum of poly(acrylic acid) on aluminum, external reflection ....	39f		
Iron ores, flotation separation .....	290		
Iron oxide(s)			
adsorption of triethylamine .....	85		
acid-base adsorption .....	82-85		

- Local geometric structure of surface species, SEXAFS and photoelectron diffraction ..... 10
- Locked mineral particles ..... 300*f*
- Locking patterns, ores ..... 299
- Locking patterns of minerals, grain size, and topography, SEM ..... 301
- Locus of failure determination, adhesive bonding ..... 136-138
- London dispersion force interaction, wet chemical analysis ..... 70-71
- Low current density sputtering, SIMS surface analysis ..... 126
- Low energy ion scattering, surface selectivity ..... 125
- Low resolution XPS spectra of a pyrolytic graphite ..... 96*f*
- Low-energy electron diffraction ..... 9  
atomic geometry ..... 2  
intensity analysis technique ..... 8
- Low-flux surface, first-wall components, magnetic fusion devices ..... 368
- Low-Z coating materials, hydrogen ion erosion yields ..... 391
- Lubricant, computer simulation of partial spectrum ..... 57*f*
- Lubricant thin film, thick, Rutherford backscattering spectrum ..... 54*f*
- M**
- Macroscopic topography, surface structure ..... 2
- Magnetic fusion devices  
conditioning studies ..... 374-386  
discharge cleaning ..... 377  
high-heat load materials, first-wall materials ..... 389  
impurity concentration for plasma ignition ..... 373*f*  
ion sputtering effects, plasma-wall  
plasma impurity effects ..... 372-374  
plasma-wall interactions ..... 368-372  
surface chemistry, first-wall materials ..... 367
- Magnetic fusion reactor technology, first-wall, erosion and radiation damage ..... 372
- Mass resolution, ISS ..... 23
- Materials, solar energy conversion systems ..... 329
- Materials analysis, energetic ion beams ..... 49
- Materials science applications, XPS, examples ..... 177
- Materials science research, interfaces ..... 331
- Mean free path length and electron kinetic energy ..... 149*f*
- Measurements  
of chemical reaction ..... 4  
of contact angles, wet chemical technique ..... 71  
of elastic electron or ion scattering cross-sections ..... 4  
of surfaces ..... 3, 4
- Mechanical requirements, solar energy conversion systems ..... 329
- Mechanisms of various subprocesses, mineral processing, surface characterization techniques ..... 301
- Mediator bonding and interaction, chemically modified electrode, analysis ..... 110
- Mediators, electron transfer bridges between electrode surface solution species ..... 89
- Melting and recrystallization of crystal-amorphous interface ..... 234
- Metal corrosion problems, surface analytical techniques ..... 251
- Metal ions adsorption in leaching ..... 306-307
- Metal oxide hydrolysis, stainless steel ..... 383
- Metal oxides, fusion device wall materials ..... 386
- Metal oxides reduction, temperature dependence ..... 387*f*
- Metallization, electronic devices ..... 243  
AES, SIMS, XPS, and RBS ..... 245
- Metals, oxidation, stages ..... 253
- Metals, spectral measurement of acid-base complexes ..... 79-80
- Metal oxides, surface sites ..... 79
- Methods of surface analysis ..... 4-5  
definitions of acronyms ..... 7*t*  
properties, experiments, and acronyms ..... 6*t*
- Microelectronic circuits, silicon ..... 236
- Microelectronics, surface structure ..... 5-9
- Microelectrophoretic techniques, zeta potential ..... 315
- Micro-x-ray diffraction, crystallographic information, minerals ..... 301
- Migration velocity, equations ..... 315
- Mineral(s)  
adsorption phenomena, wettability constant angles, wettability and flotability ..... 292  
counter ions, surface properties ..... 289  
flotation, separation ..... 289  
flotation investigations, contact angles ..... 290  
indifferent electrolytes, surface properties ..... 289  
Raman spectroscopy, solid-liquid interfaces ..... 297  
surface charge equation ..... 287

Minerals— <i>Continued</i>	
surface groups, derivative formation	296
surface potential, equation	287
surfactants, comminution process	305
surfactant adsorption	306
Mineral interface, electrokinetic	
effects	289
Mineral particle/fluid/fluid systems	288 <i>t</i>
Mineral/particle solution interfaces	288 <i>t</i>
Mineral processing	
four phase interactions	284 <i>t</i>
grinding aids for comminution	305–306
Raman spectroscopy, interfaces	297
surface characterization	283
surface characterization techniques, mechanisms of various sub- processes	301
surface or interfacial properties	285 <i>t</i>
three phase interactions	284 <i>t</i>
two phase interactions	284 <i>t</i>
Mineral processing interactions, interfacial	284 <i>t</i>
Mineral processing methodology, ore mineralogy	299
Mineral processing and surface properties	286–287
Mineral processing unit operations	286
Mineral separations, properties of surfaces and interfaces	284
Mineral/solution interfaces, analytical techniques	286
Mineral surface characterization, voltammetry	292
Mineral surfaces, IR spectroscopy, functional groups	297
Mineral/water interfaces, electrical double layer	287
Minerals and ores, surface functional groups	294
Mirror, AES depth profile	341 <i>f</i>
Mirror, deterioration, solar materials	339
Mirror degradation problem, solar materials	338
Mirror system, interfacial degrada- tion modes	340 <i>f</i>
Mobility, field dependence	319 <i>f</i> , 320
Models of electron-solid scattering	4
Models of ion neutralization	4
Modified polyester fibers, surface analysis	198
Molar absorptivity, effect of immobili- zation, chemically modified electrodes	109
Molecular beam epitaxy	
AES	235
reflection high energy electron diffractions	235
SIMS	235
Molecular speciation, chemically modified electrode, analysis	99–110
Molecular speciation, control sample surface	102
Molecular speciation, data manipulation	103
Molecular speciation information, digitized spectra	103
Monolayer emission thin film surface analysis, IR spectroscopy	40
Monolayer quantity films, stimulated Raman gain spectroscopy	45
Monolayers and thin films, Raman spectra	44
MoS <sub>2</sub> , thin film, RBS	54 <i>f</i>
Multiplet splitting, photoemission peaks	14
N	
N implantation, application to tool steel	63
N implantation example, nonresonant reactions	63
<sup>14</sup> N(d, a) <sup>12</sup> C reaction, spectrum of particles	64 <i>f</i>
Navigational computers, contacts, corrosion control	273
Near surface analysis with energetic ion beams	49–68
Neutral Red, Hammett acidity indicators	73 <i>t</i>
Neutralization of carbon black surface acids on black pearls	76 <i>f</i>
Nickel	
grain boundaries at fracture mode	265 <i>f</i>
hydrometallurgical treatment of lateritic ore, ESCA	302
lateritic ores, ESCA	304
sulfur coverages at grain boundaries	264 <i>f</i>
Nitrate and ammonium, ESCA spectra	402
<i>p</i> -Nitrobenzoic acid on copper, emission IR spectroscopic analysis	40
Nitrogen standard compounds, EGA thermograms	401 <i>f</i>
Nitrogen, atmospheric particulates, ESCA and EGA analysis	398
NO <sub>x</sub> thermogram(s)	402
of particulate sample	408 <i>f</i>
and ESCA spectra, particulate sample	403 <i>f</i>
Nonaqueous dispersions, charge transient	324
Nonaqueous fluids, charge/mass measurements	322
Nonresonant reactions, C implantation	63



- Nonresonant reactions, theory, requirements ..... 62
- Nuclear component surfaces, chlorinated hydrocarbon reaction ..... 354
- Nuclear industry, surface analysis applications ..... 345
- Nuclear reaction analysis, electronic properties, amorphous Si ..... 234
- Nuclear reaction analysis, element profile ..... 60-68
- Nuclear reaction spectroscopy, characteristics ..... 257*t*
- Nuclear related studies, AES, SIMS, and XPS ..... 346
- Nuclear waste glass, SIMS depth profiles ..... 349*f*
- O**
- O-rings, XPS analysis ..... 185-188
- Objectives, surface analysis ..... 1-3
- Optical and carbon thermogram of particulate sample ..... 400*f*
- Optical efficiency, surface electromagnetic wave propagation IR spectroscopy ..... 41
- Optical and electrical transients with high particle concentration ..... 321*f*
- Optical and electrical transients, dispersion containing relatively-high particle concentration ..... 320
- Optical and electrical transients, particle mobility ..... 321*f*
- Optical methods, surface analysis ..... 106
- Optical microscopy, macroscopic topography ..... 2
- Optical properties and film thickness ellipsometric spectra ..... 42
- Optical spectra, UV-visible reflection spectroscopy ..... 41
- Optical spectroscopy, analysis of surfaces and thin films ..... 33-48
- Optical transient measurement, particle mobility ..... 318
- Ore mineralogy ..... 299-301
- mineral processing methodology ..... 299
- Ore(s)
- atom content, bulk and surface, operating stages ..... 304*t*
- leaching, metals ..... 306
- locking patterns ..... 299
- Organic acids oxide films on aluminum, FTIR reflection spectroscopic studies ..... 79
- Organic materials, electron mean free path and electron kinetic energy through ..... 149*f*
- Organic solids, surface acidity or basicity ..... 72
- Ovalbumin, spectra from modified ..... 176*f*
- Overlapping distributions, elastic backscattering analysis ..... 55
- Oxidation
- boiler tubing, surface studies ..... 359
- of coal, Fourier transform IR spectroscopy ..... 297
- high temperature ..... 273
- high temperature gaseous ..... 254*f*
- metals, stages ..... 253
- stainless steel ..... 273
- Oxidative surface treatment, white pine, XPS analysis ..... 190
- Oxygen plasma etched (OPE) polymer anchored rhodium catalyst beads ..... 193*t*
- Oxygen plasma etching, XPS analysis ..... 189
- Oxygen reduction reaction kinetics, space charge layer of galena ..... 292
- P**
- Particle charge, nonaqueous dispersions ..... 313
- Particle mobility, optical transient measurement ..... 318
- Particle-particle stability in xylene and hydrocarbon suspensions, zeta potential ..... 316
- Particle stability and surface potential, microelectrophoresis ..... 316-317
- Particulate sample
- carbon and optical thermogram ..... 400*f*
- ESCA spectrum ..... 405*f*
- NO<sub>x</sub> thermogram ..... 408*f*
- Particulates, sulfur and nitrogen, ESCA and EGA analysis ..... 398
- Particulates, thermal analysis and photoelectron spectroscopy ..... 397
- Passivating films, electronic devices ..... 236
- Passive protective films, corrosion ..... 253
- Patterning sequence, transistor, bipolar device processing ..... 232*t*
- Patterning sequence, transistor ..... 231
- Patterning, electronic devices, AES and SIMS ..... 240
- Performance, solar energy collectors ..... 331
- Phenolic and carboxylic surface acids, aqueous titrations ..... 75
- Phenolic-OH and carboxylic surface groups, flotation rate constant ..... 298*f*
- Phenylazonaphthylamine, Hammett acidity indicators ..... 73*t*
- Phonon interactions with surfaces, UV through IR wavelengths ..... 34
- Phosphine anchored catalyst, electron lines ..... 194*f*

Phosphine anchored rhodium containing catalyst, electron spectra .....	194f	Plasma-wall interactions	
Phosphine anchored rhodium catalyst, accumulated surface scans .....	194f	hydrogen-induced changes .....	389
Photoelectron diffraction, local geometrical structure of surface species .....	10	impurities .....	372
Photoelectron spectroscopy		ion sputtering effects, magnetic fusion devices .....	371
characterization of particulates .....	397	magnetic fusion devices .....	368-372
reviews .....	145t	quiescent phase .....	371
of stainless steel surface .....	357f	spectroscopic evidence .....	370
of stainless steel surface rinsed .....	356f	surface-probe evidence .....	370
Photoelectron-induced diffraction effects, local atomic structure .....	2	Point-of-zero-charge, electrical double layer, mineral/water systems .....	287
Photoemission peaks, multiplet splitting .....	14	Point-of-zero-charge of andalusite .....	310f
Photoemission process and XPS spectrum .....	15f	Polyester fibers, chemically modified, surface analysis techniques .....	198
Photolithographic processing steps .....	232f	Polyester fibers, modified, surface analysis .....	198
Photon based techniques for interface analysis .....	10	Polyethylene fiber and graphite, ISS data .....	135f
Photon spectroscopies, requirement .....	35	Polymer anchored catalyst, XPS analysis .....	193
Photon spectroscopies, surface information .....	35	Polymer films, plasma deposited fluorocarbon coating, analysis .....	150-157
Photon spectroscopies in surface analysis, advantages and problems .....	35	Polymeric materials, core electron spectra .....	145-146
Photon spectroscopy, catalysis and corrosion .....	35	Polymer-metal interface, surface analysis .....	35
Photon spectroscopy, requirements and problems .....	34	Polymer surface, ion scattering data .....	133
Pigments, acidic and basic sites .....	83t	Polymer surfaces, O:C ratios, ISS data .....	134t
Pigments, surface acidity .....	83	Polymers, specimen charging, work function .....	136t
Plant growth regulators, biodegradable matrices, XPS analysis .....	177	Polymers, surface analysis, XPS industrial application .....	143-199
Plasma deposited films, electronic devices .....	237	Polymethylmethacrylate adsorption onto silica gel .....	81f
Plasma ignition, magnetic fusion devices, impurity concentration .....	373f	Polypropylene, ISS/SIMS data .....	135f
Plasma, impurity concentration, "effective Z" .....	374	Polystyrene, spectra from hexafluoroethane plasma polymerized onto .....	158f, 161f
Plasma impurity effects, magnetic fusion devices .....	372-374	Polystyrene latex conductometric titration .....	81f
Plasma oxidation, fibers, surface properties .....	148	Polysulfone, sulfur 2p spectra and irradiation time .....	197f
Plasma-polymerized fluorocarbon surfaces, XPS data .....	166t	Potential-determining ions electrical double layer .....	287
Plasma reactor for continuous treatment of yarn .....	151f	Potential variation through electrical double layer .....	291f
Plasma treated wool fibers		Preferential sputtering, chemical changes, sputtering process artifacts .....	28
analysis .....	157-173	Pretreatments of alloys, corrosion resistance .....	273
spectra		Pretreatments of stainless steels, crevice corrosion and high temperature oxidation, AES .....	272-273
carbon 1s electron line parameters .....	168t		
nitrogen 1s electron line parameters .....	172t		
oxygen 1s electron line parameters .....	168f		

- Principles of surface analysis ..... 3-4
- Process characterization, electronic materials, instrumental surface analysis ..... 229
- Pulse discharge cleaning, first-wall materials ..... 376
- Pulsed laser annealing, RBS ..... 243
- Pyridine adsorption onto Hi-Sil, Langmuir plot ..... 86
- Pyrite surface, ESCA ..... 302, 303f, 304t
- Pyrolytic graphite, and glassy carbon ..... 91
- Pyrolytic graphite, low resolution XPS spectra ..... 96f
- Pyrolytic graphite electrode, cyclic voltammogram ..... 97f
- Pyrolytic graphite electrode, SEM of an untreated ..... 94f
- Q**
- Q/M determination, nonaqueous fluids ..... 322-325
- Quality control, electronic materials, instrumental surface analysis ..... 229
- Quartz correlation among contact angle and adsorption density ..... 291f
- Quiescent phase, plasma-wall interactions ..... 371
- Quinones and esters of lactones, surface concentration ..... 77
- R**
- Radiation chemistry of solids, XPS ..... 196
- Radiation damage, first-wall, magnetic fusion devices ..... 372
- Radiation induced chemical reaction, sputtering process artifacts ..... 28
- Radioactive waste management, interfaces and material transfer ..... 346
- Radiofrequency (rf) plasma treatments, glassy carbon surfaces ..... 93
- Raman bands for pyridine adsorption on alumina ..... 300f
- Raman gain spectroscopy, stimulated, description, sensitivity ..... 45
- Raman scattering, characteristics ..... 257t
- Raman scattering spectroscopy, surface information ..... 35
- Raman spectra of monolayers and thin films ..... 44
- Raman spectroscopy  
 analysis of surfaces and thin films ..... 33-48  
 application of chemically modified electrode surfaces ..... 109  
 interfaces, mineral processing ..... 297  
 solid/aqueous solution interfaces ..... 297  
 solid/liquid interfaces, minerals ..... 297  
 surface information ..... 42-46
- Reactor boiler alloys, XPS studies ..... 346
- Reflectance, silver, mirror degradation, solar materials ..... 338
- Reflectance spectroscopy, internal and external ..... 41
- Reflection high energy electron diffraction, molecular beam epitaxy ..... 235
- Reflection IR spectroscopic techniques ..... 36
- Reflection IR spectroscopy, surface analysis ..... 36
- Relative intensities of Pt 4f photoelectrons ..... 101f
- Relaxation effect, electrophoretic retardation ..... 320
- Residual gas measurements, discharge cleaning processes ..... 379
- Resonant nuclear reaction  
 Cr implantation example ..... 65  
 hydrogen concentration profile, glass surface ..... 217  
 sodium concentration profile, glass surface ..... 217
- Resonant nuclear reaction profiles, glass surfaces ..... 217-219
- Reviews, photoelectron spectroscopy .. 145t
- Rhodium phosphine ligand anchored catalyst, XPS analysis ..... 193
- Rutherford backscattering spectroscopy (RBS)  
 advantages and disadvantages ..... 31  
 backscattering mechanism ..... 18  
 blocking experiments ..... 27  
 capabilities and limitations, electronic materials ..... 233t  
 channeling and blocking ..... 25  
 channeling experiments ..... 27  
 characteristics ..... 257t  
 corrosion control, gold-coated contacts ..... 273-278  
 depth profiling ..... 27  
 depth resolution ..... 25, 27  
 dopant, electronic devices ..... 242  
 dopant profile broadening, pulsed laser annealing ..... 243  
 electrostatic scattering ..... 53  
 high energy version of ion scattering ..... 18  
 kinetics, Pd<sub>2</sub>Si reaction ..... 234  
 metallization, electronic devices ..... 245  
 pulsed laser annealing ..... 143  
 quantitative elemental surface analysis technique ..... 9  
 solar materials research ..... 333  
 surface characterization ..... 13

Rutherford backscattering spectroscopy— <i>Continued</i>		Secondary ion mass spectroscopy— <i>Continued</i>	
surface sensitivities .....	24	application .....	129–132
Rutherford backscattering spectroscopy analysis, titanium implanted with platinum .....	269	adhesives and other polymers	
Rutherford backscattering spectroscopy and ion implantation, corrosion mechanisms of alloys .....	272	aqueous corrosion profiles	
Rutherford backscattering spectroscopy process .....	19f	soda-lime-silica glasses .....	214
Rutherford backscattering spectroscopy spectra for As ion-implanted Si .....	244f	basic process objectives .....	16
Rutherford backscattering spectroscopy spectrum for 2 MeV He <sup>+</sup> on a W(100) crystal .....	26f	borosilicate glass leaching .....	348–354
Rutherford backscattering spectrum of a steel sample .....	57f	capabilities and limitations,	
Rutherford backscattering spectrum for a thick lubricant thin film .....	54f	electronic materials .....	233 <i>t</i>
Rutherford backscattering spectrum thin MoS <sub>2</sub> film .....	54f	characteristics .....	257 <i>t</i>
		complementary data, dielectric, electronic devices .....	238
		contamination and dopants, electronic devices .....	235
		depth profile sodium in SiO <sub>2</sub> films ..	236
		dopant profile broadening, pulsed laser annealing .....	243
		dynamic range .....	21
		electronic properties, amorphous Si	234
		equipment .....	126
		information content .....	20
		ion microprobe .....	126
		kinetics, Pd <sub>2</sub> Si reaction .....	234
		metallization, electronic devices ..	245
		molecular beam epitaxy .....	235
		nuclear related studies .....	346
		patterning, electronic devices .....	240
		plasma-oxide interface .....	238
		sensitivity .....	128
		solar materials research .....	333
		spatial resolution .....	21
		stainless steel samples .....	379
		stainless steel surfaces .....	383
		static .....	21
		surface analysis, discharge cleaning, magnetic fusion device .....	379
		surface characterization .....	13
		surface sensitivities .....	24
		surface sensitivity adhesive bonding	123
		transitional region of SiO <sub>2</sub> -Si interface, electronic devices ..	236
		waste glass studies .....	346
		Secondary ion mass spectroscopy concentration profiles .....	22f
		Secondary ion mass spectroscopy depth profiles	
		for borosilicate glass .....	353f
		of isotopic oxygen distribution for GaAs .....	239f
		leaching of sodium borosilicate glass in simulated nuclear waste glass .....	348, 349f
		for sodium borosilicate glass .....	351f
		Secondary ion mass spectroscopy measurements, objectives, static vs. dynamic .....	21
<b>S</b>			
Sample transfer and isolation system vacuum performance, electrode analysis .....	104 <i>t</i>		
Sampled depth analysis .....	24		
Scanning Auger microscopy, surface analysis of stainless steel .....	355, 359		
Scanning electron microscopy of carbon surfaces .....	91		
chemically modified electrode, surface topography .....	112		
locking patterns of minerals, grain size, and topography .....	301		
macroscopic topography .....	2		
pin holes, polyvinyl ferrocene films on Pt .....	93		
quality of polymerically coated electrode surfaces .....	93		
of treated glassy carbon electrode ..	94f		
of an untreated pyrolytic graphite electrode .....	94f		
Scattering cross-sections for incident ion, ion scattering spectroscopy ..	23		
Scattering and emission experiments ..	4		
Scattering or emission experiments, surface sensitivity .....	3		
Schottky barrier height modulation and stabilization .....	9		
Secondary ion mass spectra of stainless steel .....	384f, 385f		
Secondary ion mass spectroscopy advantages and disadvantages .....	28, 30, 128 <i>t</i>		

- Secondary ion mass spectroscopy profiles, glass surfaces ..... 214-217
- Secondary ion mass spectroscopy spectra, aluminum alloy ..... 130
- Secondary ion mass spectroscopy static, depth profiling ..... 27
- Secondary ion mass spectroscopy studies, surface chemistry changes, glass surfaces ..... 354
- Secondary ion mass spectroscopy surface analysis, high current density sputtering ..... 126
- Secondary ion mass spectroscopy surface analysis, low current density sputtering ..... 126
- Secondary ion mass spectroscopy system, equipment ..... 127f
- Secondary ion proton spectroscopy analysis  
     compositional profile of the surface ..... 219  
     compositional profiles of cationic species in glass ..... 222  
     glass surfaces ..... 219-222
- Secondary ion proton spectroscopy techniques, concentration of alkali ..... 222
- Semiconductor industry, ion implantation ..... 56
- Semiconductor interfaces, composition, surface structure ..... 9
- Semiconductor problems, surface analytical techniques ..... 230
- Semiconductor processing, fabrication steps ..... 230-231
- Semiconductor processing technologies ..... 231-245  
     application of AES ..... 231  
     application of RBS ..... 231  
     application of SIMS ..... 231  
     application of XPS ..... 231
- Semiconductors, compound, surface and thin film analysis ..... 235
- Separation, minerals, flotation ..... 289
- SERS, surface information, description of technique, applications ..... 44
- Shake-up lines, XPS ..... 145
- Shake-up and multiplet splitting phenomena, XPS ..... 18, 20
- Side effects, energy transfer from probe to sample ..... 35
- Silica, adsorption, acidic sites ..... 85-86
- Silica-alumina catalysts,  $H_0$  values ..... 73
- Silicate glass, surface types ..... 204
- Silicon, amorphous, electronic properties ..... 234
- Silicon, microelectronic circuits ..... 236
- Siloxane urethane interpenetrating network, XPS analysis ..... 180-185, 187f
- Silver, mirror degradation, solar materials ..... 338
- Silver/glass interface, interfacial degradation reactions, solar materials ..... 338
- Silver/glass interfaces, XPS spectrum ..... 340f
- $Si_3N_4$  standard, spectrum of particles from nuclear reactions and scattering ..... 64f
- Smut, surface contamination ..... 130
- Smut on stainless steel, surface contamination ..... 130
- Soda-lime-silica glass, aqueous corrosion profiles, SIMS ..... 214
- Sodium borosilicate glass, leaching, SIMS depth profiles ..... 352f
- Sodium borosilicate glass, SIMS depth profiles ..... 351f
- Sodium concentration profile, glass surface, resonant reaction ..... 217
- Soft x-rays, AES ..... 16
- Solar energy, collection processes ..... 328
- Solar energy, conversion ..... 328
- Solar energy collectors, requirements ..... 331f
- Solar energy components, stack designs ..... 330f
- Solar energy conversion systems ..... 328  
     area-intensive nature ..... 328  
     interfaces ..... 329-331
- Solar energy conversion technologies, interface phenomena ..... 335
- Solar energy materials, application of interface science ..... 337
- Solar energy materials, surface analysis ..... 327
- Solar energy technologies, surface science research ..... 335
- Solar interface research, surface activity ..... 333
- Solar materials  
     current problems ..... 338f  
     deterioration, mirror ..... 339  
     elemental composition, interfaces ..... 333  
     interface science ..... 331  
     interface studies ..... 331-335  
     interfaces ..... 335-337  
     properties ..... 335f  
     study areas ..... 336  
     surface analytical facilities ..... 334  
     interfacial behavior, limitations of methods ..... 336  
     interfacial microstructure and microchemistry, research needs ..... 337  
     mirror degradation problem ..... 338  
     problems ..... 339  
     properties ..... 334
- Solar materials research ..... 333

Solar materials surfaces, structural determinations .....	333	Spectra— <i>Continued</i>	
Solar radiation and collection devices, description .....	328	of tetrafluoroethylene plasma polymerized onto wool .....	160f
Solid, surfaces .....	69	from wool fibers oxidized beyond the excitation region .....	164f
Solid/aqueous solution interfaces, Raman spectroscopy .....	297	from wool fibers oxidized in oxygen plasma .....	164f
Solid/gas interface, solar energy conversion systems .....	329	of wool trifluoroacetylated with ethyl thiotrifluoroacetate .....	174f
Solid interface, characterization considerations, solar energy materials .....	332	Spectral measurement of acid-base complexes on metals .....	79–80
Solid/liquid interface, mineral processing .....	284	Spectroelectrochemistry, electroactive surface mediator .....	109
Solid/liquid interfaces		Spectroscopic evidence, plasma-wall interactions .....	370
IR and laser Raman spectroscopy ..	299f	Sputter depth profile of oxide .....	275f
minerals, Raman spectroscopy .....	297	Sputter redeposition, sputtering process artifacts .....	28
solar energy conversion systems .....	329	Sputtering process artifacts	
Solid/solid interface		ion enhanced diffusion .....	28
solar energy conversion systems .....	329	knock-on effects .....	28
solar energy materials .....	332f	preferential sputtering, chemical changes .....	28
structure determination .....	8	radiation induced chemical reactions .....	28
Solid/solution interfaces, minerals analytical techniques .....	286	sputter redeposition .....	28
Solid surfaces, characterization by wet chemical techniques .....	69–89	Sputtering rate, SIMS .....	21
Someriset coal, zeta potential and flotation rate constant .....	293f	Stability, components, solar energy conversion systems .....	329
Soxhlet test, comparison of glass corrosion performance .....	208	Stack designs, solar energy components .....	330f
Space charge layer, Galena, oxygen reduction reaction kinetics .....	292	Stainless steel, AES depth-composition profiles .....	360f
Spatial location, compositional analysis .....	2	Stainless steel, chemical changes by trichloroethane .....	354
Spatial resolution, SIMS .....	21	Stainless steel, ISS/SIMS data .....	131f
Specimen charging, ion beam method .....	134–136	Stainless steel, metal oxide hydrolysis .....	383
Specimen charging, work function, polymers .....	136f	Stainless steel, oxidation .....	273
Spectra		Stainless steel, SIMS .....	384f, 385f
analysis, glassy carbon .....	106	Stainless steel, smut, surface contamination .....	130
from bovine serum albumin trifluoroacetylated with ethyl thiotrifluoroacetate .....	174f	Stainless steel, XPS .....	358f, 382f
from casein modified with ethyl vinyl sulfone .....	175f	Stainless steel alloys, corrosion resistance .....	272
from fluorocarbon coating plasma grafted to wool yarn .....	154f	Stainless steel components (nuclear), elimination of inorganic chloride contamination .....	354
from hexafluoroethane plasma polymerized onto polystyrene .....	158f, 161f	Stainless steel exposed to trichloroethane .....	358f
from hexafluoroethane plasma polymerized on wool fabric .....	159f, 163f	Stainless steel and Inconel, elemental surface composition .....	381f
from mercury papain .....	176f	Stainless steel samples, SIMS .....	379
from modified ovalbumin .....	176f	Stainless steel samples, XPS .....	379
of polyvinyl alcohol, analysis of glassy carbon surface .....	108f	Stainless steel surface rinsed, photoelectron spectra .....	356f
		Stainless steel surfaces	
		corrosion .....	354

- Stainless steel surfaces—*Continued*  
 photoelectron spectra ..... 357f  
 SIMS ..... 383  
 XPS ..... 383
- Static SIMS method ..... 21  
 modes ..... 20  
 surface analysis ..... 126
- Steel sample  
 computer simulation ..... 56  
 computer simulation of partial  
 spectrum ..... 58f  
 Rutherford backscattering spectrum ..... 57f
- Stimulated Raman gain spectroscopy,  
 description, sensitivity ..... 45
- Stimulated Raman gain spectroscopy  
 monolayer quantity films ..... 45
- Stoichiometric rations, dielectric,  
 electronic devices ..... 237
- Streaming potential, electrokinetic  
 effects, mineral interface ..... 289
- Strong electronic transitions,  
 reflectance spectroscopy ..... 41
- Structural characterization, Raman  
 spectroscopy ..... 44
- Structural determination, ISS ..... 23
- Structural determination, solar  
 materials surfaces ..... 333
- Structure of chitosan and chitan ..... 178f
- Structure of surfaces ..... 4
- Structure, chemically modified  
 electrode, analysis ..... 110–112
- Styrene divinylbenzene copolymer  
 beads, sulfonation, XPS  
 analysis ..... 188–190
- Submonolayer films, surface electro-  
 magnetic wave propagation IR  
 spectroscopy ..... 41
- Sulfide minerals, flotation, contact  
 angles and voltammetry ..... 292
- Sulfide ores, complex, flotation  
 separation, ESCA ..... 302
- Sulfonated styrene divinylbenzene,  
 electron spectra ..... 191f
- Sulfonated styrene divinylbenzene  
 cross-linked beads, intensities  
 and composition, XPS analysis .. 189t
- Sulfonation of styrene divinylbenzene  
 copolymer beads, XPS  
 analysis ..... 188–190
- Sulfone polymer radiation chemistry,  
 XPS analysis ..... 196–198
- Sulfur, atmospheric particulates,  
 ESCA and EGA analysis ..... 398
- Sulfur composition, grain  
 boundaries, AES ..... 263
- Sulfur coverages at grain  
 boundaries of nickel ..... 264f
- Sulfur intensities and radiation  
 exposure, XPS analysis ..... 198t
- Sulfur 2p spectra and irradiation  
 time of polysulfone ..... 197f
- Surface  
 atomic dynamics and electronic  
 structure ..... 3  
 concept ..... 1  
 wide scan spectra ..... 147f
- Surface acidity  
 carbon black ..... 75  
 kaolinite, attapulgite, and bentonite ..... 73  
 pigments ..... 83
- Surface acidity and basicity  
 electrophoretic methods ..... 86–87  
 indicator dye techniques ..... 72–75  
 organic solids ..... 72
- Surface activity, solar interface  
 research ..... 333
- Surface analyses, carbon blacks ..... 75
- Surface analysis  
 chemically modified electrode  
 surfaces ..... 90  
 corrosion ..... 252  
 data acquisition ..... 259  
 technique selection ..... 255  
 data analysis, corrosion ..... 261  
 definition ..... 34  
 electronic and vibrational  
 spectroscopy ..... 106  
 gold-coated contacts, AES and  
 XPS ..... 277  
 instrumental, electronic materials  
 and processes ..... 229  
 instrumentation and procedures for  
 data interpretation ..... 9  
 integrated circuit fabrication ..... 230  
 SIMS ..... 126  
 stainless steel and trichloroethane .. 354
- Surface analysis applications,  
 nuclear industry ..... 345
- Surface analysis diagnostic on  
 Tokamak ..... 380f
- Surface analysis diagnostic, wall con-  
 ditioning processes, Tokamak .... 379
- Surface analysis of modified  
 polyester fibers ..... 198
- Surface analysis studies, nuclear  
 related examples ..... 345
- Surface analysis techniques  
 AES, and semiconductor tech-  
 nologies ..... 231  
 chemically modified polyester  
 fibers ..... 198  
 RBS, and ST ..... 231  
 SIMS, and semiconductor  
 technologies ..... 231

Surface analysis techniques— <i>Continued</i>		Surface electronic structure, synchrotron radiation .....	3
using light .....	33	Surface energy, solar energy materials .....	333
XPS, and semiconductor technologies .....	231	Surface extended x-ray absorption fine structure, local geometrical structure of surface species .....	10
Surface analytical facilities, solar materials interfaces .....	334	Surface functional groups chemical modification, XPS analysis	173
Surface analytical method, ideal .....	90	coal .....	294
Surface analytical techniques, epitaxial growth of Si .....	234	minerals and ores .....	294
Surface analytical techniques, semi- conductor problems .....	230	Surface grafting, coatings to wool fibers, surface properties .....	148
Surface basicity, indicator dyes .....	73	Surface groups, chemical reactivity .....	69
Surface behavior, XPS .....	144	Surface groups, minerals, derivative formation .....	296
Surface characterization		Surface immobilization, catalysis .....	90
adhesion bonding, ISS .....	123	Surface information	
adhesion bonding, SIMS .....	125	IR spectroscopy .....	35, 36–41
flotation .....	289–297	Raman spectroscopy .....	42–46
mineral processing .....	283	UV-visible absorption spectroscopy	35
UHV techniques .....	13–32	UV-visible reflection spec- troscopy .....	41–42
Surface characterization method, adhesive bonding .....	122 <i>t</i>	Surface or interfacial properties, mineral processing .....	285 <i>t</i>
Surface characterization techniques, mechanisms of various subprocesses, mineral processing .....	301	Surface modification, XPS and AES analysis .....	93
Surface charge		Surface oxidation state, UO <sub>2</sub> , corrosion .....	266
effect of water .....	317	Surface pits, glassy carbon .....	93
minerals .....	287	Surface potential .....	313
equation .....	287	equations .....	316
Surface chemistry		minerals equation .....	287
adhesive bond formation .....	122	Surface potential and particle stability, microelectrophoresis .....	316–317
conditioning procedures, first-wall materials .....	375	Surface-probe evidence, plasma-wall interactions .....	370
discharge cleaning .....	377	Surface properties	
first-wall materials, magnetic fusion devices .....	367	C implantation .....	63
Surface chemistry changes, SIMS studies, glass surfaces .....	354	indifferent electrolytes, minerals .....	289
Surface composition		minerals, counter ions .....	289
boiler tubing .....	359	plasma oxidation of fibers, surface grafting of coatings to wool fibers .....	148
copolymers, XPS .....	180	Surface properties of mineral particles, techniques .....	286 <i>t</i>
glass .....	204	Surface properties and mineral processing .....	286–287
glassy carbon electrodes .....	103	Surface reactivity of solids .....	69
Surface composition in industrial applications .....	5	Surface roughening, sputtering process artifacts .....	28
Surface composition of pyrite, ESCA .....	304 <i>t</i>	Surface science, solar materials interfaces .....	335–337
Surface compositional data for glasses .....	208	Surface science research, solar energy technologies .....	335
Surface compositional profile, glass enamel .....	210	Surface selectivity, low energy ion scattering .....	125
Surface concentration, quinones and esters of lactones .....	77	Surface sensitive techniques, potential problems .....	259
Surface contamination .....	130		
Surface corrosion, ESCA .....	219		
Surface electromagnetic wave propa- gation spectroscopy, experi- mental configuration .....	43 <i>f</i>		



- Surface sensitivities  
 AES ..... 24  
 ISS ..... 24  
 RBS ..... 24  
 SIMS ..... 24  
 XPS ..... 24
- Surface sensitivity  
 scattering or emission experiments ..... 3  
 XPS, chemical modifications of  
 surface functional groups ..... 173f
- Surface sensitivity characteristics, RBS ..... 24
- Surface sensitivity, SERS ..... 44, 45
- Surface sites, metal-oxides ..... 79
- Surface sites on carbon blacks,  
 titration ..... 75
- Surface stability, ultra-high vacuum  
 chambers ..... 3
- Surface structure ..... 2
- Surface structure and composition  
 semiconductor interfaces ..... 9
- Surface structure in microelectronics .. 5-9
- Surface studies, boiler tubing  
 oxidation ..... 359-361
- Surface studies, Tokamaks, discharge  
 cleaning ..... 379
- Surface technique  
 characteristics ..... 257t-258t
- Surface and thin film analysis, external  
 reflection IR spectroscopy ..... 40
- Surface topography, chemically modified  
 electrode, analysis ..... 91-93
- Surface treatments, changes in  
 chemistry ..... 129
- Surfaces, analysis by IR, Raman,  
 and optical spectroscopy ..... 33-48
- Surfactant adsorption, minerals ..... 306
- Surfactants, comminution process,  
 minerals ..... 305
- Sweepout and transit light scattering  
 measurements ..... 319f
- Synchrotron radiation ..... 10  
 surface electronic structure ..... 3
- T**
- Technique selection, corrosion,  
 surface analysis ..... 255
- Techniques for surface properties of  
 mineral particles ..... 286t
- Teflon, ISS data ..... 133
- Temperature dependence for metal  
 oxides reduction ..... 387f
- Tetrafluoroethylene plasma polymerized  
 onto wool, spectra ..... 160f
- Thermal analysis, characterization  
 of particulates ..... 397
- Thermograms, sulfur and nitrogenic  
 species in particulates ..... 399
- Thick film example, elastic back-  
 scattering analysis ..... 53
- Thick lubricant thin film, RBS ..... 54f
- Thin film example, elastic  
 backscattering analysis ..... 52
- Thin films, analysis by IR, Raman,  
 and optical spectroscopy ..... 33-48
- Thin films and monolayers, Raman  
 spectra ..... 44
- Thin MoS<sub>2</sub> film, RBS ..... 54f
- Three phase interactions, mineral  
 processing ..... 284t
- TiC-coated graphite, high heat-load  
 surfaces ..... 391
- Time to depth conversion, SIMS ..... 20
- Titanium gettering, first-wall  
 materials ..... 386
- Titanium, anodic polarization curve .. 270f
- Titanium, hydrogen gettering  
 properties ..... 388
- Titanium implanted with platinum  
 current, time, and concentration .... 271f  
 RBS analysis ..... 269  
 RBS, electrochemistry ..... 267-272
- Titration  
 of ionic groups on latex particles . 77-79  
 of polystyrene latex, conductometric 81f  
 of surface sites on carbon blacks .... 75
- Tokamak(s)  
 conditioning procedures ..... 377  
 surface analysis diagnostic, wall  
 conditioning processes ..... 379, 380f  
 surface studies, discharge cleaning 379
- Tokamak Fusion Test Reactor,  
 vacuum vessel ..... 390f
- Tokamak-type fusion device ..... 369f
- Tool steel, application of N  
 implantation ..... 63
- Transient measurements, electro-  
 phoretic mobility ..... 317
- Transient measurements, insulating  
 fluids ..... 317-318
- Transistor patterning sequence .... 231, 232t
- Trichloroethane, on stainless steel .... 354
- Trichloroethane, stainless steel  
 exposed ..... 358f
- Triethylamine adsorption, onto Hi-Sil 85
- Two phase interactions, mineral  
 processing ..... 284t
- Type I glass surface ..... 204
- Type II glass surface ..... 204  
 kinetics equation ..... 206
- Type III glass surface ..... 204  
 kinetics equation ..... 206
- Type IV glass surface ..... 204  
 kinetics equation ..... 206
- Type V glass surface ..... 204  
 kinetics equation ..... 206

U	
Ultra-high vacuum, definition, uses .....	14
Ultra-high vacuum chambers, surface stability .....	3
Ultra-high vacuum techniques of surface characterization .....	13-32
Uranium oxide	
electrode, XPS spectra .....	268f
surface oxidation states .....	266, 270f
Urethane fluoroalkyl siloxane interpenetrating network, XPS analysis .....	185
UV through IR wavelengths, phonon interactions with surfaces .....	34
UV-visible absorption spectroscopy, surface information .....	35
UV-visible reflection spectroscopy, surface information .....	41-42
V	
Vacuum-baking, first-wall materials ..	375
Vacuum pump fluid and O-ring seals, XPS analysis .....	185-188
Vacuum transfer system, extended, electrode sample handling system ..	103
Vacuum vessel for Tomamak Fusion Test Reactor .....	390f
Vibrational properties of molecular structures, IR spectra .....	36
Vibrational spectroscopy	
application of chemically modified electrode surfaces .....	109
surface analysis .....	106
Vibrational spectrum, Raman spectroscopy .....	44
Voltammetry, mineral surface characterization .....	292
Voltammetry and contact angles, sulfide minerals, flotation .....	292
W	
Wall conditioning processes, surface analysis diagnostic, Tokamak ....	379
Walls, magnetic fusion devices, surface chemistry .....	367
Waste container corrosion, XPS .....	346
Water-glass reaction, boron concentration .....	348
Weathering, glass surface analysis ....	208
Wedge failure surface with ISS/SIMS data .....	139f
Wedge test, bond failure, ISS and SIMS data .....	138
Wet chemical analysis, London dispersion force interaction .....	70-71
Wet chemical analysis techniques, use and kinds of information .....	70
Wet chemical technique(s)	
characterization of solid surfaces ..	69-89
chemical reactivity of surface groups .....	69
measurement of contact angles .....	71
Wettability, minerals, adsorption phenomena .....	290
White pine, oxidative surface treatment, XPS analysis .....	190
White pine, untreated, electron spectra ..	192f
Wood surface treatment, XPS analysis .....	190
Wool	
spectra of tetrafluoroethylene plasma polymerized onto .....	160f
treated, electron spectrum .....	153f
untreated, electron spectrum .....	153f
Wool fabric, spectra from hexafluoroethane plasma polymerized onto .....	159f, 163f
Wool fiber(s)	
electron line intensities .....	172t
oxidized beyond excitation region, spectra .....	164f
oxidized in oxygen plasma .....	164f
oxygen plasma treated, spectra ..	169, 170
plasma deposited fluorocarbon coating, analysis .....	150-157
plasma treated, analysis .....	157-173, 168t, 172t
spectra of hexafluoroethane plasma polymerization .....	162f
surface grafting of coatings, surface properties .....	148
Wool fibers and film, electron lines ....	172f
Wool trifluoroacetylated with ethyl thiotrifluoroacetate, spectra .....	174f
Wool yarn	
electron spectrum .....	152f
oxygen plasma treated, spectra ..	170, 171
spectra from fluorocarbon coating plasma grafted to .....	154f
treated, electron spectrum .....	152
X	
X-ray photoemission spectroscopy ....	346
advantages and disadvantages .....	28, 29
chemical bonding .....	144
chemical composition .....	144
core lines .....	145
depth profiling .....	27
inelastic meanfree path length .....	146
instrumentation .....	145
of a pyrolytic graphite, low resolution .....	96f

- X-ray photoemission spectroscopy—  
*Continued*
- shake-up lines ..... 145
  - surface analysis, fibers and polymers, industrial applications ..... 143–199
  - surface behavior ..... 144
  - surface composition, copolymers .... 180
  - surface sensitivity, chemical modifications of surface functional groups ..... 173
- X-ray photoemission spectroscopy analysis
- block copolymers ..... 180
  - capabilities and limitations, electronic materials ..... 233*t*
  - characteristics ..... 257*t*
  - chemically modified electrode, elemental composition ..... 112
  - chromate films ..... 277
  - complementary data, dielectric, electronic devices ..... 238
  - composition bonding, and oxidation state in mineral surface layers ..... 301
  - copolymer composition ..... 180
  - core level shake-up process ..... 15*f*
  - correlated with coulometric results, film thickness ..... 99
  - corrosion studies, criteria ..... 255
  - corrosion, control, gold-coated contacts ..... 273–278
  - data analysis ..... 261
  - description of method ..... 14
  - electrochemical reactions at  $\text{UO}_2$  surfaces ..... 266
  - electrode surface modification ..... 102
  - extent of surface modification ..... 93
  - feather keratin, controlled release formulations ..... 180
  - final state relaxation ..... 14
  - final states, core-electron removal .. 16
  - fluoroalkylsiloxane ..... 185
  - growth regulators, cellulose ..... 180
  - growth regulators, encapsulated in natural polymers ..... 177–181
  - inelastic scattering ..... 24
  - information content ..... 18
  - intensities and composition, sulfonated styrene divinylbenzene cross-linked beads ..... 189*t*
  - interpenetrating networks ..... 180, 185
  - metallization, electronic devices .... 245
  - nuclear related studies ..... 346
  - O-ring seals and vacuum pump fluid ..... 185–188
  - oxygen plasma etching ..... 189
  - plant growth regulators, biodegradable matrices ..... 177
  - polymer anchored catalyst ..... 193
- X-ray photoemission spectroscopy analysis—*Continued*
- quantitative elemental surface analysis technique ..... 9
  - rhodium phosphine ligand anchored catalyst ..... 193
  - siloxane urethane interpenetrating network ..... 180–185, 187*t*
  - solar materials ..... 333
  - stainless steel samples ..... 379, 382*f*
  - structure of thin layer ..... 261
  - sulfonation of styrene divinylbenzene copolymer beads ..... 188–190
  - sulfone polymer radiation chemistry ..... 196–198
  - sulfur intensities and radiation exposure ..... 198*t*
  - surface analysis ..... 277, 379
  - surface analysis of stainless steel ..... 354, 350
  - transitional region of  $\text{SiO}_2$ -Si interface, electronic devices .. 236
  - urethane fluoroalkyl siloxane interpenetrating network ..... 185
  - use with electrochemical data ..... 95
  - vacuum pump fluid and O-ring seals ..... 185–188
  - waste container corrosion ..... 346
  - waste glass studies ..... 346
  - wood surface treatment ..... 190
- X-ray photoemission spectroscopy atomic speciation ..... 95
- X-ray photoemission spectroscopy data, plasma-polymerized fluorocarbon surfaces ..... 166*t*
- X-ray photoemission spectroscopy depth profiles, evolution of film composition ..... 361
- X-ray photoemission spectroscopy depth-composition of Iconel 600 alloy surface ..... 362*f*
- X-ray photoemission spectroscopy peaks of  $\text{Na}_2\text{CrO}_4$  ..... 279*f*
- X-ray photoemission spectroscopy process, electronic energy level diagram ..... 14
- X-ray photoemission spectroscopy signal, electrochemically determined coverage ..... 99
- X-ray photoemission spectroscopy spectrum
- at Ag/glass interfaces ..... 340*f*
  - and emission angle for Ru 3d and Fe 2p  $3/2$  ..... 100*f*
  - gold and silver ..... 277
  - intensity ratios ..... 99
  - and photoemission process ..... 15*f*
  - stainless steel surfaces ..... 358*f*, 383
  - $\text{U}^{4+}$  and  $\text{U}^{6+}$  oxidation states ..... 267

X-ray photoemission spectroscopy spectrum— <i>Continued</i> from uranium oxide electrode .....	268f	<i>Zeta potential—Continued</i> particle-particle stability in xylene and hydrocarbon suspensions	316
<b>Y</b>		Zeta potential and flotation rate constant of Somereset coal .....	293f
Yarn, plasma reactor for continuous treatment .....	151f	Zeta potential measurement, aqueous system .....	315-316
<b>Z</b>		Zr-Al getters, fusion device applications .....	389
Zeta potential .....	313	Zr-Al getters, hydrogenic loading, discharge cleaning .....	389